NASA CR-72366
AVSSD-0071-68-CR

ISOTOPE REENTRY VEHICLE DESIGN STUDY
CONCEPTUAL DESIGN -- PHASE IA -- TOPICAL REPORT

Prepared for

NATIONAL AERONAUTICS AND SPACE ADMINISTRATION

Contract NAS 3-10938

AVCO MISSILES, SPACE AND ELECTRONICS GROUP
SPACE SYSTEMS DIVISION
Lowell Industrial Park
Lowell, Massachusetts 01851

Requests for copies of this report should be referred to

National Aeronautics and Space Administration
Office of Scientific and Technical Information
Attention: AFSS-A
Washington, D.C. 20546

NASA CR-72366
AVSSD-0071-68-CR

ISOTOPE REENTRY VEHICLE DESIGN STUDY
CONCEPTUAL DESIGN -- PHASE IA -- TOPICAL REPORT

Prepared for

NATIONAL AERONAUTICS AND SPACE ADMINISTRATION

May 1968

Contract NAS 3-10938

TECHNICAL MANAGEMENT
NASA LEWIS RESEARCH CENTER
Cleveland, Ohio

BRAYTON CYCLE BRANCH
LLOYD I. SHURE

AVCO MISSILE, SPACE AND ELECTRONICS GROUP
SPACE SYSTEMS DIVISION
Lowell Industrial Park
Lowell, Massachusetts 01851

ABSTRACT

This document summarizes the Phase IA conceptual design effort on the Isotope Reentry Vehicle (IRV) study. The major objective of the study is to develop a preliminary design of a 25 KW_t Pu 238 IRV. Major design emphasis is on system safety and developability. The IRV is configured to meet minimum practical diameter and weight limits. During Phase IA various IRV, heat source, and heat-source heat exchanger concept combinations have been developed and evaluated. Three IRV systems have been recommended for detailed conceptual design evaluation in Phase IB.

EDITED BY:
EDITORIAL SERVICES SECTION
WILLIAM BARBER

CONTENTS

CONTENTS (Cont'd)

CONTENTS (Cont'd)

CONTENTS (Concl'd)

ILLUSTRATIONS

ILLUSTRATIONS (Cont'd)

ILLUSTRATIONS (Cont'd)

ILLUSTRATIONS (Cont'd)

ILLUSTRATIONS (Cont'd)

ILLUSTRATIONS (Cont'd)

ILLUSTRATIONS (Cont'd)

ILLUSTRATIONS (Cont'd)

ILLUSTRATIONS (Cont'd)

ILLUSTRATIONS (Cont'd)

ILLUSTRATIONS (Cont'd)

ILLUSTRATIONS (Cont'd)

ILLUSTRATIONS (Cont'd)

ILLUSTRATIONS (Concl'd)

TABLES

TABLES (Concl'd)

1.0 INTRODUCTION

This report presents the initial results of the Isotope Reentry Vehicle (IRV) Design Study being performed under contract NAS 3-10938 for the Lewis Research Center. The major objective of the program is to achieve a preliminary design of a $25KW_t$ (at the end of mission life) plutonium 238 IRV. The required operational lifetime is five years and major design emphasis is placed on system safety and vehicle developability. In addition, the IRV should be configured for minimum diameter and weight, and the design of the heat source heat exchanger must be compatible with the characteristics of the Brayton Cycle which is presently under investigation at NASA/Lewis.

Figure 1.0-1 shows an exploded view of an illustrative IRV and heat source heat exchanger (HSHX) configuration. The isotope heat source consists of an array of isotope capsules containing PuO_2 fuel. Approximately 164 unvented -- ORNL design -- capsules are required to achieve a thermal power output of 25 KW_{EOL}. The heat source capsule array together with its BeO heat sink is mounted on a refractory metal support plate which in turn is attached to the reentry vehicle aeroshell via a truss network. Superinsulation is used to minimize heat leaks from the heat source to the reentry vehicle and its surroundings. Crushup material is provided between the heat source support plate and the aeroshell to attenuate the g-loading of the capsules during ground impact of the IRV occurring after reentry and terminal descent. The entire IRV is attached to the parent spacecraft with a support ring which allows the IRV to be pivoted in and out of the spacecraft. Redundant and replaceable heat exchangers are provided to accept the thermal output of the heat source capsules which radiate at a maximum temperature of about 2000^oF.

Overall study ground rules are summarized in Table 1.0-I. Specific IRV design and safety criteria established at the outset of the study are listed in Tables 1.0-II and 1.0-III. In addition the structural design criteria in use in Phase IA are listed in Table 1.0-IV.

1.1 CONCEPTUAL DESIGN -- PHASE IA

During the conceptual design phase a large number of design alternatives have been considered, evaluated, and traded-off in the following design areas:

a. Aerodynamic shape and packaging

b. Aeroshell structure and reentry thermal protection

c. Heat source array configuration

d. Heat source heat exchanger configuration

e. Heat source to aeroshell attachment schemes

f. Heat source capsule retention and support schemes

g. Ground impact g-loading attenuation schemes

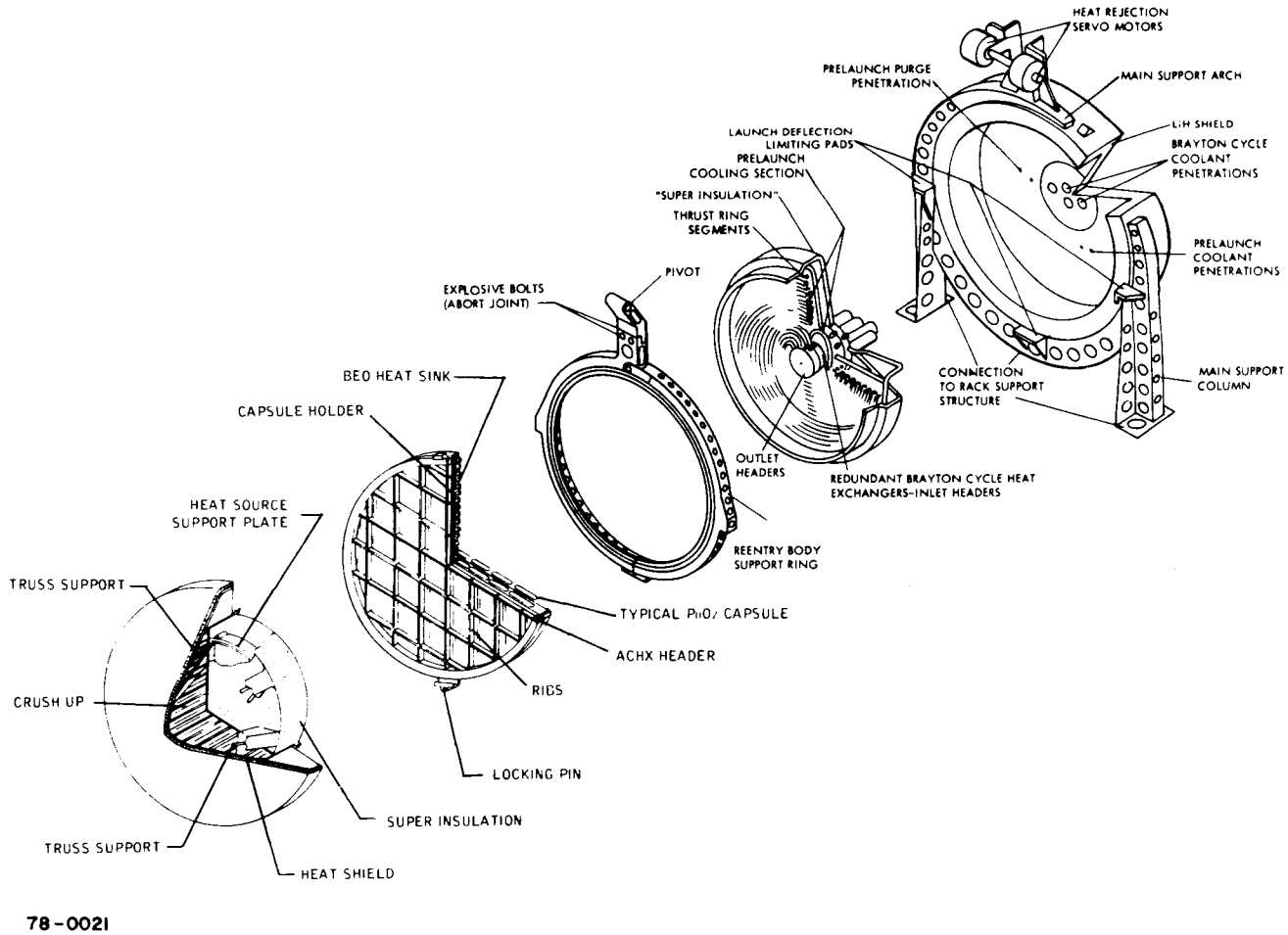

Figure 1.0-1 REFERENCE IRV AND HSHX CONFIGURATION

TABLE 1.0-I

PROGRAM GROUND RULES

1. Use ORNL isotope heat source capsule characteristics
2. Consider both separate IRV launch (Atlas/Centaur) and integral launch (Saturn 1B-MORL)
3. Consider incorporation of recovery aids for the IRV
4. Aerodynamic configurations limited to 60^{o} half-angle blunt cone and modified Apollo shape
5. HSHX to be in-place redundant and replaceable
6. Intact reentry capability during all mission phases
7. Design must provide for adequate heat rejection after impact

TABLE 1.0-II

IRV DESIGN CRITERIA

1)	Isotope Fuel	PuO_2
2)	Capsule Design	See Figure 2.1-1
3)	Fuel Loading	25 KWt (EOL)
4)	IRV Ballistic Coefficient -- $\frac{W}{C_d A}$	$\leq$ 80 lb/ft^2 (Subsonic)
5)	Heat Leak -- IRV, HSHX, and ACHX	$\leq$ 1.5 KWt*
6)	Heat Source Temperature:	
	Max Continuous, Surface	$\leq 2000^{\circ}F$
	Max Transient, Surface	$\leq 2500^{\circ}F$*
	Max Launch Pad Equilibrium (Operation with ACHX)	$\leq 1400^{\circ}F$
7)	Emergency Heat Rejection	Passive Radiation to Space by Body Deployment
8)	Thermal Storage:	
	Material	BeO
	Requirement	60 min ($1800^{\circ}F$ to $2500^{\circ}F$)
9)	Launch Abort	Rocket Ejection $\leq$ 10g Acceleration
10)	Orbital Emergency Separation	Redundant Pyrotechnic

*In the event of upside-down IRV earth impact, provision must be made to destroy or otherwise overcome the insulation and permit heat rejection without exceeding heat source temperature limits.

TABLE 1.0-III

SAFETY CRITERIA

1) Capsule design based on 10 half-life containment

2) No fuel release as a result of launch pad abort, fire, or entrapment of heat source in debris

3) Intact reentry of IRV from uncontrolled random reentry

4) Reentry vehicle ejection in the event of catastrophic launch abort

5) No burial of IRV after impact at terminal velocity

6) Radiation coupling between heat source and power conversion system - no physical connection

7) No credibility for assembly of critical mass

TABLE 1.0-IV

STRUCTURAL DESIGN CRITERIA

Launch load	10 g
Reentry load	30 g
Nominal Impact Velocity	180 fps
Vibration	natural frequency > 200 hz

h. Recovery (e.g. parachutes, ballutes) and location aids incorporation

i. Abort and deorbit rocket and separation system selection and integration

j. IRV/launch vehicle/spacecraft integration.

Several basic overall vehicle concepts were generated and examined during the early portions of the conceptual design phase. Three of these have been recommended for further study thus completing the first part of the conceptual design effort (Phase IA). This report summarizes the results of this task. The remainder of the conceptual design effort -- Phase IB -- is devoted to a more detailed analysis and comparison of the three selected vehicle concepts so that the most promising concept can be identified for the preliminary design -- Phase II.

The various vehicle concepts are compared and evaluated on the basis of several criteria, the most critical of these being:

a. Safety

b. Vehicle diameter

c. Vehicle weight

d. Reentry performance

e. Overall reliability (simplicity) and developability

f. Ability of the design to allow growth potential or changes in subsystem characteristics.

1.2 AERODYNAMIC TEST PROGRAM

The major purpose of the test program is to define a passive aerodynamic device (such as a fence or fin) which ensures that the vehicle is not stable in a rearward attitude during reentry. Consequently, if the vehicle were to initially begin reentry in such an attitude (180^{o} angle of attack) this device would guarantee vehicle "turn-around" at high altitudes prior to peak heating. Rearward (or high angle of attack) entry is undesirable because of the increased aerodynamic heating experienced by the heat source capsules which are located in the base region of the vehicle.

A number of different aerodynamic devices have been studied analytically and the most promising configurations will be tested in the free flight shock tunnel and the arc wind tunnel test facilities at NASA/Ames. These facilities are capable of achieving the appropriate Reynolds Number (10^4 - 10^5) and Mach Number conditions. Sufficient data will be collected to provide a preliminary selection of an effective turn-around device together with dimensional characteristics for use in the preliminary design phase.

1.3 PRELIMINARY DESIGN -- PHASE II

At the end of the conceptual design phase the most promising IRV concept will be selected for a more detailed preliminary design evaluation. During the preliminary

design phase the structural and thermal design of the IRV and the heat source heat exchanger will be completed. In addition, a detailed reentry performance analysis will be made to establish the performance limitations of the reference vehicle and its sensitivity to variations in the reentry trajectory, vehicle motions and vehicle physical parameters.

1.4 PROGRAM SCHEDULE

Figure 1.4-1 shows the overall study schedule together with the time phasing of the three major tasks. The two milestones shown on Phase I (conceptual design) correspond to the two oral presentations which are given at the conclusion of Phase IA and Phase IB. Topical report drafts describing these phases are due one month after the oral presentations.

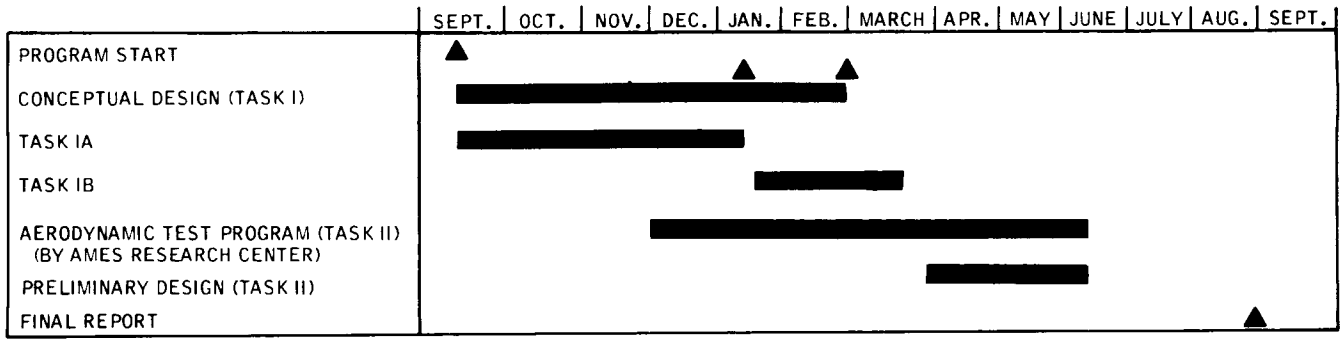

Figure 1.4-1 PROGRAM SCHEDULE

2.0 SUMMARY

During this period of the conceptual design phase three major subtasks were completed, leading to the selection of three vehicle concepts which will be evaluated further in Phase IB.

First, a systems analysis was performed resulting in the definition of the critical system design requirements for the IRV (e.g., abort requirements, reentry conditions, impact attenuation requirements, etc.) Safety considerations and examination of various failure modes played a predominant role in the system analysis.

Second, a variety of conceptual designs were considered and evaluated for each of the critical IRV subsystems. Their relative advantages and disadvantages were examined and selections of preferred design alternatives were made wherever possible.

Third, a considerable number of total IRV conceptual designs were synthesized in order to examine the impact of different design alternatives on the total vehicle system. In addition, trade-off studies were performed to evaluate the effects of different design options on critical vehicle parameters (e.g., vehicle diameter). Using several selection criteria (i.e., vehicle weight, diameter, reentry performance, safety, developability and growth potential), three vehicle concepts were recommended for further study.

The following sections describe the results of these three subtasks. In addition, the last sections of the summary contain the major conclusions and recommendations to date, together with a description of the most important problem areas which have been identified at this time.

2.1 SAFETY SYSTEMS ANALYSIS

The purpose of the systems analysis was to examine the mission sequence in detail, to determine the various possible failure modes and to determine the span of reentry conditions and other vehicle design requirements so as to provide criteria for the vehicle design which would result in satisfactory performance over the entire design envelope, including normal operations, as well as during failure modes governed by the maximum credible accidents.

The major ground rules for the analysis are listed below:

a. For the separate launch case (Atlas/Centaur) a 260 nautical mile circular orbit with a 50 degree inclination was assumed. A yaw maneuver was included in the ascent trajectory to assure that the entire ascent trajectory (to orbital insertion) would take place over deep water.

b. For the integral launch case (Saturn I-B/MORL) a 164 nautical mile circular orbit with a 50 degree inclination was assumed.

c. The nominal IRV return mode is controlled intact reentry, initiated by deorbiting the IRV from the space station.

d. The complete design envelope is defined by consideration of the maximum credible accident.

Figure 2.1-1 shows an illustrative launch, injection and docking sequence (for the separate launch case.) Figure 2.1-2 shows a nominal deorbit and recovery sequence utilizing a parachute and flotation system. A thorough analysis of the total mission sequence was performed for both the separate and integral launches, including abort condition envelopes for any point along the launch and injection trajectory, launch pad accidents, inorbit accidents, deorbit requirements, reentry trajectory perturbations, ground and water impact conditions, etc. The resulting major system design requirements are shown in Figure 2.1-3. It should be pointed out that the worst heating rate conditions (i.e., the -10 degree trajectory, Figure 2.1-3) comes from the worst credible abort condition. It is possible to postulate even worse abort conditions by assuming that the launch vehicle destruct system fails, that the IRV abort system fails, and that the launch vehicle pitches over and expends all its remaining fuel by continuing to thrust at the pitch-over angle. This can result in entry velocities of about 25-26,000 fps and entry angles considerably in excess of 10 degrees. The probability of such a failure sequence, however, appears to be very low and therefore, has not been used as a design criterion.

A complete discussion of the entire systems and failure mode analysis is contained in section 3.0.

2.2 MAJOR IRV SUBSYSTEM DESIGN ALTERNATIVES

The most critical IRV design areas where different approaches must be evaluated are listed below:

a. Aerodynamic shape selection

b. Heat source configuration

c. Heat source heat exchanger configuration

d. Heat source attachment and support

e. Impact attenuation

f. Turn-around devices

g. Recovery aid integration

h. Deorbit and abort rocket integration.

Various design concepts have been considered and evaluated for each of these areas. These concepts and the results for each area are summarized in the following sections.

2.2.1 Aerodynamic Shape Concepts

To reduce aerodynamic heating and ground impact velocities, it is desirable to achieve low vehicle ballistic coefficients (W/C_DA). Consequently, blunt, high

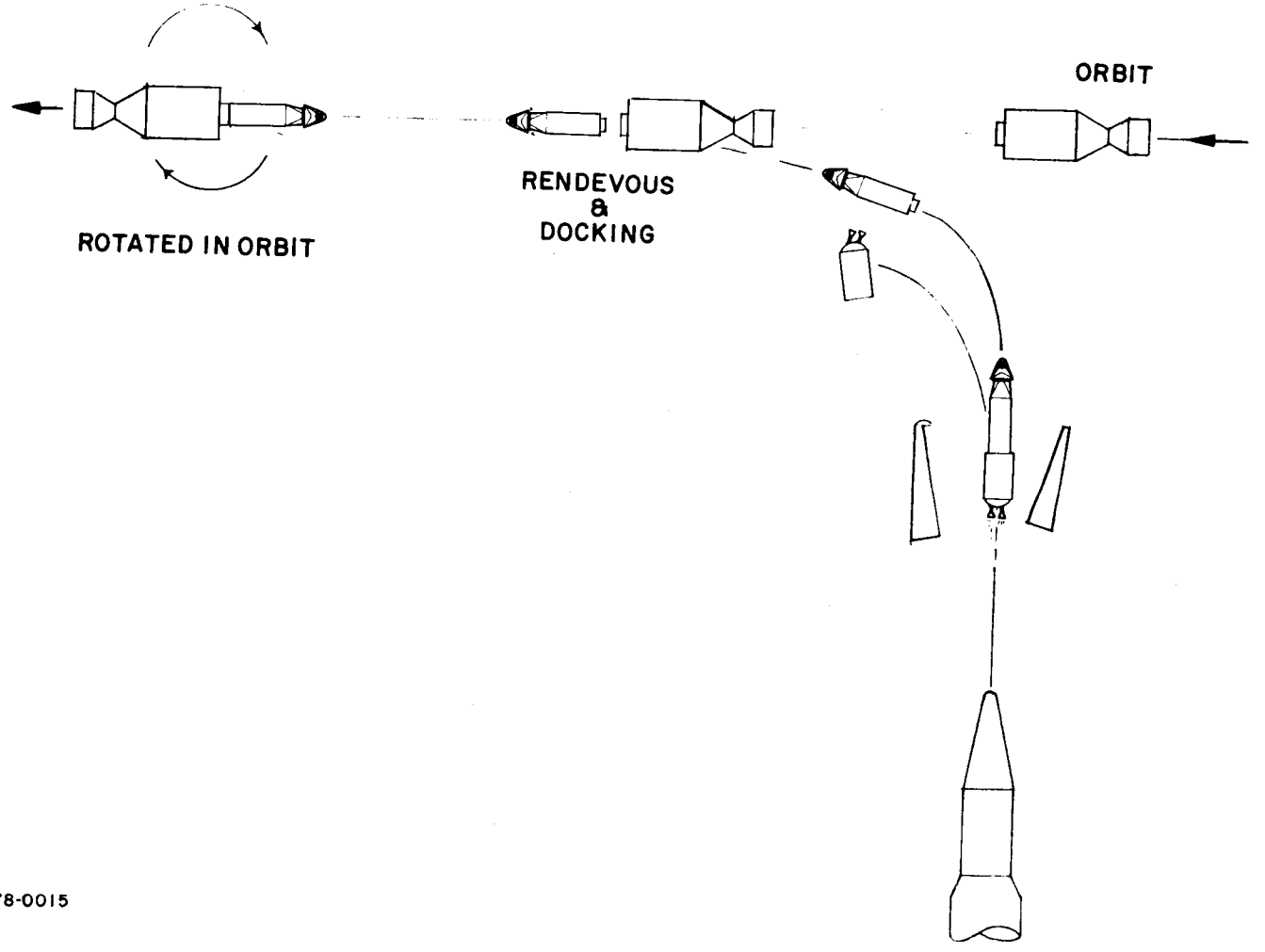

Figure 2.1-1 SEPARATE LAUNCH SEQUENCE

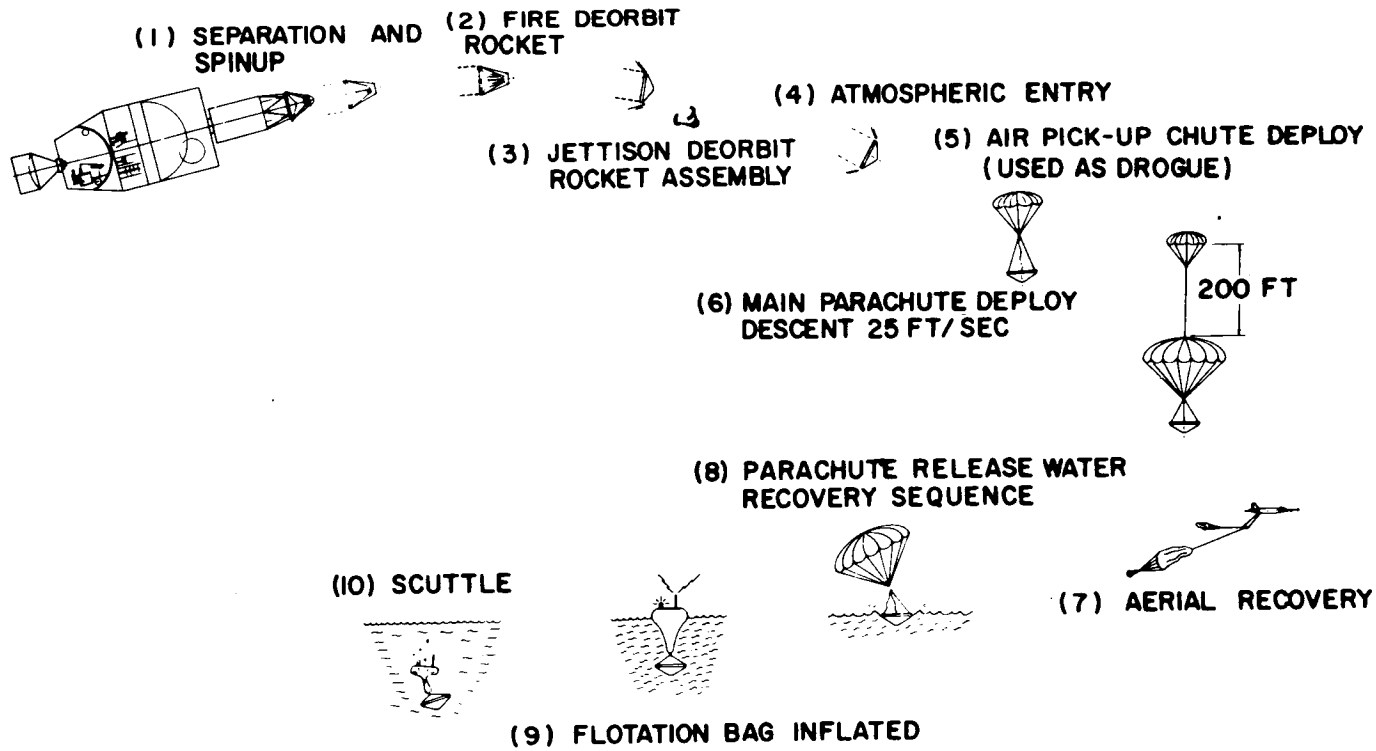

Figure 2.1-2 DEORBIT AND RECOVERY SEQUENCE

AEROSHELL	ENTRY VELOCITY	<26000 FPS
	ENTRY ANGLE	0 TO -10 DEG
	ENTRY BODY RATES	PITCH-YAW <6 DEG/SEC ROLL <6 DEG/SEC
	PEAK AXIAL LOADS	$< +10, -32$ G'S
	PEAK LATERAL LOADS	$< \pm 10$ G'S
	PEAK INTEGRATED HEATING (2 SKIP ENTRY)	$Q = 55000$ BTU/FT^2 AT $\dot{q} = 230$ BTU/FT^2 SEC
	PEAK HEATING RATE (-10° ENTRY)	$\dot{q} = 370$ BTU/FT^2 SEC AT $Q = 10,900$ BTU/FT^2
	IMPACT VELOCITY	< 150 - 200 FPS
HEAT SOURCE	MAXIMUM CAPSULE TEMPERATURE (REENTRY)	< 2500°F
	MAXIMUM CAPSULE TEMPERATURE (OPERATING)	< 2000°F
	LIMIT CAPSULE IMPACT LOAD	<1000 G'S
	REQUIRED IMPACT ATTENUATION	ROTATION SYSTEM WITH BEEFED UP HS PLATE 8 INCH CRUSHUP STROKE
ABORT AND DEORBIT ROCKETS	THRUST	2800 LB
	VELOCITY INCREMENT	500 FPS
	THRUST VECTOR ALIGNMENT	< 1 INCH
	SPIN RATE	7-10 RPM
	LAUNCH PAD ABORT RANGE	200-250 FT

Figure 2.1-3 SYSTEM DESIGN REQUIREMENTS

drag configurations are most desirable. Such configurations also provide generally good packaging characteristics and can be employed efficiently over the total range of achievable reentry conditions. Figure 2.2-1 presents the aerodynamic shape concepts which have been considered. Basically, they consist of two configurations, a 60-degree half-angle blunt cone (Figure 2.2-1(a)) and a modified Apollo shape (Figure 2.2-1(b)) where the normal afterbody has been replaced by a short cylindrical section. The drag and stability characteristics of both configurations are quite similar. The modified Apollo shape appeared to possess superior packaging characteristics for planar heat source configurations and was included for that reason. The configuration of primary interest was the blunt cone. To reduce the heating to the heat source capsules (located in the rear of the vehicle), recessing of the heat source into the vehicle was examined and the resultant configurations are shown in Figure 2.2-1(c) and (d). In addition, in the case of conical heat source configurations, the heat source can be recessed into the conical cavity of the blunt cone as shown in Figure 2.2-1(e). Investigation has shown that when impact attenuation (requiring crushup stroke), heat source recession and recovery aid integration are considered, the Apollo configuration is inferior in packaging (i.e., requires larger vehicle diameters) and center of gravity location relative to the blunt cone (for a given diameter). Consequently, the blunt cone has been recommended as the reference aerodynamic configuration for the IRV.

A treatment of the important aerodynamic characteristics of the IRV is presented in section 4.0.

2.2.2 Heat Source Configurations

The heat source configuration can have a major influence on vehicle diameter and weight, as well as seriously influencing vehicle stability (through the center of gravity location and inertias and the capsule heating environment). Furthermore, different heat source configurations will react differently to the g-loadings associated with ground impact. Several generically different capsule array configurations have been examined in order to evaluate their advantages and disadvantages. The various heat source configurations are shown in Figure 2.2-2.

The simplest configuration is the planar array (Figure 2.2-2(a) and (b)). In these two concepts the circular array results in the smallest diameter heat source, while the rectangular array facilitates incorporations of recovery and location aids within a circular vehicle configuration.

The conical and pyramidal configurations (Figure 2.2-2(c) and (d)) represent an attempt to take full advantage of the aeroshell conical shape thereby improving the center of gravity location.

The "pincushion" and stacked capsules arrays (Figure 2.2-2(e) and (f)) represent an attempt to arrive at the smallest possible heat source diameter so as to aid in minimizing total vehicle diameter.

The planar arrays are the simplest configurations. Capsule retention schemes can be used which support the capsules very uniformly (i.e., in a "cradle") thereby improving the impact resistance of the heat source. (A review of the heat source failure modes during ground impact indicated that maintaining heat source plate integrity after impact is a desirable goal.) For 164 capsules the minimum circular heat source diameter appears to be about 49 inches. Recessing

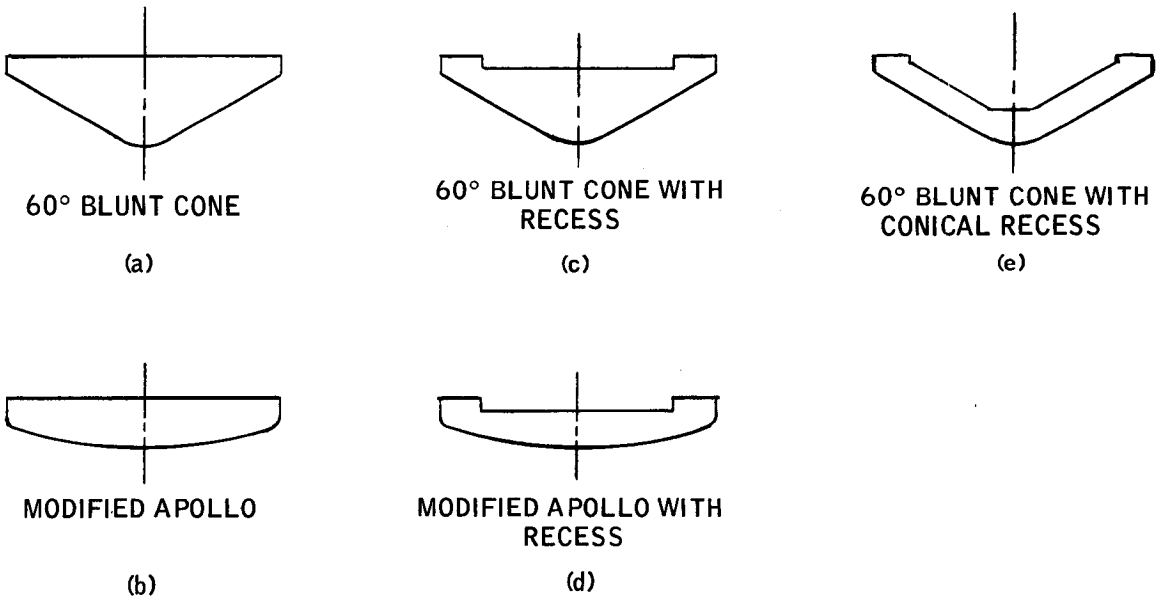

776459P

Figure 2.2-1 AERODYNAMIC SHAPE CONCEPTS

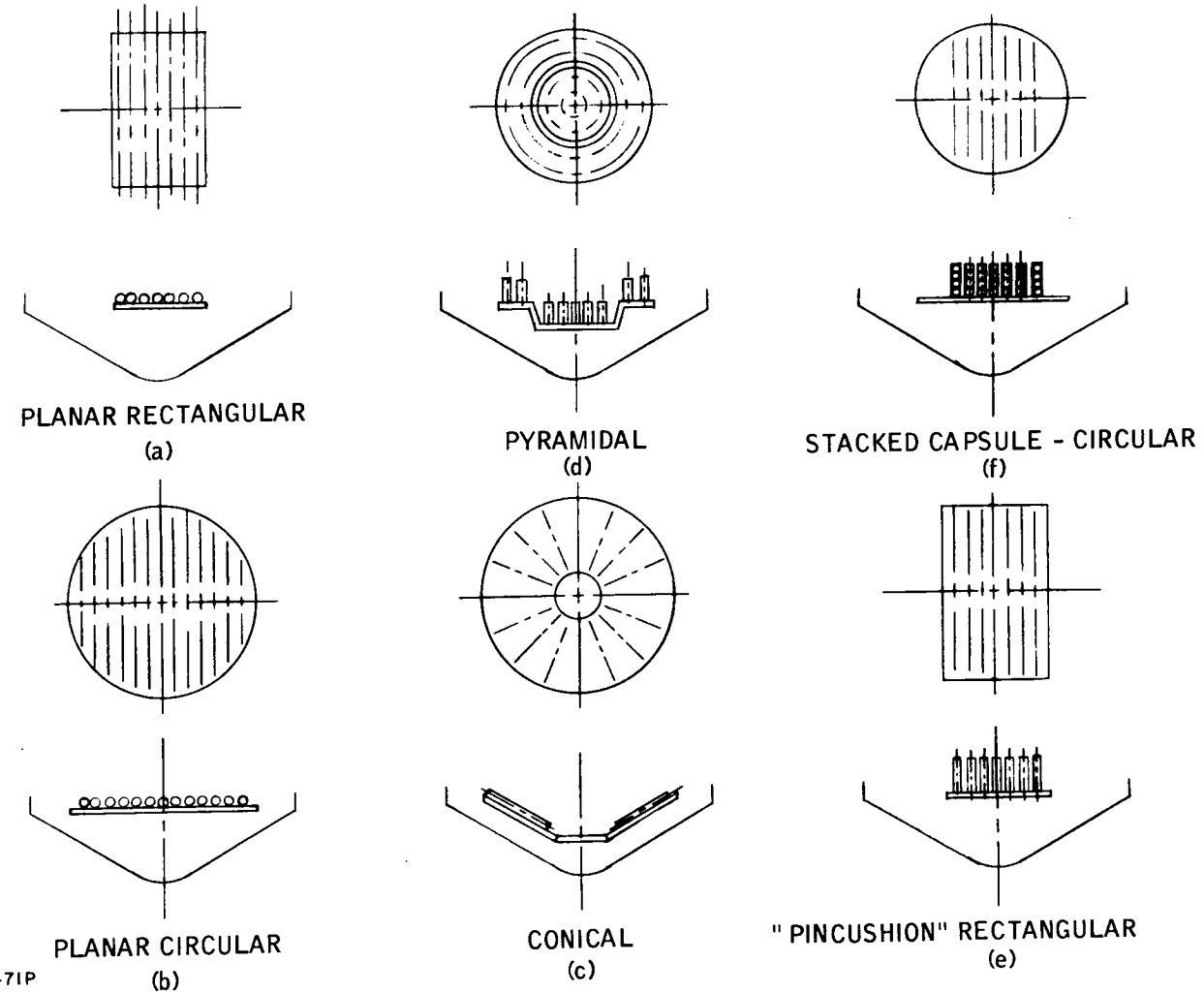

Figure 2.2-2 HEAT SOURCE CONFIGURATIONS

the array provides heat protection during reentry and, if necessary, a cover plate can be used to provide additional heating protection as well as additional impact retention protection. The disadvantage of the planar array lies in the fact that all capsules are relatively far aft in the vehicle so that favorable center of gravity locations are hard to achieve.

The conical and pyramidal arrays provide better center of gravity location and the conical array results in advantageous capsule recession and somewhat better vehicle aerodynamic turn-around capability. However, the array requires significantly larger heat source diameters (and consequently larger heat source weights) and the impact loadings at oblique angles can cause heat source break-up more readily than for the planar array. Capsule retention schemes for the pyramidal array are more complicated, auxiliary cooling on the launch pad is more difficult, aerodynamic heating on the capsules which protrude beyond the vehicle base is greater, and at oblique impact angles it is difficult to keep the upright capsule retention systems from failing under the high g-loads. Finally, in the pyramidal case the heat source heat exchanger design appears more complicated and the required capsule operating temperatures appear to be somewhat higher.

The pincushion array is quite similar to the pyramidal array and suffers from the same limitations. The stacked capsule array with rows of capsules stacked on top of each other in principle provides the smallest heat source diameter (of about 40 inches) but creates considerable difficulty in launch pad cooling, heat exchanger design, capsule operating temperatures and capsule retention and impact performance. In addition, the aerodynamic heating to the capsules during entry may be quite severe since they protrude beyond the vehicle base. It is also very difficult to achieve reasonable center of gravity locations in a minimum diameter vehicle since so many of the capsules are located at the extreme aft end of the vehicle.

At this time it appears that the planar configuration is most attractive when all factors are considered. However, the pincushion and stacked arrays must be further evaluated to determine whether they allow achievement of significant reductions in heat source diameter.

Section 5.1 contains a detailed description of the various heat sources.

2.2.3 Heat Source Heat Exchanger Configurations

To accommodate the different heat source configurations a number of HSHX configurations have been considered. Both tube fin and plate fin heat exchangers have been evaluated in both single and two-pass configurations.

The various HSHX concepts are shown in Figure 2.2-3. The tube fin devices appear easier to fabricate and are lighter than the plate fin devices. The use of a two-pass flow system minimizes the temperature gradients across the heat source and thereby result in lower maximum capsule operating temperatures. Consequently, it appears that two-pass, tube fin HSHX configurations are most attractive.

A detailed description of the various HSHX designs and analyses can be found in Section 5.2.

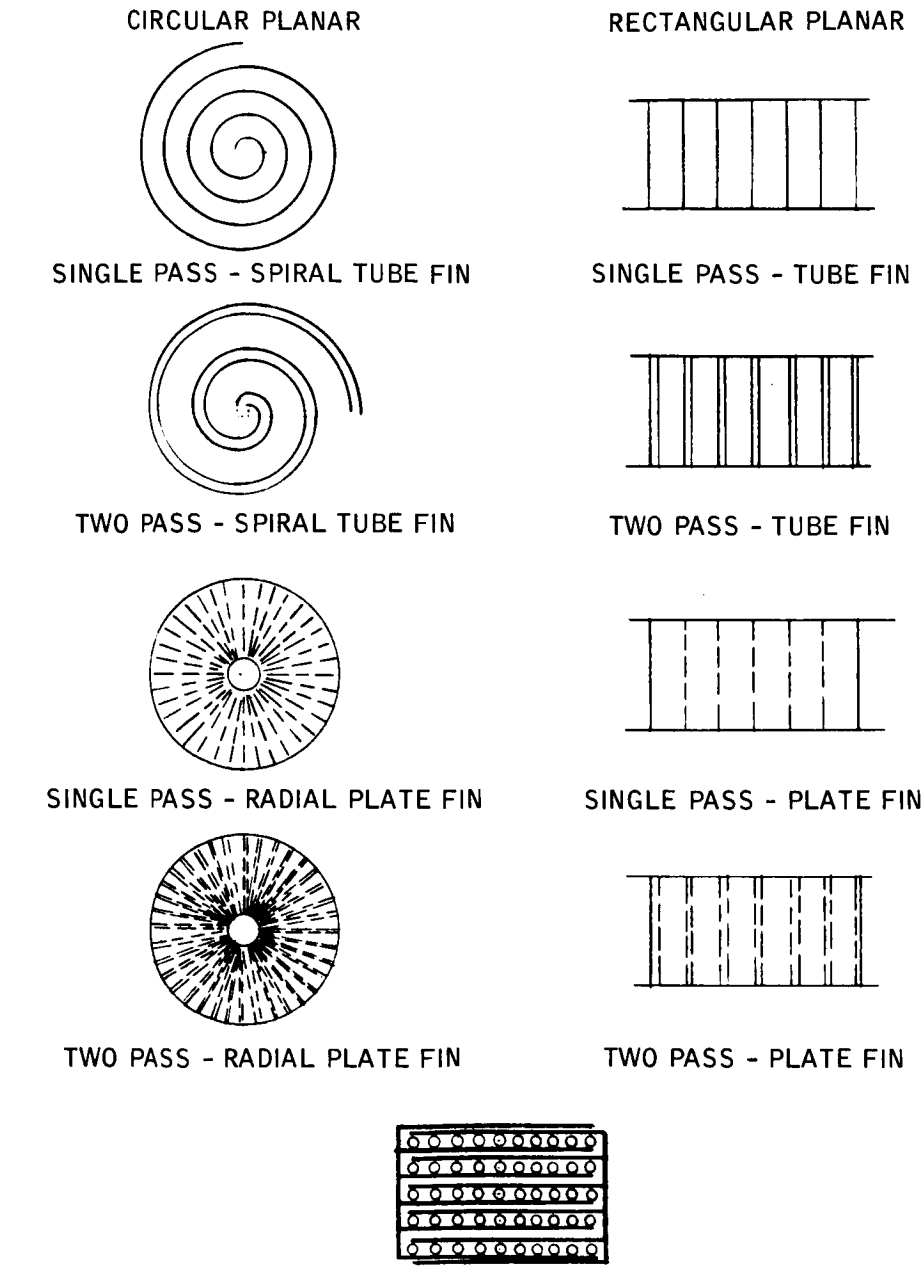

Figure 2.2-3 HSHX CONFIGURATION

2.2.4 Heat Source Support and Attachment Concepts

The heat source plate must be attached to the aeroshell and supported to withstand the launch and reentry loads. In addition, heat leaks from the heat source through the attachments and supports should be minimized and the loading distribution acting on the heat source during ground impact should be as uniform as possible.

The various support and attachment concepts which have been examined are shown in Figure 2.2-4. Four basic schemes have been evaluated. One is peripheral attachment of the heat source to the aeroshell at a few distinct points with bending of the heat source plate constrained by crushup material located beneath the plate of (Figure 2.2-4(a)). It is also possible to attach the plate at several points directly to the crushup material without peripheral attachments (Figure 2.2-4(c), or the plate can be attached peripherally to a ring structure without requiring the support by crushup material (Figure 2.2-4(d)). All of these attachment schemes result in fairly high heat leak values. Thermally, the most attractive support scheme is a refractory metal truss support which penetrates the superinsulation to attach to the heat source plate. As is discussed later, crushup support can still be provided to attenuate the ground impact g-loading.

A detailed discussion of the various attachment schemes is presented in Section 5.3.

2.2.5 Impact Attenuation Concepts

As a design goal it is desirable for the isotope fuel capsules to remain intact at all times. To meet this design goal care must be taken to assure that if the IRV impacts on land the resulting g-loads do not rupture the capsules. The impact loading tolerance of the capsules depends strongly on how the loading is applied. It is expected that for a uniform distribution of loads (i.e., in a "cradle") the capsules could survive g-loads as high as 100,000-200,000 g's. Therefore, one of the design goals is to furnish a capsule retention scheme which supports the capsules very well during impact. Cradle type retention schemes are therefore most desirable. The actual impact g-loading is of course dependent on a complex interaction between the IRV terminal velocity, the terrain, the efficacy of the retention scheme for different impact geometries and the amount and rate of impact energy absorption by the IRV. Crushup materials can be designed to be useful in attenuating the impact loading. However, further analysis (and probably testing) will be required to specify an optimum impact attenuation concept.

Figure 2.2-5 illustrates various impact attenuation concepts. The simplest concept is to fill the aeroshell with isotropic crushup material (Figure 2.2-5(a)). For non-zero angles of impact (i.e., away from vertical impact) anisotropic crushup material and the variation in crushup stroke can combine to greatly decrease impact attenuation material utility. Even for vertical impact the loads are not distributed uniformly over the heat source plate because the most forward portion of the crushup transmits high loads to the center of the plate before the material outboard of the nose region begins to crush.

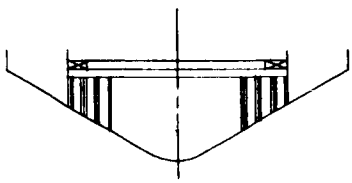

PLANAR ARRAY - PERIPHERAL ATTACHMENT AND CRUSHUP

(a)

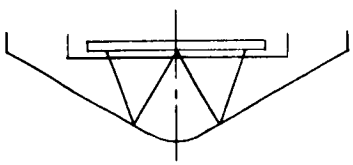

PLANAR ARRAY - TRUSS SUPPORT

(b)

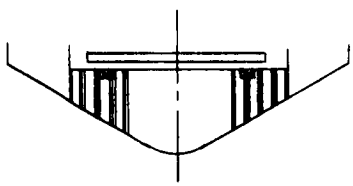

PLANAR ARRAY - FOUR POINT ATTACHMENT TO CRUSHUP SUPPORT

(c)

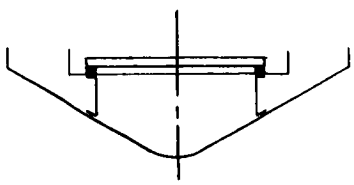

PLANAR ARRAY - PERIPHERAL RING SUPPORT

(d)

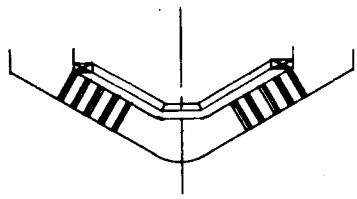

CONICAL ARRAY - PERIPHERAL ATTACHMENT AND CRUSHUP

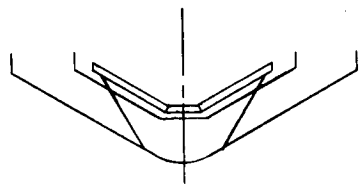

CONICAL ARRAY - TRUSS SUPPORT

776460P

Figure 2.2-4 SUPPORT AND ATTACHMENT CONCEPTS

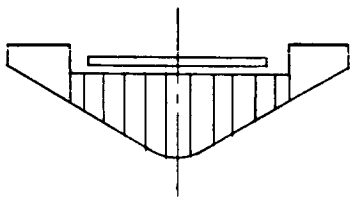

PLANAR ARRAY - NON-ORIENTATED
AND NON-LOAD DISTRIBUTING
(a)

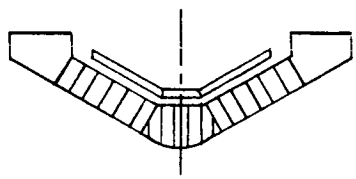

CONICAL ARRAY - ORIENTATED
AND NON-LOAD DISTRIBUTING

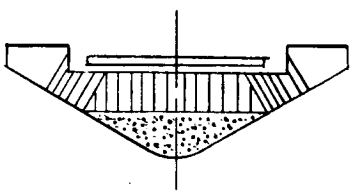

PLANAR ARRAY - ORIENTED
PLUS LOAD DISTRIBUTING
(b)

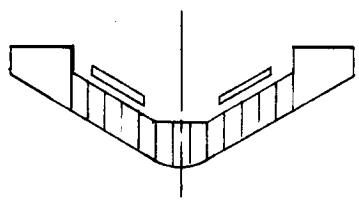

CONICAL ARRAY - NON-ORIENTATED
AND NON LOAD DISTRIBUTING

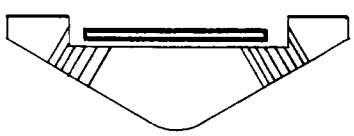

PLANAR ARRAY - ORIENTED CRUSHUP
RING PLUS "BEEFED UP" PLATE
(c)

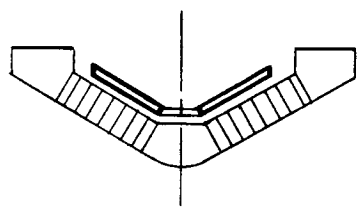

CONICAL ARRAY - ORIENTATED
PLUS "BEEFED UP" PLATE

776472P

Figure 2.2-5 IMPACT ATTENUATION CONCEPTS

The situation can be somewhat alleviated by using different crushup materials for different portions of the vehicle and by orienting the crushup material so that it performs better at non-zero impact angles. This is illustrated in Figure 2.2-5(b). However, to prevent destruction of the heat source plate and the capsule retention mechanism it is necessary to use long crushup strokes to reduce the g-loadings and this necessitates large vehicle diameters. Furthermore, the large amount of crushup material needed imposes a severe vehicle weight penalty. Consequently, an effort has been made to find an impact attenuation scheme which results in less severe vehicle design penalties. Figure 2.2-5(c) illustrates such a potentially attractive method. It consists of a ring of crushup material which supports a strengthened heat source plate. At impact angles of up to ±30 degrees this crushup ring causes the plate to rotate so that it impacts flat on the ground and absorbs the impact energy by plastic deformation. This impact geometry is most favorable for the distribution of loading on the capsules in their cradle retention. The heat source plate must be designed with sufficient strength so as not to fail due to the loads acting on it while it is rotating. This appears to be the lightest attenuation system and requires only modest crushup stroke lengths of several inches.

A discussion of the various impact attenuation schemes is contained in Section 5.4.

2.2.6 High Altitude Turn-around Devices

If the vehicle starts to reenter in a backward attitude it is desirable to cause it to right itself at high altitudes so as to minimize the aerodynamic heating to the fuel capsules.

A variety of different approaches can be used to assure that the vehicle will be unstable in rearward attitudes. Most of these are illustrated in Figure 2.2-6. The center of gravity offset is conceptually the simplest and most reliable method, but it greatly complicates the vehicle design and the deorbit system and results in trim angles of attack after turn-around. A large afterbody can be used to effect turn-around but it interferes seriously with the HSHX and heat source design and greatly degrades the transonic and subsonic vehicle stability. Fins can be used but rather large fin sizes are required for high altitude turn-around. Flaps are effective devices, but generally must be actively deployed and also result in non-zero flight trim angles. Fences appear to be the most promising devices. An aerodynamic test program is being conducted by the Ames Research Center to assist in selection of a fence configuration. Further details on the various turn-around devices can be found in section 4.0.

2.2.7 Recovery Aid and Deorbit and Abort System Integration Concepts

The incorporation of decelerators (e.g. parachutes, ballutes) and location aids (beacons, etc.) has been considered as an aid in the recovery of the IRV. These devices can be packaged either around the periphery of the IRV or they can be located in the center if a cavity is provided in the heat source. The top part of Figure 2.2-7 illustrates this schematically. The peripheral location is preferable since it eases the thermal insulation problems and imposes fewer constraints on the heat source configuration design.

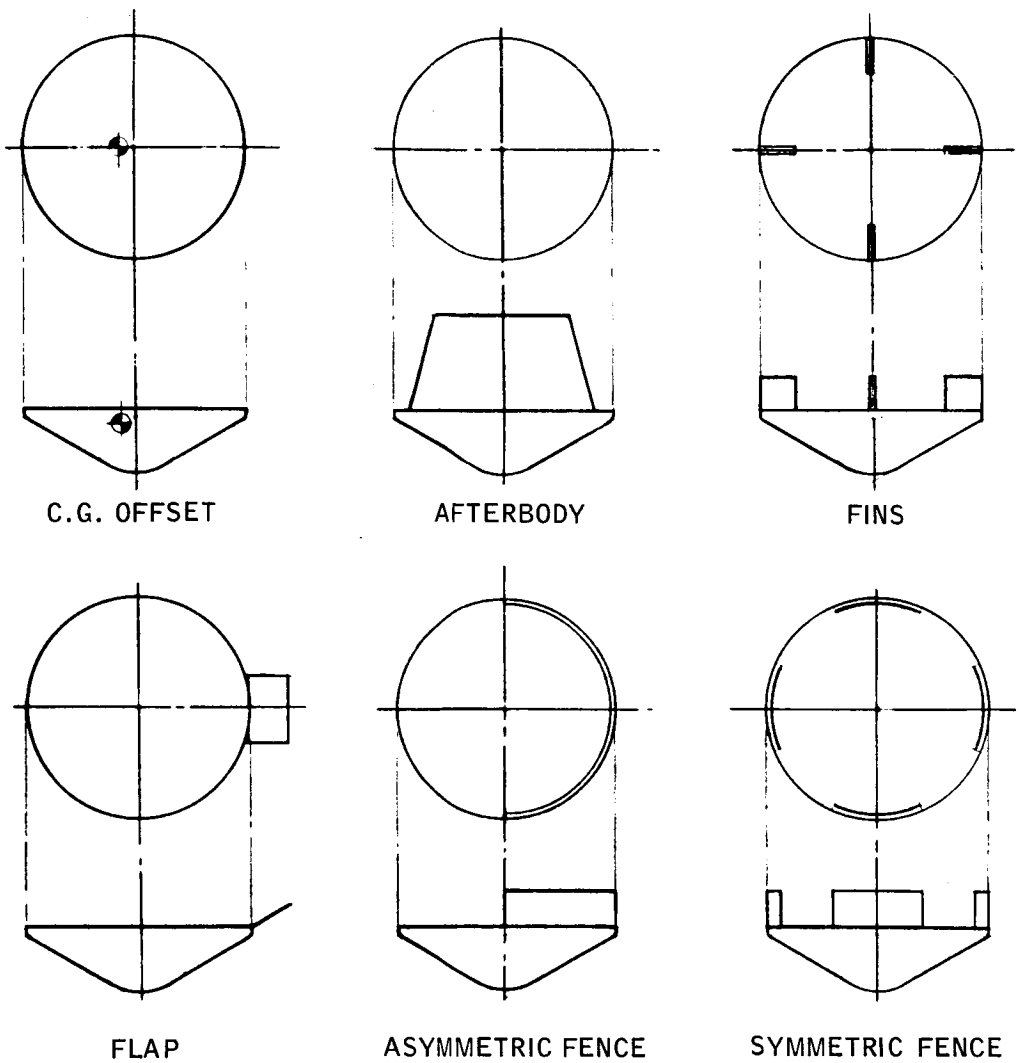

78-0017

Figure 2.2-6 TURNAROUND CONCEPTS

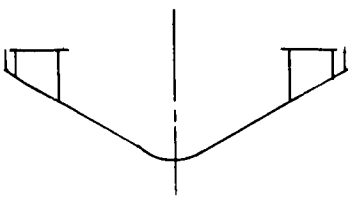

PERIPHERAL LOCATION

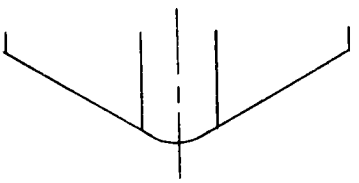

CENTRAL LOCATION

ABORT AND DEORBIT ROCKET
INTEGRATION CONCEPTS

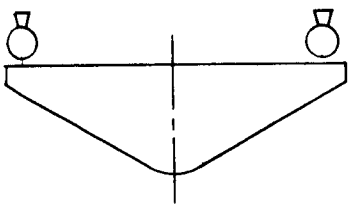

FOUR ROCKET PERIPHERAL
LOCATION

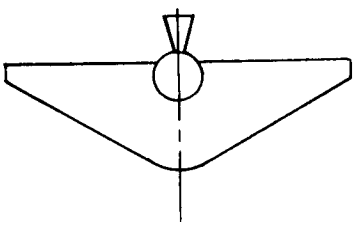

SINGLE ROCKET
CENTRAL INTERNAL
LOCATION

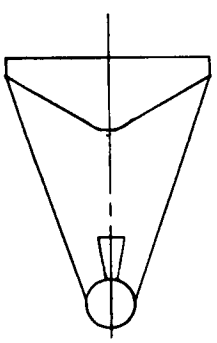

SINGLE ROCKET
TOWER SYSTEM

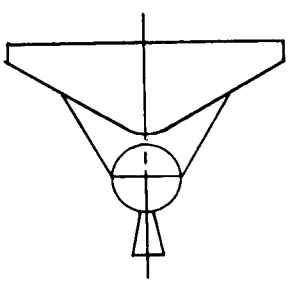

SINGLE ROCKET
HEAT SHIELD MOUNTING

776470P

Figure 2.2-7 RECOVERY AIDS AND ABORT AND DEORBIT
ROCKET INTEGRATION CONCEPTS

Several different options are also available for the integration of the abort and deorbit rocket system as illustrated in the lower portion of Figure 2.2-7. Several rockets can be located peripherally or a single rocket can be located in the center of the rear of the vehicle. The peripheral arrangement has the disadvantage that if one of the rockets fails large tumble rates are produced, while the single central rocket is very difficult to integrate within the heat source, interferes with the HSHX integration and poses a difficult thermal insulation problem. The major advantage of the central mounting is that the potentially catastrophic failure mode of the peripherally mounted deorbit rockets is eliminated. However, as shown in Figure 2.2-7 there are other ways of achieving this goal by mounting the rockets on short tower systems which are attached to the IRV. This scheme appears to be the most advantageous of those considered to date. It should be pointed out that even though it appears feasible to use the same rocket system for abort as well as deorbit a more thorough examination now underway could show that separate systems for these functions are desirable.

2.3 IRV CONCEPTUAL DESIGN SYNTHESIS AND EVALUATION

In addition to the various design alternatives associated with the IRV subsystems, several overall vehicle performance requirements must be considered in the synthesis of the different conceptual designs. The most critical requirements which influence the overall IRV design are as follows:

a. Heat source reentry heating protection

b. Vehicle aerodynamic stability

c. Ground impact attenuation

d. Incorporation of recovery and location aids.

As will be described below these factors are interrelated and often impose conflicting requirements on the vehicle design thereby necessitating trade-off studies to select the best design criteria.

2.3.1 Discussion of Interrelated Vehicle Performance Requirements

There are three ways to provide reentry heating protection for the IRV heat source. First, it is possible to reduce the heating by tailoring the vehicle reentry performance; namely, by reducing the ballistic coefficient and by providing higher forward stability so that the vehicle is at small angles of attack during the important heating period. Second, the heating to the heat source can be reduced by recessing the heat source below the base of the vehicle. Third, the capsules can be protected against heating by supplying a cover plate over them or by burying the capsules in a suitable heat block material (such as graphite). All three of these methods affect the vehicle design. Achievement of lower ballistic coefficients generally requires an increase in the size of the size of the vehicle. High stability imposes a requirement for effective turnaround devices, favorable inertia ratios, and good c.g. locations. Recessing the heat source requires either larger vehicle diameters or the addition of a cylindrical section at the rear of the vehicle. This in turn affects the vehicle transonic and subsonic stability. Cover plate protection entails some weight penalty, results in somewhat higher capsule operating temperatures and in the case of graphite adds a materials compatibility requirement.

The vehicle aerodynamic stability over the entire flight regime is primarily determined by four factors; namely, the aeroshell configuration (including the effects of any cylindrical sections), the center of gravity location relative to the diameter of the vehicle, the effectiveness of the turnaround device, and mass inertia ratio. It is desirable to minimize the height of any cylindrical sections and to locate the c.g. as far forward as possible.

Ground impact attenuation requirements are governed primarily by the allowable g-limit, the specific crush-up design selected, the terrain model, and the vehicle attitude at impact. It is desirable to provide long crush-up strokes but this greatly increases the required vehicle diameter (to provide long strokes at non-zero angle of impact) and moves the c.g. back by locating the heat source plate far aft of the vehicle nose. Good subsonic stability is desirable to minimize the angle of attack of the vehicle at impact. Finally, low ballistic coefficients are favorable since they result in lower impact velocities, but these can generally only be attained by increasing the vehicle size (it is assumed that even if auxiliary deceleration devices are used such as parachutes, the vehicle has to be designed to accept failure of the retardation device). Furthermore, the impact attenuation system generally imposes a substantial weight requirement thus making it difficult to achieve low ballistic coefficients.

The incorporation of deceleration and recovery aids requires volume and therefore generally increases the vehicle diameter as well as adding weight to the vehicle. Good transonic and subsonic vehicle stability is required for the proper deployment of parachutes.

2.3.2 Vehicle Conceptual Design Synthesis

An analysis of these various performance requirements indicates that to accommodate all of them involves increasing vehicle size and weight substantially. To better understand the trade-offs involved our approach has been to evolve four basic IRV configurations which are "bare" (i.e., do not contain recovery aids or impact attenuation) and then to examine the effect on the vehicle design of adding impact attenuation and recovery aids.

Figure 2.3-1 shows the four basic "bare" IRV vehicle concepts corresponding to the three different heat source configurations housed within the blunt cone aeroshell plus the planar heat source housed in the modified Apollo aeroshell configuration. The corresponding vehicle diameters and weights are also indicated on the figure. It should also be pointed out that the planar heat source vehicle design is derived for a heat source plate recession of one capsule diameter. This means that the top of the isotope capsules are flush with the base of the vehicle.

Figure 2.3-2 shows what the effects are on vehicle diameter and weight for additional recessing, crushup provisions, and the incorporation of recovery aids. The extreme left hand column indicates the generic heat source configurations used. The next column lists the dimensions and configuration of the heat source. The third column shows the diameters and weights for the "bare" vehicles and corresponds to Figure 2.3-1. The fourth column indicates the effects of recessing the heat source plate three (3) capsule diameters below the base. The fifth column shows the effect of adding crushup while maintaining a recess of only one capsule diameter. The sixth column shows the effect of incorporating only recovery aids (parachutes) along the periphery of the vehicle without adding

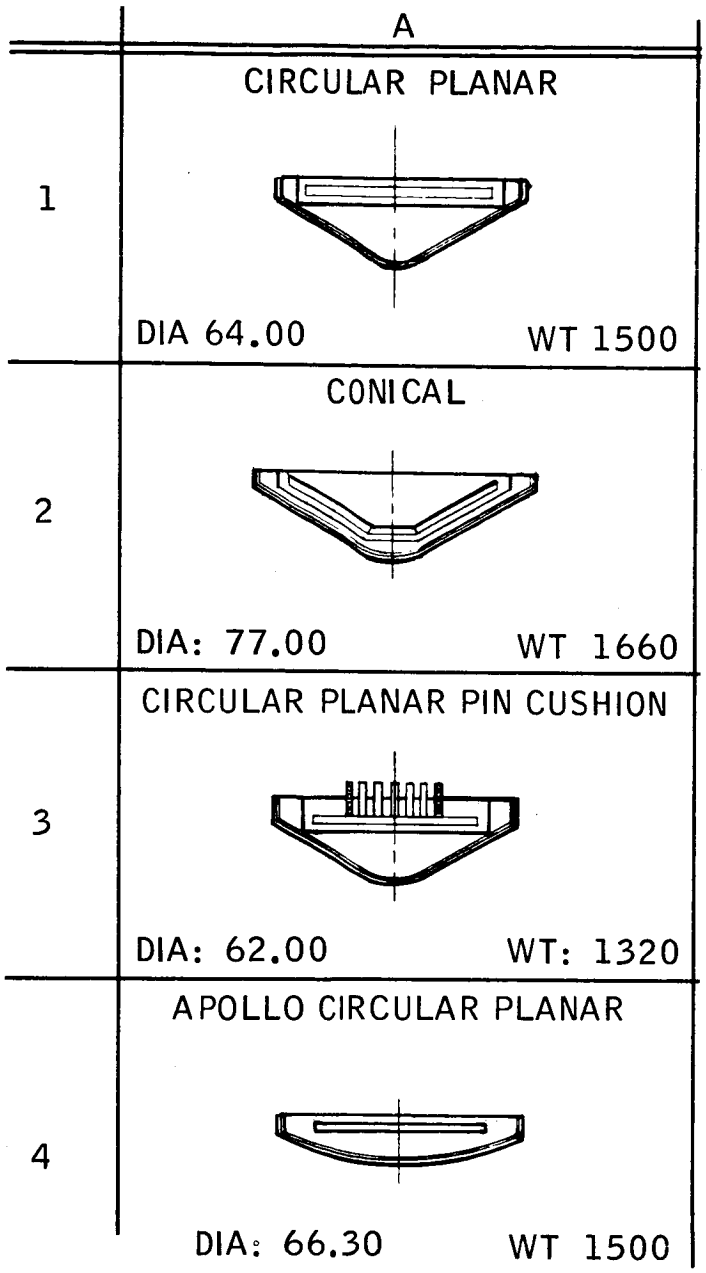

Figure 2.3-1 IRV CANDIDATE CONFIGURATION SUMMARY

CONFIGURATION	VEHICLE			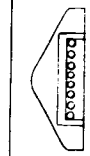		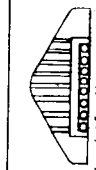				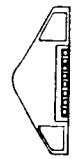		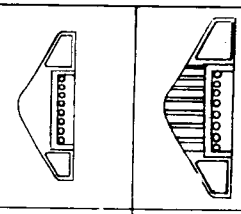		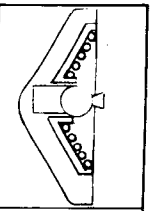	
HEAT SOURCE		FLUSH		RECESSED (3 CAPSULE DIAMETER)		CRUSH-UP		FLUSH CRUSH-UP		FLUSH RECOVERY AIDS		RECESSED RECOVERY AIDS		RECESSED CRUSH-UP RECOVERY AIDS		CRUSH-UP RECOVERY AIDS	
		DIA.	WT.	DIA.	WT.	DIA.	WT.	DIA.	WT.	DIA.	WT.	DIA.	WT.	DIA.	WT.	DIA.	WT.
	CIRCULAR 47" DIA.	64"	1500	73"	1530	89"	1900	98"	1950	84"	1690	84"	1690	98"	2080	113"	3210
	RECTANGULAR 63" X 34"	89"	1690	92"	1710	107"	2080	116"	2140	89"	1800	92"	1830	116"	2290	----	----
	CONICAL 57" DIA.	77"	1660	77"	1660	91"	2030	101"	2040	94"	1860	94"	1860	101"	2190	103"	3160
	39" DIA. 4" PROTRUSION 20% CYL.	62"	1320	----	----	----	----	----	----	85"	1520	----	----	----	----	----	----
	32x56 RECT. 4" PROTRUSION 20% CYL.	81"	1435	----	----	----	----	----	----	81"	1535	----	----	----	----	----	----
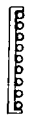	CIRCULAR 47" DIA. APOLLO	66"	1500	80"	1550	102"	1950	119"	2040	92"	1710	92"	1710	119"	2180	----	----

78-0018

Figure 2.3-2 SUMMARY OF WEIGHT DIAMETER CHARACTERISTICS

impact attenuation and still keeping the recess at one capsule diameter. The seventh column is the same as the sixth but with a three capsule diameter recess. The eighth column shows the combination of a three capsule diameter recess, crushup, and recovery aids. The last column shows the effect of locating the rocket and the recovery aids in a central cavity within the IRV.

2.3.3 Selection of Preferred Conceptual Designs

As indicated previously the selection of preferred concepts is based primarily on safety, vehicle diameter and weight, developability, reentry performance and growth potential. In addition, several other selection criteria are used for various portions of the IRV system. These criteria are indicated in Figure 2.3-3 and are largely self explanatory.

An examination of Figure 2.3-2 shows that the modified Apollo configuration does not possess any significant advantages over the blunt cone and, in fact, requires larger vehicle sizes to accommodate the various vehicle design options. Therefore, this shape will not be given further consideration in Task IB.

It was recommended that the three remaining basic vehicle concepts be further investigated with particular emphasis on the circular planar array which yields the simplest vehicle concept. The conical heat source array offers the most advantageous reentry performance configuration, but does require larger heat source diameters. The pincushion heat source array is attractive as the smallest heat source diameter, but is quite difficult to design properly and does impose more serious reentry heating problems. Therefore, to be considered as a serious candidate it must be established that the configuration does, in fact, result in significantly smaller vehicles. This requires further analysis.

Additional trade-off information and details on the conceptual design synthesis are contained in Section 6.0 of this report.

2.4 RECOMMENDATIONS AND CONCLUSIONS

The major conclusions reached to date are as follows:

a. The blunt cone aeroshell configuration is preferable to the modified Apollo configuration.

b. A graphite encapsulated "pincushion" heat source offers potential for lowest vehicle diameter and weight. Further analysis is required to evaluate this. This design is quite complicated and should be considered further only if the analysis indicates substantial diameter and weight savings.

c. The recommended HSHX concept is a two-pass, tube fin heat exchanger design.

d. The truss support for the heat source minimizes heat leakage and appears to be the best concept for the heat source attachment scheme to the aeroshell.

e. Impact attenuation imposes large vehicle size and weight penalties.

IRV SYSTEM	AEROSHELL	HEAT SOURCE	HEAT SOURCE HEAT EXCHANGER
WEIGHT	WEIGHT	WEIGHT	WEIGHT
DIAMETER	DIAMETER	DIAMETER	DIAMETER
HEAT LEAKAGE	CENTER OF GRAVITY	CENTER OF GRAVITY	
S/C INTEGRATION	TURNAROUND CHARACTERISTICS	LOWEST CAPSULE OPERATING TEMPERATURE	LOWEST CAPSULE OPERATING TEMPERATURE
ABORT AND DEORBIT SYSTEM INTEGRATION	THERMAL PROTECTION	EASE OF FABRICATION	EASE OF FABRICATION
IMPACT PERFORMANCE	ANGLE OF ATTACK ENVELOPE (THROUGH OUT MISSION SEQUENCE)	MINIMUM TEMPERATURE GRADIENT	MINIMUM TEMPERATURE GRADIENT
MATERIALS SELECTION		STRUCTURAL SUPPORT REQUIREMENTS	STRUCTURAL SUPPORT REQUIREMENTS
			IN-PLACE REDUNDANCY
			REPLACEABILITY

*ALL DESIGNS FIRST MUST MEET BASIC SAFETY AND DEVELOPABILITY CRITERIA

776448 P

Figure 2.3-3 CONCEPT SELECTION CRITERIA

f. Parachute recovery aid inclusion imposes significant vehicle penalties.

g. Pending further study the tower concept for abort and deorbit rocket integration is most attractive.

The following recommendations are made on the basis of the Phase 1A Study:

a. The vehicle concepts to be studied further should include a circular planar heat source array, a conical array and a "pincushion" array. The aeroshell configuration is a blunt cone.

b. Both circular and rectangular tube fin HSHX should be evaluated.

c. Evaluate potential gains in system performance which can be achieved if the ground rule for full power output from the secondary HSHX with primary HSHX in place.

d. Evaluate cover plates for heat source capsule retention and reentry heat protection.

e. Determine minimum impact attenuation system for the various vehicle concepts.

f. Evaluate both low density and graphitic ablative aeroshell heat shields.

A number of technical problem areas have been identified. The most important of these are as follows:

a. Post ground impact thermal energy rejection.

b. Iron titanate coating temperature limitations and stability.

c. Lack of long term low temperature ablator and thermal control coatings stability data.

d. Compatibility of graphite with capsule coatings and refractory metals at elevated temperatures.

e. Lack of heat source capsule impact resistance data for different types of load distributions.

f. Prediction of IRV ground impact response.

g. Long term (5 year) performance of IRV components.

3.0 SYSTEMS ANALYSIS

Systems analyses have been performed to establish the nominal mission profile for the Isotope Reentry Vehicle. The mission profile has been perturbed for each of the credible failure modes which can result in nuclear safety hazards. The appropriate operational response to each failure mode has been determined. Analysis of the nominal mission and of each failure mode resulted in establishing the IRV design requirements based upon accumulation of the most severe requirements from all credible situations. Requirements for safety aids and recovery aids have also been identified.

3.1 SYSTEMS ANALYSIS GROUND RULES

The ground rules used for the systems analysis are as follows:

a. Two launch concepts were considered.

1. A separate launch on an Atlas/Centaur launch vehicle into a 260-nautical-mile circular orbit inclined at 50 degrees. The ascent trajectory provided by Lewis Research Center employs a yaw maneuver to achieve instantaneous impact points which are always in deep water. After establishing the 260-nautical-mile orbit, the power supply must dock with the user vehicle (e.g. MORL). During this operation the power supply/Centaur system is assumed to be passive with the active docking role taken by the user vehicle.

2. An integral launch on a Saturn I-B launch vehicle into a 164-nautical-mile circular orbit inclined at 50 degrees. The entire power supply is launched as an integral part of the MORL. The launch trajectory provided by Langley Research Center passes over the southern tip of Africa presenting the possibility of land impact for some classes of ascent abort.

b. Nominal mission termination is accomplished by controlled intact reentry of the radioisotope heat source/IRV combination. The heat source heat exchangers and Brayton Cycle Units remain with the user vehicle.

c. The nuclear safety criteria to be met in the IRV system are as defined in Table 1.0-III. These ground rules have been followed in developing the systems safety requirement for the IRV. The items of most concern are potential criticality hazards and dispersion of fuel form fines in the biosphere. Fuel capsule burial in deep water has been assumed to be acceptable in the event of abort or eventual IRV disposal.

3.2 MISSION PROFILE

The nominal mission profile for the separate launch concept is depicted schematically in Figure 3.2-1. Similarly, the nominal integral launch mission profile is shown in Figure 3.2-2. A nominal mission termination profile, including air snatch and flotation for surface recovery, is shown in Figures 3.2-2 and 3.2-3. Several of the IRV systems design requirements are defined by analysis of the

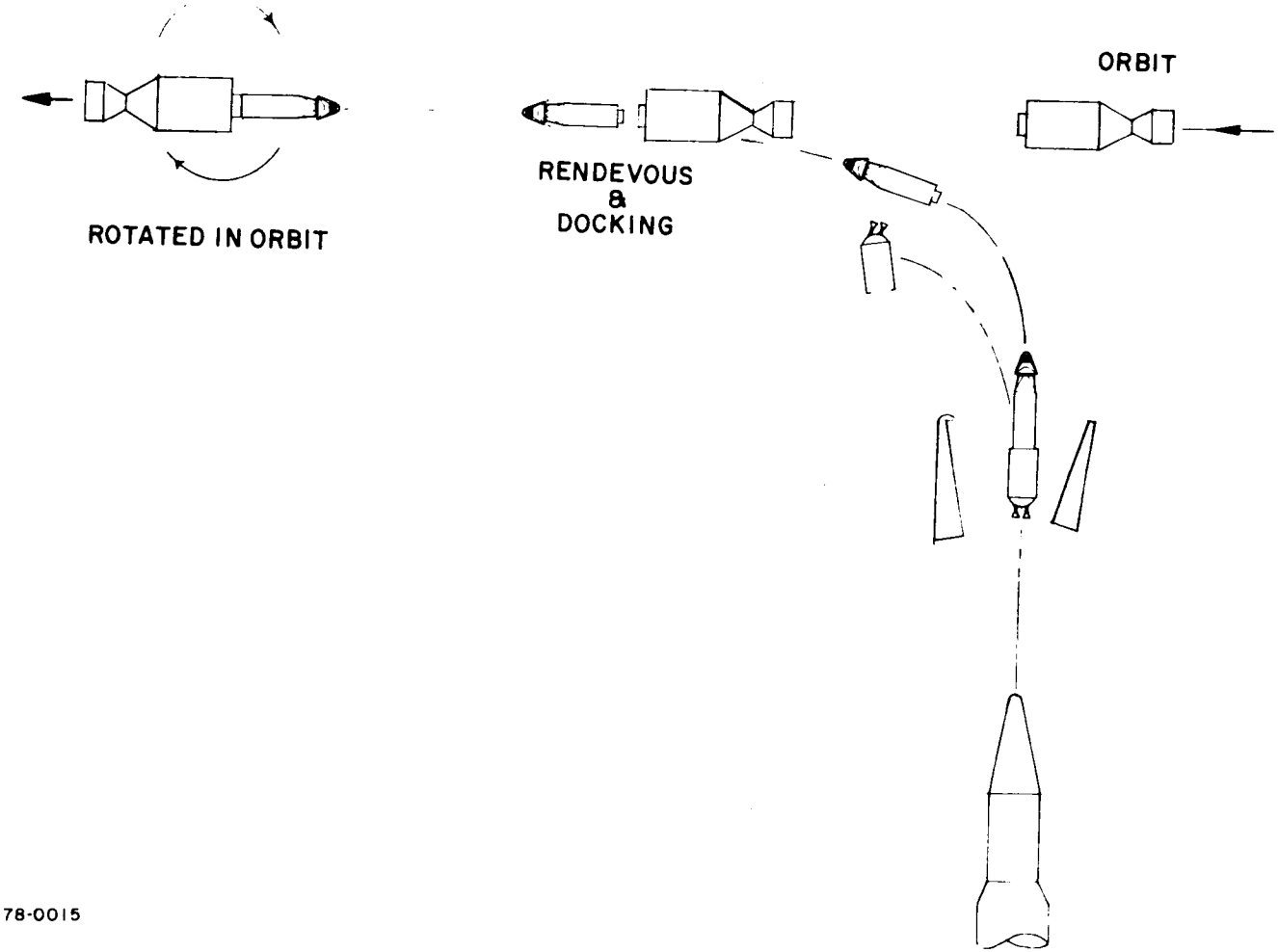

Figure 3.2-1 SEPARATE LAUNCH PROFILE

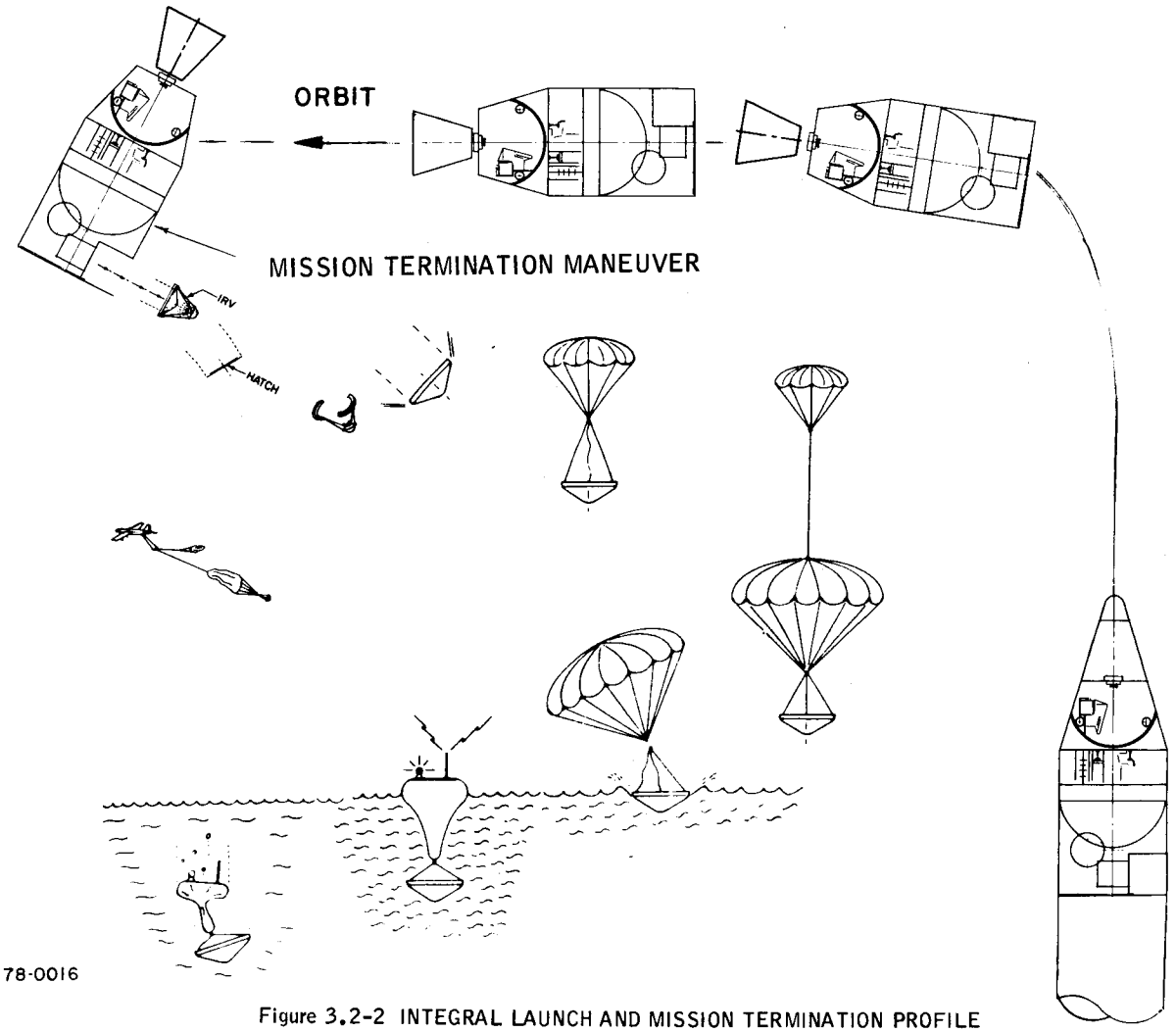

Figure 3.2-2 INTEGRAL LAUNCH AND MISSION TERMINATION PROFILE

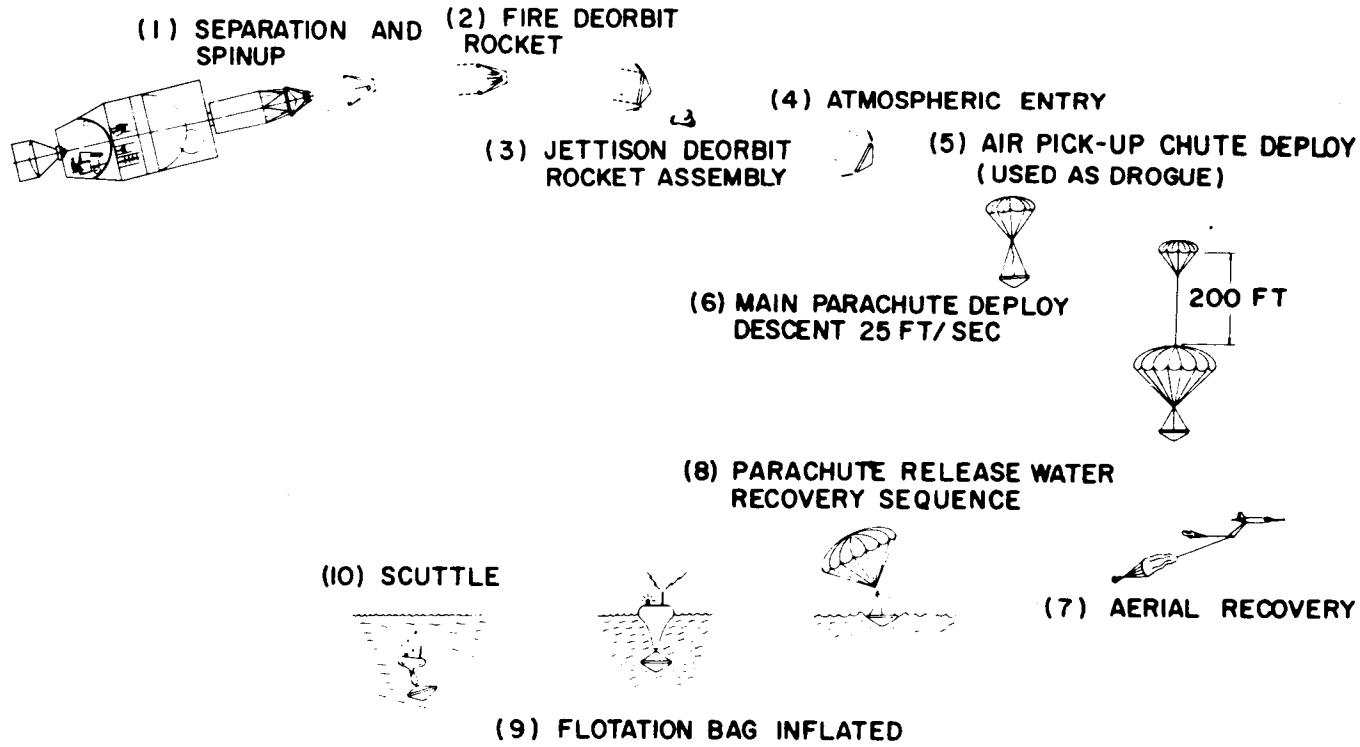

Figure 3.2-3 DEORBIT AND RECOVERY PROFILE

nominal mission profile. For convenience the mission profile has been subdivided into mission phases.

3.2.1 Prelaunch Mission Phase

During this mission phase, the Auxiliary Coolant Heat Exchanger must maintain the heat source at temperatures below the 600° F in the atmosphere, the level at which significant damage to the heat source can occur from oxidation of the columbium 1 percent zirconium heat source plate.

3.2.2 Lift-off and Ascent Mission Phases

Sufficient thermal capacity must be provided in the heat source to prevent the temperature from rising above 2500° F during launch. Once the vehicle is injected into orbit, the separate launch and integral launch concepts present distinctly different situations. For the separate launch concept, the power system with the Centaur stage must maintain themselves for several orbits before docking with a space station is accomplished. The active roll in the docking maneuver is assumed by the space station. The Centaur can accommodate the housekeeping requirements, including attitude control, for the several orbits necessary for the rendezvous. During the predocking period, the IRV heat source can be cooled by initiating operation of the BRU's or by rotating the IRV away from the HSHX on its hinge to allow radiation to space. (For more detailed description of the separate launch sequence see NASA Contract NAS9-7444, Study of the Separately Launched Multi-Use Space Electrical Power System.)

The power subsystem in the integral launch concept can perhaps be started soon after orbit injection. If the space station is launched unmanned for later rendezvous with another crew carrying spacecraft once in orbit, it may be necessary to again rotate the IRV away from the space station to provide heat rejection to space during the interval between orbit injection and rendezvous with the crew.

3.2.3 Orbital Mission Phase

During the orbital mission phase, the entire thermal output (less losses from the heat source) is used to drive the Brayton Cycle power subsystem which supplies the needs of the spacecraft. If the power system requires routine maintenance for any reason, the IRV section of the power subsystem must be rotated away to the alternate cooling mode as shown in Figures 3.2-4 and 3.2-5, where heat rejection is accomplished by direct radiation to space. As stated in the study ground rules, the entire heat exchanger-Brayton cycle unit is in-place redundant to ensure against inadvertent power loss during critical phases of the mission.

3.2.4 Deorbit Mission Phase

At mission termination, after a mission lifetime of up to 4 years, the heat source is still generating thermal energy at almost its initial rate. The IRV could be left in orbit, however, after about 4 years in a typical case (W/C_DA = 40 lb/ft^2, h = 260 n.m.), the IRV would re-enter due to natural orbital decay. To achieve an orbital lifetime approaching the level of ten half-lives, the IRV must be injected into a higher altitude orbit. A highly eccentric orbit with

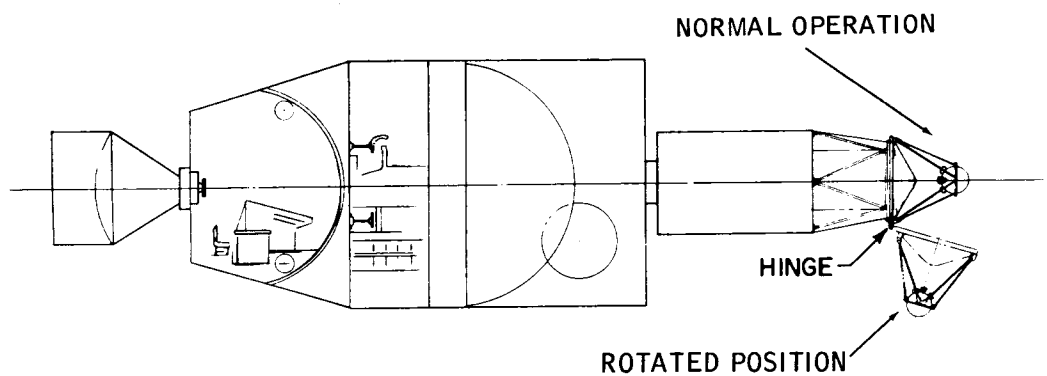

776355P

Figure 3.2-4 ORBITAL NONCRITICAL FAILURE (ALTERNATE COOLING MODE SHOWN)

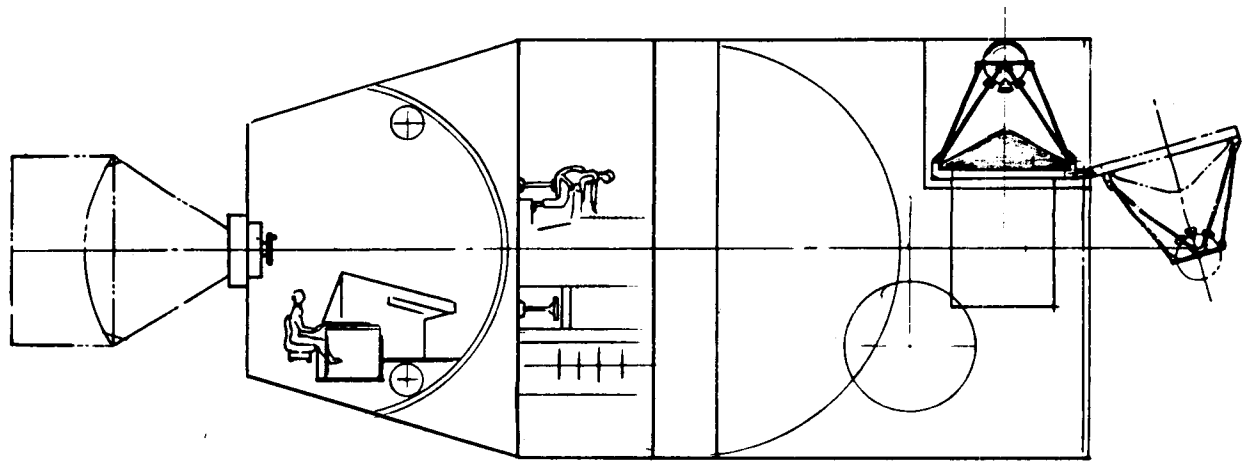

776451P

Figure 3.2-5 ORBIT-NONCRITICAL FAILURE (ALTERNATE COOLING MODE SHOWN)

perigee at the original circular orbit altitude will not suffice. A two burn (two periods of thrust application) maneuver is necessary to place the IRV in an appropriate higher altitude orbit.

There also remains the possibility of malfunction which could allow the IRV to prematurely re-enter even if the intent was to place it in a safely high orbit (e.g., the orbit injection engine could fire in the wrong direction and apply a retro velocity increment). Therefore, the nominal method of mission termination studied has been controlled intact reentry. (Deorbit velocity increment applied to control reentry and impact to a pre-selected recovery area.) However orbital decay and other random reentry mission terminal abort conditions have been considered in the IRV design.

The isotope heat source must be returned to the Earth's surface, preferably into deep water areas of the ocean where possible recovery by surface recovery teams or eventual deep water burial can be implemented. Recovery of the isotope heat source can best be accomplished by controlled intact reentry of the IRV from low altitude circular or near circular orbits which can place the IRV into a relatively small recovery area from which it can be recovered by either air snatch during descent or from the ocean after impact. Deep water burial is insured by provision of a sea water activated scuttling device.

The implementation of deorbit was examined for the two orbits specified in the Systems Analysis Ground Rules (paragraph 3.1). The geometry of deorbit is shown in Figure 3.2-6 where the IRV is shown in circular orbit. The IRV is separated from the spacecraft and immediately spun up for thrust vector control.

The spin rate necessary to achieve adequate thrust vector control is determined in Appendix F to be 7 to 10 rpm for the typical tipoff rates at IRV/space station separation, thrust vector misalignments, and IRV dynamic imbalance. This low spin rate results from the extremely favorable ratio of moments of inertia (I roll/I transverse) in the designs considered to date. A less favorable inertia ratio would result in higher spin rates.

A retro velocity increment is applied to the IRV to place it on a reentry trajectory toward the desired recovery area. The magnitude (ΔV) and direction (ϕ) of the velocity increment are as shown. The IRV traverses a geocentric angle (θ) between application of the velocity increment and reentry into the Earth's atmosphere (400,000 ft. altitude). At reentry, reentry angle (γ_E) is shown as the angle between the local horizontal and the velocity vector; the angle of attack (α_E) is shown as the angle between the IRV longitudinal axis and the velocity vector. Figures 3.2-7 through 3.2-14 show the reentry velocity (V_E), reentry angle (γ_E),reentry angle dispersion ($\Delta\gamma_E$), and reentry angle of attack (α_E) for various values of ΔV and ϕ for the 164 and 260 nautical mile circular orbits. The reentry angle dispersion shown is the result of a 1 sigma error in thrust application angle of 5 degrees and a 1 sigma error in ΔV magnitude of 2 percent.

Aerodynamic trajectories have been run for a variety of reentry angles at a reentry velocity of 26,000 feet per second. A reentry angle of at least -2.25 degrees is necessary to ensure capture and subsequent reentry on the first orbital pass. (A reentry angle of -0.73 degrees results in a two skip reentry; that is,

two orbital passes before reentry.) It is also desirable to reenter at the smallest practical angle of attack. Examination of Figures 3.2-7 through 3.2-14 shows that the angle of attack at reentry can be improved by selecting positive thrust application angles at the expense of a slight increase in ΔV, V_E, and $\Delta\gamma_E$. For example, in deorbiting from a 260 nautical mile circular orbit, a thrust application angle of 40 degrees for a reentry angle of -2.25 degrees results in a reentry angle of attack of 52 degrees rather than the 81 degrees which would result from the selection of the minimum reentry dispersion thrust application angle of 0 degrees (see Figure 3.2-9). The penalty for this improvement in reentry angle of attack is small indeed; an increase of 50 feet per second in ΔV, an increase of 100 feet per second in V_E, and an increase of 0.14 degrees in $\Delta\gamma_E$. There may be one other disadvantage associated with this plan. If the IRV cannot be mounted on the spacecraft in the proper orientation for this thrust application angle, a spacecraft maneuver will be required before IRV separation. This maneuver may be required in any case unless the IRV can be mounted in the proper orientation. The reentry conditions which result for nominal deorbit from each of the two study orbits are shown in Table 3.2-I.

TABLE 3.2-I

REENTRY CONDITIONS AT ϕ = DEGREES

Orbit (n.mi.)	ΔV (ft/sec)	V_E (ft/sec)	γ_E (degrees)	α_E (degrees)
164	425	25,540	-2.25	115
260	425	25,800	-2.25	72

3.2.5 Reentry and Descent Mission Phases

The nominal reentry and descent trajectories result from the reentry conditions of Section 3.2.4 and specification of the IRV ballistic parameter (W/C_DA). The W/C_DA must be low enough to allow subsonic conditions for parachute deployment by 50,000 feet altitude, if air snatch recovery is to be attempted using current procedures. In any event, the W/C_DA must be low enough to provide a tolerable terminal velocity at impact if no parachute is used or if a parachute failure occurs. A W/C_DA in the range from 20 to 40 pounds per square foot appears reasonable providing terminal velocities between about 160 and 240 feet per second. The resulting altitude at which subsonic parachute deployment conditions (0.8 mach) prevail is between 54,000 and 72,000 feet.

The reentry vehicle aerodynamic stability must result in turnaround before the aerodynamic heating during reentry elevates the temperature of the isotope fuel capsules to dangerous levels. If the reentry vehicle aerodynamic performance does not result in early enough turnaround, a passive aerodynamic turn-around device must be used to augment the basic reentry vehicle performance.

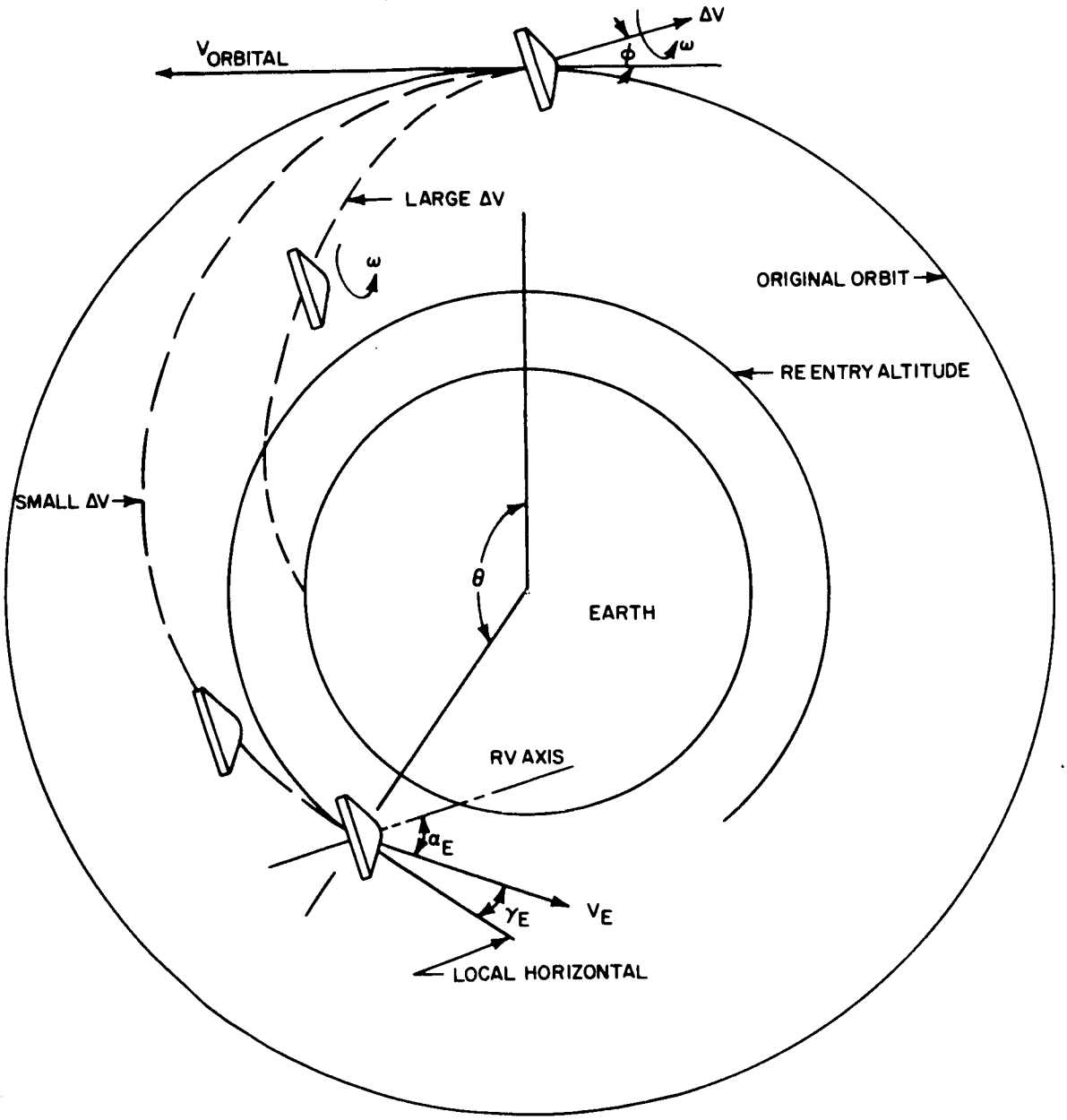

Figure 3.2-6 DEORBIT GEOMETRY

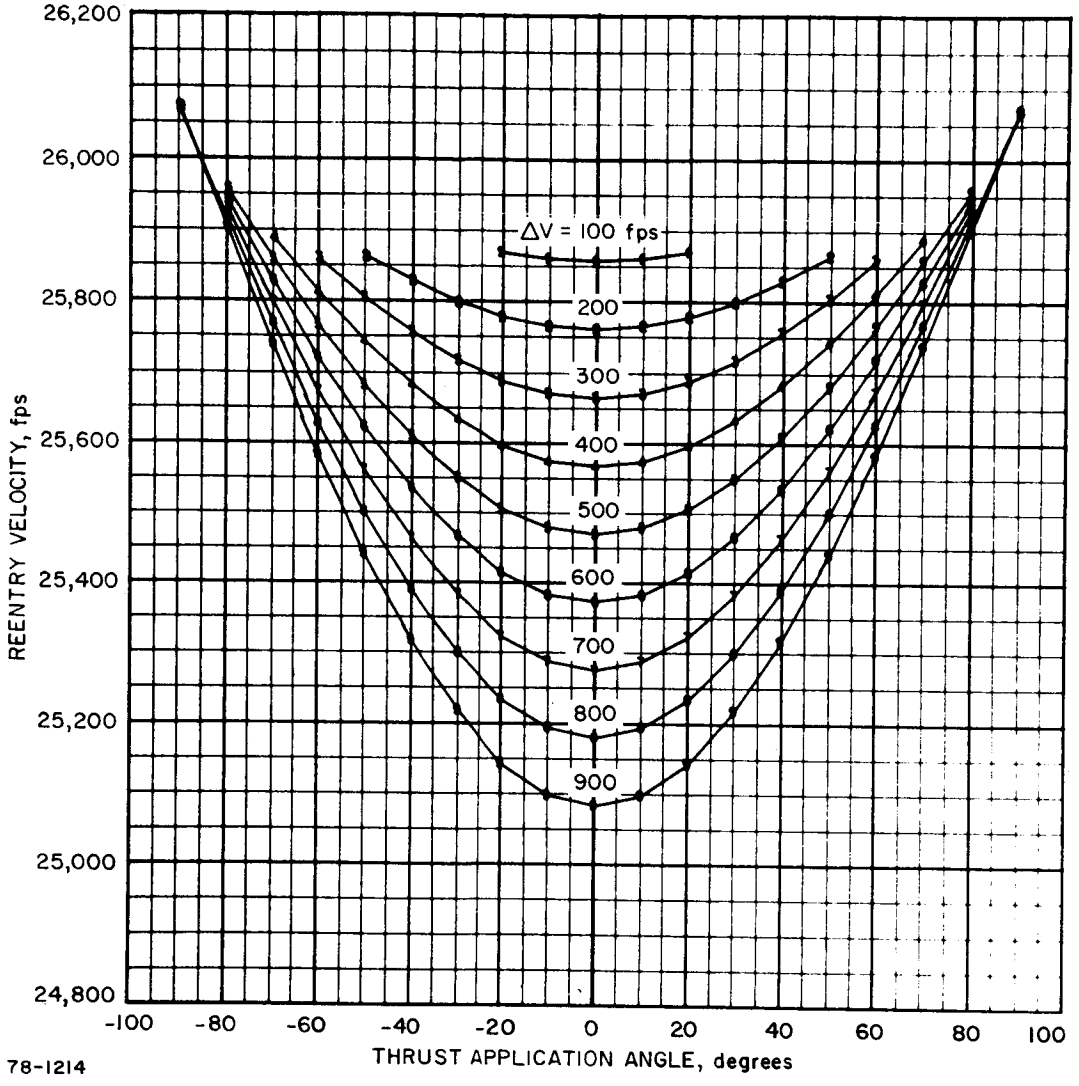

Figure 3.2-7 IRV ALT = 164 NM REENTRY VELOCITY PROFILES

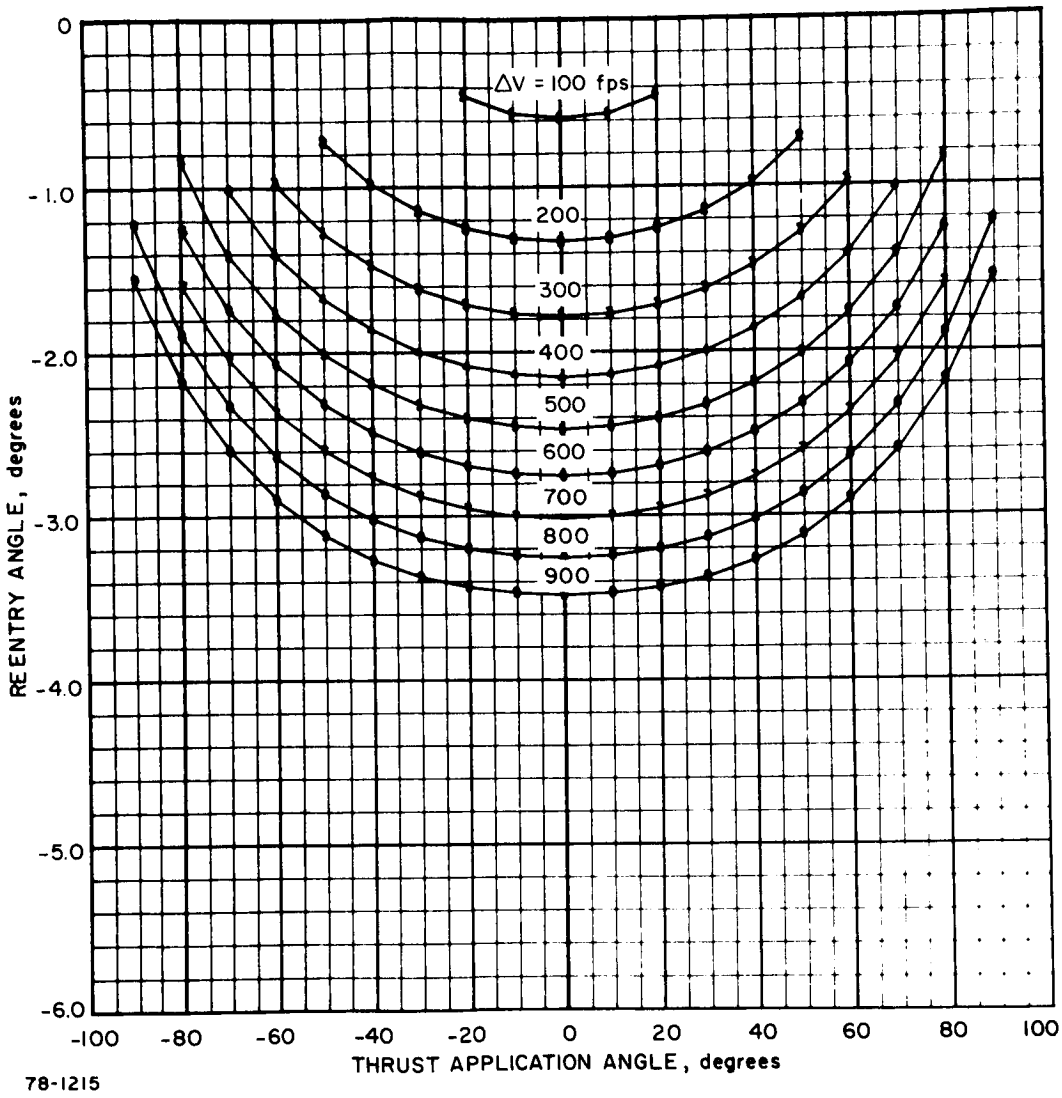

Figure 3.2-8 IRV ALT = 164 NM REENTRY ANGLE PROFILES

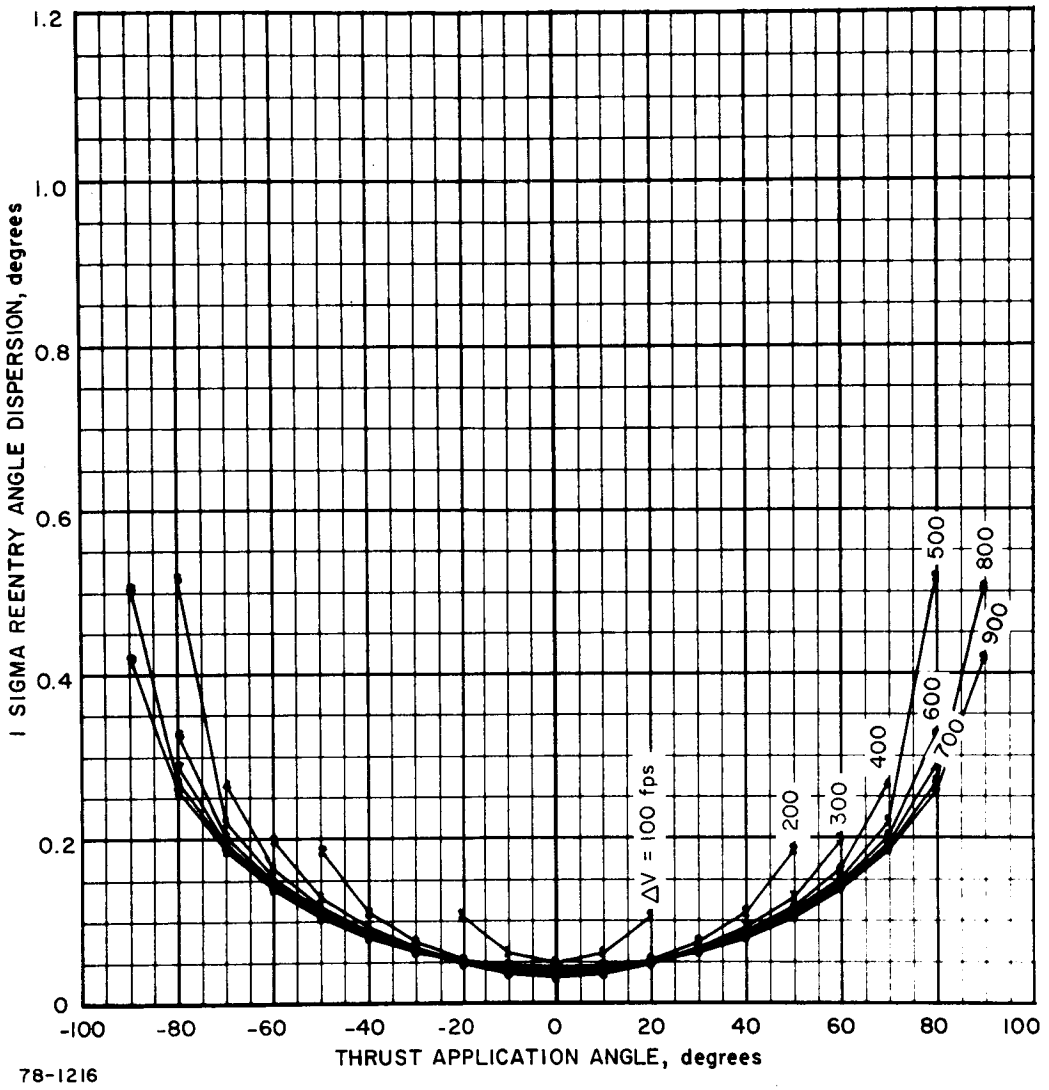

Figure 3.2-9 IRV ALT = 164 NM 1 SIGMA DISPERSION IN REENTRY ANGLE

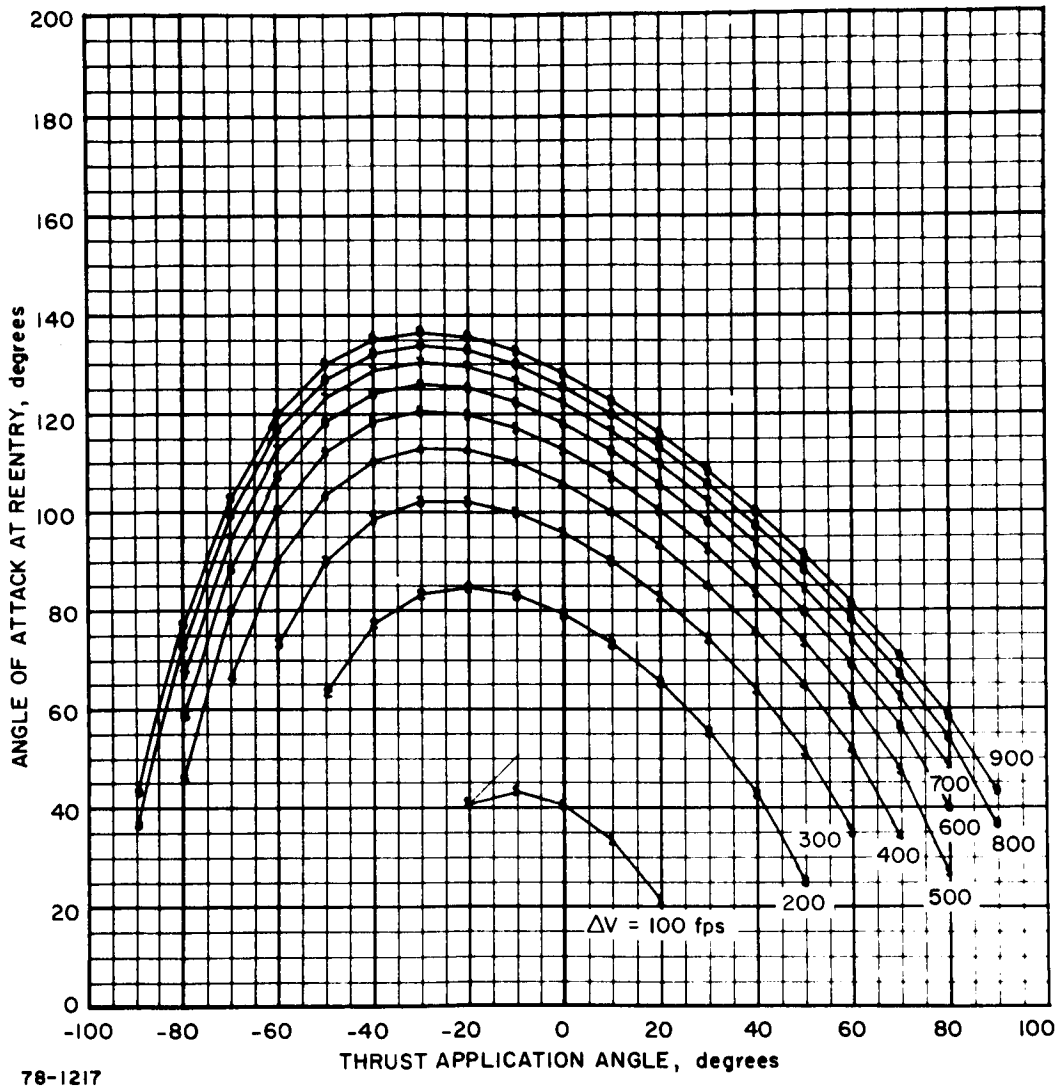

Figure 3.2-10 IRV ALT = 164 NM ANGLE OF ATTACK AT REENTRY

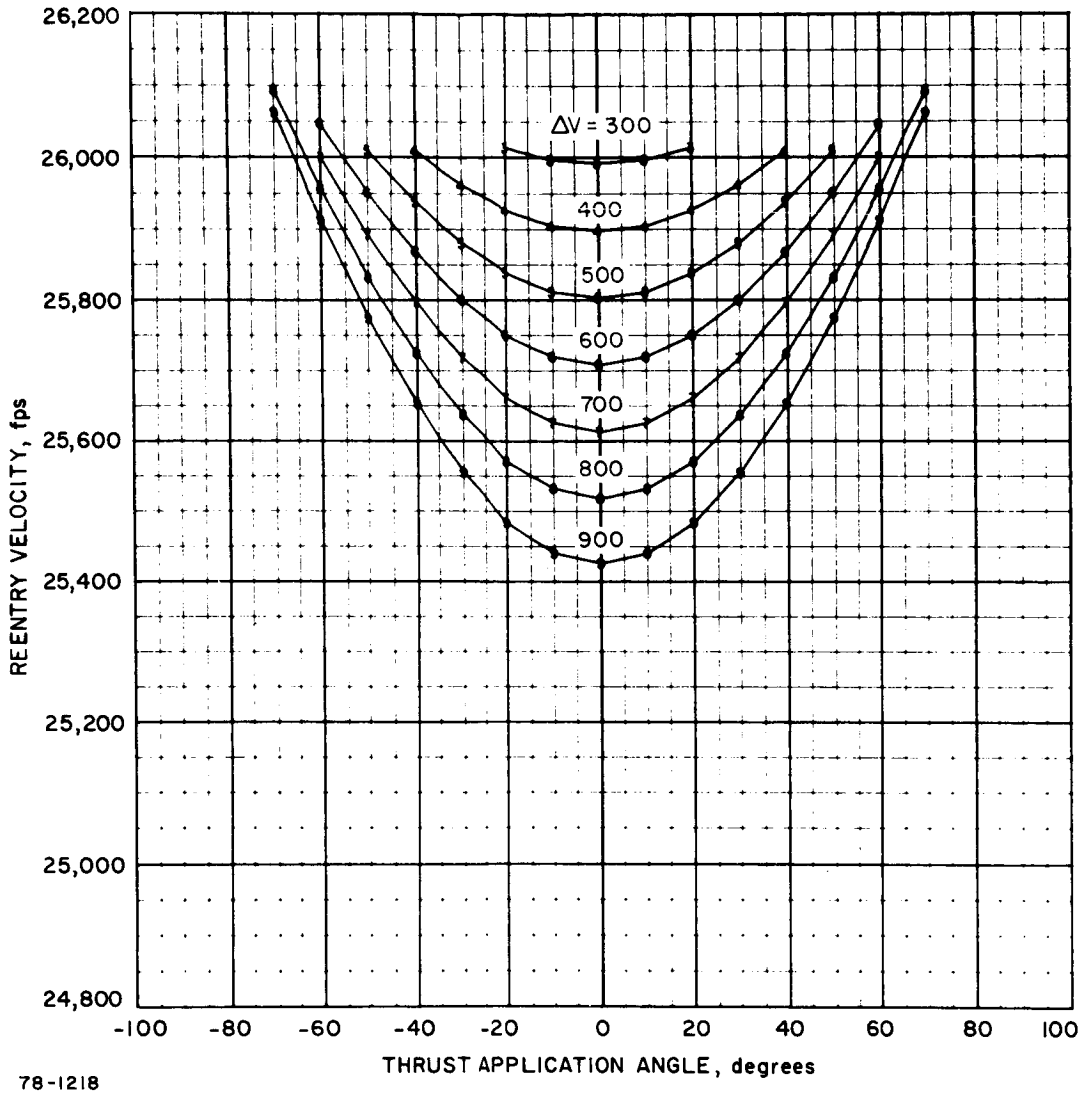

Figure 3.2-11 IRV ALT = 260 NM REENTRY VELOCITY PROFILES

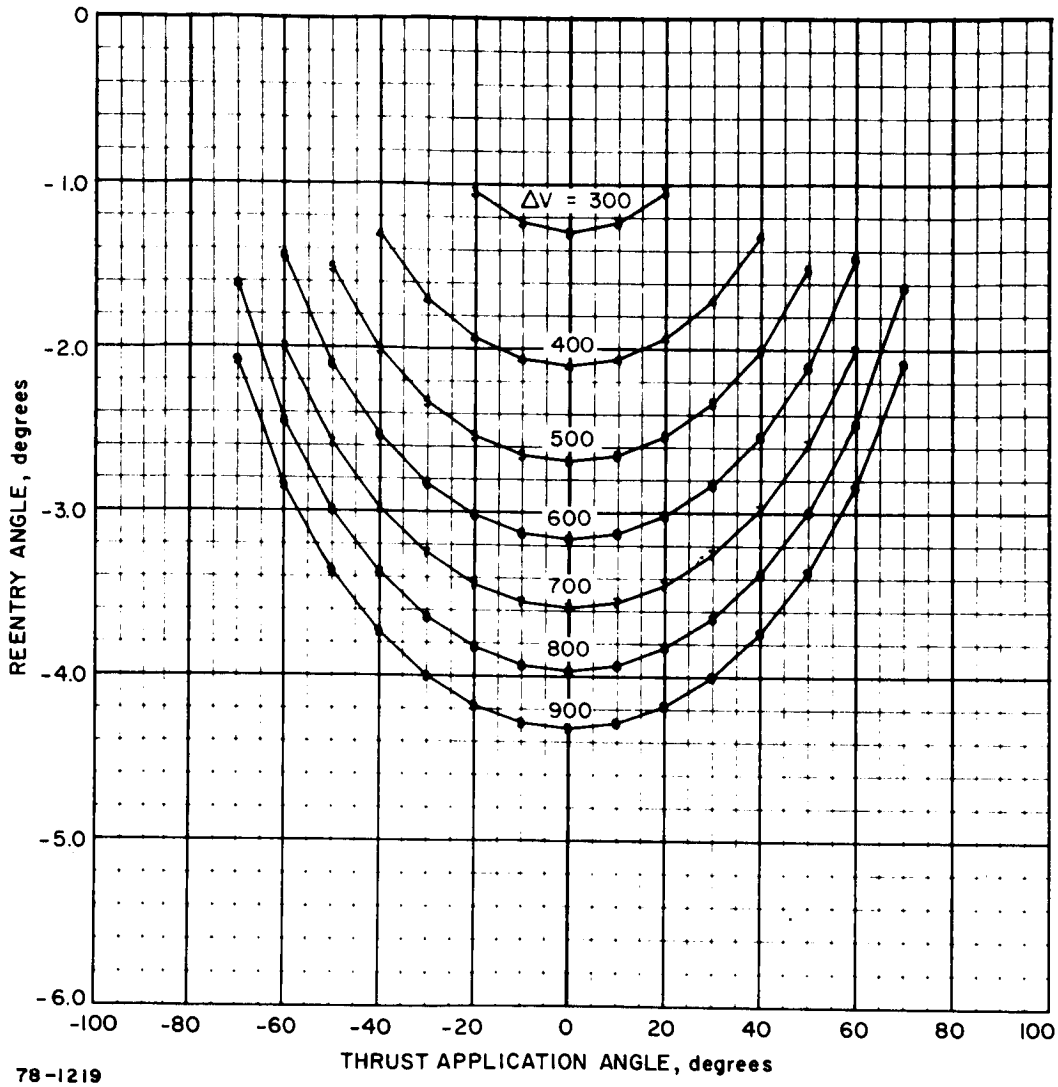

Figure 3.2-12 IRV ALT = 260 NM REENTRY ANGLE PROFILES

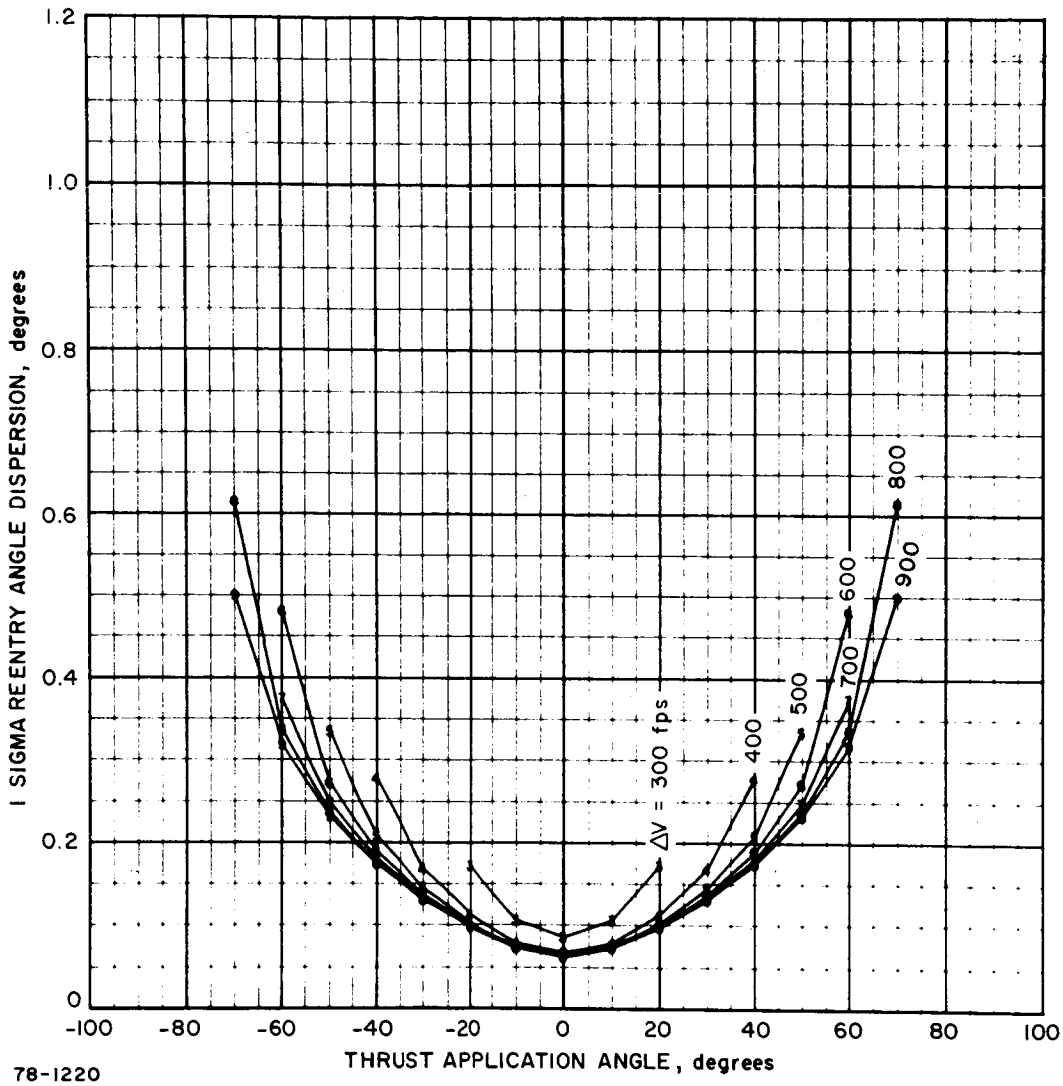

Figure 3.2-13 IRV ALT = 260 NM 1 SIGMA DISPERSION IN REENTRY ANGLE

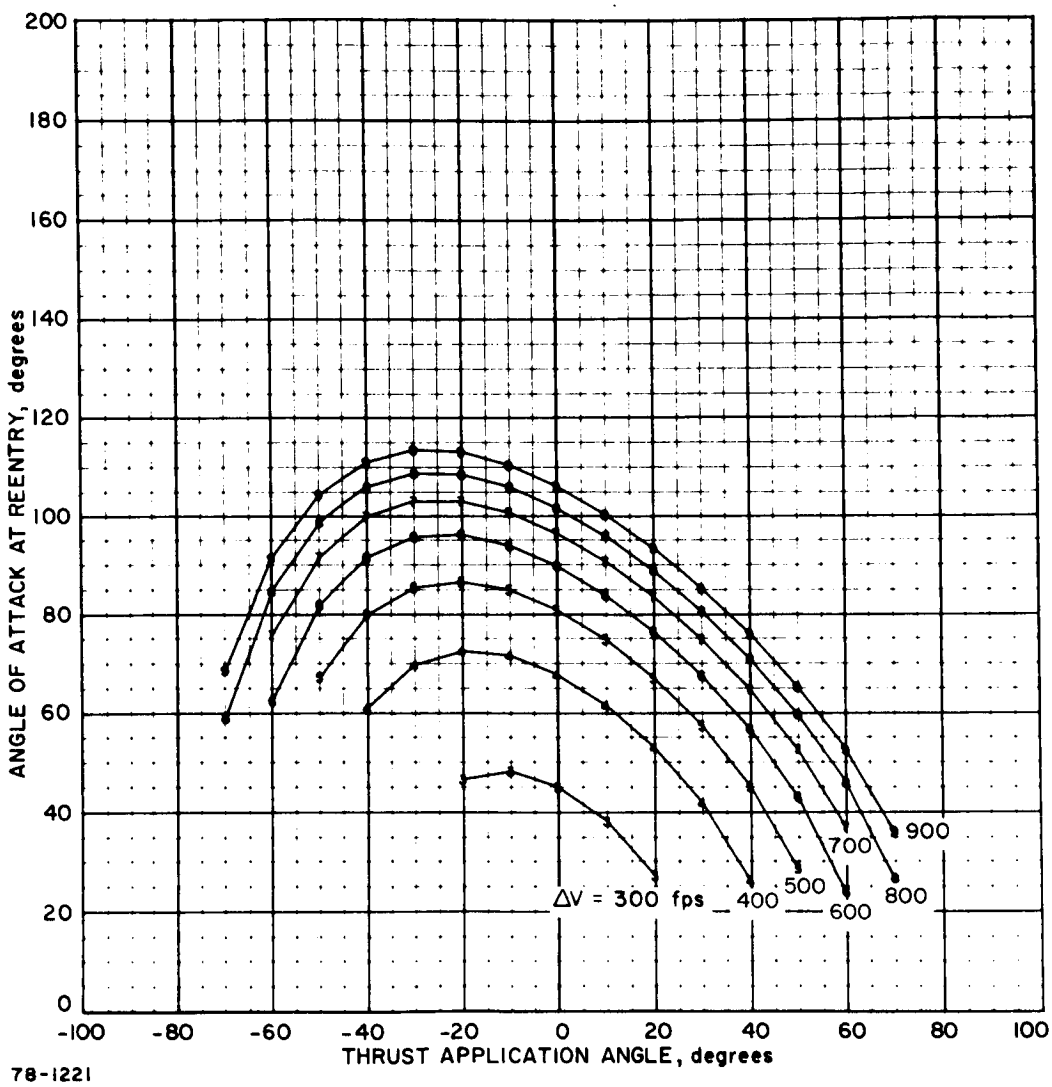

Figure 3.2-14 IRV ALT = 260 NM ANGLE OF ATTACK AT REENTRY

3.2.6 Impact Mission Phase

At impact, a flotation system with location aids may be activated. This system should be capable of operation for a period of at least 48 hours, and should provide both daylight and night location aids. After 48 to 60 hours, the flotation system can reliably scuttle the IRV for deep water burial.

If recovery is deemed unnecessary, the IRV is allowed to impact and sink in deep water. Deep water burial may be acceptable since even if containment is breeched the dissolution rate of the microsphere PuO_2 fuel form in salt water has been shown to be extremely low (Reference 1). In addition the interaction between deep water marine life and man's ecological cycle is comparatively weak. Oceanographic studies have also shown that the transfer of dissolved solids from the deep ocean to the surface waters requires a period of approximately 700 to 1000 years, a period that is equivalent to 10 half life containment (Reference 2).

3.3 FAILURE MODE ANALYSIS

The nominal mission profile has been perturbed to find the various credible failure modes which could possibly result in nuclear fuel release. For simplicity the mission has, once again, been subdivided into several phases. For each phase, the systems failure modes have been analyzed to establish the appropriate operational response; the resulting system design requirements have been defined; and the necessary safety and recovery aids have been identified.

3.3.1 Prelaunch and Lift-Off Failure Modes

The primary failure modes during prelaunch and lift-off mission phases are shown in Table 3.3-I. The system requirements are indicated for each failure mode but are not repeated even though applicable to later failure modes.

Failure mode 1 (minor failure, noncritical to the IRV) requires no action on the part of the IRV launch team unless it develops into a more serious failure mode. IRV instrumentation and monitoring Ground Support Equipment (GSE) hardware and software are necessary to determine the status of the IRV subsystems throughout the prelaunch phase to insure against undetected development of a critical failure mode.

Failure Mode 2 (minor failure - IRV cooling) can be accommodated most readily by providing in-place redundant operating capability for the Auxiliary Coolant Heat Exchanger (ACHX). A totally redundant ACHX in a ready-state throughout prelaunch and launch operations can be provided. At a minimum, the active elements of the ACHX should be redundant highly reliable components.

Failure mode 3 (minor heat source malfunction) covers the extremely unlikely prelaunch malfunctions which might occur within the heat source, thermal insulation, or radiation shielding equipment. The occurrence of such a malfunction can be detected by appropriate radiation and thermal sensors distributed throughout the IRV. In the event of such a malfunction the equipment must be repaired or replaced prior to launch. Handling equipment and techniques must be developed to enable such repairs to be accomplished with a minimum launch hold.

TABLE 3.3 - I

SYSTEM DESIGN REQUIREMENTS PRELAUNCH AND LIFTOFF FAILURE MODES

Failure Mode	Required Action	System Requirements
1. Minor Failure (Noncritical to IRV)	None	1. Instrumentation 2. GSE Hardware and Software
2. Minor Failure (IRV Cooling)	Activate Redundant Elements in ACHX	Redundant ACHX Elements
3. Minor Heat Source Malfunction	Repair, Replace --- Delay Mission	GSE Handling Equipment
4. Launch Vehicle Explosion (With Warning)	Abort	1. Sequencing System 2. Shroud Jettison System 3. Separation System 4. Thrust Vector Control 5. Abort Rocket 6. Impact Attenuation 7. Post Impact Heat Rejection 8. Flotation System 9. Location Aids 10. Recovery Teams
5. Launch Vehicle Explosion (Without Warning)	Abort	1. Automatic Sequencing 2. Fast Reaction Shroud Jettison

Failure modes 4 and 5 (launch vehicle explosion with or without warning) constitute the most severe failure modes during the prelaunch and launch mission phases. The IRV is separated and propelled away from the launch vehicle to limit exposure to the explosion fire-ball and resulting launch pad fire. The IRV must also be capable of surviving sustained exposure to the launch pad fire (>20 minutes) in the event that the abort rocket system fails.

The launch abort rocket requirements are defined primarily by the requirement to propel the IRV an adequate distance from the launch pad catastrophe. A thrust level of 2600 pounds will result in a separation distance at least 200 feet in < 20 seconds which seems adequate to escape the launch pad fire. Ascent shield abort, disconnect, and separation of the IRV can occur within a few seconds of the abort signal which could be initiated by the Range Safety officer, or automatically.

The IRV can be exposed to launch pad fire in any number of orientations including burial in the pile of rubble resulting from destruction of the launch vehicle. Two models for the launch pad fire representing the extremes are being examined. The first model allows the heat source full exposure to the fire at temperatures up to 1700° F (Reference 3) for up to twenty minutes (the longest duration of launch pad fire before access by support personnel is assumed). The heat source will rapidly assume the fire temperature. However, since the operating temperature of the heat source is about 2000° F, no damage to the heat source capsules will occur. As the fire subsides, the heat source will be cooled by convective heat transfer to the surrounding atmosphere.

The second extreme model denies convective cooling for the heat source. Under these circumstances it is also reasonable to deny heat input to the heat source from the fire. The IRV must then depend upon the built-in thermal capacity of the beryllium oxide within the heat source plate. The thermal capacity of the plate is designed by the ground rule requirement for one hour from 1800° F to 2500° F when cooling of the heat source is resumed. The beryllium oxide heat sink necessary to satisfy this operating requirement will allow a period in excess of three hours for ground crews to reach the IRV and initiate auxiliary cooling (exposing the heat source to the atmosphere is sufficient for cooling).

The IRV and heat source may also be subject to physical damage during a launch vehicle explosion. The T_{111} structure of the heat source capsules as designed appears capable of withstanding end-on impact with an unyielding surface at velocities up to 300 feet per second. Since the heat source is shielded from direct exposure to the explosion by the BHXU and HSHX as well as the intermediate structure and radiation shielding, it is not clear that more severe shock loading will be encountered during an explosion; however, more detailed analysis is required.

An additional hazard which may result from a launch pad explosion is exposure of the heat source capsules to possible corrosive action of the launch vehicle fuel or oxidizer. The outer layers of the heat source capsules should be corrosion resistant, at least for the short period involved in a launch pad explosion.

3.3.2 Ascent Failure Modes

The primary failure modes during ascent to orbit injection are shown in Table 3.3-II. Once again, only the previously unidentified system requirements are listed.

TABLE 3.3-II

SYSTEM DESIGN REQUIREMENTS ASCENT FAILURE MODES

Failure Mode	Required Action	System Requirements
1. Same as Prelaunch Failure Modes (Except IRV Cooling)	Same as Prelaunch Failures	1. Telemetry 2. Aeroshell 3. Parachute
2. Launch Vehicle Thrust Vector Control or Guidance Failure	Abort	1. Rate Instrumentation (on Launch Vehicle) 2. Automatic Ejection

Failure Mode 1 (same as prelaunch failure modes) includes the effect of all failure modes considered in Section 3.3.1 except the IRV cooling failure mode which cannot occur during ascent, at least in the same manner as previously discussed. Another difference exists for the separate launch concept, in that the dynamic pressure loading during a portion of ascent exceeds any reasonable thrust level for the abort rocket system. During this period, if a launch vehicle explosion occurs, the blast force itself may serve to jettison the IRV. The only action which can be taken is activation of the IRV separation system to make release of the IRV occur more readily during the explosion.

Additional systems requirements have been added to safely return the heat source from the higher altitudes from which the IRV may descend. The IRV status monitor requirement can only be satisfied through a radio link (possibly the launch vehicle telemetry system) to ground receiving stations or to the space station in orbit.

The entry conditions (V_E,γ_E) which result from launch abort at any point along the ascent trajectory are indicated by the lower curve in Figure 3.3-1 and Figure 3.3-2 for reentry from ascent to the 164 and 260 nautical mile circular orbit respectively. The circles indicate the time after launch in seconds at which an abort must occur to result in the reentry conditions indicated.

The upper curve represents the reentry conditions which would occur if the total remaining ΔV were applied in a fixed direction starting at a time 400 sec. after lift off. The possibility of this type of malfunction occurring to this degree is not considered credible and consequently the most severe reentry conditions chosen for design are $\gamma_E = -10^o$, $V_E = 26{,}000$ fps.

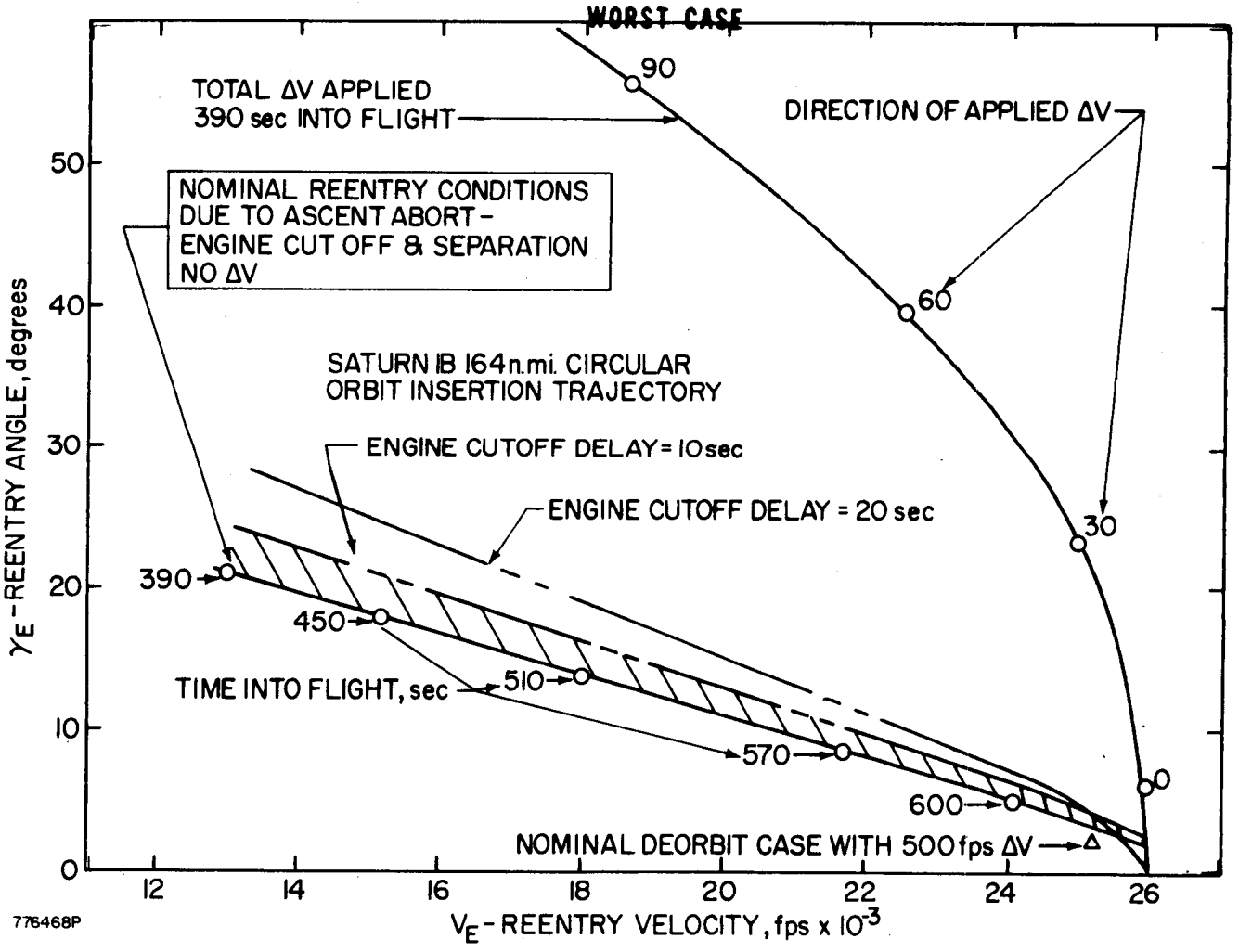

Figure 3.3-1 REENTRY CONDITIONS

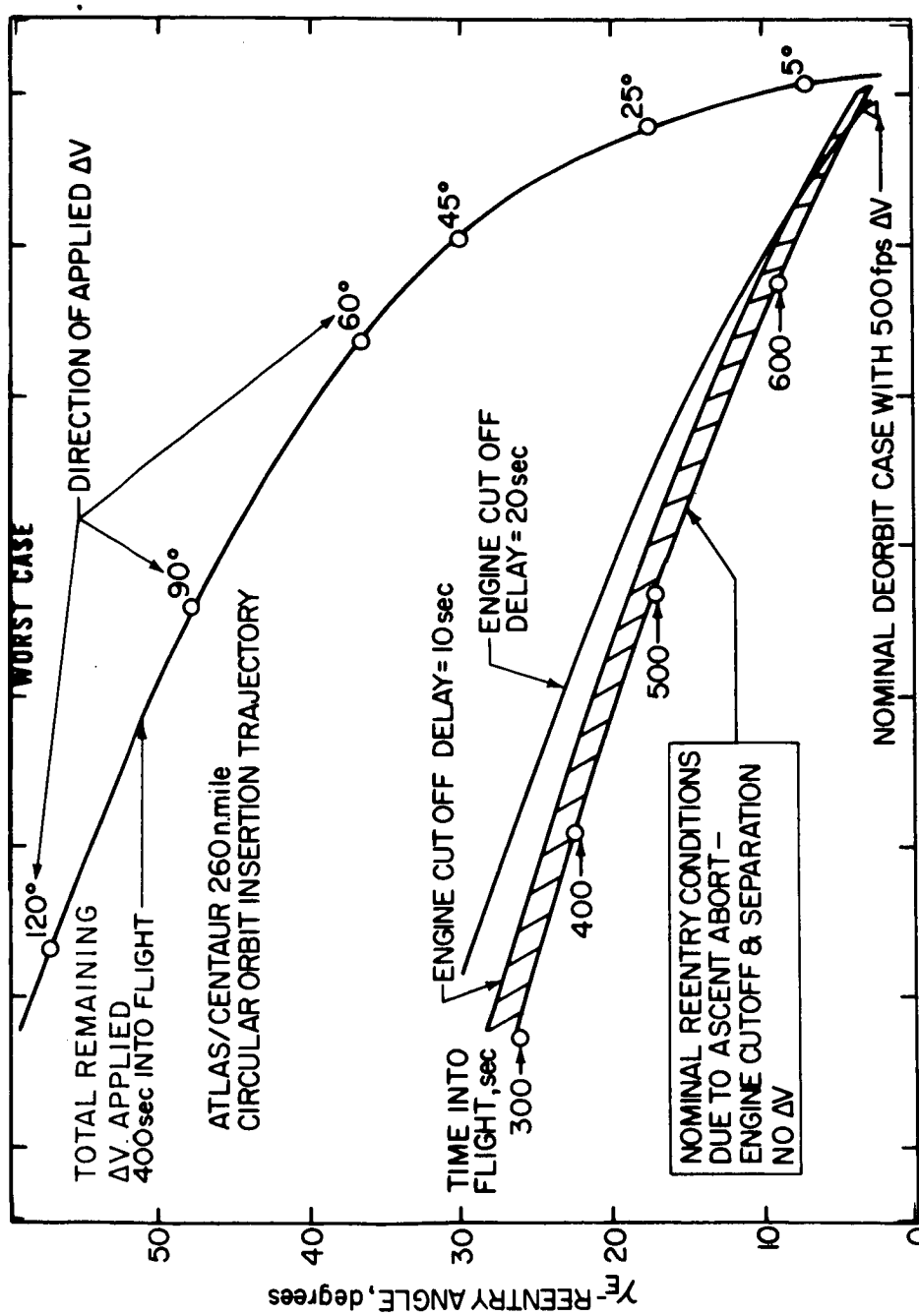

Figure 3.3-2 REENTRY CONDITIONS

The reentry conditions resulting from nominal deorbit are shown for comparison (marked with a triangle Δ).

Failure Mode 2 (launch vehicle thrust vector control (TVC) or guidance failure) is depicted in Figure 3.3-3. At some point during ascent the launch vehicle guidance system is assumed to command an unprogrammed maneuver. This will drive the launch vehicle away from the nominal ascent trajectory. The failure mode can be modeled in either of two ways. First, a pitch angular acceleration maneuver may be maintained until a destruct command is issued by Range Safety.

Assuming that a hard-over command situation arises for the Centaur by means of some malfunction, the applied torque will result in a pitch rate increase of:

$$\dot{\theta}(t) = 0.017t \text{ rev/sec}$$

where $\dot{\theta}(t)$ is the pitch rate in revolutions/second, and t is time in seconds. The resulting pitch rate will be retained by the IRV until entry. Pitch rates exceeding 2 rev/sec will most probably tumble throughout reentry; a highly undesirable but tolerable condition. This failure mode leads to a requirement for rate sensors (perhaps on the launch vehicle) which automatically initiate ejection of the IRV if the rates exceed a preselected value.

Another type of failure (also shown in Figure 3.3-3) which would cause tumbling during reentry could result from a separation system failure, or a premature booster detonation. The IRV is subjected to the blast loads and due to a tie-down bolt release mechanism malfunction, unsymmetrical loading will induce angular acceleration in the IRV. Depending upon the magnitude of the loading environment, the rotational rate will build up until the restraining tie-down bolt fails. The dynamical model analyzed is depicted in Figure 3.3-4.

The remaining tie-down bolts were assumed to have been released or to have already failed. The blast load was varied over the range of reasonable values (Reference 4) to determine the maximum angular rate possible for the model, 0.1 revolutions per second. This represents a conservative upper limit on the body rates at reentry.

3.3.3 Orbital Failure Modes

The primary orbital failure modes are shown in Table 3.3-III. As before, only the new systems requirements are identified.

Failure Mode 1 (same as prelaunch failure modes) includes once again the effects of all failure modes considered in Section 3.3.1 except, of course, the launch vehicle explosion failure mode which can no longer occur. The function of monitoring the status of the IRV now passes from the ground crews to the space station crew who periodically check the IRV behavior on the IRV monitor and control console.

Failure Mode 2 (IRV cooling failure) may result from any malfunction which causes the HSHX to stop functioning. The IRV is mounted on a ring which is hinged to the spacecraft permitting the IRV to be rotated into a position such that it can be cooled by direct radiation to space. The heat source plate, as previously

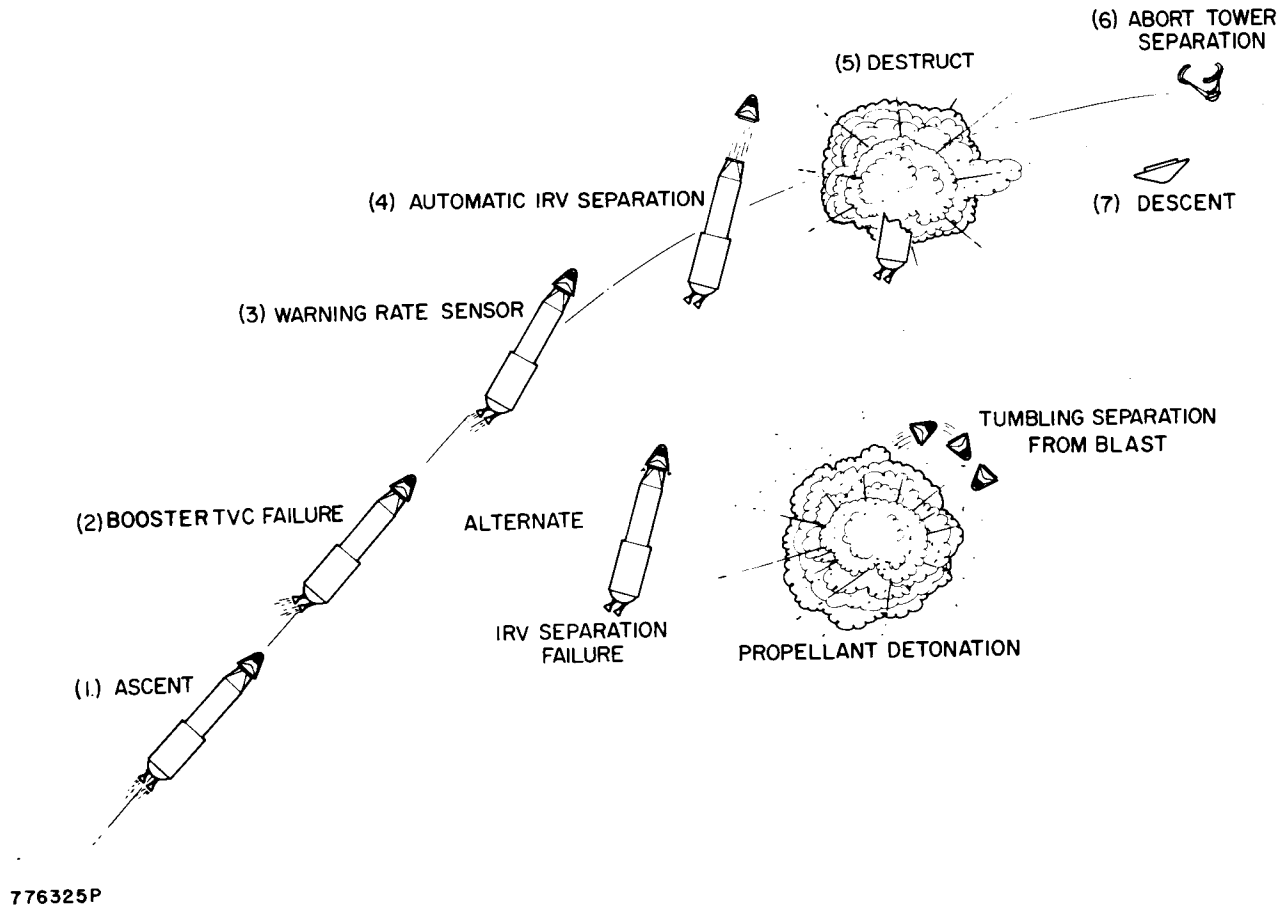

Figure 3.3-3 ASCENT ABORT SEQUENCE

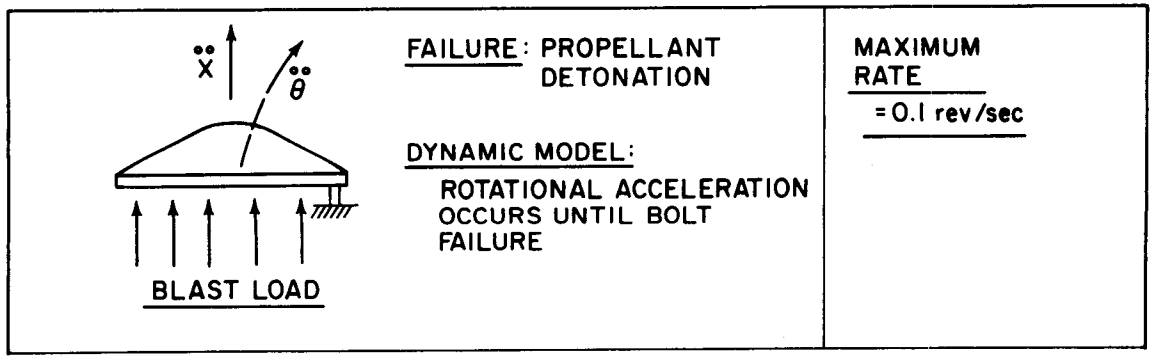

776420P

Figure 3.3-4 BLAST MODEL

TABLE 3.3 – III

SYSTEM DESIGN REQUIREMENTS ORBITAL FAILURE MODES

Failure Mode	Required Action	System Requirements
1. Same as Pre-launch Failure Modes	Same as for Pre-launch Failure Modes (Except Cooling Failure)	Spacecraft IRV Monitor and Control Console
2. Cooling Failure	Hinge IRV to Alternate Cooling Mode	Redundant IRV Hinge and Drive System
3. Failure which Requires Mission Termination	1. Establish Deorbit Point for Impact Site Control 2. Orient Spacecraft 3. Separate, Spin-up IRV Deorbit	1. Dynamic and Static IRV Balance 2. Redundant Separation System 3. Deorbit Systems a) ΔV Rocket b) Spin Rockets c) Spacecraft Maneuver for Attitude Reference
4. Failure which Requires Mission Termination without Warning	1. Disarm ΔV Rocket 2. Separate IRV	1. ΔV Rocket Arm-Disarm Capability
5. Failure which Requires Mission Termination during Spacecraft Attitude Control System Malfunction	1. Disarm ΔV Rocket 2. Separate IRV	2. IRV Design for Deorbit by Natural Decay, Random Entry, Random Impact Location

discussed, contains enough thermal capacity to allow the IRV to remain in its operational orientation for approximately 30 minutes without exceeding design temperature limits on the heat source fuel capsules. The hinge must be actuated by both electrical and mechanical drive mechanisms to insure its operation.

Failure Mode 3 (mission termination) can result from a large variety of spacecraft failure modes. It can also result from a simultaneous failure of the HSHX and the hinge and drive system, which prevent proper IRV cooling. The only remaining option is to deorbit (or separate) the IRV and terminate the mission. The operations involved are no different from a normal mission termination except as noted in Failure Modes 4 and 5. The thermal capacity of the heat source plate will provide sufficient time to select a deorbit point which results in water impact.

Failure Mode 4 (mission termination without warning) may not allow adequate time to select the impact point within one or more pre-arranged recovery areas. Failure Mode 5 (spacecraft ACS malfunction) does not allow control over the deorbit velocity thrust application angle which also results in inability to control the impact point. In either case, the deorbit rocket should be disarmed before IRV separation. The IRV can be separated and allowed to deorbit by natural decay. The resulting reentry could occur anywhere within the latitude band represented by the initial orbit inclination. The IRV would remain in orbit from about one month for the 164 nautical mile orbital altitude to 2 to 4 years for the 260 nautical mile orbital altitude. In the latter case, it may be quite practical to retrieve the system from orbit before it reenters through the use of some as yet unidentified space system. In fact, it may be possible or desirable to prepare for such an event by developing such a system if the IRV should be subjected to either of these failure modes.

3.3.4 Reentry and Descent

The primary failure modes during the reentry and descent mission phase are shown in Table 3.3-IV. During reentry and descent, there is no opportunity to react to the failure modes. The failure modes can be overcome only by conservative design and the use of redundancy where practical.

TABLE 3.3-IV

SYSTEM DESIGN REQUIREMENTS REENTRY AND DESCENT FAILURE MODES

Failure Mode	Required Action	System Requirements
1. Aerodynamic Fence Failure	None	1. Design IRV for Tumbling Throughout Reentry 2. Design IRV for Rearward Reentry
2. Aeroshell Failure	None	Design IRV with Conservative Margin
3. Aerodynamic Decelerator Failure	None	1. Design IRV for No-Decelerator Impact Velocity 2. Omit Decelerator if Serious Impact Failure Modes can Result

Failure Mode 1 (aerodynamic fence failure) leaves the IRV with a reduced capability to inhibit any tumble rates during reentry. Depending upon the aerodynamic configuration which remains after fence damage, the IRV may have an undesirable stable trim angle of attack or perhaps multiple stable trim angles of attack. The IRV must, therefore, be designed conservatively to accommodate tumbling throughout reentry or to survive reentry at any possible stable trim angle of attack.

Failure Mode 2 (aeroshell failure) can result if design margins for the IRV are exceeded during actual operation. The IRV must be designed with conservative margins to preclude this possibility. Since the conditions which establish the design levels for the IRV are, in themselves, extremely unlikely, conservative safety factors applied to the design levels should be more than adequate to insure against IRV structural failure during reentry.

Failure Mode 3 (aerodynamic decelerator failure) assumes the use of a parachute or ballute for terminal descent. The failure of such a device to deploy requires that the IRV impact attenuation system be designed to protect the heat source capsules at an impact velocity typical of the IRV alone. The decelerator must not introduce failures modes at impact which are more severe than the high velocity impact which the decelerator is designed to alleviate. The decelerator may make the IRV more sensitive to wind gusts resulting in adverse impact angles or large horizontal velocity components at impact. Investigation of the decelerator induced failures modes remains to be done, at which time a decision can be made. Selection of either no decelerator or the use of a ballute precludes the possibility of air snatch recovery but still permits consideration of surface recovery from the ocean (if a flotation bag is included).

3.3.5 Impact Failure Modes

Nominal mission termination is designed to impact the IRV in a preselected recovery area in deep water. There is, however, as a result of some launch aborts for the integral launch concept or deorbit by natural decay and random entry, the possibility of land impact. Even for these extremely limited cases, the probability of water impact exceeds that of land impact. Land impact, however improbable, must be considered in the design of the IRV.

The primary hazard which may occur on land impact is the release of fuel form fines. Although there exists slightly over two bare critical masses of the Pu-238 oxide fuel form in the Heat Source, the design of the fuel capsules and associated hardware should preclude consideration of criticality as a credible accident under any conceivable abort condition. It is clear from Ref. 5 that as long as the fuel capsules retain their basic integrity, the subcriticality of any possible array of capsules can be guaranteed. This is true for all cases including ground impact and deep water burial. If post impact (ground) heat rejection is inadequate some capsule meltdown and fuel release is conceivable, but attainment of a critical mass configuration of the fuel is considered to be an incredible event.

The design of the IRV must prevent significant deformation or physical damage to the fuel capsules at impact and must provide means for adequate post impact heat rejection. Three approaches are available to achieve this end:

a. Intact Impact--The fuel capsules are retained in a cradle in the heat source plate which, in turn, is protected at impact by an impact attenuation system. The entire assembly is designed to survive impact with neither release of the capsules nor structural damage to the capsules. The primary problem with this approach is provision for post impact heat rejection. Impact should occur nose down with a similar IRV rest attitude providing cooling by convective heat transfer to the atmosphere. However, either land or swamp burial could cause the heat source to overheat and melt. Land burial is unlikely to occur at impact but can be caused by drifting sand over an extended time period. Swamp burial appears even less likely as the swamp must have a limited supply of water and dry up due to water boil-off caused by the heat source, leaving the IRV buried in what once was mud. A third possibility would have the IRV assume an inverted rest attitude on the surface after impact. The heat source could be denied adequate cooling by convective heat transfer to the atmosphere and must rely on conduction through the heat source plate, the crushed structure and insulation, and the probably broken aeroshell. The adequacy of this heat path is difficult to assess and requires further analysis.

b. Fracturable Plate--The primary difference in this design approach is that the heat source plate is designed to fracture upon impact, spilling the capsules over the local surface. This approach provides an improved situation for post-impact heat rejection since the fuel capsules are spread out and can be treated singly or in small groups. However, the capsules may be damaged as the heat source plate fractures. The actual loads which a particular capsule may encounter are difficult, if not impossible, to predict.

c. Pre-impact Capsule Dispersion--This design approach disperses the capsules before impact and allows them to impact individually. This approach appears to overcome the problems of the previous two approaches, however it has problems of its own. The dispersion device is an active element which must survive launch, 5 years in space in the severe thermal, radiation, and hard vacuum environment, and reentry, to activate just before impact. There is no convenient physical phenomenon which occurs just before impact from which the dispersion mechanism could be directly activated. The most convenient phenomenon during reentry would be peak load or peak heating, both of which occur at too high an altitude to be useful. The high altitude dispersion results in significant reentry heating on the capsules as well as a worst case terminal veloiity of about 400 feet per second which exceeds their present capability. Lower altitude dispersion system activation can be accomplished by radar altimetry, or perhaps a deployable nose spike impact detector. The more conventional techniques such as a baroswitch or a timer from peak dynamic pressure cannot adequately disperse the capsules since the terrain altitude at the impact point is unknown.

Selection between these three approaches to impact protection is not clear cut; however, preliminary analysis indicates that the intact impact concept provides the most predictable design.

3.4 CONCLUSIONS

During each mission phase, there are several orders of safety mechanisms which act to prevent the occurrence of a nuclear hazard. Table 3.4-I shows these safety mechanisms. It is important to note that there are always at least 5 orders of safety mechanisms with 6 orders of safety mechanisms acting during the critical prelaunch, ascent, and orbital phases.

The systems design requirements are listed in three groups. Table 3.4-II includes those items which are commonly used for most launch vehicles or reentry systems and as such do not represent a departure from standard procedure. Table 3.4-III includes those items which are necessary for the IRV and are not commonly part of the launch vehicle or reentry system. Table 3.4-IV indicates the optional IRV subsystems. These subsystems are not necessary for safe reentry of the IRV but either enhance the performance of the IRV or provide for recovery of the isotope heat source. The optional equipment may be designed into the IRV or not, as the mission and safety requirements dictate. Table 3.4-V shows a summary list of abort, deorbit, separation, and recovery aids including typical weights for each item.

TABLE 3.4-I

SAFETY MECHANISMS

	GROUND HANDLING	ON THE PAD	ASCENT	ORBITAL	REENTRY	DESCENT	IMPACT
1ST ORDER SAFETY MECHANISM	SHIPPING CONTAINER	REDUNDANT AUXILIARY COOLANT SYSTEM	HEAT SINK (BeO)	ALTERNATE HEAT REJECTION SYSTEM	AEROSHELL	AIR SNATCH	WATER IMPACT
2ND ORDER SAFETY MECHANISM	BeO	ABORT & RECOVERY SYSTEM	ABORT, REENTRY AEROSHELL & RECOVERY SYSTEM	ABORT, REENTRY AEROSHELL & RECOVERY SYSTEM	BeO	IMPACT ATTENUATION SYSTEM	IMPACT ATTENUATION SYSTEM
3RD ORDER SAFETY MECHANISM	FUEL PLATE	BeO	IMPACT ATTENUATION SYSTEM	IMPACT ATTENUATION SYSTEM	FUEL PLATE	FUEL PLATE	FUEL PLATE
4TH ORDER SAFETY MECHANISM	FUEL CAPSULE	FUEL PLATE	FUEL PLATE	FUEL PLATE	FUEL CAPSULE	FUEL CAPSULE	FUEL CAPSULE
5TH ORDER SAFETY MECHANISM	FUEL FORM	FUEL CAPSULE	FUEL CAPSULES	FUEL CAPSULES	FUEL FORM	FUEL FORM	FUEL FORM
6TH ORDER SAFETY MECHANISM		FUEL FORM	FUEL FORM	FUEL FORM			

78-0003

TABLE 3.4-II

ROUTINE SYSTEMS DESIGN REQUIREMENTS

1. Instrumentation	4. Telemetry
2. GSE Hardware and Software	5. Rate Instrumentation (LV only)
3. Abort Sequencing System	6. Spacecraft Display Systems

TABLE 3.4-III

SUMMARY SYSTEM DESIGN REQUIREMENTS

Isotope R/V Subsystems
1. Disconnect and Separation Subsystem (With Redundancy)
2. Abort Rockets with TVC
3. Aeroshell-Structure and Heat Shield
4. IRV Hinge and Drive System
5. Deorbit Rocket with TVC
6. Redundant Active Elements in ACHX
7. Shroud Jettison System

TABLE 3.4-IV

SUMMARY SYSTEM DESIGN REQUIREMENTS

Optional IRV Subsystems
1. Impact Attenuation System
2. Recovery Aids
A. Parachutes B. Flotation System C. Location Aids
3. Recovery Teams

TABLE 3.4-V

ABORT, DEORBIT, SEPARATION, AND RECOVERY AIDS
SUBSYSTEM WEIGHT SUMMARY

ABORT, DE-ORBIT SEPARATION	WEIGHT (POUNDS)	**156.9**
SEQUENTIAL TIMER	1.0	
SPIN ROCKETS	1.0 (4)	
RETRO ROCKET	133.0	
SEPARATION NUT	0.3 (3)	
SYSTEM SUPPORT RING	18.0	
RECOVERY AIDS		**109.0**
THRUSTER AND MOTAR CHUTE	5.0	
DROGUE CHUTE AND LINE	50.0	
MAIN CHUTE	50.0	
BARO SWITCH	2.0 (2)	
LOCATION AIDS		**32.5**
RADAR REFLECTOR	1.0	
FLASHING LIGHT	1.0 (2)	
DYE MARKER	3.0	
BATTERY	25.0	
JUNCTION BOX	1.5	
FLOTATION		**27.5**
FLOTATION BAG	15.0	
SALT WATER SWITCH	0.25 (2)	
SALT WATER BATTERY	10.0	
SHARK REPELLENT	2.0	
SPECIAL INSTRUMENTATION		**3.0**
TEMPERATURE SENSOR	0.05 (10)	
RADIATION SENSOR	0.25 (10)	
BRACKETS AND CABLES		**15.0**

78-0060

4.0 IRV AERODYNAMICS

4.1 INTRODUCTION

The aerodynamic reentry analyses provide information in three major areas:

a. The heating and loading environment experienced by the aeroshell during reentry or abort

b. The heating environment experienced by the fuel capsules during reentry or abort

c. The hypersonic stability characteristics of the aeroshell which affect the vehicle dynamics at high altitudes (and hence can have an important effect on the capsule heating) and the transonic and subsonic stability of the aeroshell which can affect the deployment of drag augmentation devices (e.g., parachutes or ballutes) and which also affect the angle of attack of the vehicle at impact.

These three factors are quite interrelated since the reentry environments to which the aeroshell and capsules are subjected are strongly dependent upon the angle of attack history of the vehicle.

The most important IRV reentry requirement is that the maximum capsule temperature should never exceed a limiting value which, for this study, has been specified as 2500°F. It is, therefore, very desirable to minimize the reentry heating to the capsules, and since the capsules are located in the base region of the vehicle, this implies that high angles of attack during the important heating period are undesirable. Since abort and failure modes may result in tumbling or rearward entry, it is important to provide sufficient hypersonic stability so that the aeroshell will stabilize in a forward attitude at high enough altitudes to prevent exposure of the capsules to high stagnation type heating rates. Various aerodynamic devices have been investigated to provide this stabilizing capability at high altitudes. At present, fence concepts appear most promising for the elimination of stable rearward attitudes and a test program has been initiated by the Ames Research Center to evaluate fence effectiveness so as to provide guide lines for the fence design.

The aerodynamic analyses have been performed over a wide range of reentry conditions to encompass the various possible failure and abort modes. In addition, two basic aeroshell configurations have been considered (i.e., the 60° blunt cone and the modified Apollo) together with several different heat source configurations. Performance analyses were conducted for several specific IRV conceptual designs to determine the reentry performance tradeoffs for the different concepts.

The results of these investigations are summarized in the following subsections.

Section 4.1.1 describes the pertinent characteristics of the vehicle configurations considered in Phase 1A of the study with emphasis placed on the aeroshell geometry, the capsule array geometry and several different turn-around (hypersonic stability) devices. Section 4.1.2 describes the system and subsystem

constraints and requirements which result in certain reentry corridors and vehicle dynamic conditions which should be accommodated by the IRV design. Section 4.1.3 presents a summary of the environmental conditions encountered by the aeroshell and the fuel capsules as well as a brief discussion of the various turn-around devices. Section 4.2 contains the results of all the parametric studies performed to date and section 4.3 compares the reentry performance of the several different conceptual IRV design approaches. A summary of the major conclusions and the identification of the important problem areas are contained in section 4.3, also. Section 4.4 describes the aerodynamic test program being performed by the Ames Research Center. Section 4.5 discusses the methods of analysis used to perform the aerodynamic studies.

4.1.1 Configuration Description

4.1.1.1 Aeroshell

The aerothermodynamic analyses were conducted on the spherically blunt cone (R_N/R_b = 0.25) with a half-angle of 60 degrees, as well as on a modified Apollo shape, or spherical segment with R_N/R_b = 2.4 (see Figure 4.1-1). Primary emphasis was placed on the blunt cone analysis, since the modified Apollo shape appeared to offer packaging advantages only for the planar heat source arrays. The aerodynamic characteristics of the two shapes are quite comparable with the modified Apollo showing a slightly higher drag coefficient. Data for the blunt cone and modified Apollo were obtained from references 6 to 11.

The base geometry of the configurations depends on the heat source capsule array geometry and is discussed below.

4.1.1.2 Capsule Array Geometry

The capsule array geometry has a significant effect on the vehicle mass characteristics (center of gravity, moment of inertia) as well as the aerodynamic and heating characteristics of the IRV. Consideration of the dependence of the capsule heating and the vehicle aerodynamic performance on the capsule geometry, resulted in the examination of two limiting geometries, one comprising a flat base with exposed capsules mounted on it whereas the other had recessed capsules mounted on a flat plate (see Figure 4.1-2). These two capsule array configurations were used to determine the turn-around altitude requirements.

Further studies dealing with other capsule array geometries such as conical and pyramidal configurations are discussed in section 4.2.3.

4.1.1.3 Turn-around Devices

Several turn-around concepts were considered, namely:

a. Symmetrical fences

b. Asymmetrical fences

c. Fins

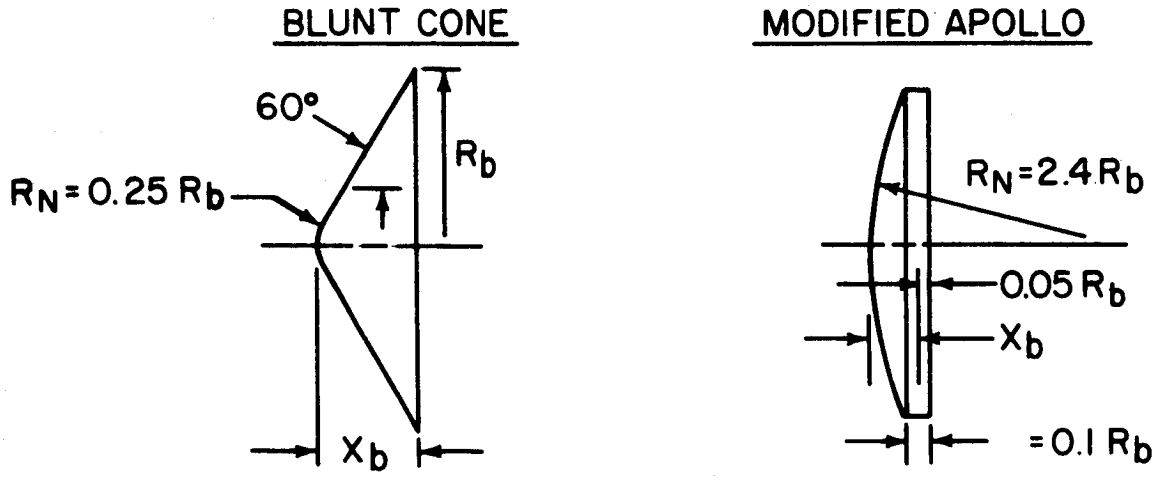

	BLUNT CONE	MODIFIED APOLLO
C_D (HYPERSONIC)	1.59	1.65
$\dot{q}_s / \dot{q}_{s_{B.C.}}$	1.0	0.35
	(HEATING OTHERWISE COMPARABLE)	
X_b	0.27	0.15
C_{m_α} (HYPERSONIC)*	0.178/rad	0.166/rad
(TRANSONIC)	0.109/rad	0.126/rad

*$X_{C.G.}$ AT X_b

78-0068

Figure 4.1-1 AEROSHELL SHAPE COMPARISON

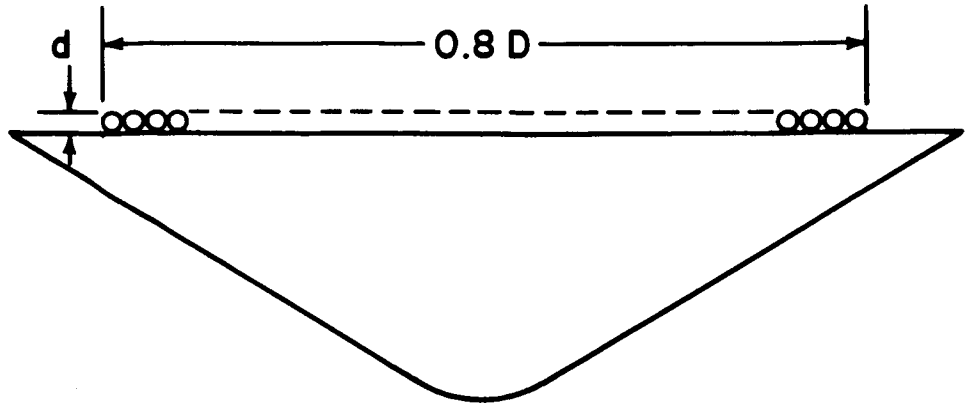

A. HEAT SOURCE CAPSULE EXPOSED

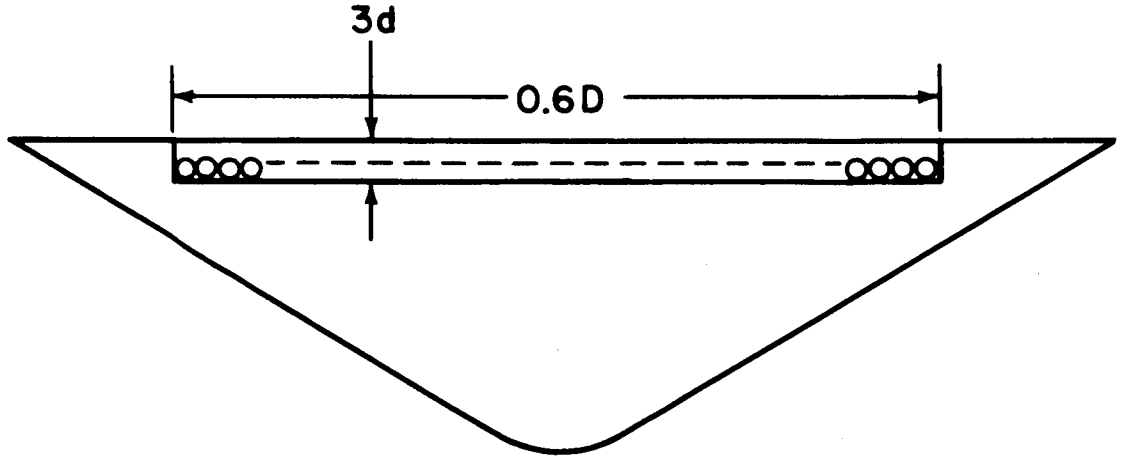

B. HEAT SOURCE CAPSULE RECESSED

78-0072

Figure 4.1-2 CAPSULE ARRAY GEOMETRY

d. Flaps

e. Afterbodies

f. Center of gravity offsets.

These concepts are illustrated in Figure 4.1-3.

The fence device is most attractive since it provides the required turn-around while being compatible with the system constraints and requirements. The various devices were required to eliminate the stability of the vehicle configuration at 180^{o} angle of attack. In addition, the interaction of the device with the basic configuration can produce a moment which is either favorable or unfavorable.

4.1.2 Mission Requirements, Constraints, and Design Criteria

There are a number of system and subsystem constraints and requirements which interact with the IRV aerodynamics. The intact survival of the isotope capsules involves not only the determination of the reentry environment (aerodynamic heating and loads) but also the evaluation of the aerodynamic stability and performance in the transonic and subsonic flight regime. This is due to the fact that the terminal descent behavior and angular motions of the IRV are quite critical for the ground impact survival of the capsules and dictate the impact attenuation requirements. The vehicle diameter influences the impact problem through the dynamic behavior as well as by controlling the impact velocity (through the ballistic coefficient, W/C_DA). The dynamic behavior is strongly influenced by the length of the vehicle skirt extending beyond the conical forebody, a limit cycle angle of attack motion being directly related to this length.

In order to insure the proper selection of the design criteria, abort at any time during the mission sequence was considered in addition to the normal IRV reentry conditions resulting from a controlled deorbit of the IRV.

Reentry from orbit (100 to 260 n.m. circular orbits) for both controlled (retro rockets) and uncontrolled (orbital decay) reentry was examined. The maximum reentry angle was -10 degrees and the entry velocities included those resulting from an extreme failure mode during the ascent trajectory. This failure mode involved a pitch-over failure maneuver of the last stage booster and results in maximum reentry velocity at a given reentry angle. The reentry envelopes for velocity and angle are presented in Figure 4.1-4. In addition, the reentry conditions for various retro rocket ΔV's are presented. The reference ΔV is 500 fps with a nominal reentry angle of -2.25 degrees. The vehicle spin rate associated with this ΔV is 7.5 RPM. The reentry condition for the ΔV of 500 fps which results in a double skip is indicated in Figure 4.1-4 ($\gamma_E = -0.73^{o}$, V_E = 26,058 fps).

An abort analysis was made for both Atlas/Centaur and Saturn I-B launches, considering simple separation as well as rocket aborts with ΔV's consistent with those considered for active entry from orbit.

In order to encompass the range of anticipated vehicle performance (ballistic coefficient, W/C_DA), the W/C_DA was varied from 20 to 40 lbs/ft^2. The reference IRV diameter was initially selected as 7.5 feet.

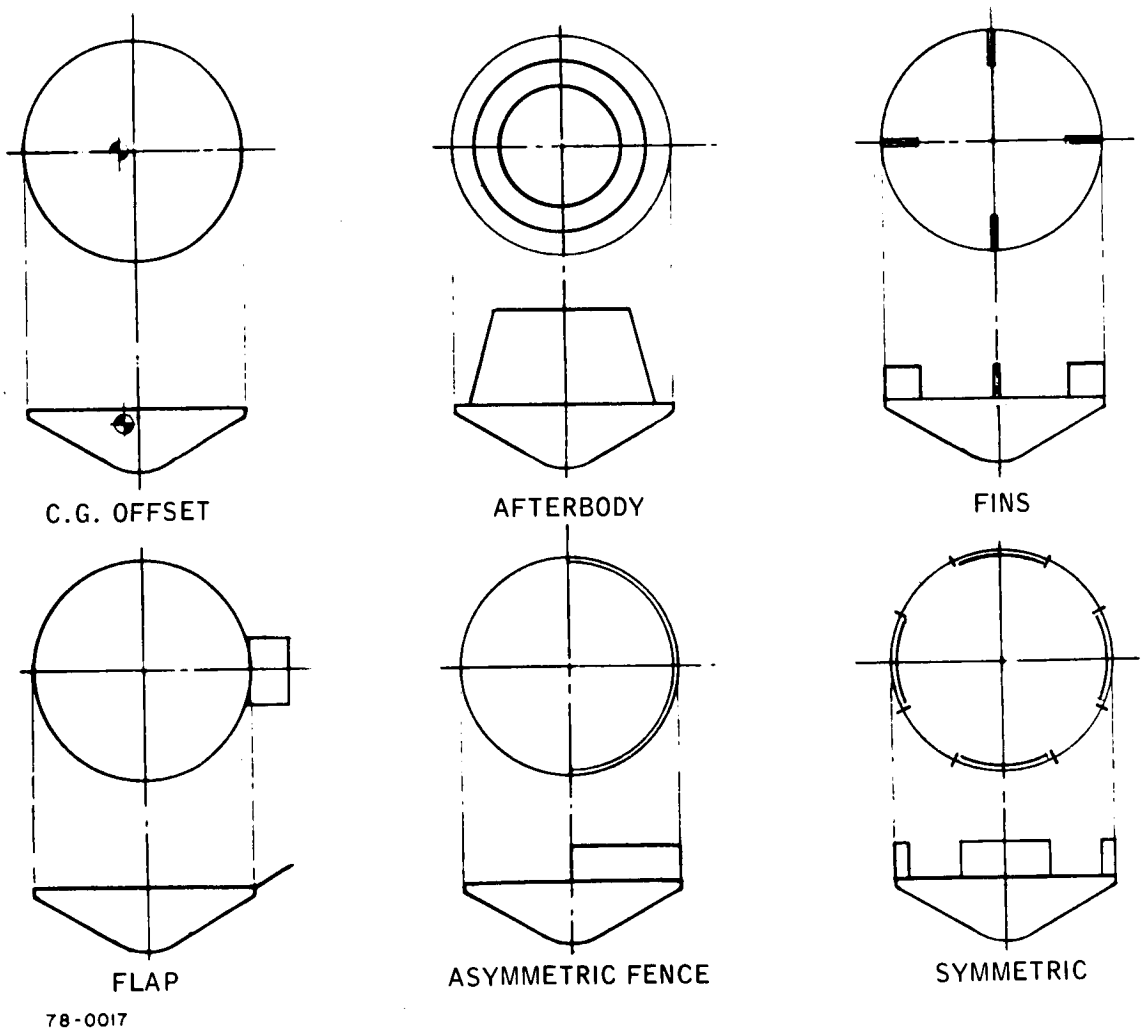

Figure 4.1-3 TURNAROUND CONCEPTS

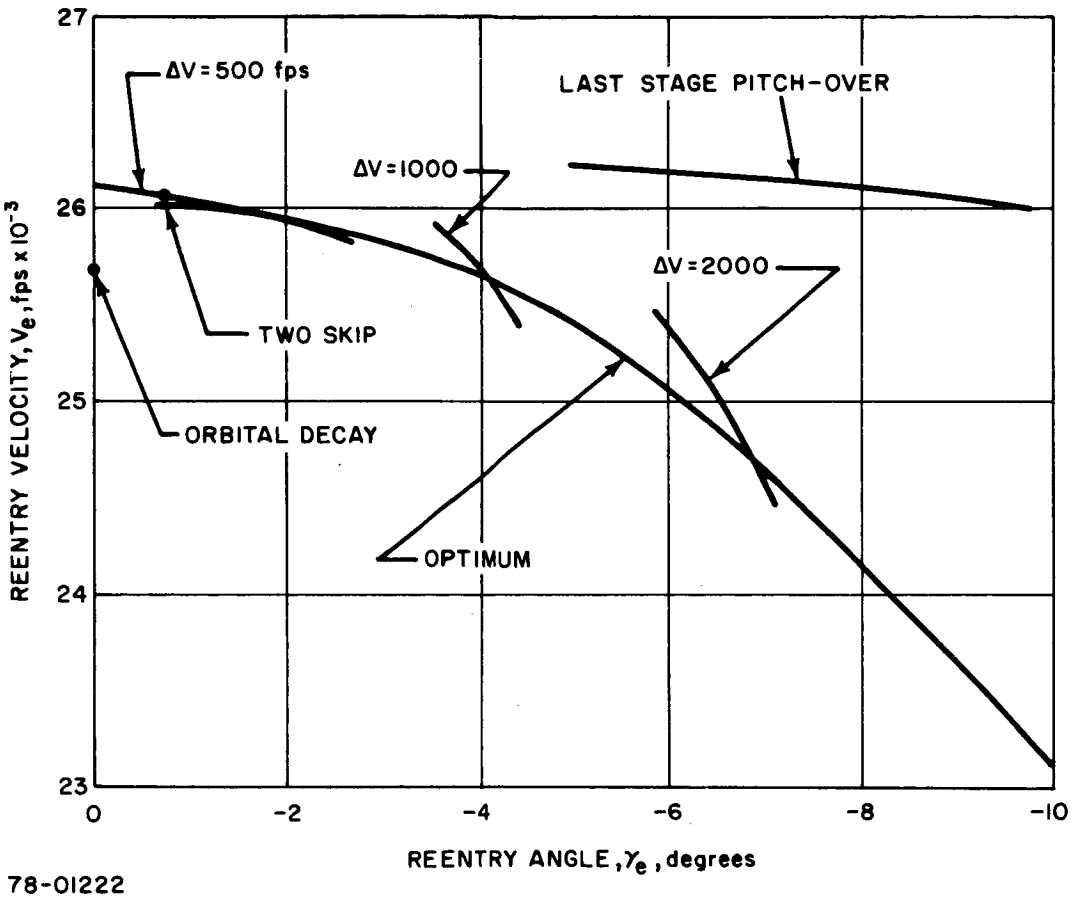

Figure 4.1-4 ORBITAL REENTRY CONDITIONS

The vehicle attitude at entry was considered random with the exception of controlled entry from orbit where, for the nominal entry condition, the initial angle of attack of the spin stabilized IRV was 78 degrees. This angle of attack varies with the thrust application angle (see Section 3.0 discussion). Two possible initial angles of attack are critical for the isotope capsule heating environment. A 90 degree angle of attack results in maximum capsule heating aggravation effects. (No turn-around device is necessary for this condition as the vehicle aerodynamic characteristics are adequate.) An initial angle of attack of 180 degrees results in lower altitude penetration into the atmosphere prior to turn-around; however, the heating aggravations are less severe. The angle of attack which results in the lowest turn-around altitude depends on the turn-around device, this angle of attack being that associated with the minimum stability point of the vehicle and the turn-around device.

Tumbling reentry was also considered with rates varying from zero to six radians per second, the nominal rate being 0.6 radians/sec. Such tumbling could occur if the spin stabilization system fails or if an explosion on the space station causes the IRV to separate with large tipoff rates.

4.1.3 Performance Summary

4.1.3.1 Aeroshell

Although the methods and techniques utilized in the analyses are discussed in Section 4.5, it is important to mention at this point the processes used to define the heating environment. Considerable data (References 12 to 16) has been obtained for the convective heating at the stagnation point and a number of theories are available for calculations (References 13, 17 to 20). The scatter in the data is evident in Figure 4.1-5 where the heat transfer parameter has been plotted as a function of the flight velocity. Although numerous curve fits to the data are available, these empirical relations are useful primarily for indicating the nominal heating. Although the relation indicated in Reference 21, that is,

$$\dot{q}_s \sqrt{R_N} = 865 \left(\frac{\rho}{\rho_{SL}}\right)^{.5} \left(\frac{V}{10^4}\right)^{3.15}$$

results in a value of the heat transfer parameter which agrees with the average of the data, the bands of uncertainty are ± 25 percent in the range of interest for the IRV stagnation point heating.

The analysis for the IRV is consistent with the upper bound of the data and utilizes methods consistent with those of Fay and Kemp (Reference 20), thereby insuring that vehicle as well as capsule design environments and subsequent indications of survival are of a high confidence level.

In addition, the heating associated with orbital reentry is subject to low density effects such as vorticity interaction which increases the heating. This vorticity correction becomes dependent upon the vehicle angle of attack as well as the flight conditions. The initial analyses considered the vorticity correction associated with the zero angle of attack stagnation point which, although adequate for low angles of attack as well as tumbling, results in conservatism

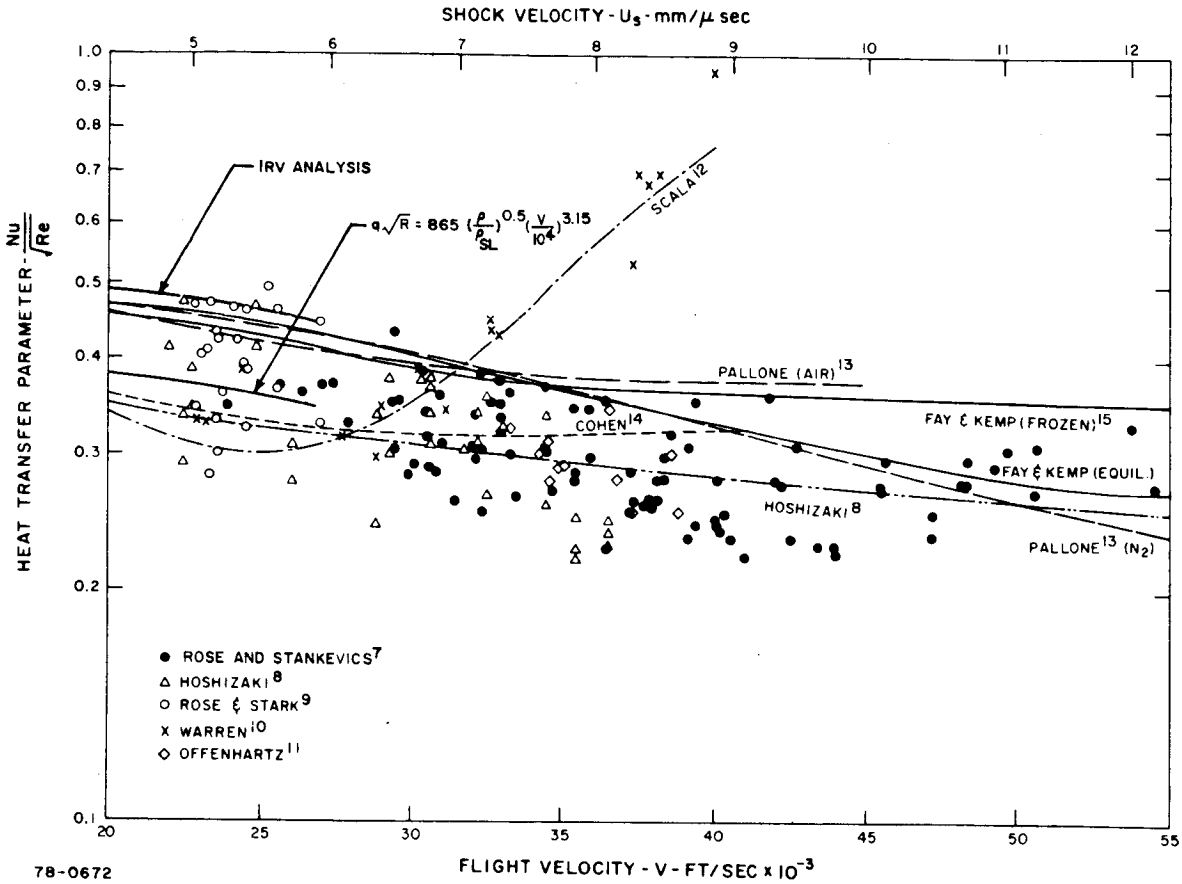

PALLONE (13), HOSHIZAKI (8) AND COHEN (14) THEORIES ARE SHOWN APPLICABLE TO A STAGNATION PRESSURE OF 1 ATM. FAY AND KEMP (15) WAS CALCULATED FOR THE EXPERIMENTAL CONDITIONS, i.e., p_1 = 0.25 mm OF Hg. SCALA (12) WAS CALCULATED FOR A FLIGHT ALTITUDE OF 240,000 FT.

Figure 4.1-5 SUMMARY PLOT OF VARIOUS EXPERIMENTAL DATA AND THEORIES FOR STAGNATION POINT HEAT TRANSFER IN PARTIALLY IONIZED AIR AND NITROGEN

(i.e., higher calculated heating) for stable rearward reentry since for that case the shock wave is considerably flatter at the stagnation streamline. This conservatism varies with the entry conditions, the maximum being about 20 percent. The complexity of the calculations for this correction precluded its use over the broad range of parameters considered for the studies. However, a number of illustrative trajectory cases were run including the effects of vorticity interaction and these are identified in the text.

The critical or design heating environment for the aeroshell is the integrated heating associated with entry out of orbit. The selection and design of the thermal protection system for the aeroshell depends primarily upon the total heating load and, to some extent, upon the maximum rates to be anticipated. The variation of the total heat load with reentry conditions resulted in large integrated heating for shallow reentry angles (see Figure 4.1-6) because of the long duration of the heating pulse. Illustrated also is the dependence of the heat load on the vehicle ballistic coefficient. (These results are for a zero angle of attack throughout entry, and in addition do not include low density effects.) The worst abort condition is also presented for comparison. The maximum heat load occurs for the double skip condition.

Although the worst abort condition does not result in the worst integrated heating, it does lead to the highest heating rates because of the higher reentry velocity (see Figure 4.1-7).

The maximum aerodynamic loads (as reflected by the maximum dynamic pressure) are associated with abort during the ascent trajectory. Two peaks in the dynamic pressure occur during the ascent trajectory histories, the first occurring at low altitudes (with low velocities), whereas the second occurs during reentry from an abort at high altitude with the corresponding high velocity. The first peak was higher for the Saturn I-B whereas the second peak was higher for the Atlas/Centaur (see Table 4.1-I). Comparative results are presented for the loads associated with orbital reentry.

TABLE 4.1-I

A SUMMARY OF THE MAXIMUM DYNAMIC PRESSURES

Trajectory	Maximum Dynamic Pressure, psf
Nominal controlled reentry	295
Orbital decay	252
γ_E = -5 degrees	490
γ_E = -10 degrees	955
Atlas/Centaur abort	980
Saturn I-B abort	610

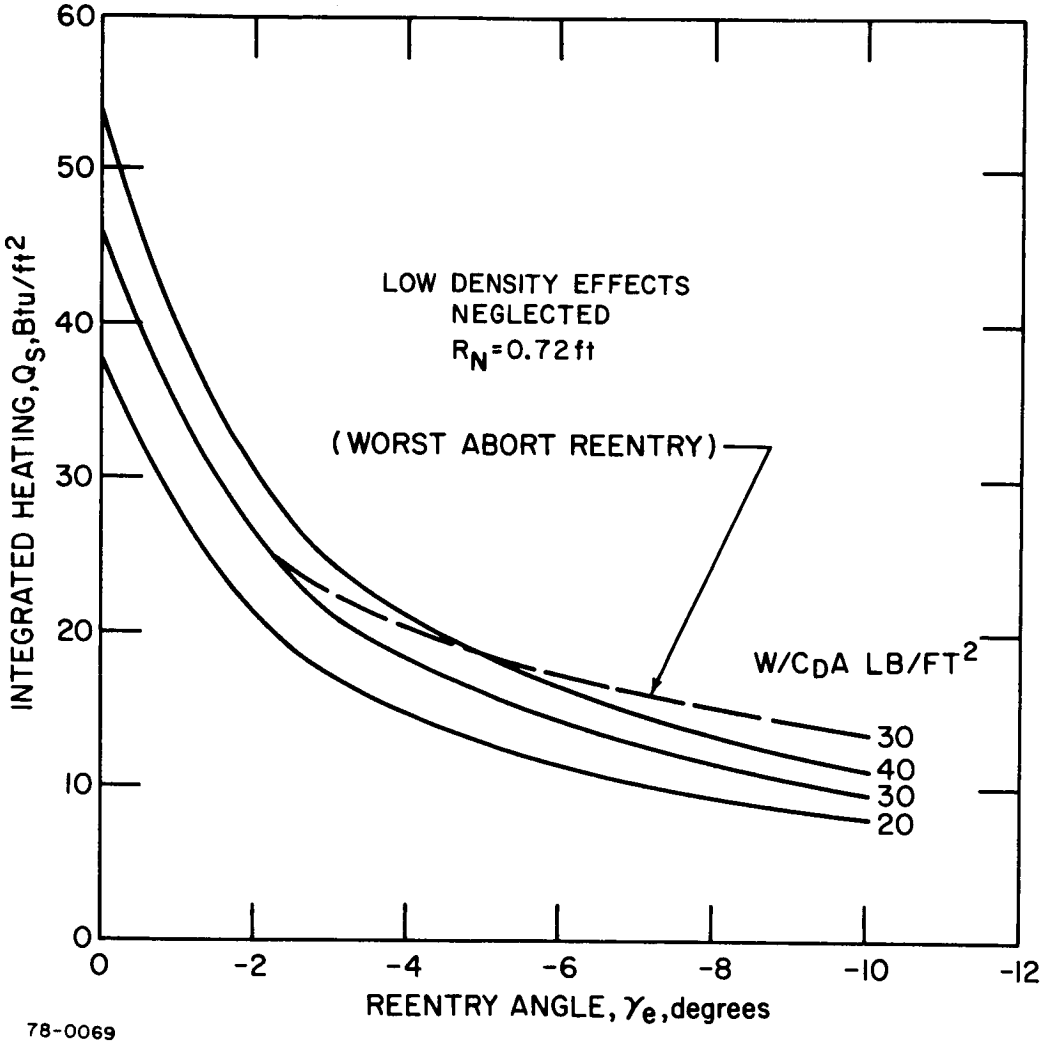

Figure 4.1-6 BLUNT CONE STAGNATION POINT INTEGRATED HEATING

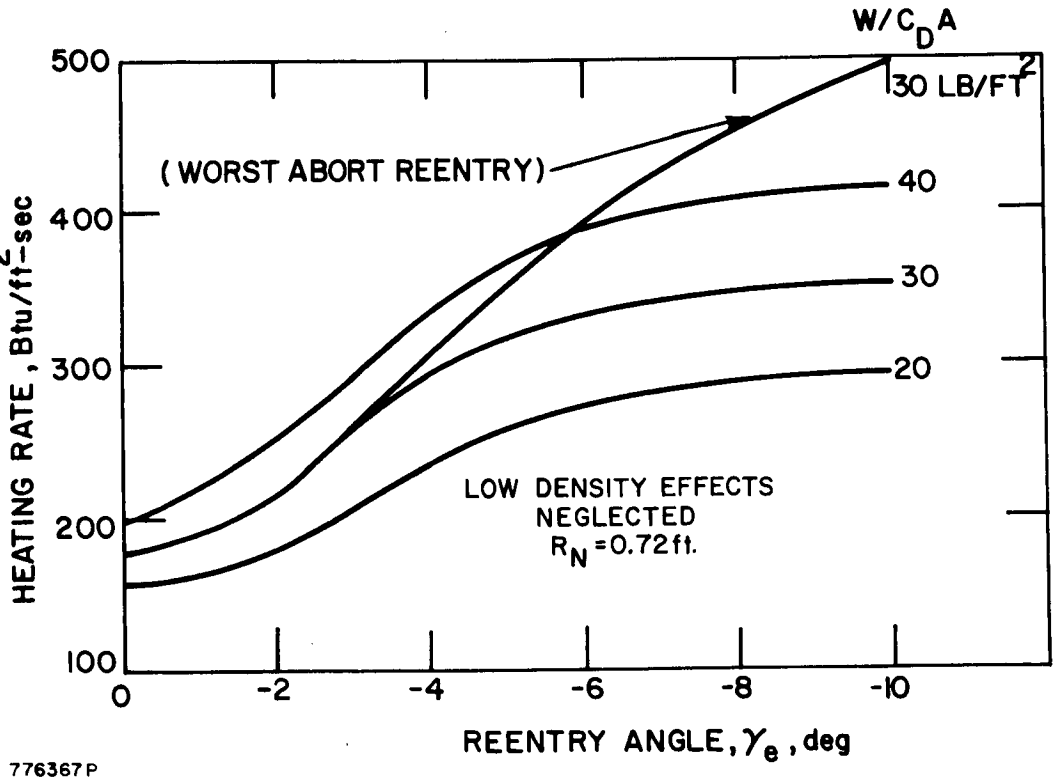

Figure 4.1-7 BLUNT CONE MAXIMUM STAGNATION POINT HEATING RATES

4.1.3.2 Capsule Heating Environment

The isotope capsule heating environment was found to be sensitive to:

a. The vehicle initial reentry conditions,

b. The capsule array geometry, and

c. The vehicle stability during early reentry.

The integrated heat load on the capsule and dependence on the vehicle stability is reflected in the variations of the heating with turn-around altitude. Little variation in the heat load is to be expected for early turn-around; however, as turn-around occurs later in time, the heat load rises very rapidly as shown in Figure 4.1-8. Turn-around altitudes as low as 300,000 feet for this case result in substantially the same heating environment on the capsules as for zero angle of attack entry. The reference fence devices analyzed resulted in turn-around altitudes for which the capsule maximum temperatures were insensitive to the early heating history. A typical heating history for the capsule (in this case an exposed capsule array) is presented in Figure 4.1-9 for the worst abort conditions. Three peaks are associated with this tumbling entry (the first is at very high altitudes and is very small). Although the second pulse has high rates, the duration is very short and, therefore, maximum capsule temperatures occur during the last pulse.

The maximum capsule temperatures and their variation with reentry conditions for the two limiting capsule array geometries are presented in Figure 4.1-10. The orbital decay reentry ($\gamma_E = 0^o$) results in minimum capsule temperatures. (It should be noted that conservatively high initial capsule temperatures have been assumed at the beginning of reentry. In reality, the initial capsule temperatures will be much lower.)

The capsule heating associated with an ineffective turn-around device or failure mode was investigated by considering two reentry conditions; the first one where the vehicle is stabilized in a rearward attitude throughout the entire reentry, and the other where tumbling occurs throughout reentry. In the latter case, the heating is cyclical with the capsule effective heating being less than that for the rearward attitude throughout reentry. (Results of this analysis are presented in Section 5.1.)

4.1.3.3 Turn-around Devices

The various devices considered were presented illustratively in Figure 4.1-3 with relative comparisons shown in Table 4.1-II. The center of gravity offset and the flap device both result in large trim angles of attack throughout the reentry trajectory. The offset center of gravity also complicates the vehicle design and deorbit system and necessitates an increased vehicle diameter (of approximately 7 percent).

A deployable flap appears unattractive from reliability considerations. The afterbody concept is unattractive since the heat exchanger-heat source interface requirements interfere with the location of the afterbody and a very large afterbody is required to assure good turn-around performance.

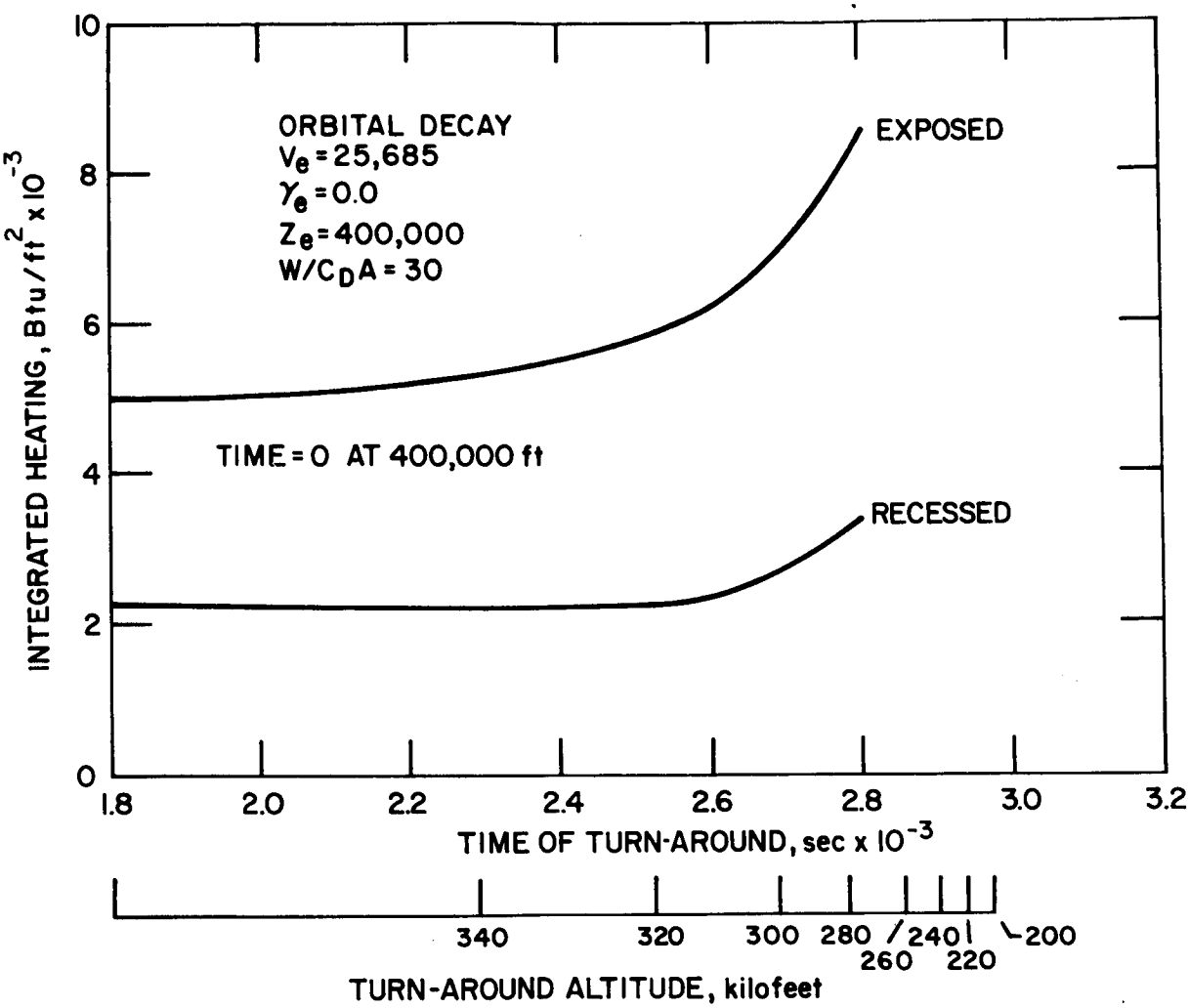

Figure 4.1-8 HEAT SOURCE CAPSULE REENTRY HEATING AS A FUNCTION OF TURNAROUND TIME (ALTITUDE)

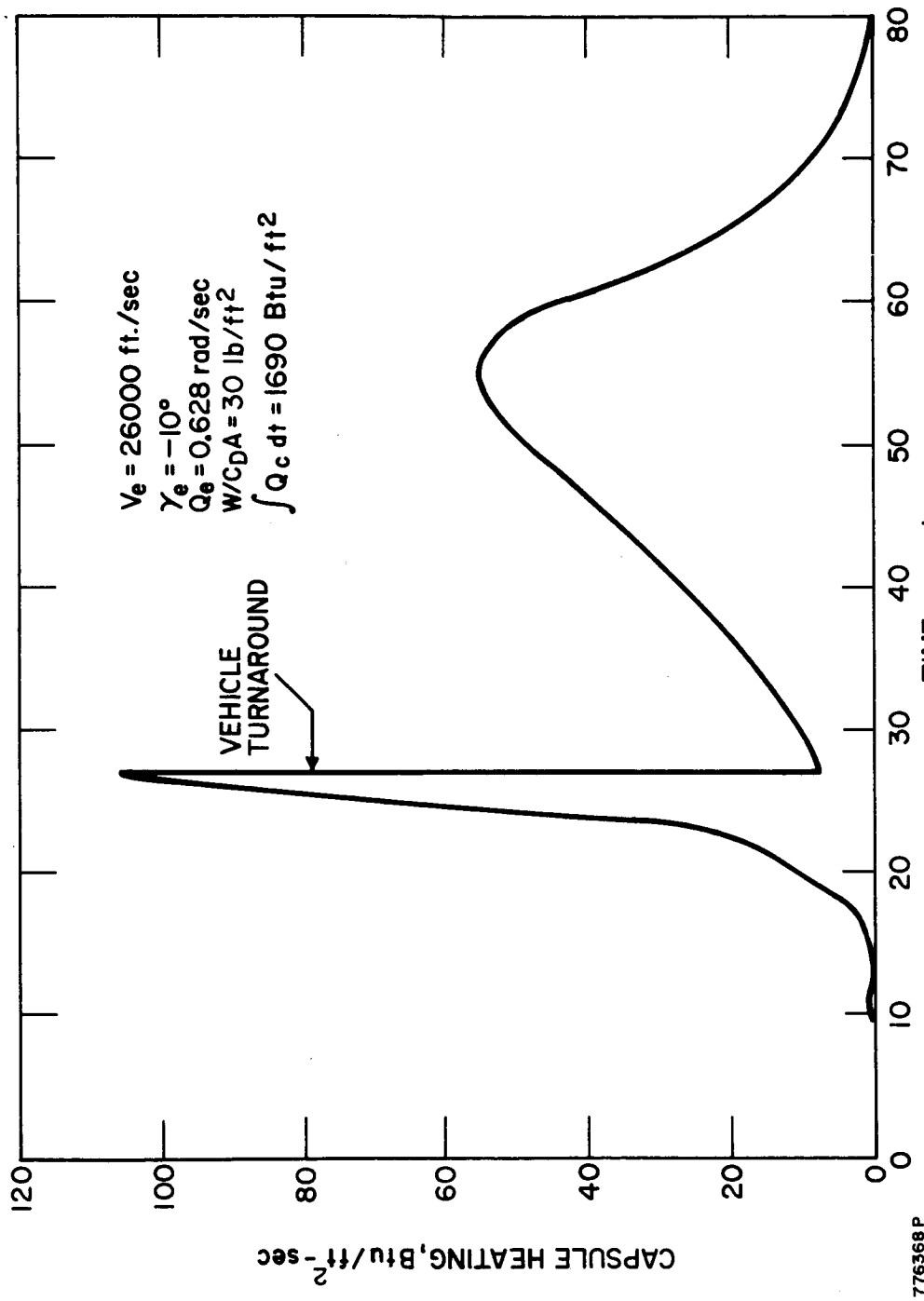

Figure 4.1-9 CAPSULE REENTRY HEATING FOR ABORT TRAJECTORY (WITH TYPICAL FENCE CONFIGURATION)

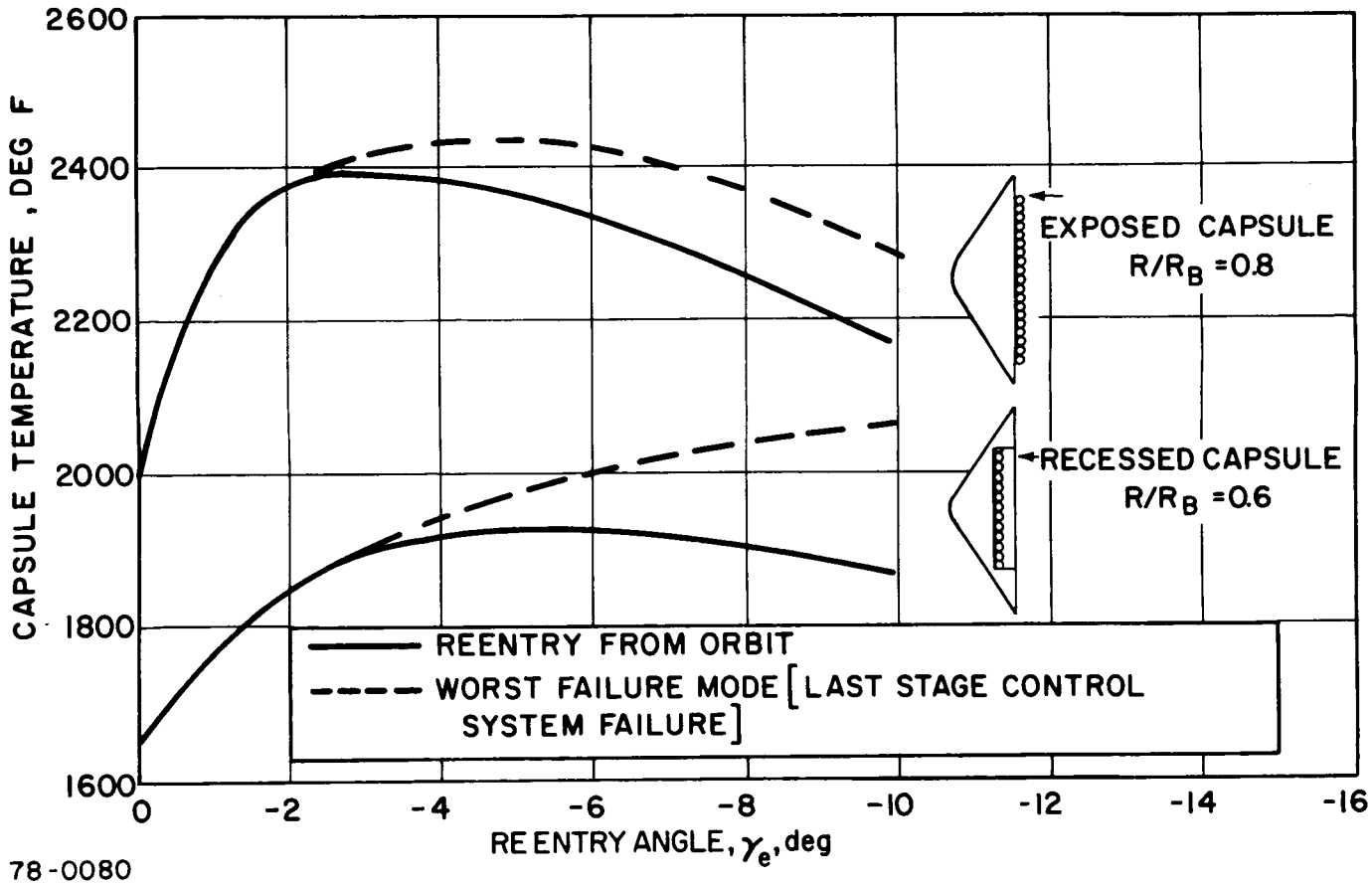

Figure 4.1-10 MAXIMUM CAPSULE TEMPERATURE

TABLE 4.1-11

TURNAROUND DEVICE COMPARISONS

CONCEPT	ADVANTAGES	DISADVANTAGES
1. CENTER OF GRAVITY OFFSET	A. SIMPLEST	A. LARGE NON ZERO ANGLE OF ATTACK
	B. HIGHEST CONFIDENCE	B. VEHICLE DESIGN AND SEPARATION COMPLEXITY
		C. DIAMETER PENALTY
2. AFTERBODY	NO ASYMMETRIC EFFECTS	A. EXCESSIVE WEIGHT PENALTY
		B. HEAT EXCHANGER INTERFACES
		C. LARGE DEGRADATION IN SUBSONIC STABILITY
3. FINS	NO ASYMMETRIC EFFECTS	A. FIN/BASE INTERACTION UNFAVORABLE
		B. LARGE FINS REQUIRED
		C. HEAT EXCHANGER INTERFACES
4. FLAP	SIMPLE (IF PASSIVE)	LARGE NON ZERO ANGLE OF ATTACK
5. FENCE (ASYMMETRIC)	ELIMINATES STABLE TRIM POINT AT 180° ANGLE OF ATTACK	A. POSSIBLE SUBSONIC STABILITY PROBLEMS DUE TO ASYMMETRIC BASE FLOW
		B. STABILITY
		C. VISCOUS EFFECTS
		D. PERFORMANCE PREDICTION IS DIFFICULT
6. FENCE (SYMMETRICAL)	A. FENCE/BASE INTERACTION CAN BE FAVORABLE	A. UNCERTAINTY IN PERFORMANCE AT 180° ANGLE OF ATTACK
	B. NO ASYMMETRICS	B. VISCOUS EFFECTS
	C. PREDICTABLE PERFORMANCE	

776462P

The limitation on the inboard location of all devices (to avoid interfering with the radiant flux from the capsules) results in large axial extensions particularly for the fin device.

The reference configuration selected for illustrative purposes during this phase, based on preliminary analysis, consists of an outboard fence perpendicular to the base and subtending an arc of 180 degrees. Final fence selection will be based on results of the Ames test program. It should be noted, however, that the turn-around requirements dictated by the aerodynamic heating are applicable to any IRV/heat source configuration independent of final fence geometry. The fence height of 0.2 R_b is selected on the basis of anticipated viscous phenomena.

4.2 RESULTS AND DISCUSSION

4.2.1 Parametric Studies

4.2.1.1 Aeroshell

4.2.1.1.1 Aerodynamic Heating -- The aeroshell parametric study was performed for the 60° blunt cone and for a modified Apollo shape, the comparisons being made on the basis of aerodynamic heating and loads assuming the same value of W/C_DA for each shape. The variations of pressures and heating distribution and the effect of the shoulder radius and of cylinder length are also included.

The results of the aeroheating parametric analysis have been shown in Figures 4.1-6 and 4.1-7 for the blunt cone configuration. The highest heating rates were obtained from the steepest abort reentry condition because of the higher reentry velocities and angles. The larger effective nose radius of the modified Apollo results in stagnation point heating of 0.35 times the blunt cone heating.

The heating distributions used in the analysis include the effect of shoulder radius. The variations in the heating and pressure distributions were developed for radius-ratio values of R_S/R_b = 0.025, 0.05, and 0.10 where R_S is the shoulder radius and R_b the base radius of the 60 degree cone.

The pressure distributions used in the analysis are shown in Figure 4.2-1. The pressure distribution for R_S/R_b = 0.1 was obtained from Reference 24. The distributions for other shoulder radii were determined by assuming that the pressure is the same when the flow is expanded through the same angle.

The convective heating distributions were obtained from similarity theory and are shown in Figure 4.2-2 for the three shoulder radius ratios. Illustrated is the influence of shoulder radius on the heating on the shoulder, which is greater than that forward of the shoulder. As can be seen, the shoulder heating increases as the radius becomes smaller, with the maximum heating always occurring at the sonic point on the shoulder.

The heating distribution for the modified Apollo configuration is shown in Figure 4.2-3 for the shoulder radius ratio of 0.05. As for the blunt cone, the maximum shoulder heating value is about 1.5 times the heating value forward of the shoulder radius. Similarly, the maximum shoulder heating ratios for other radius ratios will be the same as those presented in Figure 4.2-2 for the 60 degree cone.

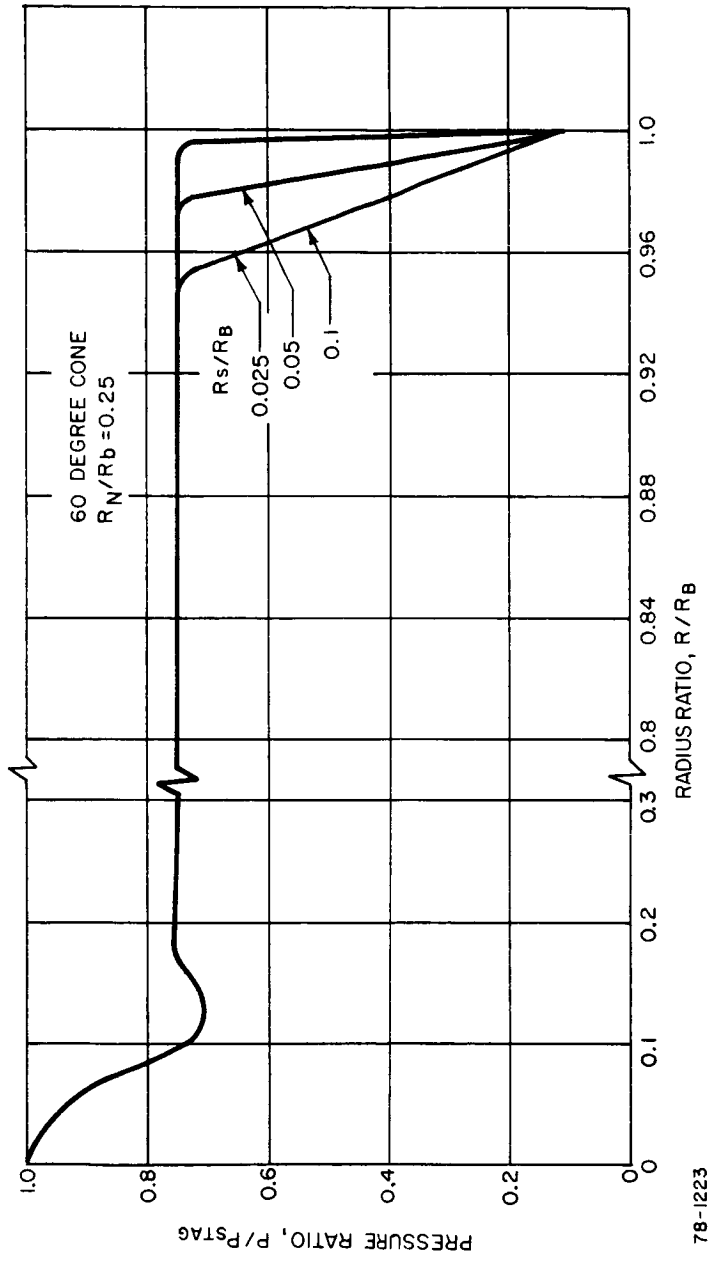

Figure 4.2-1 PRESSURE DISTRIBUTION

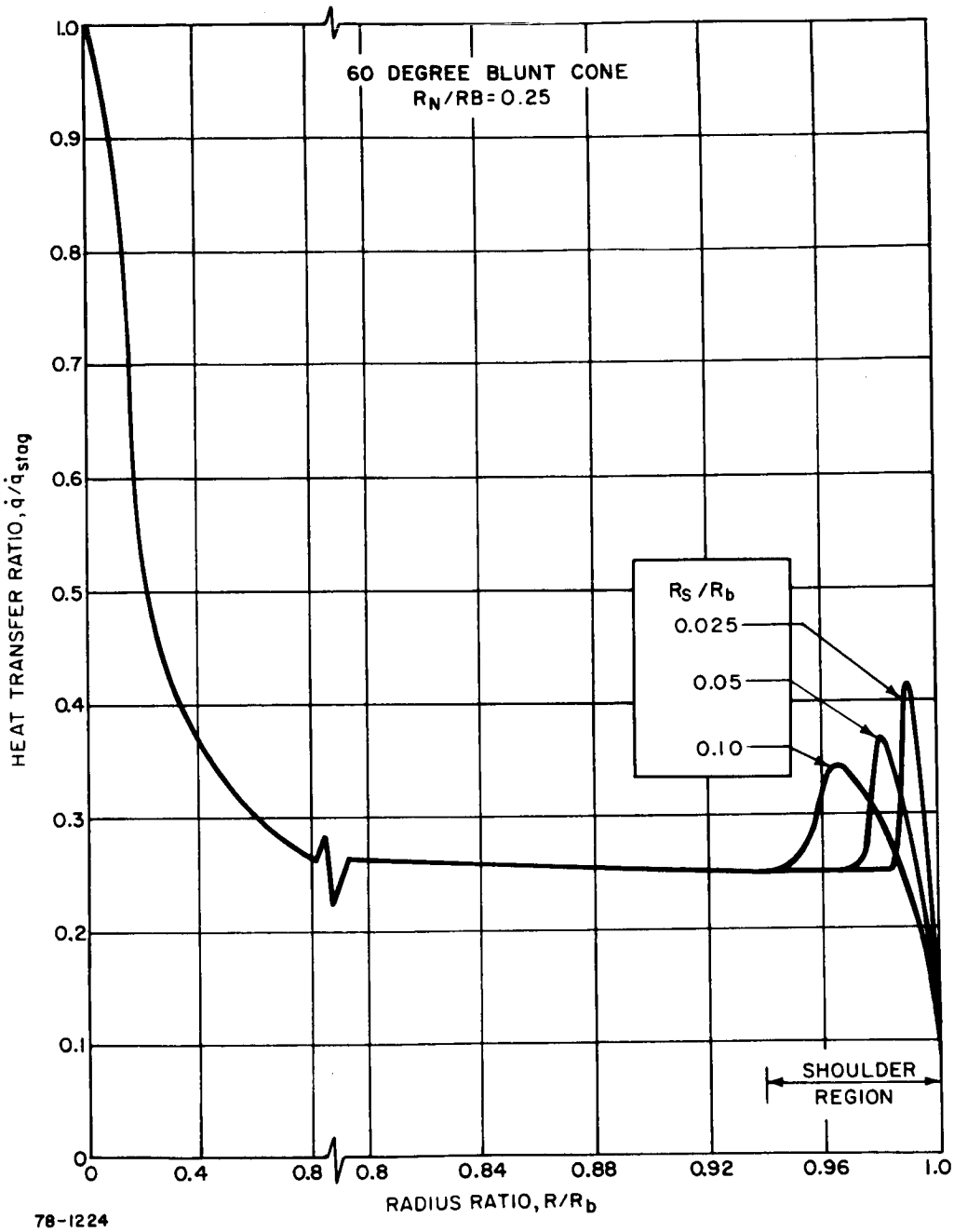

Figure 4.2-2 HEATING DISTRIBUTION

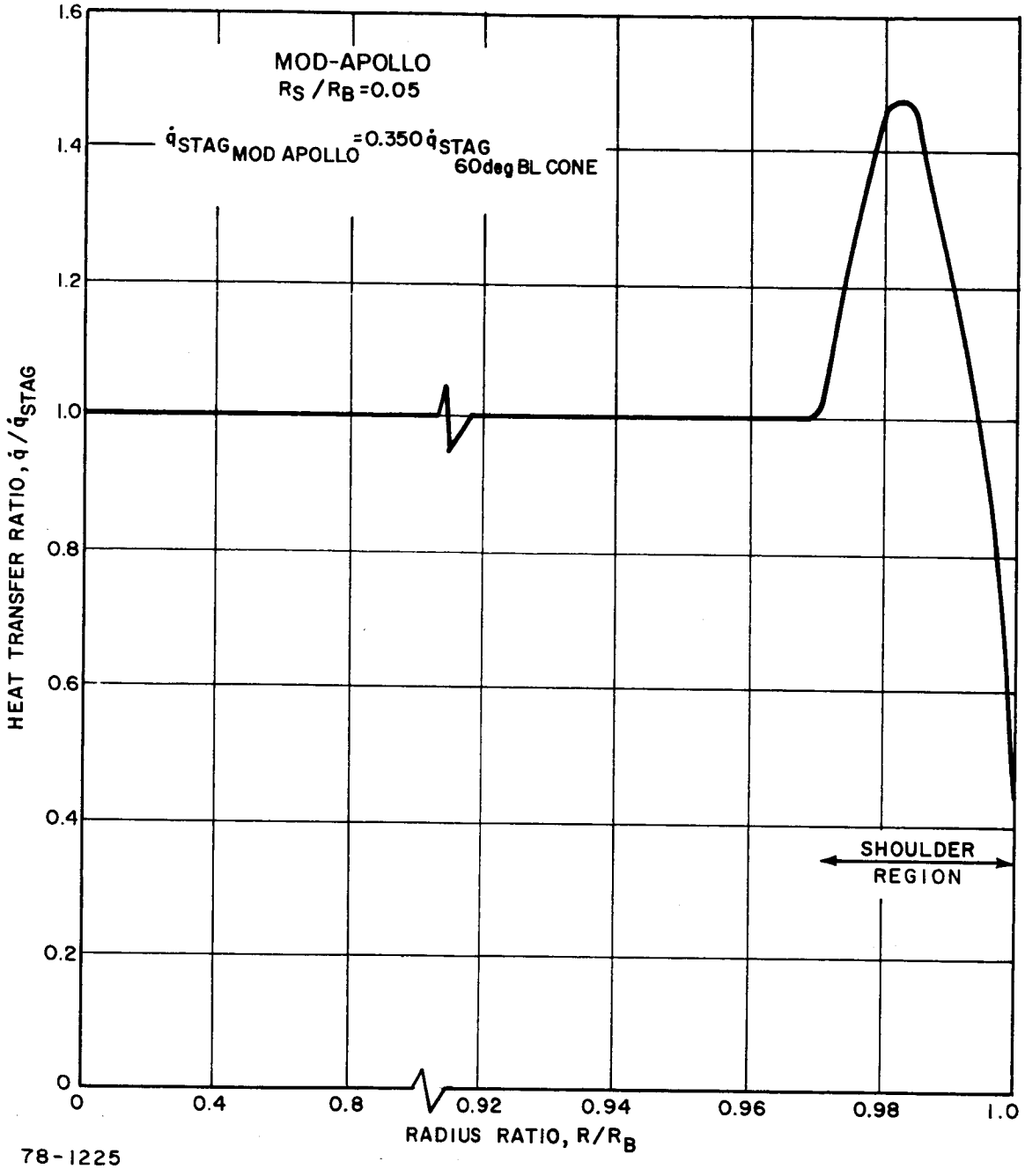

Figure 4.2-3 CONVECTIVE HEATING DISTRIBUTION

Failure mode considerations require the investigation of aeroshell heating over a wide range of angles of attack. Figure 4.2-4 shows the variation with angle of attack, α , of the heating at five stations on the blunt cone. Three radii are assumed for the aft edge of the aeroshell to demonstrate the radius effect on maximum and average heating rates (see Section 4.5).

It may be required for purposes of efficient packaging to add a cylindrical skirt section at the maximum diameter of the aeroshell. The effect of this cylinder on the high altitude turn-around capability depends on the movement of the center of gravity and the relative positions of the center of gravity and the fence location. Assuming the center of gravity remains the same, an increase in the fence moment can occur when the fence is mounted on the base of the cylinder. For the case of the center of gravity remaining at the cylinder base no increase in the fence moment arm will occur. The cylinder length can also affect the transonic and subsonic stability characteristics of the vehicle. Data from reference 9 have been utilized to determine the effects of shoulder geometry on the limit cycle amplitudes and the results are presented in Figure 4.2-5. The cylinder length selected will depend on this criterion (angle of attack amplitude at impact), as well as other systems design criteria.

4.2.1.1.2 Airloads -- Airloads for the aeroshell design were determined from the trajectories for the various reentry modes. These included controlled entry from orbit, two-skip entry, orbital decay and various abort conditions for abort during the boost phase from the Atlas/Centaur and Saturn I-B launch vehicles. The parameters used were the deorbit ΔV , the entry angle, γ_E , and the vehicle ballistic coefficient, W/C_DA.

Figure 4.2-6A shows the peak dynamic pressures for a range of entry conditions from a maximum flight path angle of γ_E = -10 degrees to -2 degrees at 400,000 feet. Entry velocities varied with entry angle consistent with deorbit from 260 nautical miles. Similar curves are shown in Figure 4.2-6B but show the peak dynamic pressures as functions of ΔV, V_E and γ_E, and extend the γ_E to -0.7 degrees. The results presented for a ΔV of 500 fps are typical of those anticipated for the reference controlled entry mode with γ_E = -2.25 degrees.

4.2.1.1.3 Boost Abort -- Figure 4.2-7 shows the maximum dynamic pressure developed assuming that abort takes place at various times during the launch trajectory. The first peak occurs when the booster is at its maximum dynamic pressure. The resulting entry vehicle trajectory shows that this point occurs at the separation of the entry vehicle from the booster. The second peak results from abort at high altitudes, where the IRV trajectory exits from the atmosphere and subsequently reenters with the peak occurring during the reentry phase. The maximum dynamic pressure values for abort are 980 psf for the Atlas/Centaur and 610 psf for the Saturn I-B. The values for the Atlas/Centaur are higher because of the steeper ascent trajectory, resulting in reentry angles higher than those for the Saturn I-B. It should be noted that the boost-abort results in loads that are greater when compared to those for the nominal reentry from orbit conditions.

Comparing all conditions, the highest dynamic pressure occurs for the worst abort reentry with a value of 990 psf.

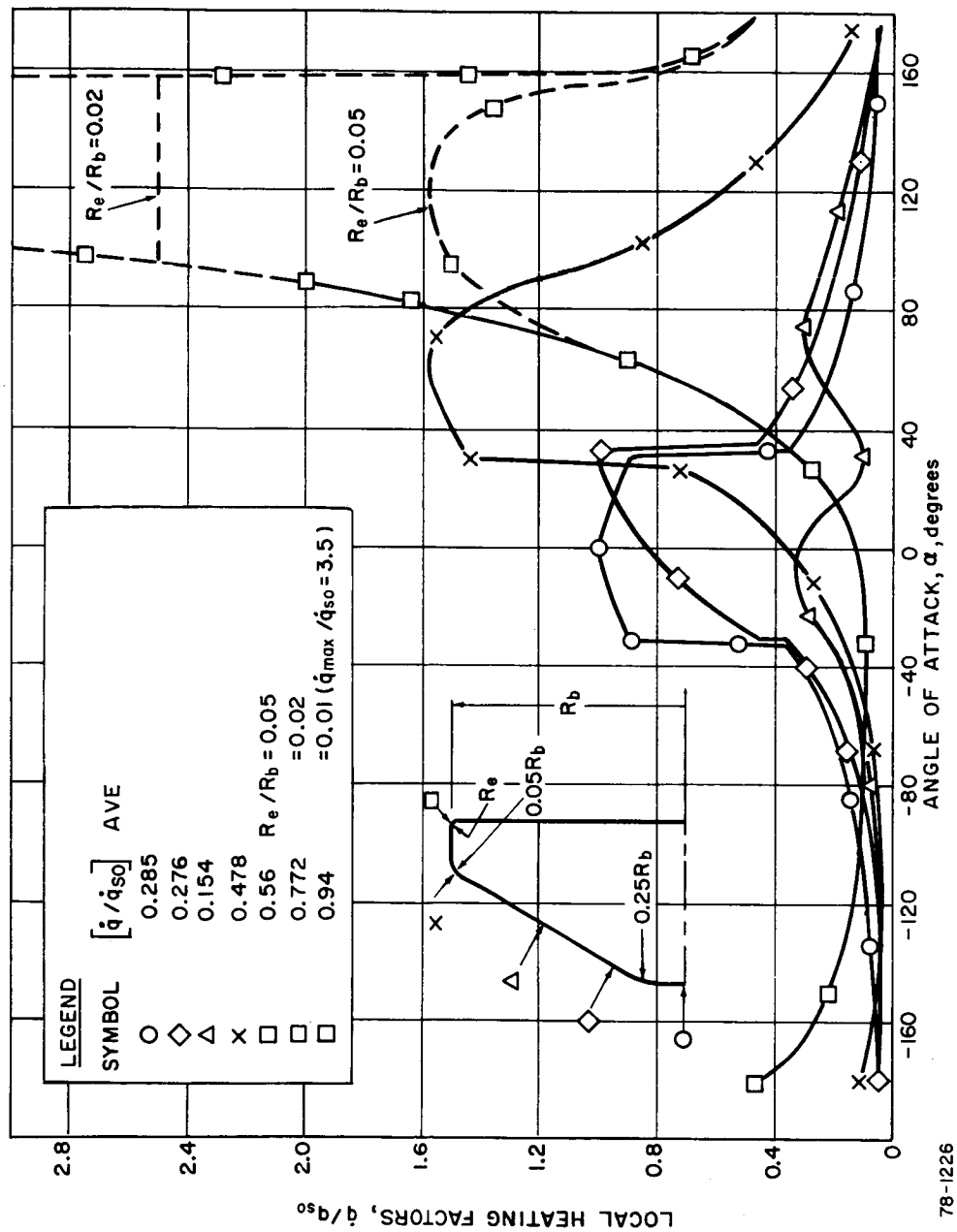

Figure 4.2-4 AEROSHELL HEATING AT ANGLE OF ATTACK

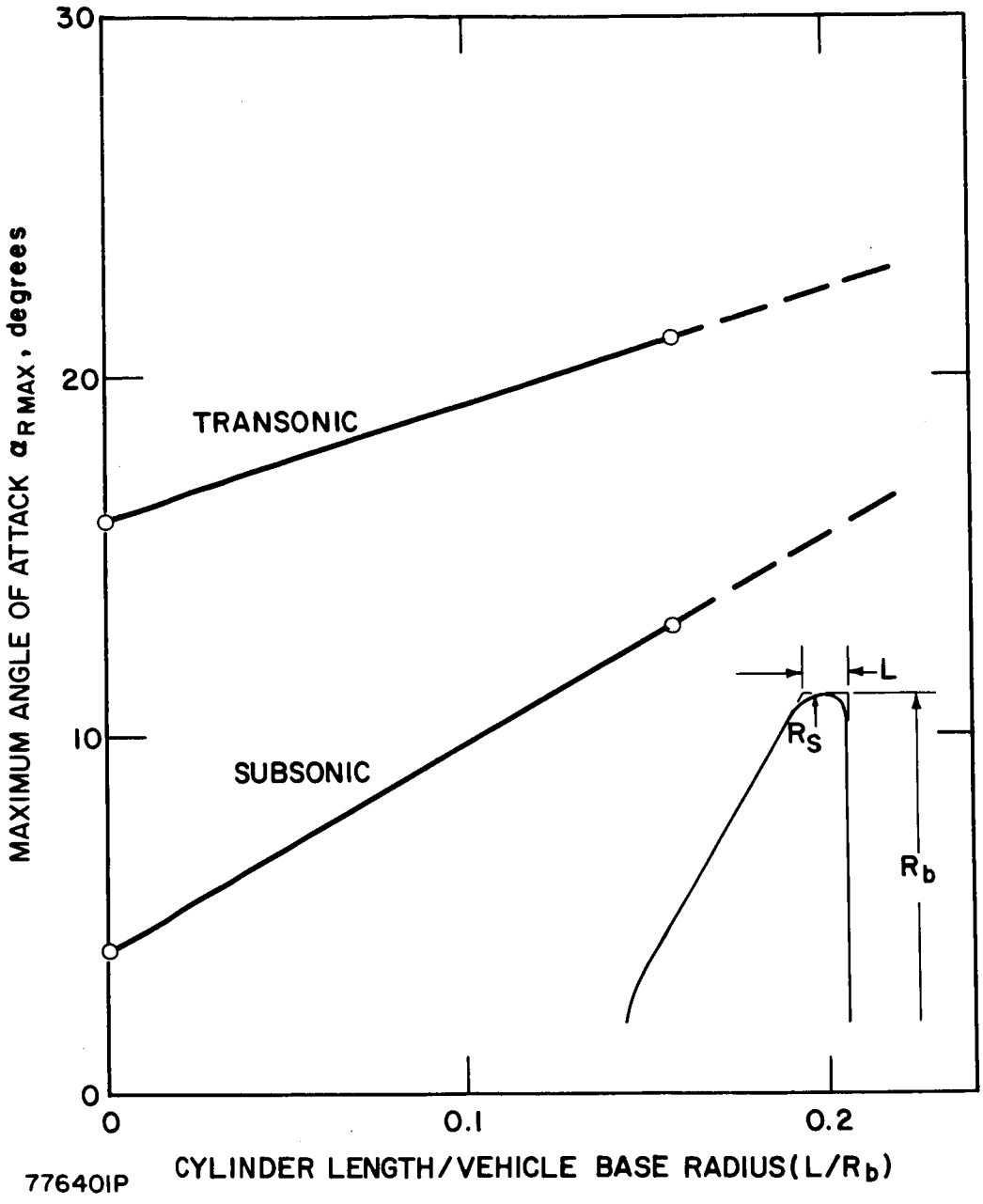

Figure 4.2-5 DEPENDENCE OF LIMIT CYCLE AMPLITUDE ON CYLINDER LENGTH

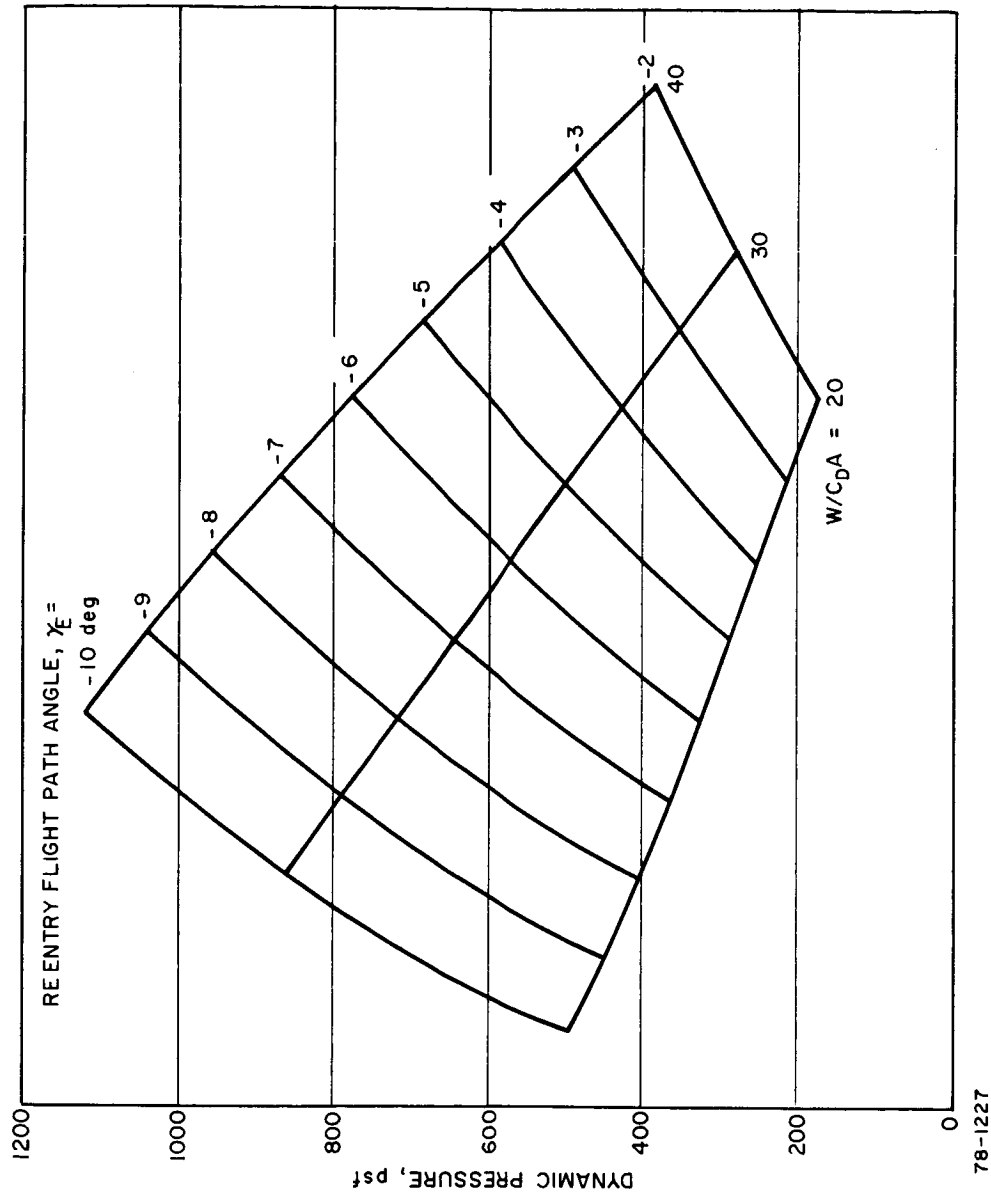

Figure 4.2-6a PEAK STAGNATION POINT DYNAMIC PRESSURE FOR CONTROLLED ENTRY

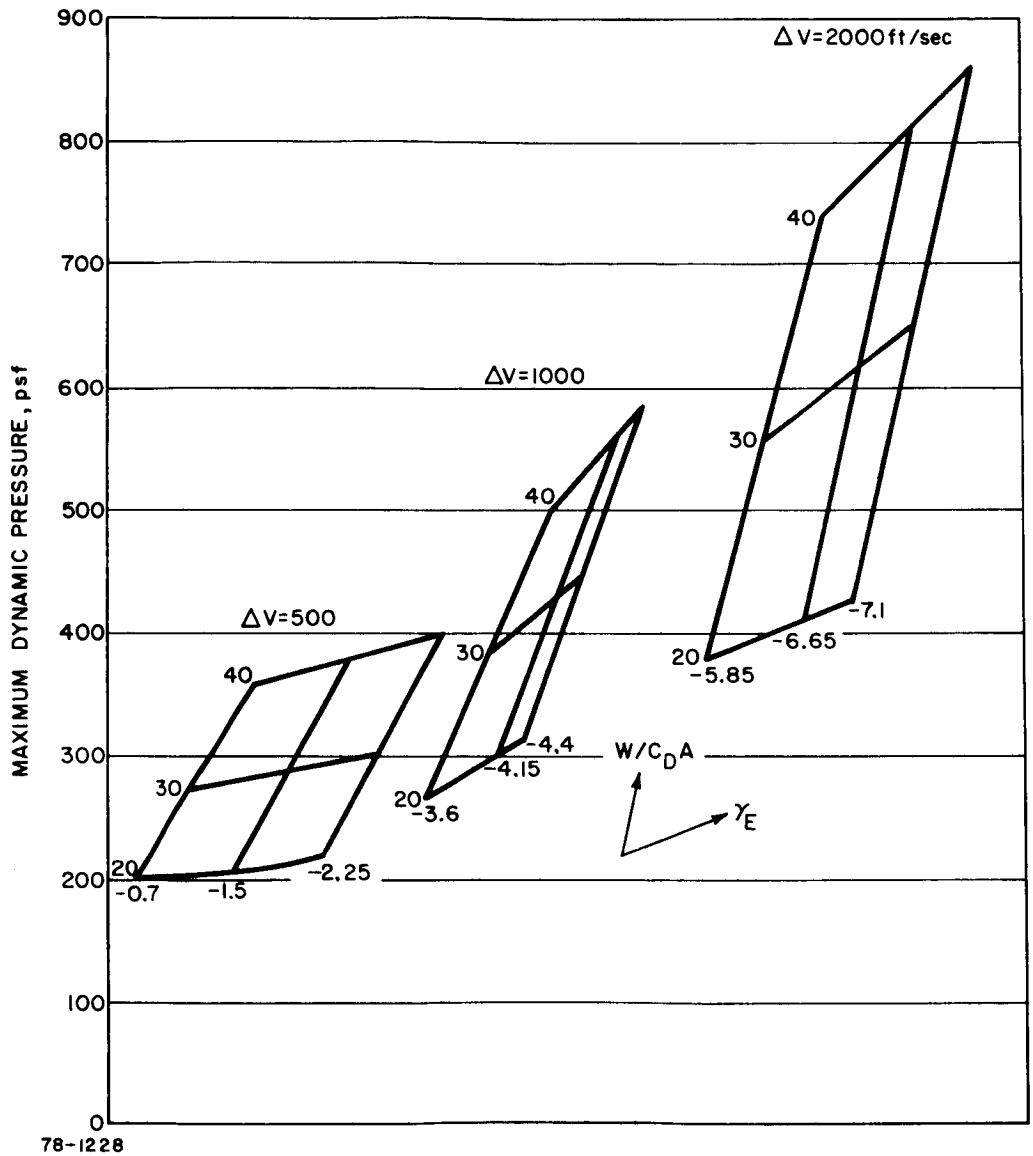

Figure 4.2-6b PEAK STAGNATION POINT DYNAMIC PRESSURE FOR CONTROLLED REENTRY

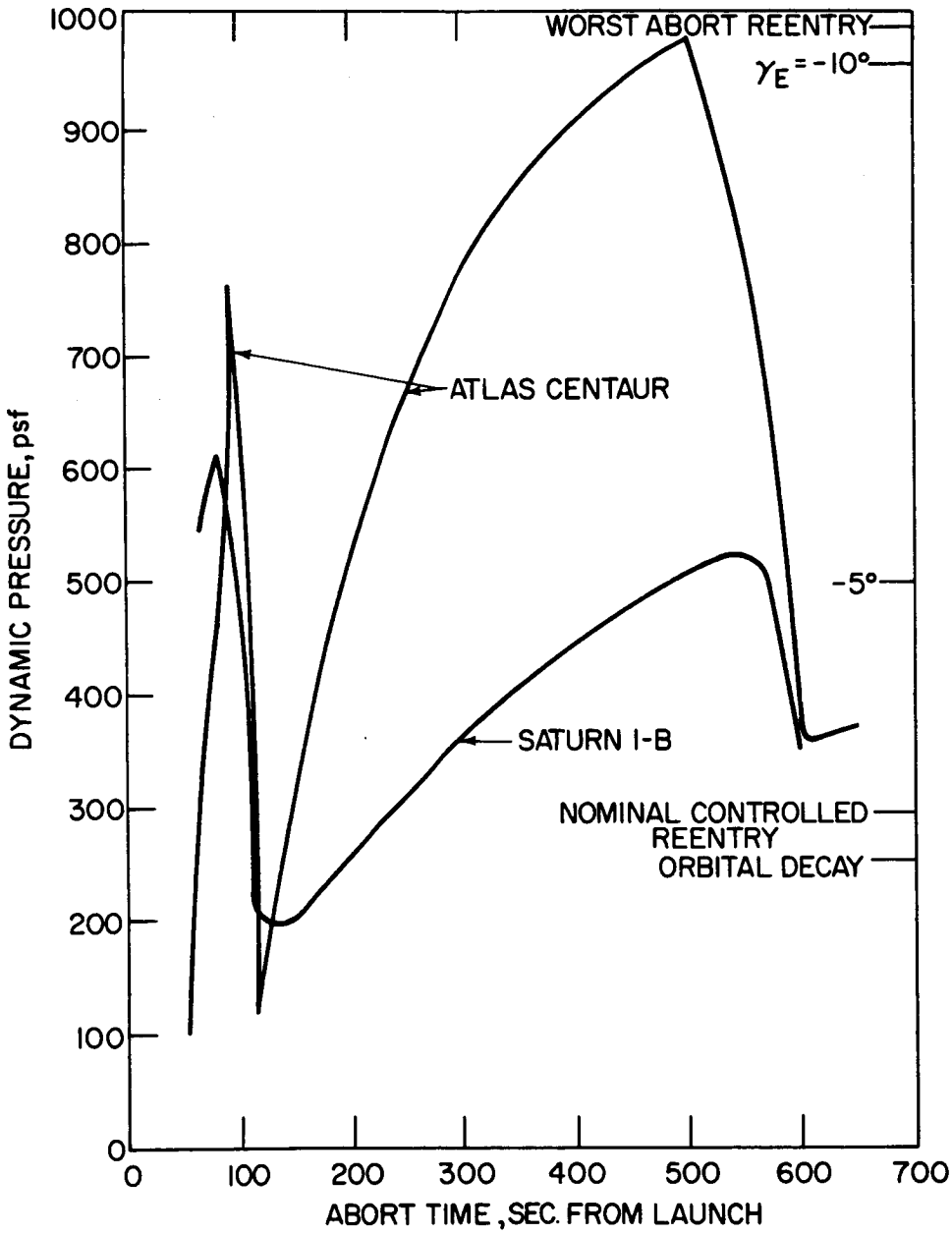

78-0070

Figure 4.2-7 MAXIMUM DYNAMIC PRESSURE - BOOST ABORT

4.2.1.2 Capsule Parametric Studies

The capsule descriptions and theoretical analysis of the base heating are described elsewhere in the report. The parametric variations included entry angle and velocity, the various modes of entry, the capsule configurations and the effects of turn-around altitude.

The base heating for the various reentry conditions are determined by applying the base heating factors obtained from early estimates of cylinder stagnation point heating and of flat faced cylinder stagnation point heating.

Capsule heating for the extreme cases of recessed and exposed capsule configurations (see Section 4.1.1) were obtained for each condition.

Figure 4.2-8 presents a typical heating history for the extreme cases for an entry angle of attack of 90 and 180 degrees (viscous interaction effects have been included). The effect of turn-around is determined by proceeding along the angle of attack heating curve and dropping to the $\alpha = 0$ curve at the time of turn-around. In all cases the integrated and maximum heating rates are higher for the exposed capsule configuration. Similar curves are shown for the two-skip entry in Figures 4.2-9 through 4.2-11 which show the heat pulse during the two skips and the final entry, respectively.

The effects of the two entry modes associated with a turn-around device failure are illustrated in Figures 4.2-12 and 4.2-13 for an entry angle of zero degrees as well as for rearward entry and tumbling entry (viscous interaction has not been included for the last two entry modes). A curve showing typical effects of turn-around time on capsule heating has been presented in Figure 4.1-8. As expected, the integrated heating increases rapidly as the turn-around time is delayed. Consequently, to avoid high heating, the vehicle should turn-around above 300,000 feet.

Recently, more refined values of capsule heating factors have been defined parametrically for the rearward entry case. Although these results have not been applied to actual trajectories as yet, they are presented here for the purpose of defining the penalties in heating associated with various parameters for exposed and recessed capsule designs. The results are shown in Figure 4.2-14 normalized with respect to the maximum heating for flush mounted capsules. The heating penalty associated with protruding capsules is seen to be large. Recessing the capsules is beneficial, but little additional benefit is gained by recessing the capsules below a certain depth corresponding to several capsule diameters.

Using the test data from Reference 22, heat transfer distributions are obtainable for various cavity depths. These are shown in Figure 4.2-15 for the rearward entry case. Again, diminishing returns are noted with respect to increasing cavity depth.

4.2.2 Destabilizing (Turn-around) Devices

The necessity for a destabilizing device is discussed in Section 4.5. Several concepts have been investigated and have been shown in Figure 4.1-3 with a brief summary of the advantages and disadvantages for each concept given in Table 4.1-II.

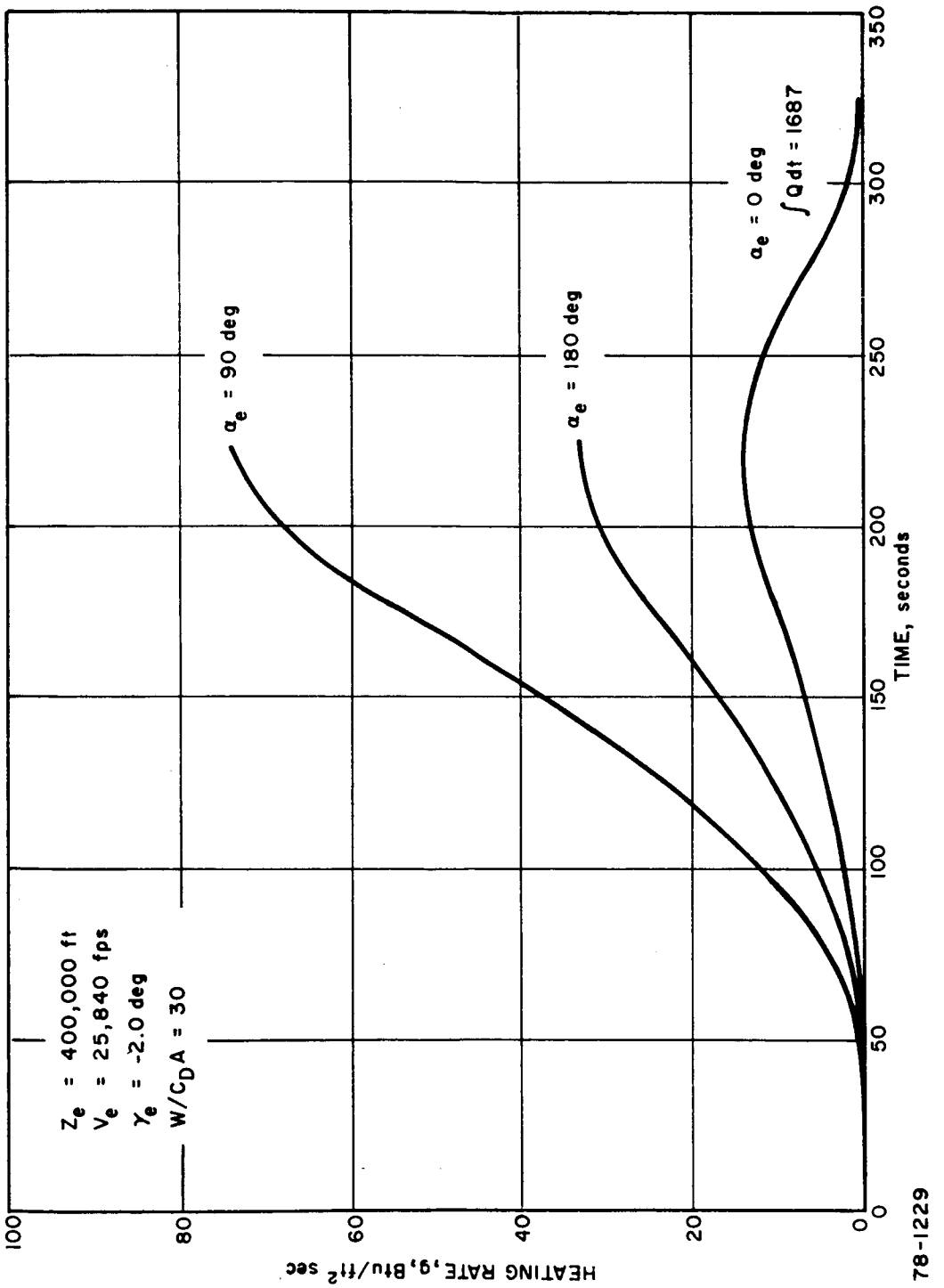

Figure 4.2-8 CONVECTIVE HEATING FOR RECESSED CAPSULES

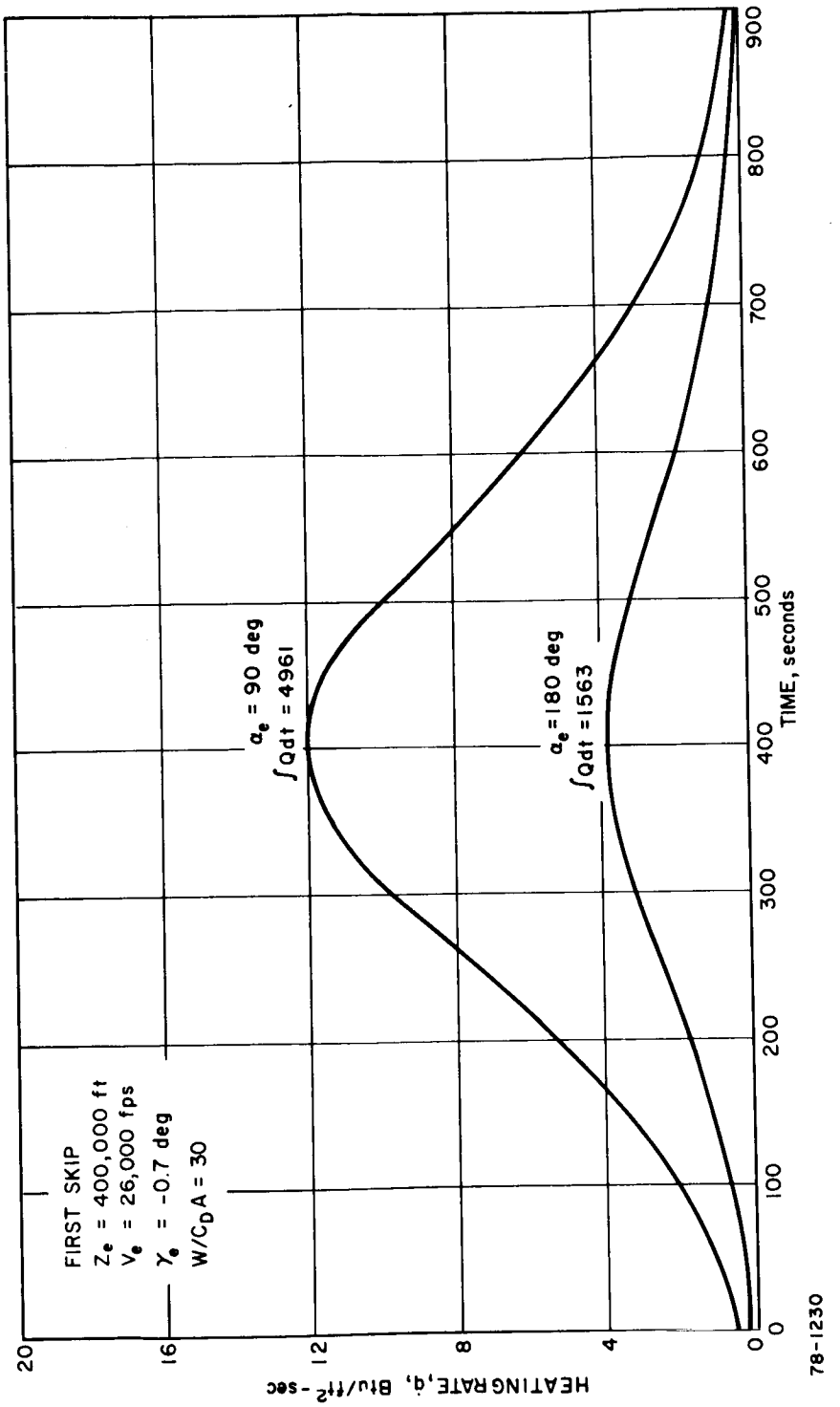

Figure 4.2-9 CRITICAL CONVECTIVE HEATING FOR EXPOSED CAPSULES

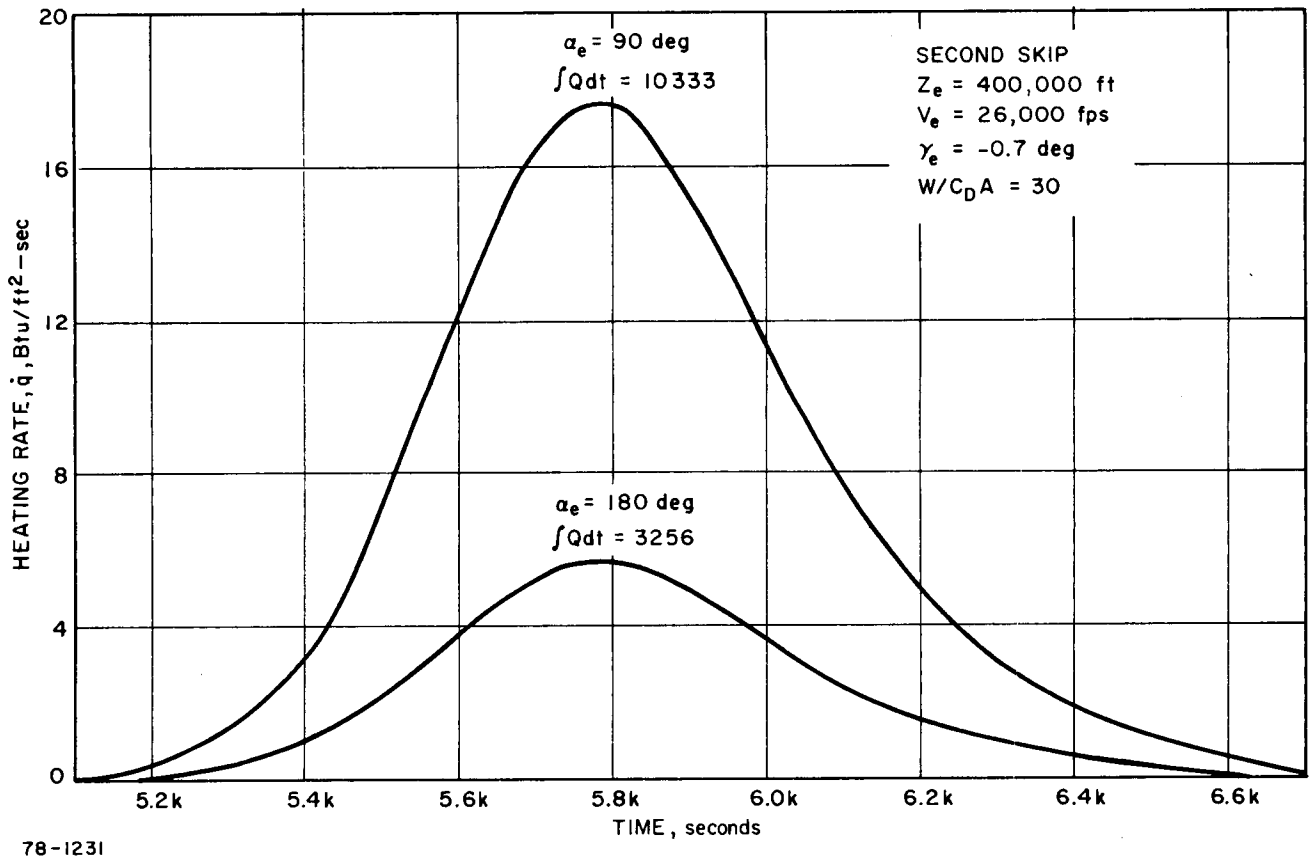

Figure 4.2-10 CRITICAL CONVECTIVE HEATING FOR EXPOSED CAPSULES

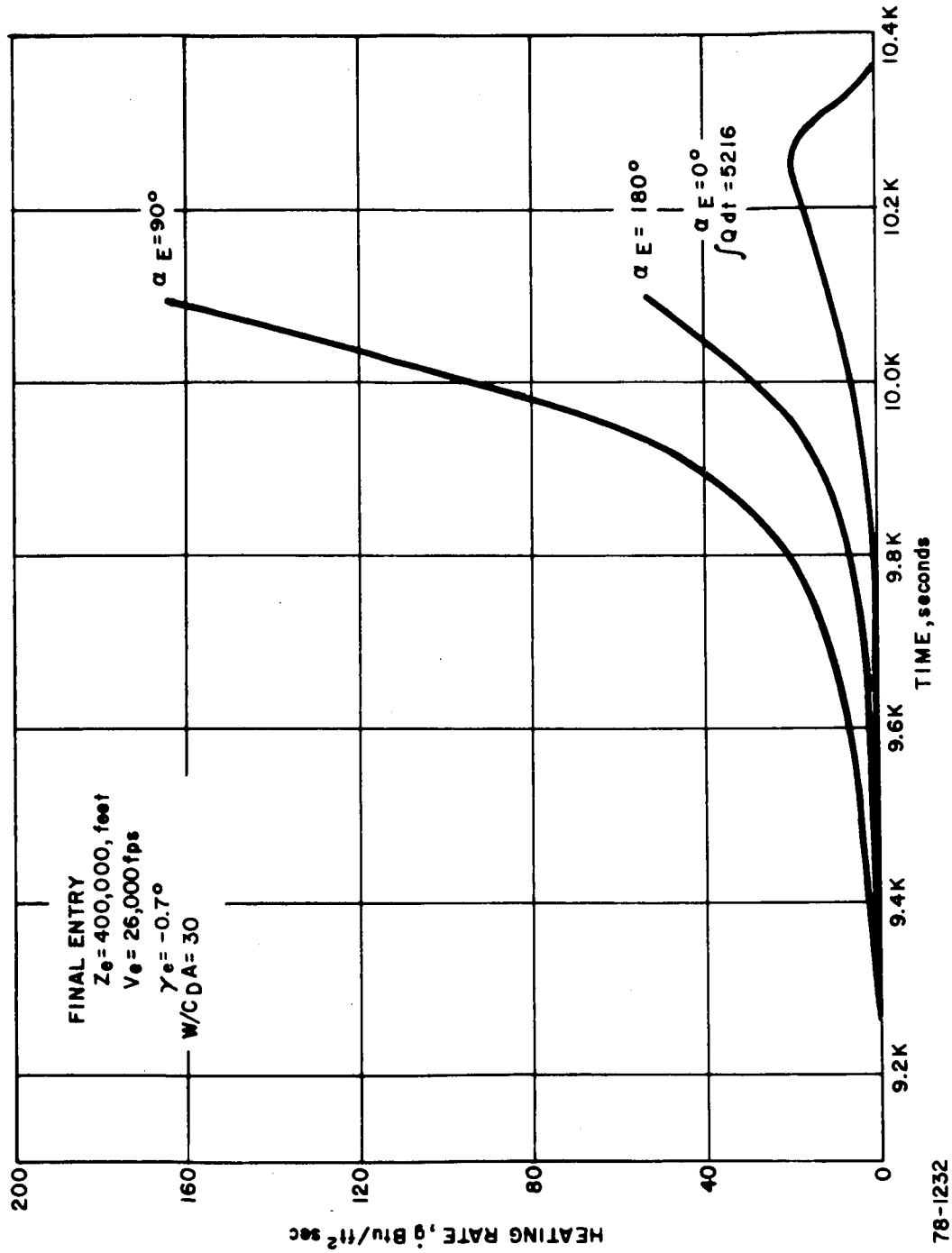

Figure 4.2-11 CRITICAL CONVECTIVE HEATING FOR EXPOSED CAPSULES

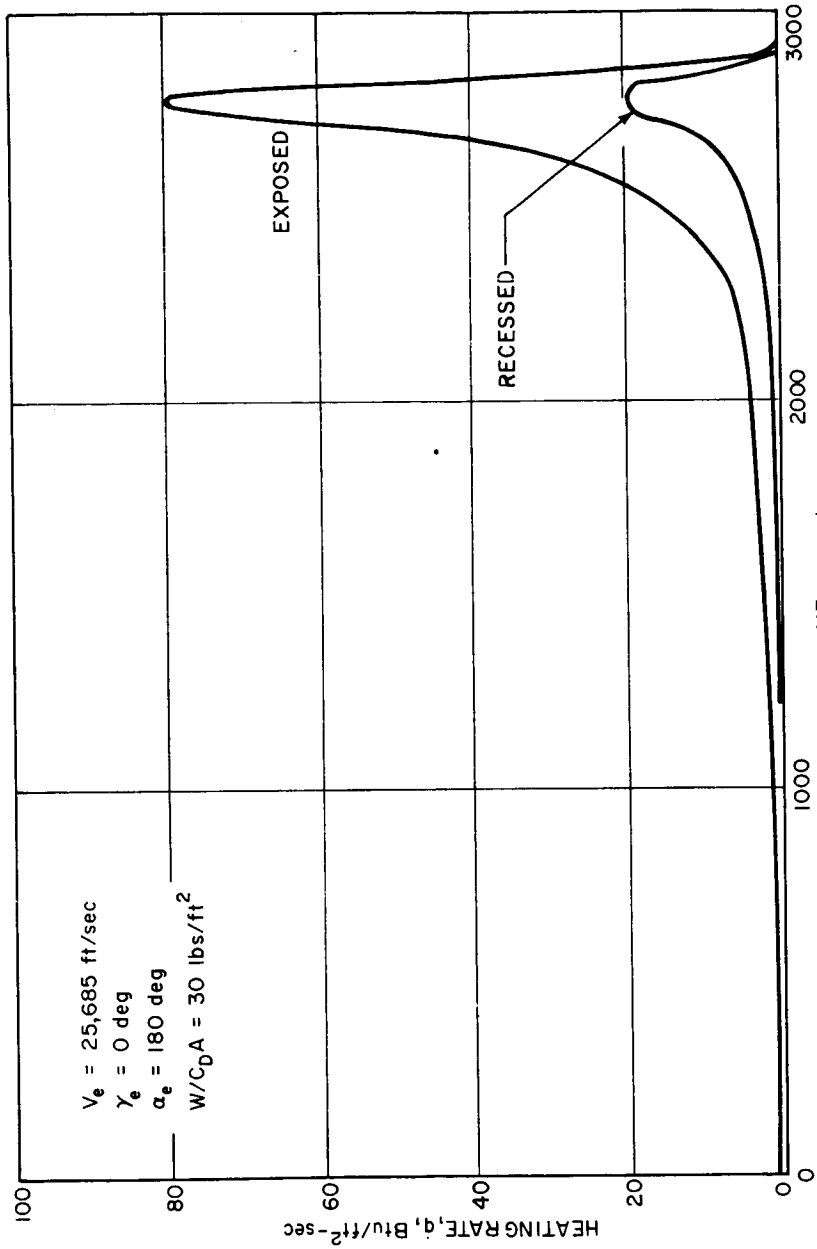

Figure 4.2-12 CAPSULE REENTRY HEATING FOR VEHICLE REMAINING AT REARWARD ATTITUDE TO IMPACT

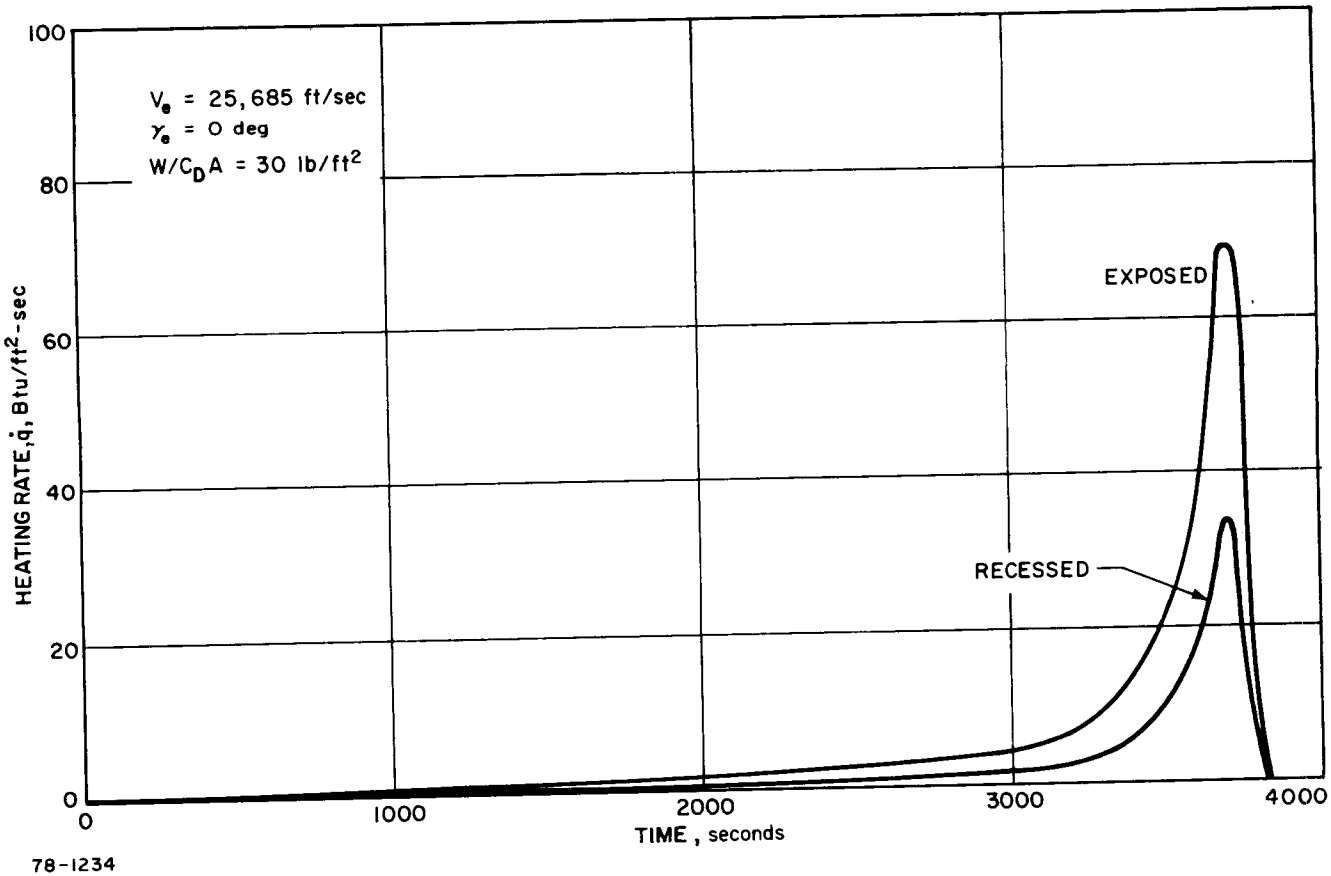

Figure 4.2-13 CAPSULE REENTRY HEATING FOR VEHICLE TUMBLING THROUGHOUT ENTRY TO IMPACT

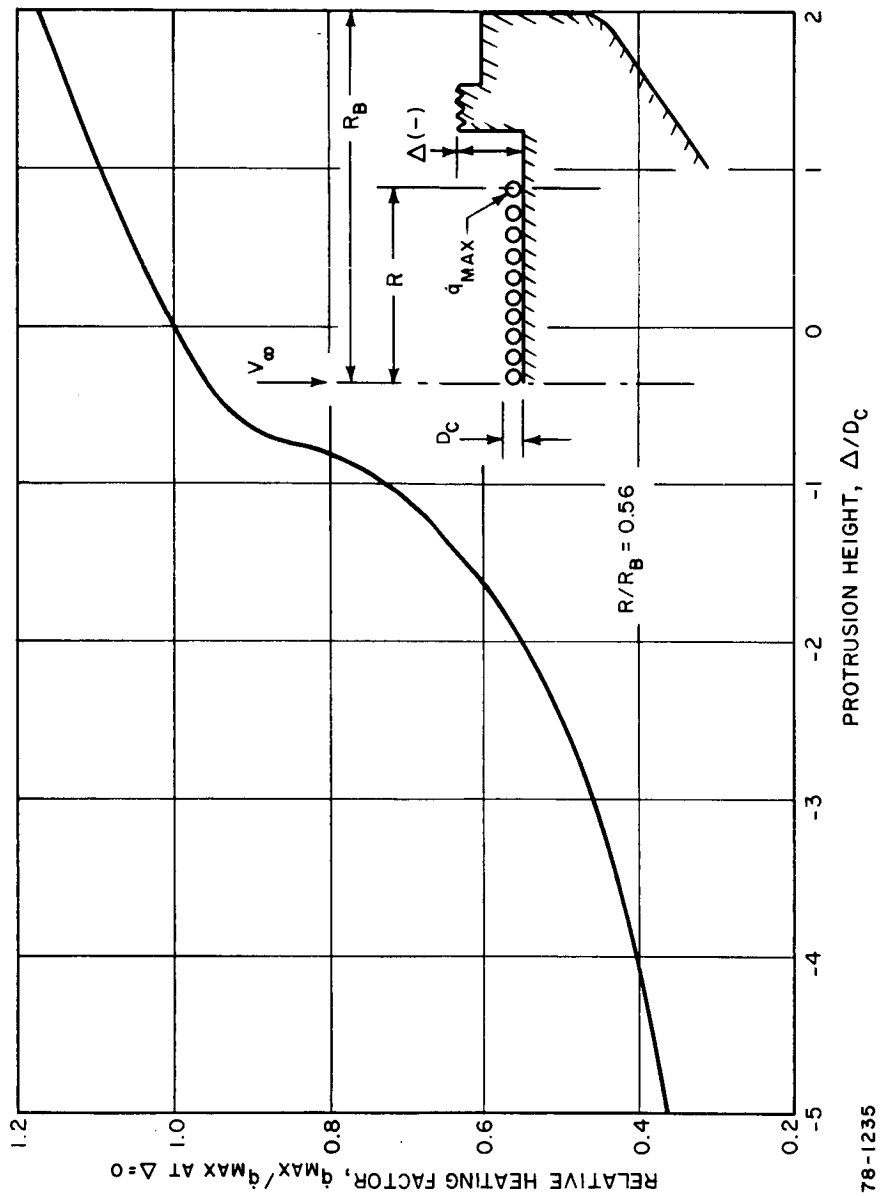

Figure 4.2-14 MAXIMUM HEATING VARIATION WITH PROTRUSION HEIGHT AT $\alpha = 180^0$

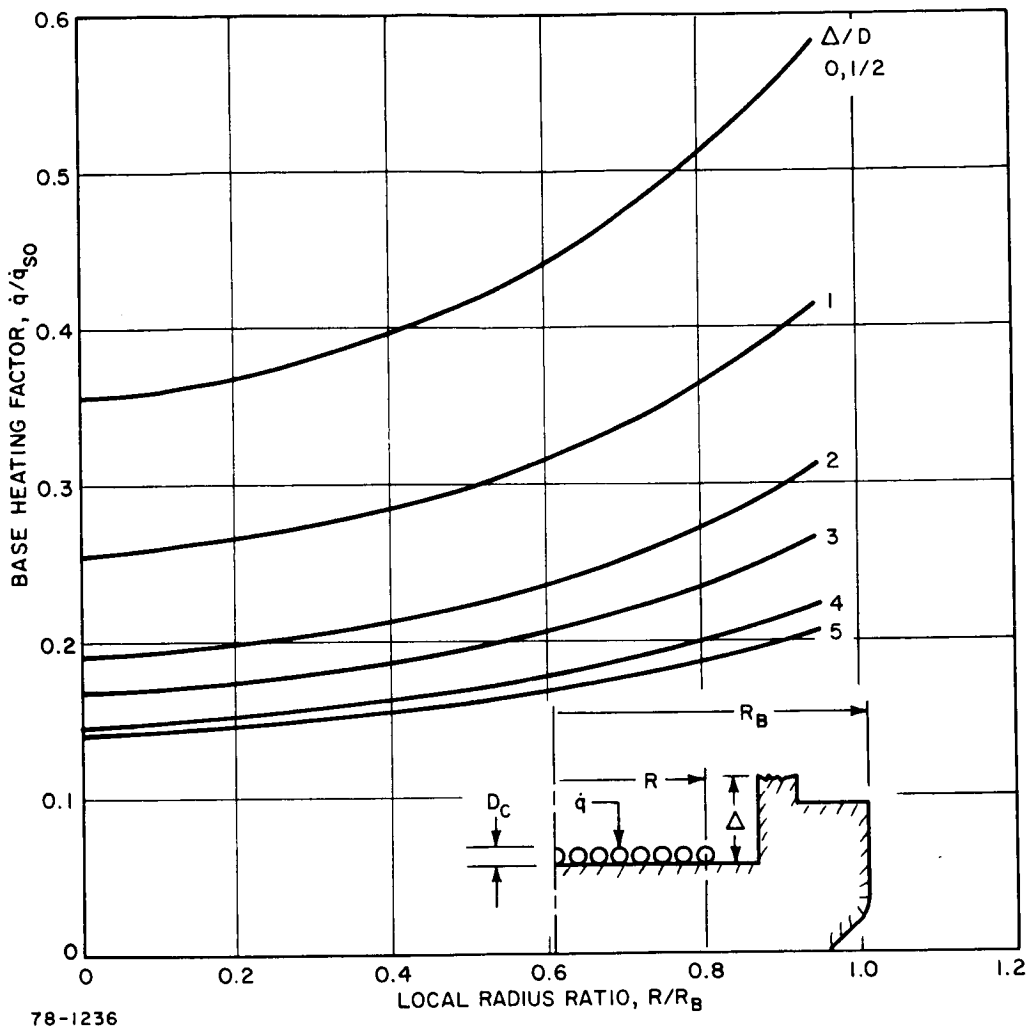

Figure 4.2-15 CAPSULE BASE HEATING FACTOR AT $\alpha = 180^{o}$

The main factors to be considered in choosing a concept for turn-around are as follows:

a. A passive concept is desired for reliability reasons

b. Minimize the trim angle of attack

c. Minimize design problems associated with the reentry vehicle

d. Minimize heat exchanger/heat source interface problems

e. Avoid reentry vehicle separation design complexities

f. Maintain minimum size consistent with adequate turn-around capability

g. Maximize performance predictability.

4.2.2.1 Center of Gravity Offset

The use of the center of gravity offset provides the simplest method with the highest degree of confidence. The turning moment is provided primarily by the drag force acting about a center of gravity which is offset from the vehicle axis.

At entry, the minimum offset distance required to destabilize the rearward attitude is approximately 0.032D in the plane of offset. Figure 4.2-16 shows the hypersonic pitching moment coefficient as a function of angle of attack with both a zero offset and 0.032D. It is seen that in addition to destabilizing the rearward attitude, there is a change in the forward trim angle of attack due to the offset center of gravity. The variation of this forward trim with Mach number is plotted in Figure 4.2-17. The trim angle is large being of the order of 14 degrees at hypersonic speeds with a maximum angle of attack of 18 degrees transonically. As mentioned previously, the offset center of gravity also significantly complicates the overall IRV design including the deorbit system.

4.2.2.2 Afterbody

An alternate device which was investigated was an afterbody shown in Figure 4.2-18. The analysis assumed that the minimum static margin was the same as for the asymmetric fence design. The center of pressure for the afterbody was obtained from reference 11. The required afterbody is large, resulting in an excessive weight penalty together with other disadvantages associated with the heat exchanger interface problems and a large degradation in subsonic stability due to the afterbody.

4.2.2.3 Fins

An analysis of the fins indicates immediately that zero moment would be obtained at α = 180 degrees because each fin would be at zero angle of attack. At angles of attack between 90 and 180 degrees the interaction of the fin with the base produces pressure distributions requiring excessively large fins to produce sufficient overturning moments.

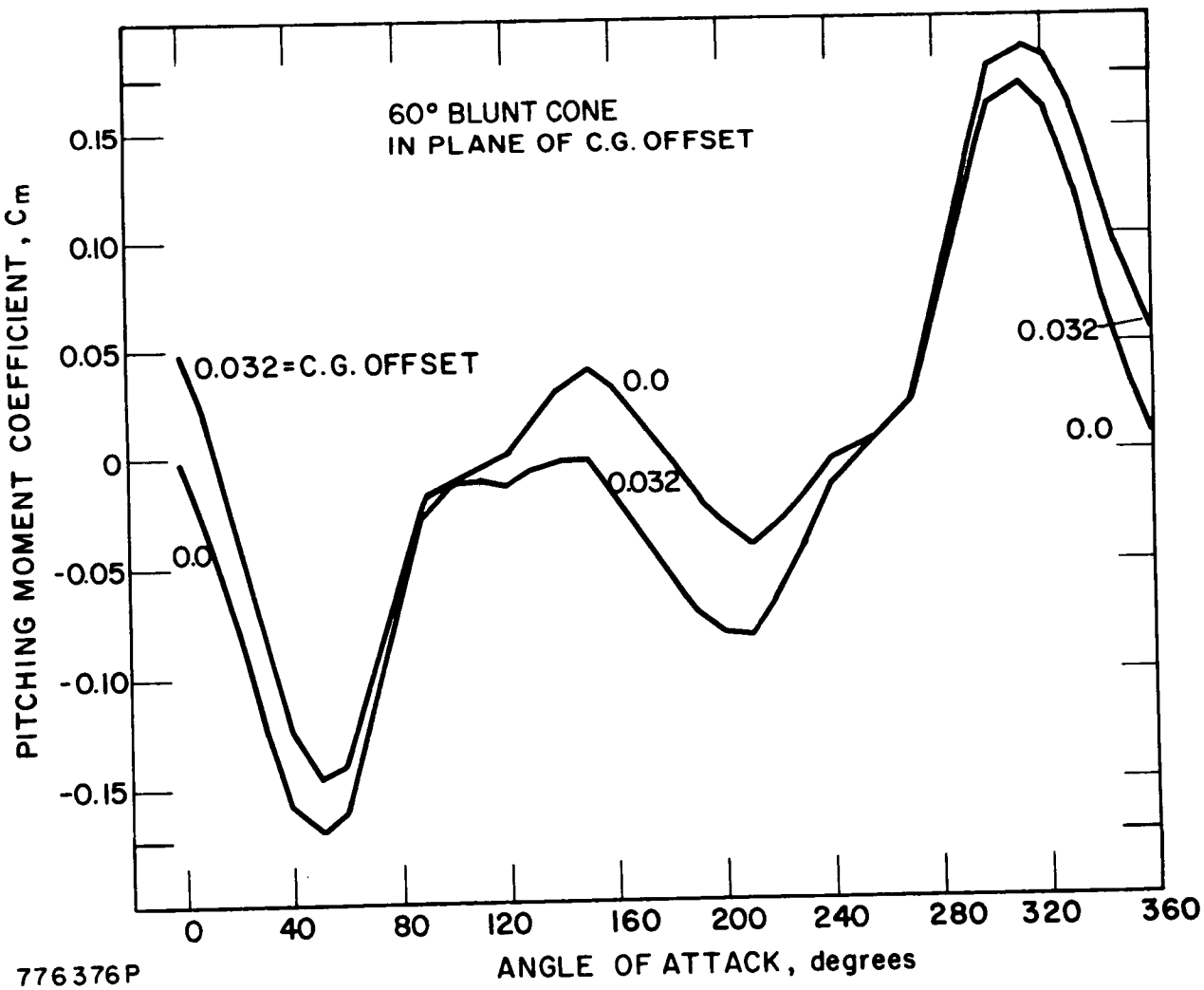

Figure 4.2-16 PITCHING MOMENT COEFFICIENT VARIATION WITH C.G. OFFSET

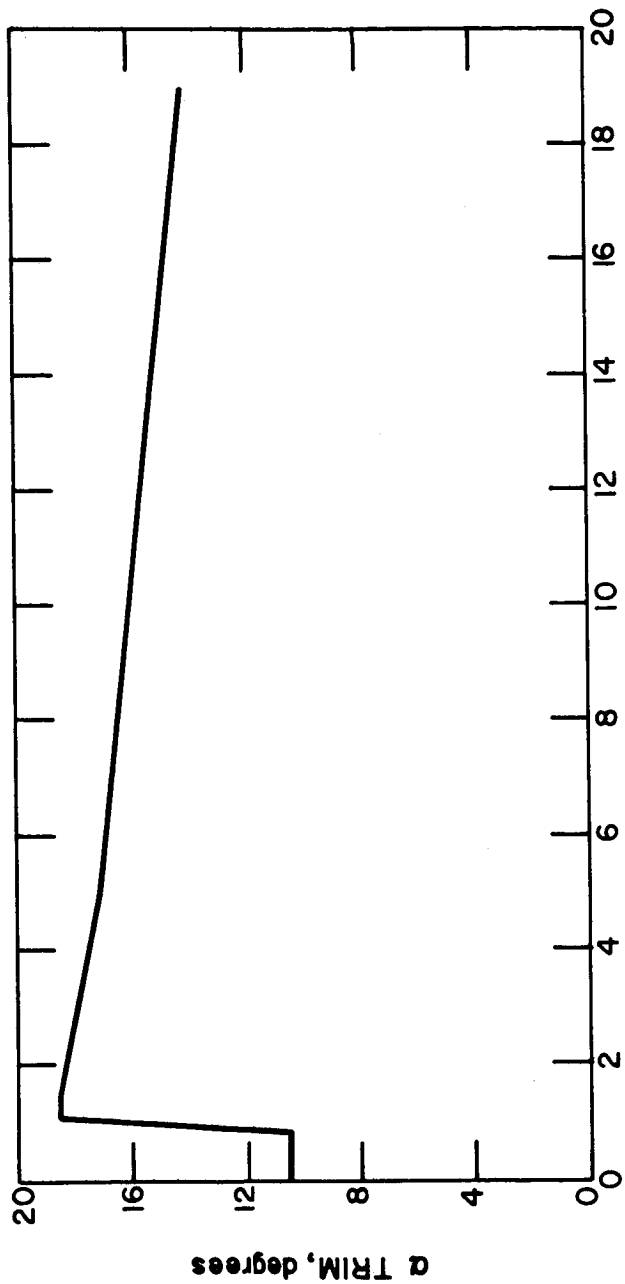

Figure 4.2-17 TRIM ANGLE OF ATTACK (0.032D C.G. OFFSET)

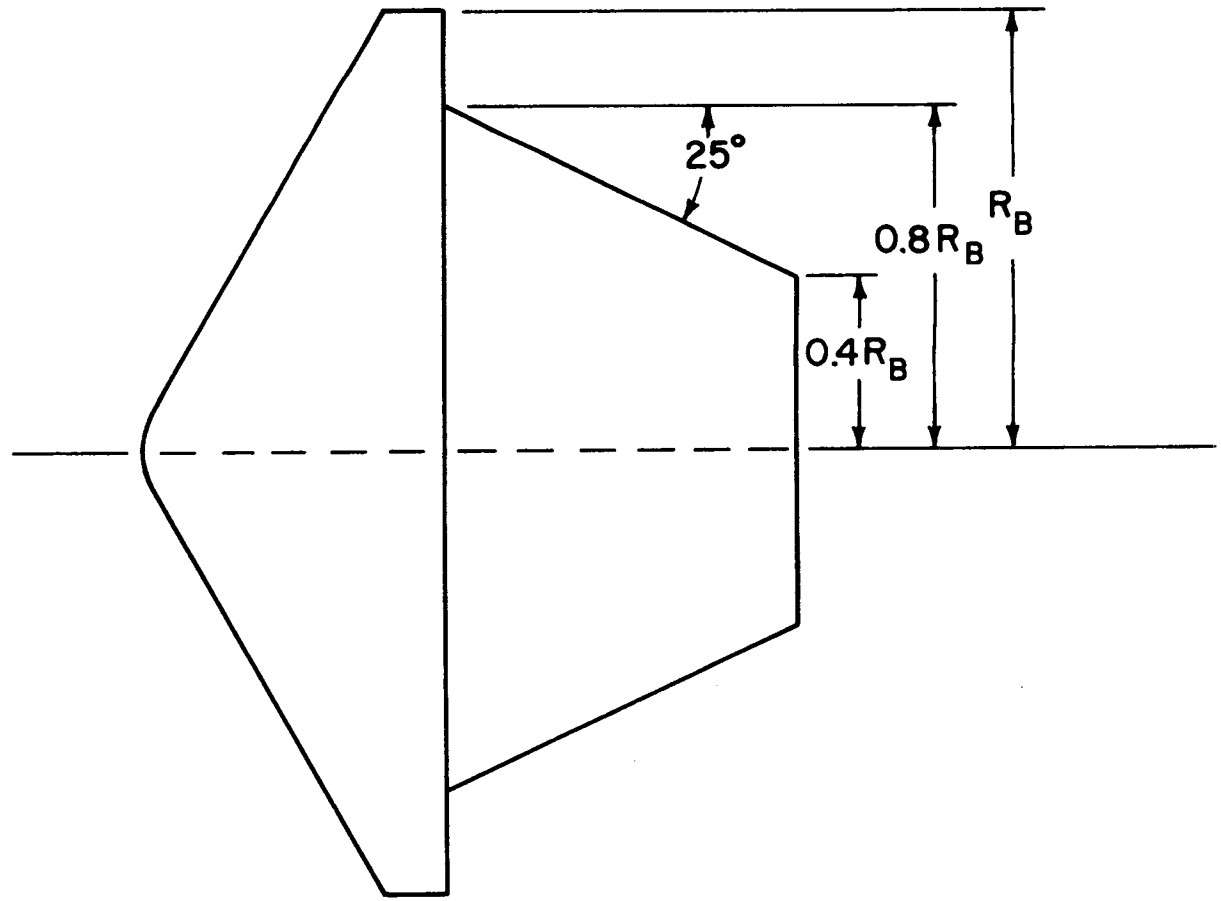

Figure 4.2-18 AFTERBODY CONFIGURATION

4.2.2.4 Flaps

The flap would provide a very simple method if it were a passive device. It would, however, produce excessively large trim angles of attack, comparable to those associated with the center of gravity offset.

4.2.2.5 Symmetric Fence

The symmetric fence has been analyzed in some detail and the results in Figure 4.2-19 show that a reasonable size fence will produce sufficient moment to provide favorable turn-around capability. There is also the advantage of no asymmetries and performance predictability.

The moment coefficient due to added fences as shown in Figure 4.2-19 is a function of fence length for the two extreme conditions of continuum and free molecule flow. The incremental moment coefficient due to the side fences, i.e., the two fences between the windward and leeward sides, has been neglected in these calculations, and is assumed to be very small since these two fences are centered on the moment axis. In continuum flow, an optimum fence length is seen to occur approximately at L_F/R_b of 0.1. This phenomenon is due to the high base pressure shift toward the windward side for shorter fences and due to the shading effect for longer fences. Examination of the equation below shows that the contribution of the windward fence is destabilizing. Further, as fence length is increased, the base contribution and the leeward fence contribution are both decreased. Therefore, lengths greater than those considered in this study are probably of little value.

The free molecule moment curve shows a monotonic increase in the length range considered. Moment coefficients in free molecule flow are lower up to L_F/R_b of 0.2. It can be shown that by differentiating the moment equation for the fence one obtains:

$$\left(\frac{L_F}{R_b}\right)\left[\frac{P_1}{P_S}+\frac{P_4}{P_S}-\frac{P_3}{P_S}\,\mathrm{TAN}^2\left(\alpha-\frac{\pi}{2}\right)\right]+\frac{P_3}{P_S}\,\mathrm{TAN}\left(\alpha-\frac{\pi}{2}\right)=0$$

which provides a maximum moment for

$$L_F/R_b = 1.75$$

Beyond this length, the windward fence (which contributes a stabilizing moment in free molecule flow) shades the base entirely, and begins to shade the leeward fence.

Available envelope considerations alone may preclude the use of long fences. Because the absolute magnitude of the pressure encountered in the free molecular regime is very low, it is likely that the vehicle will not be turned around and stabilized until some degree of continuum flow is encountered. On this basis, fence lengths L_F/R_b of about 0.15 appear to be the most judicious selection for the four-part symmetric fence configuration.

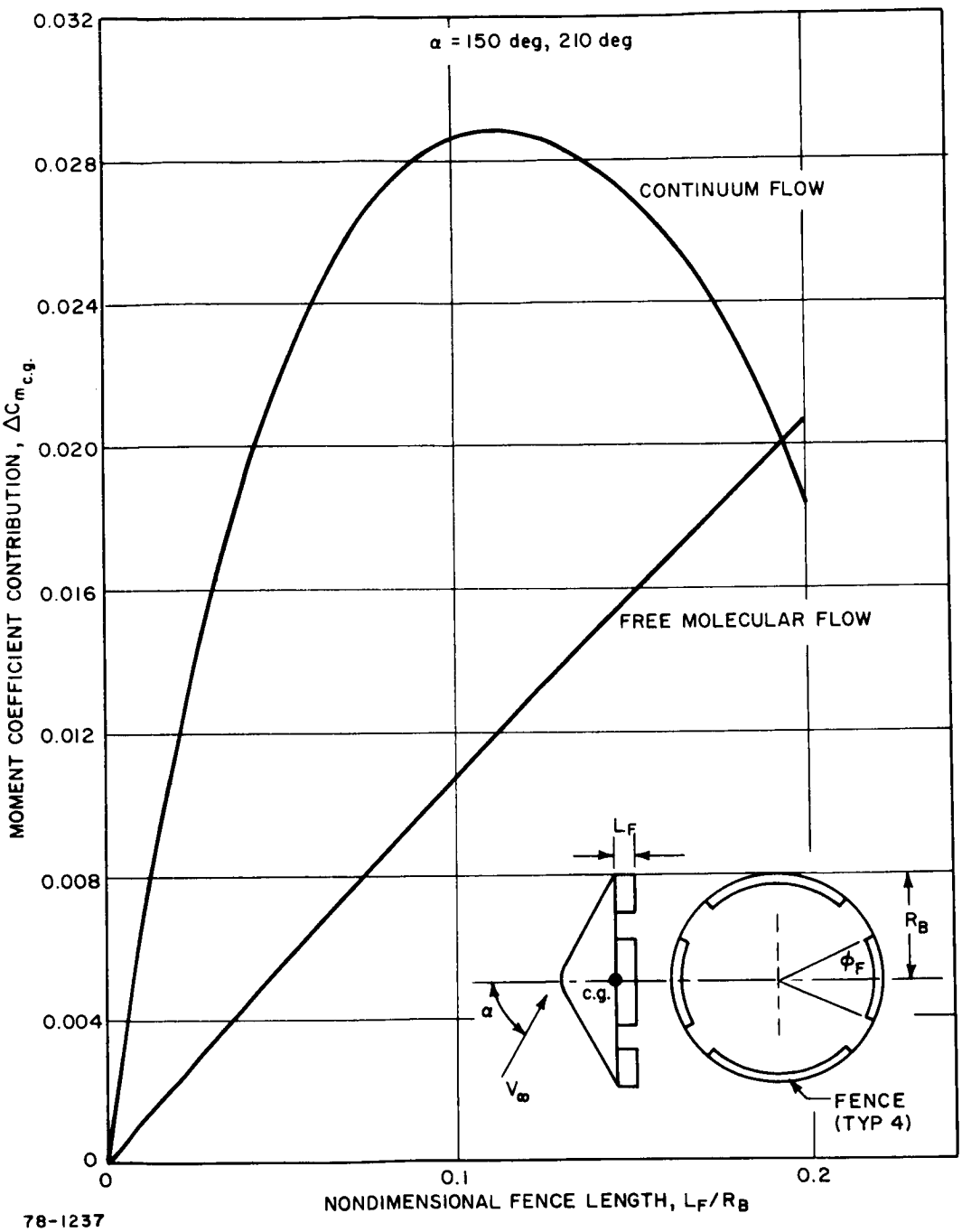

Figure 4.2-19 PITCHING MOMENT INCREMENT DUE TO SYMMETRICAL FENCE

4.2.2.6 Asymmetric Fence

A typical asymmetric fence is shown in Figure 4.2-20.

The effect of the fence/base interactions is shown in Figure 4.2-21 which indicates the moment coefficients which must be overcome by the fence at α = 150 degrees. The variation with fence location shows that the fence must overcome a greater pitching moment as the fence is moved inboard. With the fence located at the edge of the base, the moment on the base area is actually favorable so that the fence is required only to produce this pressure distribution. The pressures acting on the fence surface itself are of additional benefit.

The trim angles due to the fence are shown in Figure 4.2-22. As might be expected, the $\delta_F = 0$ fence produces the least asymmetry since these fences are "shaded" or hidden from the primary flow field at small angles of attack. Increasing the fence height and the protrusion angle increases the trim angle of attack significantly. The most desirable fence would be one for which $\delta_F = 0$.

4.3 IRV CONCEPTUAL DESIGN PERFORMANCE COMPARISON

A comparison of five conceptual design configurations is presented to evaluate their relative turn-around characteristics. This turn-around capability is desirable in order to achieve a single trim point near zero angle of attack and to reduce base heating problems for initial rearward entry. The five configurations that were evaluated are as follows:

a. Circular planar heat source array, 60 degree cone - without recovery aids

b. Rectangular planar heat source array, 60 degree cone - with recovery aids

c. Conical heat source array, 60 degree cone - without recovery aids

d. Conical heat source array, 60 degree cone - with centrally mounted recovery aids

e. Pincushion heat source array, 60 degree cone - without recovery aids.

The mass characteristics for these configurations are shown in Table 4.3-I.

4.3.1 Configuration Comparison

As stated previously, the turn-around capability of the five configurations must be adequate to rotate the vehicle and converge the angle of attack sufficiently to reduce base heating problems. Figure 4.3-1 shows parametrically the fence configurations required to overcome the static moment coefficient and to produce a single trim point. Superimposed are the allowable fence heights which ensure that the fence does not extend beyond the maximum vehicle radius. Fence heights greater than these minimum values must be used to provide sufficient turning capability. Configuration 1 has been used as the basis for comparison. The asymmetric fence is located at the maximum diameter and is perpendicular to the base (δ =0) with a height to base radius ratio, H/R_b , of 0.2 and a 180 degree arc.

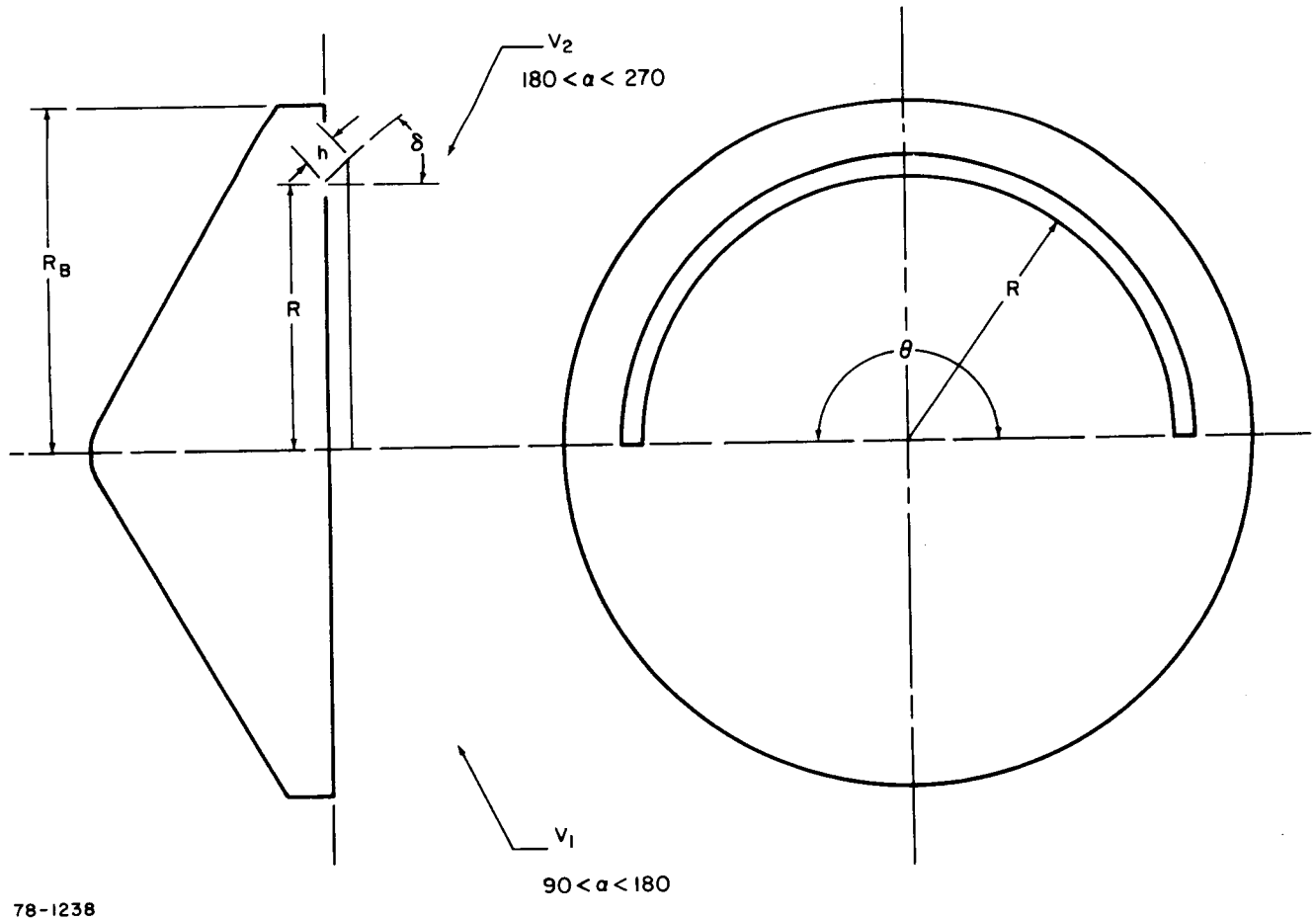

Figure 4.2-20 FENCE CONFIGURATION

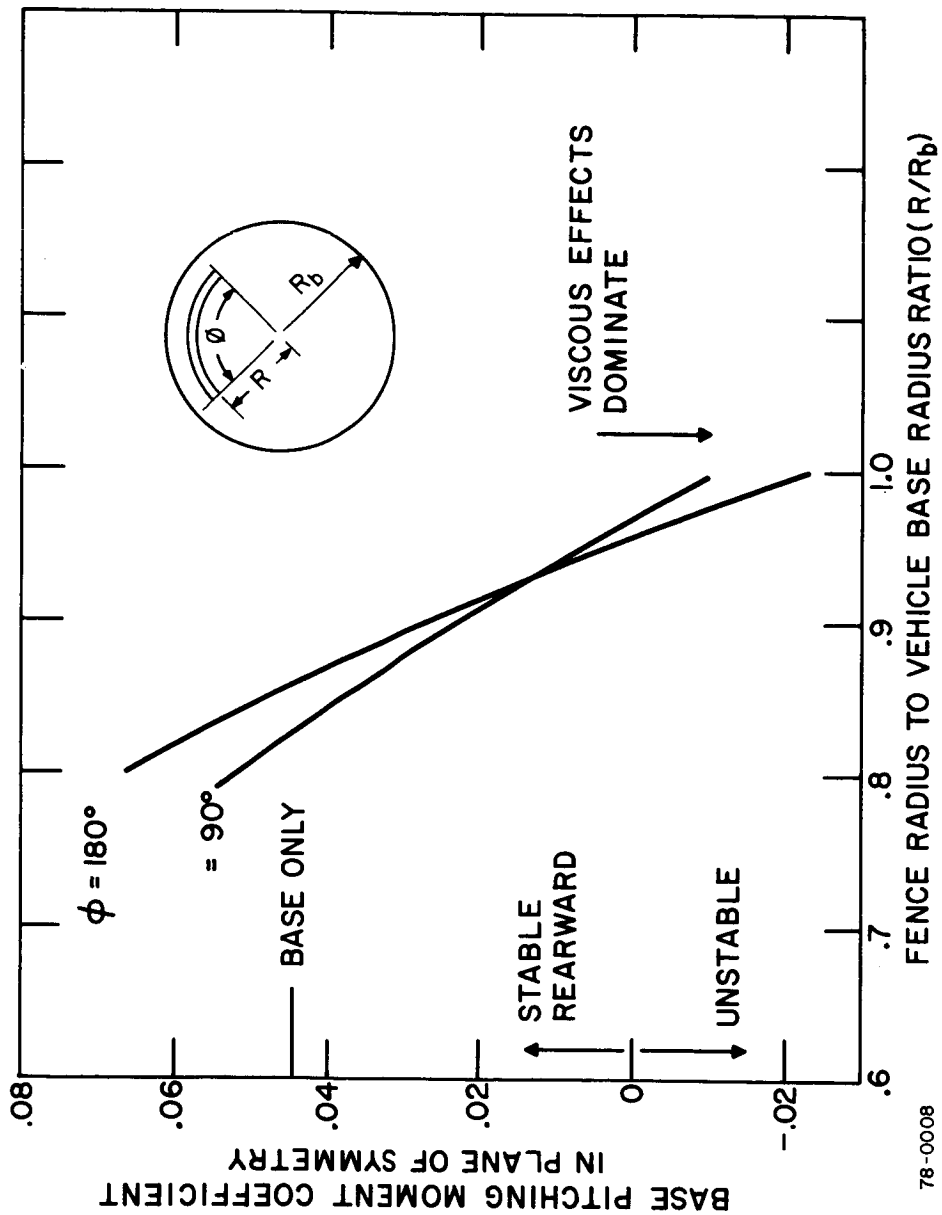

Figure 4.2-21 FENCE REQUIREMENT VARIATION WITH FENCE LOCATION

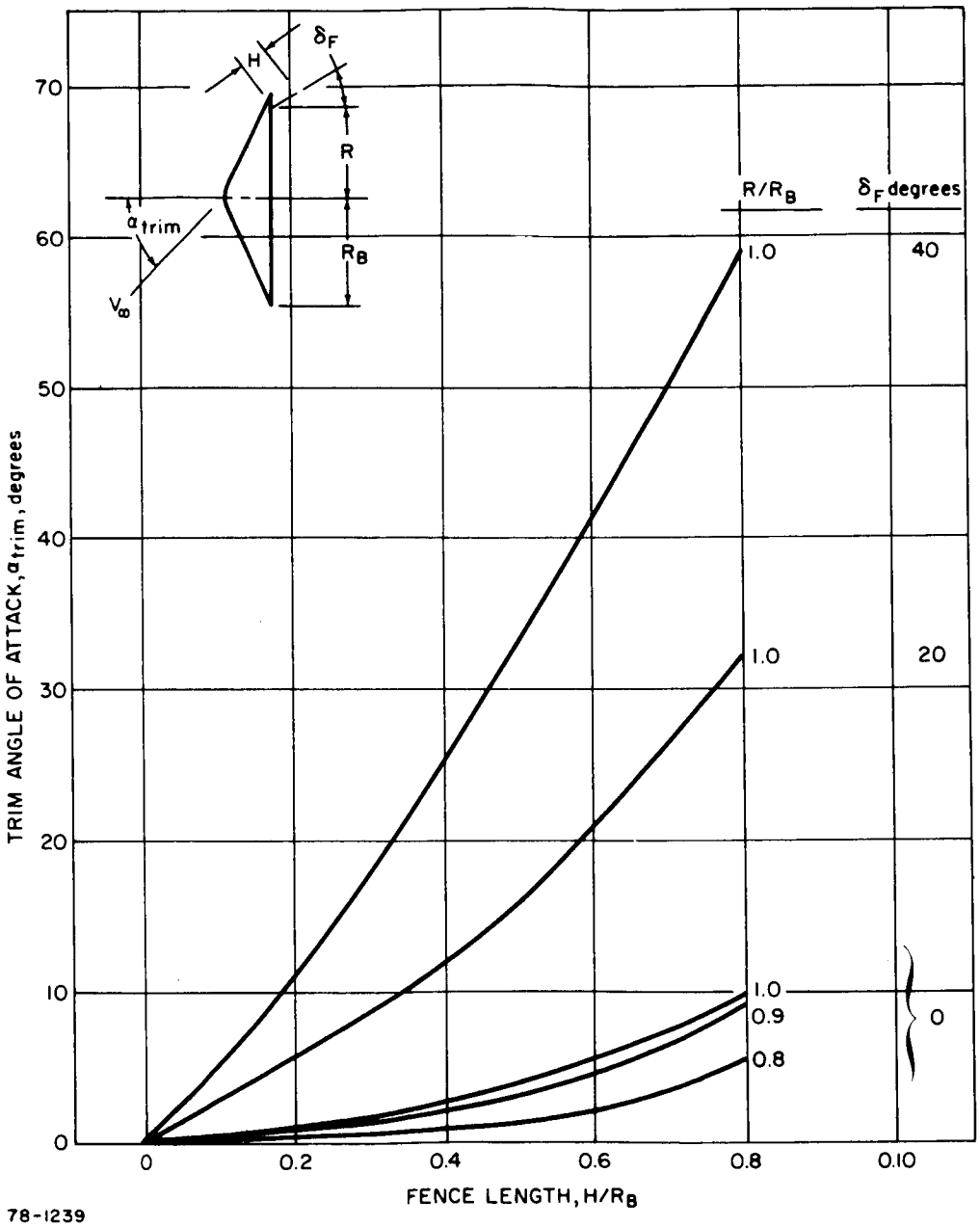

Figure 4.2-22 TRIM ASYMMETRY DUE TO FENCE (IN PLANE OF SYMMETRY)

TABLE 4.3-I

MASS CHARACTERISTICS OF FIVE CONCEPTUAL DESIGNS

Design Shape	Mass Slugs	XCG/D	I_{xx} Sl-Ft^2	I_{yy} Sl-Ft^2	I_{zz} Sl-Ft^2	Diameter feet	W/C_DA
1	41.5	0.333	130	70	70	5.75	32.4
2	45.8	0.293	152	74	105	6.25	30.4
3	42.1	0.314	117	66	66	5.75	32.8
4	49.2	0.295	261	146	146	7.33	23.6
5	42.6	0.352	133	75	75	5.83	32.4

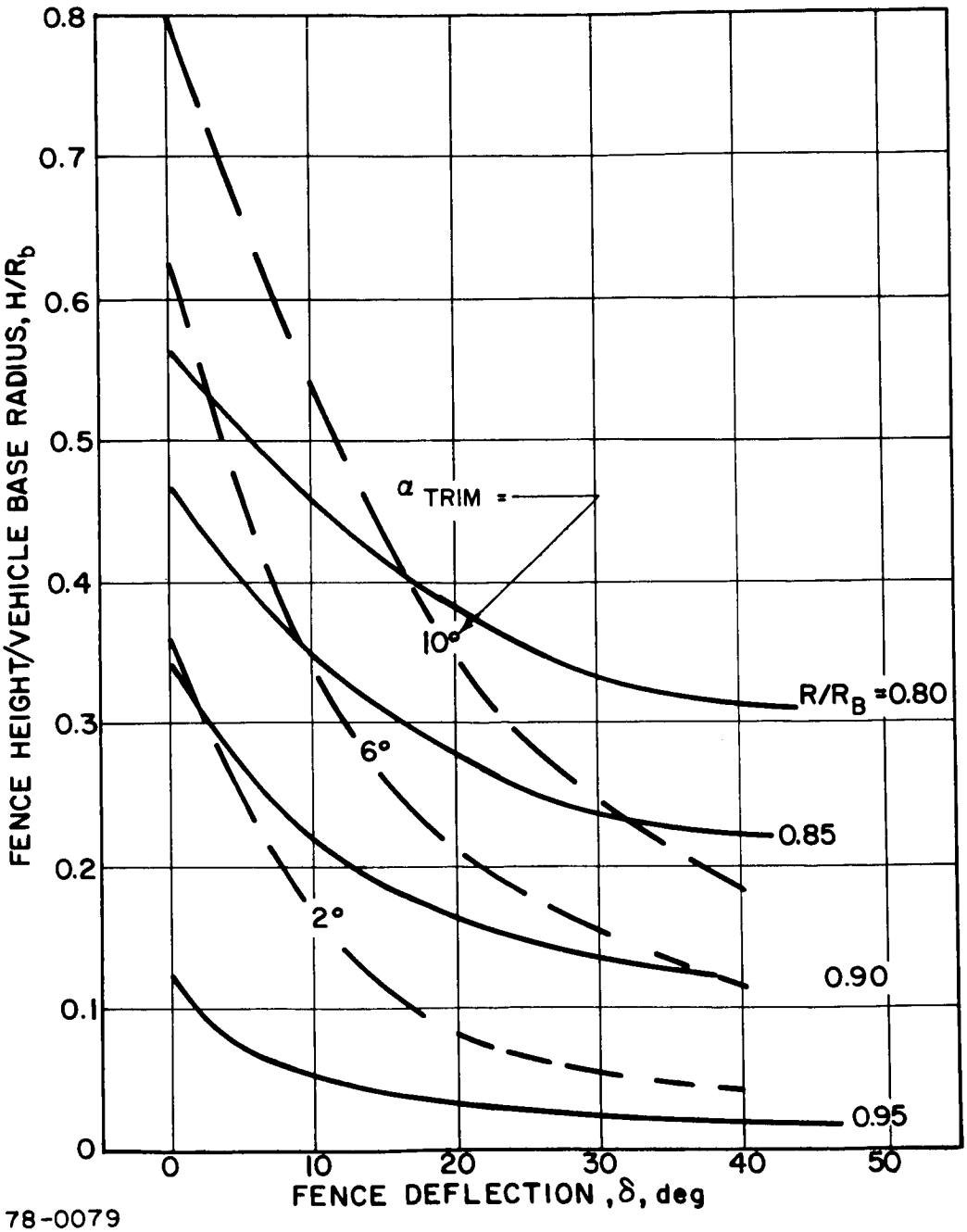

Figure 4.3-1 FENCE REQUIREMENT FOR TURNAROUND

For the highest heating rate trajectory (reentry angle of -10 degrees and reentry velocity of 26,000 fps) the turn-around characteristics are shown in Table 4.3-II. An exposed capsule array was selected for illustrative purposes. Its maximum heating effects occur at an angle of attack of 90 degrees and the data of Table 4.3-II indicate the heating rates when the angle of attack envelope attains this value. Two comparisons are made; the first is for Configuration 1 with different fence heights, and the second is a comparison of the five configurations for a fixed fence height ratio of 0.2.

As expected, the first comparison shows that the turn-around times and the capsule heating decreases as the fence size is increased (see Figure 4.3-2). This is caused by the higher effective pitching moment as the fence size is increased. The comparison of configurations in Table 4.3-II shows that the lowest heating is obtained with Configuration 3 and the highest with Configuration 2. Although the turn-around capabilities are a function of several variables, the predominant parameters are the pitching moment variation and the moment of inertia. The lowest heating is obtained for Configuration 3 with its low moment of inertia and favorable pitching moment variation with angle of attack. From this analysis a selection of the configuration for greatest turn-around capability should be based on low moments of inertia and high turning moments. An attempt should be made to minimize the vehicle moments of inertia in order to improve the turn-around times and thus decrease the base heating.

The effect of center of gravity location on the maximum base heating rate is shown in Figure 4.3-3 for Configuration 1 which shows that as the center of gravity is moved aft the heating rate increases. This aft movement in effect results in a degradation in the pitching moment characteristics causing lower turn-around altitudes and consequently higher heating rates.

4.3.2 Conclusions and Problem Areas

The vehicle stability, particularly that at transonic and subsonic speeds, imposes a constraint on the allowable extension of the vehicle shape beyond the conical forebody. The recommended cylinder limit of 0.15 R_b is based on limited test data. The influence of either the symmetric or asymmetric fence on this limitation is uncertain, although some degradation in the stability is to be expected from the trends indicated by the available data. A test program (discussed below) is being performed by the Ames Research Center to define the hypersonic turn-around characteristics. Additional testing is also recommended over the complete speed range to obtain transonic and subsonic stability data.

The predicted fence performance results in a sufficiently high altitude at turn-around. The preliminary analyses of the fence device indicate favorable interaction with the base thereby minimizing the fence height requirements. However, in order to ensure this favorable interaction the fence height must extend beyond the boundary layer. The dependence of the boundary layer thickness upon Reynolds Number and hence altitude, indicates a strong dependence of fence effectiveness on altitude. Since in the turn-around analysis constant coefficients were considered, the performance associated with varying the effectiveness with altitude requires further analysis, especially since this variation will somewhat reduce the turn-around altitude.

TABLE 4.3-II

TURNAROUND CHARACTERISTICS FOR THE HIGHEST HEATING RATE TRAJECTORY OF FIVE CONCEPTUAL DESIGNS

Trajectory

γ_E = -10 deg.

V_E = 26,000 Ft/sec

For Shape 1

Fence Height H/R_B	Time at $\alpha = 90^o$ sec	Q_{base} at α = 90 deg.* Btu/ft^2-sec
0.116	25.2	137
0.195	23.8	106
0.31	22.6	88
0.41	21.3	66

For H/R_B = 0.195

Shape	Time at $\alpha = 90^o$ sec	Q_{base} at α = 90 deg.* Btu/ft^2-sec
1	23.8	106
2	25.3	142
3	22.1	79
4	22.8	87
5	24.8	126

*An exposed capsule has been assumed.

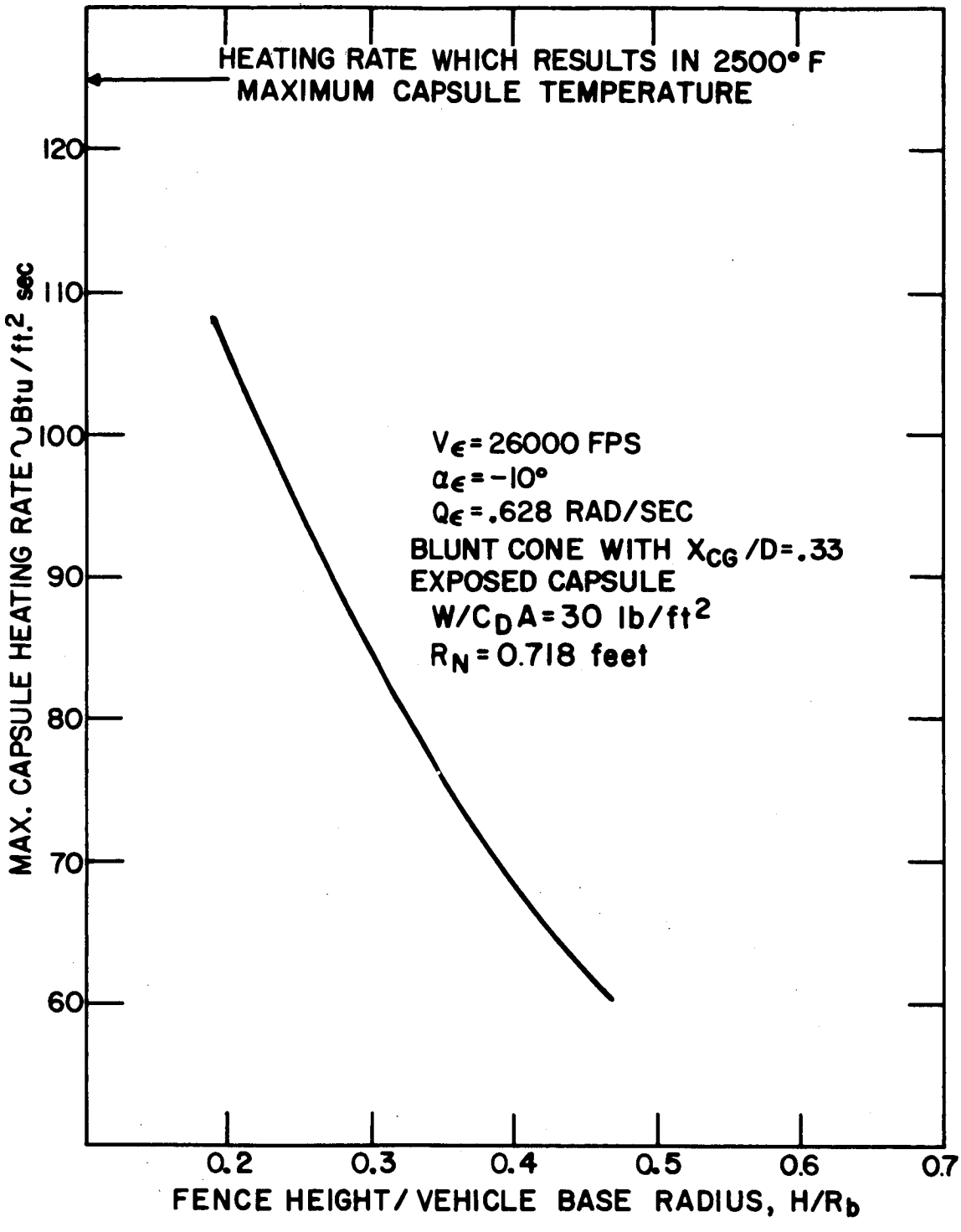

78-0010

Figure 4.3-2 EFFECT OF FENCE HEIGHT ON MAXIMUM CAPSULE HEATING RATE

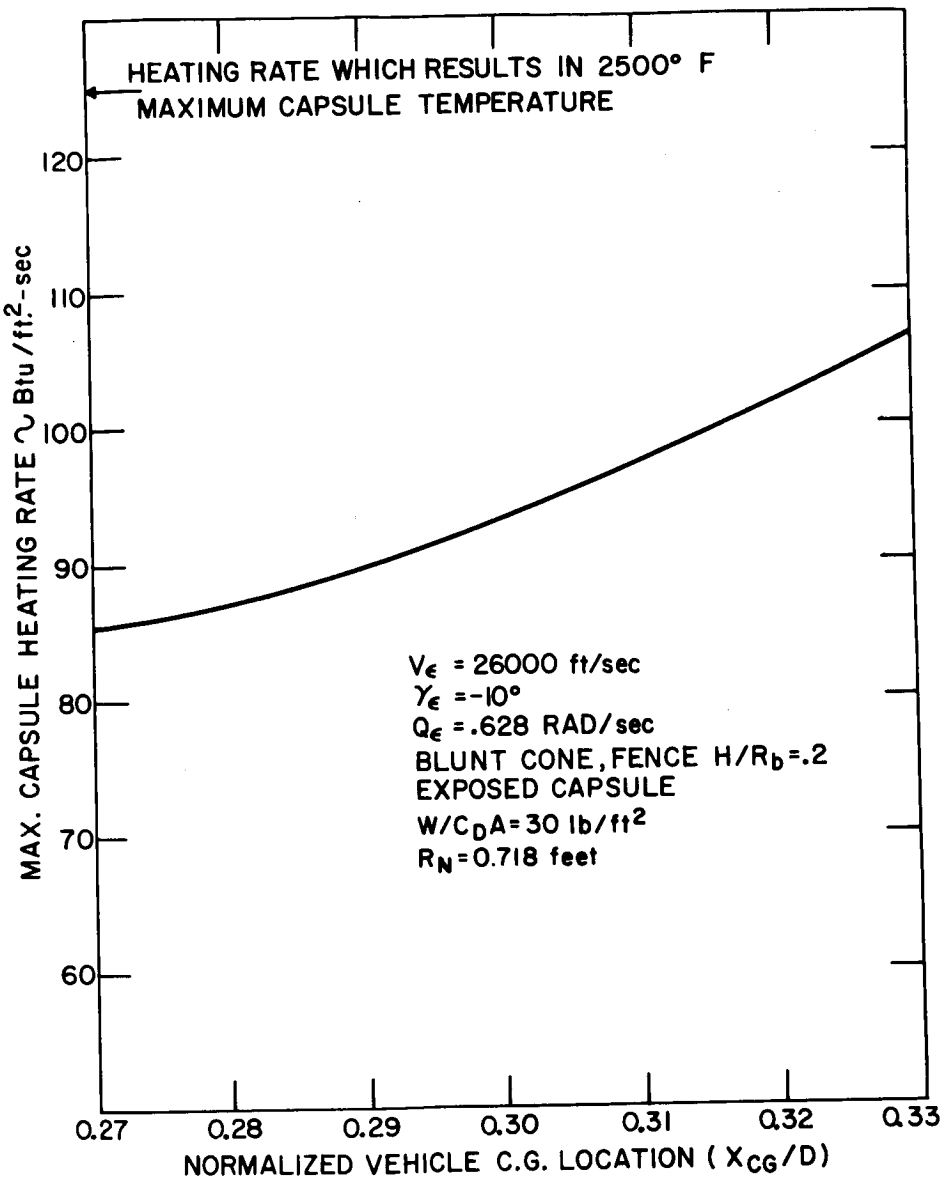

78-0012

Figure 4.3-3 EFFECT OF VEHICLE C. G. LOCATION ON MAXIMUM HEATING RATE

The capsule heating environment, being sensitive to the geometry of the capsule array, requires analysis for specific configurations in addition to the limiting environments considered so far in the study. This is due to the fact that the dynamic behavior and the turn-around altitude depends upon the aerodynamic and mass characteristics of the reentry vehicle which in turn depend critically upon the capsule array geometry.

The conical array geometry results in a desirable aerodynamic configuration since a more favorable center of gravity location is possible. Also favorable are the pitching moment characteristics associated with the dish shape which results in superior performance for random attitude reentry.

Little difference exists between the modified Apollo and the blunt cone configurations, although the available data indicates a possible slight advantage in hypersonic stability for the modified Apollo.

Considerable testing is required for the two most critical aerodynamic problem areas, i.e., the vehicle stability with turn-around devices and the capsule heating. A test program to evaluate the efficacy of fence devices has been initiated by Ames. The objectives and procedures of this test program are described below.

4.4 AERODYNAMIC TEST PROGRAM

The test program is designed to define the turn-around capability of various fence devices on a 60 degree blunt ($R_N/R_b = 0.25$) cone. The recommended program is conducted in two phases. Static tests at moderate Reynolds Numbers in the NASA/Ames arc jet facility are desired for geometry variation effects, while low Reynolds Numbers effects will be determined in the NASA/Ames shock tunnel facility by means of free flight models.

The arc jet wind tunnel test program will determine the high angle of attack variation of the pitching moment coefficient (in addition, drag and normal force will be measured). Variations in the fence geometry (angle, length and subtended arc for the fence) will be investigated to establish the dependence of the moment characteristics on these parameters. Preliminary analyses indicate that the continuum flow performance is inferior to that for free molecular conditions since the base is neutrally stable in the free molecular flight regime.

4.4.1 Simulation Requirements

The broad spectrum of reentry conditions results in a wide range of flight conditions for which turn-around occurs. Figure 4.4-1 presents the variation of Reynolds Numbers with the reentry angle for which the capsule maximum temperature becomes sensitive to the turn-around altitude. These curves for the limiting capsule environments reflect the maximum Reynolds Numbers of interest.

The Aerodynamic Arc Jet will be used to evaluate the effectiveness of the fence devices, particularly the height requirement. The Shock Tunnel is utilized in the program to obtain the variation of the effectiveness at reduced Reynolds Numbers.

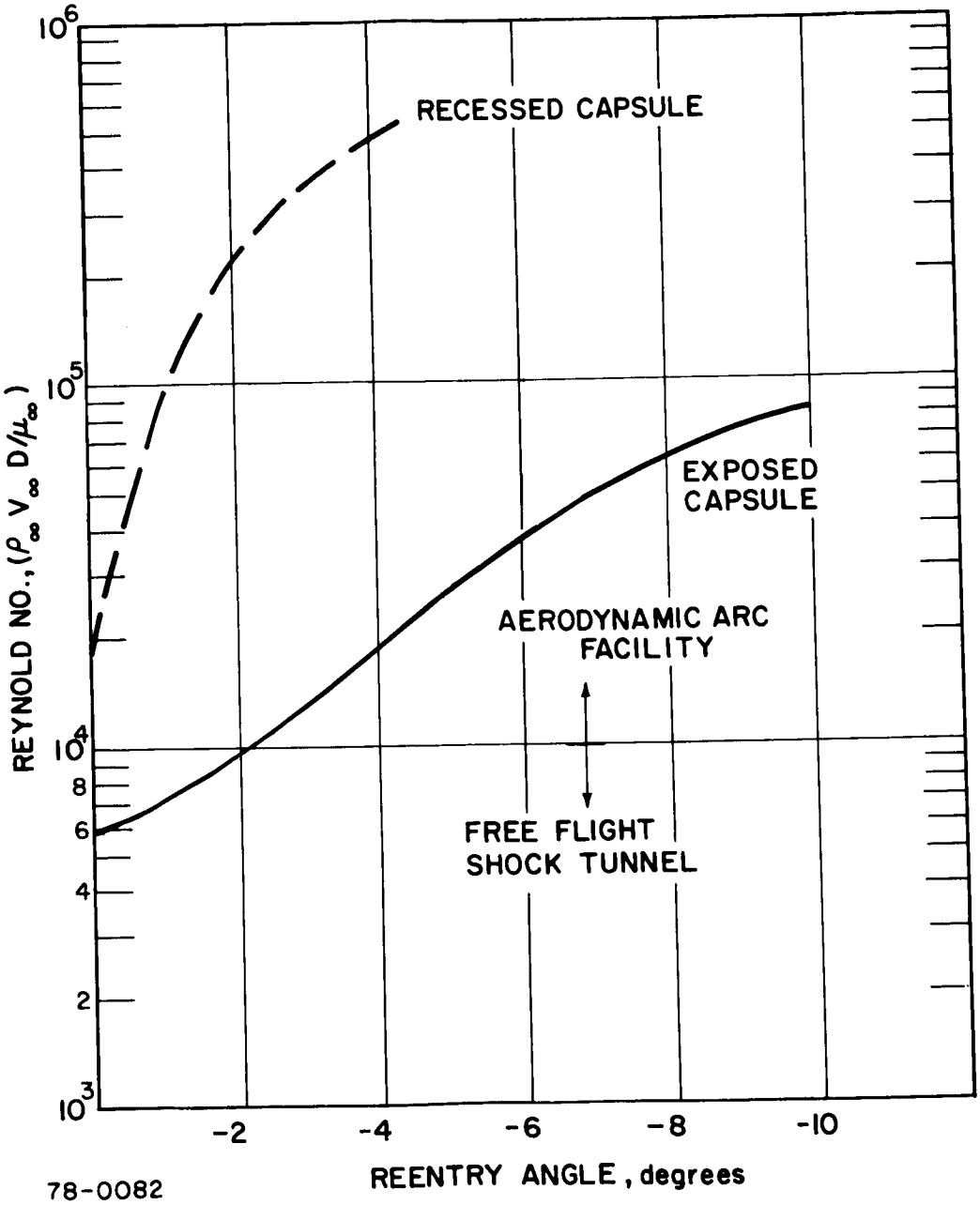

Figure 4.4-1 REYNOLDS NUMBER AT TURNAROUND

4.4.2 Test Models

4.4.2.1 Wind Tunnel Model

The test configuration is the blunt (R_N/R_b = 0.25) 60 degree half angle cone. There are variations in the IRV configuration which alter the base region geometry and the associated flow. Three base geometries will be considered:

a. A flat base

b. A cylindrical recess

c. A conical recess.

These variations in geometry are accommodated by means of interchangeable plates (see Figure 4.4-2). Variations in fence geometry are also accomplished by means of interchangeable plates. The fence plates are attached by means of screws with a 45 degree spacing providing a means for altering the angle between the fence axis and the pitch plane. An additional advantage in this arrangement is the elimination of the need for many different model and sting arrangements. The present model-sting combination is limited to two, one for $135^o < \alpha < 225^o$ and one for the $90^o < \alpha < 180^o$ and $180^o < \alpha < 270^o$ ranges. The model-sting arrangement for these two combinations is shown in Figures 4.4-2 and 4.4-3. Two cone models are required which utilize the same interchangeable plates. Complete angle of attack variations are accomplished by rotating the fence plate 180^o. The test matrix is arranged such that model set-ups can be accomplished while conducting a test without duplicate parts or assemblies.

The sting influence on the model has been minimized by means of an adapter section between the balance and the model. This is particularly important for the 90^o angle of attack. A shroud is utilized on this adapter to eliminate the introduction of the aerodynamic forces acting on this section into the model forces as well as to minimize the heat flux to the balance.

4.4.2.2 Free Flight Models

These models will comprise one symmetrical and one asymmetrical fence configuration with the recessed base vehicle configuration. To ensure sufficient angular motion, the moment of inertia must be low. In addition, to keep the model in the field of view, the mass must be high. These two requirements are satisfied by a nonhomogeneous model. A model diameter of one inch is generally used to permit several models to be used in the test section during a single test run.

All models will be devoid of instrumentation. The wind tunnel data will consist of the force and moment coefficients while the free flight data consists of qualitative turn-around motion data and, if possible, estimates of the pitching moment coefficient near the initial angle of attack. The qualitative data would indicate angles of attack which are suspect relative to stability, as well as delineate areas for further wind tunnel tests.

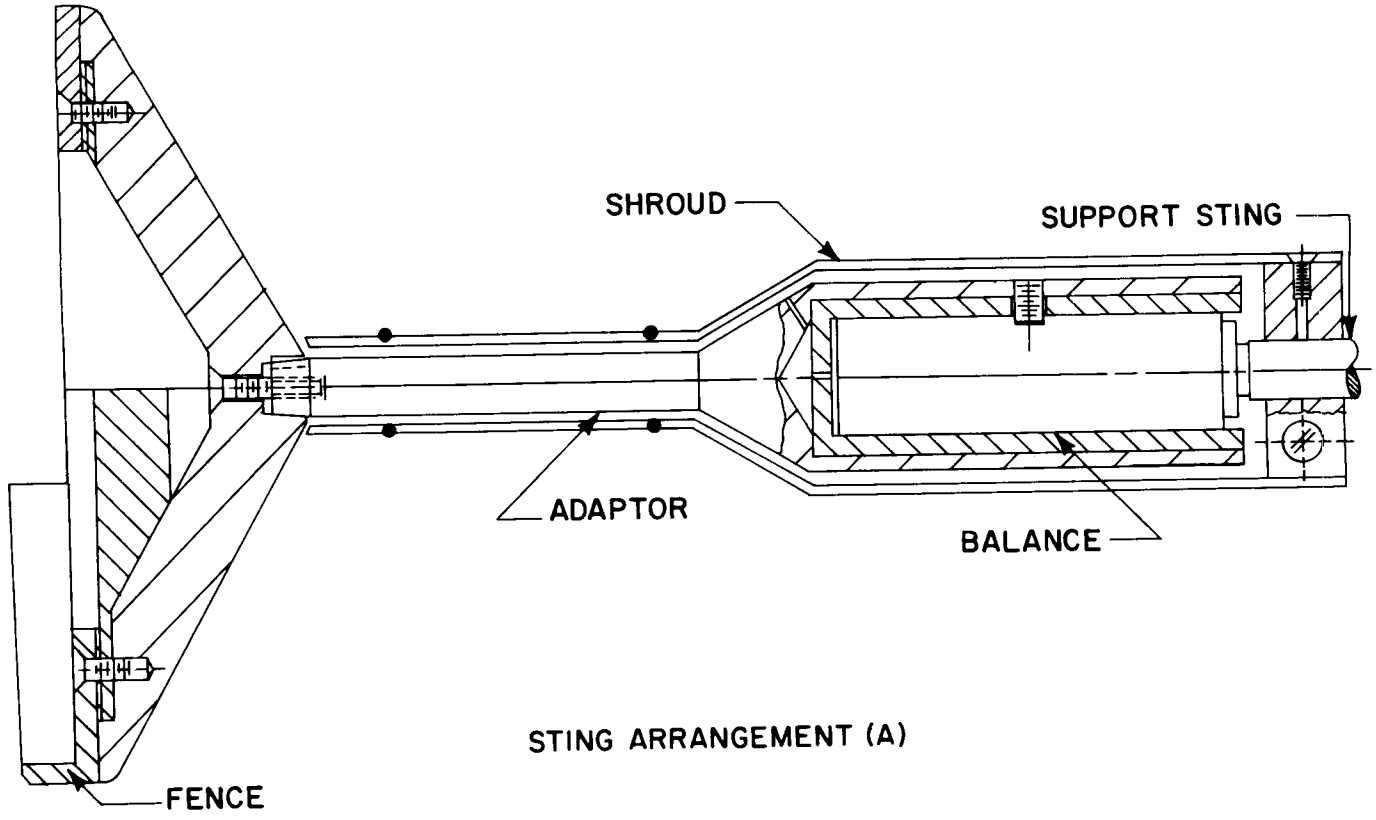

Figure 4.4-2 TEST MODEL ($135 < \alpha < 225$) -- STING ARRANGEMENT (A)

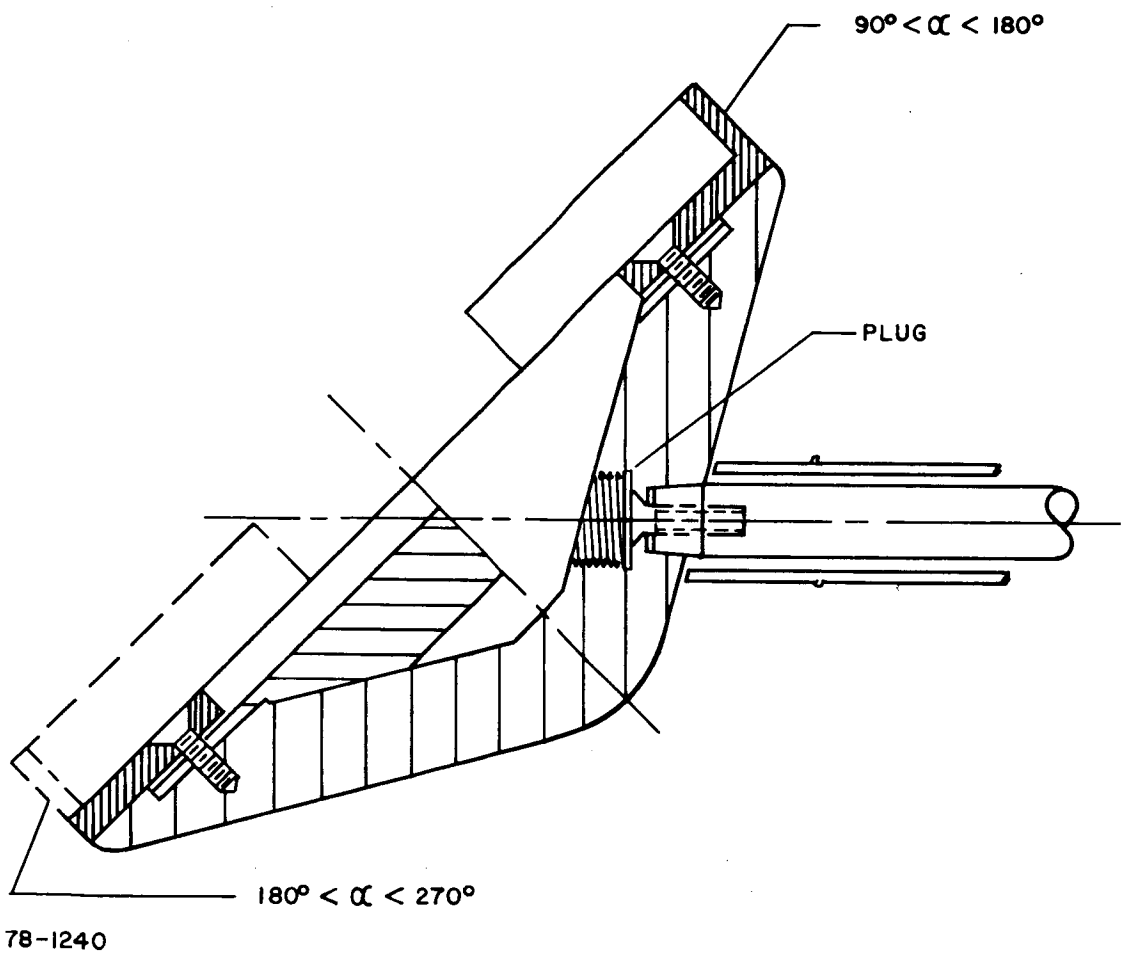

Figure 4.4-3 TEST MODEL -- STING ARRANGEMENT (B)

4.4.3 Test Program Definition

4.4.3.1 Wind Tunnel

The variation in the pitching moment coefficient will be obtained for a 60 degree blunt cone with fences or flaps at a Mach Number of 14 and a Reynolds Number per foot of 2×10^4 in the hypersonic wind tunnel (see Table 4.4-I). The angle of attack variation will be from 90 to 270 with emphasis on the minimum stability angle (this angle at present appears to be near that for which the flow is perpendicular to the fence). The pitch plane will be in the plane of symmetry of the fence as well as out of plane.

TABLE 4.4-I

ARC JET TUNNEL FLOW CONDITIONS

D	=	0.4
H_T	=	3000 Btu/lb
M	=	14
$R\infty/Ft$	=	21,000
$q\infty$	=	0.2 psi

4.4.3.2 Free Flight

Initial free flight tests (already in progress) will consider various turn-around devices. Free flight testing in the shock tunnel will be performed on the reference symmetrical and asymmetrical fence configurations or other fence configurations based on the results obtained in the wind tunnel tests and the initial free flight tests.

4.5 METHODS OF ANALYSIS

4.5.1 Aerodynamic Coefficients

The aeroshell aerodynamic evaluation relied wholly on the available data. Considerable test effort has been expended toward defining the aerodynamic coefficients for the blunt cone. These tests, encompassing the complete Mach Number range from subsonic to hypersonic speeds, are summarized in references 6 through 10.

The modified Apollo coefficients presented in Reference 11 have been adjusted for the flat base and in addition the data of Reference 9 have been incorporated into the analysis.

4.5.2 Pressure and Heating Distribution

The methods used to determine the pressure and heating distributions differ greatly for different parts of the IRV aeroshell. The discussion is therefore

divided into an aeroshell section concerned with the heating on the forebody of the vehicle, and an isotope capsule section wherein the heating to the heat source capsules is defined.

4.5.2.1 Aeroshell Analysis

The flow field about the sixty-degree blunt shape poses a difficult test for analytical techniques by virtue of the fact that the entire flow field is transonic. At hypersonic speeds, the bow shock lies very close to the body. The curvature of the shock in the nose region produces a sonic point very close to the central axis of the vehicle. The sonic point on the body, however, lies at the shoulder near the outer extremity of the flow. The sonic line, therefore, lies very close to the body over a considerable portion of the flow. This phenomenon suggests that any small disturbance, such as the presence of a thin boundary layer, will alter the flow. It must be assumed, however, that a steady-state, inviscid flow field exists. Further complicating the problem is the existence of the over-expansion region at the nose sphere-cone junction. At the transonic condition this over-expansion can cause the existence of a locally supersonic condition followed by a normal shock. This condition, complicated by the theoretically discontinuous velocity gradient at the junction is difficult to circumvent in computer-based calculation procedures. Inverse blunt body solutions generally are ruled out by the boundary condition that the body sonic point lie on the shoulder of the shape. And the near-sonic condition at the sphere-cone juncture often causes interaction techniques to diverge at this point unless the juncture is artificially smeared by use of an exponential fairing.

The forebody flow field and pressure distribution were obtained with a direct solution of the type given by Godunov, et. al. (Reference 23). This type of solution, as modified by Masson (Reference 24) incorporates the unsteady equations of fluid dynamics and describes the steady-state flow field as an asymptotic limit for long duration flight at a constant free stream condition. A floating mesh is employed which always covers exactly the shock layer. Given arbitrary initial conditions at all points on the network, the amount by which the data do not satisfy the equations of motion defines the time derivative of the flow field. The time derivative then determines a new set of values for the network. The flow field dynamics and ideal gas thermodynamics are therefore determined as time dependent functions. The actual pressure distribution used in these studies is modified from that presented in Reference 24 for various shoulder geometries. Coupling these pressure distributions with the free stream dynamic pressure history from the trajectory analysis provides the necessary information on aero-loads for design purposes, assuming a constant ratio of stagnation pressure to dynamic pressure. For air this ratio is approximately 1.98 over the hypersonic portion of the trajectory where maximum loads occur.

The same pressure distributions form a basic part of the data required to compute the aerodynamic heating distributions over most of the trajectories. The aerodynamic heating rates on the aeroshell are obtained from Avco computer code 873C on the basis of laminar similarity theory. The local heat transfer rate, in ratio to the stagnation point heat transfer is

$$\frac{\dot{q}}{\dot{q}_s} = \frac{\rho_w \mu_w U_e r^a}{2\,\frac{1+a}{2}\sqrt{\rho_{w_s}\mu_{w_s}\left(\frac{dU_e}{d_x}\right)_s \xi}} \left(\frac{1 + 0.096\sqrt{\beta}}{1.068}\right) \tag{1}$$

where, following reference 25.

ρ_w = density

μ_w = viscosity

Ue = velocity at edge of boundary layer

r = local body radius

$(dUe/dx)_s$ = stagnation point velocity gradient (modified Newtonian)

x = local surface distance

a = 0 for a cylinder, 1 for a sphere

and

$$\xi = \int_o^x \rho_w \, Ue \, \mu_w \, r^{2a} \, dx \tag{2}$$

$$\beta = \frac{2\xi}{Ue}\,\frac{dUe}{d\xi} \tag{3}$$

The computer program computes the thermodynamic state at specified body points using the pressure at that point and assuming the entropy remains constant, along the body streamline, at its normal shock value.

It has been found that the heating distribution obtained at various altitudes is sufficiently constant over the greatest portion of the trajectories, so that a single distribution usually suffices for the design evaluation. This distribution is, therefore, applied to the stagnation point heat pulse over the entire trajectory.

At extremely high altitudes, the stagnation point heat flux is computed, assuming purely diffuse free molecular flow, from

$$\dot{q}_s = \frac{1}{1556}\,\rho_\infty \, U_\infty^3 \left(\frac{BTU}{sec - ft^2}\right) \tag{4}$$

where

ρ_∞ = free stream density in slugs/ft^3

$U\infty$ = vehicle velocity in ft/sec

In the transition regime between free molecular and continuum flows, a semi-empirical expression, including vorticity interaction, provides the heating:

$$\dot{q}_s = k_1 Hs\, P_s^{1/2} \left(\frac{dUe}{dx}\right)_s^{1/2} [Erf(x)] \tag{5}$$

and

$$Erf(x) = k_z Z H_s k_{3z} \tag{6}$$

$$Z = f(P_s) \tag{7}$$

wherein

H_s = stagnation enthalpy

P_s = stagnation pressure

k_1, k_2, k_3 = constants

The constants are adjusted so that this expression for heating in the transition regime fairs smoothly into the free molecule and continuum values. The continuum heating is computed by the 1880 program from the semi-empirical expression

$$\dot{q}_s = (1.1 + 0.075M)\, k \sqrt{\frac{\rho_\infty}{U\infty}\left(\frac{dUe}{dx}\right)_s}\, (U\infty)^{3.909 - 0.0229M} \tag{8}$$

where

k = constant, and

M = molecular weight of the atmosphere.

This analysis, then, provides a definition of the heating distribution over the aeroshell in normal flight, i.e., at zero angle of attack. Since the vehicle may tumble over a portion of the trajectory, or may enter at $\alpha = 180^o$ which is a pseudo-stable position, the heating distribution at all angles of attack must be investigated. This is done by obtaining, at several aeroshell stations, the ratio of local heating to the stagnation heating rate on the nose at zero angle of attack ($\dot{q}/q_{so}$). This multiplier can then be applied to any trajectory stagnation heating pulse. In order to proceed with the analysis, the stagnation point must be located at all angles of attack. Between 0^o and 30^o, the

stagnation point lies on the nose cap of the vehicle, and the heating distribution may be taken as the equivalent tangent cone value. From 30° to nearly 90°, the stagnation point lies on the shoulder radius. At this point the heating is cylindrical in nature, and the distribution may be shown to be similar to that on a tangent wedge. At α = 90°, and beyond to nearly 180°, the corner at the maximum diameter of the vehicle becomes the stagnation point. If the corner is sharp, the heating at this point is theoretically infinite. But by assuming various corner radii, the heating levels can be calculated. Similarly to the shoulder position, the cylinder-tangent wedge approximation is used.

At any angle of attack other than zero, a portion of the aeroshell is shaded from the on-coming flow and effectively from the base of the vehicle in that attitude. The heating on this virtual base is a relatively low fraction of the overall heating, and therefore an approximation may be applied safely. Avco test data indicates a monotonic increase in heating from 0.04 $\dot{q}_{so}$ at the base center to 0.125 $\dot{q}_{so}$ at the outer edge of the base.

4.5.2.2 Isotope Capsule Analysis

The complex geometric configurations which comprise the several IRV base designs negate the use of computerized, or highly theoretical methods. Computer methods are generally limited to fairly simple geometries, and pure theoretical models would entail excessive time for the conceptual design purpose. Nevertheless, heating levels on the capsules must be obtained which are indicative of the actual levels to be encountered in flight, since the whole feasibility of the concept depends upon the survival of the isotope capsules. It should be stated strongly that no theoretical or practical approach can be entirely adequate for this purpose, and well instrumented, simulated ground testing is a necessity for a final design.

Pressure distribution, or aerodynamic loads, on the various capsule arrays can, in general, be ignored in the conceptual design phase. At any given altitude, the pressures experienced by the capsules will not exceed the nose stagnation pressure. After the vehicle has turned around, and the angle of attack is less than, say, sixty degrees, the capsule pressure level will not exceed three or four percent of stagnation value. These values suffice for design loads. Heat transfer considerations also do not require exact specification of pressure levels other than the stagnation value.

The heat transfer to several capsule arrays was investigated during the course of study. Those results were discussed above. The general ground rules for these analyses are discussed here. Published test data were relied upon as much as possible as a starting point for simple geometric shapes. Thus, the data of Nestler (Reference 22) and the data and very excellent matching theory of Marvin (Reference 26) provided the basic heating distributions for flat and concave cylinders, corresponding to a smooth-based IRV at 180 degrees angle of attack. For configurations where the capsule array protruded from the base, but did not disturb the shock shape (still at α = 180°), a simple linear interpolation of the velocity gradient between body and shock was assumed. Since

$$\dot{q}_s \sim \sqrt{\left(\frac{dUe}{dx}\right)_s} \qquad (9)$$

the heating was perturbed accordingly.

Where the capsule protruded beyond half a capsule diameter, heating to the capsule was increased by a factor of $\sqrt{2}$. The model for this was a simple cylinder in a potential flow corresponding to the subsonic flow over the vehicle base by which it may be shown that the local velocity (and therefore the stagnation point velocity gradient) is increased by a factor of 2. This factor is not applied to capsules which can be considered recessed relative to the vehicle base, since in this case the flow is more nearly uniform.

4.5.3 Stability and Performance

4.5.3.1 Fence Requirements

The vehicle design requirement for a single trim point necessitates the use of a fence or other device in order to prevent a trim point other than at zero angle of attack for the rearward entry conditions. This requirement is shown in Figure 4.5-1 for the flat base vehicle. The curve shows a trim point at α = 180 degrees and is stable about this point from 120 degrees to 240 degrees. If the vehicle should enter at any angle of attack between 120 and 240 degrees it would stabilize at 180 degrees. The corrective device must, therefore, provide a pitching moment capable of overcoming this stability. For a concave base shape the situation is similar except that the stable angle of attack range extends from 140 degrees to 220 degrees.

4.5.3.2 Fence Analysis

The fence configuration which was analyzed is shown in Figure 4.2-20 and is canted at some angle δ and located a distance R from the vehicle centerline. It extends over an arc angle of ϕ. The analysis assumed subsonic flow behind the shock impinging radially on the fence. The result of deflecting the fence provides a larger moment arm which increases the effective pitching moment coefficient. Newtonian flow was used for the data at angle of attack of 90 degrees. In order to determine the effective angle of attack on the deflected fence, it is necessary to know the streamline pattern. As no data was immediately available, two values were assumed, namely 20° and 30°, which appear to be realistic for the low deflection angles. It is possible, however, that for the high deflections the effective angle of attack may be higher, thus decreasing the pitching moment coefficient. A more detailed study of the streamline pattern is necessary to accurately determine the effective angle of attack. This analysis of the fence was applied to angles of attack from 90 to 180 degrees. The velocity vector is shown in Figure 4.2-20 as V_1. Angles of attack from 180 to 270 degrees depicted as V_2 in Figure 4.2-20 were analyzed by assuming that the outboard face of the fence was subjected to a pressure equal to stagnation pressure. The inboard pressure was determined by assuming an oblique shock with leading edge separation. The flow deflection angles due to separation were determined from Reference 27.

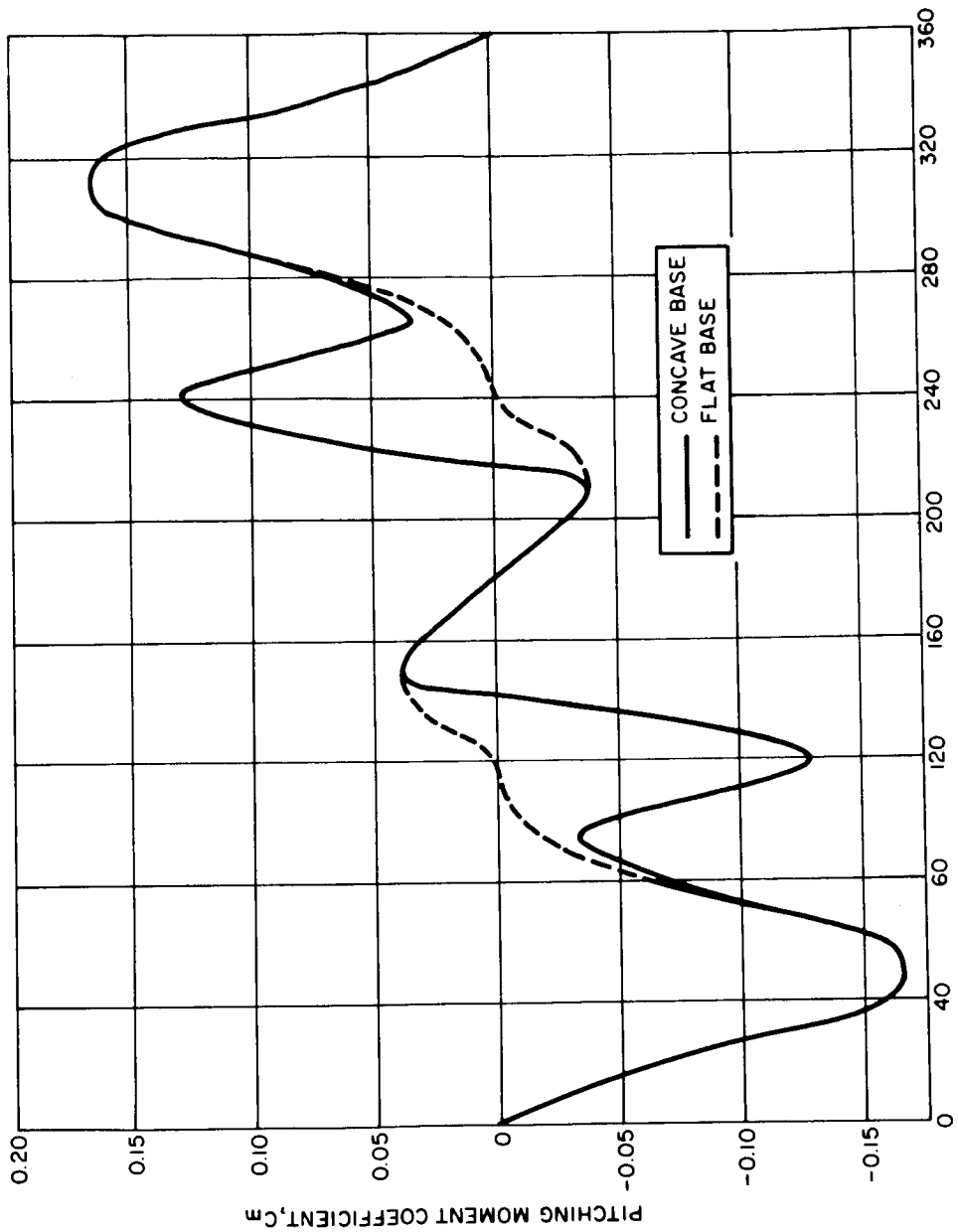

Figure 4.5-1 PITCHING MOMENT CHARACTERISTICS -- 60^0 BLUNT CONE

The analysis of the fence effectiveness has been expanded to include the changes in the pressure distribution on the vehicle base as a result of the addition of the fence. The two additional effects are the shadowing effect which is an adverse effect and the pressure buildup in front of the fence which produces a favorable moment. These base effects were determined by integrating the pressure distributions of Figure 4.5-2 at the particular fence location point, the outboard part being the shadowed effect and the inboard part the pressure increase over the configuration minus the fence.

4.5.3.3 Dish Effects

The effect of the shape change in the base area can be determined by comparing essentially two shapes; a flat base configuration to simulate the planar heat source arrays and a dished out base to simulate the concave heat source arrays. The effect of the dished out base is twofold; the effect on the basic body coefficients and its effect on the flow field impinging on the fence. The effects occur between angles of attack of 80 and 180 degrees and decrease the axial force, increase normal force and add negative pitching moment. The effect on the fence effectiveness is to reduce the effective angle of attack on the fence because of the reverse flow at the surface of the dish. The overall effect of the concave shape on the pitching moment can be seen in Figure 4.5-1. The angle of attack convergence will occur sooner in a trajectory if the area under the pitching moment curve can be increased. The concave area under the pitching moment curve is enlarged and the angle of attack convergence will occur sooner than for the flat base, assuming that the fence effectiveness is the same.

4.5.3.4 Turnabround Capability

The turnaround device must not only produce a single trim point but must rotate the vehicle fast enough so that it minimizes heating problems in the base area. From Reference 28 the turnaround time and the resulting oscillation for an atmospheric entry is a function of pitching moment coefficients, the mass characteristics and the vehicle size and shape. Within our present study for a fixed forebody shape and assuming fixed entry conditions, the turnaround time and oscillation for a tumbling body become a function of the parameter

$$\left(\frac{I}{ALC_{m_{max}}}\right) = k$$

where

I = Moment of inertia

A = Reference area

L = Reference length

$C_{m_{max}}$ = The maximum value of a sine curve evaluated so that its area equals the area under the actual pitching moment curve.

Using the pitching moment curves of Figure 4.5-1, the fence effects on the base pressure and the effect of the fence surface the value of $C_{m_{max}}$ can be determined.

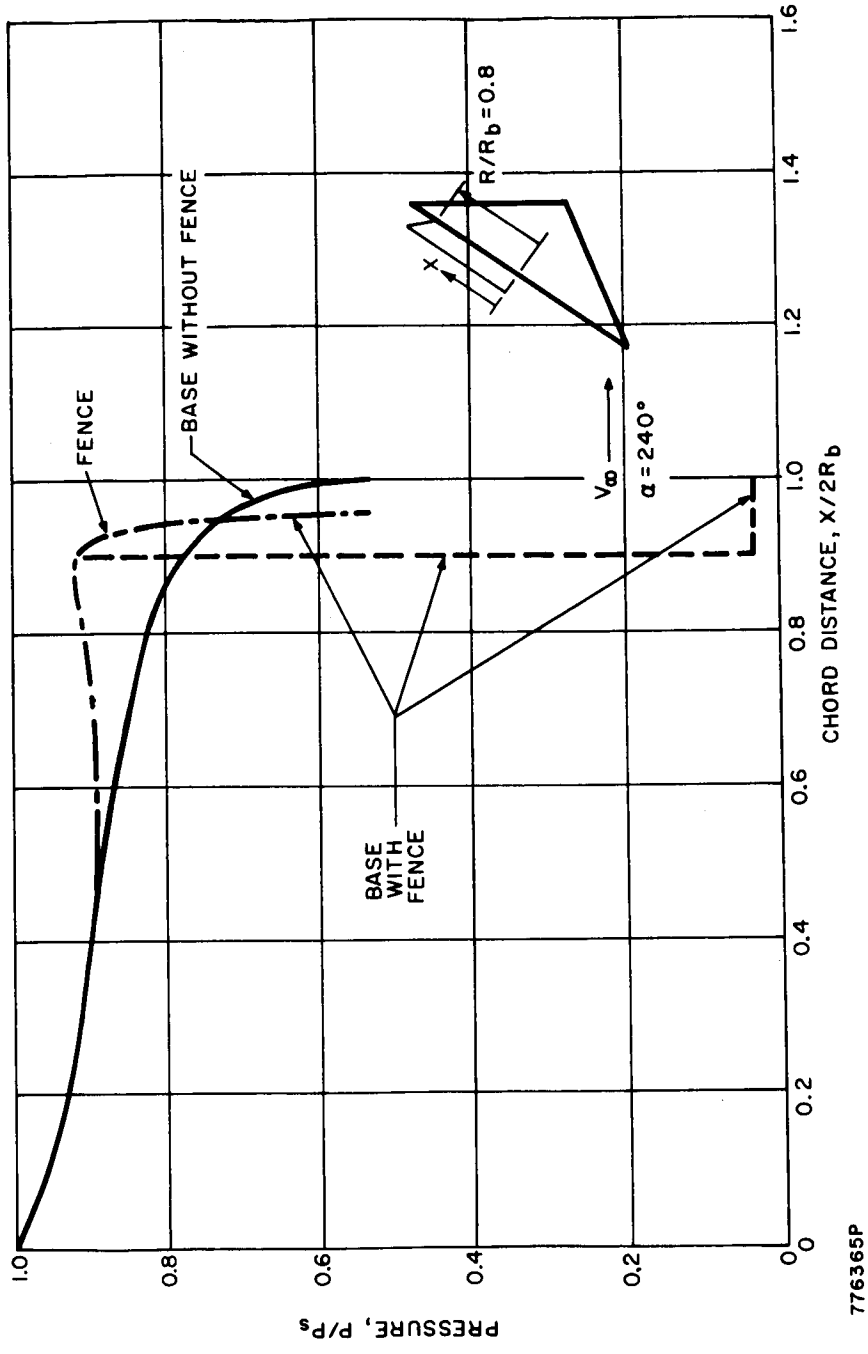

Figure 4.5-2 FENCE AND BASE PRESSURE DISTRIBUTIONS

This together with the physical characteristics of the vehicle configuration enables K to be determined. Various configurations can therefore be compared by using this parameter.

4.5.3.5 Symmetrical Fence

Four symmetrically located fences have been analyzed as a turnaround device.

Because the isotope capsules should not be exposed to a high heat pulse, the IRV must be turned around at high altitudes. The minimum altitude limit is a function of the reentry conditions, but will, in general, be specified to occur above 300 K ft. At these altitudes, the question arises of whether the flow about the IRV is continuous or free molecular in nature. The characteristics of the two flow regimes are entirely different, as indicated in Figure 4.5-3. Certainly free molecular flow will be encountered initially in reentry. And it is also quite possible that continuum flow will be encountered before the IRV turns around. Therefore, both cases, representing the practical extremes of performance, are investigated.

4.5.3.6 Continuum Flow

The continuum flow field shown in Figure 4.5-3 indicates, under the assumption of 2-dimensional flow along the surface center line, a strong shock wave standing forward of the RV and subsonic flow over the entire base region. The flow over the body surface is shown to separate from the leading fence and to re-attach to the base, and then to reseparate in the presence of a strong adverse pressure gradient due to the "aft" fence. An iterative procedure was utilized for the calculations. It was first assumed that the leading edge separation was supersonic and that the shock wave was attached to the fence. Brower's supersonic solution (Reference 29) was iterated for a free stream Mach Number of 30 and for several separation angles, and was found to be divergent, but with a trend toward convergence in the subsonic detached shock zone. The method given by Chapman, et al. (Reference 30) for the limiting case of subsonic flow was then applied and found to give reasonable results for the first separation zone. The subsonic character of the first separation zone requires that the second separation zone, which must be accompanied by a pressure rise, must also be subsonic. Currently, only supersonic laminar separation analytical techniques are available, and subsonic data are limited. Therefore, for the second separation zone, the subsonic pressure distributions of Charwat, et al. (Reference 31) were modified to accommodate the initial pressure level at the re-attachment point. The resulting pressure distributions over the IRV base are presented in Figure 4.5-4 for four fence lengths. Also shown is the Newtonian base pressure level (P_B/P_S) in the absence of a fence.

The fence pressures are taken as follows: P_1/P_S is assumed to be Newtonian: P_2/P_S is taken to be equal to the pressure level at an R/R_B of 1.0 to the windward side, or 0.624; P_B/P_S is equal to the base pressure at R/R_B =1.0 on the leeward side; and is variable; P_4/P_S is assumed to be zero.

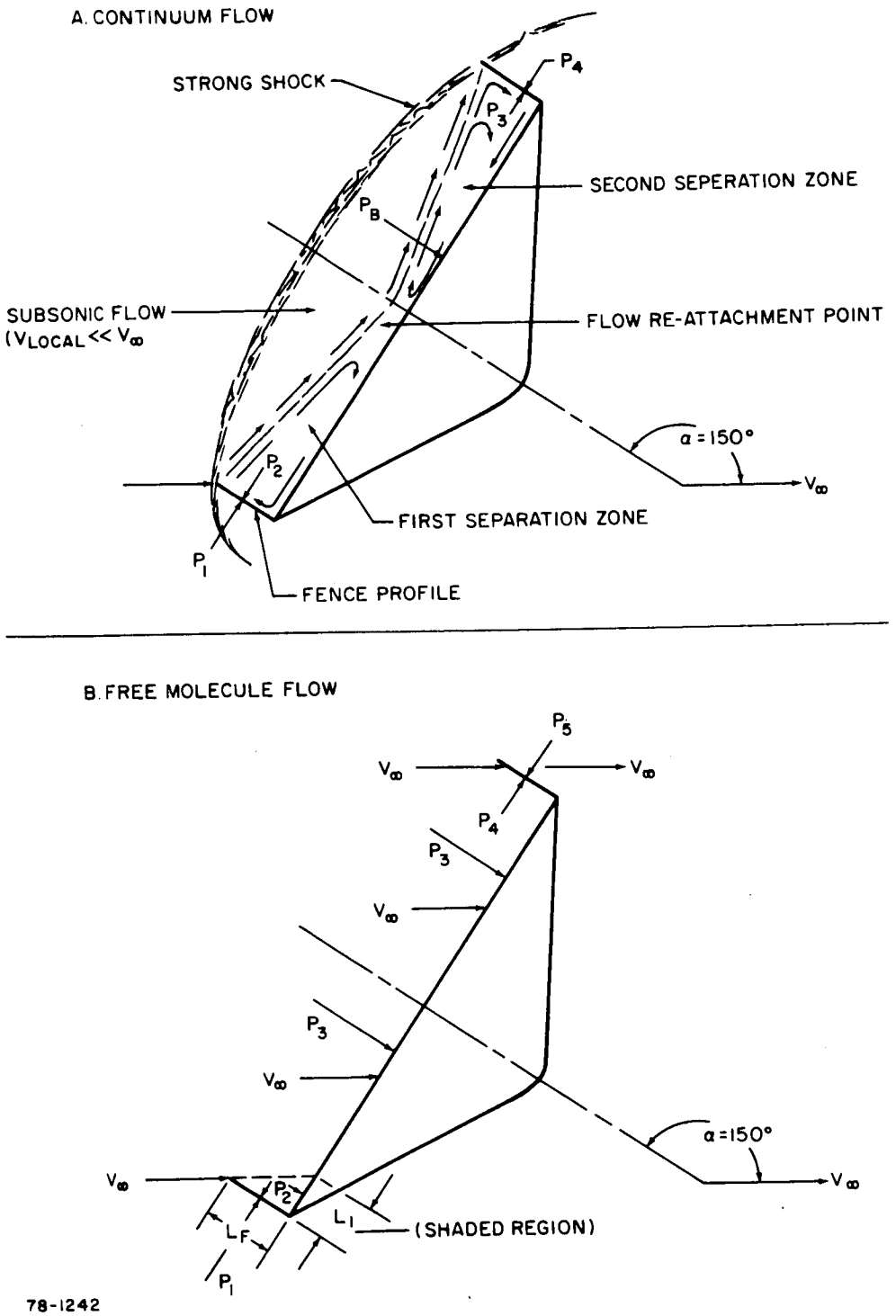

Figure 4.5-3 FLOW FIELD SKETCHES

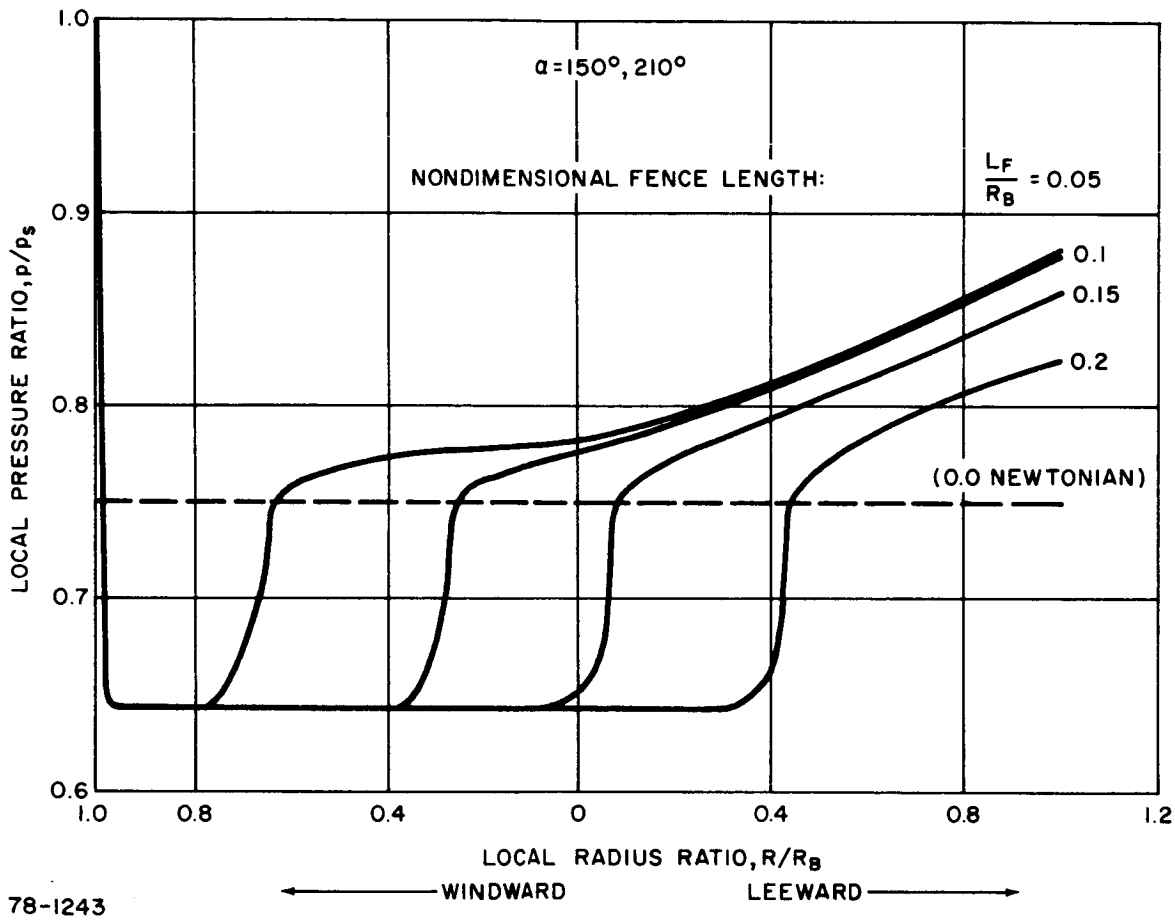

Figure 4.5-4 CONTINUUM BASE PRESSURE DISTRIBUTIONS

The moment coefficient due to fences may be written as

$$C_{m_{C.G.}} = \frac{P_S/q_\infty \sum M/P_S}{2\pi R_B^3}$$

where the ratio of stagnation pressure to free stream dynamic pressure is 1.94. With the vehicle center of gravity at the intersection of the central axis and the base plane, the moment sum in Equation 1 is expressed as

$$\sum M/P_S = \left[\frac{P_1}{P_S} - \frac{P_2}{P_S} + \frac{P_3}{P_S}\right] L_F^2 \sin\frac{\theta_F}{2} \sum\left(\frac{P}{P_S} - \frac{P_B}{P_S}\right) A_{B_{eff}} \bar{X}$$

where the first expression on the right side of the quality represents the fence contribution, and the right hand summation is an approximate form of the pressure-moment integral over the base.

4.5.3.7 Free Molecular Flow

A far less complex flow picture occurs under the free molecule premise. The fluid medium forward of the vehicle is sufficiently rarified that no shock wave or deflecting flow field is encountered at any point on the vehicle (Figure 4.5-3). The "free stream" impinges directly on all parts of the body except those hidden behind other body surfaces, and the local pressure can be expressed purely as a function of free stream conditions and local body geometry. At high velocities the pressure is given by:

$$P = (2 - f_n)\,\rho_\infty\,\phi_B^2\,\sin^2\theta$$

where θ is the local inclination of the body surface to the velocity vector, and f_n is the free molecule accomodation coefficient. Purely diffuse flow is assumed herein, for which

$$f_n = 1$$

On this basis the pressures acting on the IRV are computed to be

$$P_1/P_S = 0.25$$

$$P_2/P_S = 0$$

$$P_3/P_S = 0.75$$

$$P_4/P_S = 0.25$$

$$P_5/P_S = 0$$

These are the only pressures acting on the body: the forebody is hidden from the on-coming flow and therefore "feels" zero pressure, as also occurs in the areas on which P_2 and P_5 act. The shaded portion of the base is easily shown to be

$$L_1 = L_F \tan(\alpha - \pi/2)$$

and the moment equation becomes

$$\sum \frac{M}{P_s} = \left(\frac{P_1}{P_S} + \frac{P_4}{P_S}\right) L_F^2 \, R_B \sin \frac{\theta_F}{Z} + \frac{P_3}{P_S} L_F R_B \sin \left(\frac{\theta_F}{Z}\right) \tan \left(\alpha - \frac{\pi}{2}\right) \, 2R_B$$

$$- L_F \tan \left(\alpha - \frac{\pi}{2}\right)$$

This quantity is substituted into Equation 1 to obtain the moment contribution. It may be noted that without flaps, the moment contribution of the base is zero and the total moment coefficient for the body is also zero.

In free molecular flow, the pressure forces are generally low enough that the shear forces may represent an appreciable fraction of the total forces acting on the body. For this special case, however, where the vehicle c.g. lies in (or very close to) the base plane, it is easily shown that

$$\sum \frac{M_T}{P_S} = 0$$

4.5.3.8 Trim Angles of Attack for Asymmetric Fence

By adding a 180° fence to the aft surface of the IRV 60° blunted cone, the resulting reentry vehicle is asymmetric with respect to the central axis. With the fence weight component balanced to obtain a zero c.g. offset, the aerodynamic moment asymmetry will produce a trim angle of attack after the vehicle has righted itself. The purpose of this discussion is to present, on a somewhat crude basis, the values of trim angles to be expected for various fence geometries.

The sketch on Figure 4.2-22 defines the three geometric parameters varied in the study; these being h, the fence height, δ_F the fence protrusion angle, and R, the radius at which the fence is attached. The range of these parameters is as follows:

$$0 \leq h \leq 0.8 \, R_s$$

$$0.8 \leq R/R_o \leq 1.0$$

$$0° \leq \delta \leq 40°$$

The vehicle diameter was D = 5.75 feet and the c.g. location was assumed to lie in the base plane. A single flight condition was considered corresponding to the point where α becomes less than ten degrees for the V_e = 23,000 fps, γ_e = -10° entry trajectory. Free stream conditions were calculated for an altitude (Z) of 133,319 feet, and a velocity of 16,847 fps. The local flow conditions at the IRV shoulder were a Reynolds Number (R_{e_L}) of 2.2 x 10^5, a Mach Number (M) of 1.99, a pressure ratio (P/P_s) equal to 0.13; and boundary layer thickness (δ_o) of 0.08 ft, assuming laminar flow.

The method for obtaining the trim angle of attack is relatively straight-forward. One defines the incremental moment coefficient due to the fence as

$$\Delta C_{m_{C.G.}} = \frac{4}{\pi} \frac{P_S}{q_\infty} \frac{\sum M}{D_B^2}$$

Where the quantity $P_s/q_\infty = 1.94$, and the sum of the moments is

$$\sum M/P_S = \int \frac{P}{P_S} \times dA_{eff}$$

P/P_s = Local pressure ratio

A_{eff} = Effective area on which the pressure acts

X = Moment arm

This requires evaluation of the pressures on each side of the fence and on the base between the fence and the maximum body diameter. Except for the $R/R_B = 1.0$ geometries, a separated flow analysis is required. The methods of Erdos and Pallone, References 32 and 33, were used to define the separation geometry and pressures. The trim angle of attack was obtained from

$$\alpha_{TRIM} = \frac{\Delta Cm}{(Cm_\alpha)_o}$$

in which $(C_{m_\alpha})_o$ is the static stability at zero angle of attack. The trim angle of attack will, of course, be some value other than zero, so that the use of $(C_{m_\alpha})_o$ introduces an error because the pitching moment curve is non-linear. The error is small at small angles of attack (less than 30 degrees). At higher angles of attack a larger error occurs, but the results show the general order of trim angles to be expected.

5.0 IRV SUBSYSTEM DESIGN ALTERNATIVES

This section contains a discussion of the various subsystem design alternatives together with the analyses and trade-offs which are necessary to select the most promising concepts.

Under subcontract to Avco the Astronuclear Laboratory of Westinghouse Corporation is responsible for the heat source design and the Air Research Division of Garrett Corporation is responsible for the heat source heat exchanger (HSHX) design. Consequently, sections 5.1 and 5.2 have been provided in their entirety by Westinghouse and Garrett respectively. (It should be noted that both Garrett and Westinghouse were required to complete HSHX related parametrics to evaluate significant effects. This approach was necessary until sufficient initial data had been generated to provide a basis for more detailed analysis in Phase IB. For the same reason AVCO and Westinghouse both were required to develop initial analyses in the areas of impact attenuation and Heat Source/ aeroshell attachment.)

5.1 HEAT SOURCE

5.1.1 Design Requirements

The isotope heat source assembly discussed in this report consists of fuel capsules, capsule retention hardware, a heat source plate assembly, heat sink material, a thermal insulating system, an auxiliary cooling heat exchanger (ACHX) system for launch pad operation and heat source support structures. A number of heat source configurations and variations in these components were developed, resulting in a large number of heat source designs. In all cases, these designs were evaluated on the basis of several design criteria and goals. The basic design and safety ground rules followed were defined in the contract work statement and are shown in Tables 1.0-II and 1.0-III. Structural load criteria based on preliminary analysis are shown in Table 1.0-IV. The system modifications required to attenuate impact velocity induced loadings are discussed in section 5.4 following.

Long-term operation at high temperature and stress necessitates the use of refractory metal alloys for the fuel capsule, retention hardware, and the heat source structure. This requires that the ACHX maintain the heat source assembly at temperatures below 600° F to prevent oxidation during ground handling and launch pad operation.

Besides these design requirements, there are several additional performance objectives for an optimum design:

a. Minimum heat source (and IRV) size

b. Minimum heat source weight

c. Provision of a favorable center of gravity location (as near to the IRV nose as possible)

d. Ease of assembly and handling

e. High reliability.

Since the heat source is thermally coupled (by radiative heat transfer) to the heat source exchanger (HSHX) with an in-place redundant unit, the heat source design (and configuration) must be compatible with the HSHX design and preferably simplify the design of the HSHX. It is also necessary to provide an acceptable load transmission path to the aeroshell to avoid localized loads and local high temperatures. A tentative temperature limit of 300° F was used at the reentry vehicle interface (backside of honeycomb structure).

Efforts were made to reduce the thermal losses through the heat source sides of the insulation system to less than about 600 watts, since it was anticipated that the heat loss on the HSHX side would be substantial due to the penetration of the insulation with relatively large diameter pipes.

The fuel capsule used for these design studies is the ORNL non-vented design defined in the contract work statement (Figure 5.1-1). No modification of the fuel capsule was made. The nominal number of capsules required for the heat source is 164.

5.1.2 Candidate Designs

5.1.2.1 Overall Configuration

After a series of preliminary studies, six candidate configurations were selected for continued investigation:

1. A circular planar heat source with a 60 degree cone aeroshell (Figure 5.1-2)

2. A rectangular planar heat source with a 60 degree cone aeroshell (Figure 5.1-3)

3. A conical heat source with 60 degree cone aeroshell (Figure 5.1-4)

4. A conical heat source with centrally located recovery and abort rocket space within a 60 degree cone aeroshell (Figure 5.1-5)

5. A rectangular planar "pin cushion" array (capsules standing on end, with HSHX penetrating between rows of capsules) heat source with a 60 degree cone aeroshell (Figure 5.1-6)

6. A reduced diameter, circular planar, heat source with a 60 degree cone aeroshell (Figure 5.1-7)

Configuration 1 (circular planar) is the simplest heat source design and is rather straight-forward to fabricate and handle. The ACHX system can be easily provided because of simplicity of aligning coolant channels within the linear capsule arrangement.

Configuration 2 (rectangular planer) and its variations were studied because of potentially more efficient utilization of volume for recovery aids which might result in a relatively smaller overall IRV diameter.

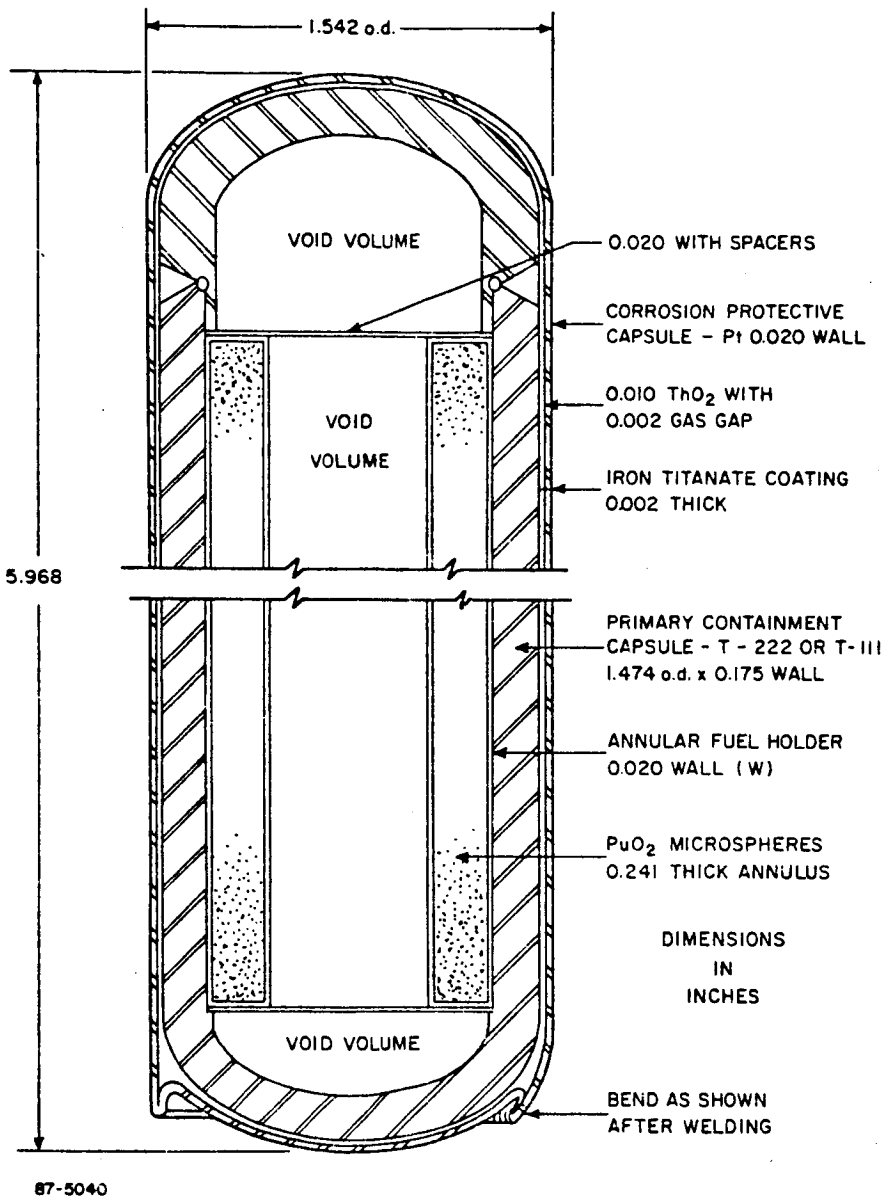

Figure 5.1–1. Conceptual Design of the Pu-238 Fueled Capsule - 164 Capsules Required

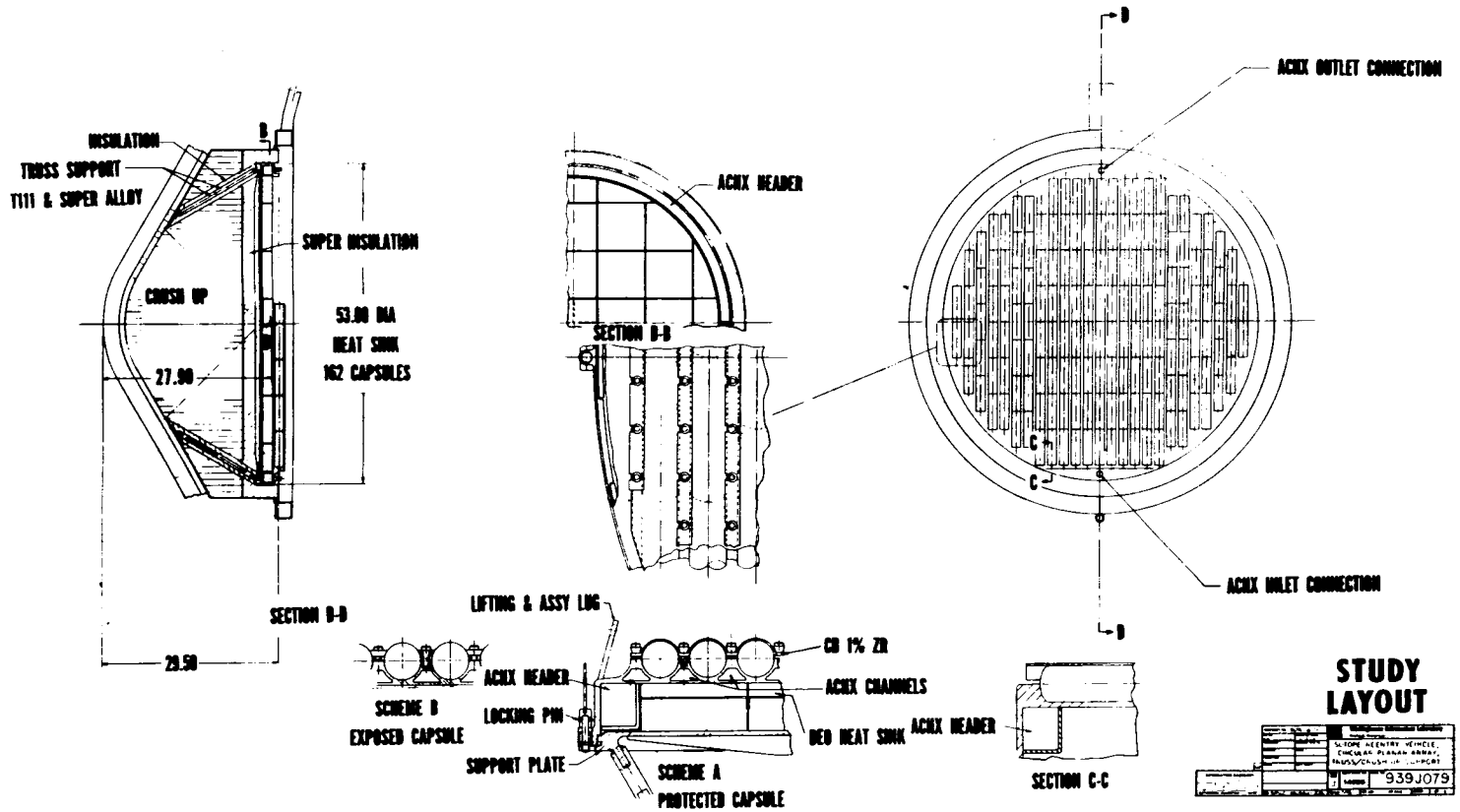

Figure 5.1–2. Circular Planar Heat Source

Configuration 3 (conical arrangement) results in the most favorable location of the center of gravity as anticipated. The conical support plate structure also offers a more rigid structure compared to the circular or the rectangular planar arrangements. Some of the drawbacks are that it is a more complex structure to fabricate, and its geometry offers less available volume for impact attenuating material. This geometry requires a more complex capsule arrangement to minimize the wasted space, and as a result the design of the ACHX coolant channels is more difficult than in the planar designs.

Configuration 4, resulted from a desire to incorporate a single abort rocket and recovery aids at the center of IRV. The notable drawbacks with the central recovery aid location are larger heat loss and excessive weight, as well as difficulty in keeping these recovery aids and the rocket at a relatively low temperature ($<300^{o}$ F) during the long-term normal operating conditions.

Configuration 5, the pin cushion design, is potentially the most compact and light-weight design. A compatible HSHX design has each row of capsules surrounded by a primary HSHX on one side and a secondary HSHX on the other. This results in constant thermal performance regardless of whether the primary or secondary heat exchanger is in operation. On the other hand, this configuration presents a more complex mechanical interface with HSHX.

The maximum capsule temperatures under launch pad and normal operating conditions are somewhat higher than the other designs but are acceptable. A major difference in design of the pin cushion arrangement is the use of graphite heat blocks rather than the refractory metal alloy heat source support plate with beryllium oxide heat sink design used for all other configurations.

Configuration 6 represents an attempt to tightly package the fuel capsules, thereby minimizing heat source diameter. The theoretical minimum diameter of this circular planar arrangement is about 47.0 in., corresponding to the capsule spacing of 1.6 in. between centerlines. Preliminary investigation indicated that this is only achievable at the cost of a significant increase in ΔT between the HSHX side and the ACHX side of the capsule wall. This temperature difference as a function of capsule centerline spacing has been calculated and is shown in Figure 5.1-8. (The optimum design appears to be at 1.75-inch capsule spacing, which gives a 4-inch reduction in heat source diameter, when compared to Configuration 1, at the expense of 25^{o} F in peak capsule temperature.)

5.1.3 Heat Source Component Design Study

Exploratory design analysis of the key components of an isotope heat source have been completed and are presented here in support of the development and comparison of candidate heat source designs. The components to be discussed in the order of presentation are as follows:

1. Fuel capsule
2. Capsule Retention System
3. Heat Source Plate Structures

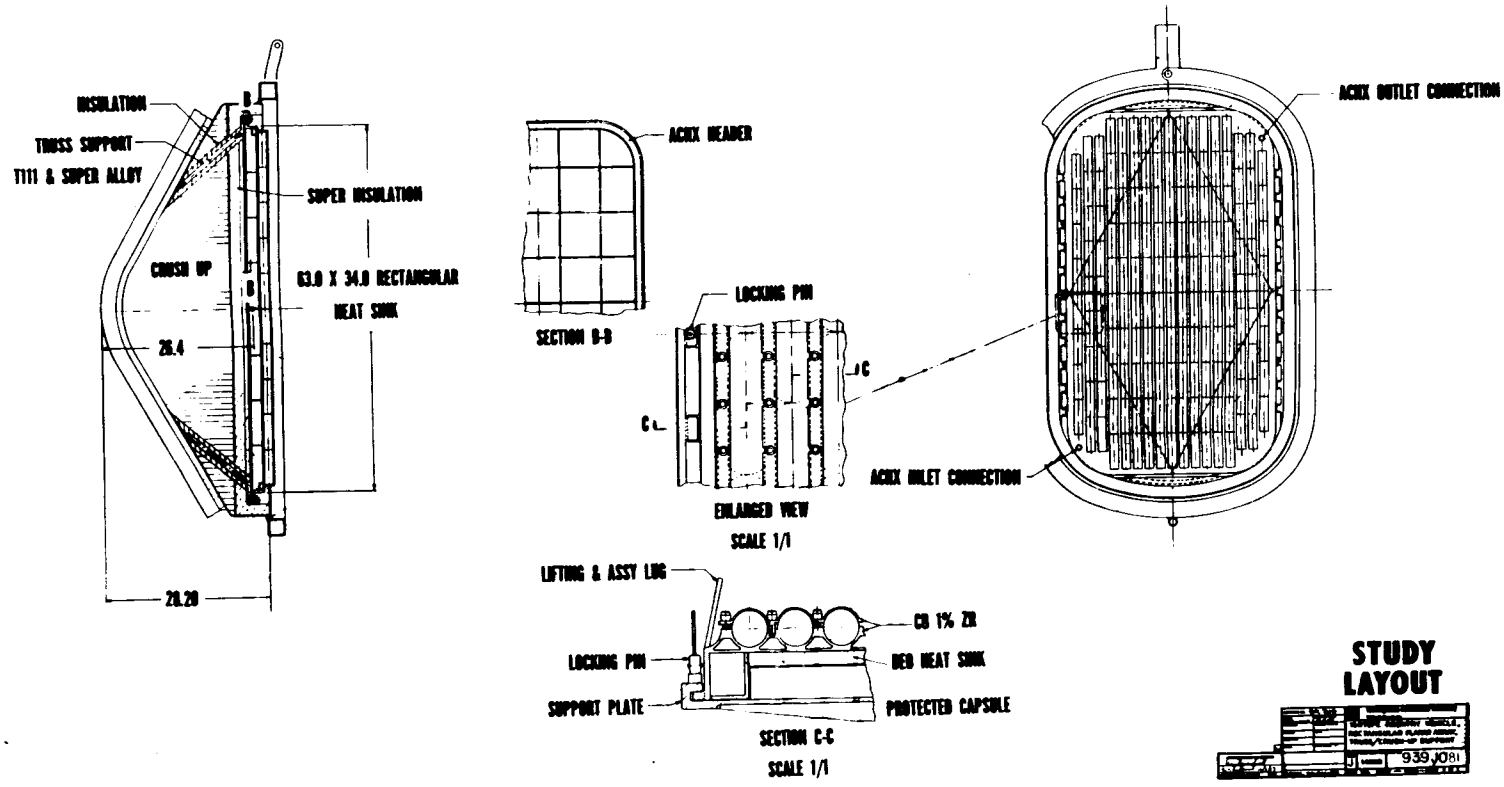

Figure 5.1–3. Rectangular Planar Heat Source

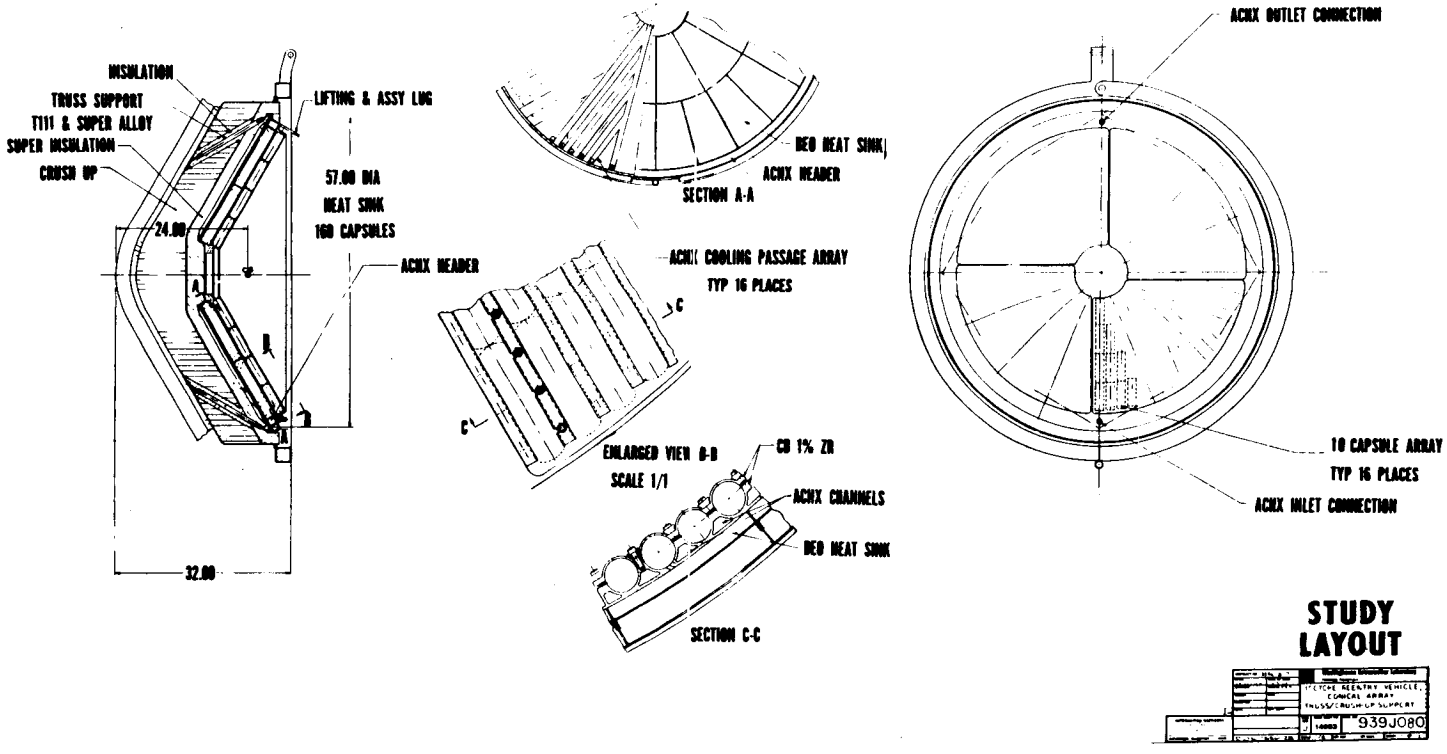

Figure 5.1–4. Conical Heat Source

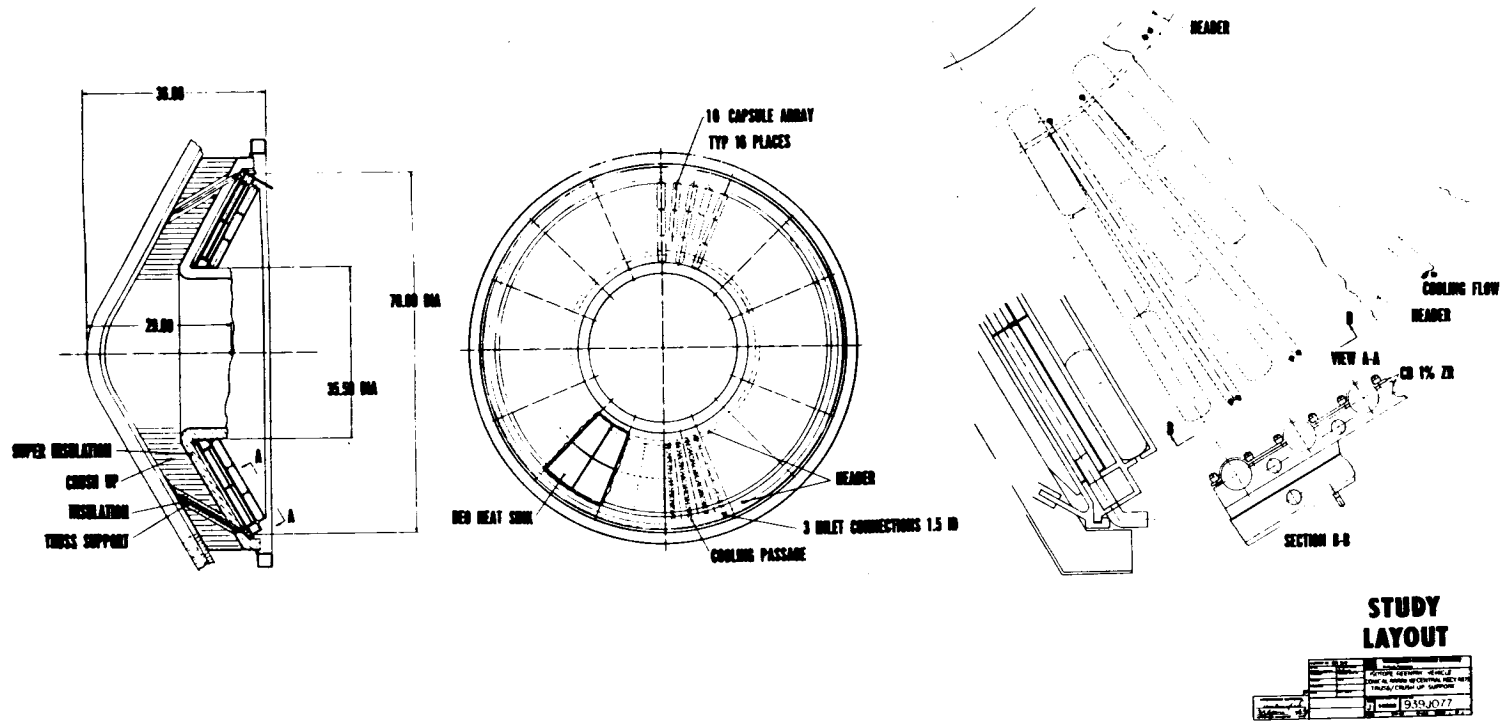

Figure 5.1–5. Conical Heat Source with Centrally Located Recovery and Abort Rocket Space

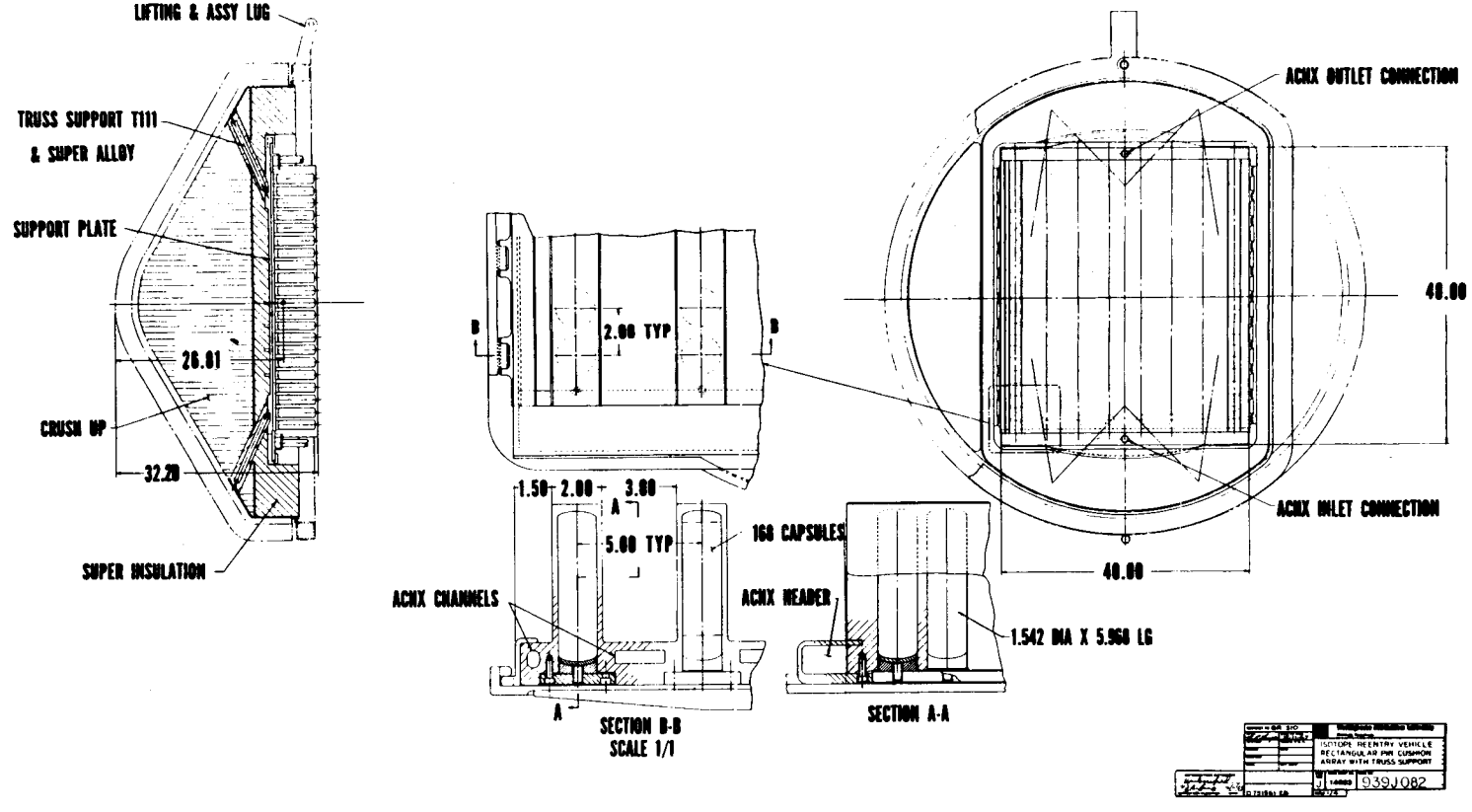

Figure 5.1–6. Rectangular Planar "Pin Cushion" Array Heat Source

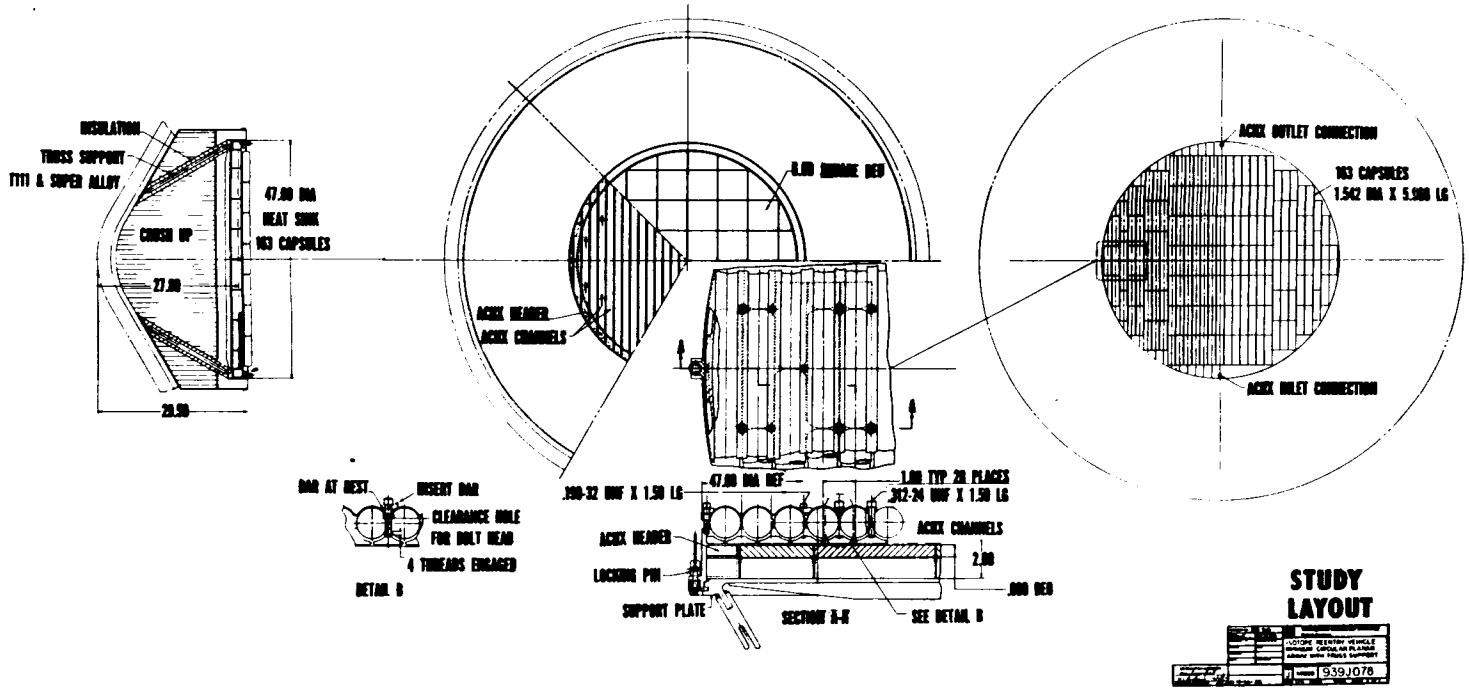

Figure 5.1–7. Reduced Diameter, Circular Planar Heat Source

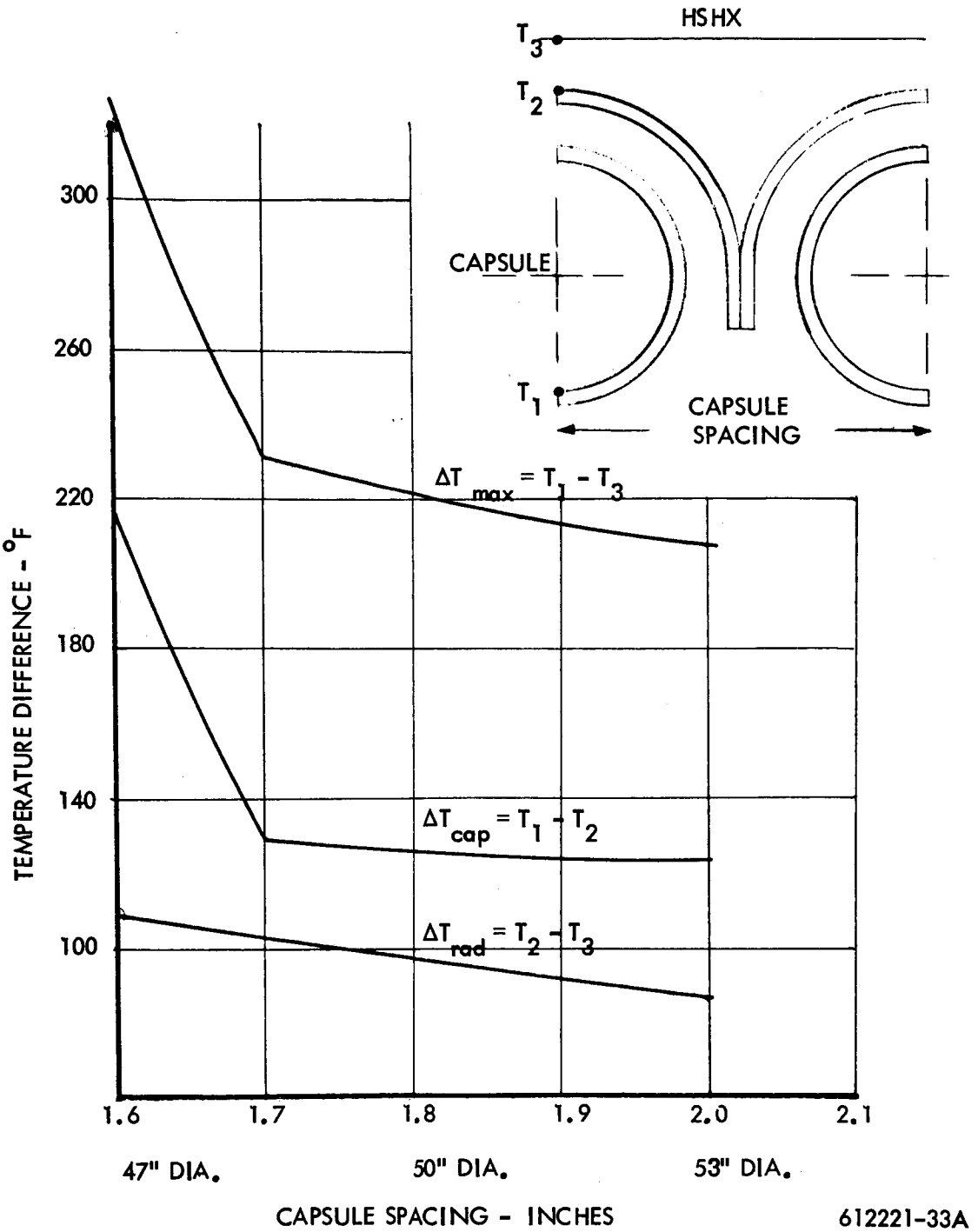

Figure 5.1–8. Effect of Capsule Spacing on Peak Capsule Temperatures

4. Heat Sink

5. Insulation System

6. Auxiliary Cooling Heat Exchanger (ACHX)

These components are illustrated in a typical configuration Figure 5.1-9.

A brief mechanical design description is followed by structural and thermal analysis. However, it is not always convenient to separate thermal analysis by component, and where necessary, thermal analyses including more than one component are grouped under a convenient component heading. Consequently, reentry heating analysis is presented under the capsule retention system. Similarly, thermal loss analyses, including those through the heat source support structure, are presented under the insulation system.

5.1.3.1 Fuel Capsule

5.1.3.1.1 Mechanical Design -- Pu-238 was selected as the fuel for this application in order to meet the long-term service life (five years) and to minimize the heat source system weight. A prior safety consideration that the fuel capsule be designed for absolute containment of the fuel for 10 half-lives (890 years) under all operating or abort conditions, including ground impact, ground burial, and ocean immersion, led to a capsule design as shown on Figure 5.1-1 previously.

The basic capsule design shown employs a multi-layer capsule construction where each layer of material is optimized for specific functions; that is,

a. a fuel liner material is selected for chemical compatibility with the fuel (W);

b. a container structure material is selected mainly for desirable creep rupture properties and strength at high temperature with a thick wall for impact survival (T-111, T-222); and

c. a noble metal clad is selected to protect the container structure from oxidation (Pt or Pt plus Rh).

The container structure is coated with a diffusion barrier (such as Al_2O_3 or ThO_2) to prevent embrittlement of the container structure, while the outside surface of the oxidation resistant cladding is coated with a high emittance material to enhance the radiative heat transfer.

5.1.3.1.2 Impact Analysis -- The fuel capsule is the most critical component of the IRV during impact. Failure or deformation of any IRV component can be tolerated with the exception of the fuel capsule. The integrity of the capsule must be maintained.

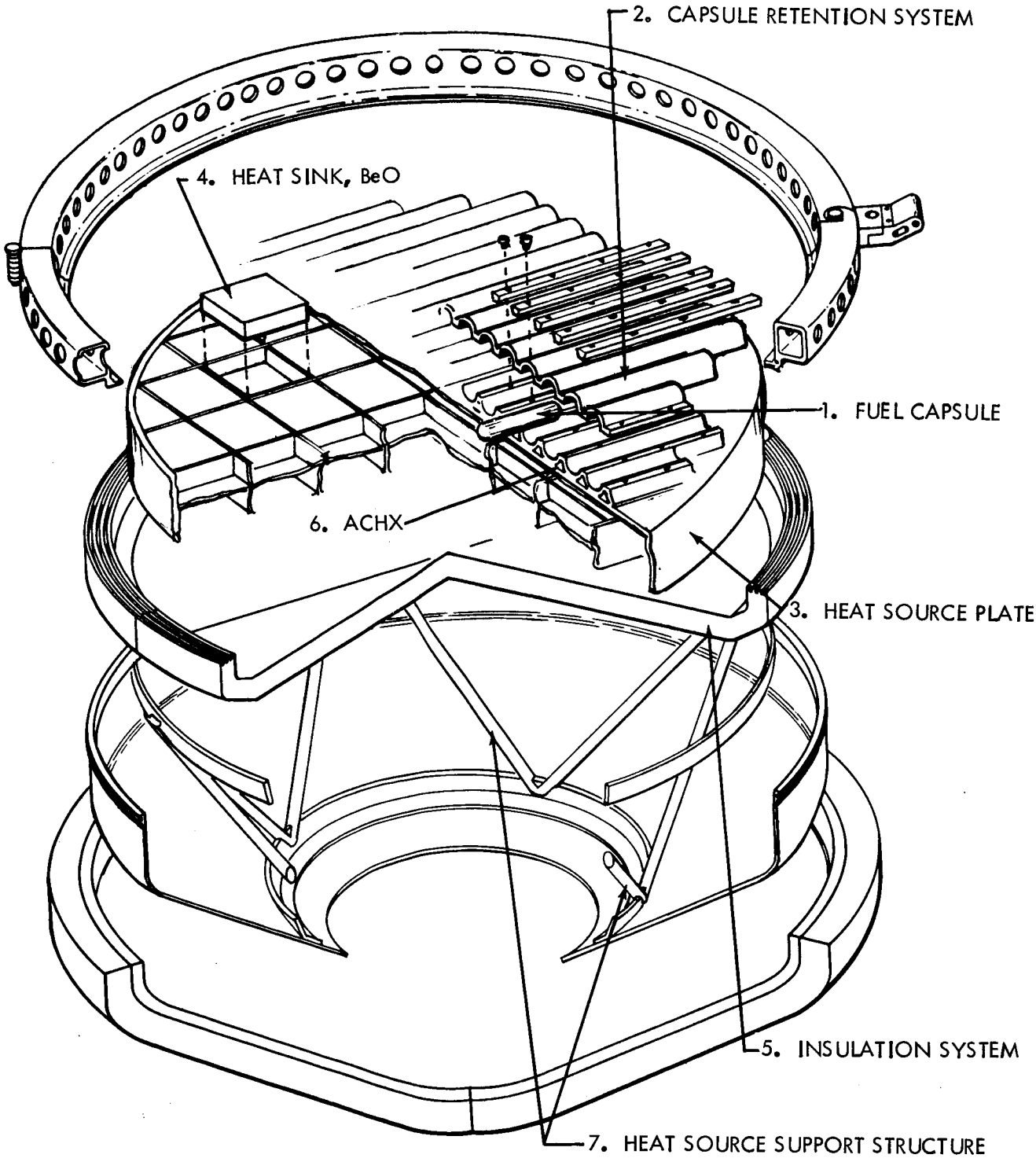

Figure 5.1–9. Circular Planar Array Exploded View

A brief analysis of the capsule structural response has been completed during Phase IA. The results of this analysis have been factored into the development of the impact attenuation scheme detailed in Section 5.4. Appendix A treats the analytical approach employed in evaluating capsule behavior. It should be noted that a truly comprehensive study of capsule response during impact should include an impact test program.

The results of the analysis are summarized in Figure 5.1-10. They indicate that a uniform cradle support is superior to any flat surface support, and suggest that 1100g is the minimum capsule impact load capability. It should be noted that the ORNL capsule seems to be able to survive a head-on impact velocity consistent with worst case terminal velocity of the IRV at impact (150-200 fps).

5.1.3.2 Capsule Retention Systems

Preliminary evaluation of various capsule retention schemes resulted in the choice of two classes of retention for protected capsule and exposed capsule designs as shown in Figure 5.1-11. These designs are applicable to all configurations described in previous sections except for the pin cushion array. Reentry heating analysis indicates some advantage of the protected capsule design (cover plate) over the bare capsule design. Also, when one considers that loss of several retention bolts during reentry could disperse capsules in the upper atmosphere in the case of the bare capsule retention, the cover plate design offers considerably increased reliability of intact reentry. Both designs can be adequately cooled by the ACHX during the launch pad operation. A typical temperature distribution with air coolant is shown in Figure 5.1-12.

With the pin cushion array, it was felt that a graphite block type structure, rather than a metal structure, will yield a simpler and light-weight design. A conceptual design is shown in Figure 5.1-13, indicating vertical and horizontal orientation of capsules. Precise reentry heating information is not available for this design to date. Based on the reentry heating rate data for the other configurations, the capsule heating problem would appear to be comparable to the cover plate design. Thermal analysis under a launch pad condition reveals some temperature penalty at the top of the graphite block as shown in Figure 5.1-14. However, this design also meets the criteria of maintaining heat source maximum temperatures below 600° F.

A discussion of the mechanical and thermal characteristics of candidate capsule retention schemes follows. The thermal analysis of backside heating effects on capsule retention and capsule is also described. This analysis is based on reentry heating inputs described in section 4.0. It includes a review of the heating history consistent with the various possible systems failure modes.

5.1.3.2.1 Capsule Retention System - Mechanical Design -- One fuel capsule retention scheme considered is based on attaching a tubular holder to the fuel plate, with a 1-inch-wide by 1/16-inch-thick Cb 1 percent Zr strip in semicircular corrugated clips. These clips were fastened to the surface of the heat support plate by plug welding in the corrugations. Securing the capsules in the tubular holder was accomplished by deforming an omega-shaped longitudinal upset on the tubular holders and crimping off the ends.

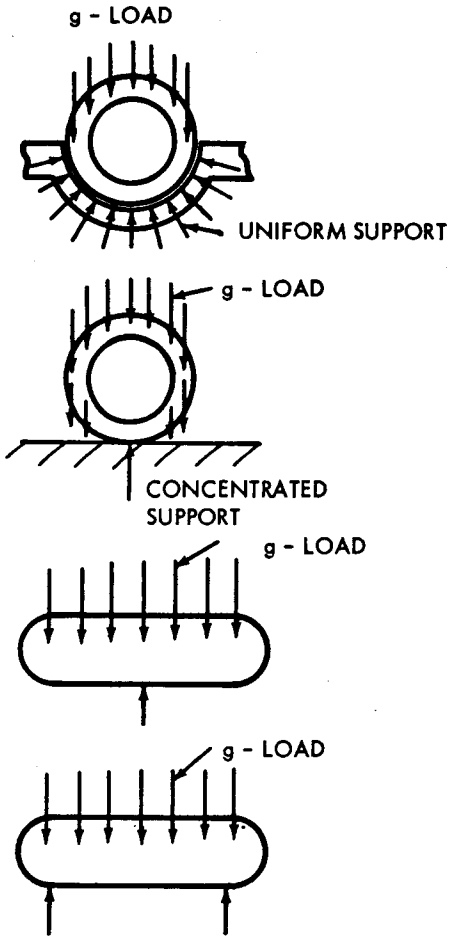

		g-LOAD
1	UNIFORM CRADLE SUPPORT	> 27,300g
2	CONCENTRATED SUPPORT FROM FLAT PLATE	1110g
3	BENDING LOAD-CENTER SUPPORT	2800g
4	BENDING LOAD-SUPPORT AT ENDS	2800g

NOTE: EFFECT OF INTERNAL PRESSURE INCLUDED

612204-1B

Figure 5.1–10. G-Load Capability of Capsule Side-On Impact

PROTECTED CAPSULE

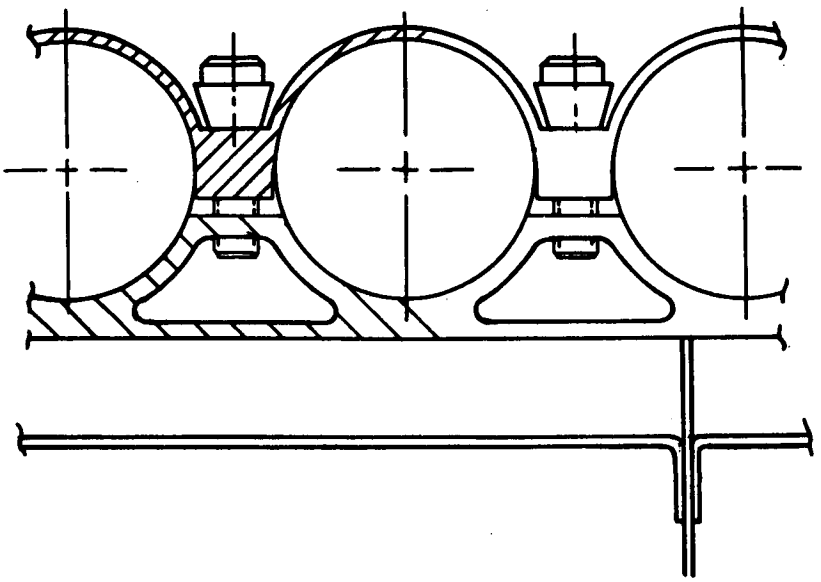

EXPOSED CAPSULE

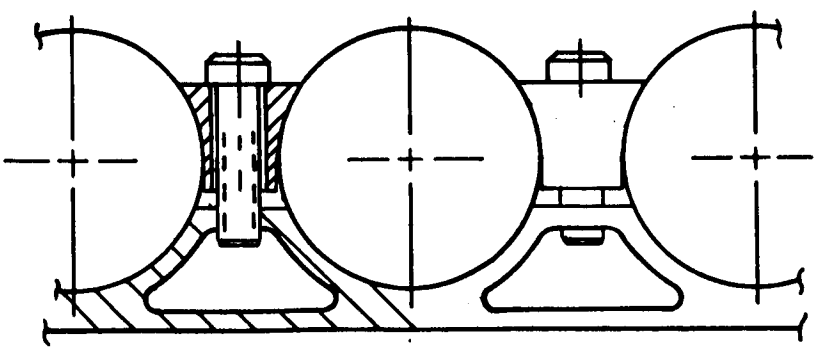

612221-2B

Figure 5.1-11. Retention Schemes

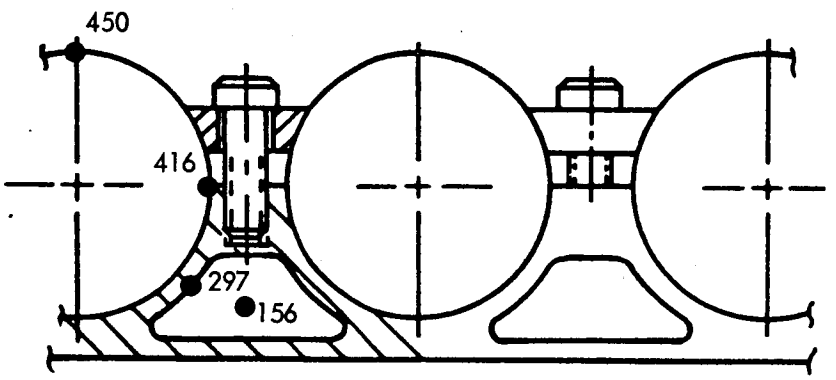

612221-24B

Based on Coolant Inlet Temperature of 80°F.

Figure 5.1–12. Capsule Temperature Distribution at Heat Source Hot Spot Circular Planar Array – ACHX Operation

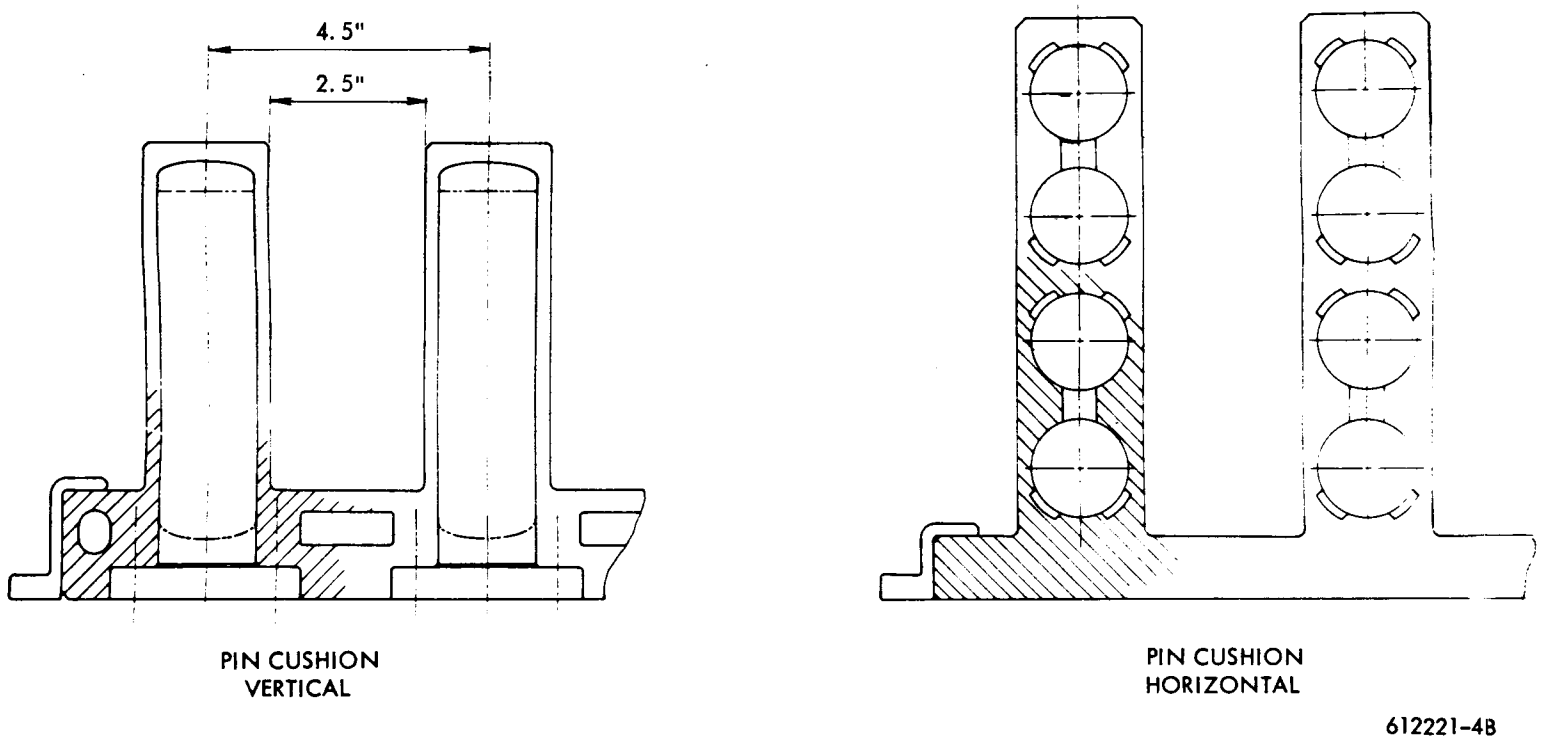

Figure 5.1–13. Retention Schemes

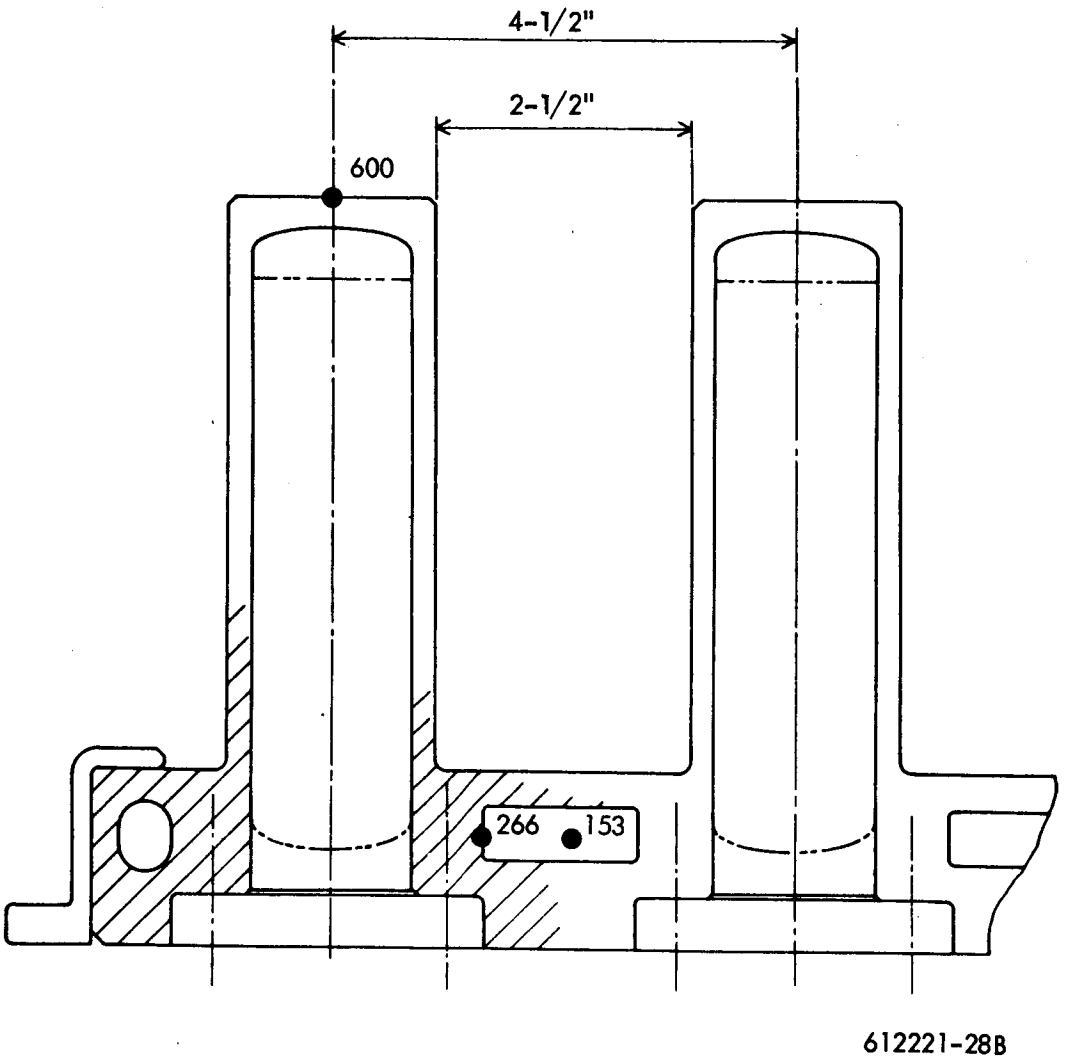

Based on Coolant Inlet Temperature of 80°F

Figure 5.1–14. Capsule Temperature Distribution at Heat Source Hot Spot Pin Cushion Array – ACHX Operation.

Although flattening the upset reduced the diameter of the tubular holders, thus holding the capsules in place, the differential coefficient of thermal expansion between the fuel capsule and the capsule holder and the long term creep at operating temperatures could loosen the capsules in holders. Problems of capsule movement during the life of system were anticipated. These problems, together with the launch pad cooling and remote handling problems dictated sophisticated retention system designs.

Early designs included both "bare" and covered capsule retention. In both schemes the capsules were retained in grooved channels. For the "bare" capsules retention was achieved by a triangular shaped bar which exposed the major portion of the capsule surface area, (Figure 5.1-15 and 5.1-16). In the covered case retention is achieved by a corrugated plate which completely contains the capsule (Figure 5.1-17). In both cases, a bolted locking bar was used to sandwich in the capsules between the heat source plate and the retention mechanism. Figure 5.1-18 shows a retention scheme generated for planar designs, in which the capsules are contained within a heat block of BeO or graphite.

Pyramidal and pin cushion retention schemes were also generated, including the bare and protected capsule type, and a heat block concept. Figure 5.1-19 and 5.1-20 show the bare and protected configurations relying mainly on a tie bolt to contain the capsules. Launch pad cooling and reentry heating create problems with these concepts and therefore a heat block system was developed. This consists of capsules located in vertical rows within a graphite block, as shown in Figure 5.1-13. The capsules are loaded from the bottom of the heat source and retained with a graphite plug bolted at the base.

The final selection of a retention scheme, for the circular planar, and conical arrays from the mechanical standpoint has been based on the advantages and disadvantages of the three (3) schemes investigated. From this the choice was the covered capsule, which offered the maximum protection to the capsules with only a minimal weight penalty.

Bare Capsule

Advantages	Disadvantages
Light weight	Possible capsule damage during impact.
Capsule distribution $\Delta T = 75^{o}$ F	Possible scatter of capsule during re-
Simple assembly	entry if hold down bolts are lost.

Covered Capsule

Advantages	Disadvantages
Capsule protection during reentry.	Higher capsule distribution ΔT = 105F.
Simple assembly.	Heavier weight.
Capsule protected at impact.	

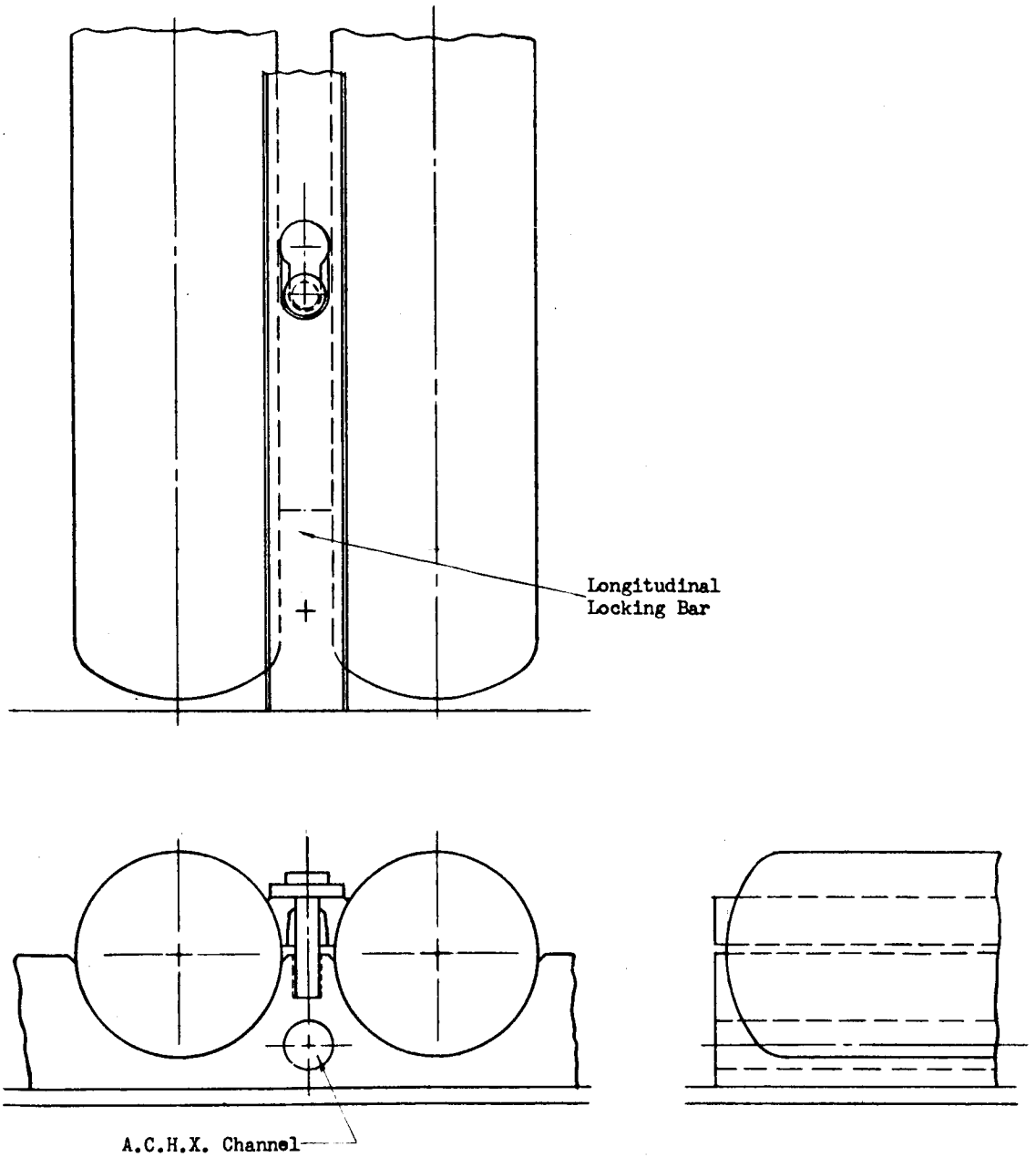

Figure 5.1-15. Exposed Capsule

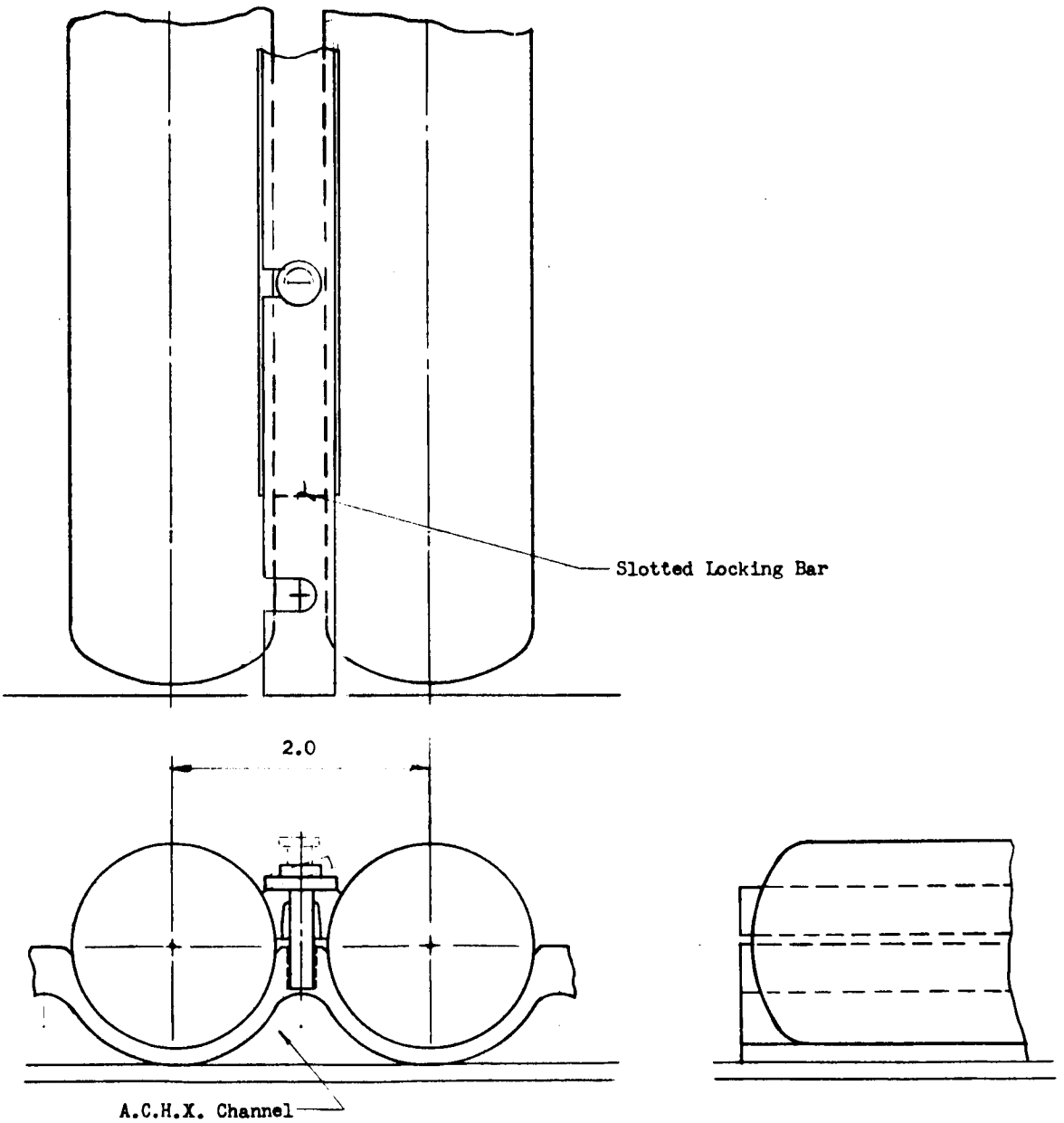

Figure 5.1-16. Exposed Capsule

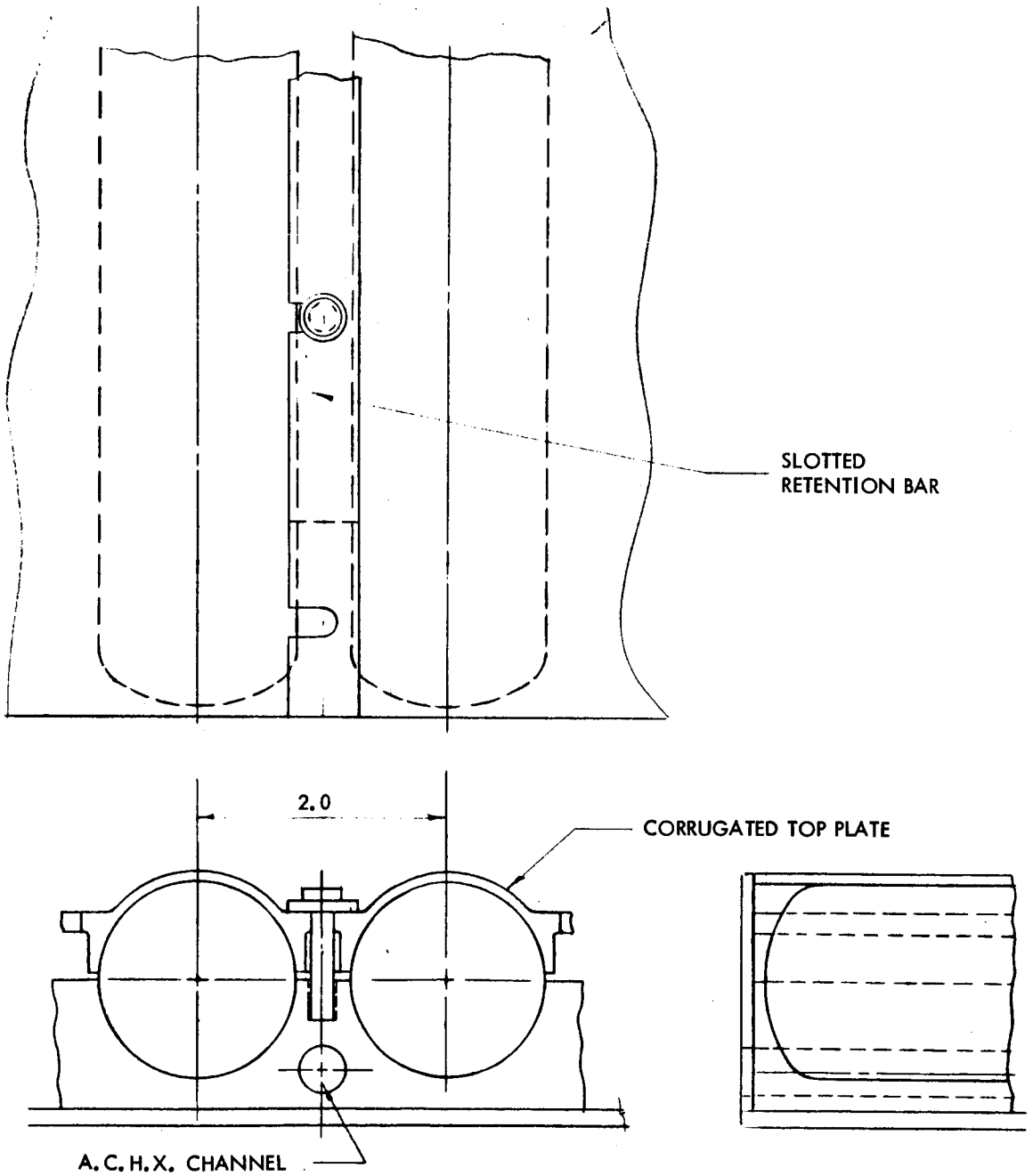

Figure 5.1-17. Protected Capsule

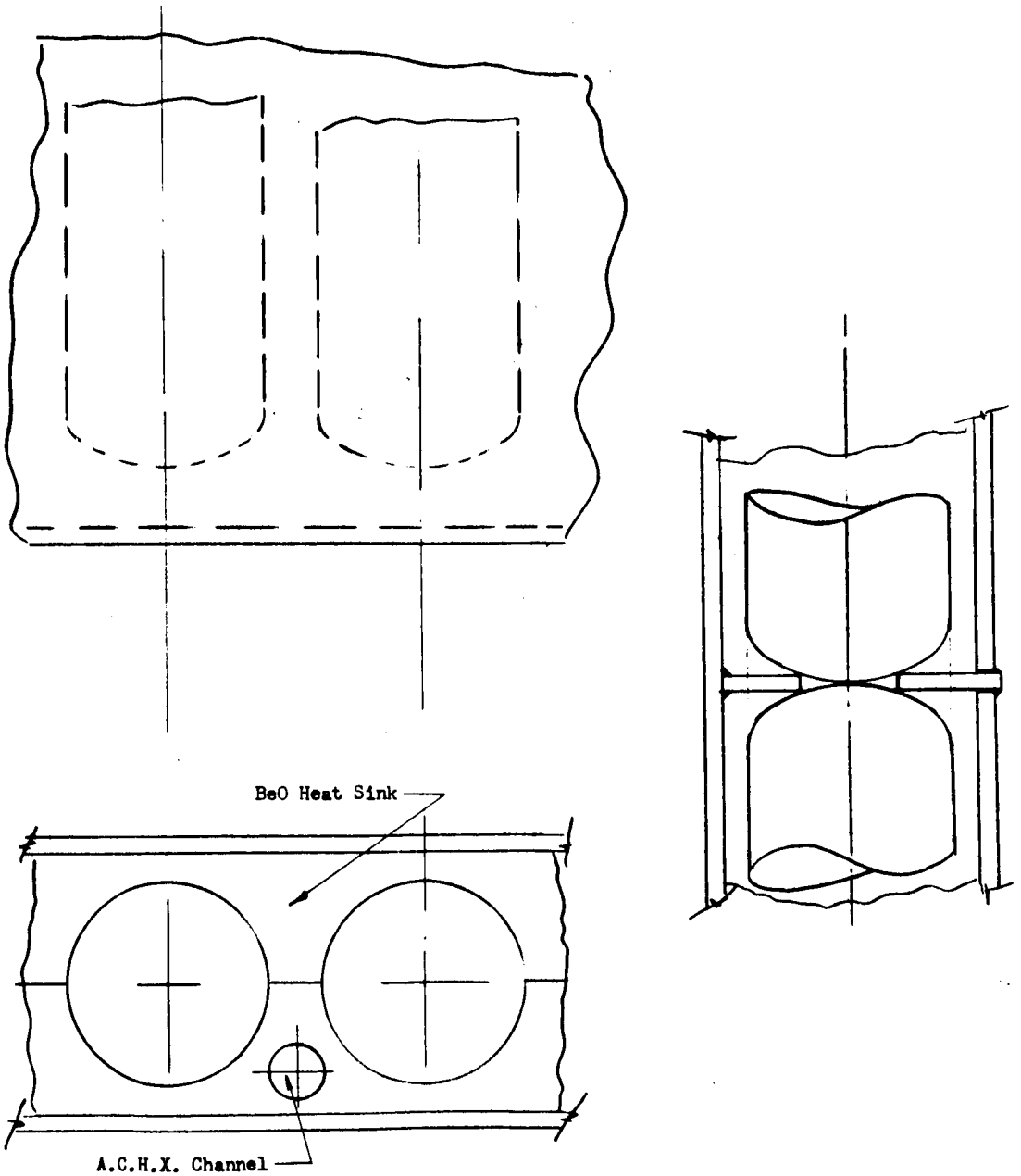

Figure 5.1-18. Heat Block

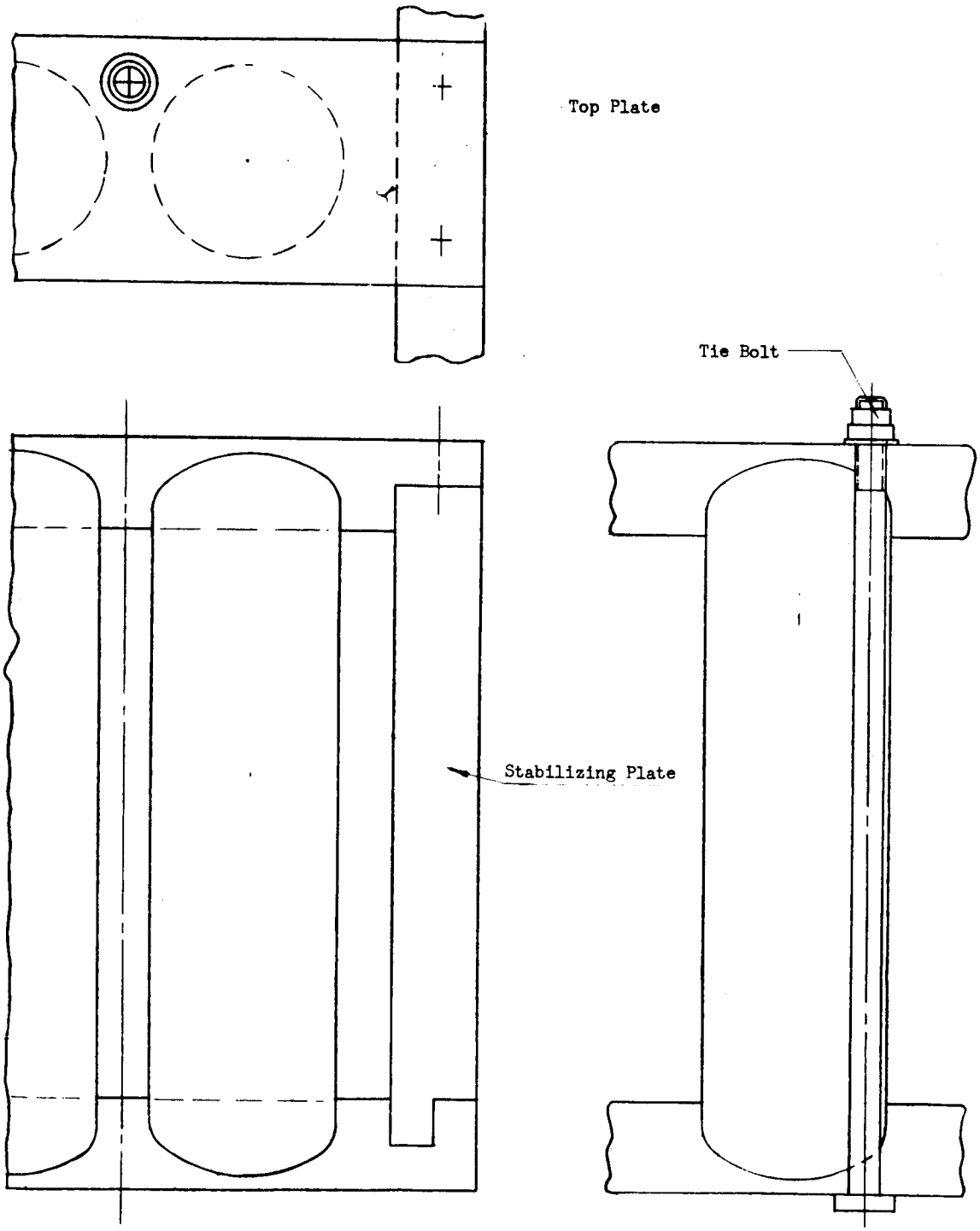

Figure 5.1–19. Pyramidal Array Exposed Capsule

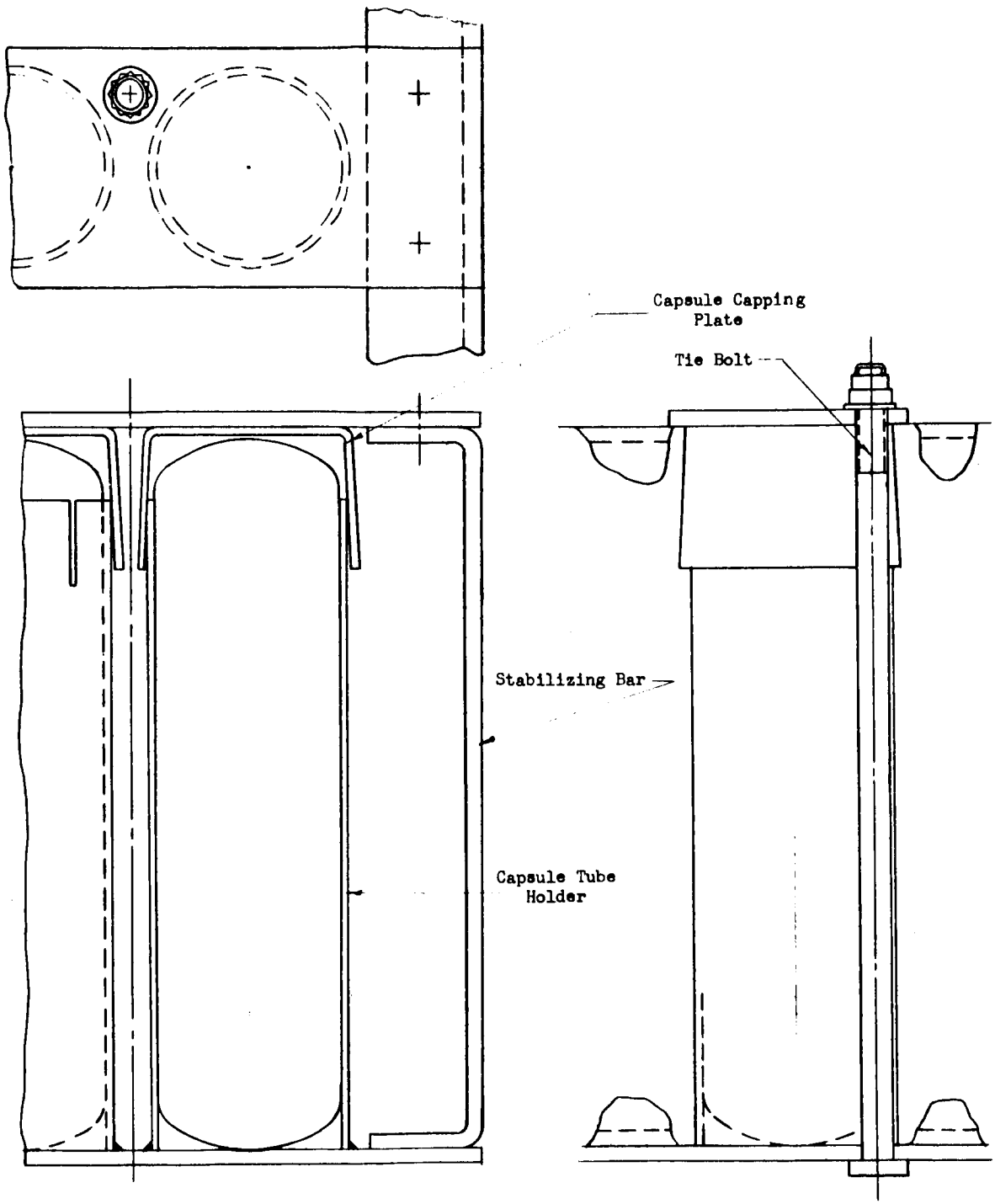

Figure 5.1–20. Pyramidal Array Protected Capsule

Heat Block

Advantages	Disadvantages
Lighter weight structure.	Fabrication and assembly problems
Complete capsule protection during reentry.	Capsule distribution ΔT = 100F.
Lower C.G.	
Retention problems minimized.	

For the pin cushion array present philosophy is to reevaluate the use of graphite as a structure, and to design a system from Cb 1 Zr, with integrated cooling channels forming the structure.

5.1.3.2.2 Thermal Analysis

a. Steady-State Performance -- Estimates have been made of temperature profiles from the base of the capsules to the surface of the capsules, or cover plate facing the HSHX, for the six configurations, based on simple conduction models assuming a radiation gap exists between the capsule and cover plate on the covered capsule designs. Although this model provides reasonable estimates of temperature profiles around the capsule, a more detailed model based on the application of an existing conduction analysis computer code (TOSS) will be used to accurately determine detailed design effects on thermal performance.

Figure 5.1-21 compares the temperature drop across the capsule support plate and retention scheme for a bare capsule, capsule with cover plate, heat block enclosed capsule, and a heat block with a stacked capsule arrangement in a circular planar heat source design. These are compared on the basis of a peak HSHX cooling fluid exit temperature, with the secondary heat exchanger in operation and with appropriate HSHX conduction and radiation ΔTs obtained through iteration based on expected heat fluxes. For the first three cases, the peak capsule temperatures are within 35 degrees of each other. For the latter case, the peak capsule temperature is considerably higher, due in part to higher surface heat fluxes and larger conduction path. The stacked heat block arrangement was deemed unacceptable. Figure 5.1-22 shows the steady-state temperature profile from the peak HSHX fluid temperature to the capsule temperature for a pin-cushion array.

Table 5.1-I compares the steady-state performance of the six configurations under consideration. Temperature profiles are shown for each design for the three capsule retention schemes, with the Primary HSHX and the Secondary HSHX in operation. All designs indicate the ability, with minor mechanical changes, to operate at or below 2000° F peak capsule temperature, from the layouts shown, with the exception of the minimum size circular planar array which will operate at 50° to 75° F higher than other designs. The use of the three retention schemes provide only a 35° F variation in steady-state operation.

Conclusions from this analysis are as follows:

1) There is little difference in steady-state thermal performance (35° F) between bare capsules, cover plates, and heat block design.

2) With the secondary HSHX in operation, maximum capsule temperatures can all be maintained at approximately 2000° F.

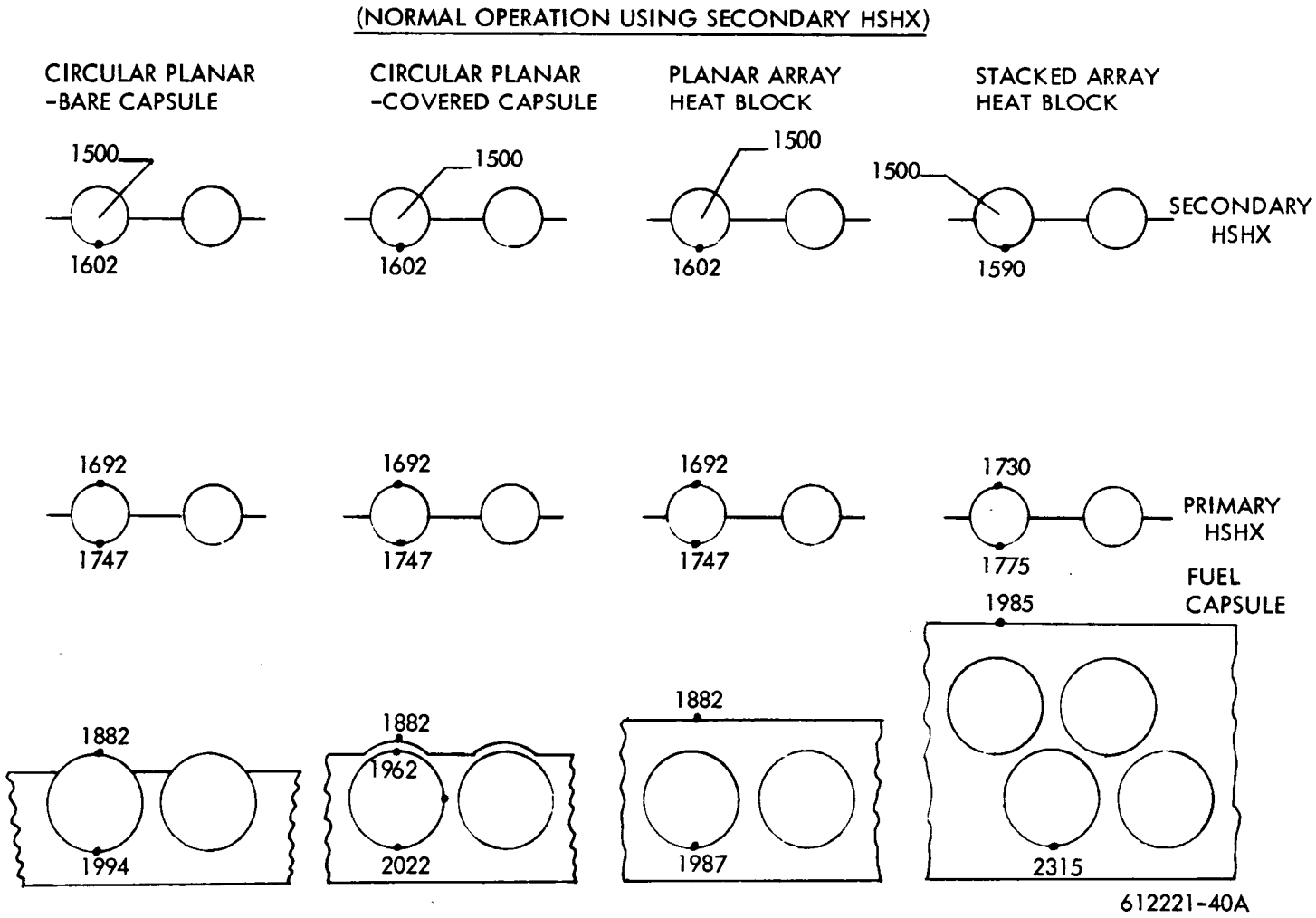

Figure 5.1–21. **Temperature Distribution Diagram**

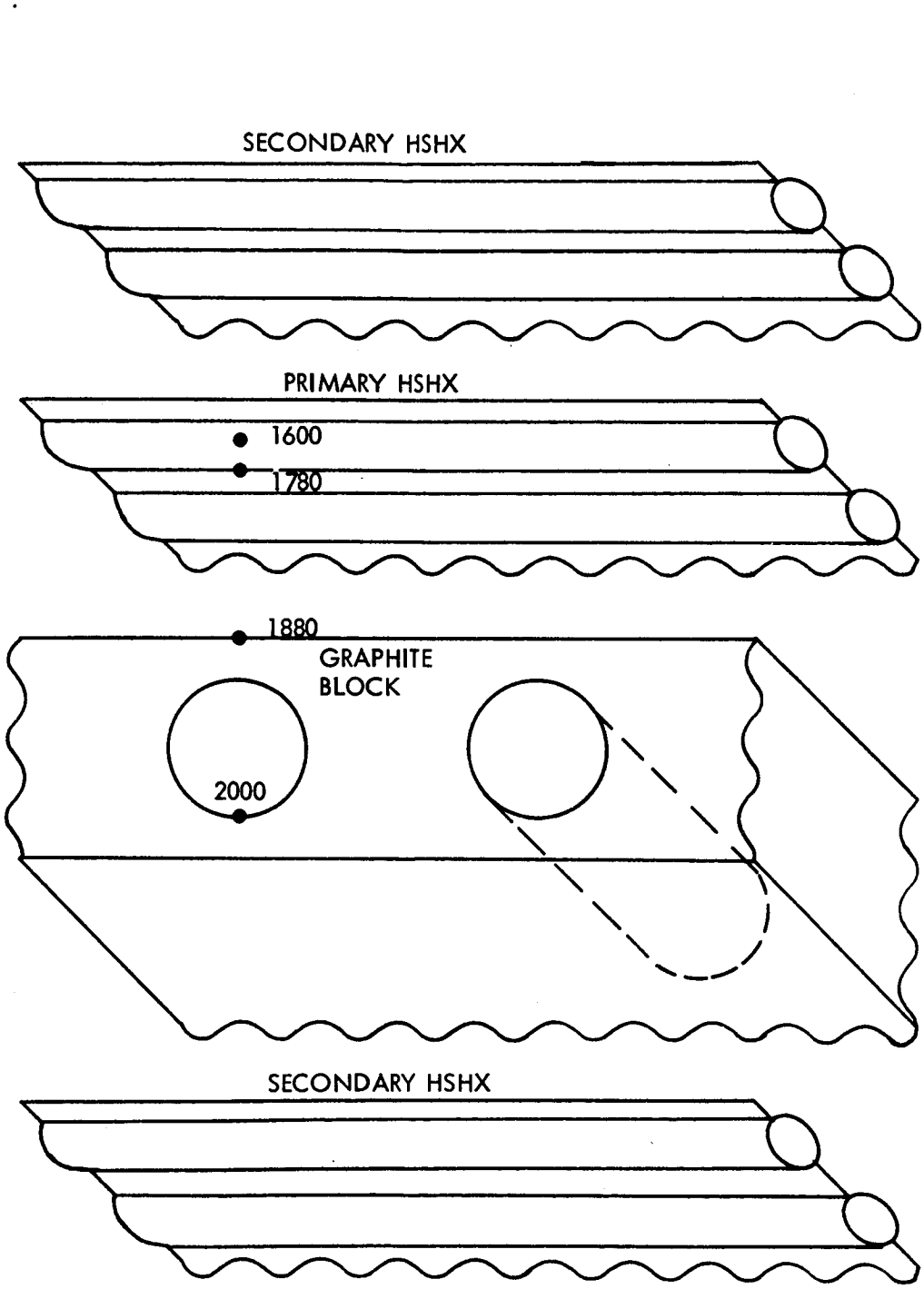

Figure 5.1-22. Temperature Distribution Diagram Pin Cushion Array (Normal Operation)

TABLE 5.1-I
IRV HEAT SOURCE THERMAL DESIGN SUMMARY

	No. 1A		No. 1C		No. 2A	No. 2B	No. 3C	No. 1A
	Circular Planar		Rectangular Planar		Conical	Conical-Cent. Rec. Aids	Pin Cushion	Min. Size Circular Planar
Heat Exchanger Operating Mode	Primary	Secondary	Primary	Secondary	Secondary	Secondary	Secondary	Secondary
Heat Source & HSHX Size (in)	53" D	53" D	34x63	34x63	57 D	70 D	40x48	47 D
Fluid Temp at Hottest Capsule (^{o}F)	1500	1500	1600	1600	1500	1500	1600	1500
HSHX Film & Wall ΔT	122	102	119	99	102	135	120	60
HSHX Gap Rad. ΔT	0	90	0	60	90	80	0	110
Primary HSHX Cond. ΔT	0	55	0	50	55	45	60	30
HS-HSHX Rad. ΔT	103	135	108	90	135	110	100	160
Heat Source Surface Temp (^{o}F)	1725	1882	1827	1899	1882	1870	1880	1860
Maximum Capsule Temp. (^{o}F)								
A. Bare Capsule	1837	1994	1939	2011	1994	1982	----	----
B. Covered Capsule	1865	2022	1967	2039	2022	2010	----	2076
C. Enclosed In Graphite	1830	1987	1932	2004	1987	1975	2000	----

612221-25B

b. Backside Heating Effects -- During reentry into the atmosphere, the array of fuel capsules will be exposed to the atmosphere on the backside of the reentry vehicle. Dependent upon the reentry angle of the vehicle and the orientation of the vehicle during reentry, the capsule array will be exposed to varied aerodynamic heating rates. The magnitude of some of these heating rates are large enough for the capsules to heat to temperatures in excess of material melting points.

To determine the magnitude of the problems associated with reentry heating, an analysis was performed to determine the capsule temperature response to the convective heating rates. Transient temperature profiles of the fuel region were obtained for reentry angles of 0, -2, -2.25 (nominal), -5, and -10 degrees and for a two skip reentry. Results were obtained for three orientation angles of 0, 90, and 180 degrees where a 0-degree orientation represents the vehicle shield facing the direction of motion. Also, a tumbling vehicle reentry was analyzed. For this analysis, an exposed fuel capsule array and a recessed array shown schematically in Figure 4.1-2 (Section 4.0) were analyzed.

Transient temperature calculations were based on a model of a typical cross section in the active region of the capsule, as indicated in Figure 5.1-23, which included the effects of convective heating, cooling by radiation, internal heat generation, and heat storage. The assumptions for this model are presented in Table 5.1-II.

Table 5.1-III presents the actual volume, density, and heat capacity which were used. For cases considering heating of the top retention plate only (Figure 5.1-17), a heat capacitance of 0.0106 Btu/in.^{o} F (corresponding to 0.100-in.-thick T-111) was used. For cases considering heating of the fuel capsule only, a heat capacitance of 0.0357 Btu/in.^{o} F was used. When considering heating of both top retention plate and fuel capsule, a heat capacitance of 0.0463 Btu/in.^{o} F (corresponding to the capsule plus a 0.100-in. T-111 container) was used.

The model considers only the capacitance in the local element of volume adjacent to the surface area, receiving convective heat and rejecting radiative heat. The effect of the capacitance of the base of the capsule and the BeO adjacent to the capsule is not included. Preliminary calculations of conduction rates indicated that the steep heating rates which are present in the worst reentry cases are much greater than the allowable conduction rates across the support structure; thus BeO heat-up may lag the capsule heat-up by a considerable margin. A more sophisticated model utilizing general computer codes for transient conduction will be used in the detailed design analysis in Phase II to obtain a more accurate estimate of the capsule thermal response.

Figure 5.1-24 presents a typical heating rate curve for a recessed fuel capsule array entering at an angle of -2.0 degrees at three different orientation angles. The temperature histories of the fuel capsule corresponding to this heating rate are presented in Figure 5.1-25 for an initial capsule temperature of 2000^{o} F. Typically during the initial period of reentry when the convective heating rates are negligible, the capsule array is cooled by radiation to space. As the convective heating rate increases with time, it exceeds the radiation cooling rate and produces a steep temperature

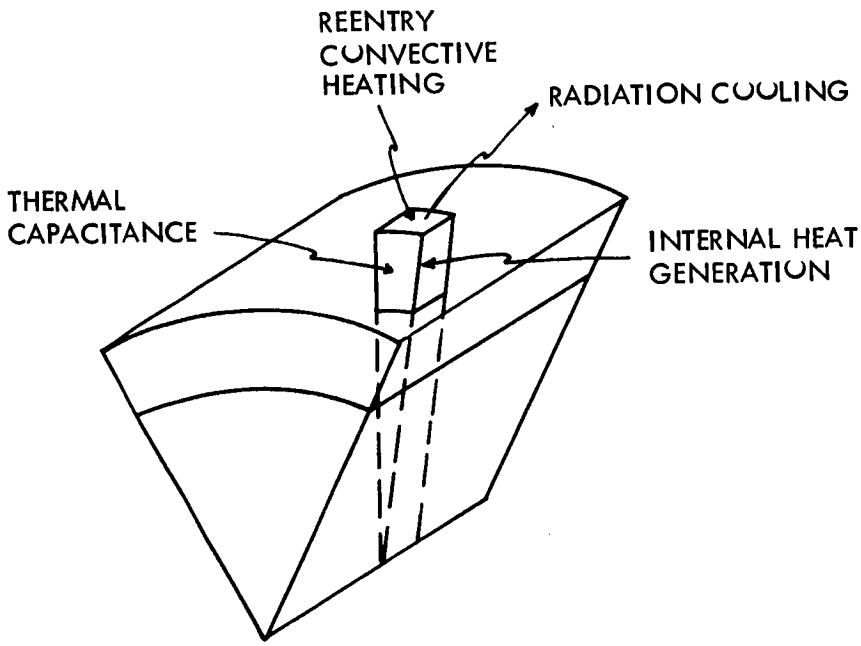

612221-36A

Figure 5.1–23. Reentry Analysis - Model Diagram

TABLE 5.1-II

REENTRY ANALYSIS-ASSUMPTIONS

1. THE MODEL REPRESENTS MOST ACTIVE AREA WITH HIGHEST AIR FRICTION HEATING RATES.

2. INFINITE CONDUCTIVITY WITHIN THE CONTROL VOLUME.

3. NO HEAT FLOW BY CONDUCTION TO SURROUNDING MATERIALS.

4. PHYSICAL PROPERTIES DO NOT VARY WITH TEMPERATURE.

5. SURFACE EMISSIVITY IS 0.85.

6. THE CAPSULE IS 1.542 INCHES IN DIAMETER, 4.537 INCHES IN LENGTH, AND HAS A POWER OF 157 WATTS.

7. THE TIME STEP (Δt) IS CHOSEN SUCH THAT THE TEMPERATURE CHANGE IS ALWAYS VERY SMALL.

8. INITIAL TEMPERATURE WAS 2000° F IN ALL CASES EXCEPT FOR THE TWO-SKIP REENTRY WHERE THE INITIAL TEMPERATURE WAS 1000° F.

9. HEATING RATES AND TIME BASED ON RN = 8.625 IN, RN/RB = 0.25, BASE DIAMETER = 69 IN.

10 REENTRY TIME INITIATED AT ALTITUDE OF 400,000 FT.

TABLE 5.1-III

CAPSULE PARAMETERS
(per inch of capsule)

Material	Thickness (in)	Volumes (in^3/in)	Specific Heat (Btu/lb °F)	Density (lb/in^3)	Heat Capacity$_3$ (Btu/in °F x 10^3)
Tungsten	0.020	0.039	0.032	0.697	0.9
PuO_2	0.241	0.599	0.056	0.414	13.9
Tungsten	0.020	0.069	0.032	0.697	1.5
T-111	0.175	0.714	0.034	0.604	14.7
Gap	0.002	0.009	----	----	----
ThO_2	0.010	0.047	0.065	0.350	1.1
Pt	0.020	0.095	0.044	0.720	3.0
$FeTiO_3$	0.002	0.010	0.210	0.284	0.6
Gap	0.004	0.019	----	----	----
Cb-1%Zr	0.100	0.518	0.083	0.310	13.3
or					
T-111			0.034	0.604	10.6

	$\sum \rho CV$ (Btu/in °F)
Capsule alone	35.7×10^{-3}
Cb-1%Zr Container (0.100 in)	13.3×10^{-3}
T-111 Container (0.100 in)	10.6×10^{-3}

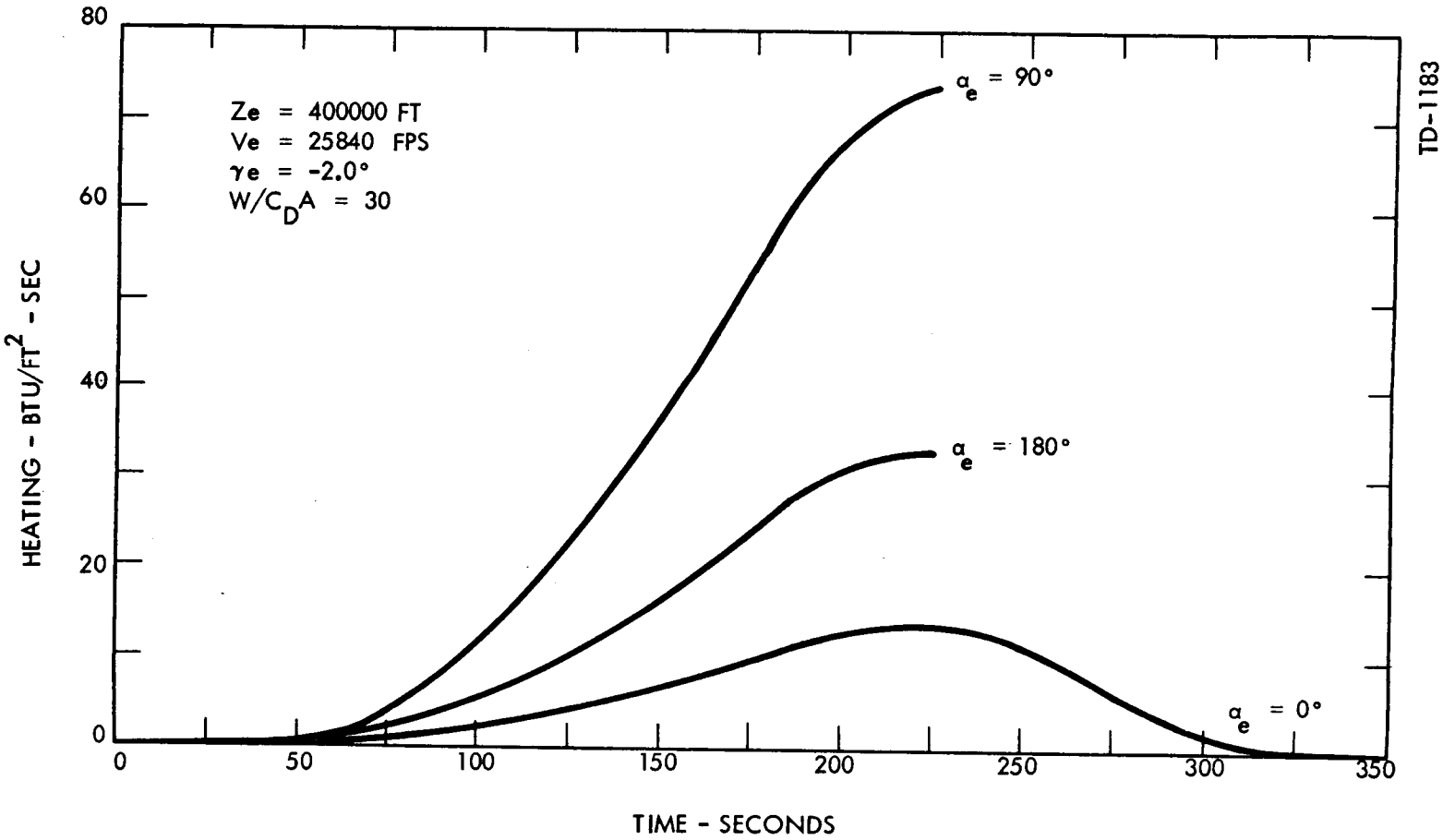

Figure 5.1-24. Convective Heating Rate for Recessed Capsules

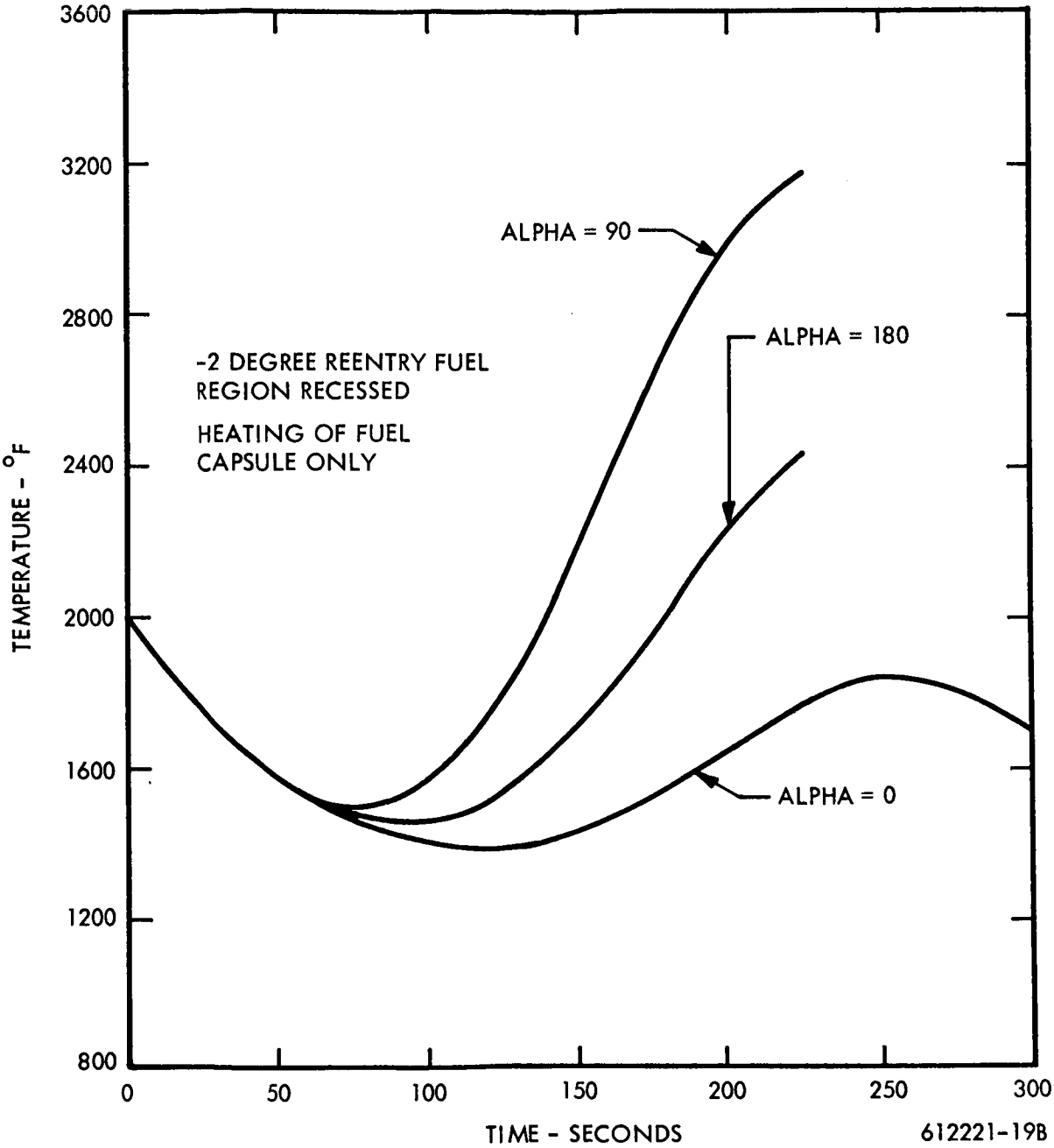

Figure 5.1–25. Reentry Temperature History

rise in the capsule temperature. The magnitude of the four components affecting the temperature history are shown in Figure 5.1-26 for an exposed capsule array oriented at 180 degrees and entering at -2 degrees. This figure illustrates the fact that the convective heating and radiation cooling terms dominate the thermal response of the capsule after the initial period of reentry. The radiation loss was evaluated for an assumption that the capsules could be maintained at 2000° F by conduction from the BeO until the heating rates exceed the cooling rates. This conduction requirements is shown for the first 80 seconds. The thermal absorption rate for the capsule is shown for the latter part of the heating period indicating a capsule temperature response rate that is decreasing with time. As shown in this figure, the internal heat generation rate is negligible throughout the reentry period. Figures 5.1-27 and 5.1-28 compare the capsule and cover plate temperature profiles for the case where the capsules are allowed to cool by radiation and the capsules remain at a constant temperature due to conduction from the BeO as may be the actual case. The two profiles converge very rapidly in the steep region of the temperature rise due to the fact that the convective heating rate and radiation cooling rates are much greater than the capacitance of the capsules as shown in Figure 5.1-26. Therefore, the profiles developed by the model should be fairly accurate. If the additional heat that can be conducted to the BeO as the capsule undergoes a rapid thermal transient is of the same magnitude as the heat absorbed by the capsule as shown in cursory calculations, convection and radiation still dominate and the peak temperature profiles are realistic. Referring to Figure 5.1-25 the capsule temperature exceeds the limiting temperature of 2500° F (established as a ground rule) for the more severe cases of heating experienced with the vehicle entering at orientations of 90 and 180 degrees. The time required for the capsules to reach this temperature establishes the time allowed to correct the orientation of the vehicle.

Figure 5.1-29 contains curves of the temperature history of a covered and bare capsule in an exposed fuel region for a vehicle with a reentry angle of -5 degrees, and an angle of attack of 180° degrees. This reentry profile represents conditions under which a steep temperature rise occurs, therefore requiring the correction of the vehicle orientation in a short time. For this case, the time to reach peak heating is 95 seconds. The first line represents the thermal response at the cover surface of a covered capsule with heat absorbed by the cover plate only. Line 2 represents the thermal response of the bare capsule with heat absorbed by the capsule. Line 3 represents the thermal response of the cover surface of a covered capsule with heat absorbed by the capsule and cover.

Line 4 represents the thermal response at the capsule surface of a covered capsule with heat absorbed by the capsule, assuming a radiation gap exists between the cover plate and the capsule. The effect of the placement of the cover plate provides some reduction in the response of the capsule temperature to the convective heating; however, it does not significantly alter the time allowed to correct the orientation from 180 to 0 degrees. Similar trends were observed for the rearward and edgewise reentry at other reentry angles. Therefore, for those conditions during which the orientation righting time is too short with bare capsule, a covered capsule will provide a small extension of correction time.

Heating rate curves and temperature histories for the other variations in reentry angle and capsule arrangements described above, presented in Table 5.1-IV and 5.1-V, summarize the peak temperatures experienced for each

of the variations considered. In those cases, where the capsule temperature exceeded 2500° F, a ratio of the time required for the capsule to reach 2500° F versus the time for the heating rate to peak is noted to indicate the serverity of the transient. For all reentry angles with the vehicle in a zero degree orientation, the capsules remained below 2500° F. The steepest temperature transients were observed for -2, -5, and -10 degree reentry angles with the vehicle oriented in a 90 degree position. For the exposed capsule regions the capsules exceeded 2500° F early in the reentry period which may impose severe correction time requirements. The 180 degree orientation is less severe than the 90 degree, but for the exposed capsule regions, short orientation correction time allowances are still imposed. With a zero degree reentry angle and a 2 skip reentry angle and a 2 skip reentry, the exposed capsule temperatures also exceed 2500° F for 90 degree and 180 degree angles of attack; however, this occurs after a relatively long period of time when the heating rate is very near its peak, indicating that overheating may not be severe. In all cases, recessing of the capsule resulted in significant reduction of the peak capsule temperatures and an increase in allowable time to correct the vehicle orientation. Table 5.1-V summarizes the peak temperatures expected for a rearward orientation and a tumbling vehicle with a zero degree reentry angle. For an exposed capsule the temperature exceeded 2500° F at a time near to peak of the heating rate curve. The heating rates for these two cases are more severe than for the other three orientations considered, indicating the steeper temperature response histories can be expected.

The following conclusions were reached from the reentry heating analysis:

1) The peak capsule temperature can be maintained below 2500° F for a (nominal) zero degree orientation for both the exposed and recessed capsules and for all reentry angles considered.

2) Reentry at angles from -2 to -10 degrees for orientations of 90 and 180 degrees impose severe righting requirements for the exposed capsule regions (40 to 56 percent of the peak heating time) thereby dictating inclusion of some type of righting aid in the IRV design.

3) Recessing of the capsules results in considerable reduction in the peak temperature and increases the allowable time to correct the vehicle orientation.

4) The effect of convective and radiation heating are much greater than the effect of capacitance and heat generation and therefore dominate the response of the capsule to reentry heating.

5) The cover plates on heat blocks do not provide significant increases in the permissible IRV turn-around times for those cases where steep heating rates are imposed on the capsules.

5.1.3.3 Heat Source Support Plate

5.1.3.3.1 Mechanical Design -- The heat source support plate is required to support and contain the fuel capsules, the BeO heat sink, and the ACHX flow passages and headers. A lightweight structure, of minimum size, is mandatory from the standpoint of system weight and efficiency.

Early designs generated employed a box girder structure with radial ribs designed to contain the BeO, and with tubular holders attached to the top plate for capsule containment. With the inclusion of the ACHX cooling channels a more sophisticated design has been generated. The corrugated top plate contains the capsules, and cooling channels are located parallel with the capsule rows. Inlet and outlet headers are combined within the support plate, and a grid structure is included to strengthen the plate and to house the BeO heat sink.

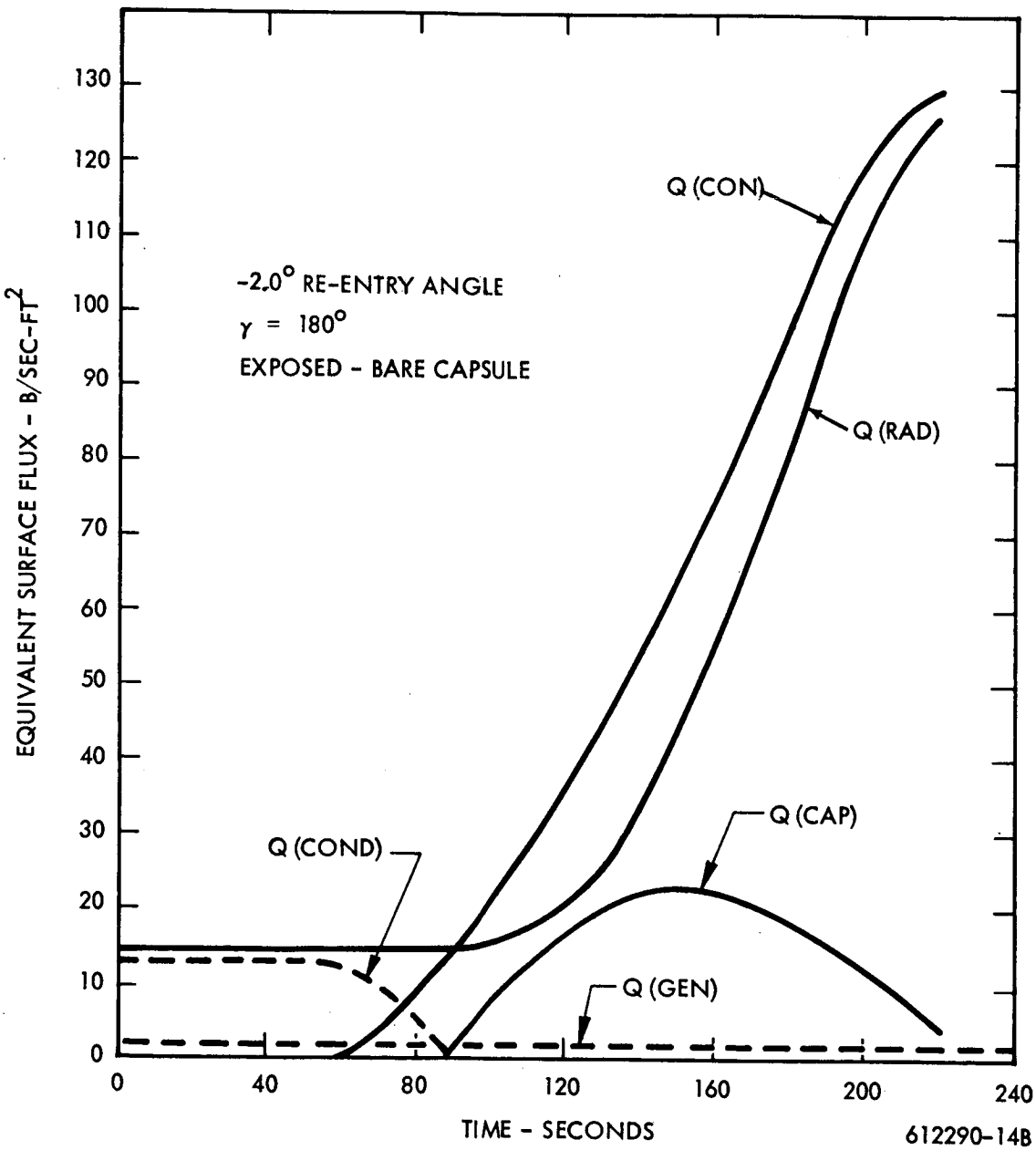

Figure 5.1–26. Component Breakdown of Heating Rates during Reentry

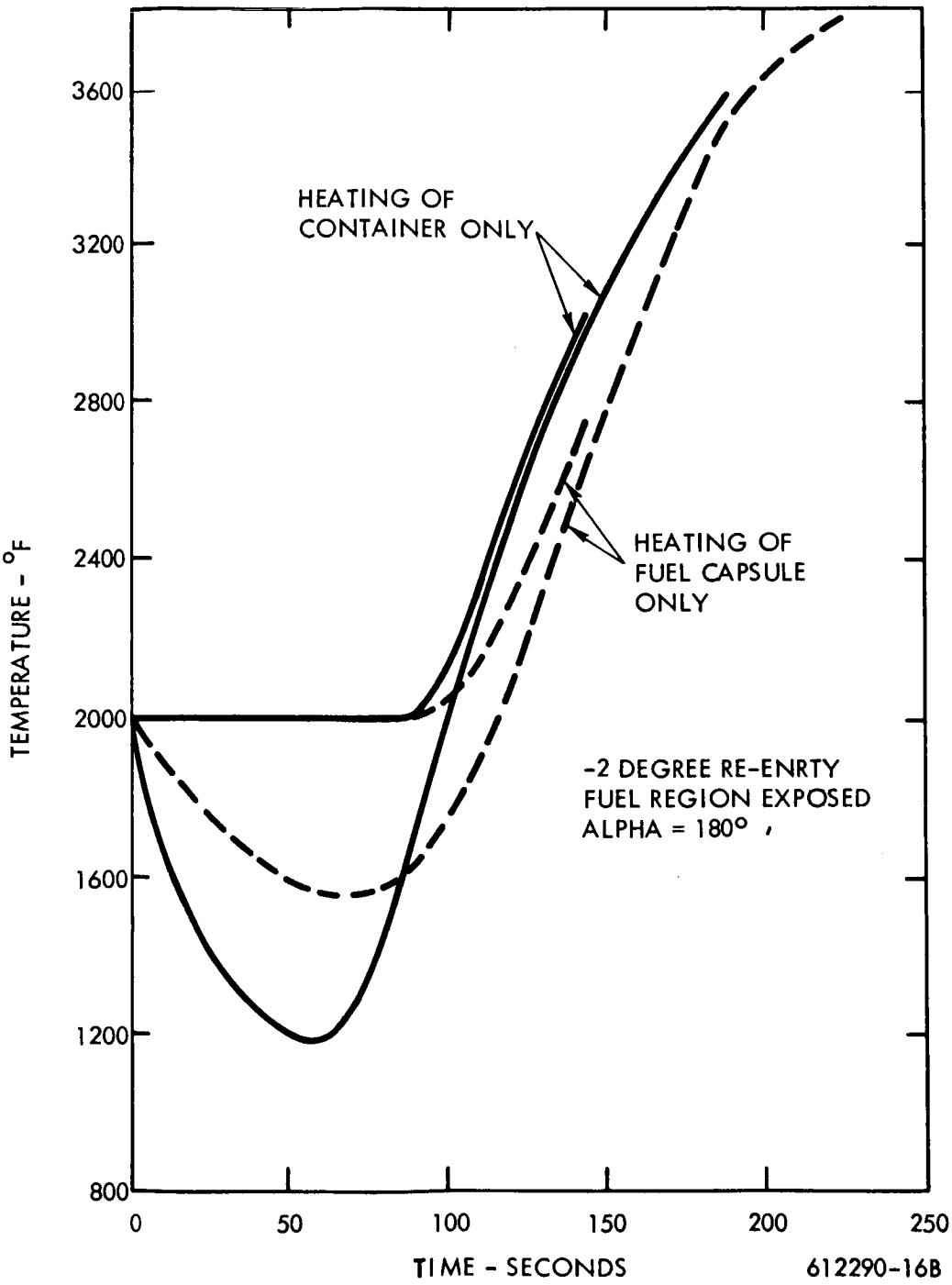

Figure 5.1-27. Effect of Initial Heating Rate on Temperature History (Alpha 180°)

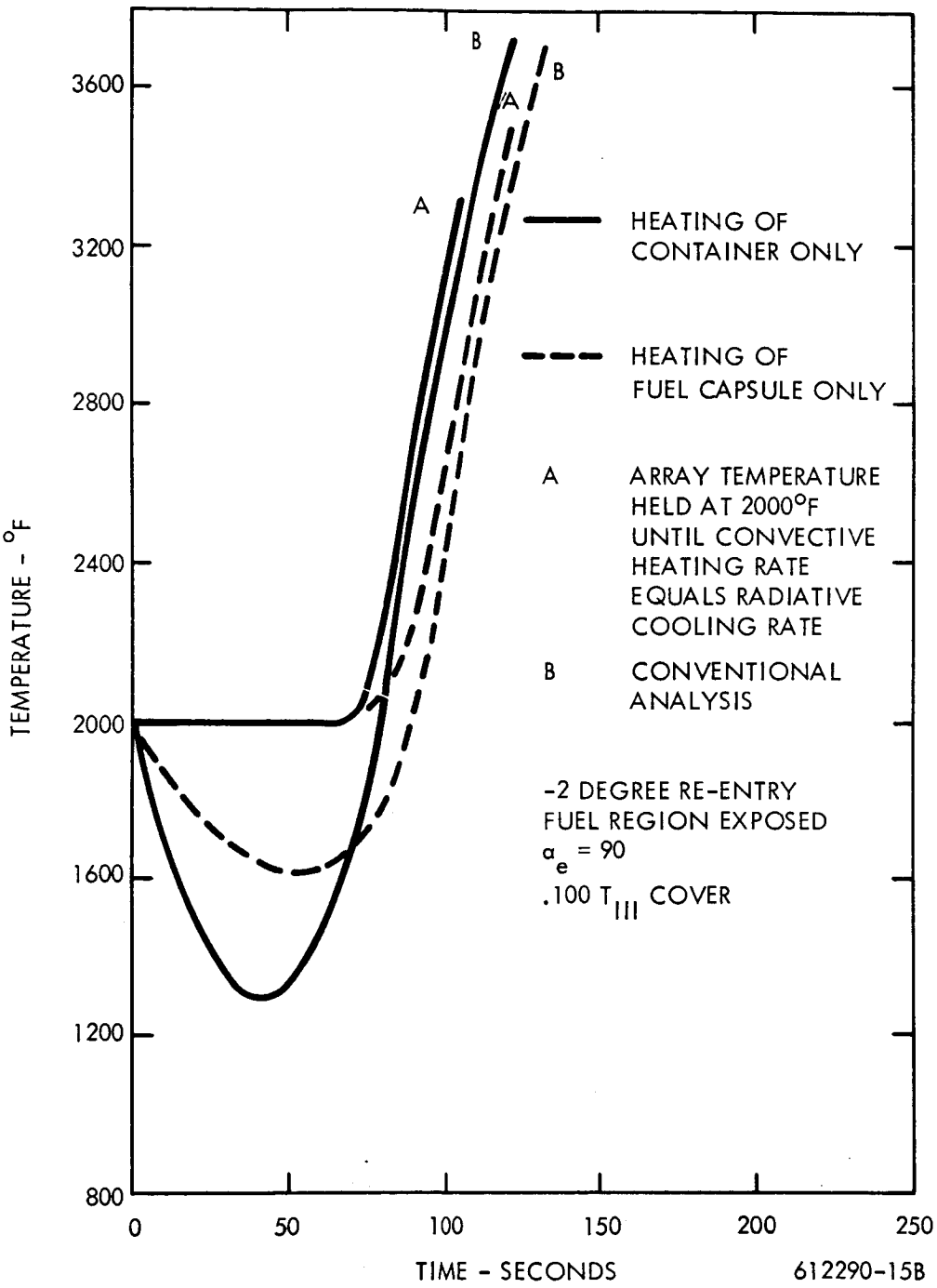

Figure 5.1–28. Effect of Initial Heating Rate on Temperature History (Alpha 90°)

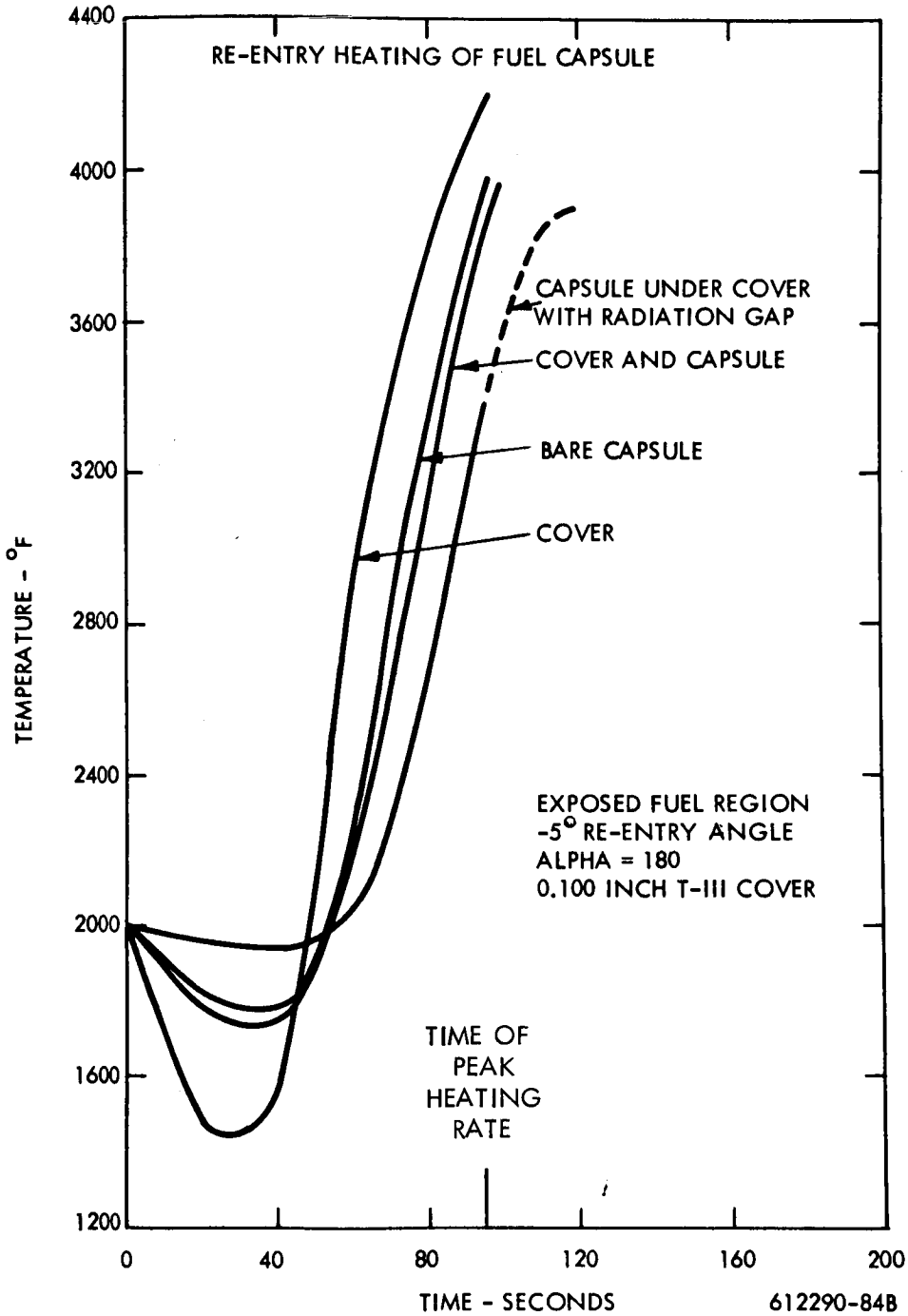

Figure 5.1-29. Reentry Heating of Fuel Capsule Array

TABLE 5.1–IV

CAPSULE REENTRY HEATING SUMMARY*

PEAK BARE CAPSULE TEMPERATURE - °F OR
RATIO OF TIME TO 2500°F/TIME TO PEAK TEMPERATURE

	EXPOSED CAPSULE REGION (←.8D→, d)			RECESSED CAPSULE REGION (←.6D→, 3d, d)		
VEHICLE REENTRY ORIENTATION (°)	90 ▷	180 △	0 ▽	90 ▷	180 △	0 ▽
REENTRY ANGLES (°) 0	0.87	0.93	1980	2540	2340	1640
-2	0.40	0.56	2380	0.67	2500	1840
-5	0.45	0.65	2360	0.72	2580	1920
-10	0.43	0.61	2160	0.86	2440	1860
2-SKIP (-.7)	0.98	0.99	2120	2350	1740	1680

* Nominal fence designs meet required turnaround times

612221-17A

TABLE 5.1-V

CAPSULE REENTRY HEATING SUMMARY - (0°, 0°, AND -2.25° REENTRY ANGLE)

REENTRY ORIENTATION	REENTRY ANGLE	PEAK BARE CAPSULE TEMPERATURE - °F OR RATIO OF TIME TO 2500°F/TIME TO PEAK TEMPERATURE	
		EXPOSED CAPSULE REGION	RECESSED CAPSULE REGION
NOMINAL	-2.25°	2300	1820
REARWARD	0°	2960 (.94)	2050
TUMBLING	0°	2900 (.98)	2400

612221-39A

The material selected for the support plate is Cb-1 percent Zr, which has a tensile yield of approximately 20,000 psi at 2000° F which is the maximum normal operating temperature specified for the system.

Five typical heat source configuration layouts were investigated:

a. A 60-degree blunted cone aeroshell of circular planar configuration with truss support (Fig. 5.1-2)

b. A 60-degree blunted cone aeroshell with rectangular planar configuration with truss support (Fig. 5.1-3)

c. A 60-degree blunted cone aeroshell of conical configuration with truss support (Fig. 5.1-4)

d. A 60-degree blunted cone aeroshell pin cushion configuration with truss support (Fig. 5.1-6)

e. A 60-degree blunted cone aeroshell conical configuration with central recovery aids and truss support (Fig. 5.1-8)

Weights, mass moments of inertia, and centers of gravity have been calculated for these five configurations. These are summarized in Table 5.1-VI.

A sixth layout has also been prepared to investigate the feasibility of reducing over-all diameter of a circular array to a mimimum. See Fig. 5.1-7.

Of the five IRV heat source configurations selected for review, two are planar, a 53-inch circular, and a 34 x 63-inch rectangular heat source containing 162 fuel capsules. The circular planar array consists of 164 fuel capsules arranged in parallel rows with the minimum acceptable distance between capsules. Of several configurations studied, with capsule centers ranging from 1.6 inches to 2.0 inches, the optimum distance based on thermal and mechanical requirements has been established as 1.75 in. resulting in a heat source support plate diameter of 49 inches.

The conical arrays are a 57-inch diameter cone and 70-inch diameter cone. The 70-inch cone has a 35.5-inch central void section which houses the recovery aids. Capsule arrangement is limited to 160 for the 57-inch diameter cone, but the number of capsules could be increased for the larger cone.

The circular conical array has one distinct advantage in that it brings the center of gravity closer to the nose of the vehicle. The fuel capsules are arranged in 16 typical arrays of 10 capsules each. With conical arrays the effect of distance between capsules does not play a large factor in reducing overall diameter but some reduction can be achieved by rearranging the capsules into a non-uniform pattern. This reduces the basic heat source support plate diameter from 57 to 51 inches.

The pin cushion array has the fuel capsule arranged on end in a rectangular graphite heat sink 48 x 40 inches with a minimum of 3 inches between capsule rows to accommodate the heat exhanger.

TABLE 5.1 – VI

SUMMARY COMPARISON OF HEAT SOURCE CONFIGURATION

PHYSICAL PROPERTIES	1A  CIRCULAR PLANAR ARRAY	1C  RECTANGULAR PLANAR ARRAY	2A  CONICAL ARRAY	2B  CONICAL ARRAY WITH CENTRAL HOLE	3C  RECTANGULAR PINCUSHION ARRAY	1A  REDUCED CIRCULAR ARRAY
WEIGHT (EXCLUDING RE-ENTRY VEHICLE STRUCTURE LBS)	1579	1578	1514	1910	1397	1490
HEAT SOURCE SIZE (INCHES)	53 DIA	63 x 34	57 DIA	70 O. D. x 35. 5 I. D.	48 x 40	47. 0 DIA
OVERALL HEIGHT (INCHES)	30. 5	29. 25	32	36	32. 2	30. 5
C. G. FROM APEX OF NOSE CONE (INCHES)	27. 9	26. 4	24	29	26. 81	27. 8
MASS MOMENTS OF INERTIA						
POLAR (SLUG FT^2)	103	119. 2	136. 3	398	51. 2	92. 3
TRANSVERSE (SLUG FT^2)	50	81. 2 (MAX) 28. 6 (MIN)	73. 0	204	38. 5	53. 9

The pin cushion configuration was basically a 40 in. x 48 in. rectangular graphite block machined and drilled for interface with the HSHX and the fuel capsules. The 168 fuel capsules are arranged in 7 rows of 24 capsules per row with a 3.0 in. space between rows for the HSHX interface. This will be re-evaluated for a circular plate, of 38-in. diameter for 167 capsules. (The 38-in. dimension depends largely upon the feasibility of reducing the space between capsule rows to 1.0 in. and using a Cb 1 percent Zr structure rather than graphite.)

The assembly and handling of the heat source is accomplished with a minimum of remote handling. The designs shown allow assembly of the fuel capsule to the heat source support plate in a remote handling area. The assembly is then transported and assembled to the support structure already installed at the launch pad.

Included in the heat source support plate is a breech type locking mechanism, which is used to assemble the field heat source to the support structure on the launch pad. The circular planar and circular conical heat sources are assembled with a rotating type mechanism, while the pin cushion rectangular configuration is assembled with a sliding breech type mechanism. Spring loaded lock pins finally secure the heat source at final assembly. During emergencies the heat source can be quickly removed by releasing the lock pins and disengaging the breech mechanism.

5.1.3.3.2 Structural Analysis -- The fuel capsules are retained by the heat source plate, presently planned to be fabricated of columbium 1 percent zirconium. The plate will also contain the beryllium-oxide. Various ribbed plate structures have been contemplated but essentially three shapes include all configurations. The three general shapes are planar circular, planar rectangular, and a conical structure.

From a structural standpoint, the larger the diameter of each structure, the lower the load capability and the resonant frequency. Hence, a 53-inch circular plate, a 63 inch x 44 inch rectangular plate, and a 60° semi-apex angle conical structure have been considered to represent the lower bounds of all the numerous configuration and sizes which have at one time or another been under consideration. The rectangular plate, in essence, is also an approximation for the integral capsule-plate block concept.

Structurally, the support plate should

a. withstand reentry loads (30 gs),

b. help to contain the fuel capsules during impact, and

c. have a fundamental frequency of over 200 hertz.

Consequently, the structural performance has been analyzed under reentry, impact, and vibratory conditions.

The load capability calculations, based on designs as shown in Figures 5.1-2 through 5.1-7, indicate the following:

a. The circular plate with radial ribs can withstand about 170 g-load without yielding,

b. The rectangular plate with four-point support of corners will yield a g-load range of 16.5 to 34. Relocating the support points from the corners to midpoints of each section, yielding load is estimated to be 45 gs, while a 60-g capability results with the edges uniformly supported.

c. The conical plate will yield at loads greater than 230 gs while a collapsing load is estimated to about 435gs.

d. The conical plate with center hole has not been analyzed, but it is expected to be somewhat weaker than the conical plate.

e. The pin cushion array in graphite block has not been analyzed; however, it is believed to be capable of withstanding the reentry loads.

f. The reduced diameter circular plate would be somewhat stronger than the larger circular plate.

The impact analysis of the plate is obviously subject to comparable limitations to those detailed in the analyses of fuel capsule performance during impact (Appendix A). In addition, the support plate design is significantly affected by the philosophy and final choice of impact attenuation system goal and requirements. An analysis of the final design performance will be completed during phase II of the study. A brief study supporting the impact attenuation system review discussed in section 5.4, has been completed.

This analysis was based on the assumption of isotropic crushable material filling the conical void below the heat source plate, heat sink, and insulation system. The result of bending stress on a circular plate (equivalent in inertia to the design concept) with uniform crushable material distribution is presented in Figure 5.1-30 as a function of crushing stroke.

Since there is no material which will take over a half million psi bending stress at temperature, the plate will breakup on impact with the use of uniform crushable material even though the g-load on the plate only reaches a maximum of 875 g's during impact.

With a judicious selection of stages of crushable materials, with decreasing effective yield stress from the apex towards the heat source support plate, it is theoretically possible to get the crushable material to all collapse uniformly over the entire depth and hence eliminate such a bending stress in the plate. However, the weight cost of such a system (e.g. foamed aluminum) is excessive. It should also be noted that the above analysis treats only the case of vertical (angle of attack - 0^{o}) impact. Non-vertical impacts result in even worse conditions (higher g loads). Therefore, effort has been continued to develop a more optimum (in terms of weight) attenuation system concept. One potential concept is described in section 5.4.

A brief dynamic analysis of the three classes of fuel capsule support plates has been completed. The analysis is described in Appendix B. The results indicate that the resonant frequencies of these heat source plate structures are below 200 hertz. Resonant frequencies of the plate structure can be raised by optimizing rib sizes and spacing. Further detailed analysis of the support plate will be completed in Phases IB and II of the study.

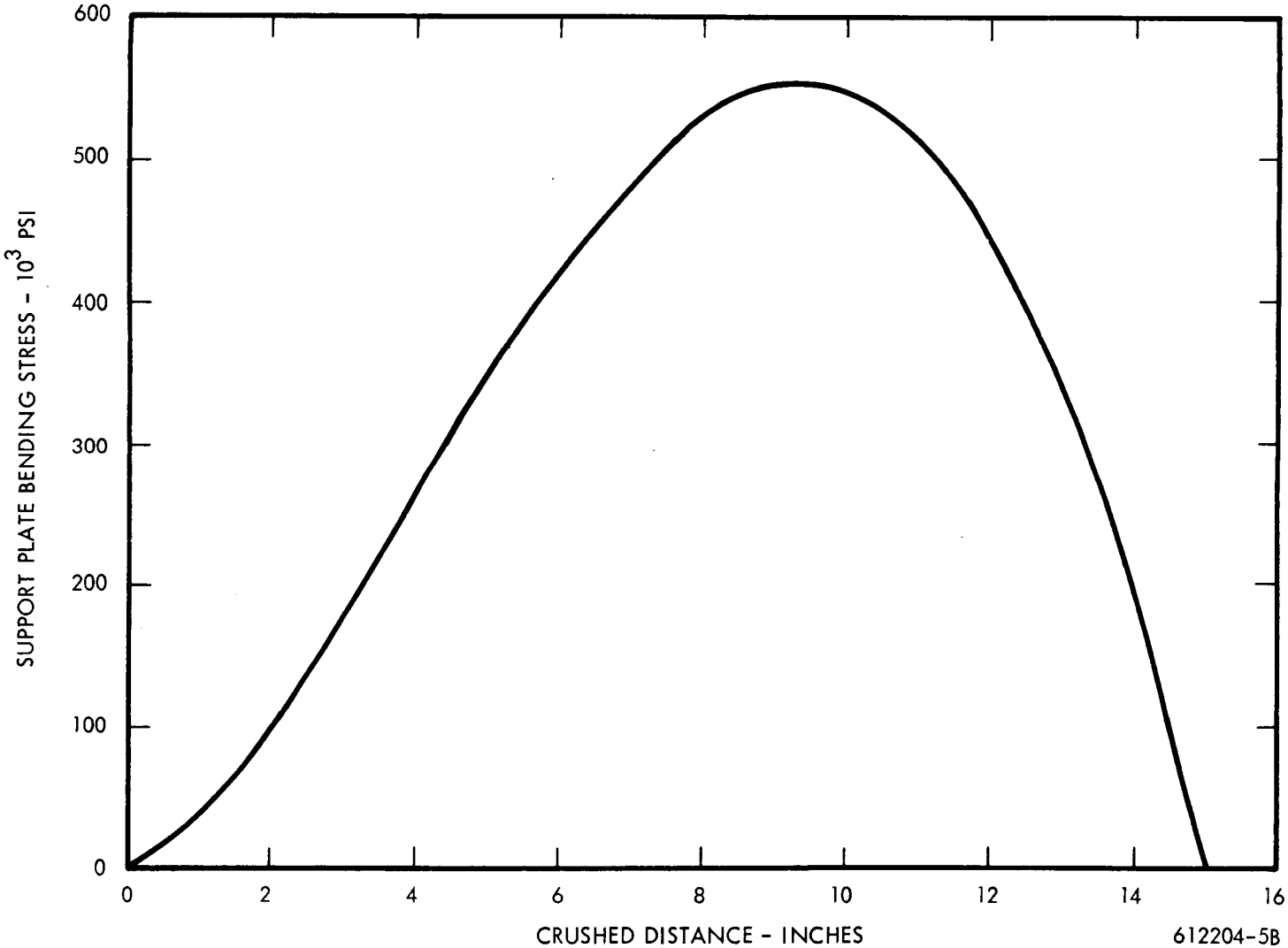

Figure 5.1–30. Theoretical Elastic Bending Stress History of a Circular Planar Support Plate for Vertical Impact

5.1.3.3.3 Heat Source Radiation Heat Transfer Analysis -- During steady state operation of the power conversion system, the heat source will be radiating thermal energy to the heat source heat exchanger (HSHX). For a planar fuel capsule array, the heat exchanger will be facing the heat source in parallel. The temperature profile of the heat source and the heat exchanger will be dependent upon several factors including, in part, geometry variation in the heat source and heat exchanger, heat exchanger coolant passage and fin arrangement variation, coolant temperature level and temperature rise, and material surface characteristics. One of the important design problems for the heat source and heat exchanger is to attempt to achieve a flat temperature profile across the heat source (thus minimizing the peak fuel capsule temperatures).

An analysis of this problem has been performed to evaluate the effect of several heat source designs on fuel capsule temperature profiles. The configurations that have been evaluated in detail are the circular planar fuel capsule array facing a circular planar heat exchanger of equal diameter with an involute array of tubes, and the rectangular planar array of fuel capsules facing a rectangular shaped heat exchanger with finned tubes connected in parallel across the width of the heat exchanger.

A calculational model has been developed based on the following assumptions:

a. Capsule array and heat exchanger tubes are arranged on plane surfaces of equal diameters and parallel to each other.

b. Both planes are divided for calculation purposes into 4 or 5 sections of equal area. Each area is allowed to assume one discrete temperature.

c. Negligible edge heat losses occur in the system (the surrounded walls were assumed at a uniform temperature such that the heat radiated to the surface was absorbed and radiated to colder surfaces).

d. Plane diameter is 53 inches for circular case and 63 inches x 34 inches for rectangular case. Spacing between planes is 5 inches.

e. Emissivity of all surfaces is 0.85 and emissive power is 0.74.

f. Initial coolant temperature profile is based on Q/A equal to a constant.

g. Initial film drop and conduction temperature difference from heat exchanger tube wall outer surface to coolant mean temperature is 50^{o} F.

h. Coolant inlet temperature is 1200^{o} F.

i. Heat source heat flow into the heat exchanger is 23.5Kw.

Figures 5.1-31, 5.1-32, and 5.1-33 present temperature profiles and heat flux profiles in the heat source and heat exchanger for the circular planar geometry. Calculations were performed for the coolant flowing radially inward and outward through an involute array of tubes. The solid lines represent the temperature profile of the coolant, heat exchanger wall, and capsule surface for the initial assumption of uniform heat flux. Because of the spacing considered, the heat flux varied by a factor of 2 about the assumed mean heat flux due to the capsules being able to see the entire temperature profile of the heat exchanger.

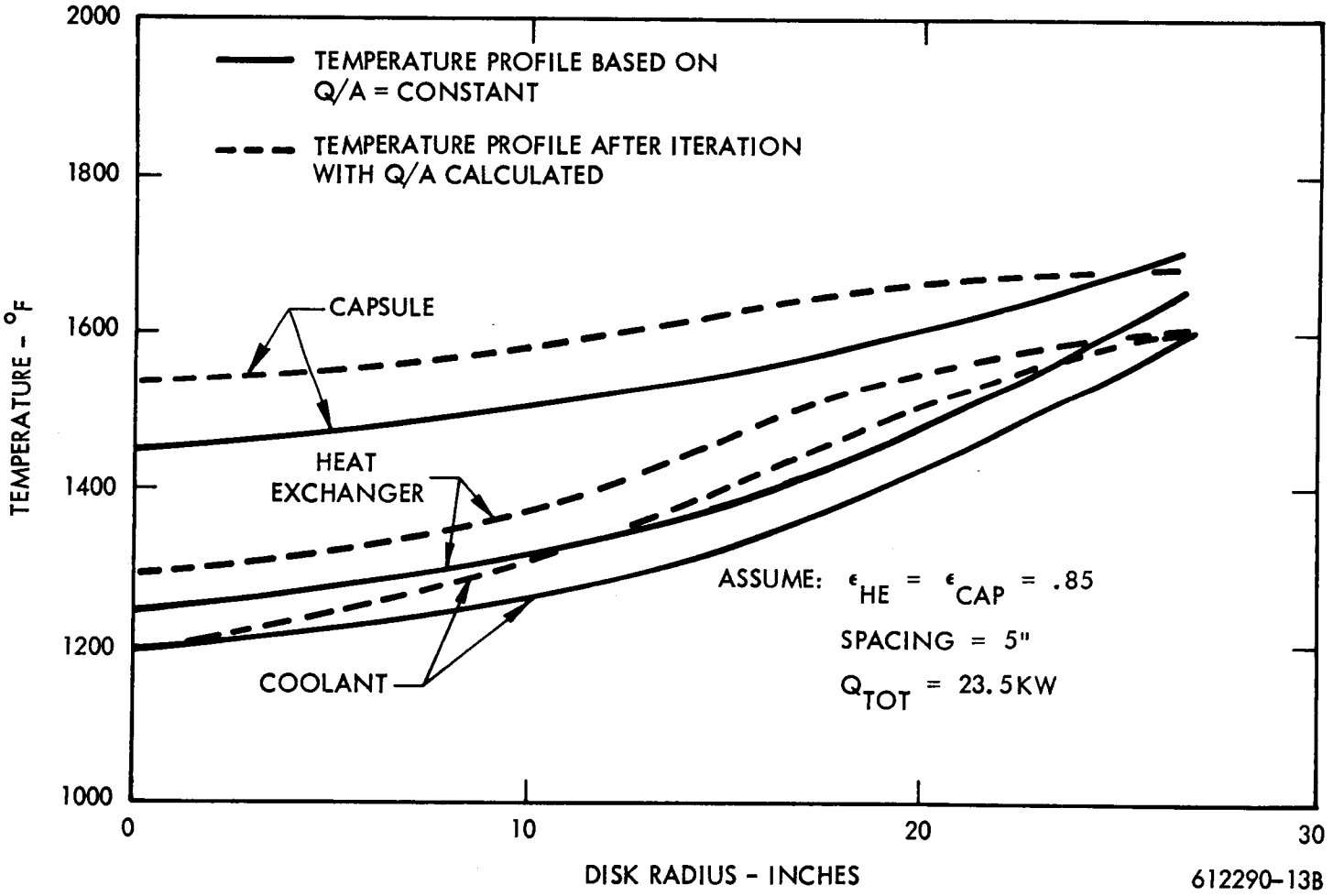

Figure 5.1–31. Temperature Profile for Circular Planar Fuel Capsule Array
(Flow Direction is Radially Outward.)

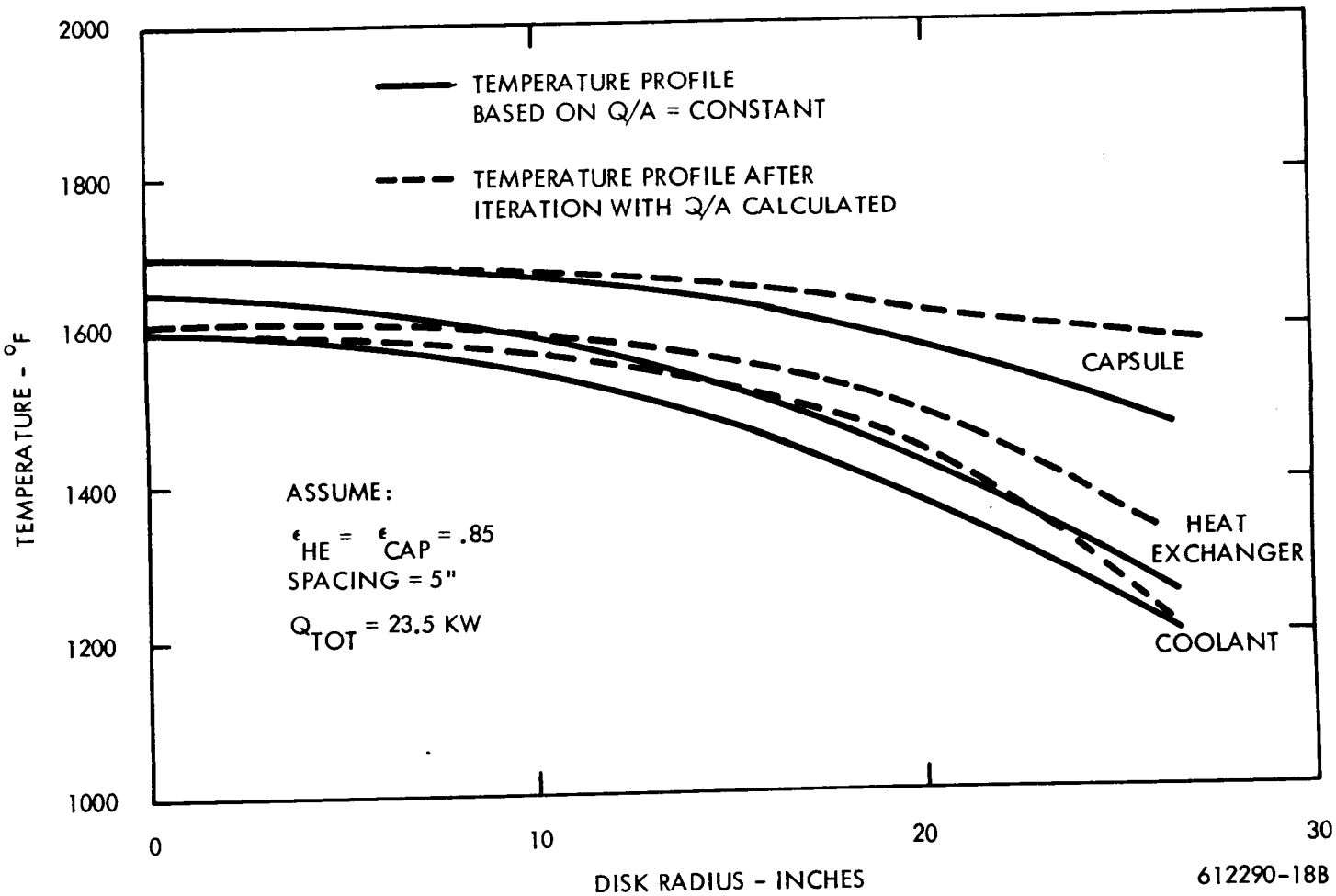

Figure 5.1–32. Temperature Profile for Circular Planar Fuel Capsule Array
(Flow Direction is Radially Inward.)

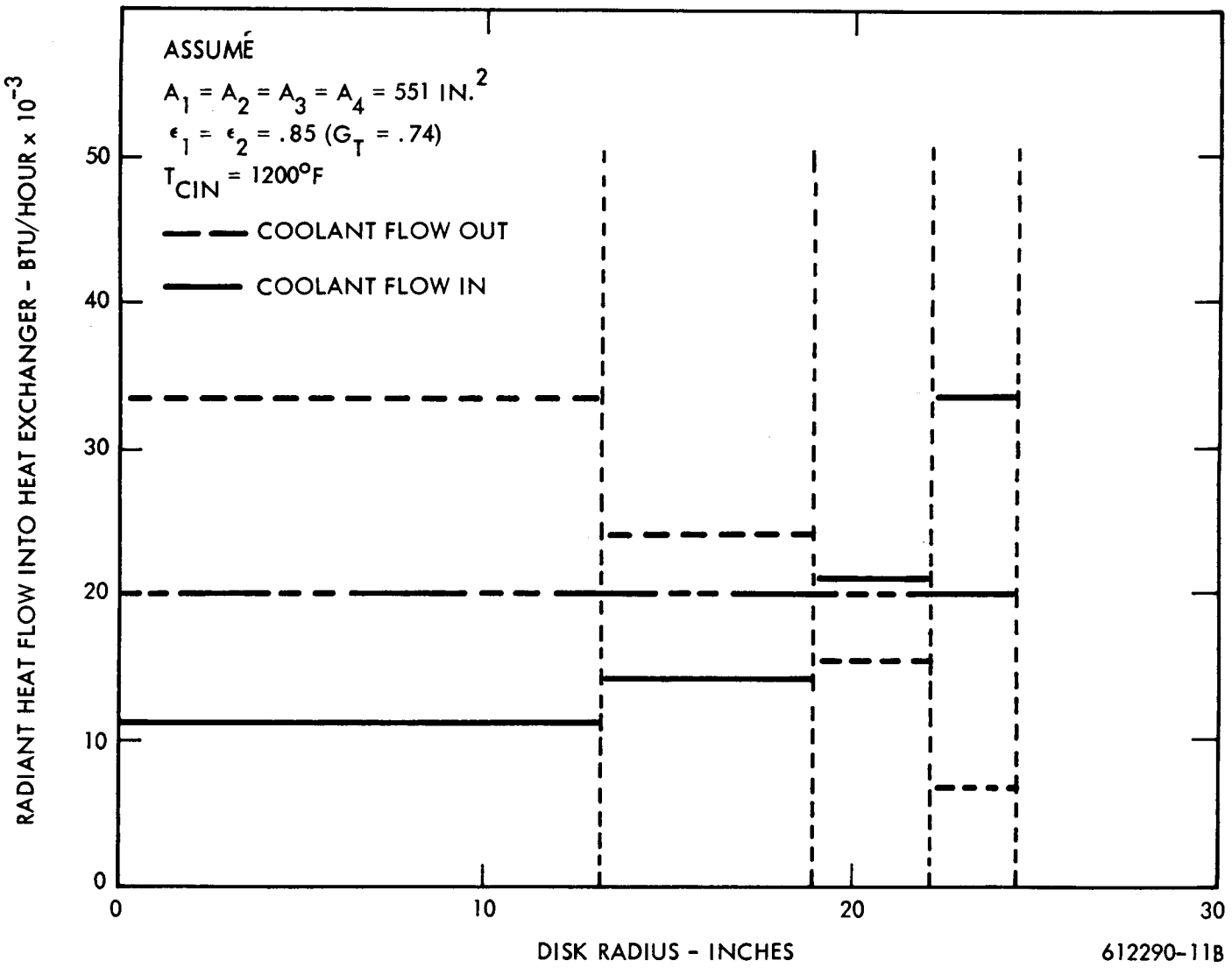

Figure 5.1–33. Heat Flux Profile for Circular Planar Fuel Capsule Array

An iteration was performed on the sensible heat rise of the coolant stream with a varied temperature drop from the heat exchanger surface to fluid based on Q/A= constant to determine the effect of a non-uniform heat flux. The dashed lines represent the temperature profiles after matching the heat transfer rate with the sensible temperature rise of the coolant. Figure 5.1-33 represents the heat transfer rate to each of the four sections of the heat exchanger after iterating the analysis to convergence.

The next set of two curves, Figures 5.1-34 and 1.1-35, present the temperature profiles and heat flux profiles for a rectangular planar array of fuel capsules facing a rectangular shaped heat exchanger. As with the circular planar geometry, Figure 5.1-34 shows that the heat flux varied considerably across the face of the heat exchanger. Therefore, the coolant temperature profile was adjusted to match the heat flux profile. The dashed lines represent the temperature profile after matching the heat transfer rate with the sensible temperature rise of the coolant. Figure 5.1-35 presents the heat flux profile after the iteration was completed.

As indicated in both geometries the effect of a non-uniform heat flux is to flatten the temperature profile in the fuel capsule thus reducing the peak temperature of the fuel capsules. The non-uniformity of the heat flux is attributed to the ability of the entire heat source to "see" the coolant inlet section of the heat exchanger because of the 5-inch spacing between units.

A parametric analysis of the circular planar fuel capsule array is presented in Figures 5.1-36 through 5.1-46. Variations in the heat exchanger wall temperature, the heat source to heat exchanger spacing, the coolant flow direction, and the surface emissivities are compared. The effect of reducing the spacing was to linearize the heat flux and thus increase the temperature drop across the heat source. The temperature profiles are all presented for the constant heat flux assumption without the iteration on coolant temperature rise as described previously.

It was concluded that a five-inch spacing provides sufficient flattening of the heat source temperature profile to maintain peak temperatures at tolerable levels. Heat Source Heat Exchanger (Section 5.2) results have indicated that additional flattening of the temperature profile is obtained.

Although a detailed study with a conical heat source has not been performed, a similar result as that for a planar heat source is expected. It is believed that a planar HSHX facing a conical heat source will perform satisfactorily and a conically dished HSHX is not necessary.

5.1.3.3.4 Capsule Spacing Analysis -- An important design parameter in the overall system design is the minimization of the heat source support plate size. Implicit to this criteria is the minimizing of the capsule spacing which will be at the expense of increased conduction and radiation temperature drops from the base of the capsule to the HSHX surface. An analysis was performed to determine effects of capsule spacing on peak capsule temperatures for a capsule with an 0.060-inch cover plate, the results of which have been shown in Figure 5.1-8. In this analysis, the internal heat generated at the base of the capsule was assumed to be conducted around the capsule periphery to a point where the cover plate is attached. From this point to the top of the capsule, the generated heat and the heat conducted from the base would be uniformly radiated to the cover plate and then radiated to the HSHX.

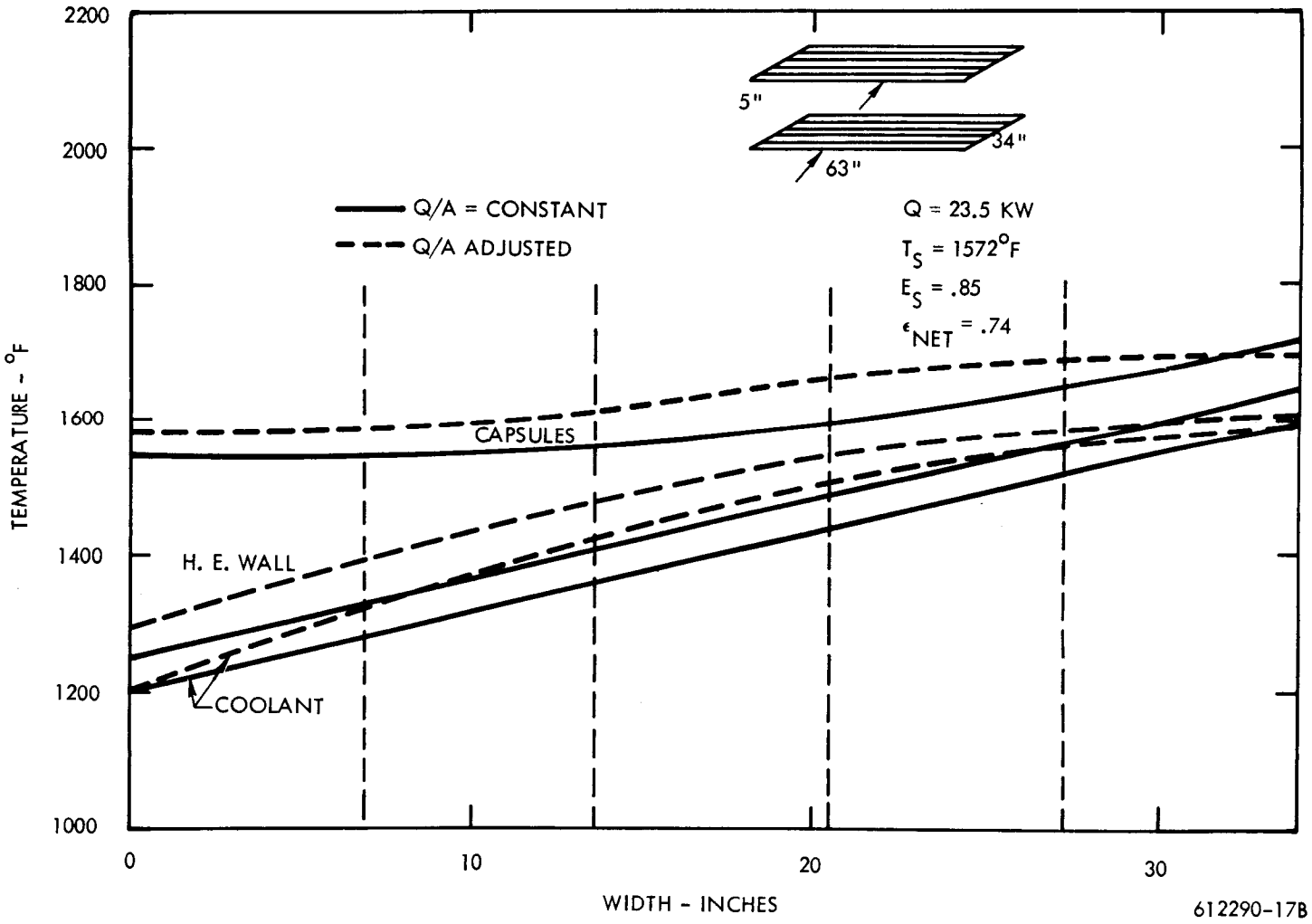

Figure 5.1–34. Temperature Profile for Rectangular Fuel Capsule Array

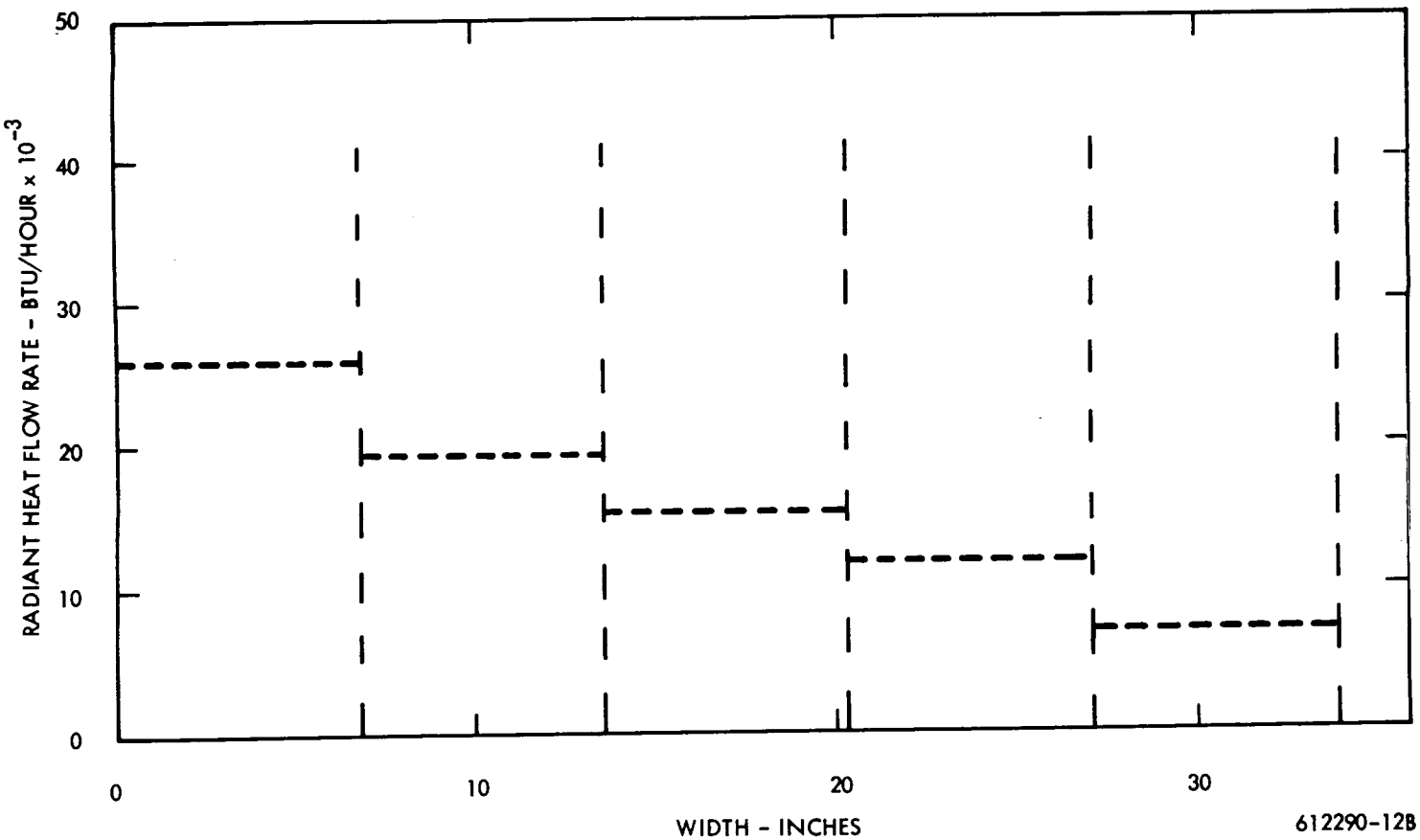

Figure 5.1–35. Heat Flux Profile for Rectangular Fuel Capsule Array

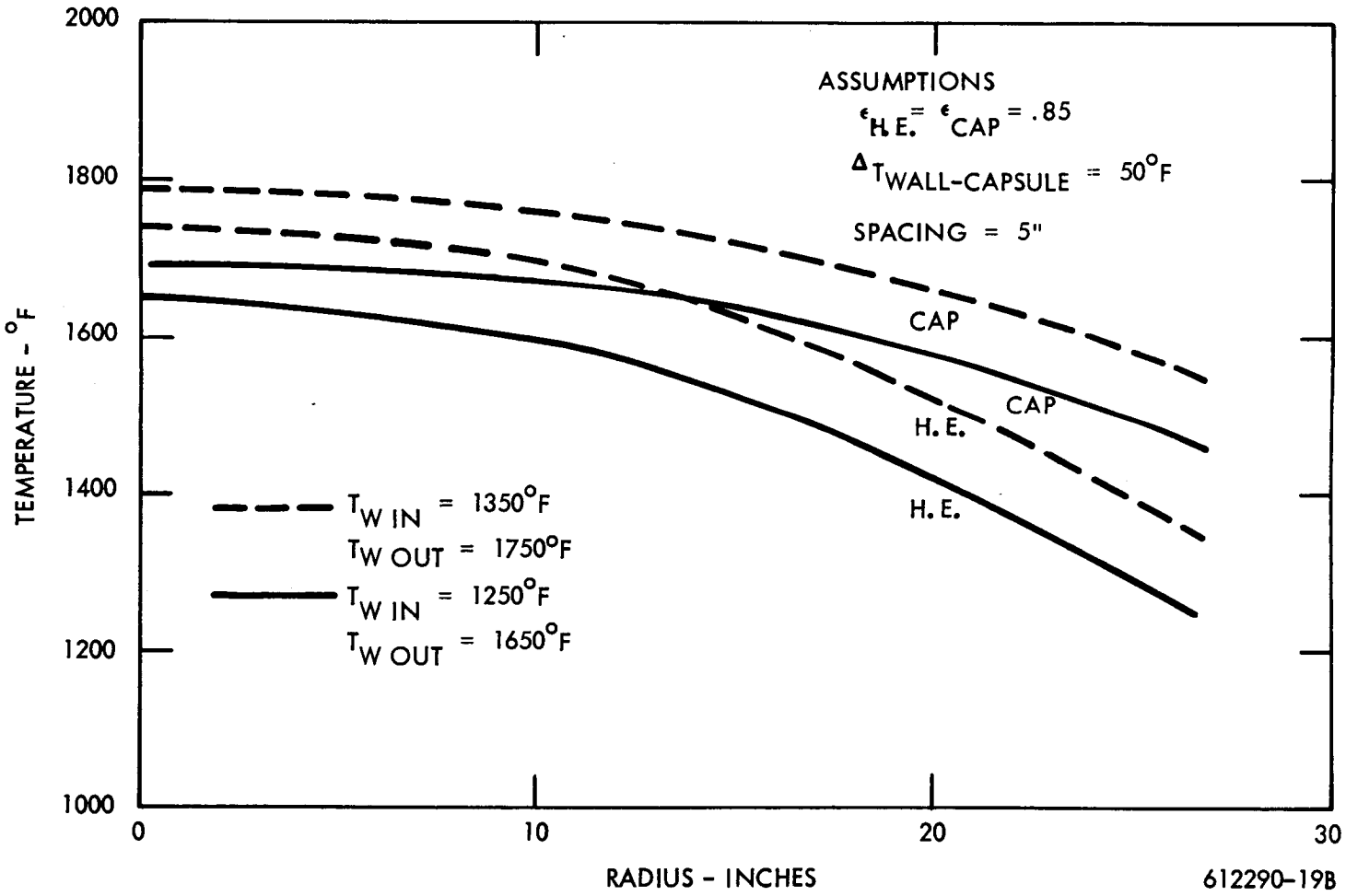

Figure 5.1–36. Temperature Profiles in Disk Capsule Array and Involute Shaped Heat Exchanger

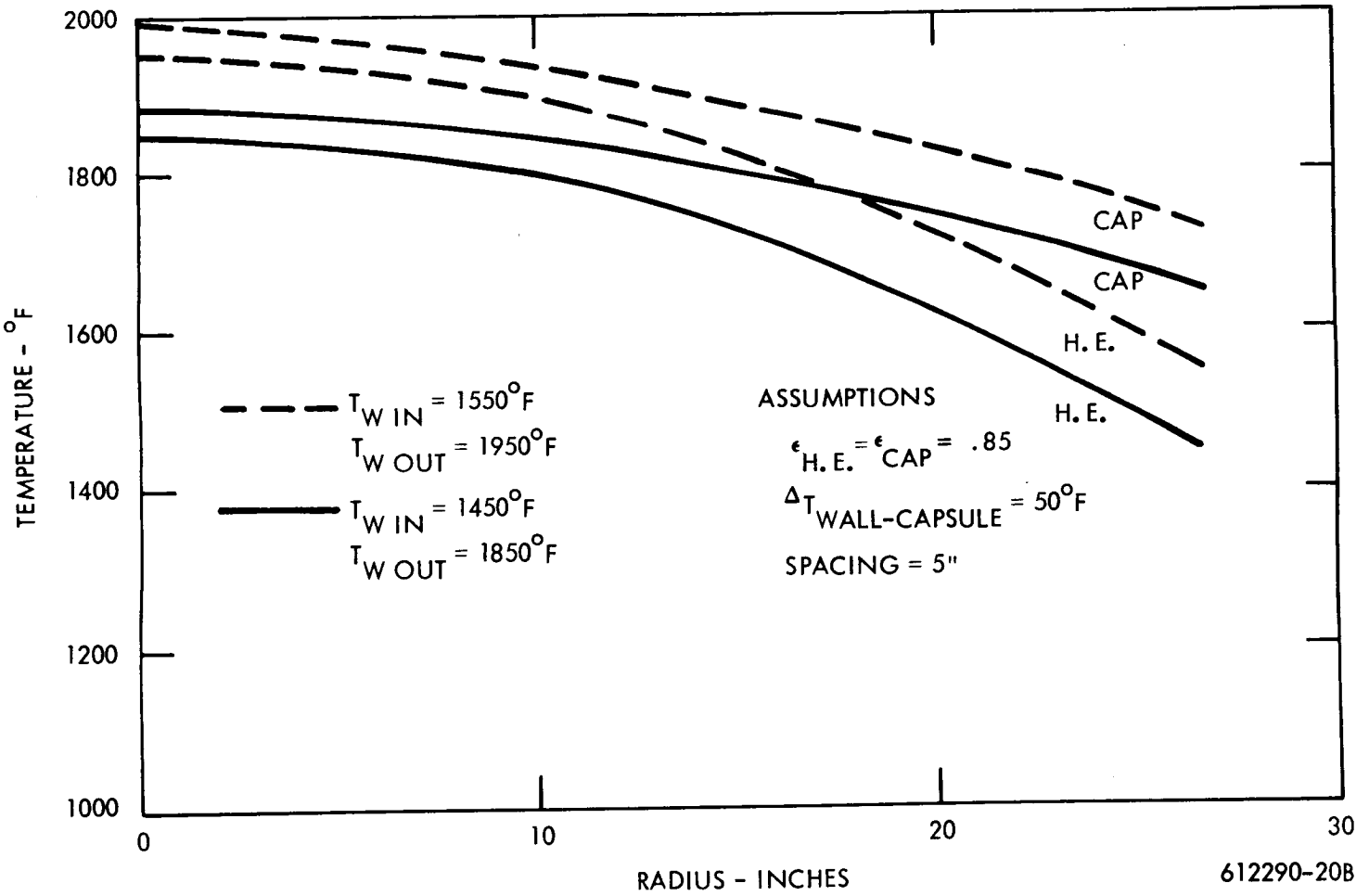

Figure 5.1–37. Temperature Profiles in Disk Capsule Array and Involute Shaped Heat Exchanger

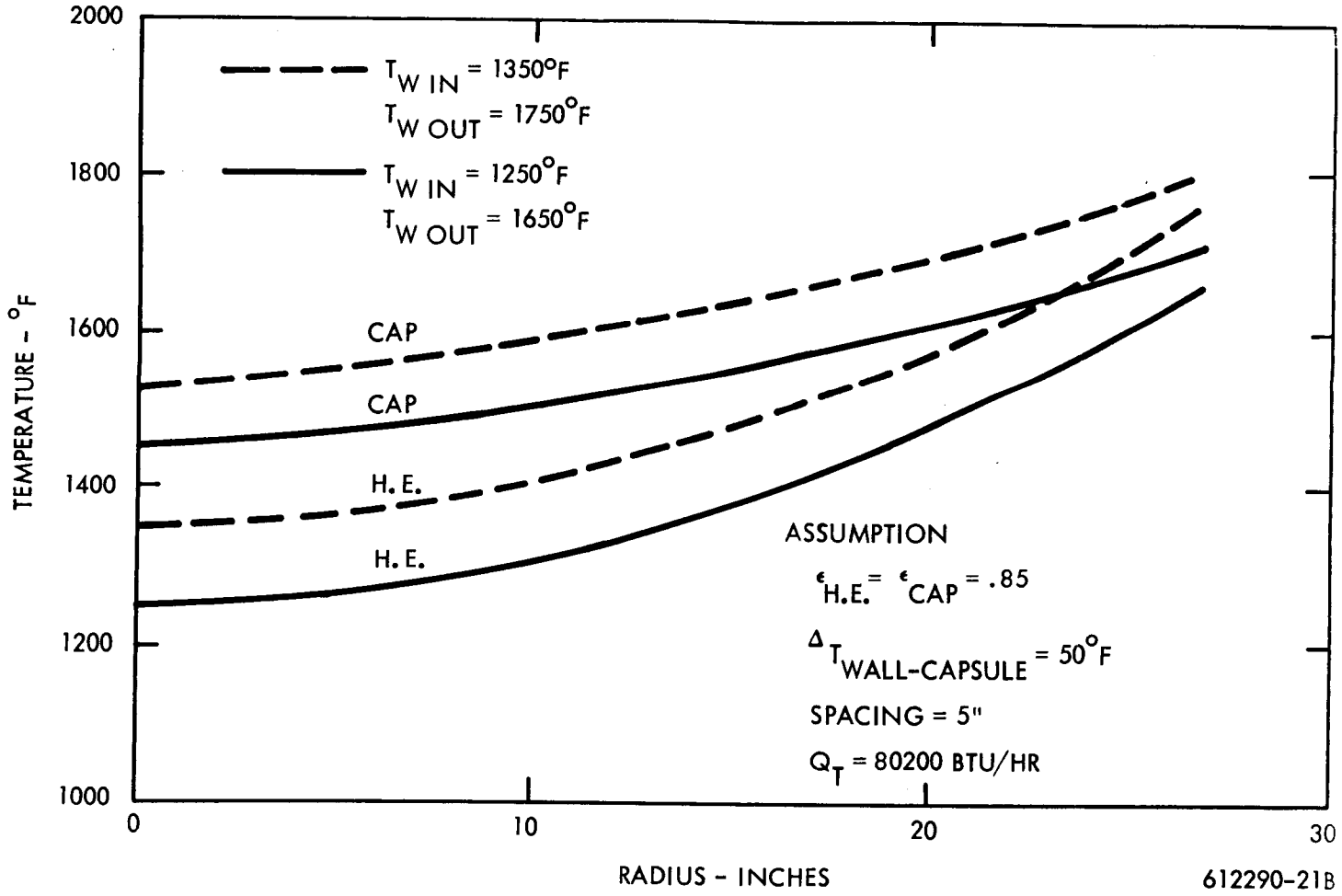

Figure 5.1–38. Temperature Profiles in Disk Capsule Array and Involute Shaped Heat Exchanger

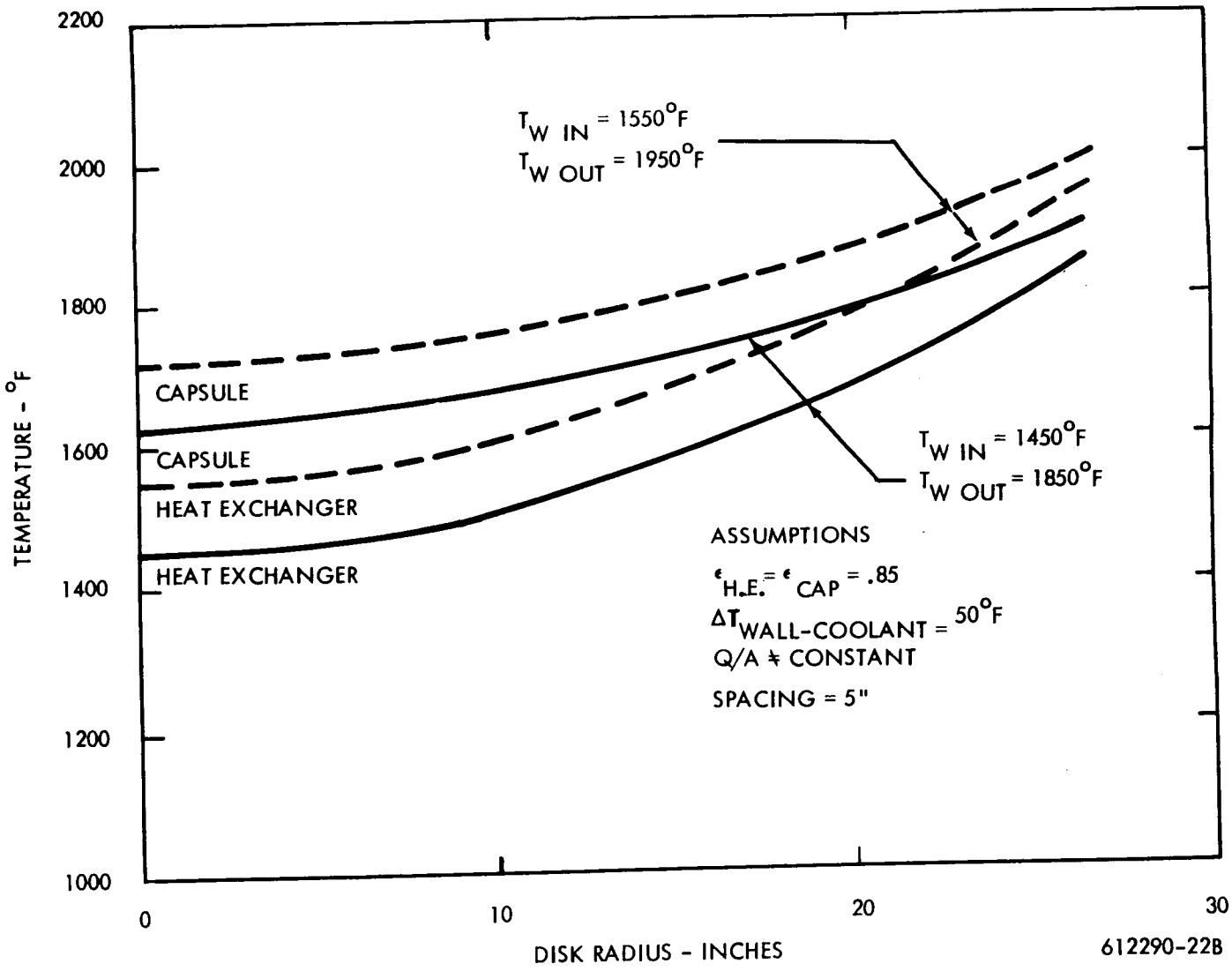

Figure 5.1–39. Temperature Profiles in Disk Capsule Array and Involute Shaped Heat Exchanger

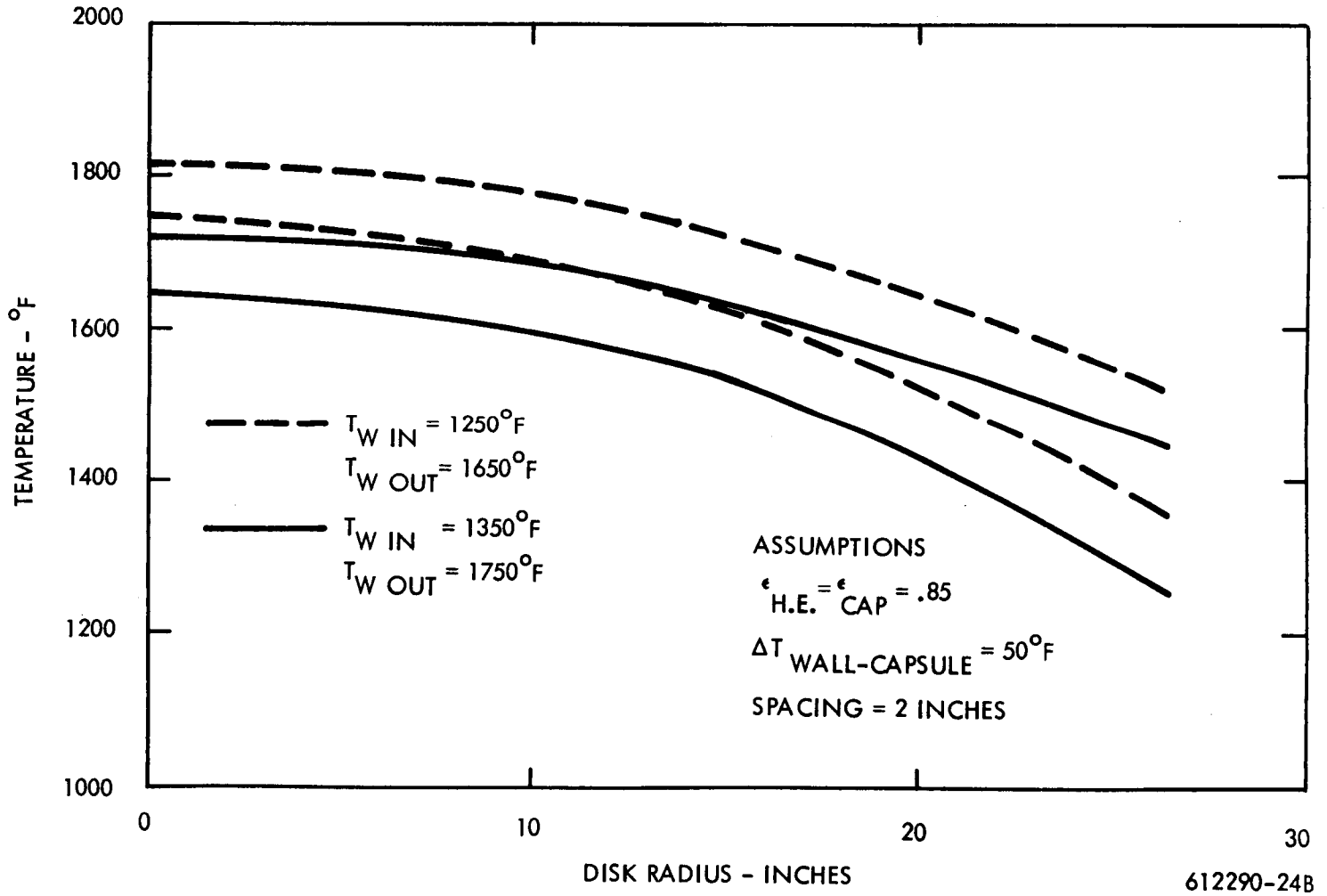

Figure 5.1–40. Temperature Profiles in Disk Capsule Array and Involute Shaped Heat Exchanger

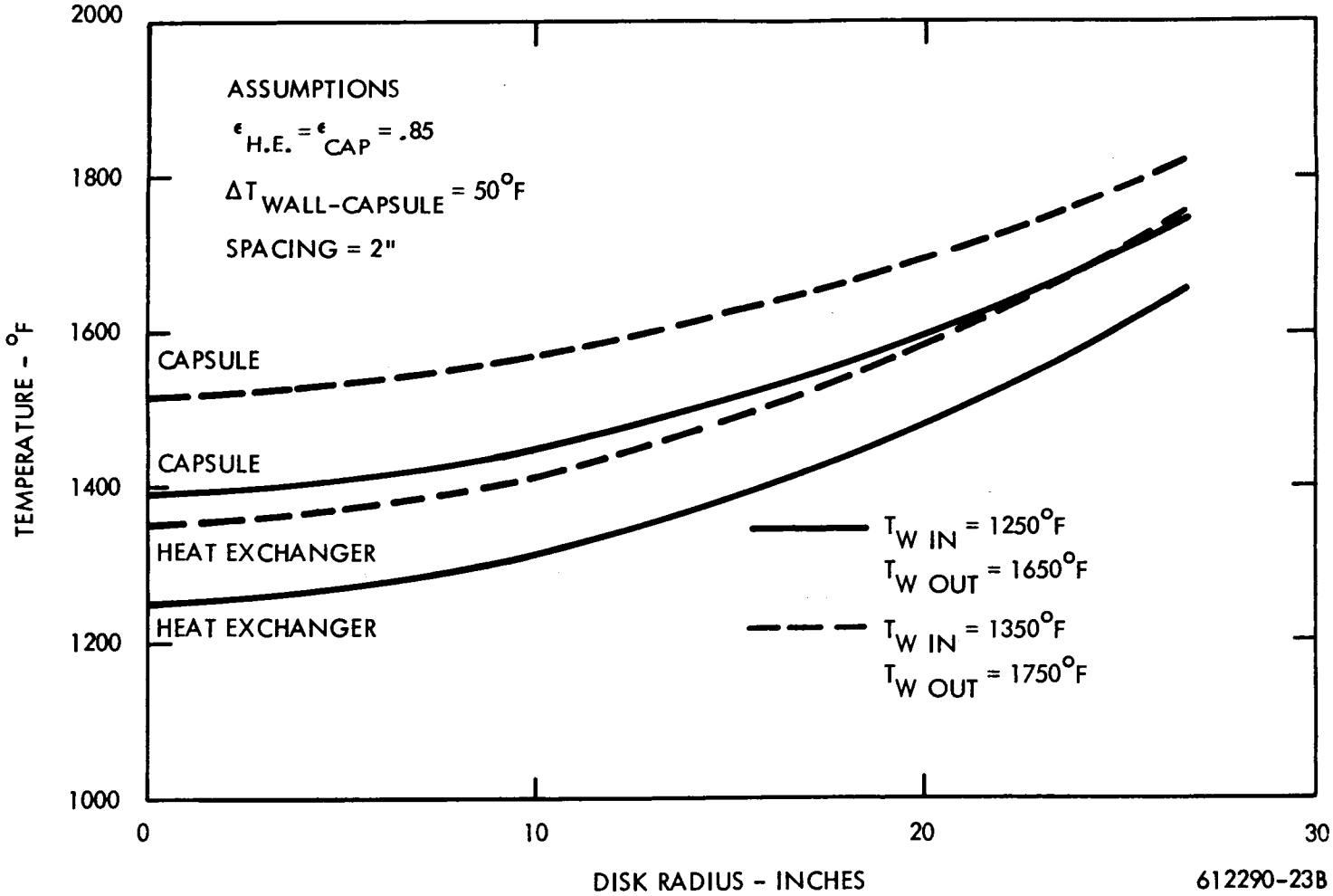

Figure 5.1–41. Temperature Profiles in Disk Capsule Array and Involute Shaped Heat Exchanger

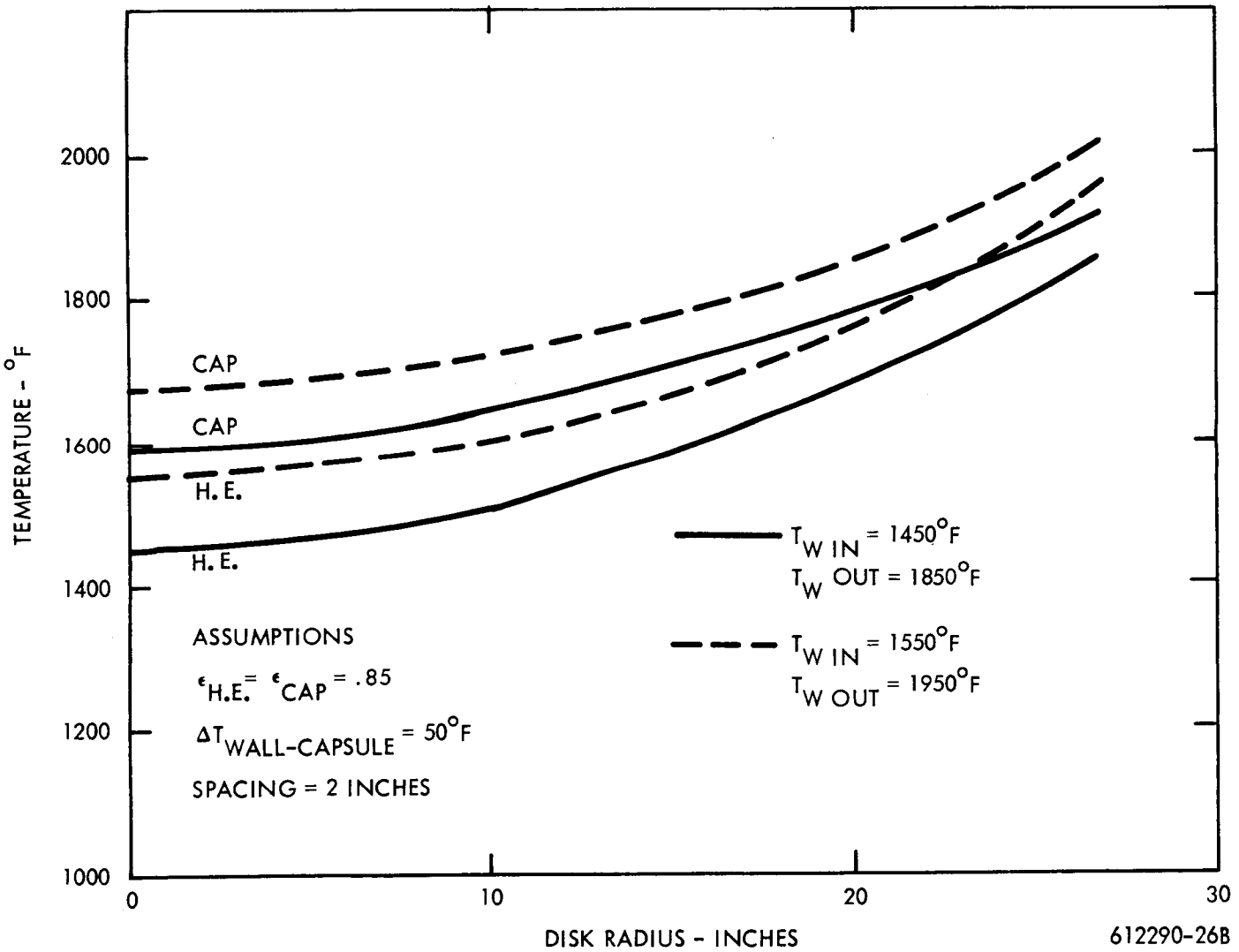

Figure 5.1–42. Temperature Profiles in Disk Capsule Array and Involute Shaped Heat Exchanger

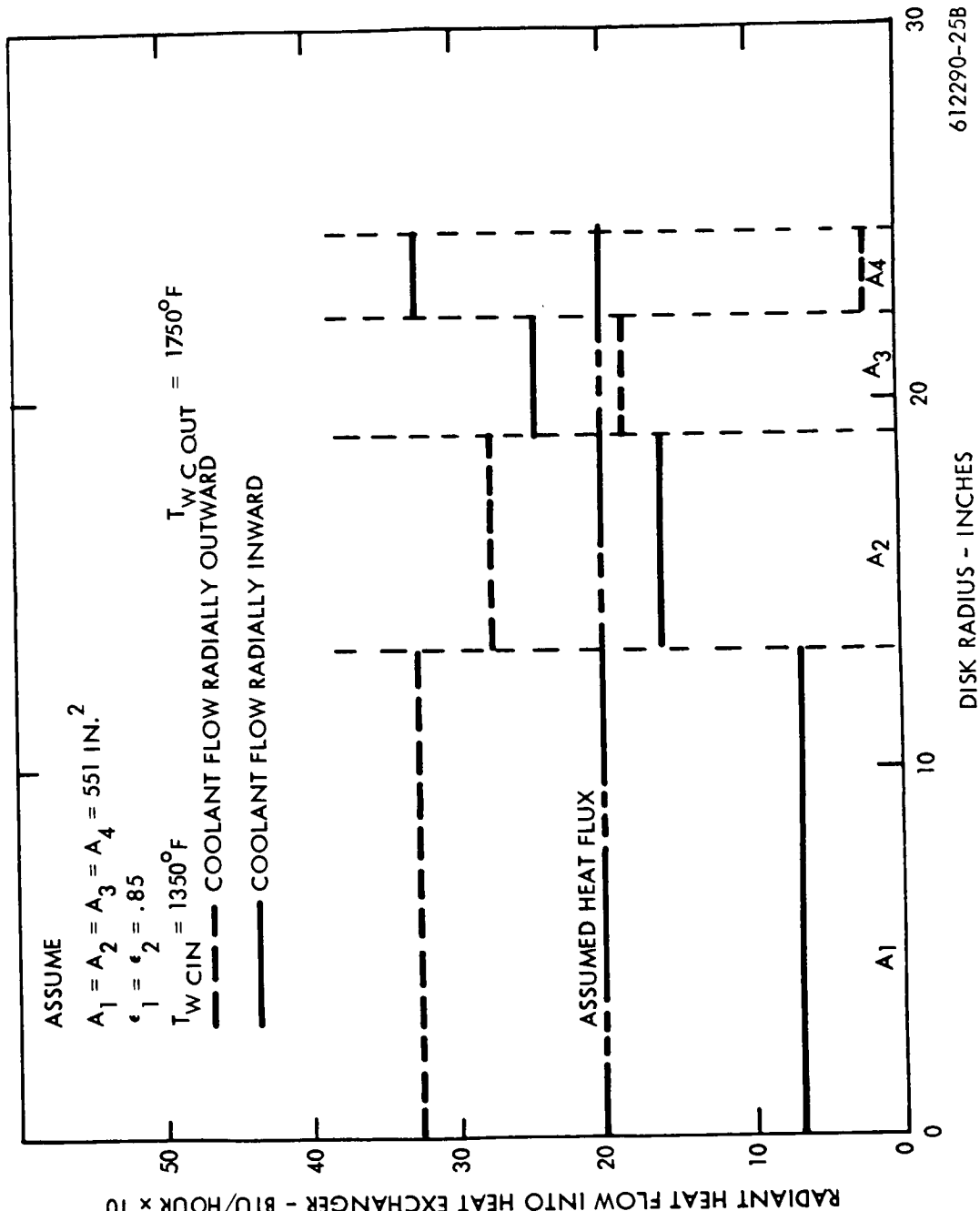

Figure 5.1-43. Calculated Heat Flow Rates to Heat Exchanger

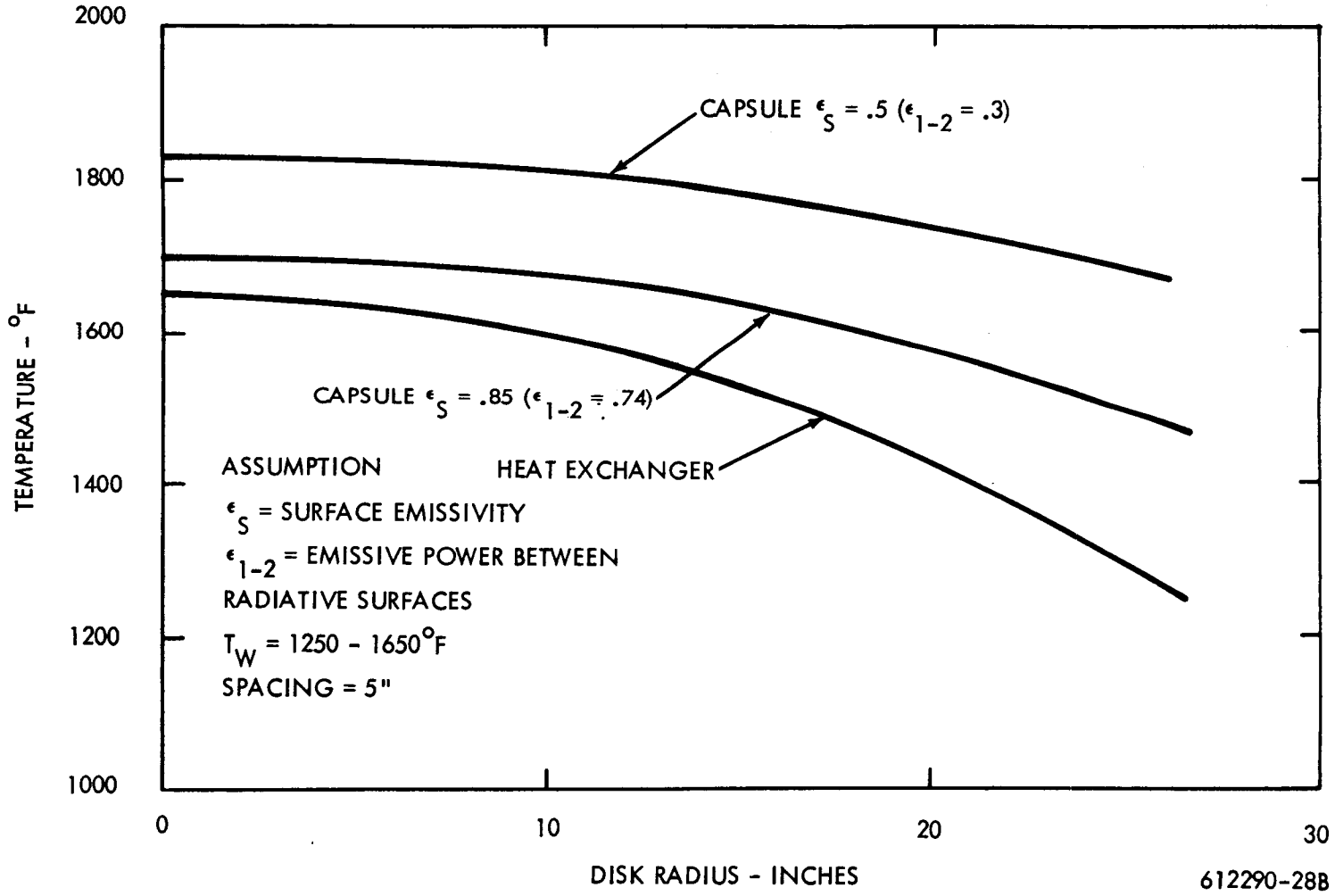

Figure 5.1-44. Effect of Surface Emissivity on Capsule Temperature with Flow Direction Radially Outward

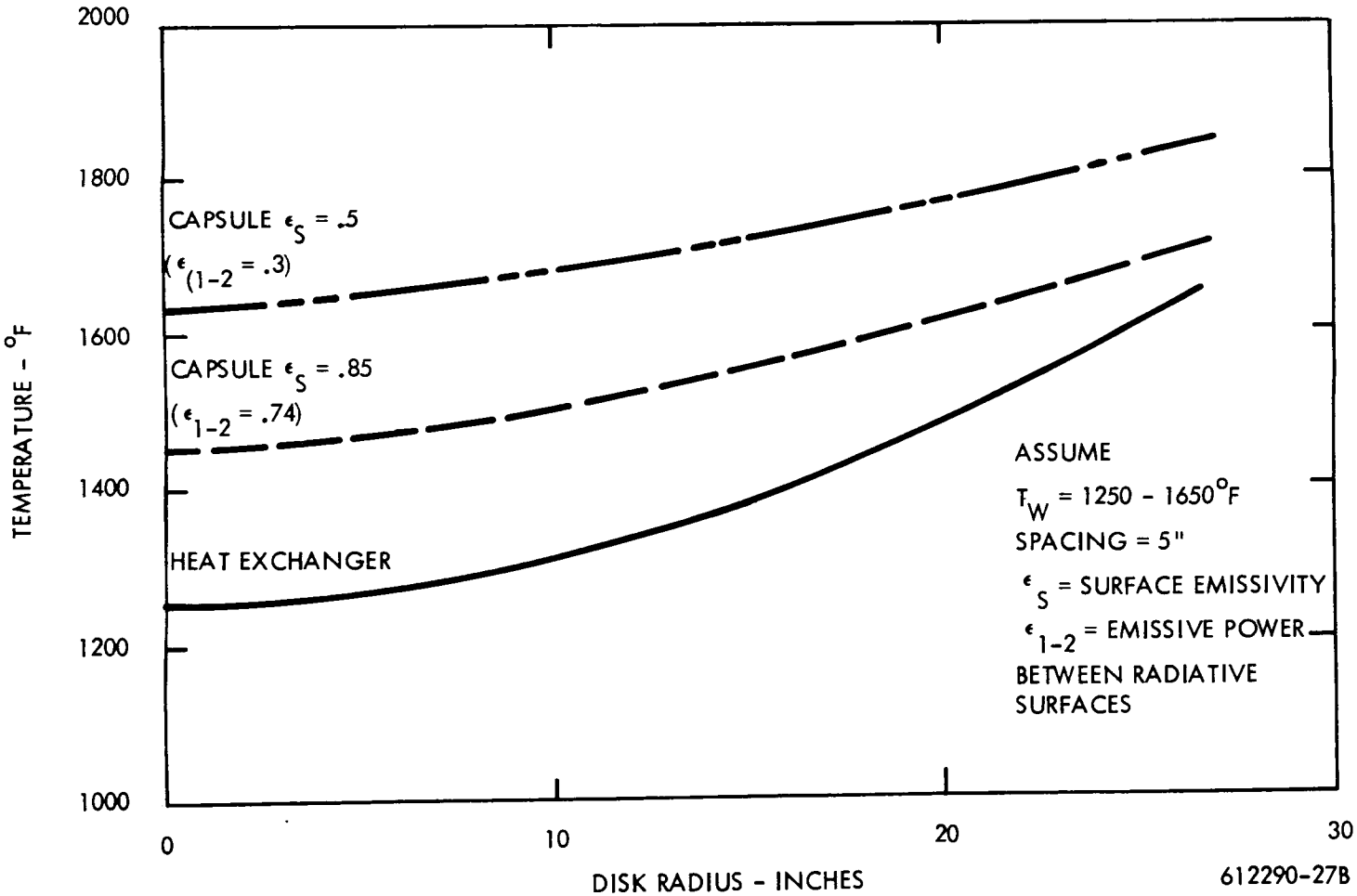

Figure 5.1–45. Effect of Surface Emissivity on Capsule Temperature with Flow Direction Radially Inward

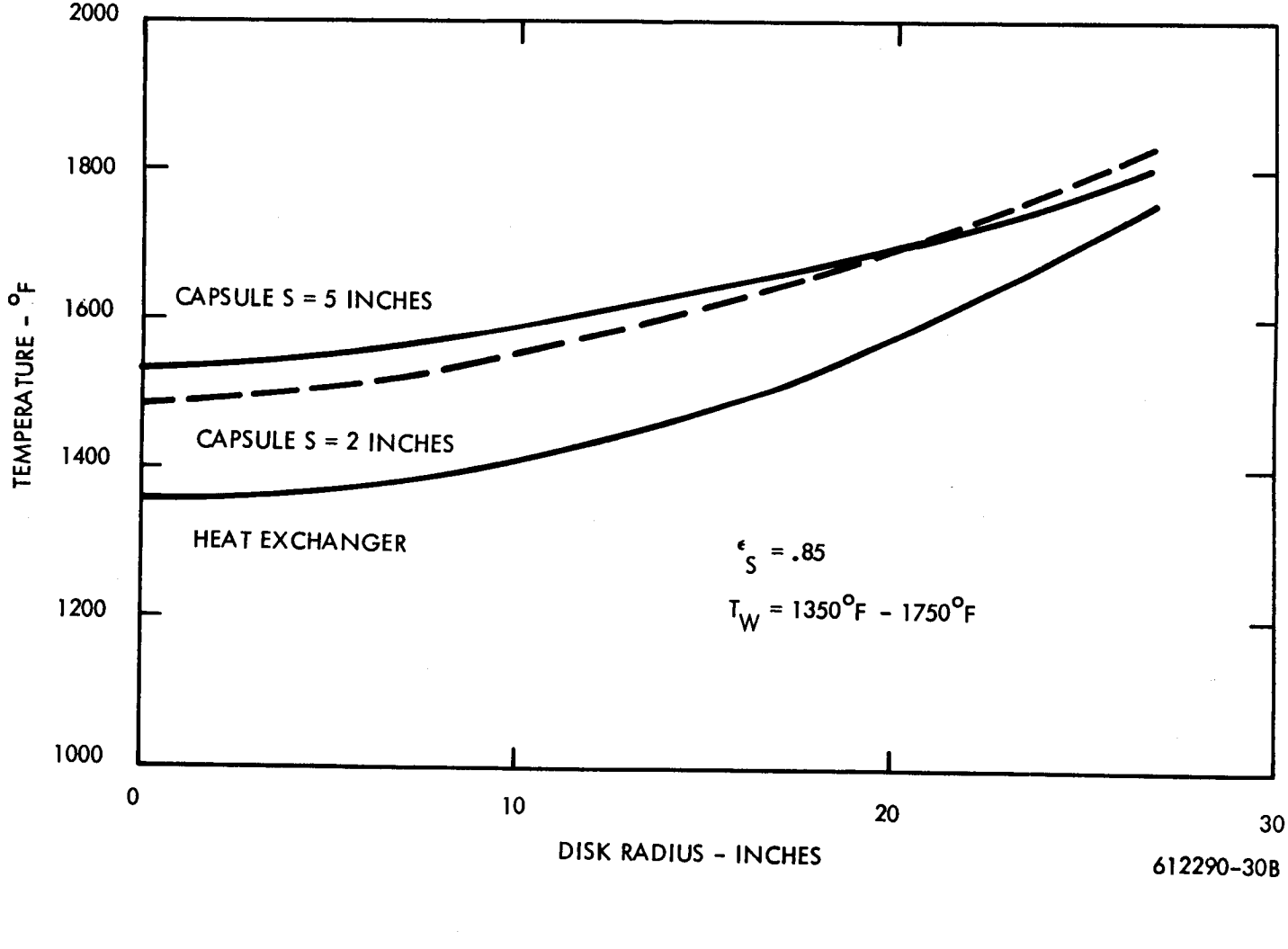

Figure 5.1–46. Effect of Spacing on Capsule Temperature Profile

The results shown in Figure 5.1-8 indicated these factors that influenced the increase in the temperature drop from capsule base of the HSHX with a decrease in spacing.

The first factor represented by the lowest line is the radiation temperature drop from the heat source to the HSHX. A decrease in spacing and this heat transfer resulted in a gradual increase in radiation ΔT to approximately 250° F from a 2.0-inch spacing to a 1.6-inch spacing.

The second factor is the influences of the gap radiation between the capsule and the cover plate. For spacings greater than 1.7 inches, sufficient space was available for positioning the cover over a 210 degree arc of the fuel capsule array thus providing a maximum in gap radiation area. Decreasing the spacing below 1.7 resulted in decreasing the arc over which the cover could be positioned, thus increasing the gap radiation, $\Delta T_{cap} = T_1 - T_2$. This resulted in a rapid increase in the temperature drop. The third factor is the influence of conduction path temperature drop. For large spacing, additional material could be placed between the capsules resulting in a slight reduction in ΔT as shown in the figure for the line $\Delta T_{cap} = T_1 - T_2$ for spacings greater than 1.7. This effect was negligible compared to effects of the capsule area over which the cover could be placed. It was concluded that for a covered capsule the minimum allowable spacing would be that spacing which would not require a sacrifice in the capsule surface area over which the cover could be placed.

For the cover considered, the optimum spacing was determined to be 1.75 inches. Thinner covers result in a larger conduction ΔT and less support bearing capability. A bare capsule array will also be subject to the penalties of increased conduction ΔT and the increase in radiation ΔT.

5.1.4 Heat Sink

Functional requirements for a heat sink are specified in the IRV design criteria:

a. Normal Operation -- Maintain minimum capsule heating rate of 700° F/HR from initial temperature of 1800° F.

b. Launch Pad Operation -- Maintain capsule at sufficiently low temperature while in the atmosphere after launch to prevent excessive oxidation of the support structure.

The selection of beryllium oxide as the heat sink material for the planar and conical array was based on its high heat capacity and its compatability with the refractory materials used in the heat source support plate fabrication.

The retention of the beryllium in the heat source support plate is accomplished as shown on Figure 5.1-47 where the beryllium oxide block is fitted between the grid structure of the heat source support plate.

A good mechanical interface between the beryllium and heat source is required to ensure good thermal conductance and a light retention plate is welded to the grid support sandwiching the beryllium in place.

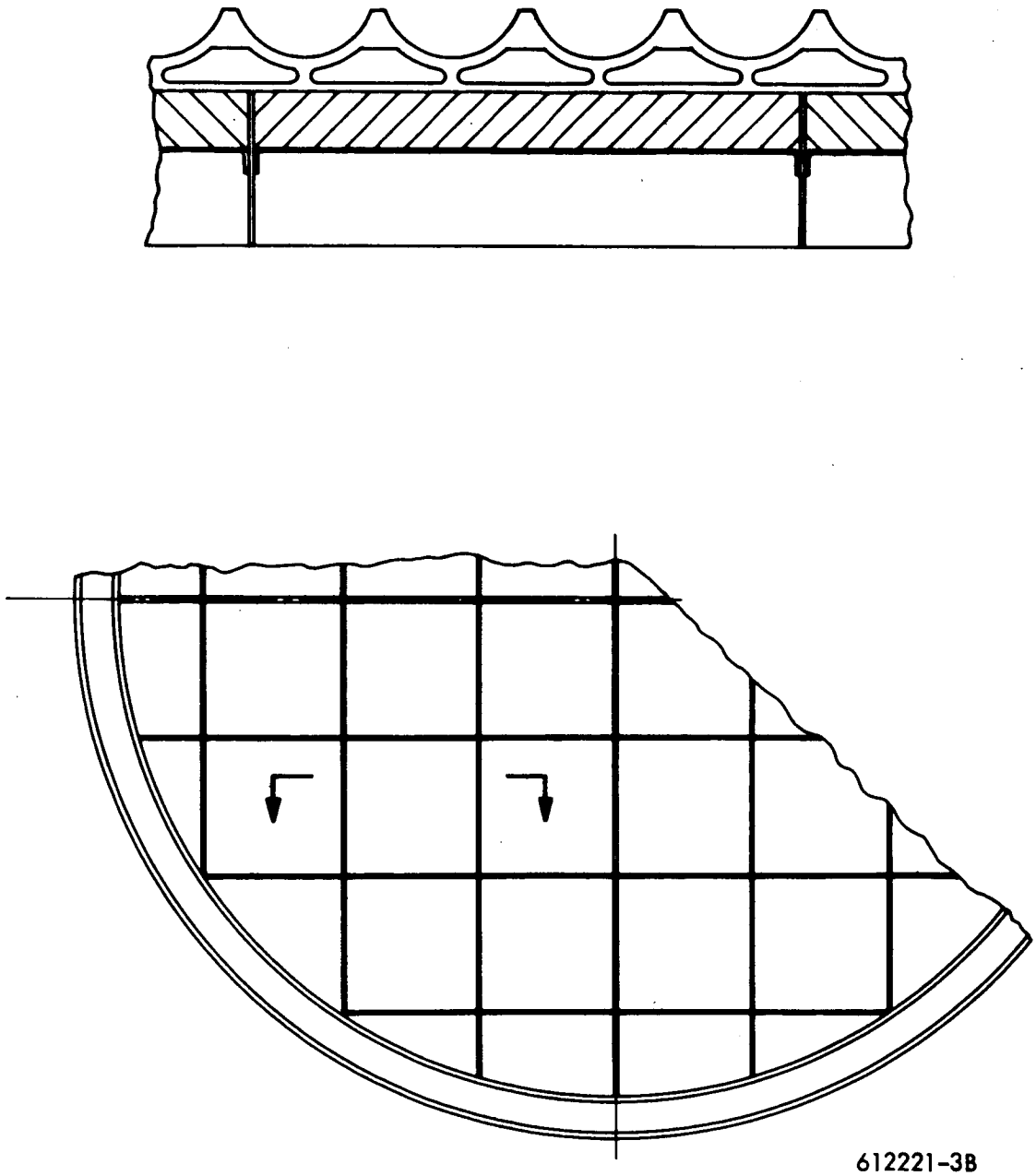

Figure 5.1-47. BeO Integration

In the graphite block pin cushion array concept no beryllium is required as the graphite heat source support plate thermal capacity is sufficient to meet the heat sink thermal requirements.

During steady state operation of the heat source and the Brayton cycle equipment while in orbit a possible source of fuel capsule damage is the overheating of the heat source to a level such that structural weakening occurs as a result of Brayton cycle equipment malfunction. To alleviate this problem, a design requirement was established to provide sufficient thermal capacity in the IRV fuel capsule assembly to limit the time for the capsule temperatures to rise from 1800° F to 2500° F in no less than one hour, thereby providing time to respond to the problem.

Figure 5.1-48 shows the effect of varied weights of beryllium oxide combined with 450 lbs of support structure and 700 lbs of capsules on the heat source heating rates for initial temperatures of 1800° F and 300° F. Providing a 10 percent margin in heating rate, 140 lbs of beryllium was selected for the designs which would provide a maximum of 630° F per hour from an initial temperature of 1800° F.

Another possibility of fuel capsule damage due to overheating exists while the missile is on the launch pad in air. While there, the heat source assembly must be maintained at as low a temperature as possible to minimize oxidation and possible structural damage. An auxiliary heat exchanger with air or nitrogen supplied from ground control is used to remove the heat generated by the capsules. Prior to launch, the heat exchanger is disconnected. A maximum time requirement for the heat source to reach an oxygen free atmosphere is therefore required to prevent the capsules from reaching excessive temperature levels.

The rate of temperature rise from a uniform temperature of 500° F is presented in Figure 5.1-49 for a heat source containing 140 lbs of beryllium oxide, 700 lbs of capsules, and 450 lbs of support structure made of Cb-1 percent Zr alloy.

A heat block design, which is used in the planar and pin cushion arrays, utilizes graphite which has a thermal capacity approximately equivalent to that of BeO at 1800° to 2500° F; therefore, a minimum of 140 lbs of graphite is required for structural use, and sufficient thermal capacity is available without the use of BeO.

Conclusions from this analysis are as follows:

a. 140 lbs of BeO provides sufficient heat capacity to limit the time for the planar and conical heat sources to rise from 1800° F to no less than one hour.

b. Designs utilizing graphite heat block will not require the use of BeO for thermal capacitance requirements.

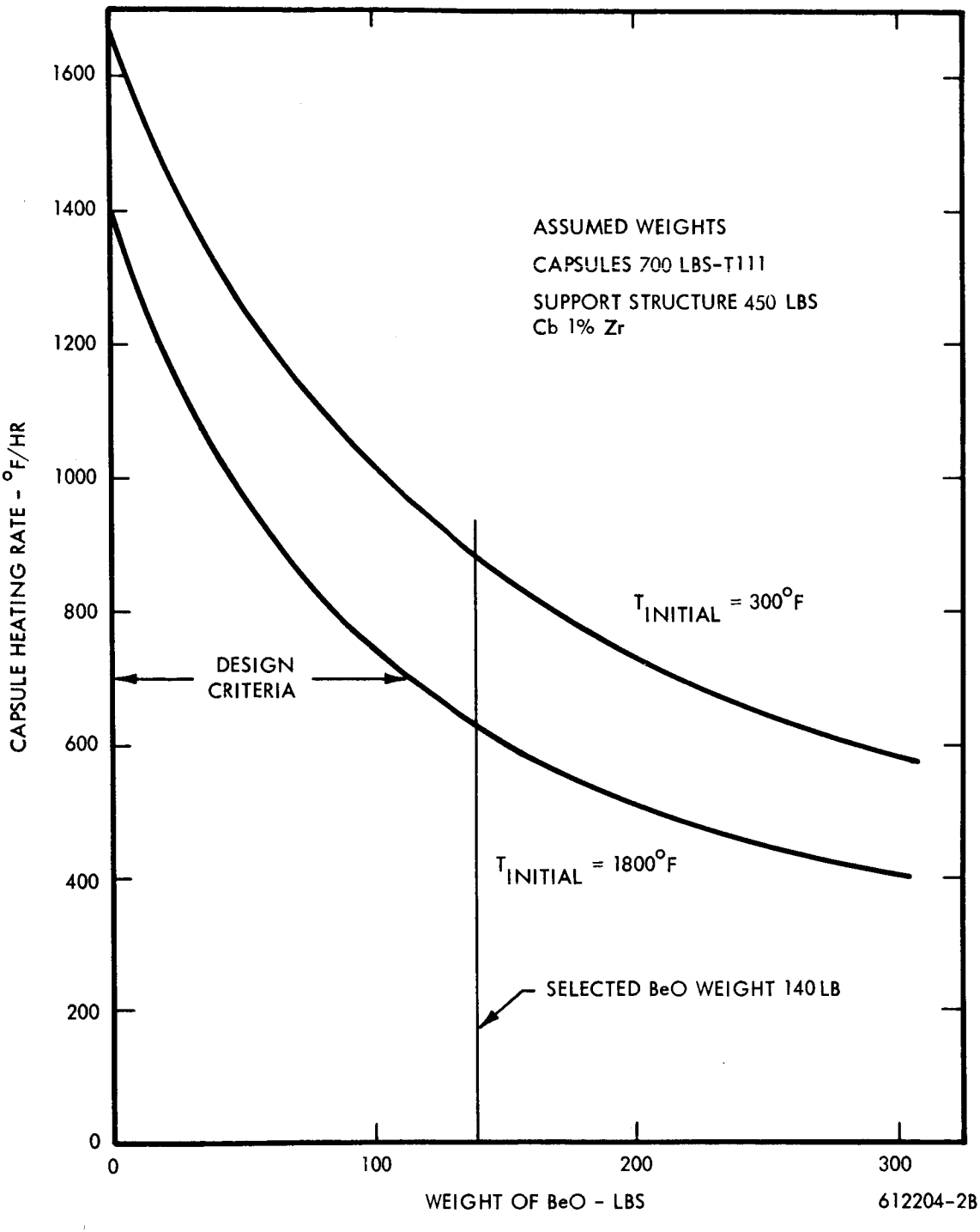

Figure 5.1-48. Capsule Heating Rate vs BeO Weight

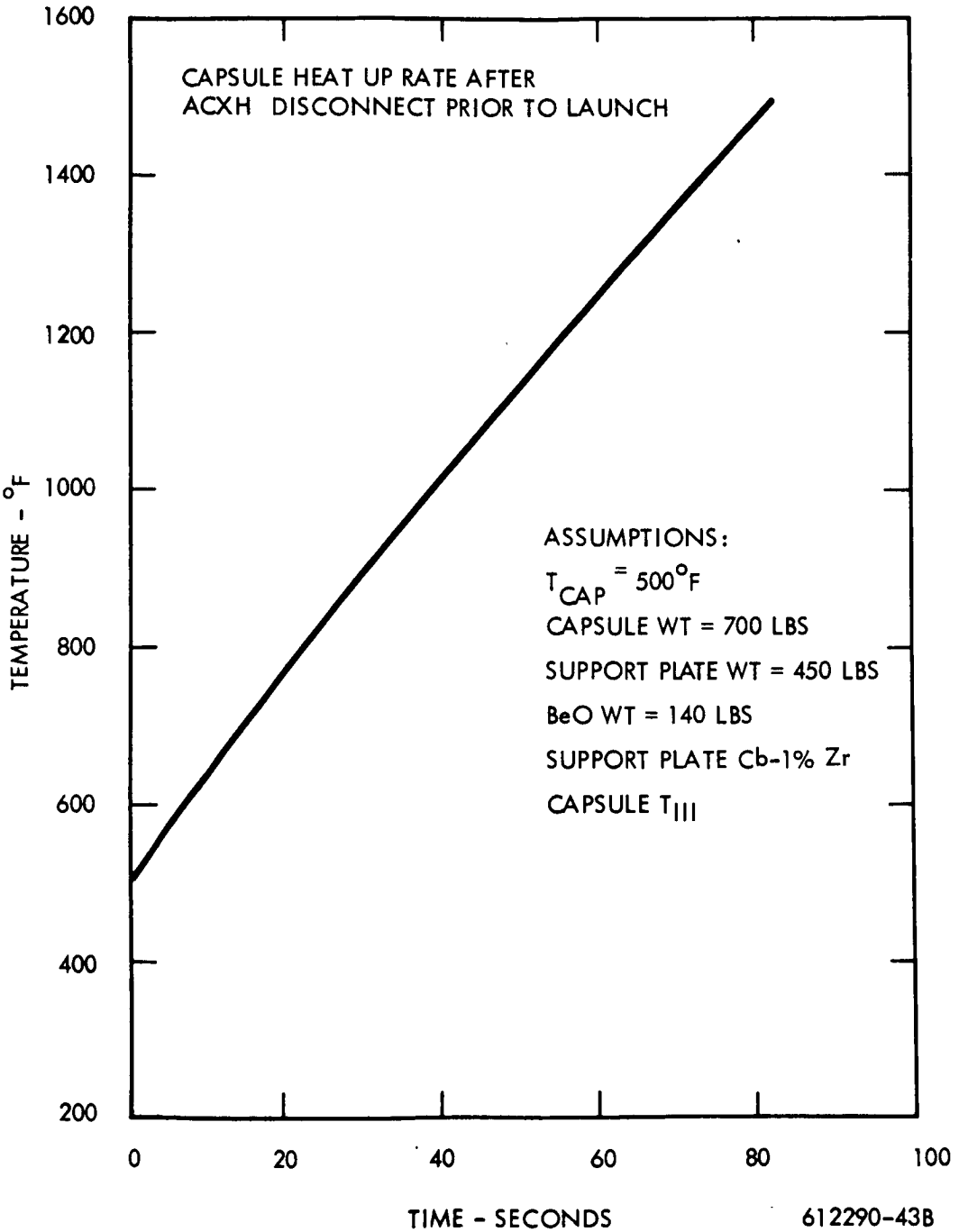

Figure 5.1-49. Capsule Heat Up Rate After ACHX Disconnect Prior to Launch

5.1.5 Insulation System

5.1.5.1 Mechanical Design

The need for a minimum heat loss system requires that an insulation capable of operating for long periods of time at high temperatures is required. To accommodate these requirements, an insulation system based on the Linde Superinsulation concept was selected as a representative material for preliminary analysis. Finally, comparisons were drawn between competitive insulation systems.

The insulation is located directly below the heat source support plate and around the sides to mate with insulation arranged around the HSHX. This completely insulates the system.

It is essential that the number of penetrations through the insulation be kept to a minimum; but, as with the truss support structure where this was unavoidable, additional insulation is located around individual struts to minimize the heat loss. The possibility of using Battelle structural insulation instead of Superinsulation has been considered. This could possibly have eliminated the separate truss support structure and insulation.

Battelle Memorial Institute has reported on a honeycomb-like structural insulation for use in thermoelectric devices, "A Thermal Insulation and Structural Support for Thermoelectric Devices" by J. Ketchman and R. Wittman, BMI. A much higher heat loss would occur in using Battelle insulation with no real structural gain. It, therefore, appears that retaining the Superinsulation is desirous.

The factors considered in the comparison were as follows:

a. Insulation thickness for given heat loss for Battelle versus Linde insulation

b. Structural attachment requirements

c. Impact attenuation capability

The apparent advantages of the Battelle concept are that it combines the crushable material and insulation functions in one material, and it adds approximately two inches to the stopping distance on impact which theoretically could decrease g-load on the heat source by 10 to 20 percent. However, the disadvantages are as follows:

a. Limited design parameter data is available.

b. There is limited material selection, since approximately 500 psi minimum capability is desired for impact effective yield strength and the design allows (σ/σ honeycomb material in compression) maximum = 0.018 (See Reference 1); hence, the material yield stress at temperature must be approximately 28,000 psi and consistent with temperature.

c. The maximum insulation capability is not as good as superinsulation, and the maximum energy absorbing capability is probably not as good as the recommended crushable materials.

d. Design provides that insulating capability and structural capability are inversely related; i.e., the better the insulator, the worse the load capability, and vice versa.

e. Battelle structures are anisotropic thermally and impact-wise.

The Linde Superinsulation system has been sized to provide a total heat leak of 250 watts. Equivalent thickness of the best Battelle material described in the above reference 1 would be 81.6 inches. That is, from table 4 reference 1, the best structure use in the IRV would be structure B, with yield strength of 360 psi at 1200°K, and

$$\text{Effective } K = 75 \quad (10^{-4}) \quad \text{watts/in}^{\circ}\text{K}, \quad 500\text{-}800^{\circ}\text{K}$$

$$\text{Effective } K = 84 \quad (10^{-4}) \quad \text{watts/in}^{\circ}\text{K}, \quad 500\text{-}1200^{\circ}\text{K}$$

$$q = KA\left(\frac{\Delta T}{h}\right)$$

$$\text{thickness} = h = \frac{KA\,\Delta T}{q}$$

a. For T = 1700° F ≈ 950°K, round plate 53-inch diameter.

h = 70.5 inches (uniform thickness about heat source)

b. For T = 1700° F ≈ 950°K, rectangular plate 40 by 64 inches

h = 81.6 inches (uniform thickness about heat source)

These thickness values are too large to be feasible, besides which a yield strength of only 360 psi is too low to provide adequate energy absorption on impact.

5.1.5.2 Heat Loss Analysis

An analysis has been performed, to evaluate thermal losses from the fuel capsules during steady state operation while in orbit, on the six designs under consideration. Preliminary estimates of thermal losses were made for conduction and radiation through the insulation strut supports, and one-half of an insulation seal connecting the reentry vehicle to the Brayton cycle equipment using the model shown in figure 5.1-50. Calculations were performed on the circular and rectangular planar arrays for two temperatures of 1800° F and 2000° F on the hot side of the insulation and truss supports and for a range of temperatures at the cold surface of the insulation and strut bases.

Based on a model sketched in figure 5.1-51, figure 5.1-52 presents heat loss through eight 22-inch struts. The same strut design is used for all six configurations. The losses through the truss are conservative for two reasons:

a. A mean thermal conductivity of 40 Btu/hour ft ^{o}F corresponding to T-111 at 1800^{o} F was used for the entire truss, whereas the design calls out the use of a super alloy with a lower thermal conductivity in a section of the truss. Figure 5.1-53 presents the heat losses for a composite strut containing T-111 and Rene-41, based on a conservatively assumed junction temperature of 1000^{o} F. Comparing figure 5.1-52 and 5.1-53 for a cold side temperature of 100^{o} F indicates that the heat losses will be reduced by 80 watts with the use of a composite strut.

b. The heat loss is based on axial conduction through the truss and radial conduction through Superinsulation around the truss. The truss is assumed to be in contact with the crush-up material which is assumed to be a porous aluminum material with a sufficiently high thermal conductivity (1-8 Btu/hour ft ^{o}F) to provide a cold heat sink. In the actual design, a radiation gap will exist between the truss and crush-up material. The actual truss heat loss will, therefore, be up to 27 percent lower (corresponding to a perfectly insulated strut) for the particular design considered.

Figure 5.1-54 summarizes the assumptions used in calculating insulation losses. Figure 5.1-55 presents the losses through the circular planar array and a rectangular planar array as a function of cold side temperature, based on the assumptions listed in figure 5.1-54. These calculations were performed based on the properties of Linde Superinsulation. The thermal losses were greater in the rectangular array because of the greater surface area. The effect of varying the insulation thickness on heat losses is shown in figure 5.1-56 for a circular planar array with a temperature drop from 1800^{o} F to 100^{o} F, and 2000^{o} F to 100^{o} F. It is shown that a 2-inch insulation thickness represents a reasonable compromise between minimizing thermal loss and minimizing insulation thickness.

An estimate of the heat losses through a Min-K seal connecting insulation layers for the IRV and the HSHX are presented in figure 5.1-58 based on a model described in figure 5.1-57. The total thermal losses are shown in figure 5.1-59 versus cold-side temperature. Estimates of the heat loss for all six arrays are presented in table 5.1-VII for a hot side temperature of 1800^{o} F and a cold side temperature of 100^{o} F. The total heat loss for all designs vary from 500 to 650 watts, with the exception of the conical array with the central recovery aids for which the heat losses are approximately 850 watts attributed to the increased surface area that requires insulation. The use of composite T-111 - Rene-41 struts results in a decrease in loss of approximately 85 watts

With a hot-side temperature of 2000^{o} F, the thermal losses for each design increase by 12 percent.

The thermal conductivity for Linde Superinsulation was used in this analysis, based on Linde's empirical relationship for evaluating a mean thermal conductivity between hot and cold surface temperatures:

$$k = 0.31 \times 10^{-6} \frac{T_1^2 - T_2^2}{T_1 - T_2} + 1.47 \times 10^{-13} \frac{T_1^4 - T_2^4}{T_1 - T_2}$$

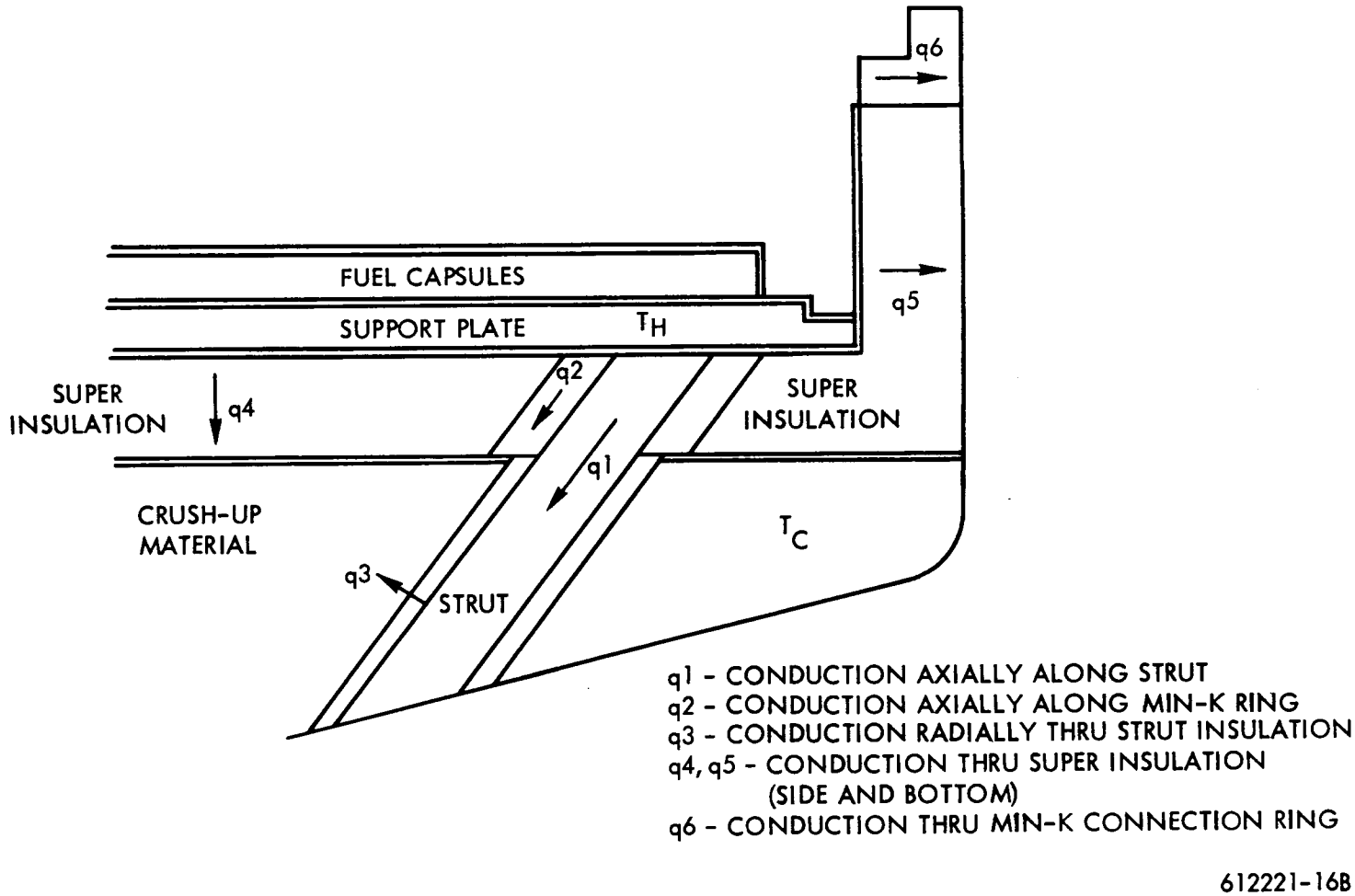

Figure 5.1–50. Insulation System - Heat Flow Model

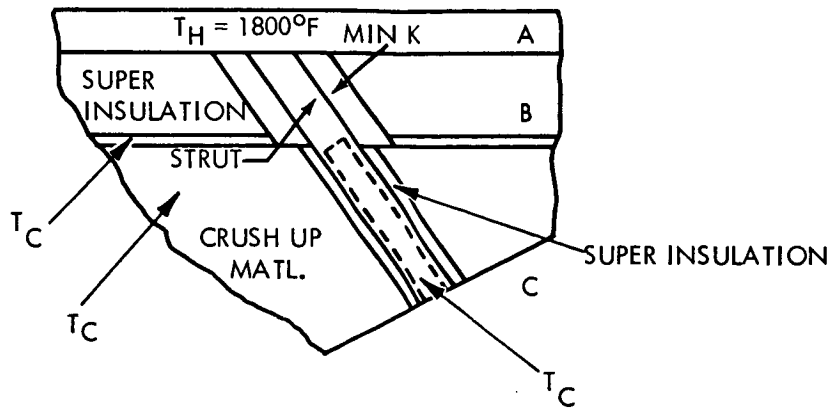

Assumptions:

Strut

OD = .75 inch

ID = .4375 inch

Matl. T_{111}

k = 40 Btu/(hr ft °F)

8 Struts

Strut Insulation

MIN-K Plug Adjacent to Superinsulation

OD = 2.75 inches L = 2.83 inches

Superinsulation Adjacent To Crush-up Material

OD = 1.25 inches L = 19.17 inches

Calculation Assumptions

(1) One Dimensional Conduction Through Strut and MIN-K Plug from Surface a-b

(2) From Surface b-c Combined Axial Conduction Through Strut and Radial Conduction Through Insulation

a. Assumed Insulation In Contact With Crush-up Material

Figure 5.1-51. Model for Strut Losses

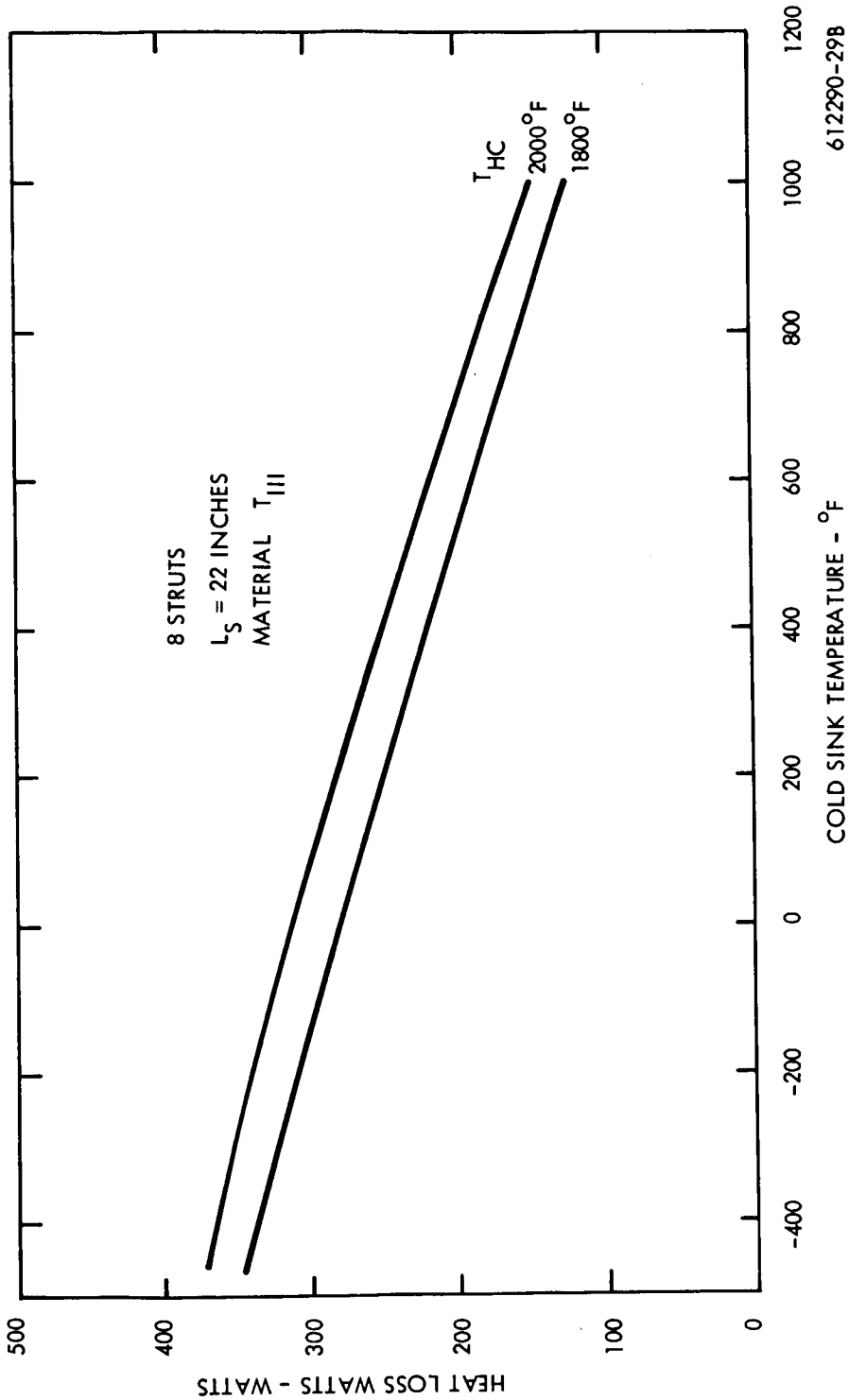

Figure 5.1-52. Heat Loss Through Struts

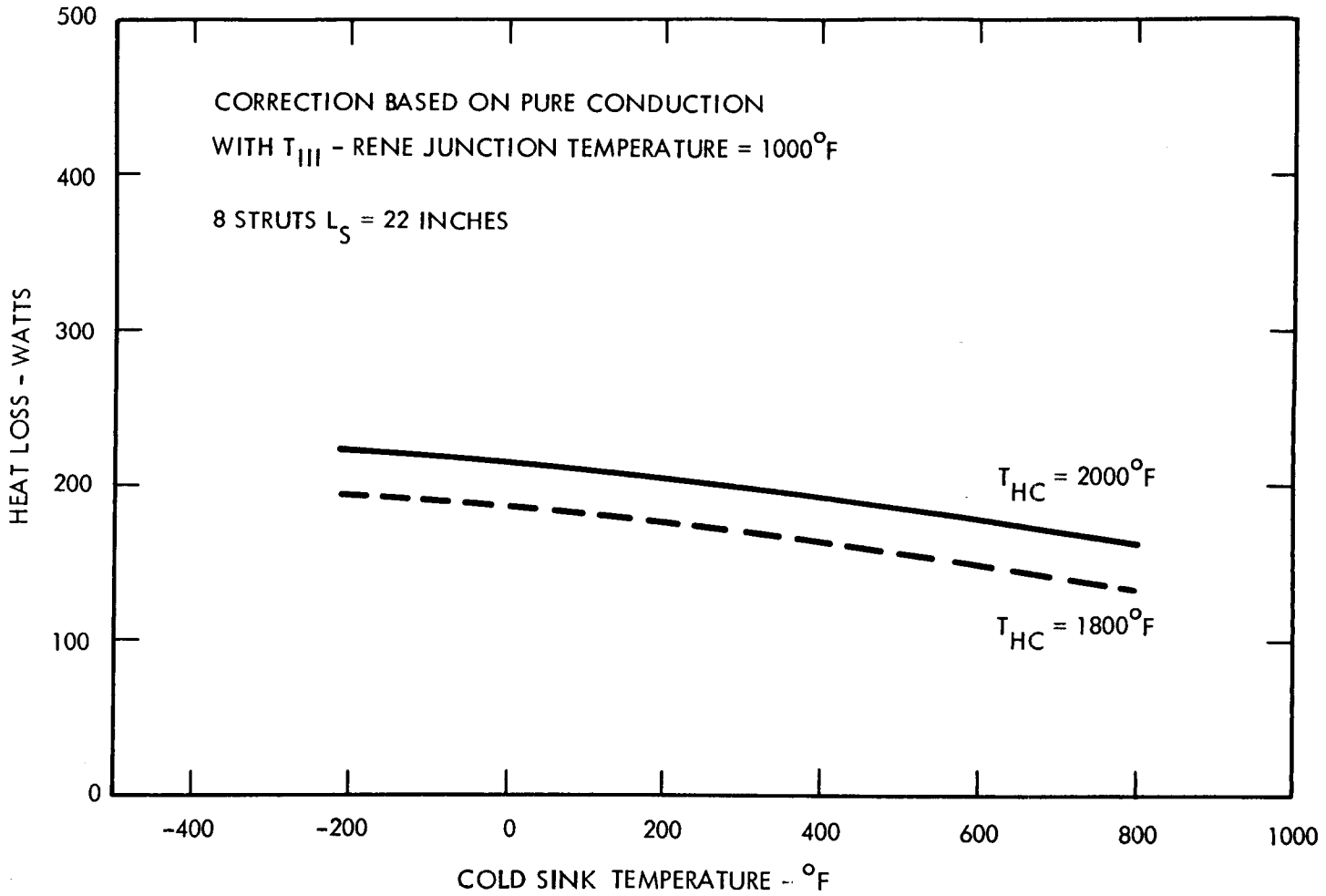

Figure 5.1–53. Heat Loss Through Struts for T_{111} - Rene 41 Struts

Circular Geometry

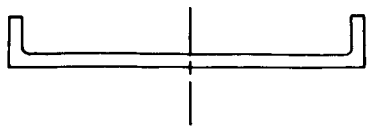

Assume:

1. Superinsulation
2. Vary k with temperature
3. Thickness = 2 inches
4. Diameter = 53 inches
5. Height of side insulation = 7 inches
6. One dimensional conduction

Rectangular Geometry

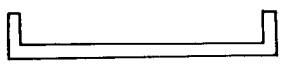

1. Same as above
2. Same as above
3. Same as above
4. Base plate = 67 inches x 38 inches
5. Height of side insulation = 7 inches
6. One dimensional conduction

Figure 5.1-54. Model for Insulation Losses

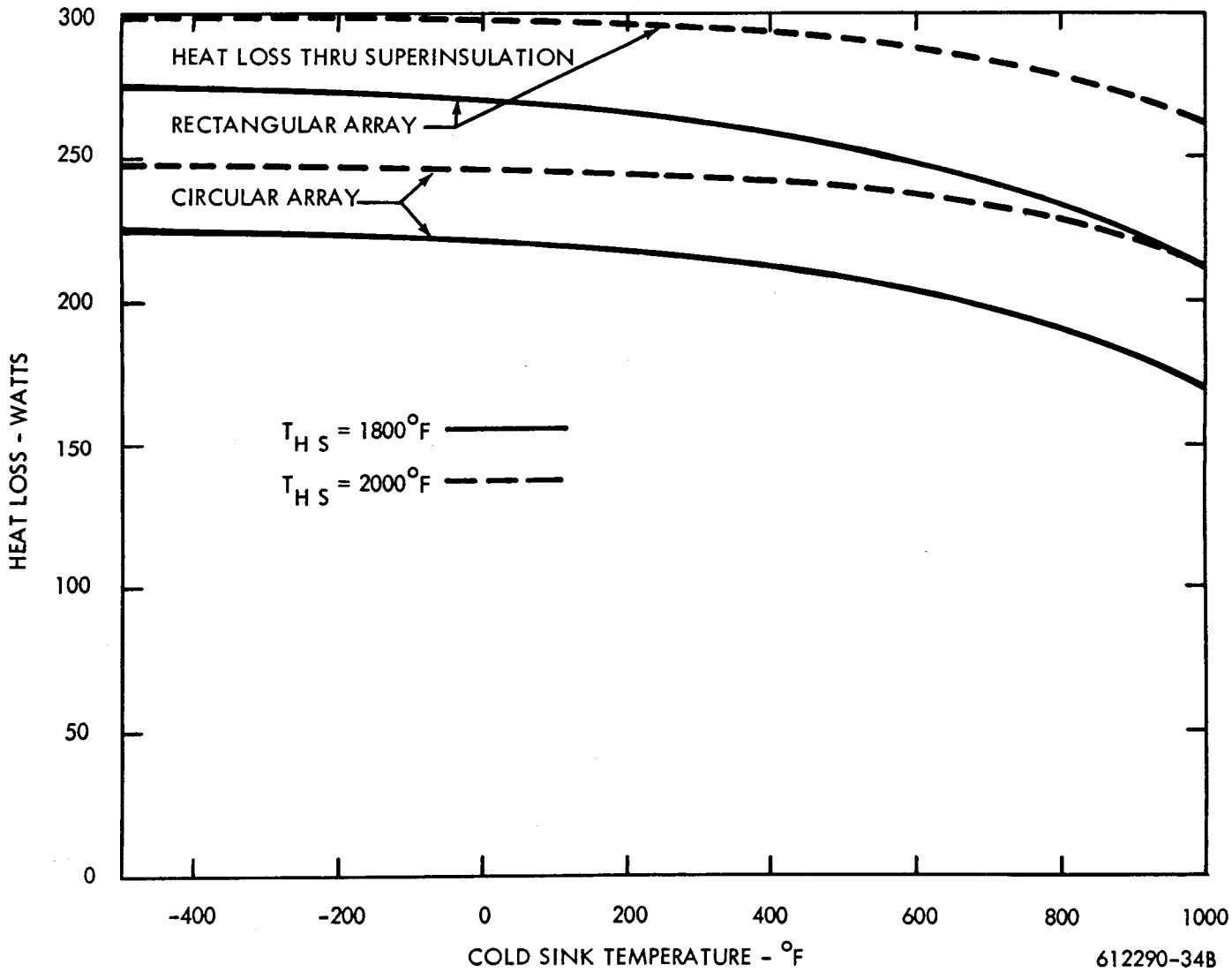

Figure 5.1–55. Heat Loss Through Superinsulation

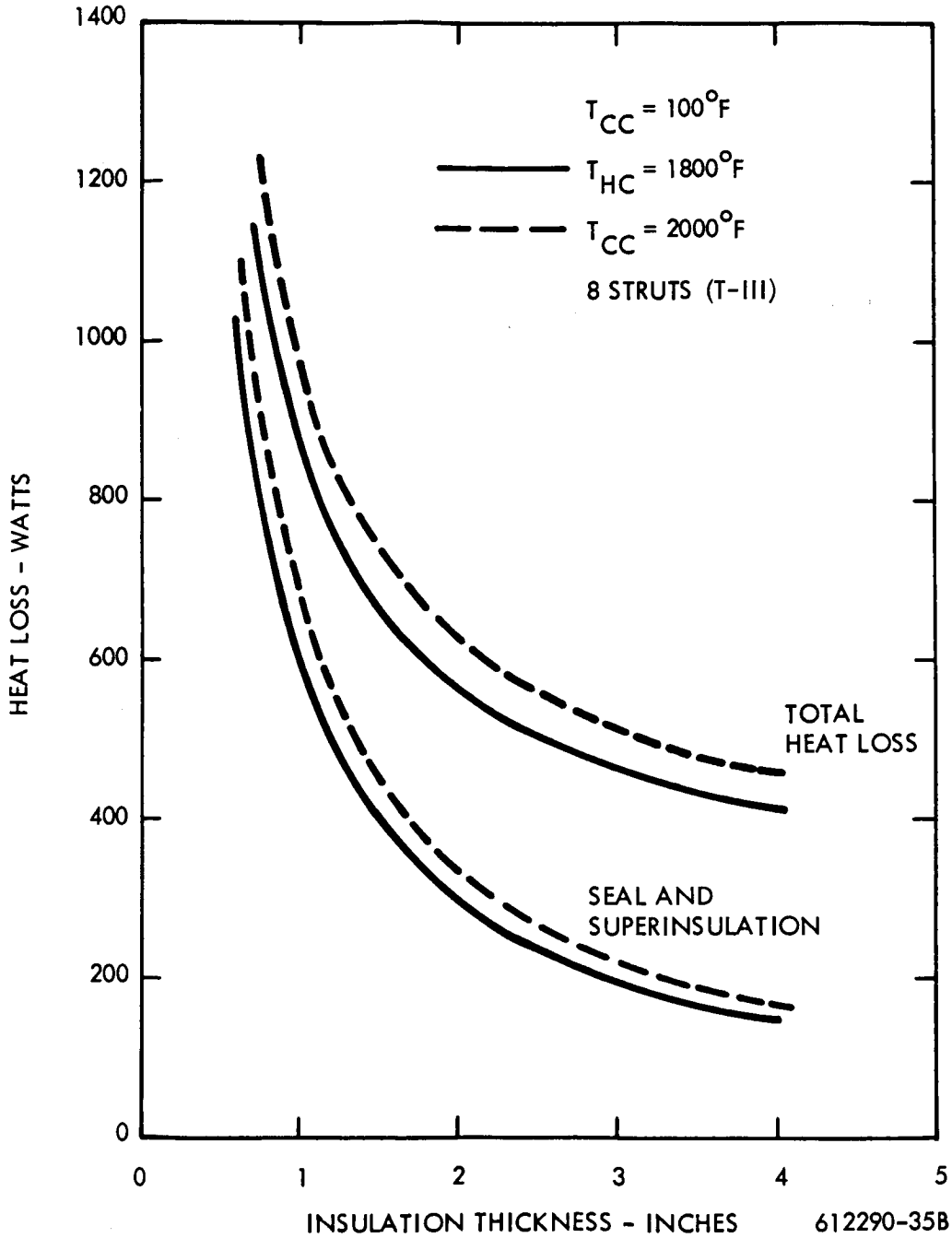

Figure 5.1–56. Effect of Insulation Thickness on Heat Source Losses (Circular Planar Array)

Circular Array

Assume:

1. Min-K 2000
2. Vary k with temperature
3. Thickness = 2 inches
4. Inner Diameter = 53 inches
5. Mean height = 1 inch
6. One dimensional conduction

Rectangular Array

Assume

1. Min-K 2000
2. Vary k with temperature
3. Thickness = 2 inches
4. Mean height = 1 inch
5. Seal around 67 x 38 rectangular perimeter
6. One dimensional conduction

Figure 5.1-57. Model for Min-K Seal

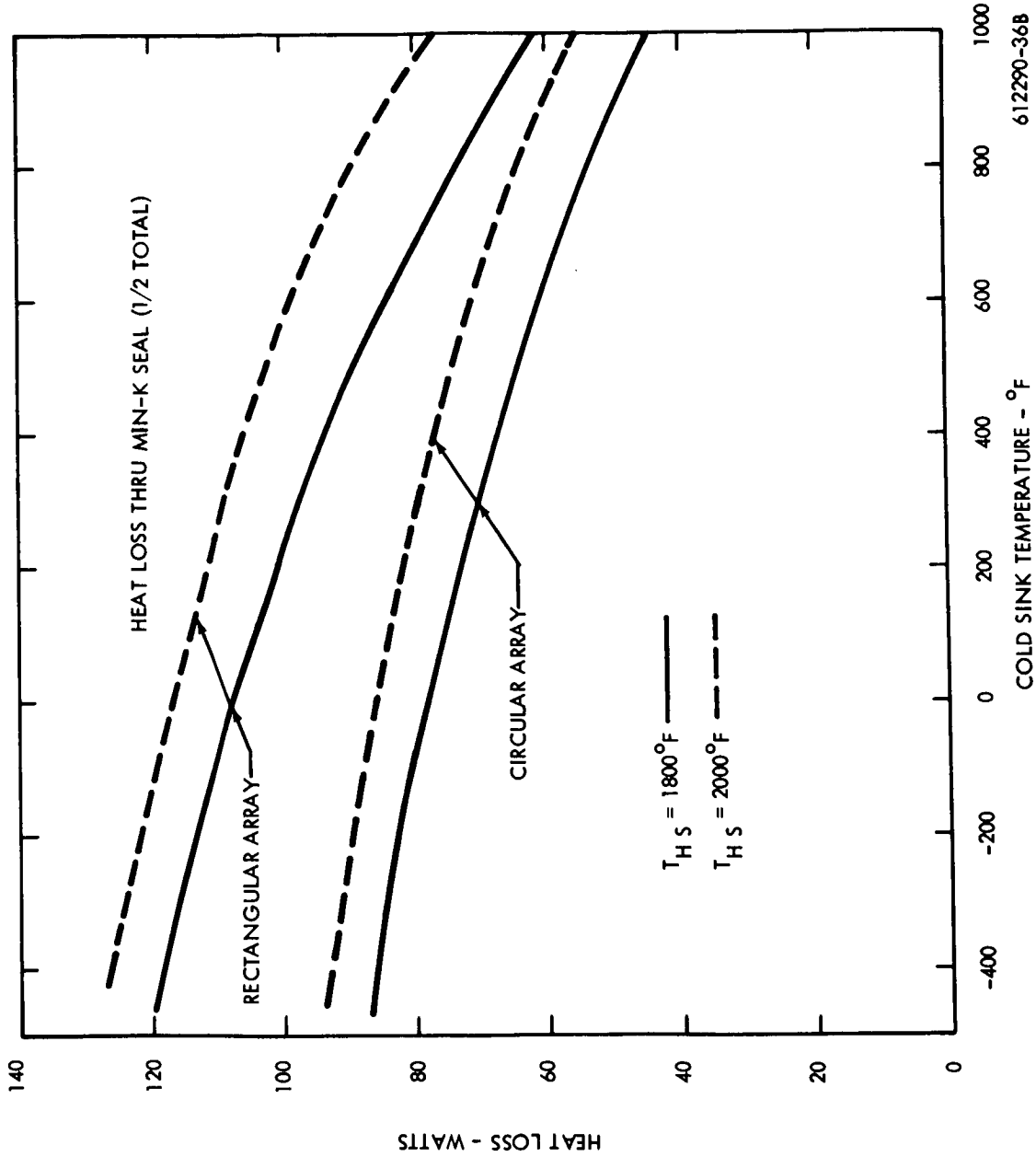

Figure 5.1-58. Heat Loss Through Min-K Seal (1/2 Total)

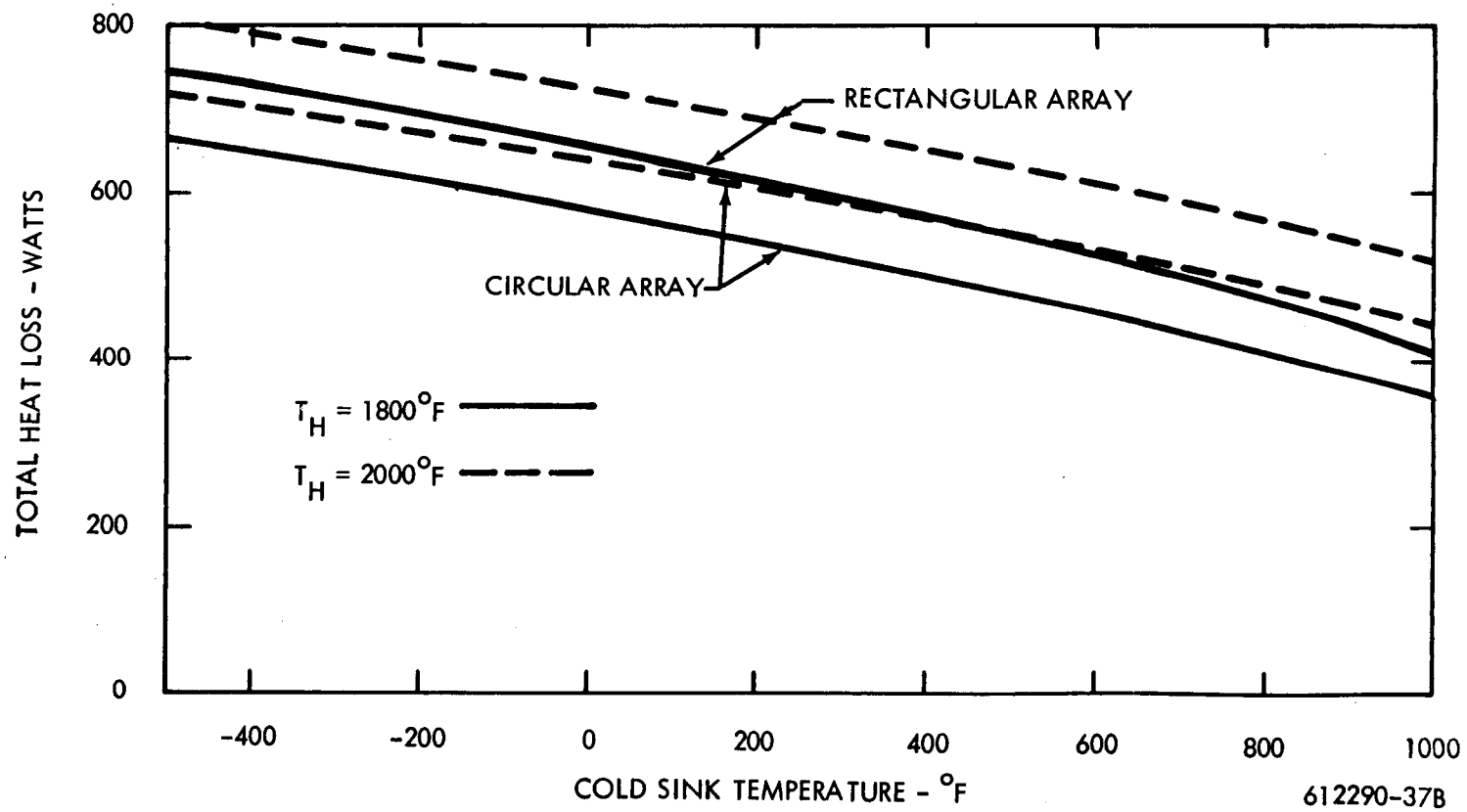

Figure 5.1–59. Total Heat Loss Through Insulation, Struts, and 1/2 of Seal

TABLE 5.1 – VII

IRV SUMMARY OF THERMAL LOSSES

TEMPERATURE 1800 – 100°F

	DESIGN NO.					
	1A	1C	2A	2B	3C	1A
	CIRCULAR PLANAR	RECTANGULAR PLANAR	CONICAL	CENTRAL RECOVERY CONICAL*	PIN CUSHION	MINIMUM SIZE CIRCULAR PLANAR
THERMAL LOSSES (WATTS)						
SEAL	76	104	82	100	81	67
STRUTS**	249	249	249	249	249	249
STRUT INSULATION	17	17	17	17	17	17
SUPER-INSULATION	218	267	271	488	211	184
TOTAL	560	637	619	854	558	517

* DONUT DESIGN INSULATION ASSEMBLY

** CONDUCTION AND RADIATION FROM EIGHT 22-INCH STRUTS

612204-13A

The thermal conductivity obtained from this correlation was compared to data for TEECO Superinsulation and Min-K 2000 data, presented in table 5.1-VIII, which indicated a factor of up to about five in reduced conductivity values for higher temperatures using TEECO data. It is felt that TEECO insulation is more effective; however, a multiple difference of five in thermal conductivity may not be realistic. For the present analysis, the Linde data was used for conservatism, but the TEECO appears to be a more efficient insulation.

From the thermal conductivity standpoint, either Linde or TEECO Superinsulation appears to be acceptable. However, TEECO Superinsulation appears preferable for this application due to design and testing experience for systems in the 2000° F plus temperature range.

Conclusions from the thermal analysis are as follows:

a. The total heat loss for all configurations range from 500 to 650 watts across a ΔT of 1800° F to 100° F, with the exception of the conical array with central recovery aids which will lose 850 watts. For a hot side temperature of 2000° F, the thermal loss will increase by 12 percent.

b. The use of a composite T-111 - Rene-41 strut will decrease the thermal losses by 85 watts across a ΔT of 1800° F to 100° F.

c. TEECO Superinsulation appears preferable to Linde Superinsulation and Min-K 2000 because of its lower thermal conductivity and because design and testing experience for the high temperature (2000° F +) range.

Total heat losses for composite strut systems for 1800° F and 2000° F hot side temperatures are shown in figures 5.1-60 and 5.1-61.

5.1.6 Auxiliary Coolant Heat Exchanger (ACHX)

5.1.6.1 Mechanical Design

Launch pad cooling of the heat source must take into consideration two separate modes of operation: fuel capsule loading and launch hold. During capsule loading operation, cooling of the capsules may be affected by natural convection and radiation or forced cooling and radiation. By either method, the heat source structure temperature must be kept relatively low to prevent oxidation of the refractory metals used. Heat transfer calculations indicate that with natural convection and radiation the heat source structure temperature may be maintained at approximately 600° F. However, by using forced convection and radiation, temperatures of approximately 450° F or lower can be maintained. This temperature level is sufficiently low to prevent oxidation of the refractory metals.

Upon completion of the fuel capsule loading operation and integration of the heat source into the launch vehicle, the heat source must be cooled continuously to accommodate varying standby and launch requirements and emergencies. The ACHX was integrated with the heat source as shown in Figure 5.1-62.

This design has the advantages of forced convection and radiation during fuel capsule loading, transportation, assembly, launch hold, or emergencies. Disconnects of umbilicals prior to launch increase safety and reliability during

TABLE 5.1 – VIII

INSULATION THERMAL CONDUCTIVITIES

MEAN THERMAL CONDUCTIVITY (BTU/HR FT °F) $T_c = 100°F$

HOT SIDE TEMPERATURE (°F)	MIN-K 2000 (AIR)		MIN-K 2000 (VACUUM)	SUPERINSULATION LINDE - VACUUM		SUPERINSULATION TEECO - VACUUM
	Perpendicular	Parallel	Perpendicular	Perpendicular	Parallel	Perpendicular
500	0.017			0.00018		
900	0.019	0.025	0.011	0.00031		0.00020
1200	0.020		0.012	0.0005	0.1	0.00026
1500	0.021			0.0015	0.3	0.00037
1800				0.0031	0.4	0.00058
2500						0.0014

612221-31A

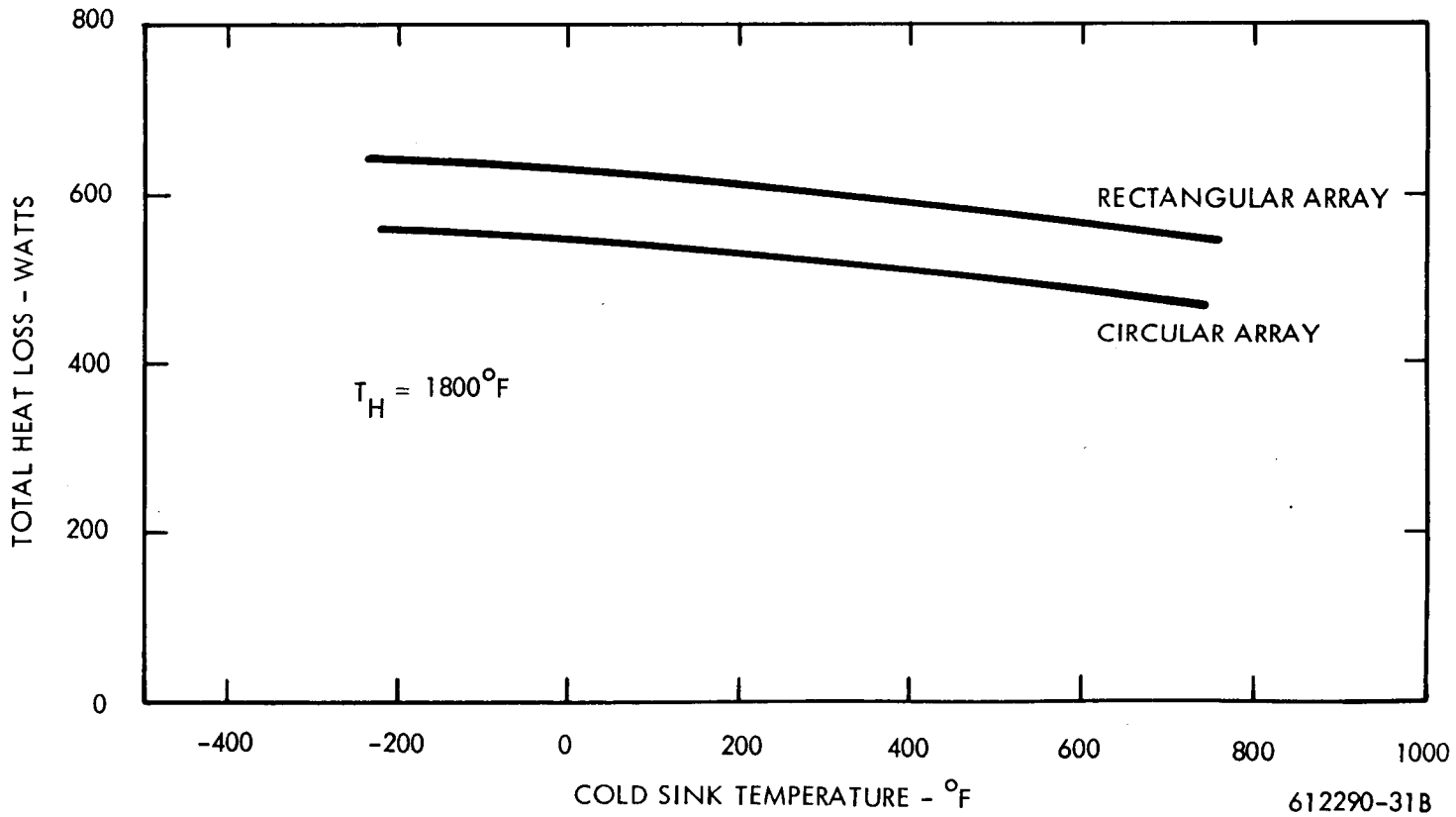

Figure 5.1–60. Total Heat Loss Through Insulation, Composite Struts, and 1/2 of Seal

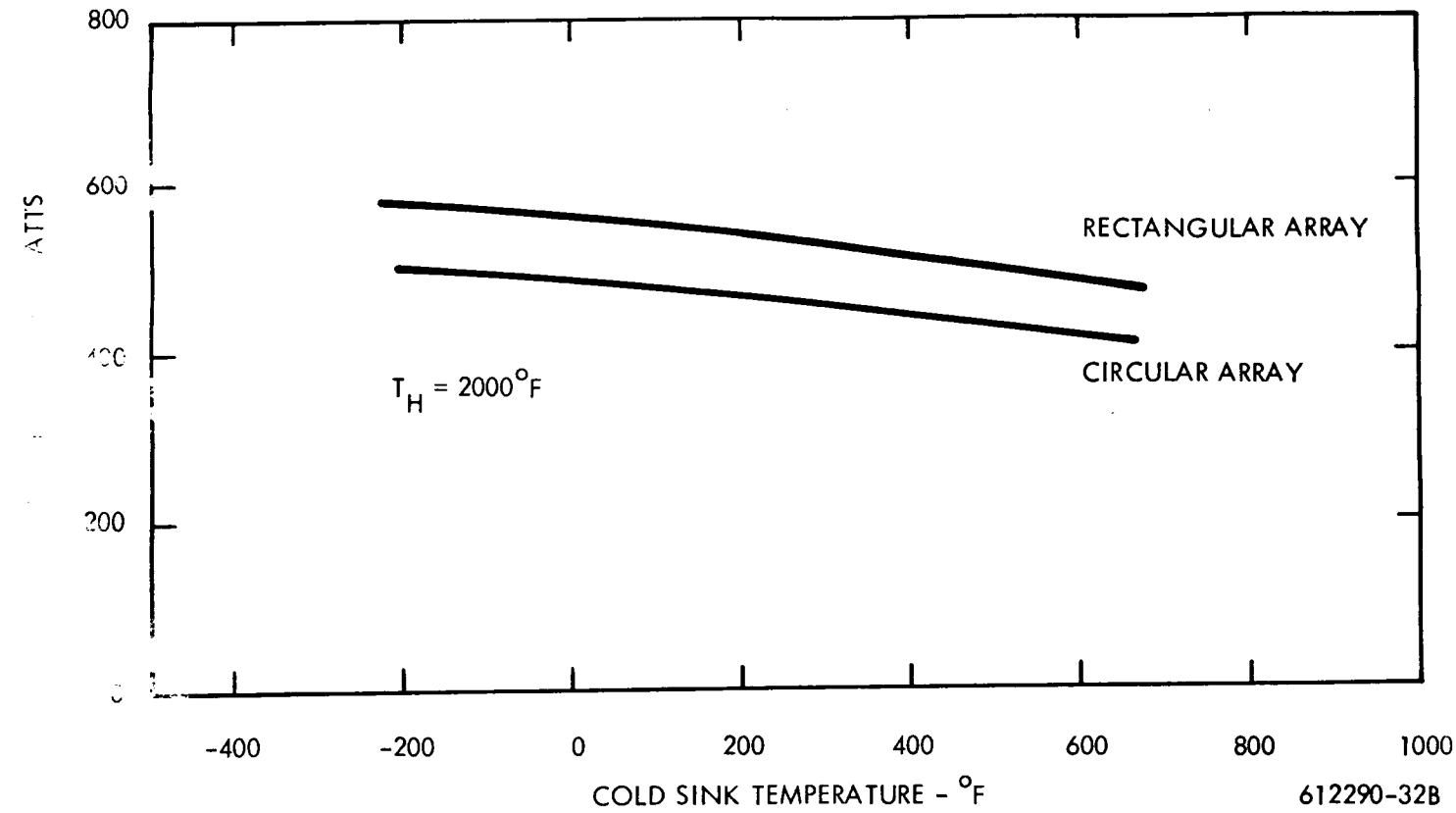

Figure 5.1-61. Total Heat Loss Through Insulation, Composite Strut, and 1/2 of Seal

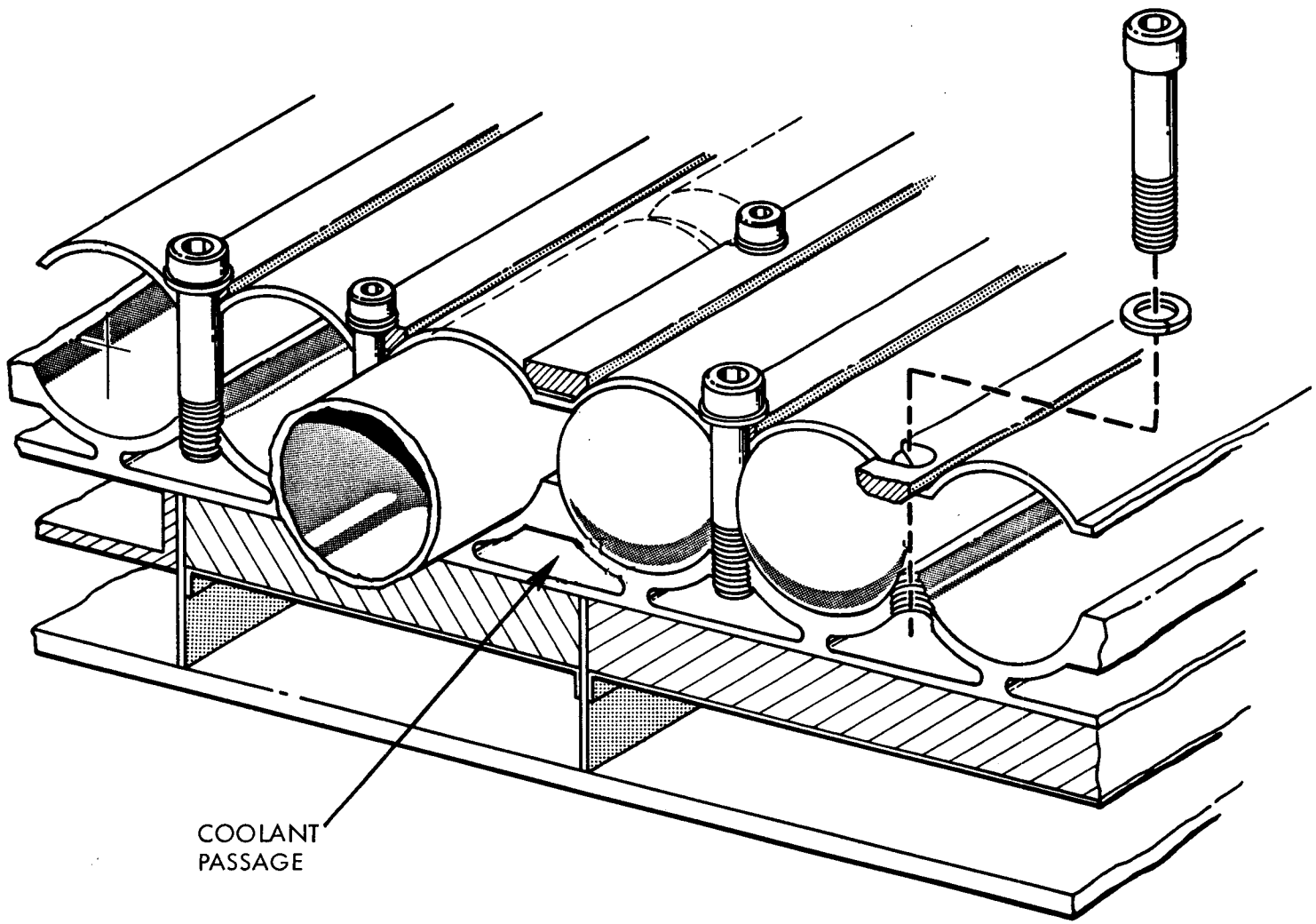

Figure 5.1–62. ACHX Coolant Flow Passages

612221-37B

launch pad operation. The ACHX flow channels as shown in Figure 5.1-62 run parallel with the fuel capsules and into distribution headers on each side of the heat source.

5.1.6.2 Thermal Analysis

An auxiliary heat exchanger located adjacent to the fuel capsule array is required in the IRV design to remove the heat generated by the fuel capsules prior to launch and to prevent overheating of the capsules and support structure. The heat exchanger consists of flow channels adjacent to each row of fuel capsules as indicated in Figure 5.1-62. Coolant is routed in parallel through each channel. A parametric analysis was performed on a typical array of fuel capsules consisting of 24 rows of capsules with 7 capsules in each row (see Figure 5.1-63). The effects of varying channel size, gas passage and velocity, and the number of passages per channel on the axial temperature rise of the gas stream, the film temperature drop from the wall to the coolant channel, and the pumping power requirements through the channels were analyzed and are presented.

Figure 5.1-64 shows the effect of gas pressure and channel size on the film temperature drop and the axial gas temperature rise for a fixed velocity. For a fixed velocity, increasing the size and pressure increases the mass flow rate and thus the heat transfer coefficient which results in a smaller gas temperature rise and film drop. As seen in this curve, maximum gas passages are desirable. Figure 5.1-65 presents the effect of velocity and pressure on the axial temperature rise of the gas and the film temperature difference. This curve indicates the necessity of pressurizing the gas and the desirability of maintaining as high a velocity as possible. Figure 5.1-66 combines the axial temperature rise and the film drop to yield the difference between coolant inlet temperature and the maximum coolant wall temperature existing at the outlet of the heat exchanger. To maintain the capsule peak temperature at 500° F will require a peak coolant wall temperature of not more than 400° F. This curve demonstrates that for a 0.78-inch channel with an inlet temperature of 80° F, this wall temperature can be readily maintained with a pressurized gas system. Figure 5.1-67 shows the pumping power requirements for the channel flow only, indicating the desirability of minimizing the velocity.

To maintain a peak temperature of the channel at 300° F and to maintain reasonable pumping power requirements suggests a pressurized gas system. In particular, a representative design would consist of 0.78-inch channels with air or nitrogen flowing with a velocity of 60 ft/sec at a pressure of 3 atmospheres. This would yield peak channel temperature of 330° F at a power requirement of 140 watts per channel.

The effect of replacing a single passage channel with a channel consisting of several cylindrical passages is shown in Figure 5.1-68 in dimensionless form. The axial temperature rise, film temperature drop, and pumping power for a varied number of coolant channels are presented in ratio form to the value corresponding of a single passage. These are plotted versus the ratio of the total free flow area for a number of passages (N_T), over the free flow area of a single passage. Based on the assumption that the maximum free flow area is obtained for a single passage, using several passages results in an increased coolant temperature rise. The film temperature drop can be decreased by increasing the number of passages, however. This curve shows that if a single passage channel can be replaced with

a multiple passage channel without a large sacrifice in the free flow area, the wall can be maintained at a lower temperature at the expense of a larger power requirement. Since the wall temperature can be readily maintained at a desirable temperature level with a single passage channel, however, multiple passages are not recommended.

The results of the parametric study indicated that a single tube channel with a minimum free flow area in the order of 0.5 in^2 using pressurized air or nitrogen will provide sufficient cooling without severe pumping power requirements. The results of this study were applied to the six configurations under consideration. Table 5.1-IX summarized the thermal and hydraulic performance of the ACHX for each configuration. As shown all designs can be maintained at a peak capsule temperature of 450° F with 30 psig air or inert gas flowing at 1 to 5 lbs/sec, with the exception of the pin cushion array which may have a 600° F peak capsule temperature. It is expected that with proper redesign this temperature can be lowered to a more desirable level.

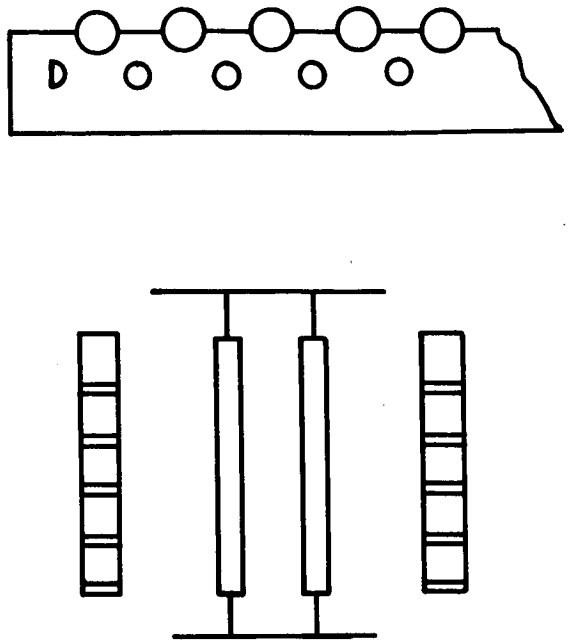

ASSUME:

24 ROWS OF FUEL CAPSULES

7 FUEL CAPSULES PER ROW

24 COOLING CHANNELS

L_{CH} = 42 INCHES

P, V, D OF EACH CHANNEL IS SAME

Q_{CH} = 1100 WATTS

PARALLEL FLOW

$T_{COOLANT\ IN}$ = 80°F

612290-42B

Figure 5.1-63. Model for ACHX Performance Calculation

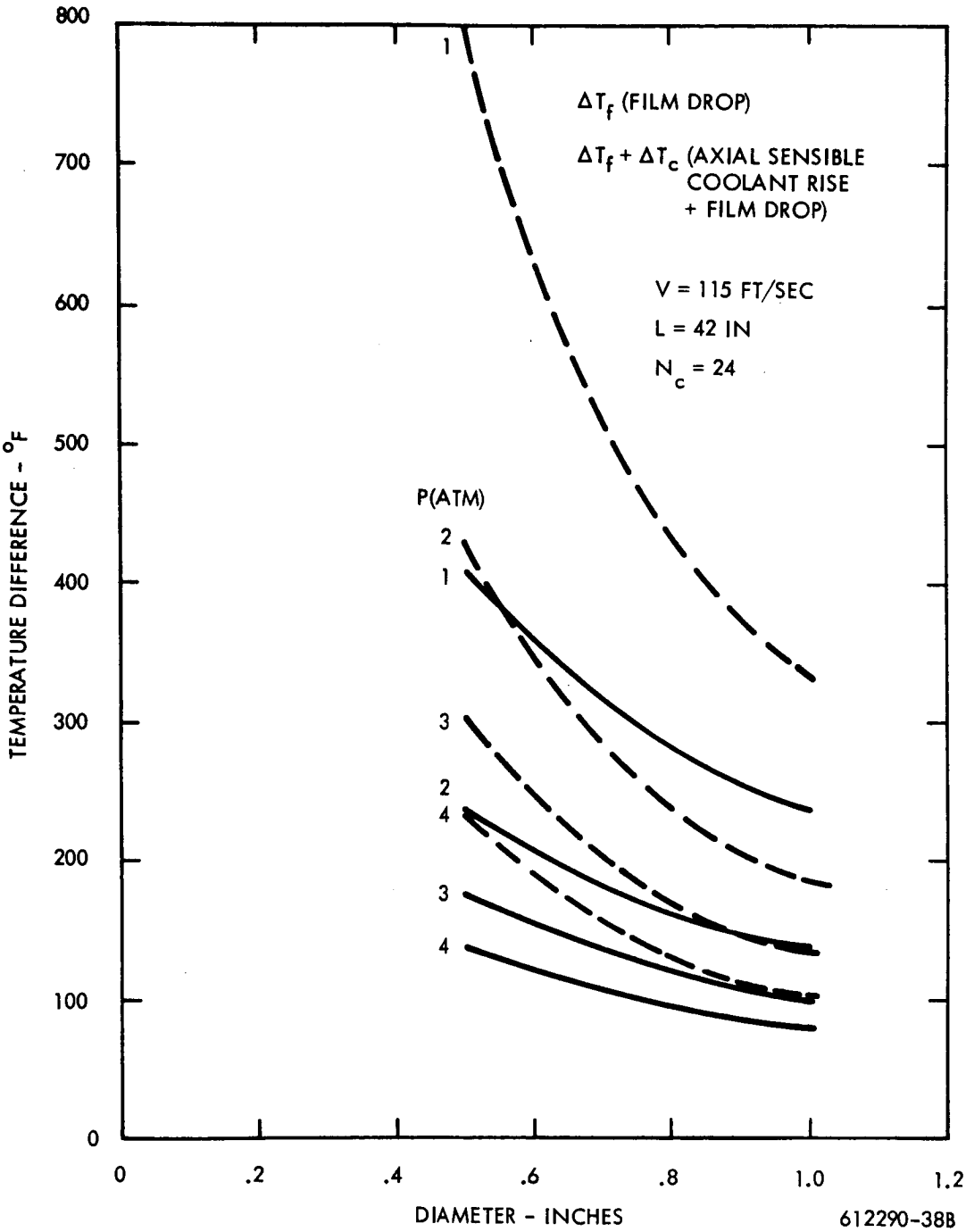

Figure 5.1–64. Effect of Tube Diameter on Film Temperature Drop and Sensible Coolant Temperature Rise

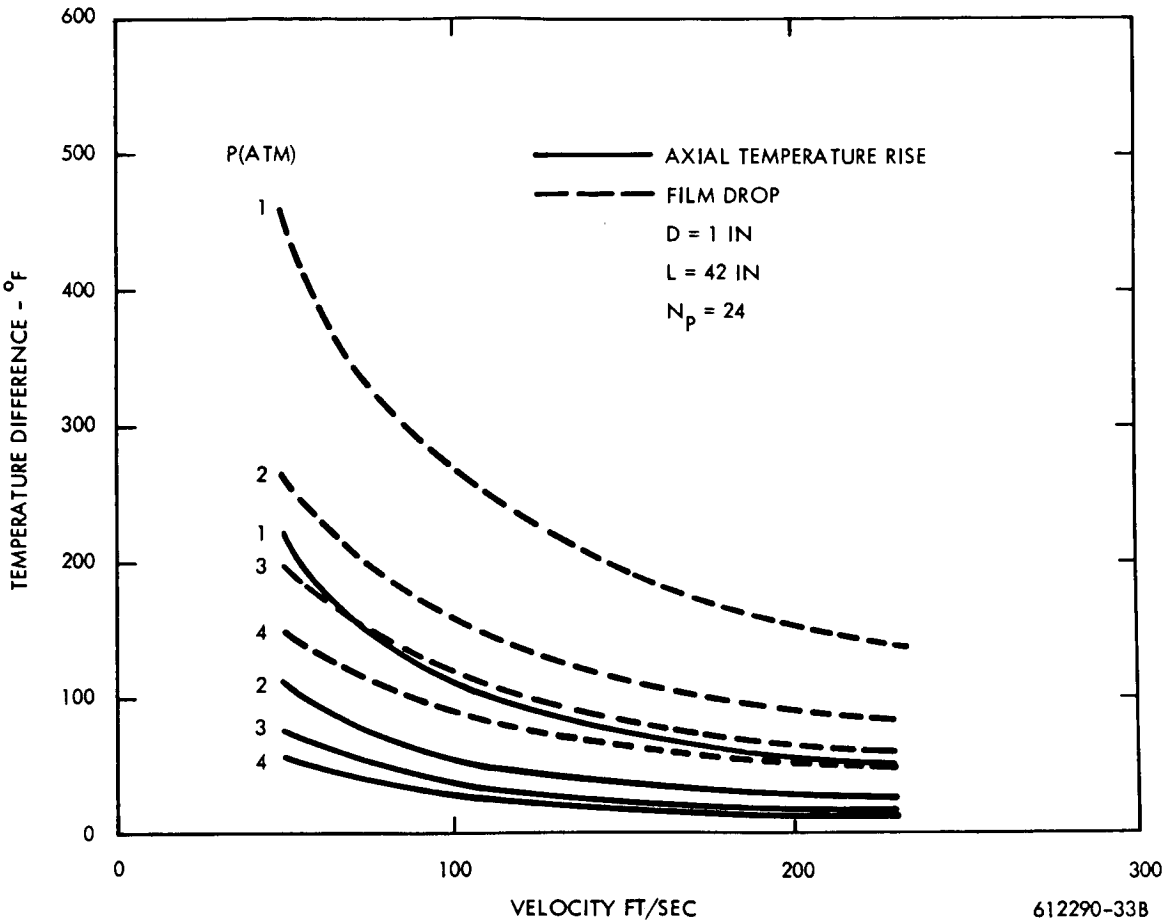

Figure 5.1–65. Effect of Fluid Velocity on Film Temperature Drop and Sensible Coolant Temperature Rise

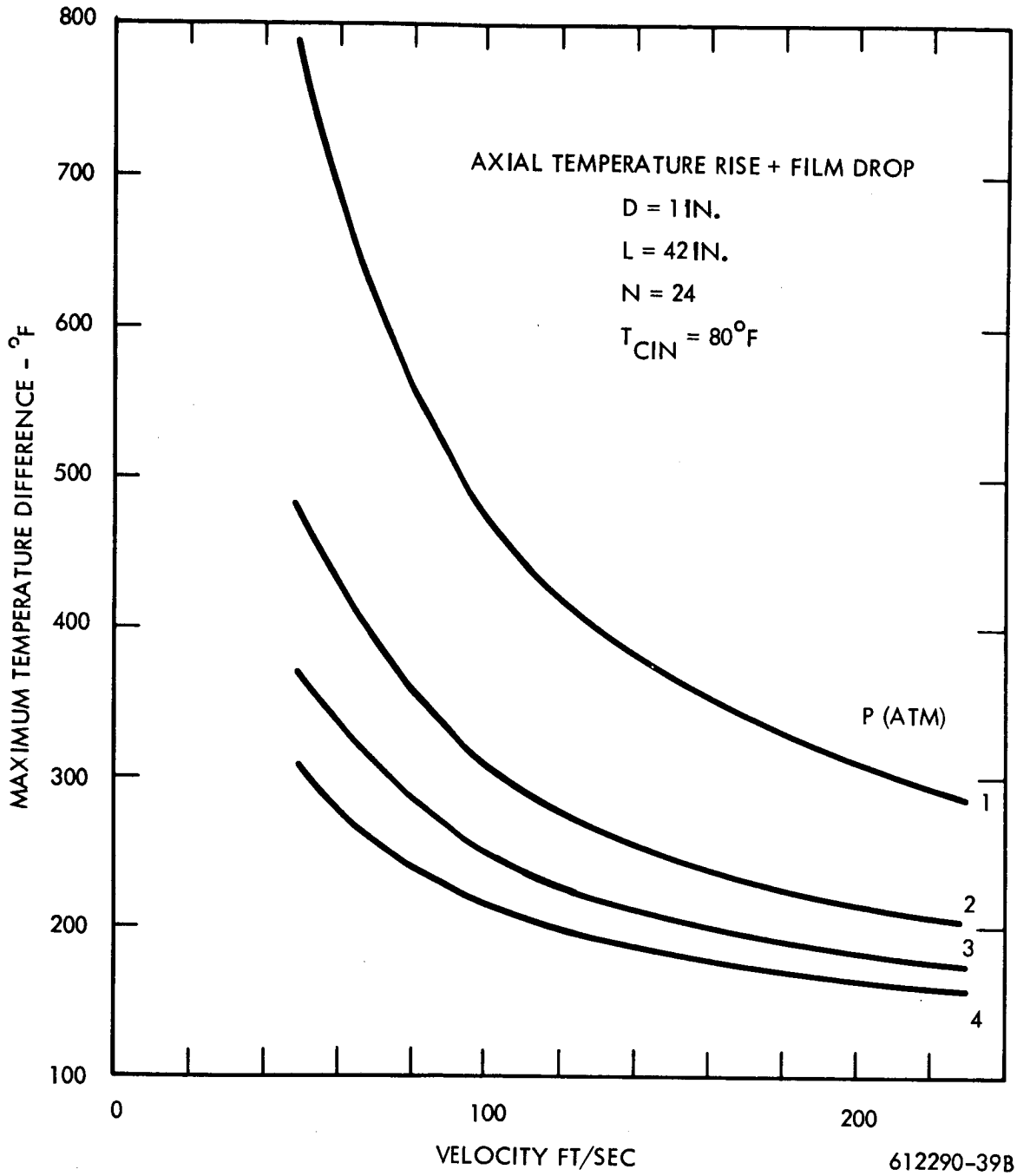

Figure 5.1–66. Effect of Fluid Velocity on Peak Capsule to Fluid Inlet Temperature Difference

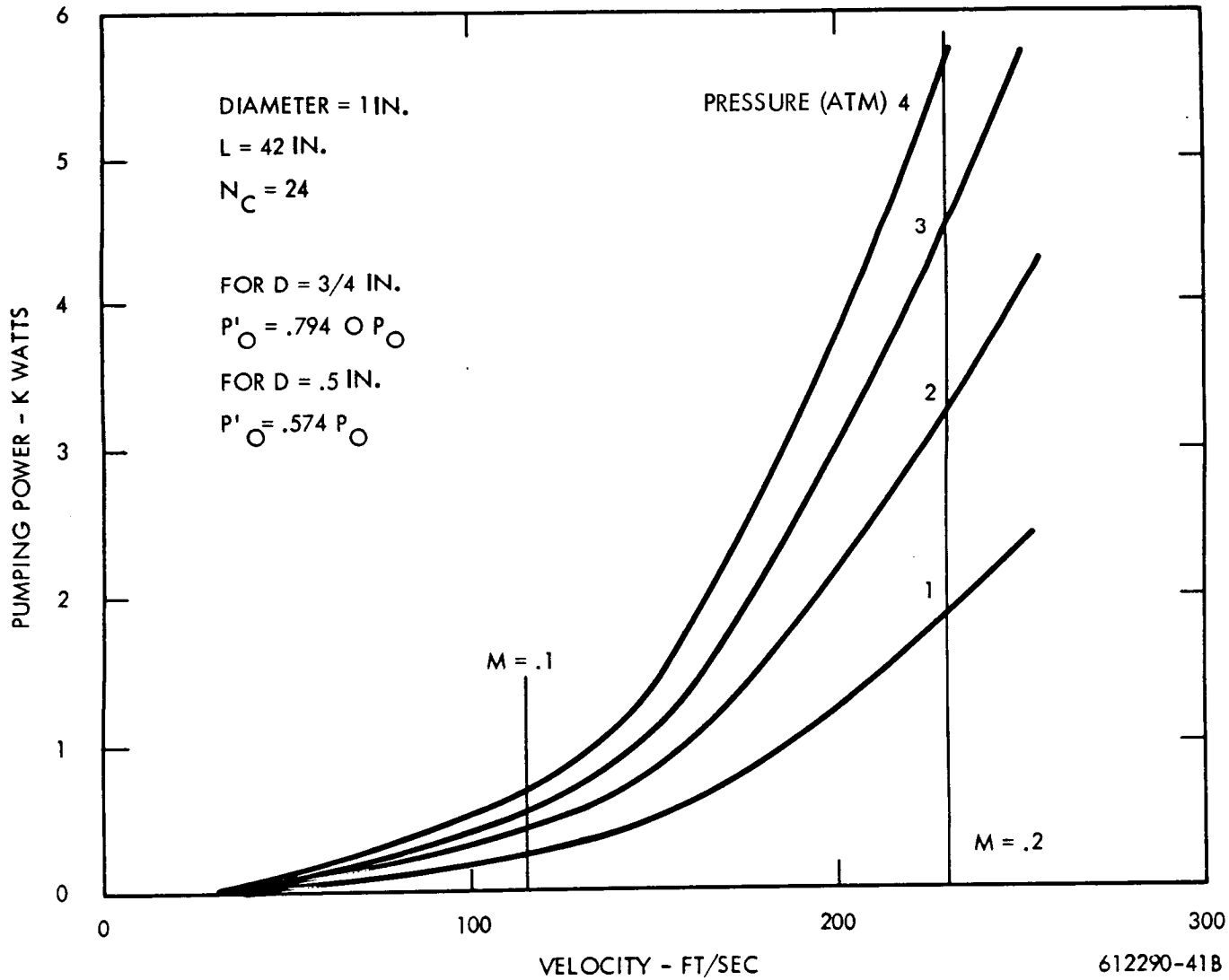

Figure 5.1–67. Effect of Fluid Velocity on Pumping Requirements

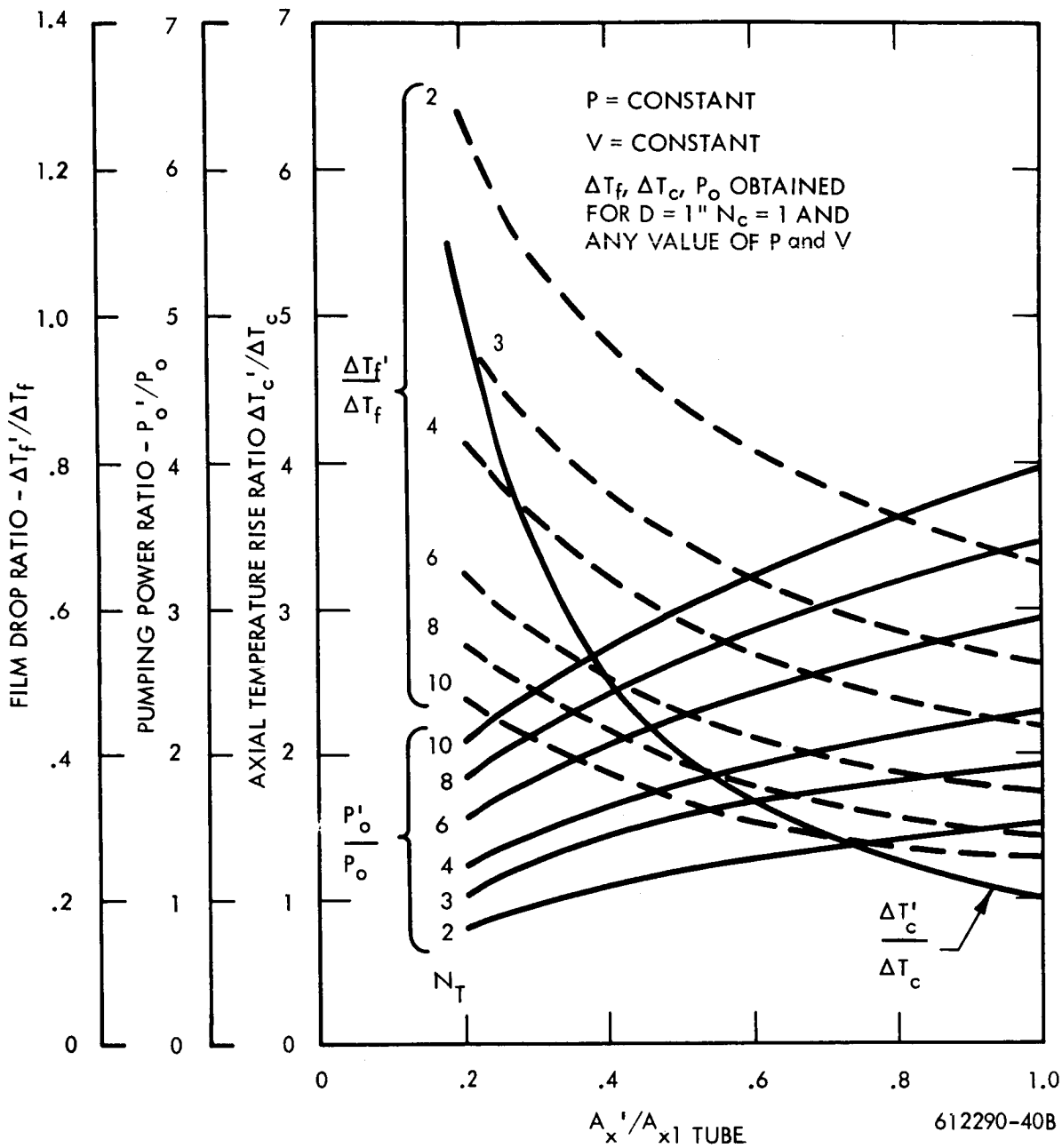

Figure 5.1-68. Effect of Increasing Number of Coolant Passages Per Channel (N_t)

TABLE 5.1 – IX

ACHX THERMAL AND HYDRAULIC DESIGN DATA

	CONFIGURATION NO.					
	1A	1C	2A	2B	3C	1A
	CIRCULAR PLANAR	RECTANGULAR PLANAR	CONICAL	CONICAL WITH CENTRAL RECOVERY AIDS	PIN CUSHION	MINIMUM SIZE CIRCULAR PLANAR
COOLANT INLET TEMP. (°F)	80	80	80	80	80	80
COOLANT TEMP. RISE (°F)	76	88	50	26	73	46
COOLANT FILM DROP (°F)	141	134	172	196	113	87
CAPSULE AND CONVECTION PATH ΔT (°F)	153	148	148	148	334	237
PEAK CAPSULE TEMP. (°F)	450	450	450	450	600	450
PRESSURE (ATM)	3	3	3	3	3	3
VELOCITY (FT/SEC)	105	115	81	49	240	198
TOTAL MASS FLOW (LB/SEC)	1.57	1.25	2.08	4.75	3.75	2.62

5.2 HEAT SOURCE HEAT EXCHANGER

5.2.1 Introduction

The heat source heat exchanger (HSHX) is an integral component of the Brayton cycle power conversion system (PCS). This heat exchanger accepts the heat from the isotope heat source and transfers it to the closed loop Brayton cycle working fluid, at a prescribed rate and temperature level. The HSHX is the interface between the Brayton cycle power conversion system and the isotope reentry vehicle (IRV), and as such exerts a major design influence on both systems. Radiation, which provides a relatively clean physical interface, is the prescribed mode of heat transfer between the isotope heat source and the HSHX. However, this interface is deceptively simple; complex radiant heat interchange relationships strongly couple the heat source temperature characteristics to the HSHX. In fact, the isotope heat source temperature level and temperature distribution are largely determined by the design, performance and location of the HSHX. Thus it is imperative that the different approaches to the isotope heat source/ HSHX be analyzed and evolved in unison to effect a reasonable design for each of these conponents.

5.2.1.1 System Definition

The HSHX is a part of the closed gas loop of the Brayton cycle power conversion system. The other major elements of the Brayton cycle gas loop are contained in a package as illustrated in Figure 5.2-1. They consist of the BRU (Brayton cyle rotating unit), recuperator, and heat sink exchanger. This package is referred to as the BHXU (Brayton cycle heat exchanger unit). For the purposes of this study the BHXU package is assumed to be mounted in a rectangular frame with the dimensions as noted in the figure.

The HSHX system includes the following items:

a. The HSHX itself

b. The ducting between the HSHX and the BHXU package

c. The structural support between the HSHX and the BHXU package

d. That portion of the insulation system which is removable with the complete closed gas loop

The elements of the HSHX system are illustrated in Figure 5-2.2. It is seen that the HSHX, ducts, structure, BHXU package and insulation form a single integral unit.

5.2.1.2 System Requirements

The requirements imposed on the HSHX are summarized in Table 5.2-I and consist of specified operational and performance goals. The overall power system is comprised of a single IRV-isotope heat source and two independent Brayton cycle power conversion systems (PCS) shown schematically in Table 5.2-I. Each of the PCS is capable of delivering full output power (6.85 KWe); however, only one of the systems is in operation at a given time. In order to provide inplace

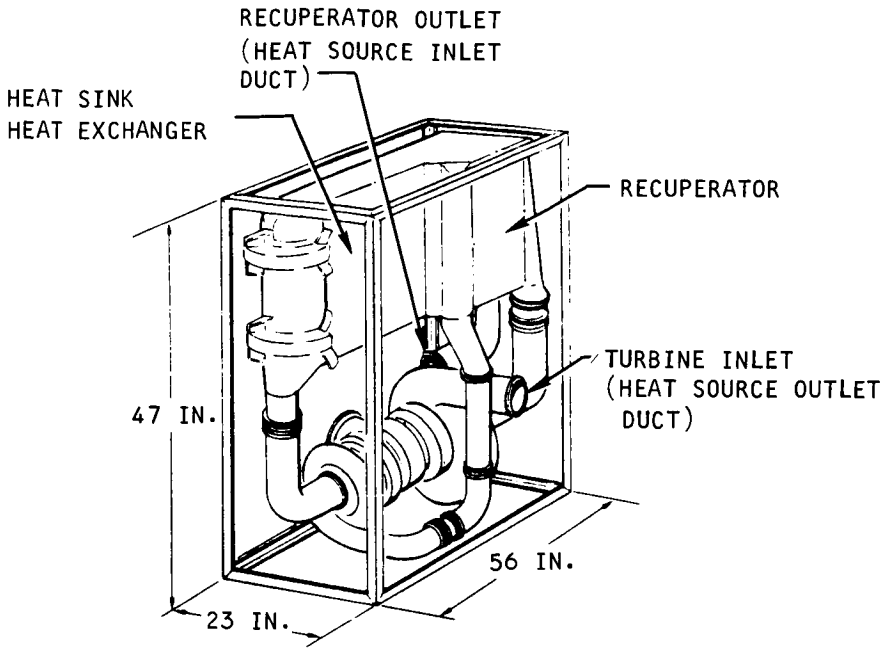

Figure 5.2-1. Brayton Cycle Power Conversion Package

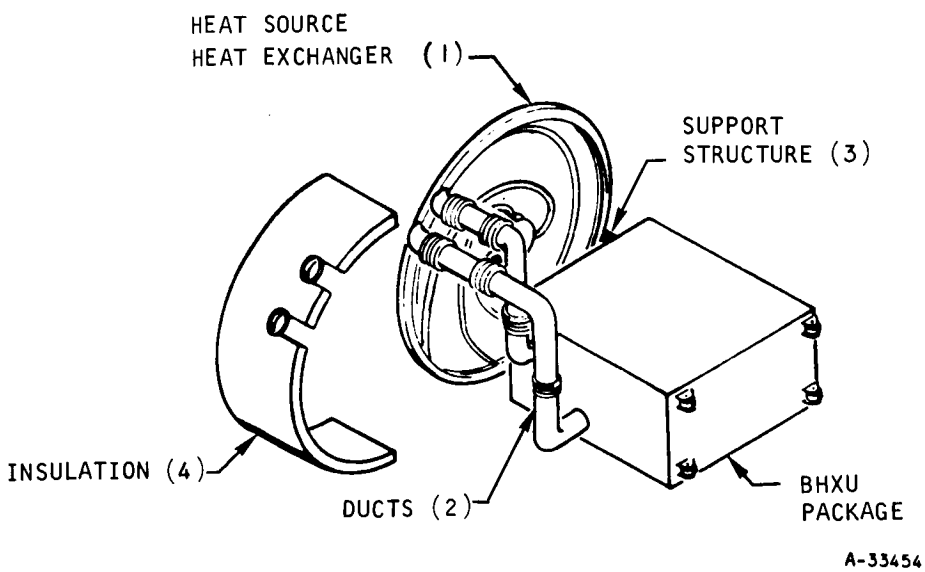

Figure 5.2-2. HSHX System

TABLE 5.2-I

HSHX - SYSTEM REQUIREMENTS

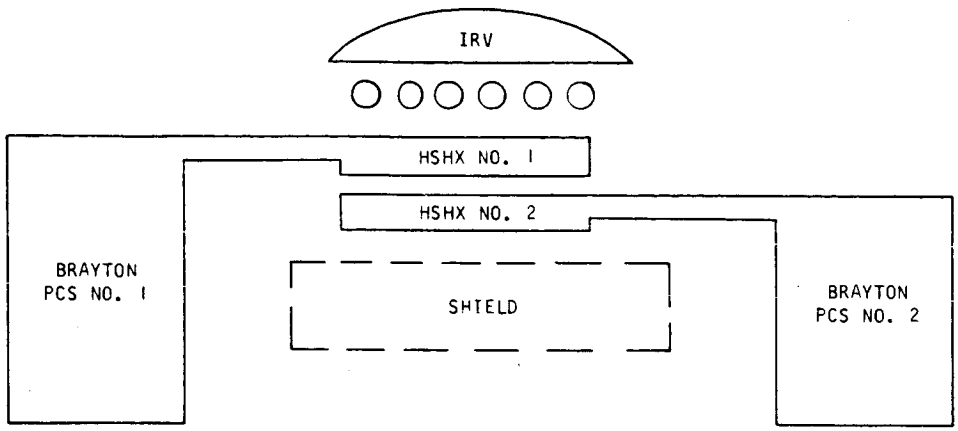

OPERATIONAL

- INPLACE REDUNDANCY

  EITHER SYSTEM NO. 1 OR NO. 2 CAPABLE OF FULL POWER OPERATION WITHOUT MOVEMENT OF MAJOR COMPONENTS

- REPLACEABILITY

  PCS'S INCLUDING HSHX'S TO BE REMOVABLE AS A COMPLETE UNIT

- INTERCHANGEABILITY

  PCS NO. 1 AND NO. 2 TO BE INTERCHANGEABLE

- COMPATIBLE WITH

  ATLAS/CENTAUR (SEPARATE LAUNCH)

  SATURN 1-B (INTEGRAL LAUNCH-MORL)

PERFORMANCE

- RADIATION HEAT TRANSFER FROM ISOTOPE SOURCE
- 1600°F EXIT GAS TEMPERATURE
- 1200°F INLET GAS TEMPERATURE
- 23.5 KW_t TRANSFERRED TO GAS
- MAX OPERATING SOURCE TEMP $\leq$ 2000°F
- $\Delta P/P \leq 3.3\%$ (1.05 PSI)
- Xe-He, (83.8 MWt) @ 0.94 LB/SEC
- HEAT LEAK $\leq$ 1.0 KW_t

A-33455

redundancy of the power conversion system, both PCS number 1 and PCS number 2 must be capable of full power operation without removal of the other. PCS number 1 and PCS number 2, including the HSHX's are to be separately removable as integral units. PCS number 1 and number 2 are to be interchangeable; or, stated another way, one PCS must be able to be utilized as either PCS number 1 or number 2. The packaging configurations of the BHXU-HSHX are to be compatible with the Atlas/Centaur separate launch to orbit vehicle, and the SATURN-1B integral launch MORL type installation. The differences between these two installations would be confined to the ducting and HSHX-BHXU interface only.

The performance requirements imposed on the HSHX are also listed in Table 5.2-I, and consist of a set of specified temperatures, flow rates, pressure drops, etc., which are required to obtain full electrical output power. In addition to the internal performance of the HSHX, the HSHX system must keep the maximum fuel capsule temperature below 2000° F during normal operation, and the heat leaks associated with the HSHX system to less than 1 kwt.

For most of the systems investigated, the ground rules were maintained through this portion of the study. However, for some systems it was necessary to relax one or more of the ground rules to provide an acceptable design solution.

5.2.1.3 Summary

Initially the HSHX design study consisted of two parallel efforts. One was concerned with the source geometry effects (i.e., planar, conical, pyramidal arrays of fuel capsules, separation distance, etc.) and how they influenced the operating temperatures of the source. The results of these analyses are presented in Section 5.2.2 of this report. The other initial effort involved the development of parametric HSHX data over a wide range of heat source areas and operating temperatures. This was done to identify the area and operating temperature requirements imposed on the heat source in order to meet the HSHX design objectives. The type of HSHX selected for this parametric analysis was of a tube-fin construction, since previous work had indicated a preference for this type of HSHX. Parametric data was prepared for both circular and rectangular heat exchangers over the range of source temperatures and source areas of possible interest. This data is given in Section 5.2.3 of this report.

On the basis of the heat source studies which were being conducted in parallel with this effort, it became apparent that in order to meet the HSHX requirements, no increase in heat source area was required over that which was necessary for the fuel capsules and the various attachment schemes under investigation. This was due mainly to the low power density associated with the fixed fuel capsule design. As a result of this, our attention turned to investigating the potential benefits derived from different flow configurations, such as multipassing the Brayton cycle fluid in the HSHX. In addition, it became necessary at this point to incorporate more sophisticated heat transfer models and analysis to more accurately assess the temperature levels and distributions associated with the heat source and HSHX's. The flow configuration analysis is described in Section 5.2.4 of this report, and the analytical methods developed for obtaining the system temperature distributions are presented in the appendices.

At this juncture of the study, five specific heat source geometries were selected for more detailed study. These were as follows:

a. Circular Planar — 53 inch diameter

b. Rectangular Planar — 63 x 34 inch

c. Conical — 53 inch diameter

d. Doughnut — 62 inch diameter

e. Pin Cushion — 48 x 40 inch

A variety of HSHX's were designed for each of these heat sources, including both tube fin and plate fin type heat exchangers employing both single and multi-pass flow geometries. On the basis of these designs, a single HSHX was selected for each of the heat sources listed above. All the designs were based on a maximum source temperature of 2000° F for normal operation of power conversion system number 2. The selection criteria employed in choosing these HSHX's were as follows:

a. Low heat source temperature gradients

b. Low HSHX temperature gradients

c. Advantageous ducting configurations

d. Ease of fabrication

e. Weight

A summary of the HSHX designs is presented in Table 5.2-II. With the selection of the specific HSHX designs, preliminary installation drawings appropriate for an Atlas/Centaur type vehicle were prepared for each, in order to identify differences in the structural, insulation, and installation characteristics. Structural concepts were developed for the attachment and support of the HSHX's to the BHXU package as well as with the different IRV designs. Insulation systems were developed and estimates of the heat leaks associated with each system were made. All operational and performance requirements could be met with the five designs considered, except that the conical and pin cushion designs required a rotation of the IRV to effect the removal of the HSHX's. However, since all the heat source designs have the capability of being rotated to permit the fuel capsules to see space for emergency heat rejection, using this mechanism to effect HSHX removal and replacement would appear reasonable. Figure 5.2-3 shows a schematic of the arrangement of the HSHX-BHXU package and the installation concept developed for an Atlas/Centaur type vehicle. The design studies for these five systems is presented in Sections 5.2.5, 5.2.6, 5.2.7, and 5.2.8 of this report.

5.2.1.4 Conclusions

The conclusions reached thus far in the study are as follows:

TABLE 5.2-II

SELECTED HSHX DESCRIPTION

HEAT SOURCE GEOMETRY	SELECTED-HSHX-DESCRIPTION						
	HSHX	FLOW CONFIGURATION	CORE WEIGHT, LB	CORE DIMENSION	NO. OF TUBES	TUBE DIAM IN.	HEAT LEAK, WATT
CIRCULAR PLANAR 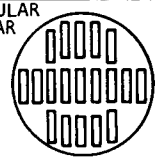		2-PASS INVOLUTE	63	53 IN. DIA	30	0.834	988
RECTANGULAR PLANAR 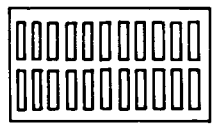	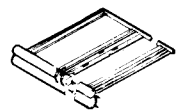	2-PASS RECTANGULAR	48	63 X 34 IN.	54	0.639	884
CONICAL 	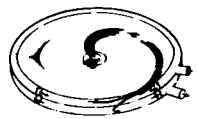	2-PASS INVOLUTE	63	53 IN. DIA	30	0.834	966
DOUGHNUT 		2-PASS INVOLUTE	71	62 IN. O.D. 30 IN. I.D.	170	0.389	1016
PINCUSHION 		SEGMENTED 2-PASS RECTANGULAR	91	9 LEGS 40 IN. BY 6 IN.	54	0.705	847

B-13907-A

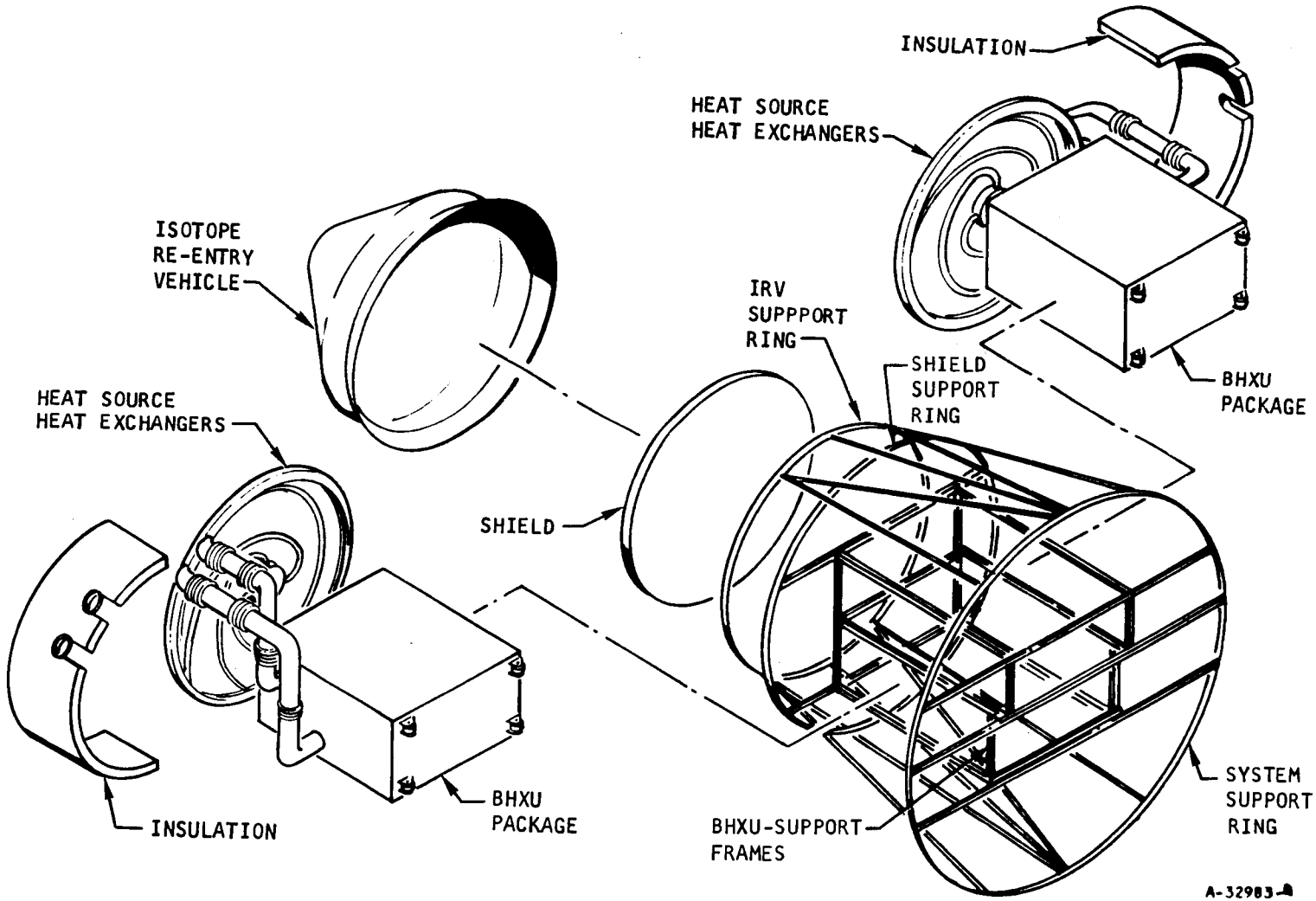

Figure 5.2–3. Circular Planar HSHX-Atlas/Centaur Installation Concept

a. Source size is determined by capsule/capsule-attachment schemes and the HSHX's do not impose an increase in source area to meet performance requirements.

b. Tube-fin HX's are preferable because they

(1) Are generally lighter than plate-fin,

(2) Utilize simple all welded construction, and

(3) Are more reliable than plate-fin

c. Two-pass heat exchangers are preferable

(1) Low ΔT across source

(2) Lower maximum source temperature

(3) Lower ΔT across HX

(4) Offer more attractive ducting arrangements

d. Rectangular HX's with high aspect ratios $\left(\frac{\text{Flow Width}}{\text{Flow Length}}\right)$ offer lowest weight and greatest potential for reducing source temperature ($\approx 100^{o}$ F)

e. On specific designs presented, source temperature can probably be reduced (50-100° F) at some increase in HX weight.

f. Can meet performance and operational requirements imposed on HSHX with any of the five specific IRV designs considered.

5.2.2 Source Geometry Effects

The three reference heat source design configurations selected for preliminary investigations are represented schematically in Figure 5.2-4 and are described in detail in Section 5.1.

5.2.2.1 Fundamental Geometric Effects

Heat is transferred from the heat source to the heat source heat exchanger (HSHX) solely by radiation. Therefore, an improvement in the geometric shape factor between the heat source and the HSHX results in an increase in the radiant heat reaching the HSHX and a decrease in the heat source temperature.

An approximate analysis was carried out to compare the effect of the geometry of the heat source and the HSHX on the heat source temperature. The following assumptions were made:

a. Each surface of the enclosure is isothermal.

b. Each surface is gray.

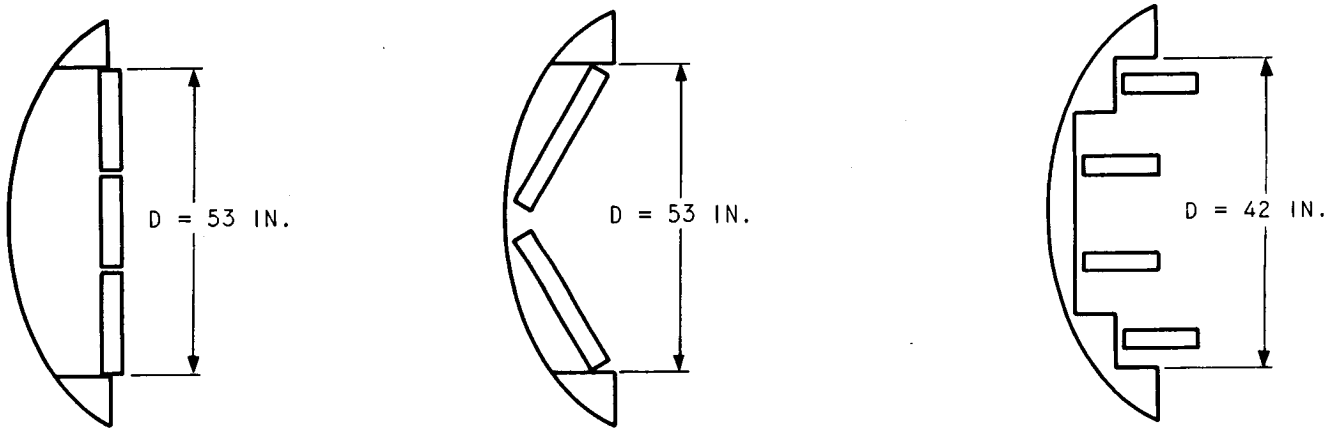

a. PLANAR ARRAY
A_0 = 15.3 SQ FT

b. CONICAL ARRAY
A_0 = 15.3 SQ FT

c. PYRAMIDAL ARRAY
A_0 = 9.6 SQ FT

A-32317

Figure 5.2-4. Heat Source Geometries

c. The radiation reflection from any surface is diffusely distributed. Under this assumption, all incident radiation is reflected with a uniform intensity regardless of the direction from which it came.

d. The radiation emitted from any surface is diffusely distributed.

e. The radiosity of any surface is constant along that surface. This assumption is necessary in order that the angle factors be independent of the magnitude and surface distribution of the energy flux.

f. HSHX 1 is assumed to be in operation and its surface facing HSHX 2 is assumed to be perfectly insulated.

The results of this analysis are shown in Figure 5.2-5. The primary heat source heat exchanger (HSHX 1) was always assumed to have the shape of a plane circular disk. The wall temperature of the heat exchanger was assumed to be equal to 1700° F which is 100° F above the outlet gas temperature. The temperature distribution over the heat source, the side walls and the HSHX were not taken into consideration. Hence the temperatures shown in Figure 5.2-5 may be regarded as average temperatures.

Four configurations for the heat source array are shown in Figure 5.2-5. In Configuration 1, the heat source has the shape of a segment of a sphere. Configurations 2 and 3 represent the case of a planar array or a pyramidal array with internal fins (in this case the radiating surface is a plane circular disk). The only difference between Configurations 2 and 3 is the presence of reradiating walls in Configuration 3. In other words, it is assumed in Configuration 3 that there is no heat lost to the environment. In Configuration 4, the heat source has the shape of the curved wall of a frustum of a cone, and it represents the case of a conical array.

Figure 5.2-5 shows that the larger the ratio D/2L, the lower the source temperature becomes, up to a value of D/2L $\cong$ 4.5. A comparison of Configurations 2 and 3 reveals the effect of the heat lost to the environment on the heat source temperature. This effect becomes negligible for D/2L > 4. In Configuration 4 the cone angle as well as the smaller base area are kept constant. Figure 5.2-5 shows the effect of the larger base area, which simulates HSHX 1, and the distance between HSHX and the highest point in the heat source array on the average source temperature. In both Configuration 4 and Configuration 1 the heat source can "see" itself, resulting in higher source temperatures. This factor is shown, however, in Figure 5.2-5 to be significant only for small values of D/2L. It is of interest to note that the conical and planar source configurations present the same average source temperatures for values of D/2L greater than 3.5.

Figure 5.2-6 shows the effect of the cone angle ($2\alpha_o$) on the heat source temperature for the case of a conical array. Both L and D are kept constant as shown in Figure 5.2-6. The same assumptions mentioned before were used in obtaining the data presented in this figure. The lowest source temperatures are obtained for cone angles greater than or equal to 120 degrees.

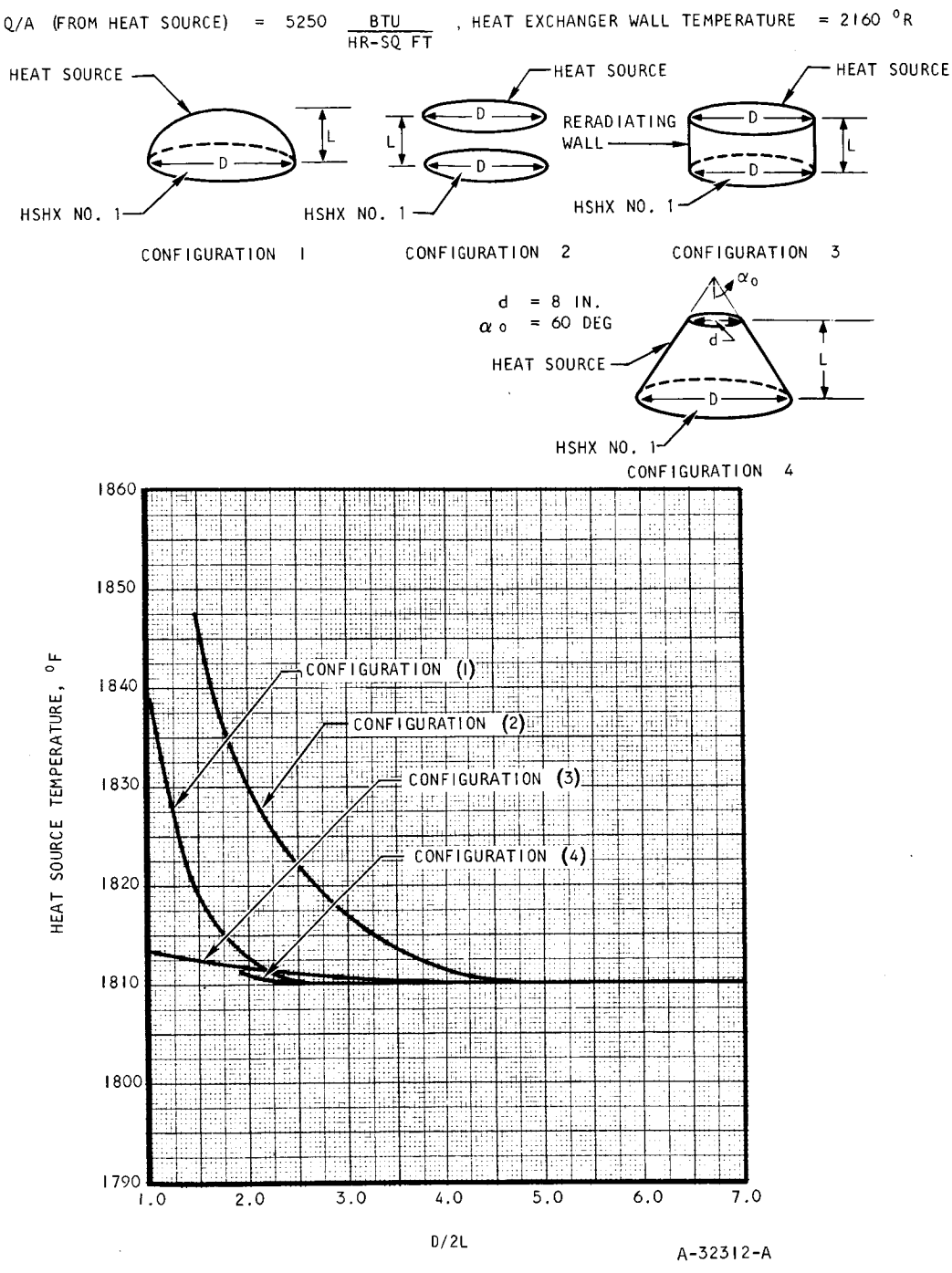

Figure 5.2–5. Effect of Geometry on Heat-Source Temperature

Q/A (FROM HEAT SOURCE) = 5250 $\frac{\text{BTU}}{\text{HR-SQ FT}}$, HEAT EXCHANGER WALL TEMPERATURE = 2160°R

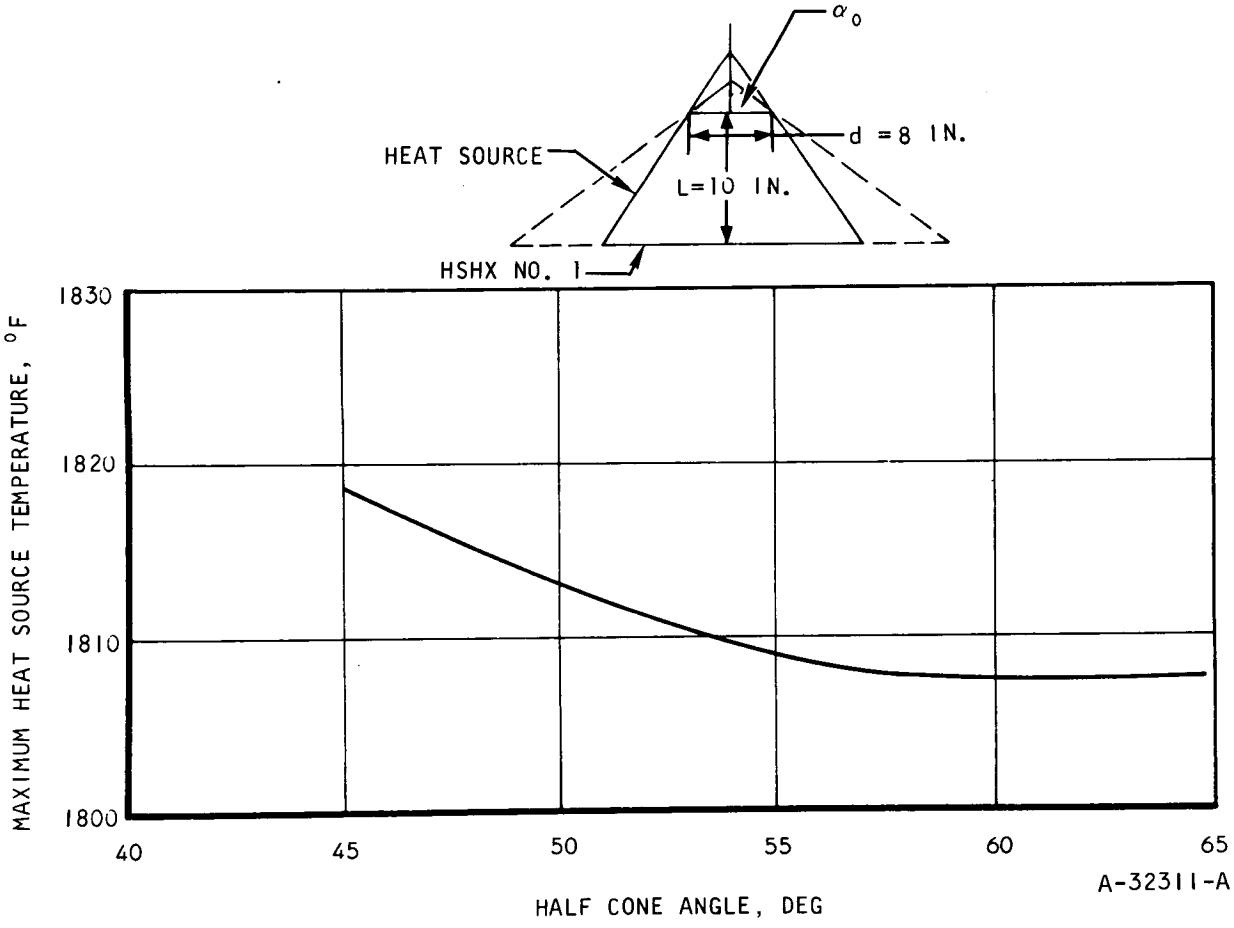

Figure 5.2-6. Effect of the Cone Angle For a Conical Array on Heat-Source Temperature

For a planar heat source array, for the case when HSHX 2 is in operation and HSHX 1 is in place, the average heat source temperature is shown in Figure 5.2-7 as a function of the ratio D/2L for various values of the HSHX 2 wall temperature. A temperature drop of 50° F, due to conduction, is assumed in HSHX 1. Again, it is shown in this figure that, neglecting the temperature change over the heat source, the lowest heat source temperatures are obtained for $D/2L > 4$. It is therefore desirable to have the HSHX close to the heat source. On the other hand, the closer the HSHX to the heat source, the more severe is the temperature change over the heat source, a factor which was not considered in the comparisons shown in Figure 5.2-7. Hence, the final selection of D/L will have to consider the average temperature as well as the temperature distribution over the heat source.

So far, in treating the radiant heat interchange between the heat source and the HSHX's, the spatial changes in the temperature and heat flux were not taken into consideration. Therefore, the temperature results presented in Figures 5.2-5, 5.2-6, and 5.2-7 may be regarded as a first approximation towards the exact temperatures. Now, to determine the effect of the separation distance L on the temperature distribution over the heat source, a more exact analysis has to be followed. Figure 5.2-8 shows the results of an approximate analysis which is discussed in Appendix C and which was used in obtaining the various designs presented in Section 5.2.5. In this analysis, the surface temperatures are allowed to change over both the heat source heat exchangers as well as over the heat source. The HSHX 2 is assumed to be in operation while HSHX 1 is in place. The variation of the heat flux along the surface of HSHX 2 has been taken into consideration. A planar-circular array is assumed for the heat source with a diameter of 53 in. The conduction temperature drop across HSHX 1 is assumed to be equal to 50° F and the side walls are assumed to be perfect reradiators with no heat lost to the environment. Two separation distances, L = 1 in. and L = 5 in., are presented in Figure 5.2.-8. The results show that by decreasing the separation distance from five to one inch, the maximum source temperature increases, while the average source temperature decreases. However, the changes in these temperatures are not appreciable. On the other hand, the temperature variation over the heat source becomes more pronounced for small values of L. Decreasing the separation distance L further would not result in any significant changes in the source temperature. It is also of interest to note that the heat flux over HSHX 2 varies by a factor of about 3 for L = 5 in. and it tends to be uniform for L = 1 in.

Finally, it may be emphasized that the results presented in Figure 5.2-8 were obtained for a one-pass radial HSHX and may not be valid for other flow configurations.

5.2.2.2 Axially Oriented Fuel Capsules

One of the heat source design approaches selected for investigation employed axial mounted fuel capsules (see Figure 5.2-4c, pyramidal array) arranged in circular rows. This type of geometry poses a severe design problem on the heat source heat exchangers.

5.2.2.2.1 Internal and External Fins -- One approach which was investigated was the use of fins to aid in the heat transfer from the fuel capsules to the HSHX. Two basic approaches employing fins are illustrated in Figure 5.2-9. One employs fins attached to the HSHX and heat is radiated from the surface of the fuel capsule, and then conducted along the fin to the HSHX. In the second approach, the fin is attached to the fuel capsule and heat is conducted along the fin to the top of the fuel capsule where it is radiated to a planar heat source heat exchanger.

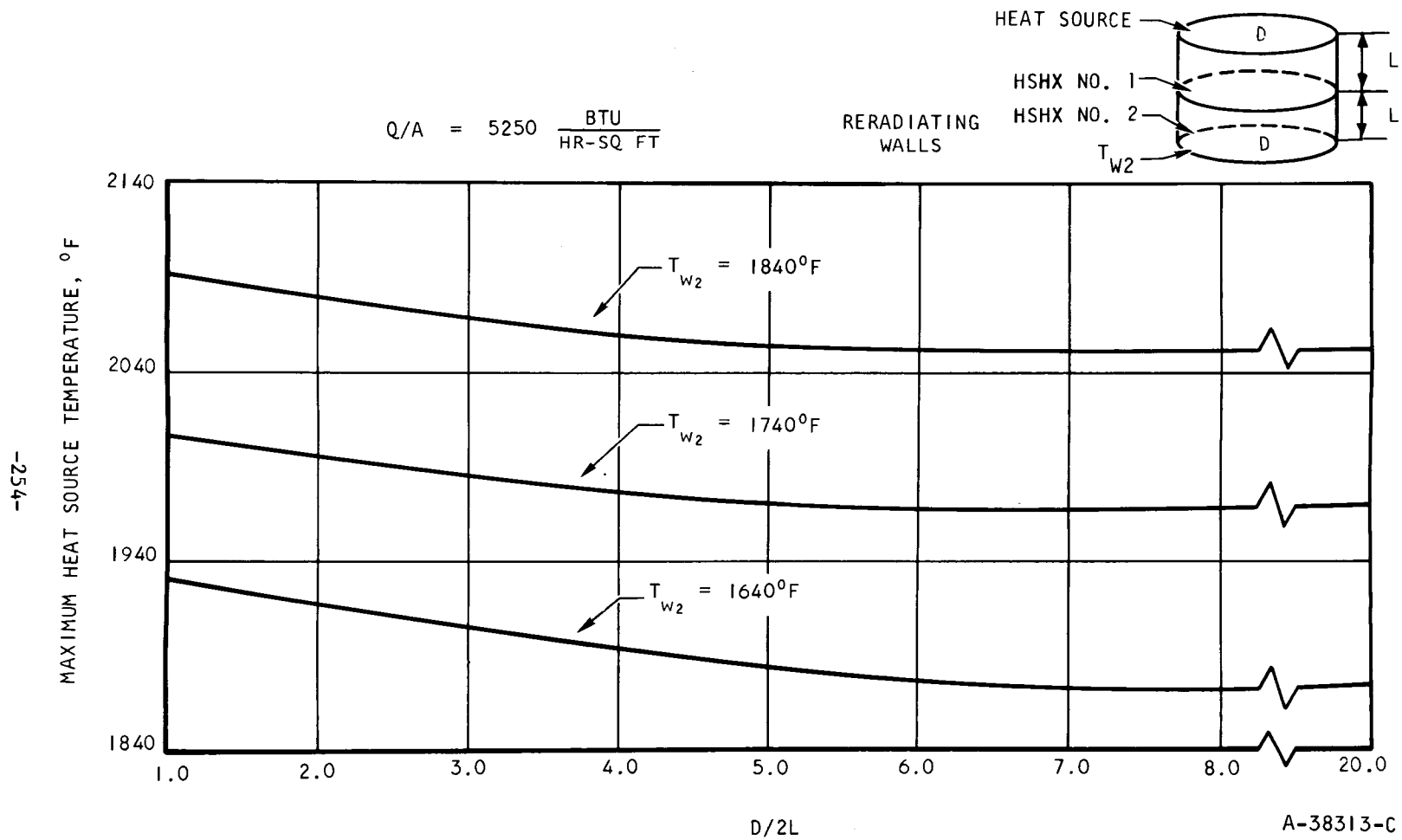

Figure 5.2–7. Effect of D/L Ratio on Heat-Source Temperature

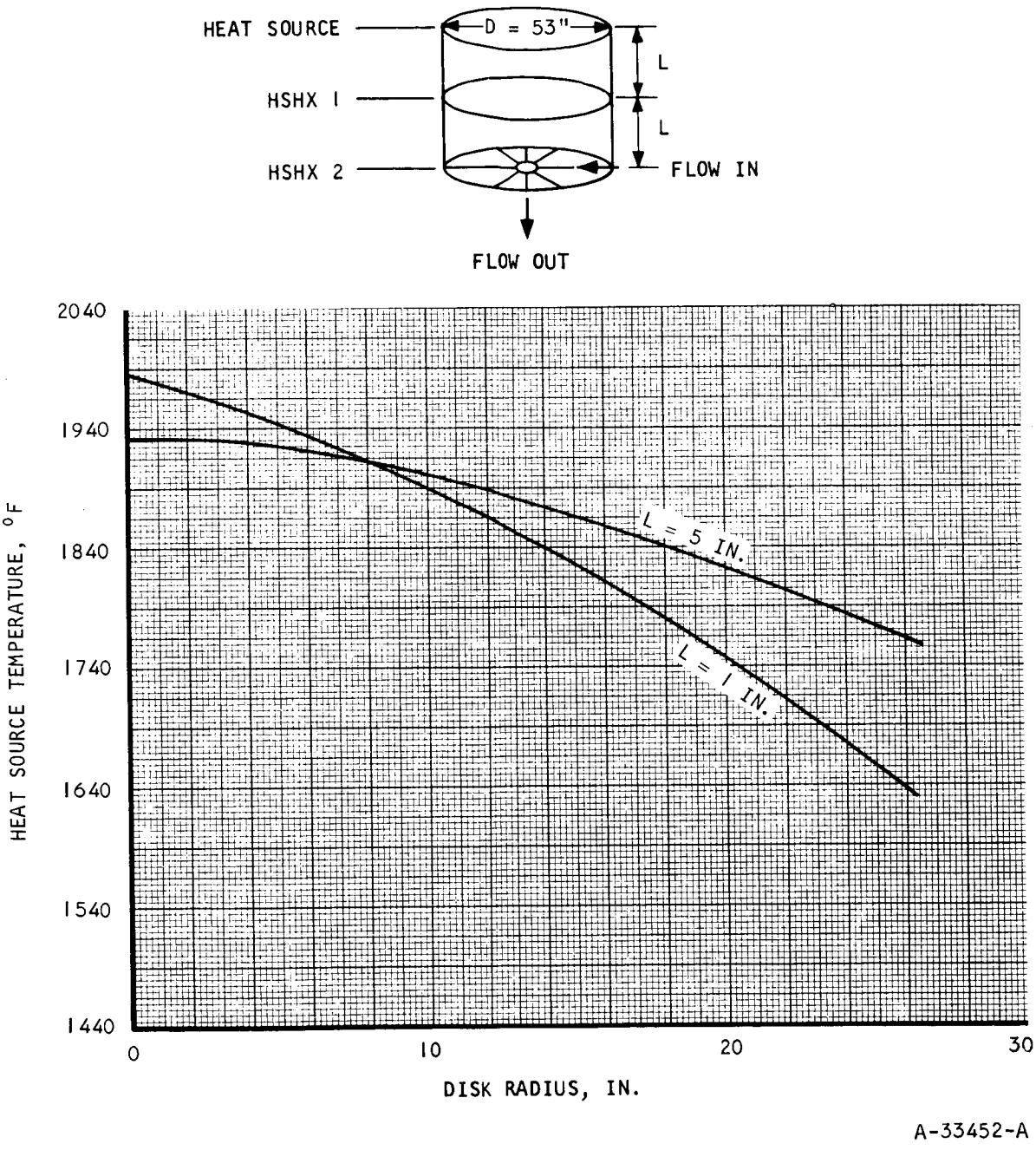

Figure 5.2-8. Effect of Separation Distance L on Temperature Distribution on the Heat Source

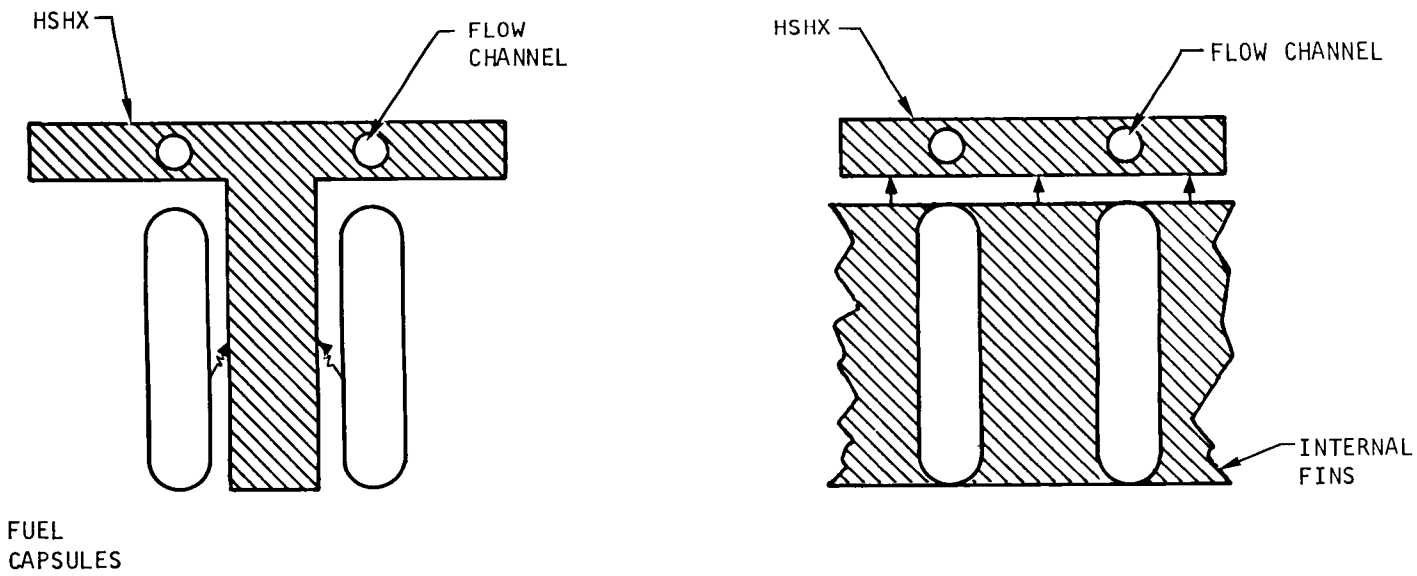

Figure 5.2-9. Axially Mounted Fuel Capsules Employing Fins

The source model assumed to evaluate these concepts has the following assumptions:

a. One-dimensional fin analysis

b. Heat source -- HSHX 1, view factor of one

c. HSHX 1--HSHX 2 view factor of one

d. 50° F conduction temperature drop across HSHX 1

e. Fin material Cb-1-Zr

f. Design for full-power operation of HSHX 2 with HSHX 1 in place

The results of the analysis are shown in Figure 5.2-10 in terms of maximum source temperature, area of the heat source heat exchangers, and required fin material weight. The conclusions reached from this study are as follows:

a. External fins result in

   1) Violation of the interchangeability of heat source heat exchangers, since HSHX is finned and HSHX 2 is not

   2) Movement of the IRV (or HSHX in two directions) is necessary to remove heat source heat exchangers

   3) Large weight penalty for fins

   4) Reduction in heat source projected area negligible over planar array.

b. Internal fins result in

   1) Reduction of heat source projected area negligible over planar array

   2) Large weight penalty for fins.

As a result of these conclusions, no further attention was given to this design approach.

5.2.2.2.2 Internal Heat Source Heat Exchanger -- A better approach to the HSHX design for axial mounted capsules is to place the HSHX between the rows of capsules. Some configurations employing this approach are illustrated in Figure 5.2-11. For the integral HSHX (Figure 5.2-11a) heat exchanger No. 1 and No. 2 are connected by common fins and together comprise a single heat exchanger panel. Thus for this case, the two heat exchangers are inseparable and violate the ground rule for separate removal of the individual heat source heat exchangers.

The independent integral HSHX (Figure 5.2-11b) employs a U-tube flow geometry and separate heat exchanger legs which fit between the individual rows of fuel capsules. For the situation depicted for configuration b, heat is extracted from both sides of the fuel capsule with either HSHX 1 or HSHX 2 in operation. However (i.e., ≈ 85 percent) flows in the direction of the operating HSHX directly adjacent to the fuel capsules.

The third configuration is depicted by Figure 5.2-11c, where the same U-type flow geometry is employed but with the legs of HSHX 1 and HSHX 2 inserted between alternate rows of capsules.

Configurations b and c permit the independent removal of either HSHX 1 or HSHX 2 as required, since the heat exchangers can be extracted from opposite sides of the heat source. Whether they can be extracted without requiring axial movement of either the IRV or the HSHX will depend upon the design of the IRV heat source array and the degree of recessment of the isotope array in the IRV.

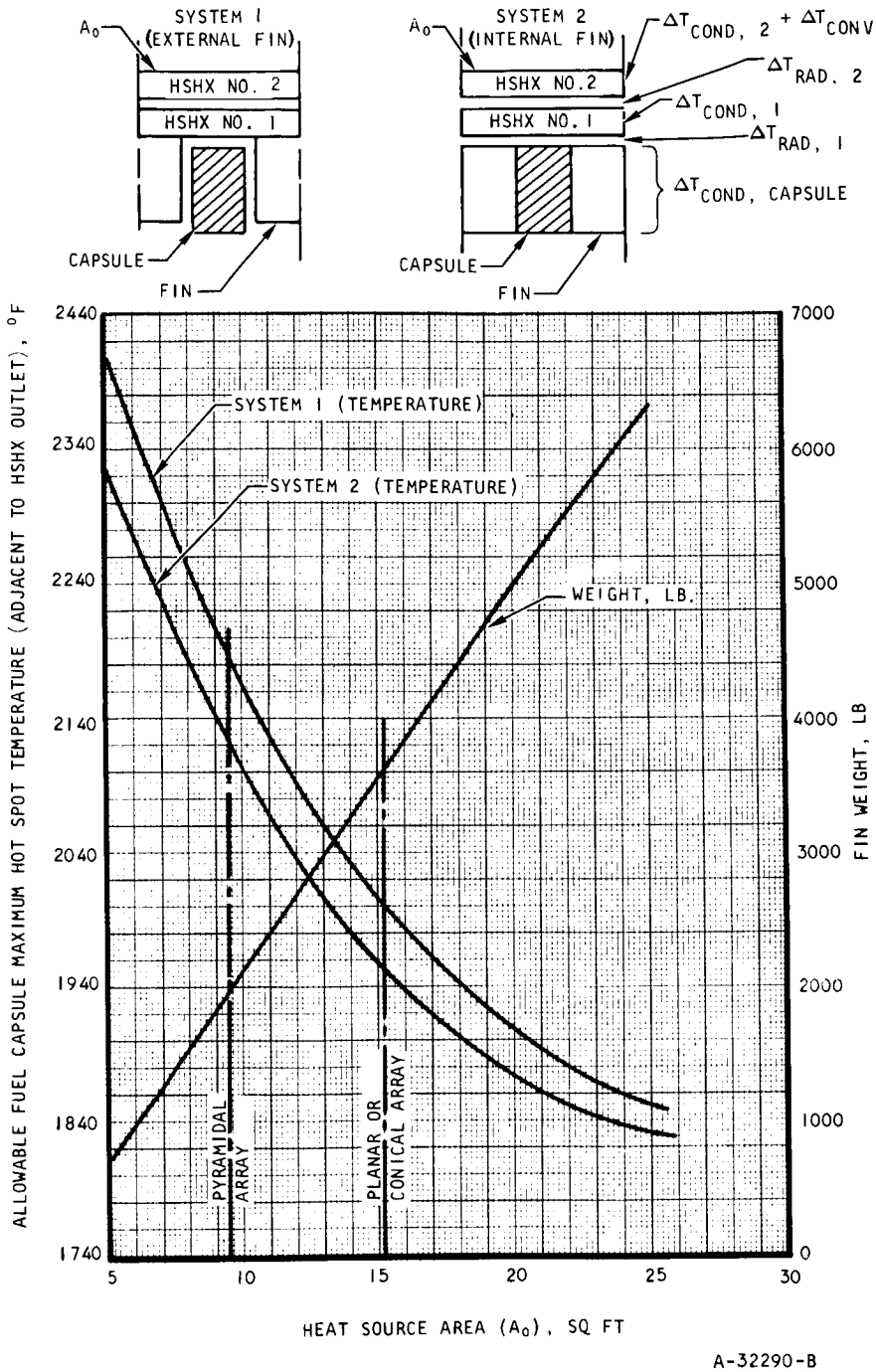

Figure 5.2–10. Axially Oriented Fuel Capsules

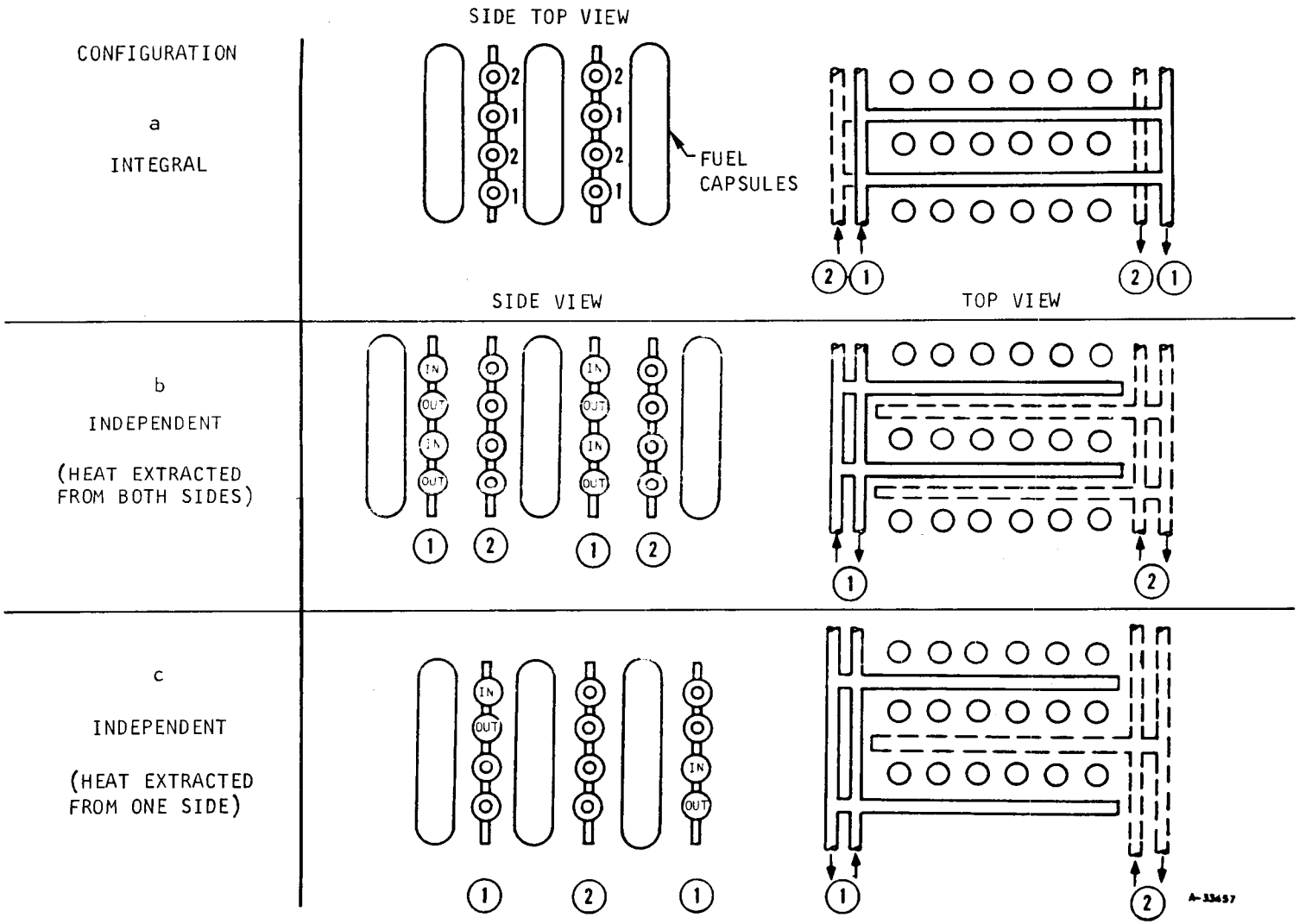

Figure 5.2-11. Internal HSHX's

5.2.3 Parametric Study of the Heat Source Heat Exchanger

In order to establish the basic relationships governing the interaction between the heat source and the Brayton cycle system and to define the operational and physical design limits imposed on the heat source heat exchanger by the set of assumed ground rules, a parametric study was performed on circular planar and rectangular tube-fin heat exchanger configurations. This study resulted in the definition of design envelopes within which heat exchanger designs existed that would offer acceptable thermal and hydraulic performance. The results of this study clearly demonstrated that the heat source heat exchangers did not set the minimum allowable size for planar heat source configurations. Rather, it was the fuel capsule and its retention requirements that established this minimum size.

The set of operational ground rules that was assumed for the study is as follows:

a. In-place system redundancy is required.

b. Independent system replaceability is required.

c. Full-power Brayton cycle operation must be obtainable from both primary and secondary systems without exceeding a specified fuel capsule maximum temperature.

d. The Brayton fluid pressure drop in the HSHX must not exceed 1 psi.

5.2.3.1 Circular Planar Configuration

The study of circular planar configurations was initiated by assuming the involute flow configuration illustrated in Figure 5.2-12. The Brayton cycle fluid was assumed to be distributed uniformly around the periphery of the heat exchanger and to trace an involute path towards the center, where it entered a header and left through an outlet duct. This flow concept was utilized because it appeared to be the most promising from the standpoint of heat transfer and pressure drop performance.

The in-place-redundancy and independent replaceability requirements resulted in the system concept shown in Figure 5.2-12. The additional temperature degradation associated with operating the secondary system establishes that mode of operation as the system design point. The second heat exchanger (HSHX 2) must be capable of maintaining the isotope capsules at a maximum specified temperature (source temperature) upon failure of the first heat exchanger (HSHX 1). To meet the above requirement, heat must be transferred through one radiation gap, then by conduction through the first heat exchanger (HSHX 1), and finally through a second radiation gap to the second heat exchanger (HSHX 2). The temperature drop associated with this heat transfer must be minimized so that a sufficient temperature difference (ΔT_2) exists between the fluid and the wall of the second heat exchanger to transfer the required amount of heat.

Since the physical size limitations of the heat exchanger would be a result of the study, it was desirable to develop a design envelope which would establish minimum heat exchanger size limits at various maximum source temperature and fixed operating conditions. Figure 5.2-13 illustrates the tube-fin geometry that was analyzed, and also defines terms used in the subsequent discussion.

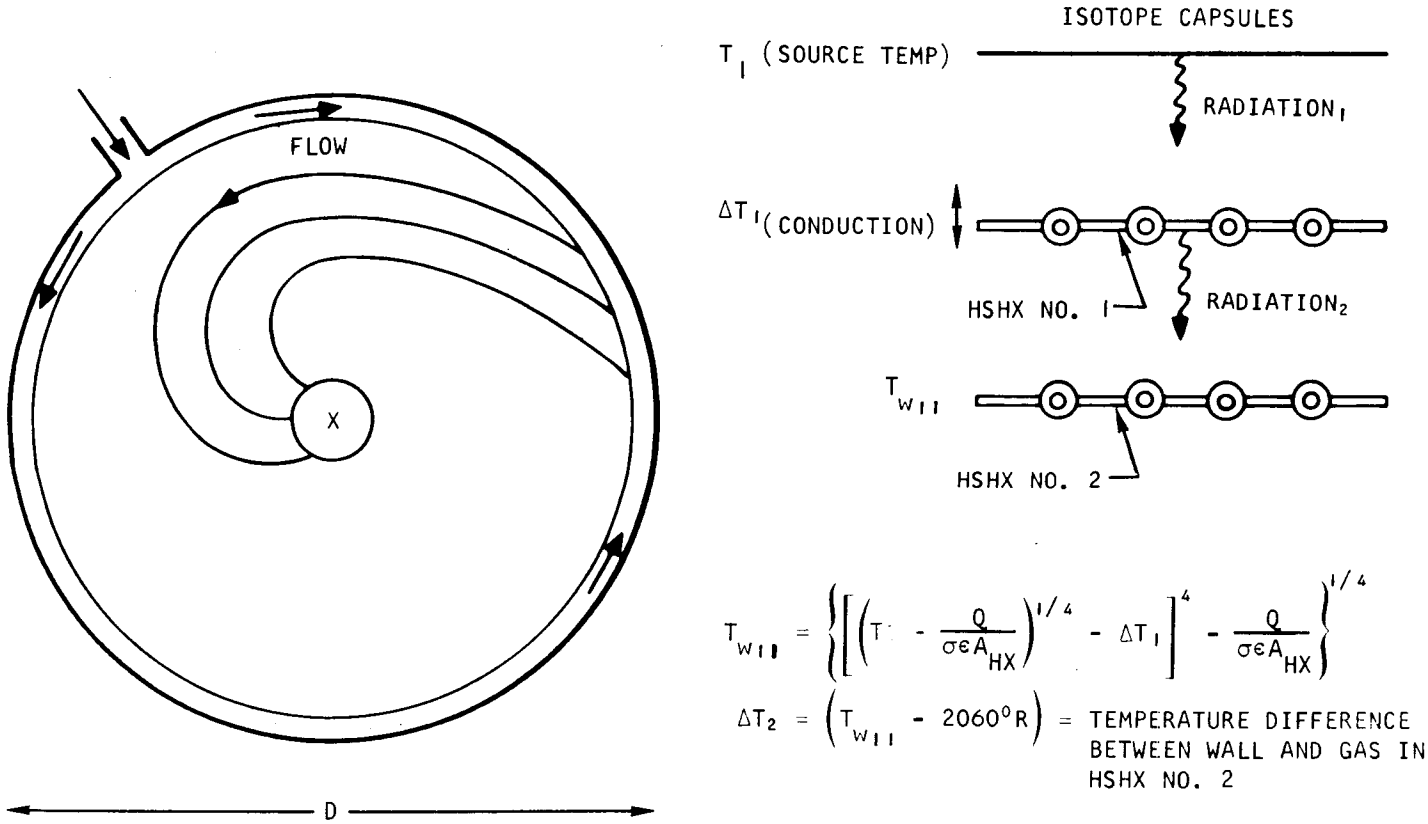

Figure 5.2–12. HSHX-Model for Parametric Study

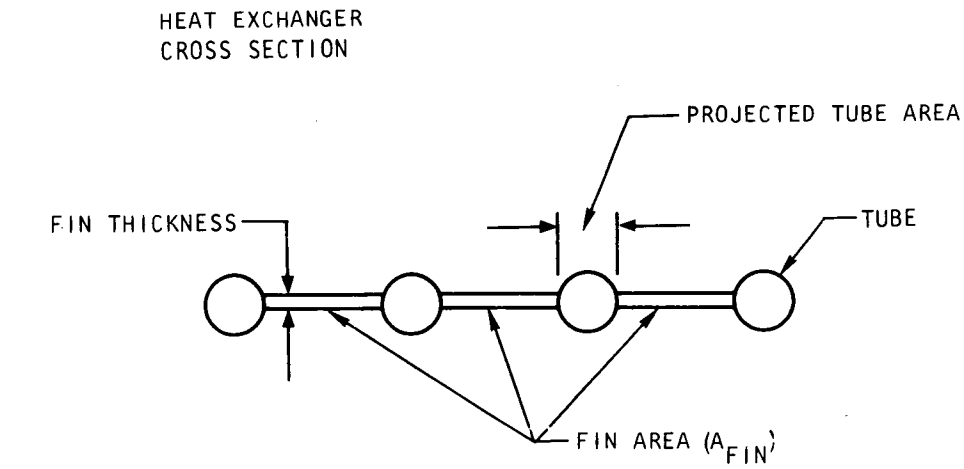

NOTE:

1. PROJECTED TUBE AREA = (TUBE DIA) x (TUBE LENGTH) x (NO. OF TUBES)
2. FIN AREA = (TOTAL HX AREA) - (PROJECTED TUBE AREA)

A-32319

Figure 5.2–13. Tube Geometry

A simple radiation analysis was performed to determine the wall temperature which would be attained by the second heat exchanger for various maximum capsule temperatures. The following assumptions were used:

a. Uniform radiation heat flux over the heat exchanger surface

b. Fin effectiveness = 1.0 (see Figure 5.2-13)

c. All surfaces are gray and diffuse.

Based on the above assumptions, the following equation is obtained for the wall temperature of the HSHX 2.

$$T_{W_{11}} = \left\{ \left[\left(T_1^4 - \frac{(2-\epsilon)\, Q}{\sigma \epsilon\, A_{HX}} \right)^{1/4} - \Delta T_1 \right]^4 - \frac{(2-\epsilon)\, Q}{\sigma \epsilon\, A_{HX}} \right\}^4 \qquad (5\text{-}1)$$

where

$T_{W_{11}}$ = second heat exchanger wall temperature

T_1 = maximum fuel capsule temperature

Q = total heat transfer rate

A_{HX} = heat exchanger surface area

ΔT_1 = conduction temperature drop across the first heat exchanger

σ = 1.714×10^{-9} Btu/hr-ft^2-$^\circ$R^4

ϵ = 0.8 (assumed emissivity)

By specifying the conduction temperature drop across the first heat exchanger (ΔT_1) and the maximum source temperature (T_1), curves of $T_{W_{11}}$ as a function of heat exchanger surface area can be generated. For this analysis, conduction temperature drop in the tube walls of the second heat exchanger was neglected, and the temperature drop between the fluid and wall was taken as the difference between the calculated wall temperature in Equation (5-1) and the specified fluid outlet temperature. The requirement of full power performance from the Brayton cycle translates into a fluid outlet temperature of 2060° R. This, in effect, means T_1 is the maximum temperature on the source adjacent to the outlet of the heat exchanger. The resulting curves are shown in Figures 5.2-14 through 5.2-18 (broken lines) for various values of ΔT_1.

The convective heat transfer and pressure drop requirements determine the projected tube area of the heat exchanger. Figure 5.2-19 shows the projected tube area versus the temperature drop between the fluid and the wall (ΔT_2). This relationship was obtained on the basis of a turbulent-flow analysis. Figure 5.2-19 is incorporated in Figures 5.2-14 through 5.2-18. Each value of ΔT_2 fixes the required heat exchanger tube area. Hence, by specifying the ratio A_{FIN}/A_{HX}, the total area of the HSHX is determined. This results in the curves

shown in solid lines, Figures 5.2-14 through 5.2-18. The curve $A_{FIN}/A_{HX} = 0$ represents the smallest involute tube design, as this design is made entirely of tubes.

The two sets of curves, which are based on the radiant heat exchange in Equation (5-1) and on the heat transfer and pressure drop requirements for the HSHX, establish the design envelopes shown in Figures 5.2-14 through 5.2-18. The cross-hatched area in each case represents the range of acceptable heat exchanger areas, the corresponding temperature differences (ΔT_2) for various A_{FIN}/A_{HX} ratios, and a source maximum effective radiating temperature of 2460° R.

Finally, curves for the maximum source temperature versus acceptable heat exchanger area may be obtained by cross-plotting points within the cross-hatched areas of Figures 5.2-14 through 5.2-18. Figure 5.2-20 shows such a cross-plot for the case of $\Delta T_1 = 25^{\circ}$ F and is derived from Figure 5.2-14.

5.2.3.2 Rectangular Configuration

In a manner similar to that utilized for studying the circular involute, tube and fin design, a parametric survey of rectangular once-through flow, tube and fin heat exchanger designs was made. Figure 5.2-21 illustrates the thermal model assumed for the heat source HSHX system. Based on the assumption of a uniform heat flux over the projected surface area of the heat exchanger and the requirement of a 1600° F Brayton fluid outlet temperature with the backup unit operating, Figures 5.2-22 through 5.2-33 were derived to present the operating envelope within which heat exchanger designs are possible. All ground rules that were assumed for this study correspond to those employed in deriving the circular planar HSHX design envelopes.

For the rectangular heat exchanger parametric survey, the effect of another variable, in addition to those considered for the involute tube study, was investigated. This variable was designated the heat exchanger aspect ratio and is defined in Figure 5.2-21. The two values for aspect ratio that were selected for the study correspond to a 31- by 64-inch rectangular heat source.

The cross-hatched area in Figures 5.2-22 through 5.2-33 represents the design envelope defined by the physical limit of no fin between tubes and by a maximum source temperature of 2460° R.

5.2.4 Flow Configurations

As a result of the studies described in the previous sections and the concurrently developed heat source designs, it became apparent that a variety of heat source heat exchangers could be designed within the required area, temperature, and operational limitations imposed on the HSHX. At this point, our attention turned to consideration of ways of reducing the source temperatures levels as well as the temperature gradients across the source and HSHX. In addition, it was necessary to develop more sophisticated analytical techniques to accurately predict the interchange of radiant energy (temperatures, heat fluxes, etc.) between the heat source and heat source heat exchangers, since this interchange is exceedingly complex and the results are very sensitive to the assumptions and models employed.

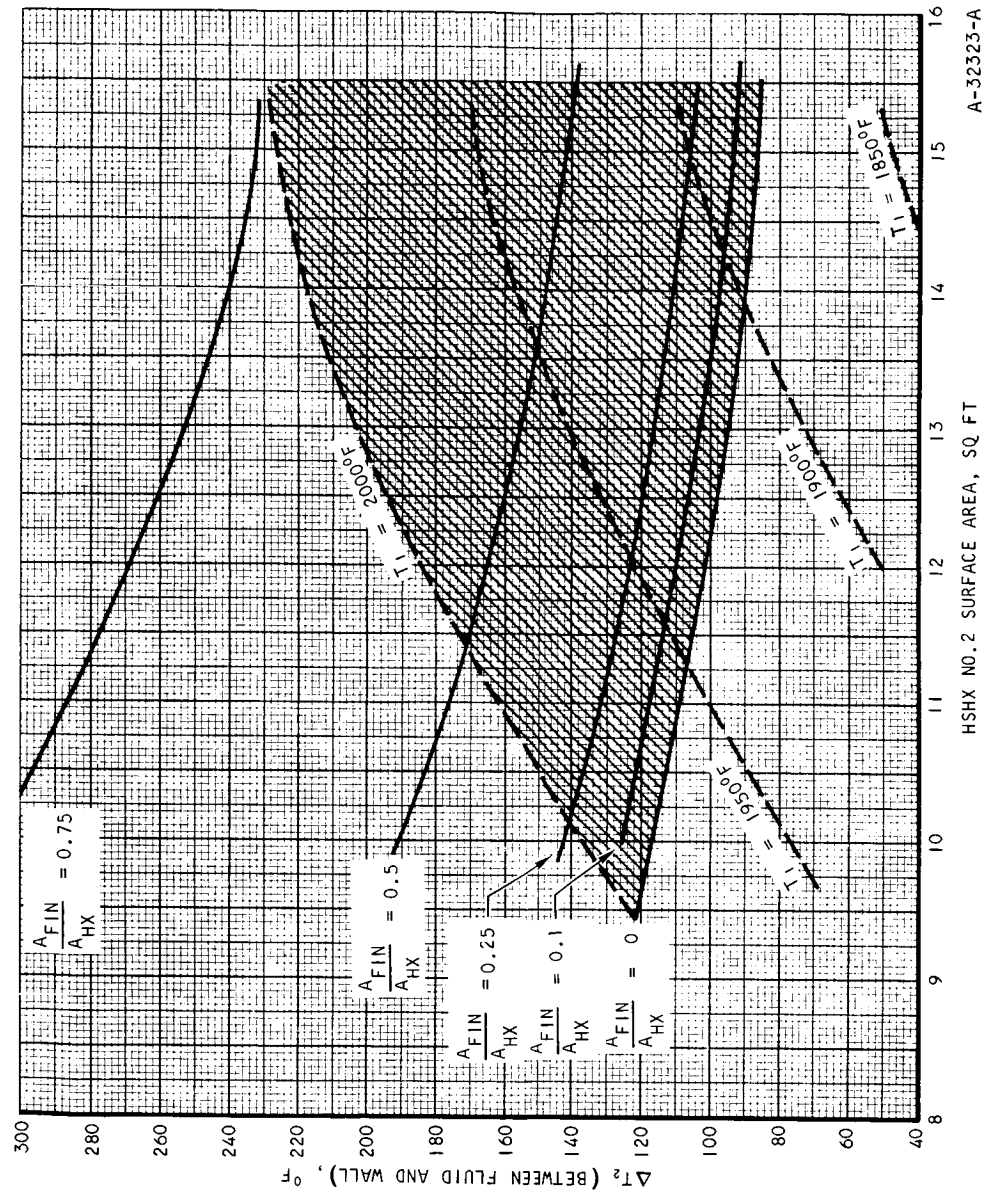

Figure 5.2-14. Heat-Source Heat Exchanger No. 2 Design Envelope ($\Delta T = 25^{\circ}F$)

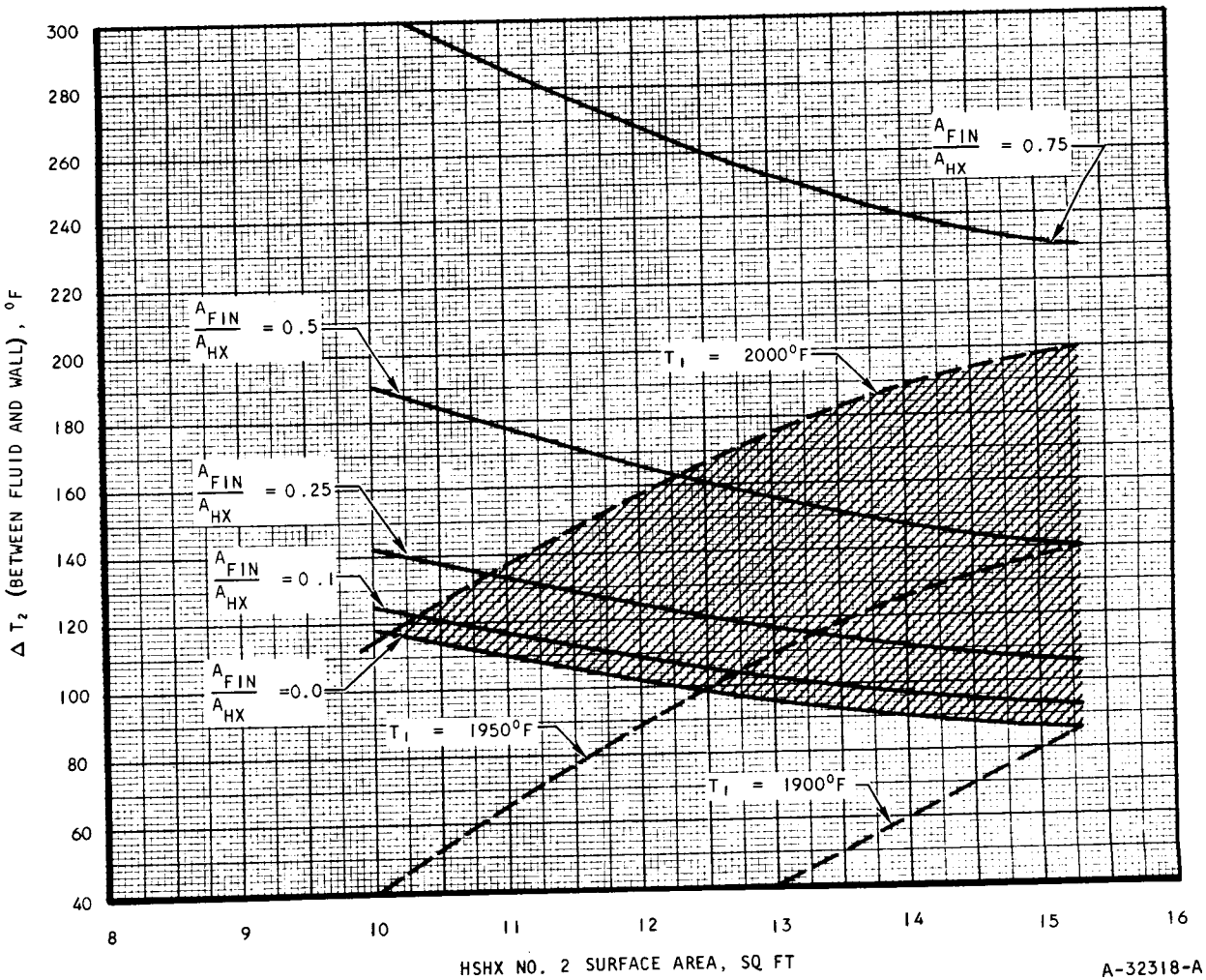

Figure 5.2–15. Heat-Source Heat Exchanger No. 2 Design Envelope ($\Delta T = 50^{\circ}F$)

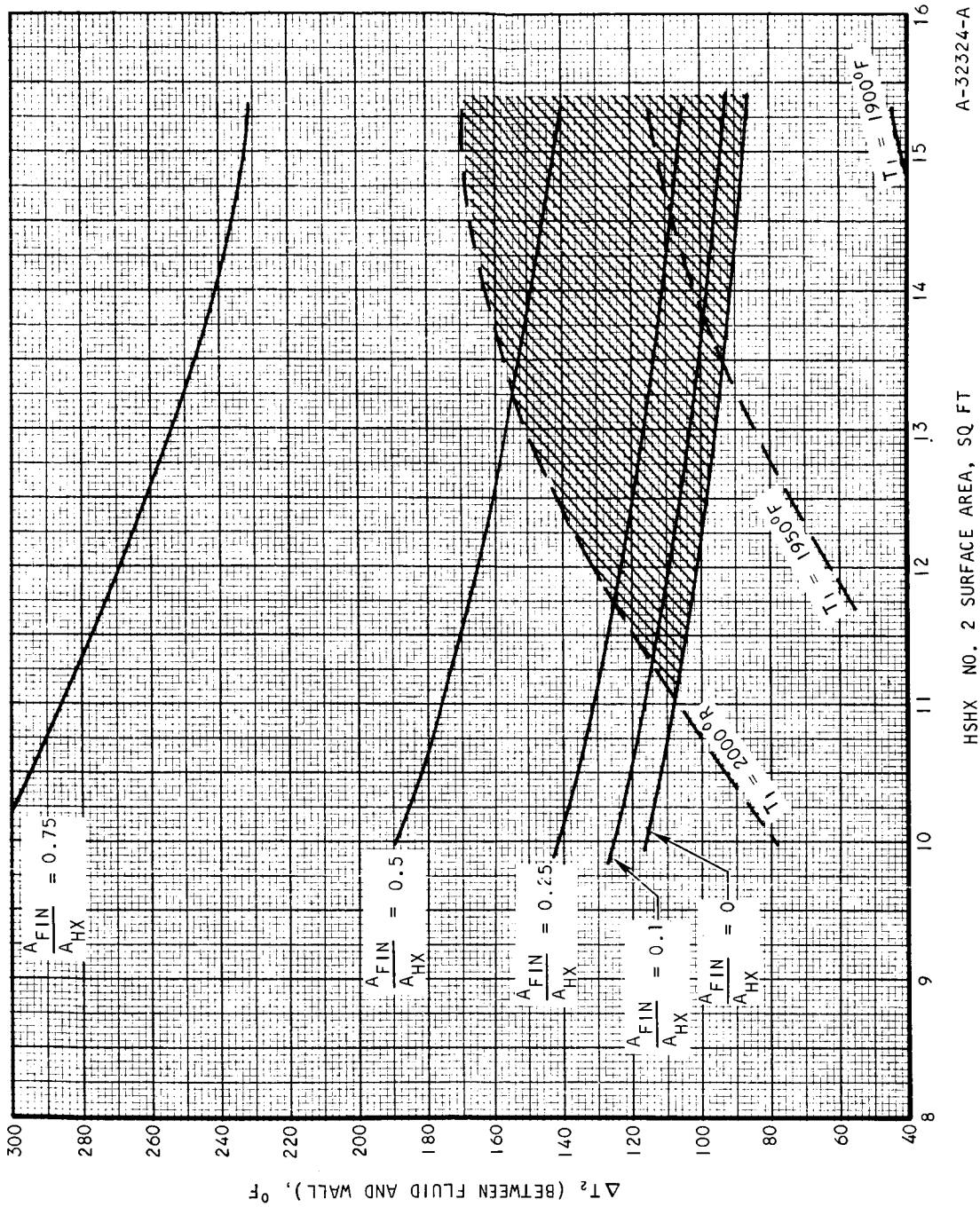

Figure 5.2-16. Heat-Source Heat Exchanger No. 2 Design Envelope ($\Delta T = 75°F$)

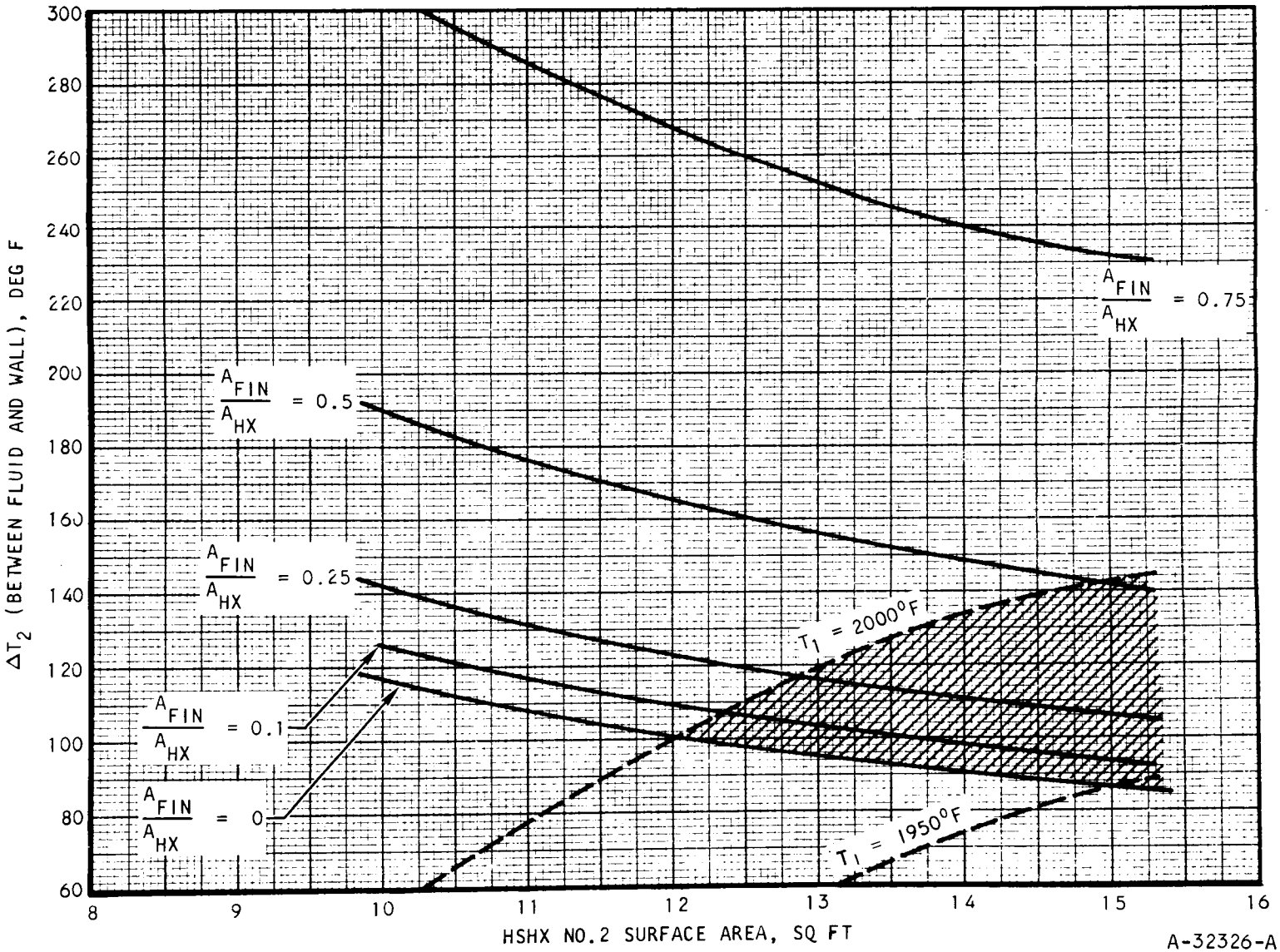

Figure 5.2–17. Heat-Source Heat Exchanger No. 2 Design Envelope ($\Delta T = 100^{\circ}F$)

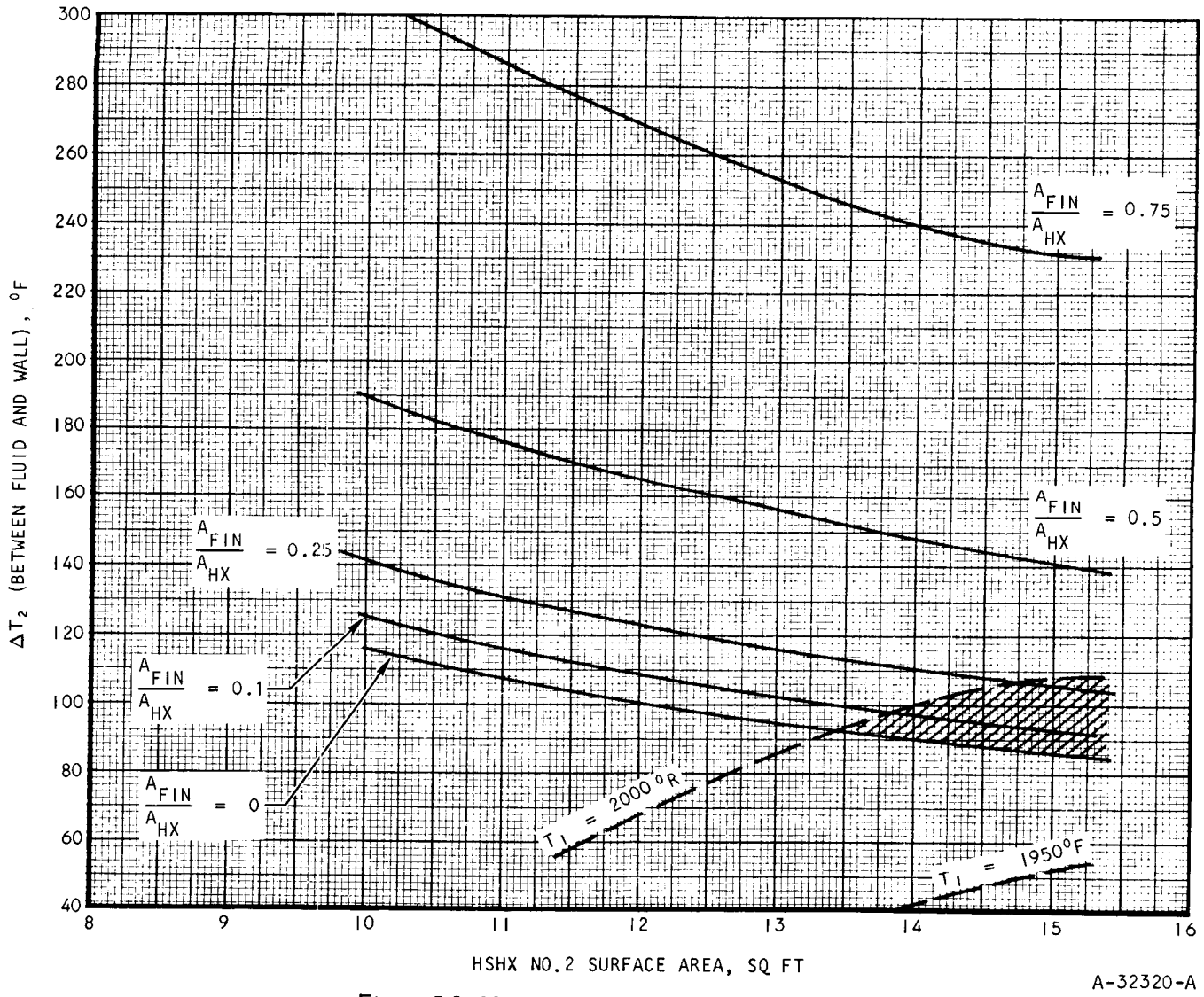

Figure 5.2–18. Heat-Source Heat Exchanger No. 2 Design Envelope ($\Delta T = 125^{\circ}F$)

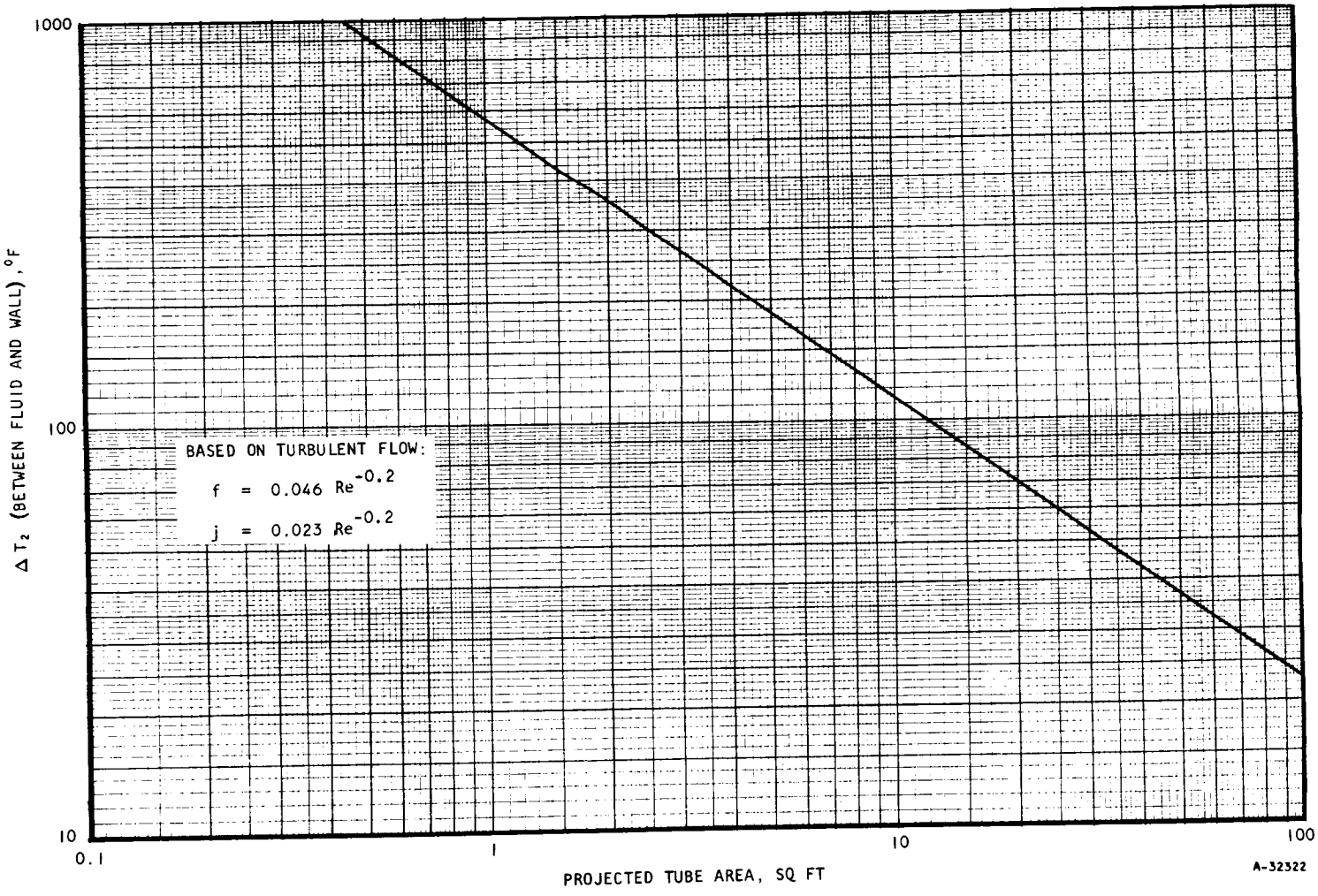

Figure 5.2-19. Projected Tube Area vs Temperature Difference (Between Wall and Fluid)

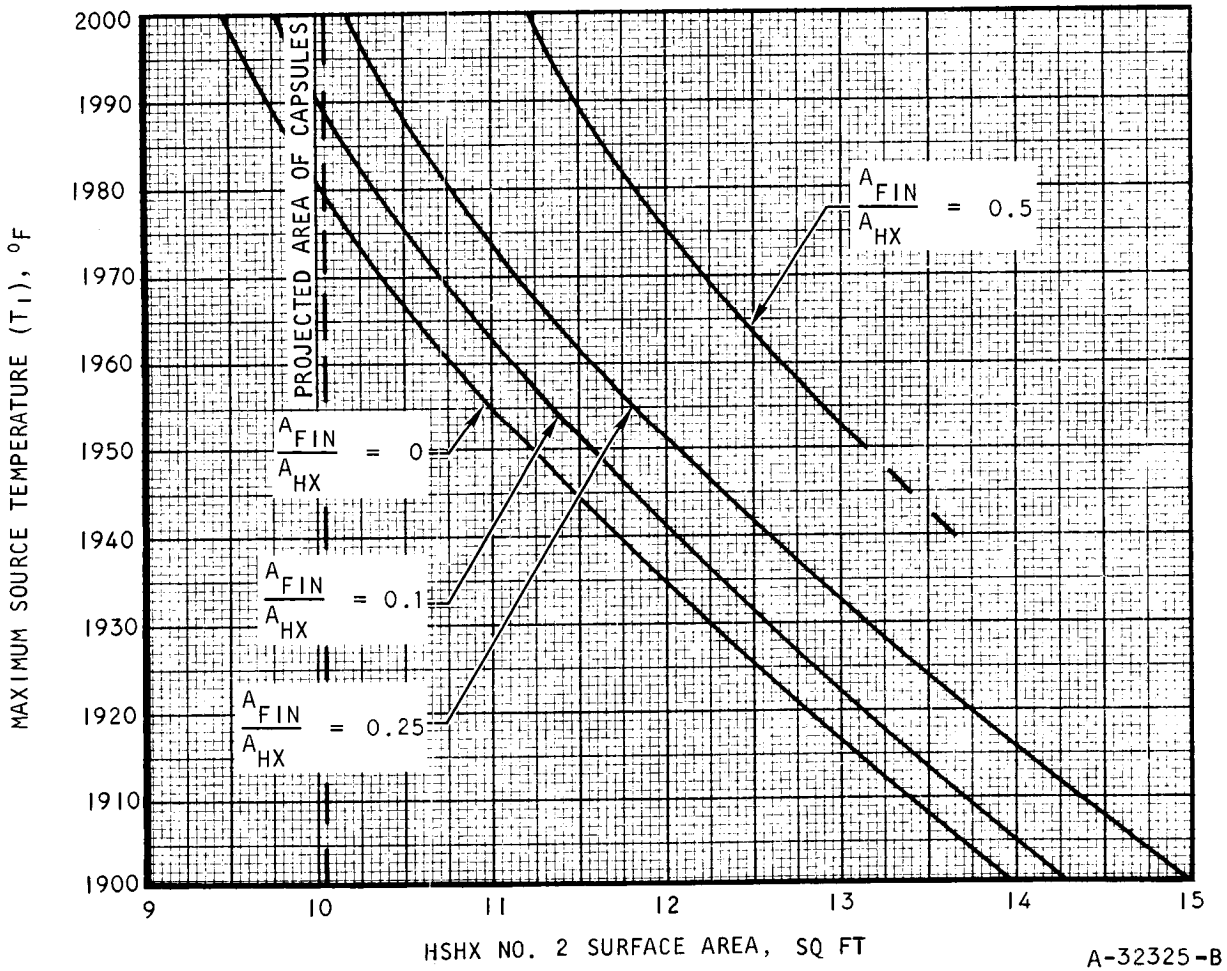

Figure 5.2-20. Maximum Source Temperature vs Heat-Source Heat Exchanger No. 2 Surface Area for $\Delta T = 25^{\circ}F$ (Envelope Designs)

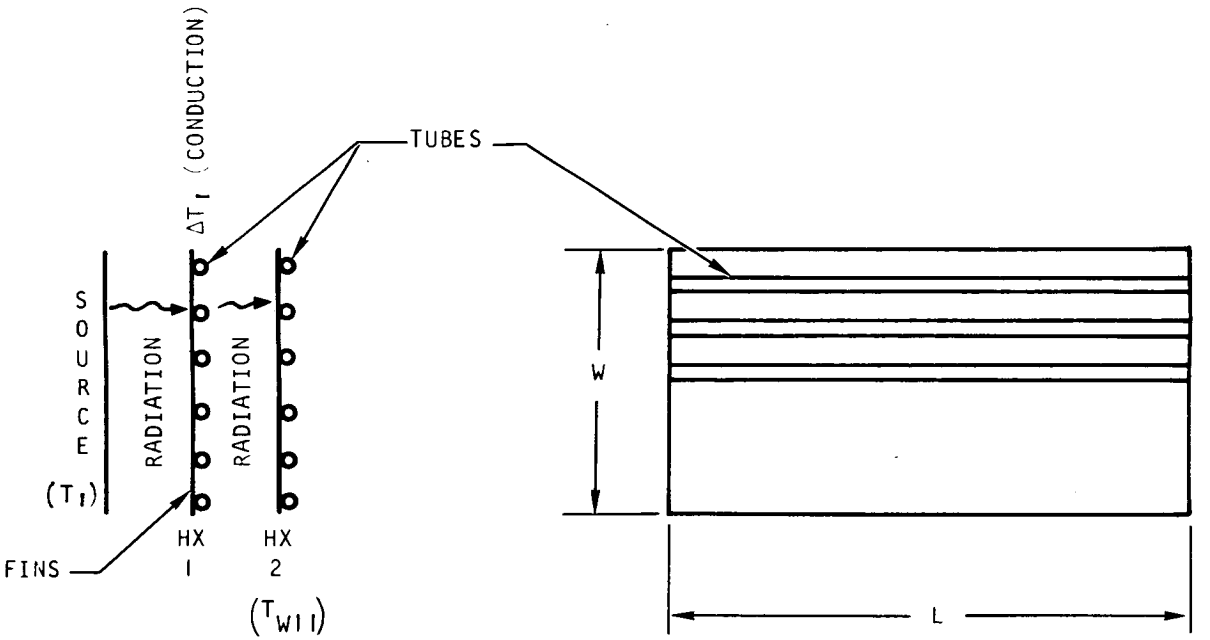

$$T_{W11} = \left\{\left[\left(T_1^4 - \frac{Q}{\sigma\epsilon A_{HX}}\right)^{1/4} - \Delta T_1\right]^4 - \frac{Q}{\sigma\epsilon A_{HX}}\right\}^{1/4}$$

ASPECT RATIO = $\frac{W}{L}$

$\Delta T_2 = (T_{W11} - 2060^{\circ}R)$ = TEMPERATURE DIFFERENCE. BETWEEN WALL AND GAS IN HSHX NO. 2

A-32614-A

Figure 5.2-21. Rectangular Tube-Fin Heat Exchanger

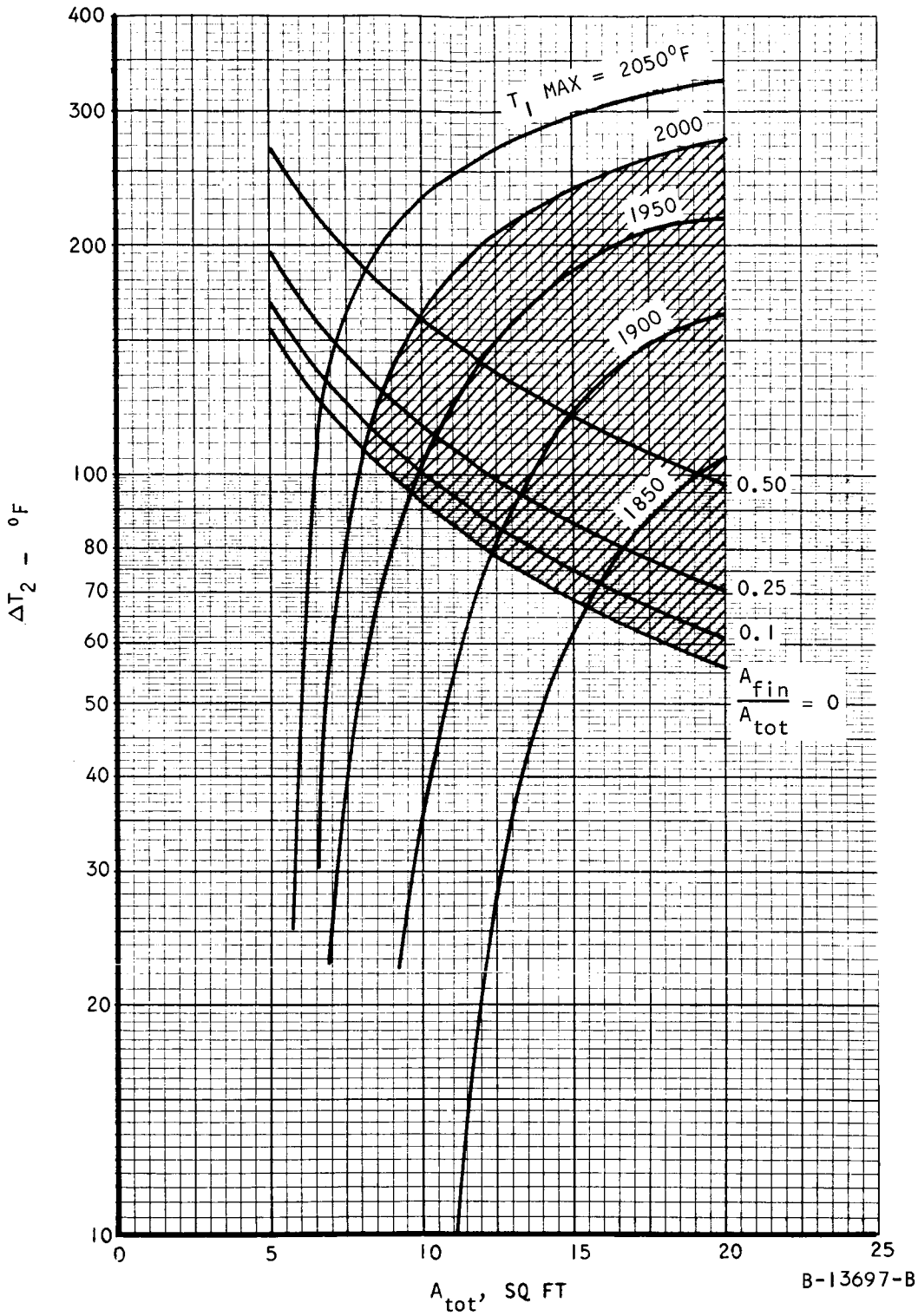

Figure 5.2–22. Parametric Data for Rectangular Tube-Fin Heat Exchanger, ΔT_{cond} = 25°F, Aspect Ratio = 0.485

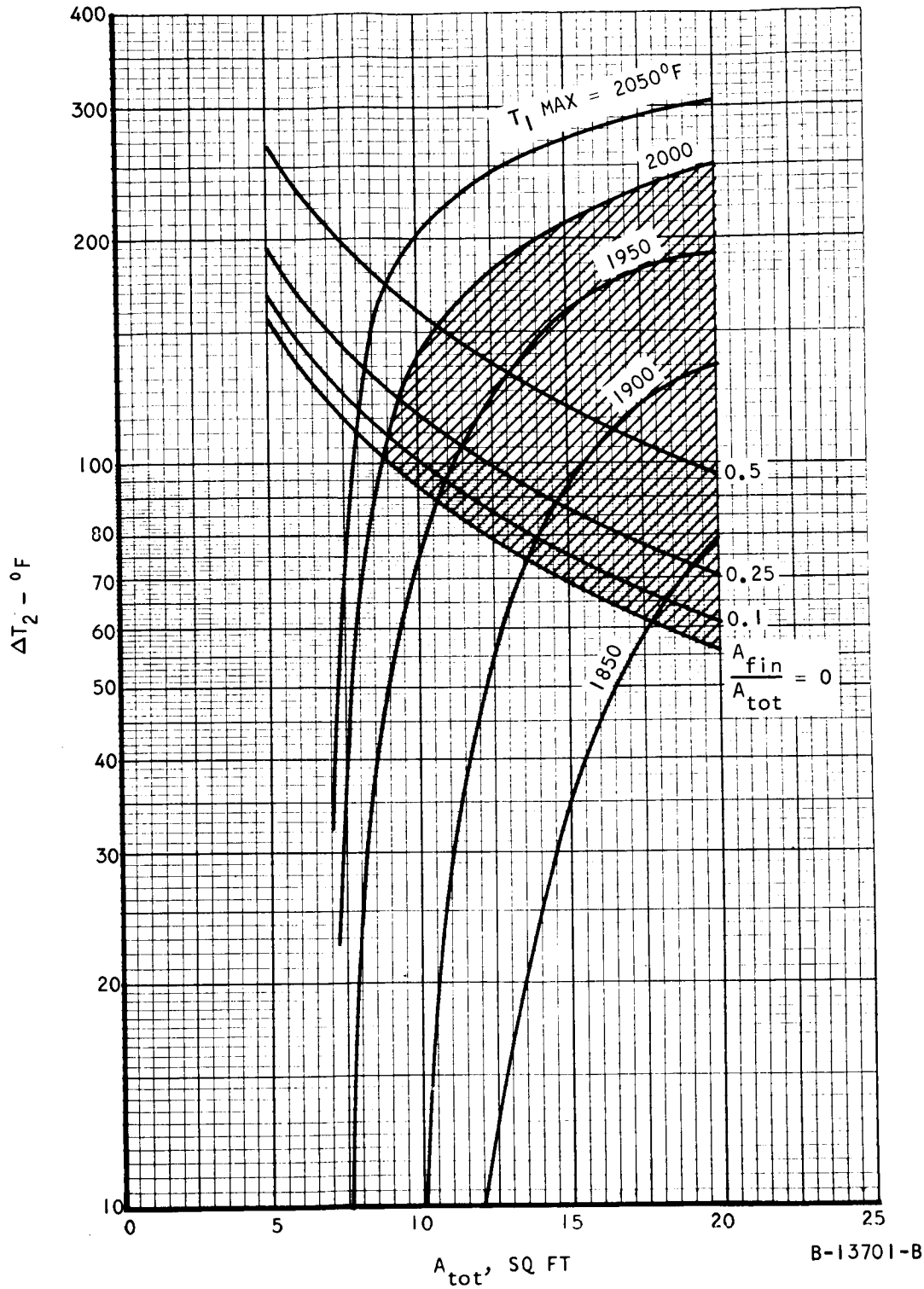

Figure 5.2-23. Parametric Data for Rectangular Tube-Fin Heat Exchanger, ΔT_{cond} = 50°F, Aspect Ratio = 0.485

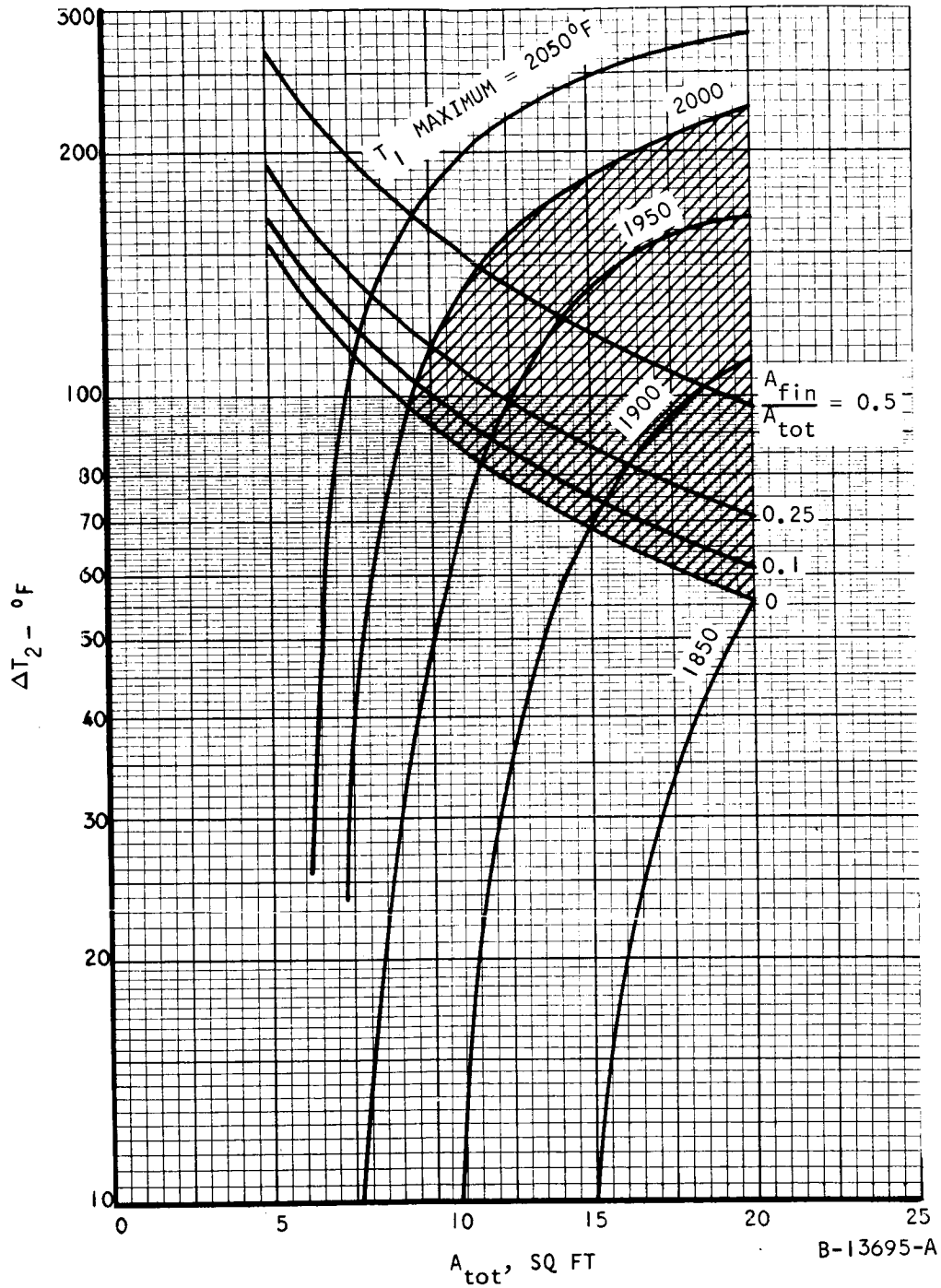

Figure 5.2-24. Parametric Data for Rectangular Tube-Fin Heat Exchanger, ΔT_{cond} = 75°F

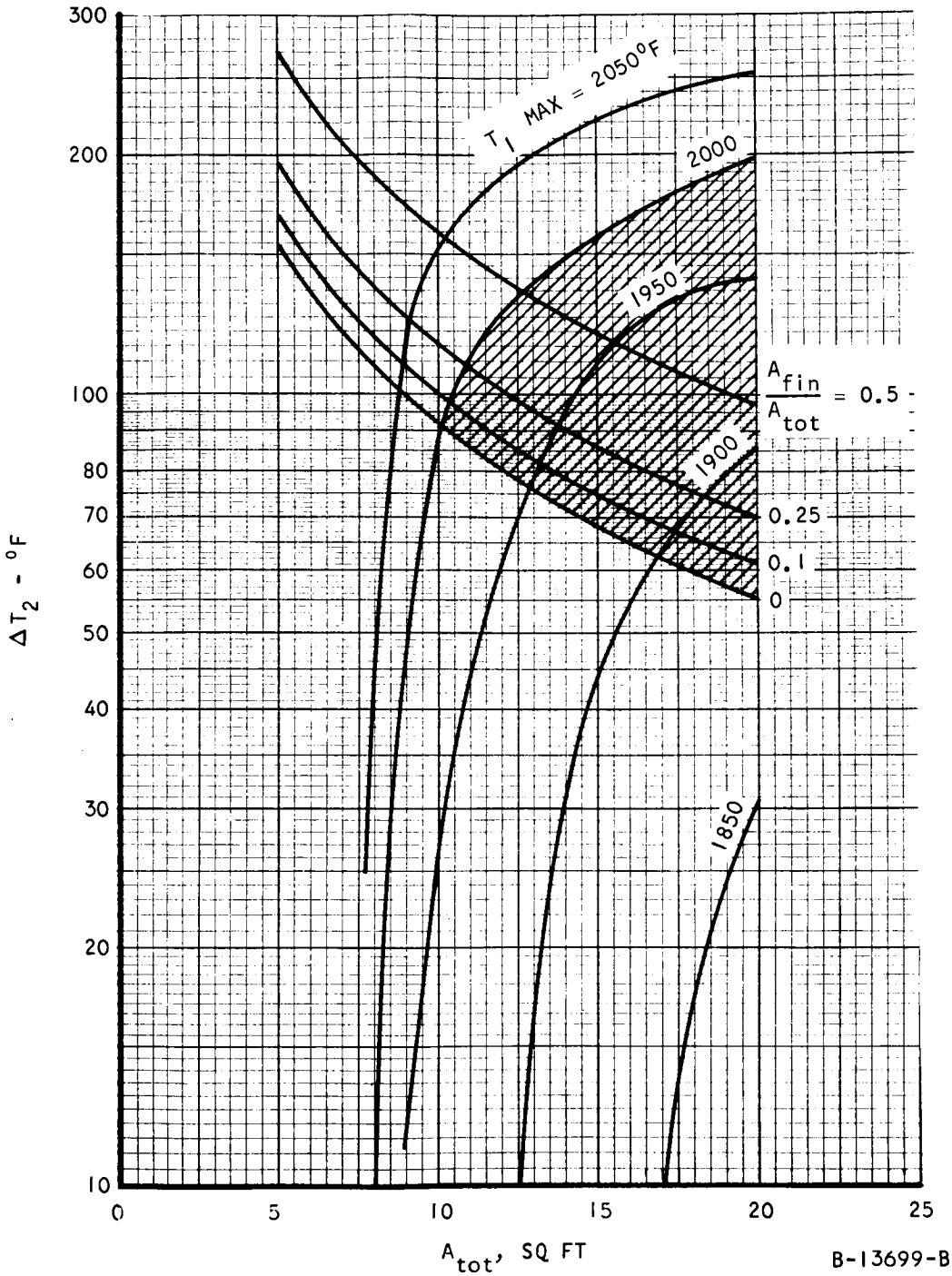

Figure 5.2–25. Parametric Data for Rectangular Tube-Fin Heat Exchanger, ΔT_{cond} = 100°F, Aspect Ratio = 0.485

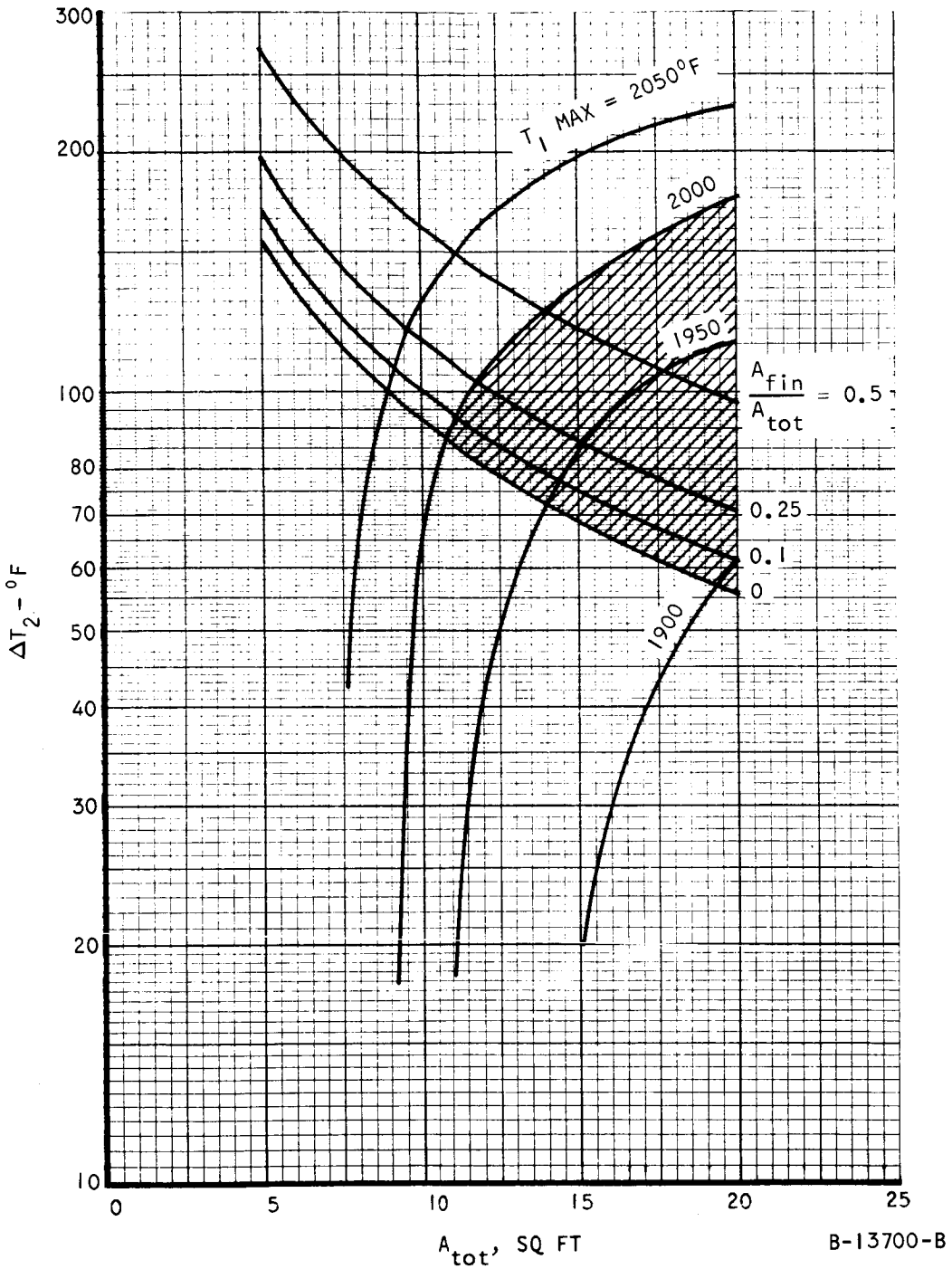

Figure 5.2-26. Parametric Data for Rectangular Tube-Fin Heat Exchanger, ΔT_{cond} = 125°F, Aspect Ratio = 0.485

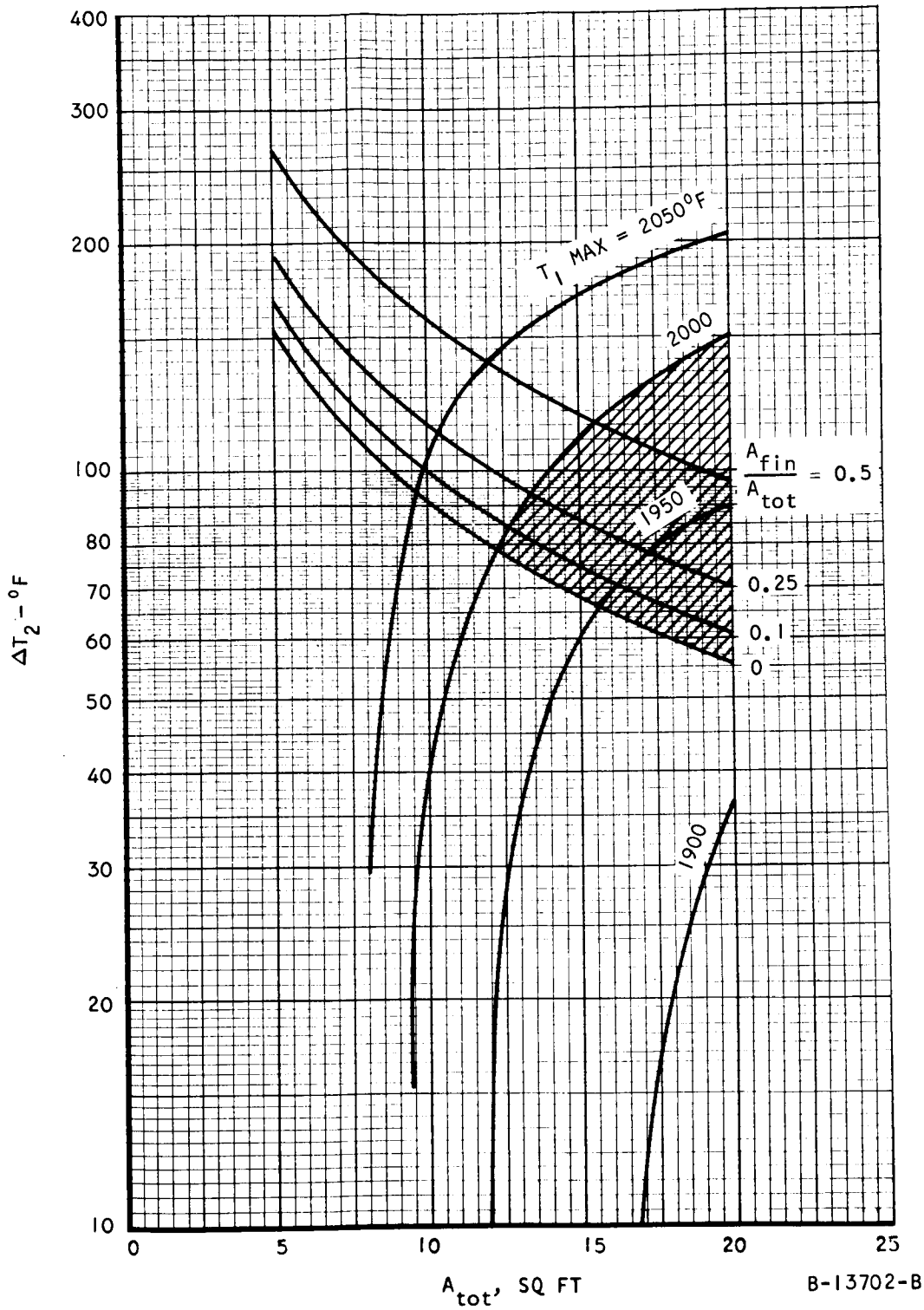

Figure 5.2-27. Parametric Data for Rectangular Tube-Fin Heat Exchanger, ΔT_{cond} = 150°F, Aspect Ratio = 0.485

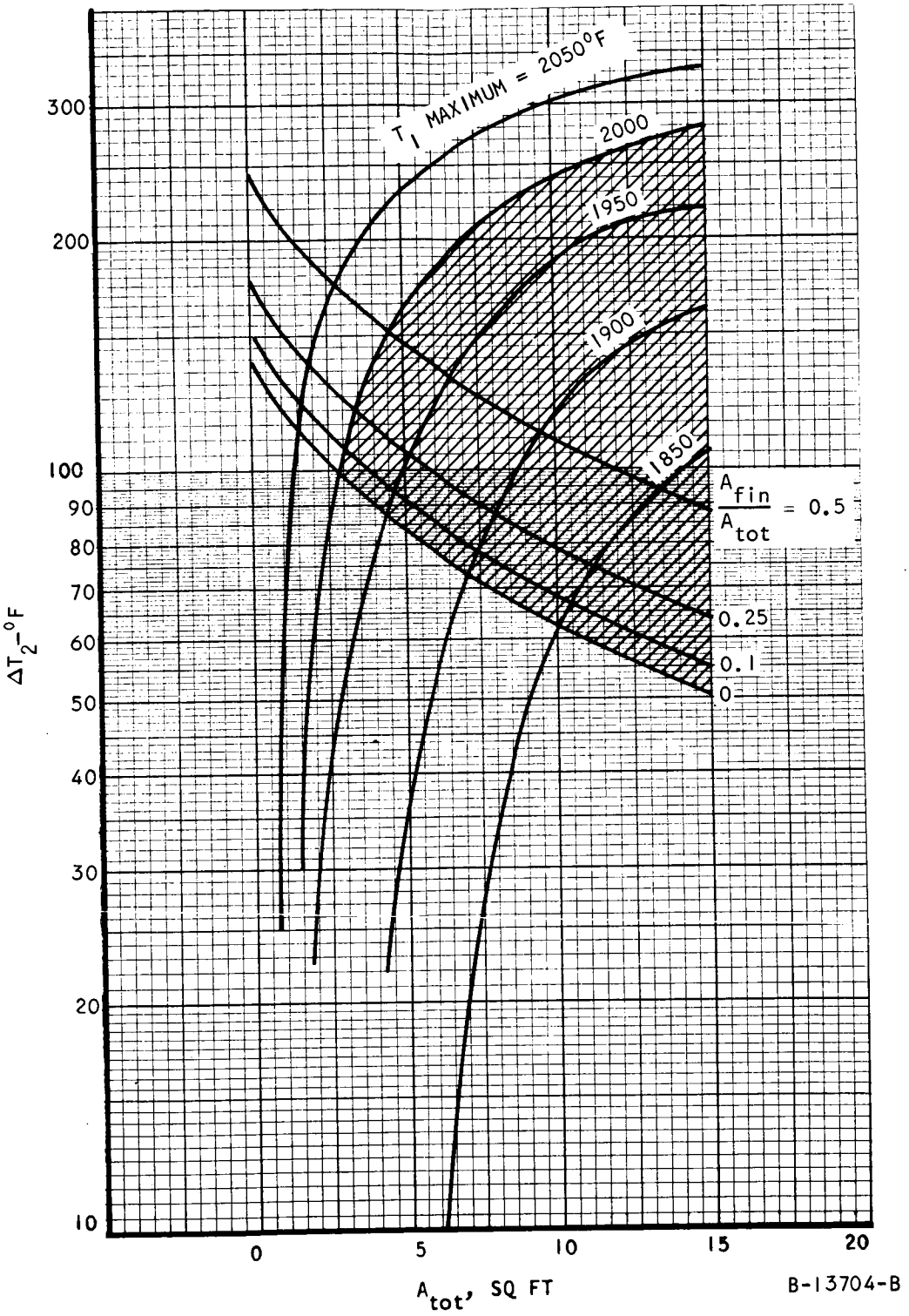

Figure 5.2–28. Parametric Data for Rectangular Tube-Fin Heat Exchanger, ΔT_{cond} = 25°F, Aspect Ratio = 2.065

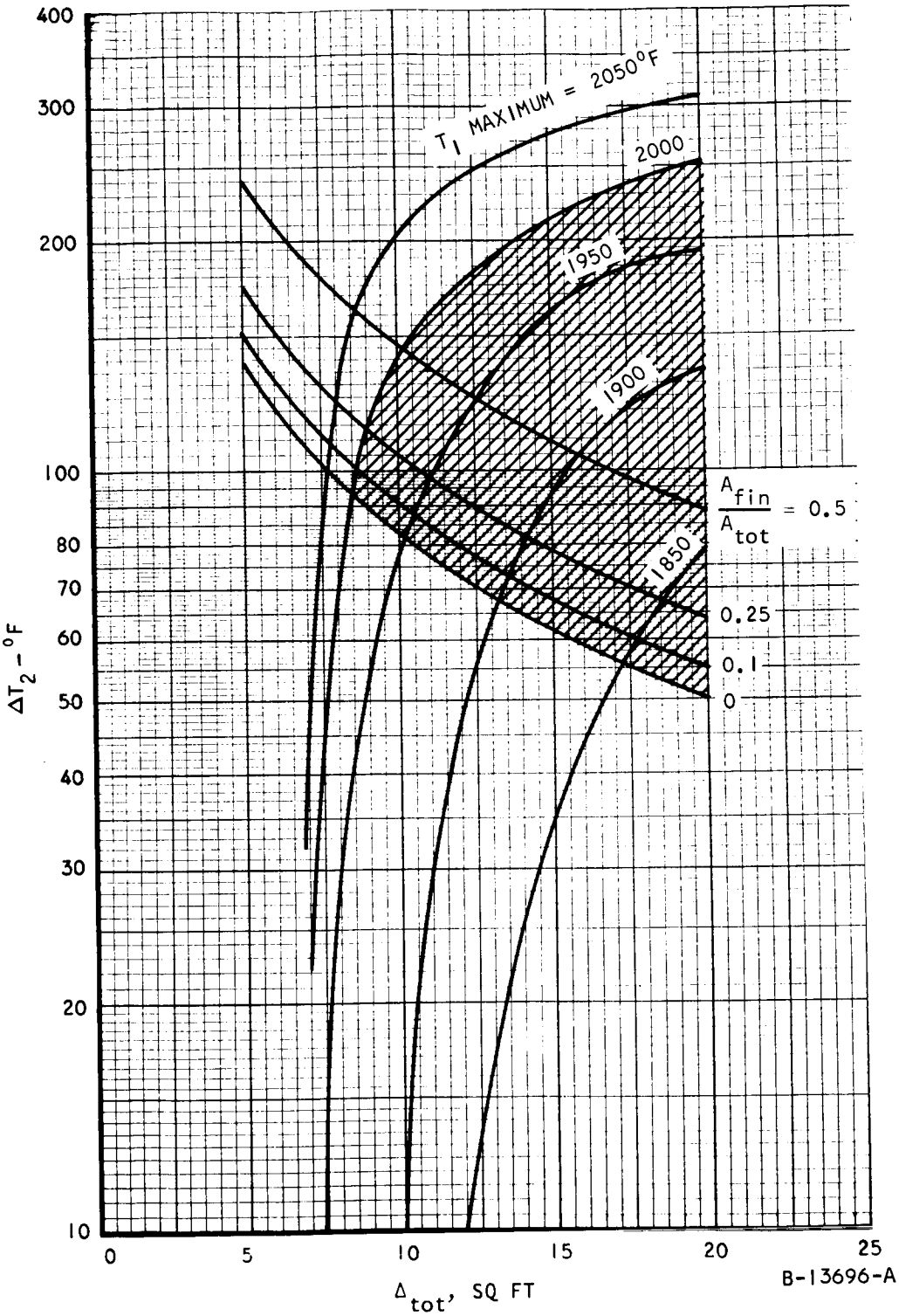

Figure 5.2–29. Parametric Data for Rectangular Tube-Fin Heat Exchanger, ΔT_{cond} = 50°F, Aspect Ratio = 2.065

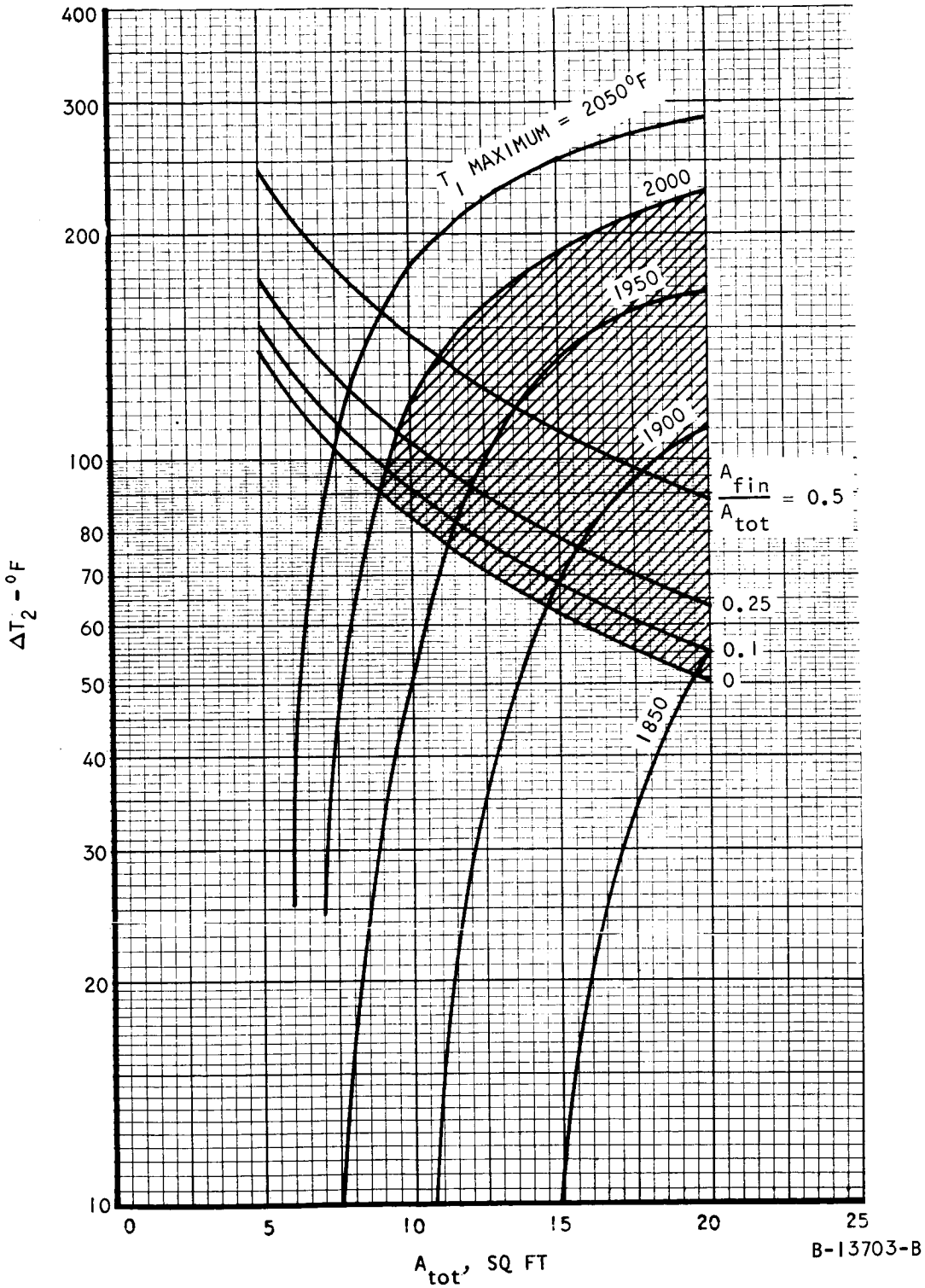

Figure 5.2–30. Parametric Data for Rectangular Tube-Fin Heat Exchanger, ΔT_{cond} = 75°F, Aspect Ratio = 2.065

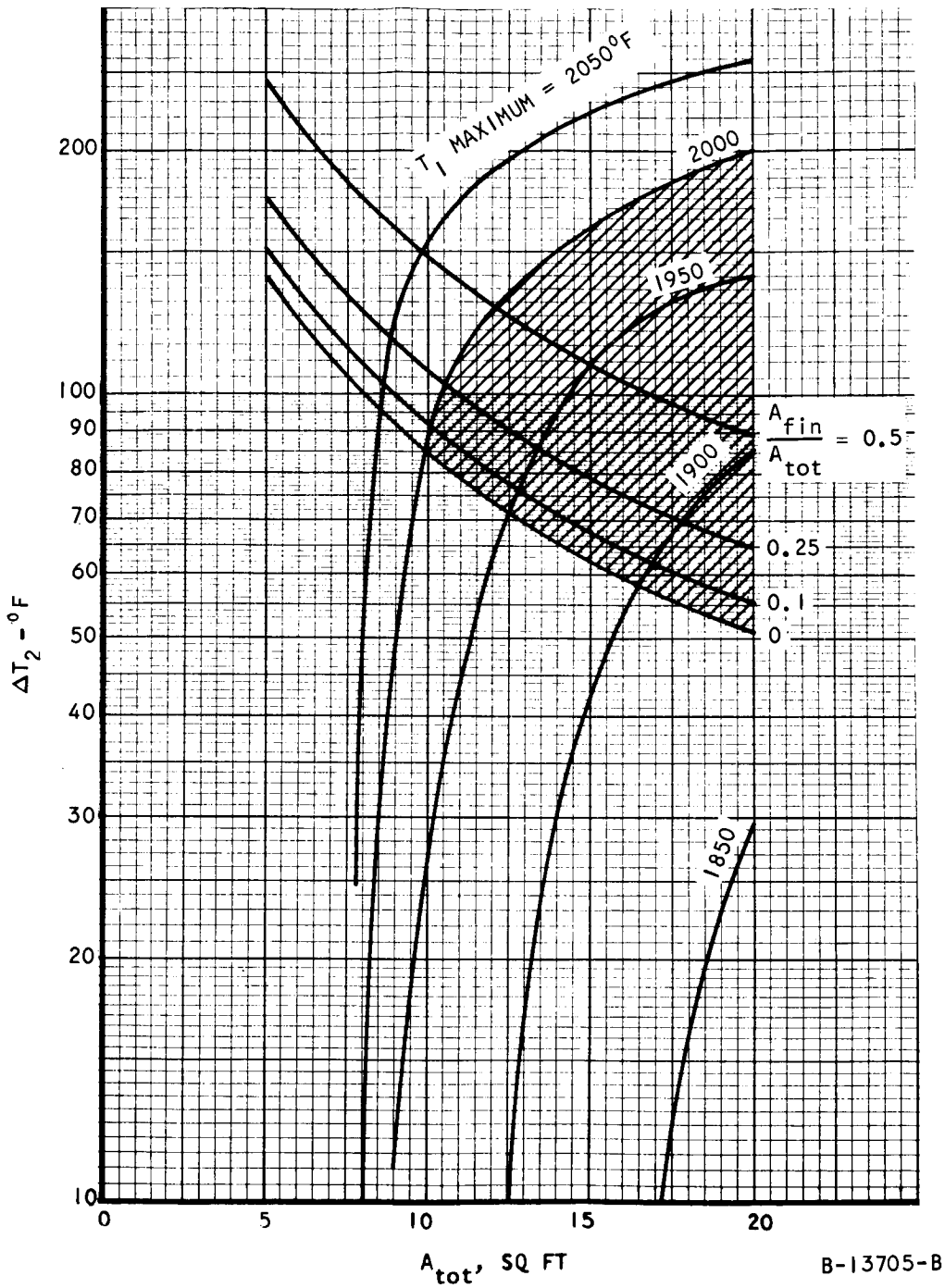

Figure 5.2–31. Parametric Data for Rectangular Tube-Fin Heat Exchanger, ΔT_{cond} = 100°F, Aspect Ratio = 2.065

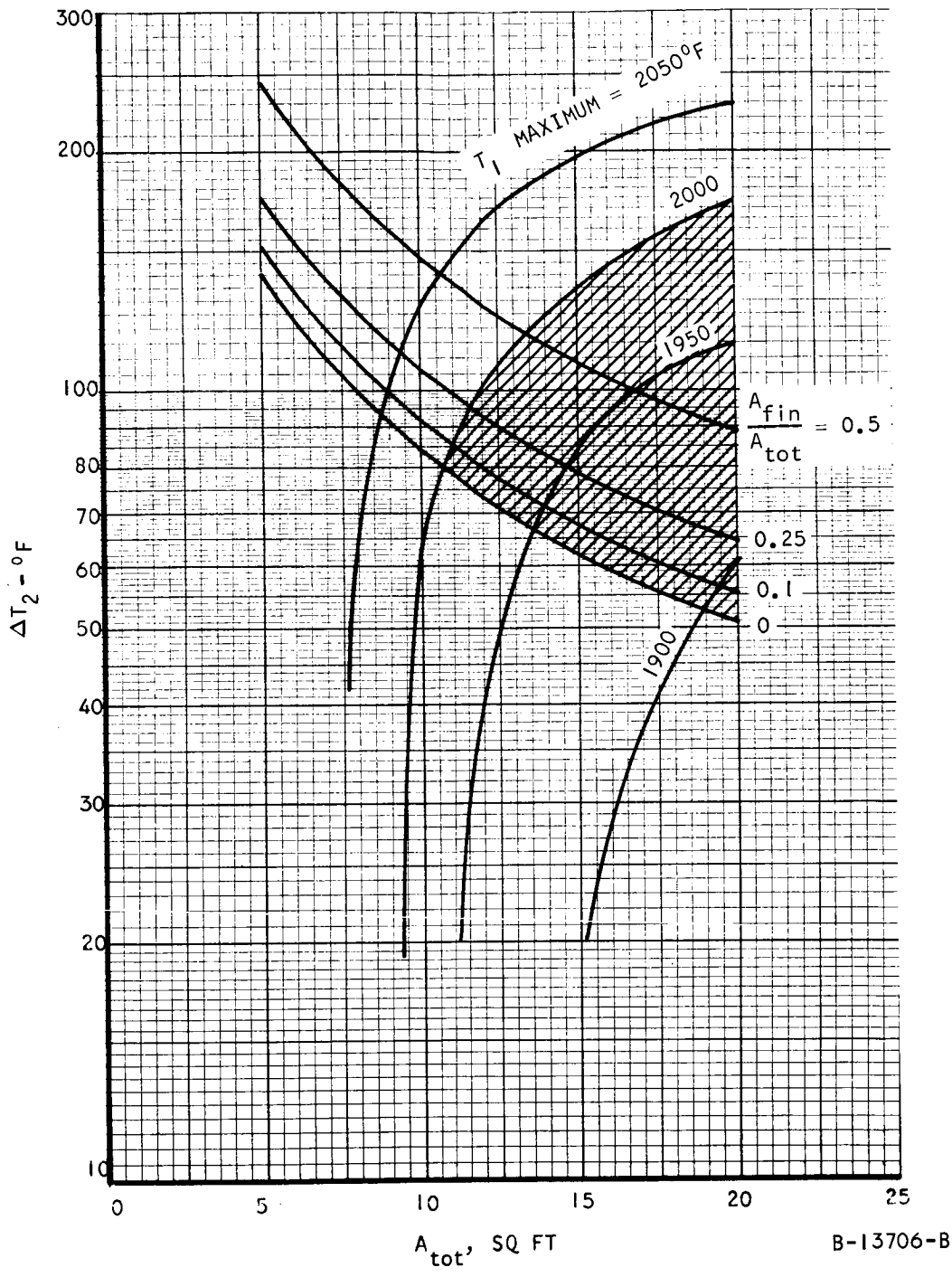

Figure 5.2–32. Parametric Data for Rectangular Tube- Fin Heat Exchanger, ΔT_{cond} = 125°F, Aspect Ratio = 2.065

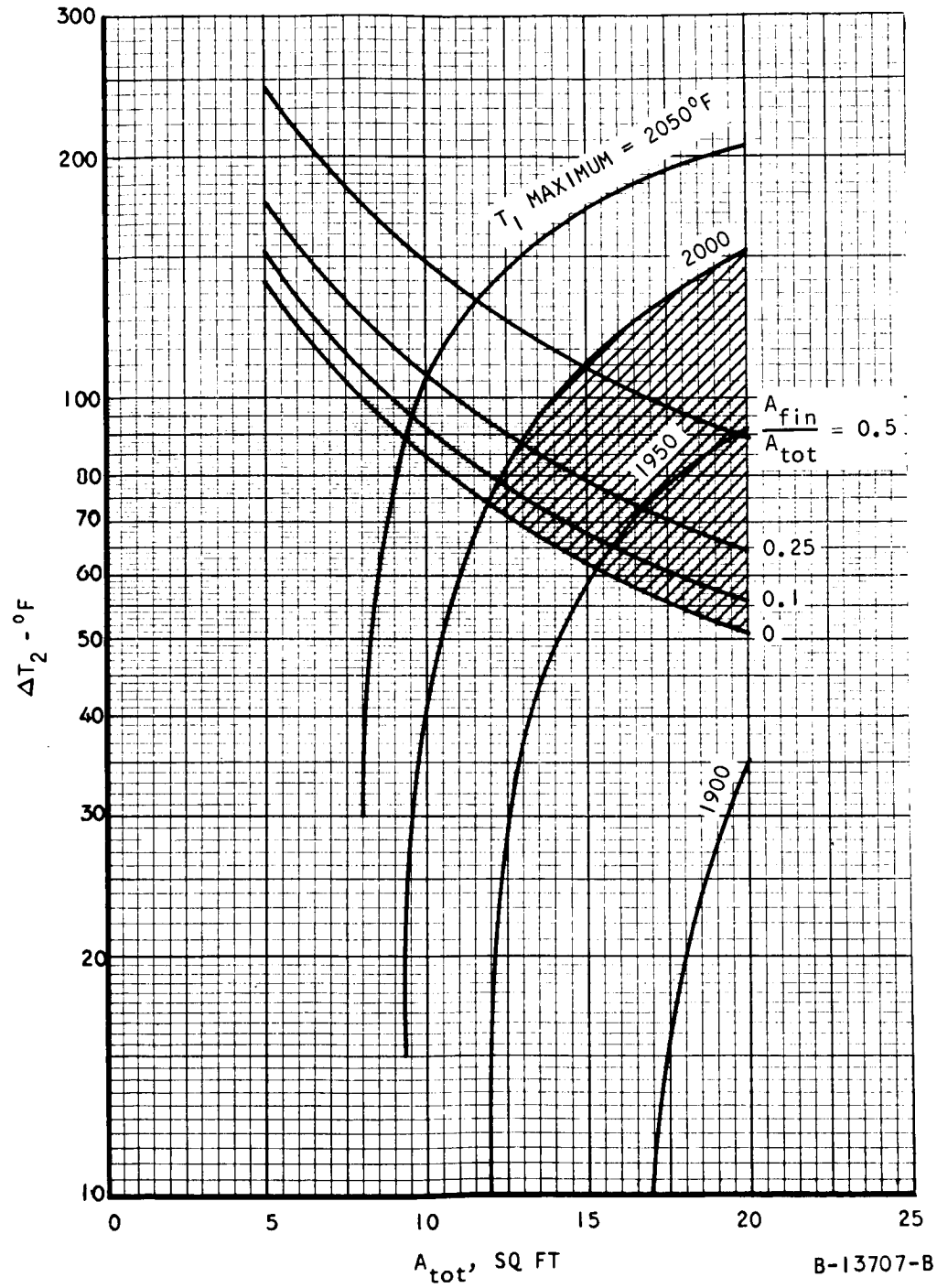

Figure 5.2–33. Parametric Data for Rectangular Tube-Fin Heat Exchanger, ΔT_{cond} = 150°F, Aspect Radio = 2.065

5.2.4.1 Effect of Flow Direction

Figure 5.2-34 shows the effect of the flow direction in the heat exchanger on the temperature distribution over the heat sources for a planar array. The solid lines are for the case when the gas flows in at the center and flows out at the outer circumference. The wall temperature of the HSHX is assumed to have the profile shown. Figure 5.2-34 reveals that if the flow enters at the outer circumference of the heat exchanger and exits at the center (dotted lines), a better temperature distribution and a lower maximum temperature in the heat source can be achieved. The possible changes in the assumed temperature rise in the heat exchanger should not affect the general conclusion indicated by this figure.

5.2.4.2 Comparison Between Single and Two-pass HSHX

Another approach to reducing source temperature levels and gradients is to go to a two-pass HSHX. In the two-pass heat exchanger, the flow is folded back on itself in a U-flow geometry; thus the flow enters and exits from the same side of the heat exchanger.

The configuration selected for this comparison, for both the heat source and the HSHX, is a 31- by 64-inch rectangular configuration. In the single-pass concept (Figure 5.2-35), the heat exchanger is made of parallel tubes connected by rectangular fins. The fluid flows once through the HSHX, and therefore the inlet and outlet manifolds are on opposite sides of the heat exchanger. In the two-pass concept (Figure 5.2-36), the tubes have a U shape, and they are also connected by rectangular fins. In this case, both the inlet and the outlet manifolds are on the same side of the HSHX.

An analysis was conducted to compare these two concepts. The analysis accounted for the conduction between the two legs of the U-tube and for the hot portions of the tube "seeing" the cold portions in the two-pass HSHX. The resulting profiles for the fluid temperature, the wall temperature, and the effective source temperature for the single-pass and two-pass systems are shown in Figures 5.2-35 and 5.2-36.

The design of the HSHX's is based on an effective source temperature which is defined as

$$T_{EFF} = \left[\frac{1}{AC} \int_{AC} T_S^4 \, dAC \right]^{1/4}$$

where

T_{EFF} = effective source temperature

AC = source surface area

T_S = point source surface temperature

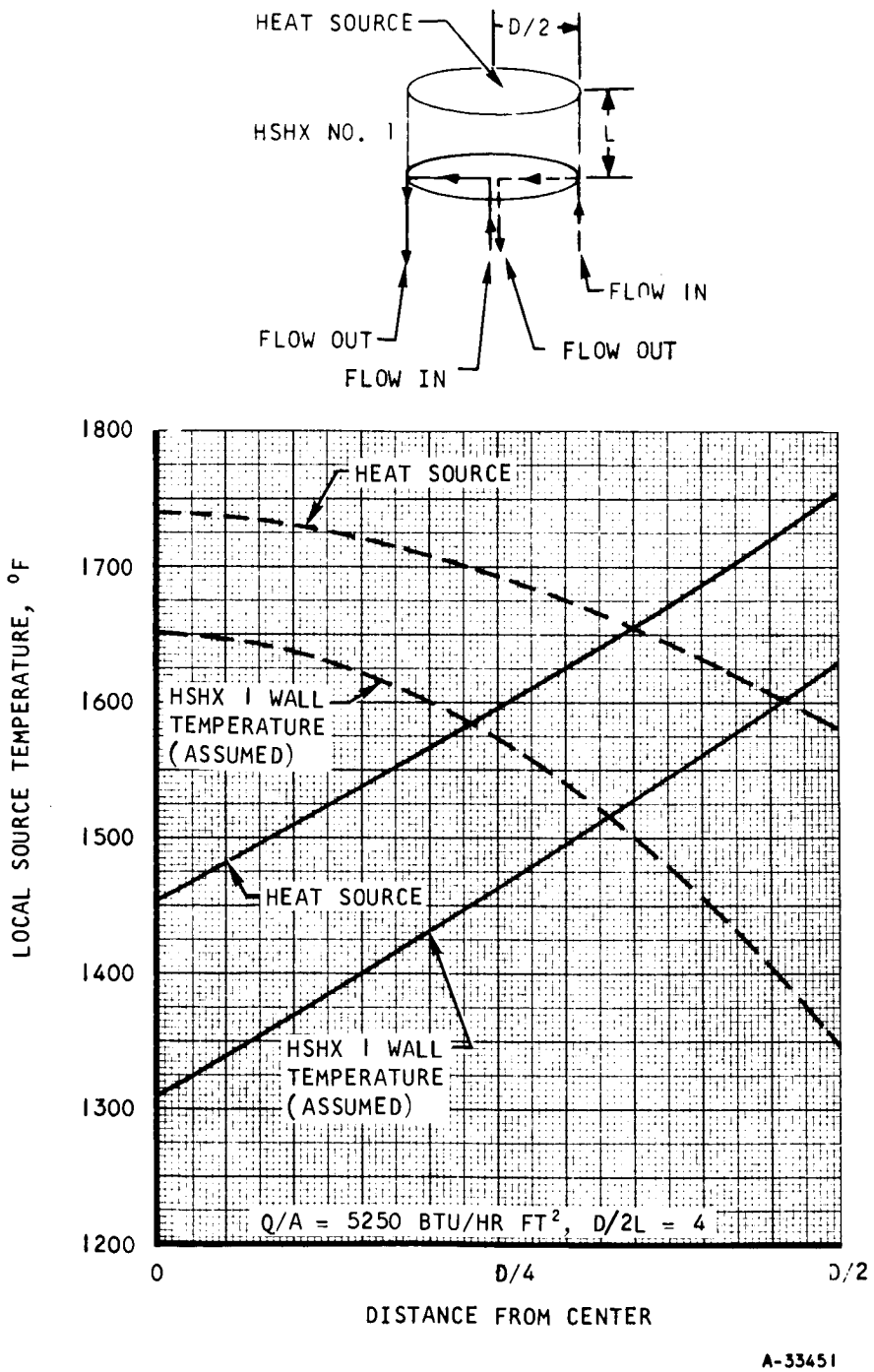

Figure 5.2–34. Effect of Flow Direction on Heat-Source Temperature Distribution

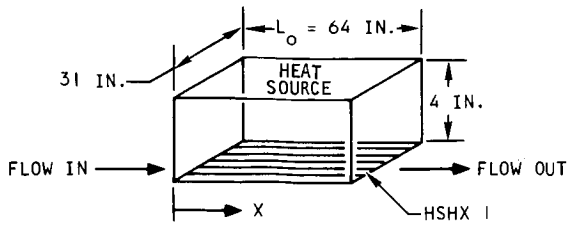

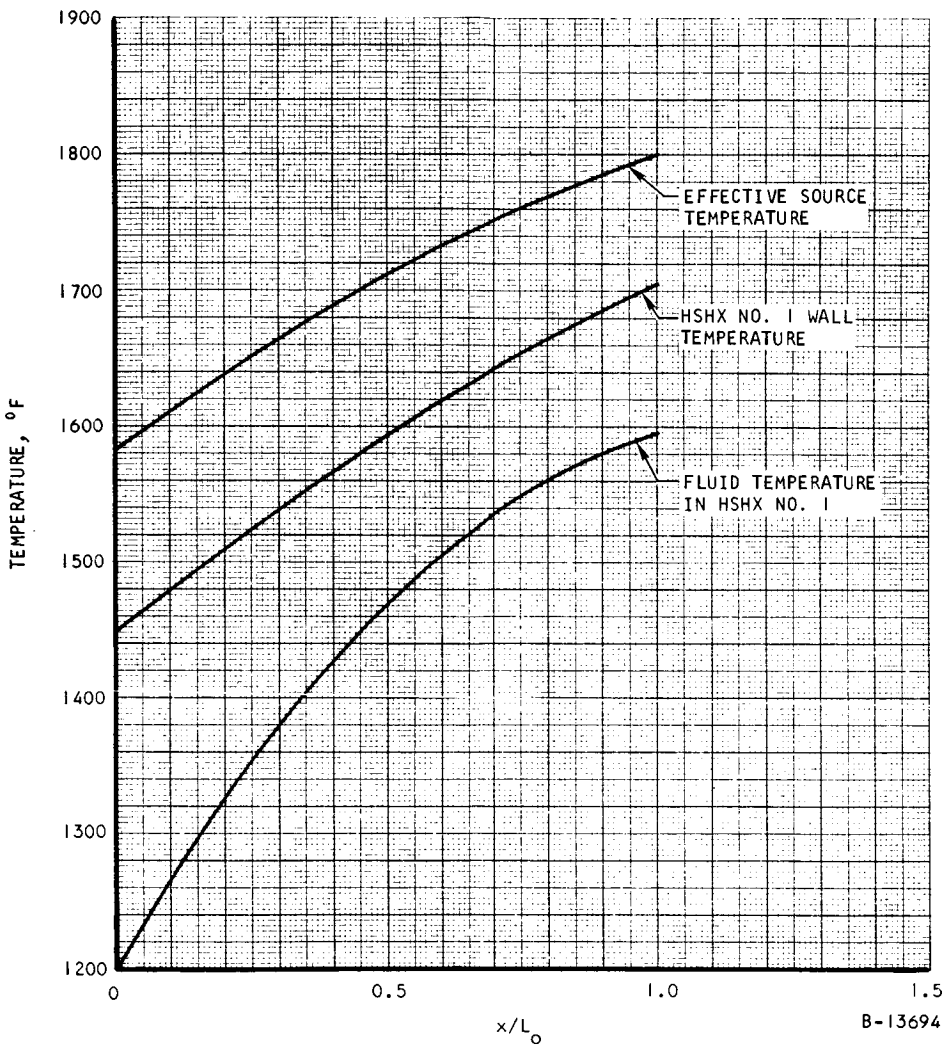

Figure 5.2-35. Approximate Temperature Distribution in 1-Pass Heat Source Heat Exchanger

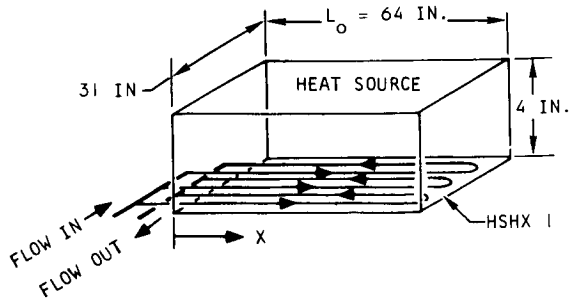

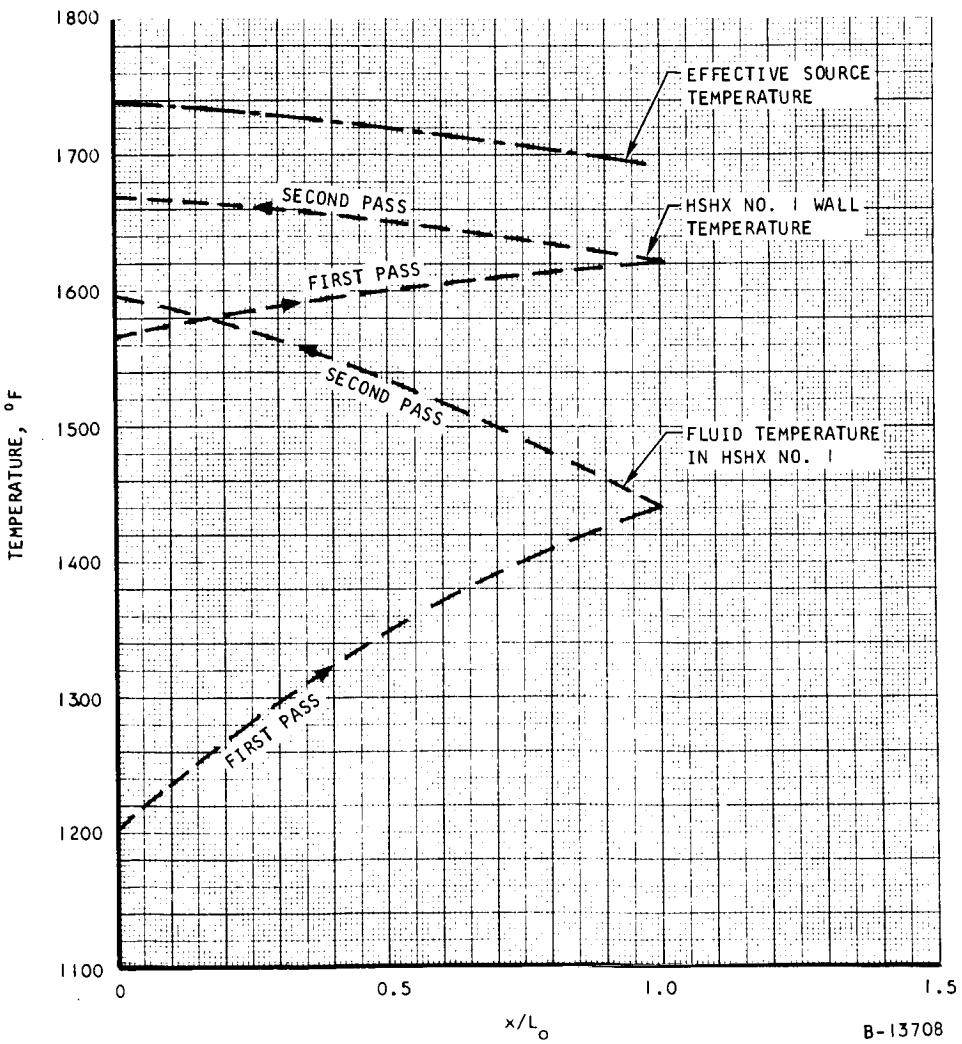

Figure 5.2–36. Approximate Temperature Distribution in 2-Pass Heat Source Heat Exchanger

The effective source temperature was taken to be equal to the minimum temperature existing on the capsule cover plate.

The effective source temperature of the two systems is compared in Figure 5.2-37, which clearly shows that the two-pass system results in a more uniform effective source temperature, as well as a lower maximum heat source temperature. The analysis used in obtaining this data is outlined in Appendix C of this report.

The analysis depicted in Figures 5.2-35 through 5.2-37 only considered a single HSHX adjacent to the heat source. The performance comparison of the single-pass and two-pass heat exchangers with both heat exchangers in place and with HSHX 2 in operation is presented in Figure 5.2-38. In this figure, the HSHX surface area is shown as a function of the effective source temperature for both the single-pass and two-pass systems. This figure reveals that, at a maximum effective source temperature of 1960° F, the surface area of the two-pass HSHX is about 25 percent less than that of the one-pass HSHX. Or if the area is fixed, the two-pass HSHX can provide the same performance on the gas side, with the heat source operating at 50° to 75° F lower temperatures than the single-pass HSHX.

5.2.4.3 Relaxation of the Full-Power Requirement on HSHX 2 with HSHX 1 Inoperative

The studies conducted thus far had adhered to the ground rule requiring that full output power be required from PCS No. 1 or No. 2; thus, the HSHX design point was the design of HSHX 2 for 1600° F gas outlet temperature and a maximum source temperature of 2000° F when HSHX 1 is inoperative. However, it should be remembered that in normal operation (i.e., with HSHX 1 in operation) the heat source temperatures are considerably below the 2000° F maximum temperature ($\approx$ 1850° F), and the 2000° F is reached only in a failure mode. A brief investigation was undertaken to reveal the effect of removing this ground rule on reducing source area and/or temperatures. Several possibilities are immediately apparent if HSHX 1 fails, such as: (1) leave HSHX 1 in place and operate HSHX 2 at reduced temperature, or (2) remove HSHX 1 prior to startup of HSHX 2.

These two situations are illustrated in Figure 5.2-39. If HSHX 1 is left in place (System 1) and the area of the heat source HSHX is reduced, the gas outlet temperature of HSHX 2 is reduced as shown. If the HSHX is reduced in size to the physical area (i.e., projected area) of the fuel capsules ($\approx$ 9.2 sq ft) the turbine inlet temperature falls from 1600° to about 1400° F.

For System 2, wherein HSHX 1 is removed upon failure, HSHX 2 can operate at design turbine inlet temperatures for all areas in excess of 8.5 sq ft. In this case the operating points for HSHX 1 and HSHX 2 are identical.

The data presented in Figure 5.2-39 was obtained from Figure 5.2-19 and the following equation.

$$T_{W_{11}} = T_1^4 - \frac{(2 - \epsilon)\, Q^{1/4}}{\epsilon \sigma A_{HX}} \qquad (5\text{-}2)$$

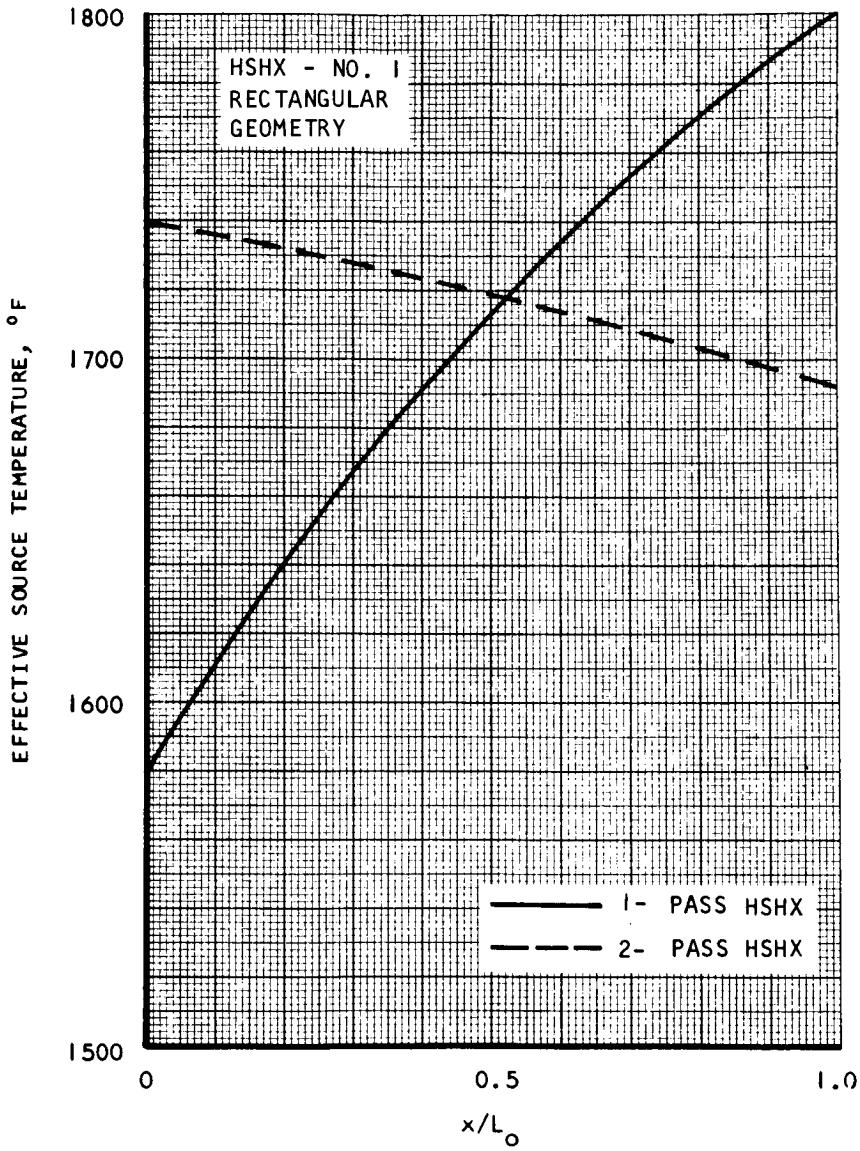

A-32611-A

Figure 5.2-37. Comparison Between the Effective Source Temperature of 1-Pass and 2-Pass HSHX

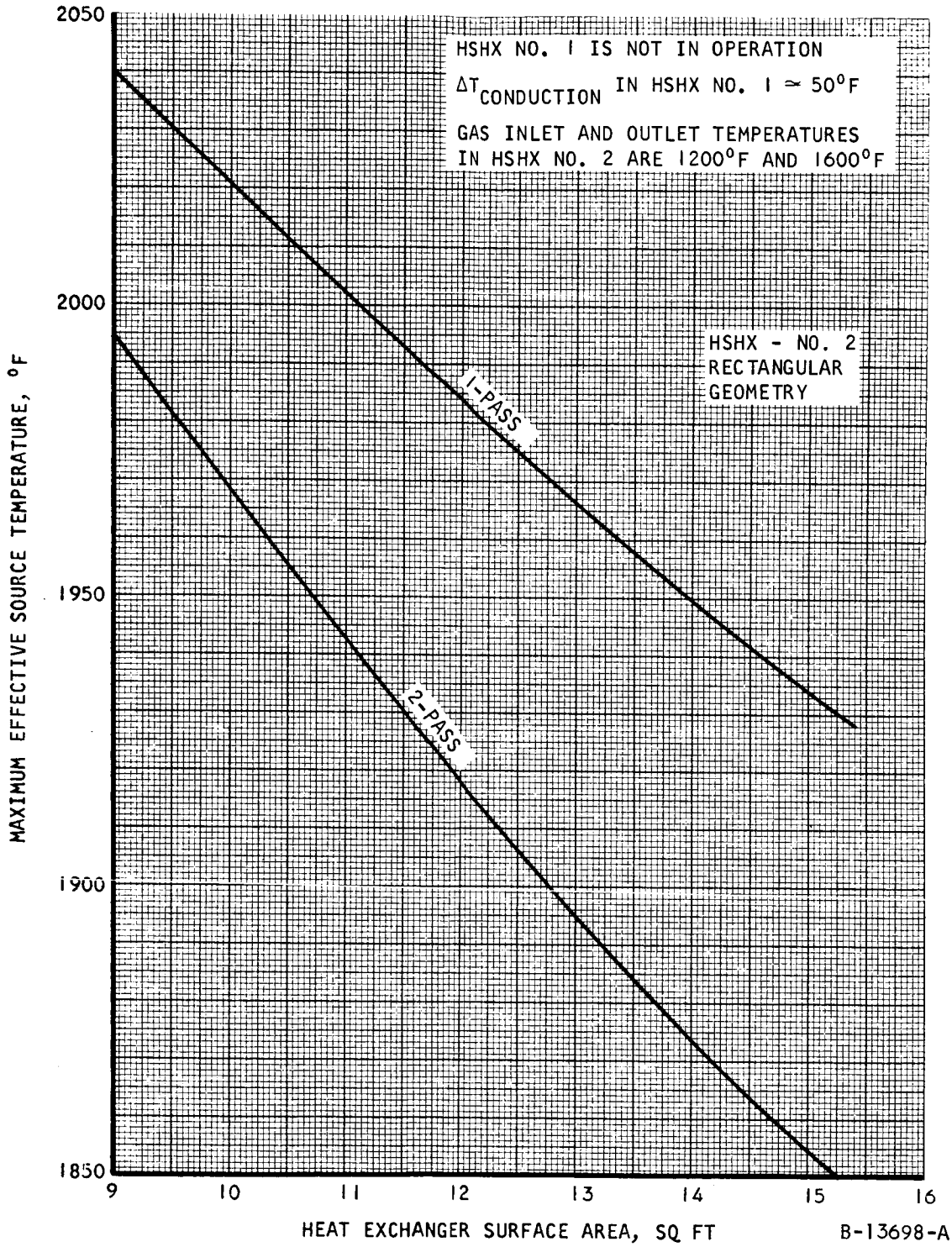

Figure 5.2–38. Comparison Between 1-Pass and 2-Pass Heat Source Heat Exchangers

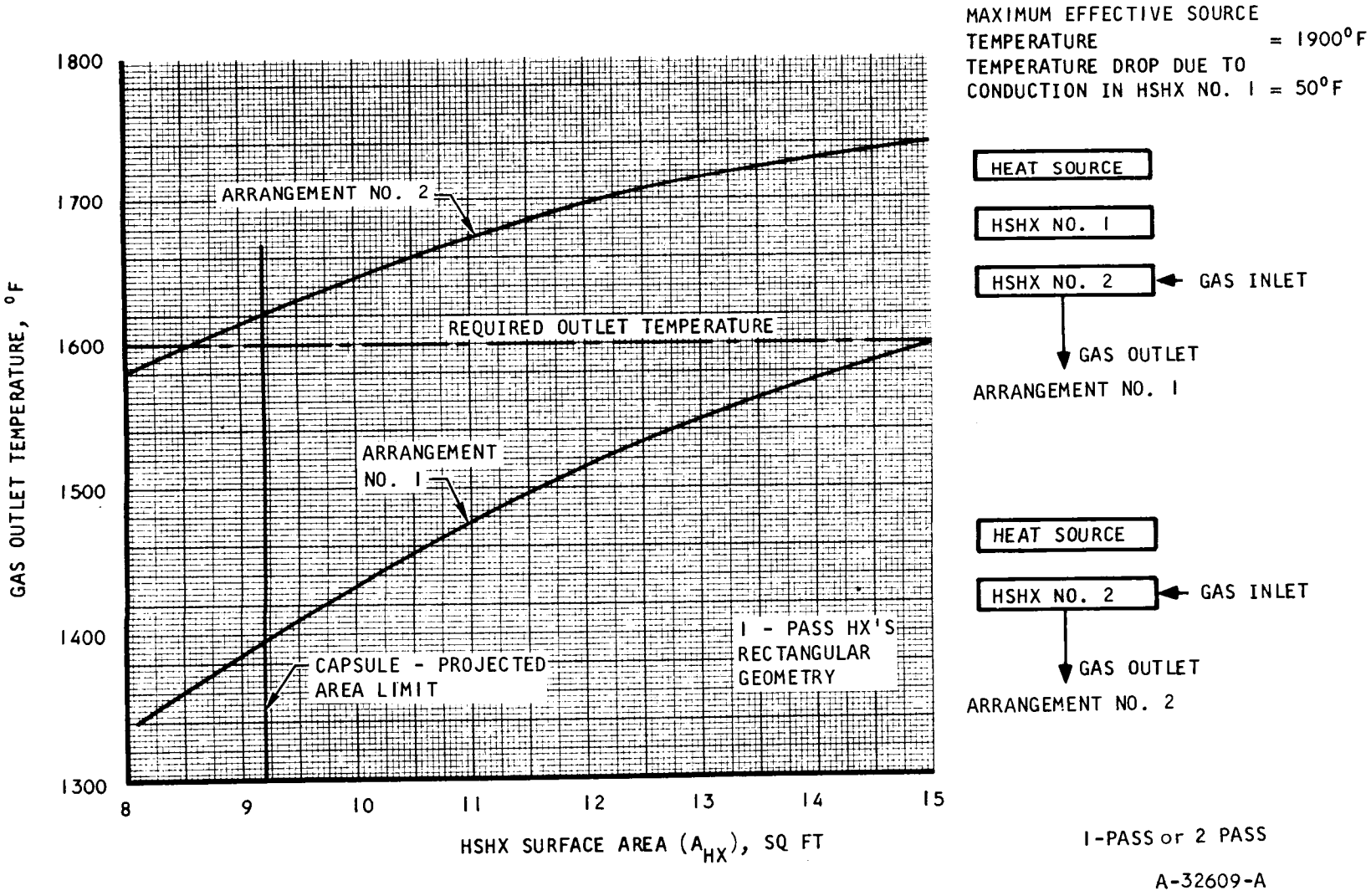

Figure 5.2-39. Relaxation of Full Power Requirements on Both Units

The heat exchangers were assumed to be of the single-pass, involute design, consisting entirely of tubes, i.e., no fins. The conduction temperature drop through HSHX 1 (ΔT_1) is taken as 50° F, and the effective source temperature is assumed to be equal to 1900° F (allowing a 100° F ΔT around the fuel capsule).

It is clear from Figure 5.2-39 that allowing HSHX 1 to be removed when it fails results in a potential of lowering the source area required by about 40 percent. This same area reduction can be obtained if a 200-deg drop in turbine inlet temperature is an acceptable condition when HSHX 1 fails. Figure 5.2-40 illustrates the effect of turbine inlet temperature variation on system performance for a typical Brayton system. A reduction of the turbine inlet temperature from 1600° to 1400° F results in a reduction of electrical power output of about 27 percent (from 6.85 to 4.0 Kwe) as indicated in Figure 5.2-40. This reduction might be acceptable until HSHX 1 could be removed and/or replaced and placed in operation. In any event, this approach offers a potential for reducing source temperatures at some penalty of operational capability.

5.2.5 Specific Heat Source Heat Exchanger Design Study

At this juncture of the study, five isotope heat source configurations were identified as meriting further detailed analysis. These heat source configurations were

	Source Geometry
Circular	53-in. dia
Rectangular	63 by 34 in.
Conical	53-in. dia
Doughnut	62-in. dia
Pincushion	48 by 40 in.

The heat source heat exchangers were required to exhibit in-place redundancy and replaceability and full power output from PCS No. 2 with PCS No. 1 in place. The latter objective had to be met within the 2000° F temperature limitation imposed on the fuel capsules, and therefore represented the HSHX design point.

The effort to this point of the study had concentrated solely on the tube fin type HSHX, primarily because a small amount of previous work had indicated a superior performance for this type of heat exchanger. However, a plate-fin type heat exchanger in many cases presents a very attractive design approach. It was decided, therefore, that a parallel design effort would be taken to the designs of the heat source heat exchangers for the above listed heat sources, one directed toward the tube-fin approach and the other involving the plate-fin approach. By contrasting the resulting two design approaches, a decision could be reached as to the relative merits of the two.

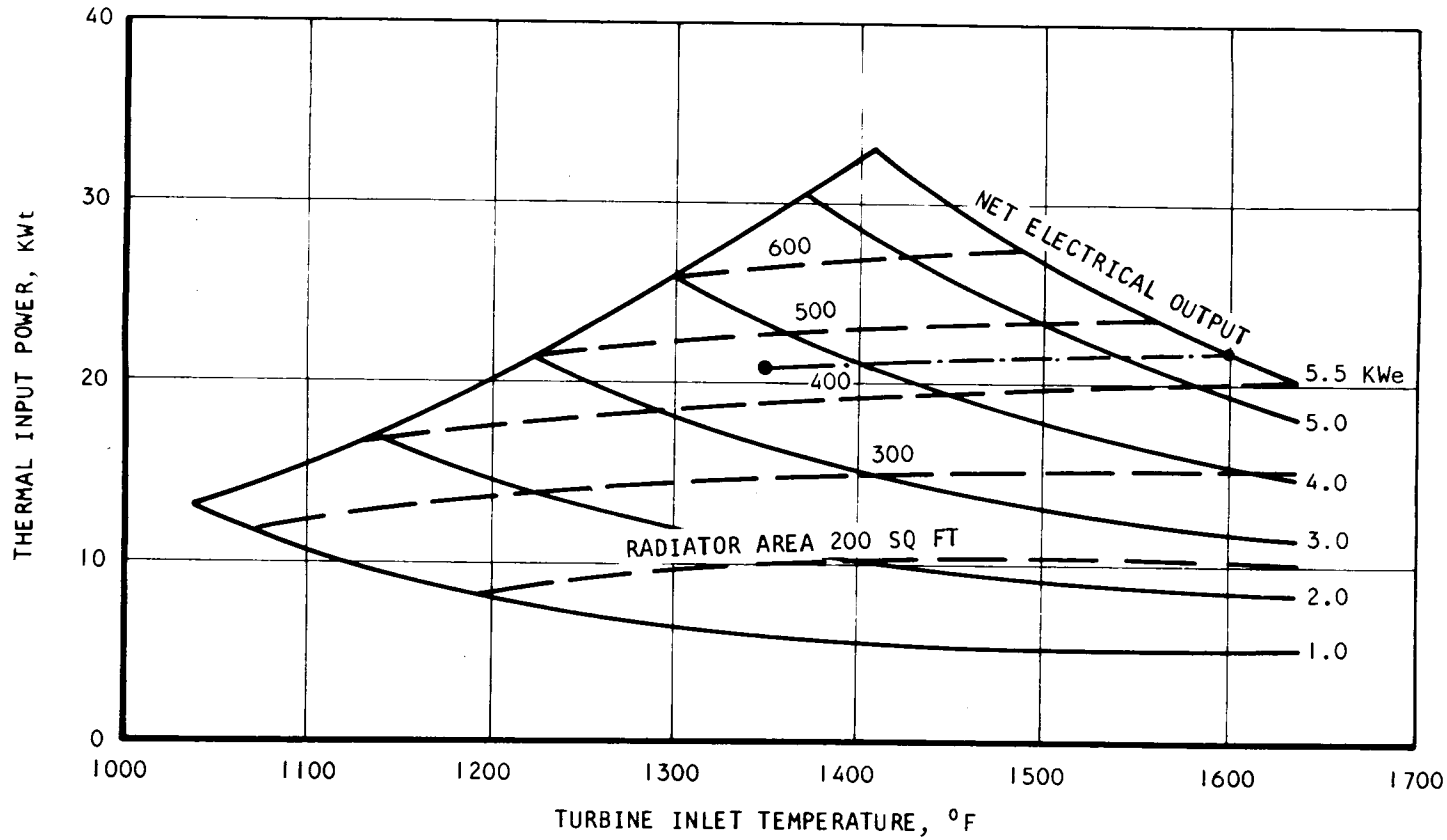

Figure 5.2-40. Effect ot Turbine Inlet Temperature on Brayton System Performance (Typical)

To design the heat exchangers it was necessary to determine the distributions of the wall temperature and heat flux for each combination of heat source array and heat exchanger flow configuration. The boundary conditions of the radiation calculations were the maximum allowable effective radiation temperature in the hottest region of the heat source array, the dimension that defined the heat source/heat exchanger system, and the 1600° F outlet temperature for the fluid in HSHX 2.

On this basis, HSHX designs were obtained that met the Brayton fluid pressure drop and fuel capsule maximum temperature limits. In addition, attention was given to sizing the manifolds so that the flow maldistribution can be maintained below 5 percent. The types of heat source heat exchangers developed for the five specific heat sources were as follows:

a. System 1: Circular planar, 60-deg cone, without recovery aids

   System 1A Single-pass, involute, tube-fin

   System 1B Two-pass, involute, tube-fin

   System 1C Single-pass, radial, plate-fin

   System 1D Two-pass, radial, plate-fin

b. System 2: Rectangular planar, 60-deg cone, with recovery aids

   System 2A Single-pass, tube-fin

   System 2B Two-pass, tube-fin

   System 2C Single-pass, plate-fin

   System 2D Two-pass, plate-fin

c. System 3: Conical, 60-deg cone, without recovery aids

   The various HSHX designs are the same as in the circular-planar array, i.e., System 1.

d. System 4: Conical, 60-deg cone, with central deorbit rocket and recovery aids

   System 4 Two-pass, spiral, tube-fin

e. System 5: Pincushion array, 60-deg cone, without recovery aids

   System 5 Two-pass, tube-fin

The physical description of each of the above heat exchangers is given in the following paragraphs. Pertinent design data is included with sketches of each design.

5.2.5.1 System 1: Circular Planar

System definition:

a. Circular planar, 60-deg cone

b. 53-in.-dia source

The main assumptions used in developing the heat source heat exchangers are as follows:

a. The separation distance between the heat source, HSHX 1, and HSHX 2 is equal to 5 in.

b. Conduction temperature drop in HSHX 1 = 50° F.

c. Surface emissivity = 0.85.

d. Maximum source temperature = 2000° F with HSHX 2 in operation at full power.

5.2.5.1.1 System 1A: Single-Pass, Involute, Tube-Fin -- Profiles of the fluid temperature, the average wall temperature of HSHX 2, and the effective source temperature are shown in Figure 5.2-41. The effective radiating wall temperature of HSHX 2 was taken as 30° F higher than the indicated wall temperatures. Figure 5.2-41 shows also the heat flux distribution over HSHX 2.

The values shown in Figure 5.2-41 were obtained using the approximate method outlined in Appendix C. The surfaces of the heat exchangers were divided in three annular sections of equal area. Since the tubes are spiraled, there is heat transfer by conduction and radiation between the tubes in each annular section. This effect, which tends to flatten the temperature distribution over both the HSHX and heat source, is accounted for approximately in the calculations.

A sketch of System 1A is shown in Figure 5.2-42. It is a circular, tube-fin configuration, with the Brayton fluid entering at the periphery and following an involute path towards the center, where it enters a header box and exits from the heat exchanger through an outlet duct on the under side. The basic drawback with this design is that the position of the outlet duct interferes with the radiant heat to the secondary HSHX.

5.2.5.1.2 System 1B: Two-Pass, Involute, Tube-Fin -- Figure 5.2-43 shows the distribution of the average wall temperature of HSHX 2 and the effective source temperature. The large heat flux shown in the first pass as compared to the heat flux in System 1A is mainly due to the additional heat transferred by conduction and radiation from the hot tube to the cold tube. This heat transfer between the two passes results in a more uniform temperature distribution over the heat source and heat exchangers and a lower maximum source temperature as compared to System 1A.

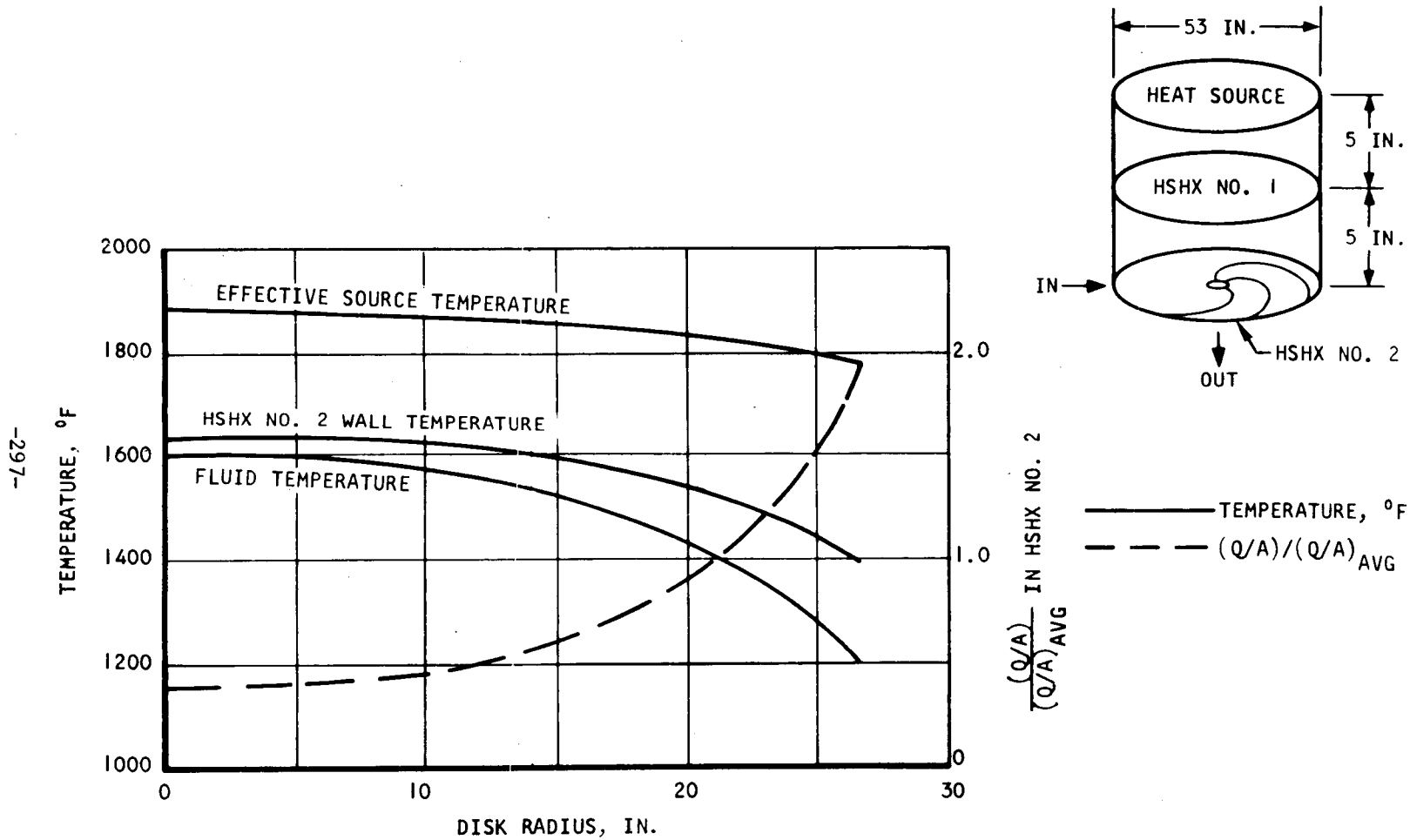

A-32973

Figure 5.2-41. Temperature Distributions, One-Pass, Involute HSHX

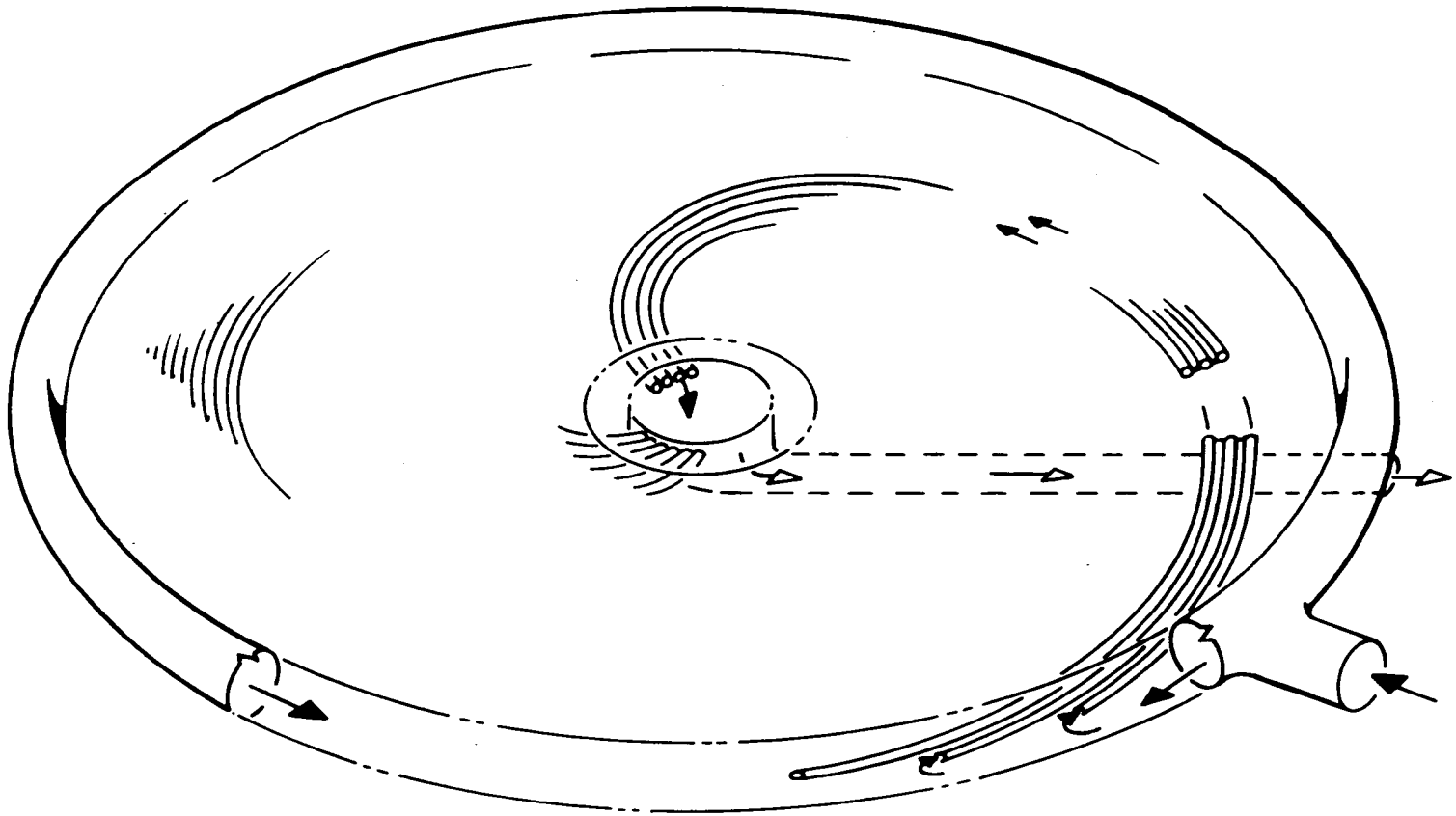

WEIGHT = 63 LB
NO. OF TUBES = 57
TUBE DIAM = 0.4675 IN.
TUBE LENGTH = 68 IN.

FIN THICKNESS = 0.040
A_f/A_t = 0.15
$\Delta P/P$ = 1.6 PERCENT

A-32974

Figure 5.2–42. Single-Pass, Involute, Tube-Fin HSHX

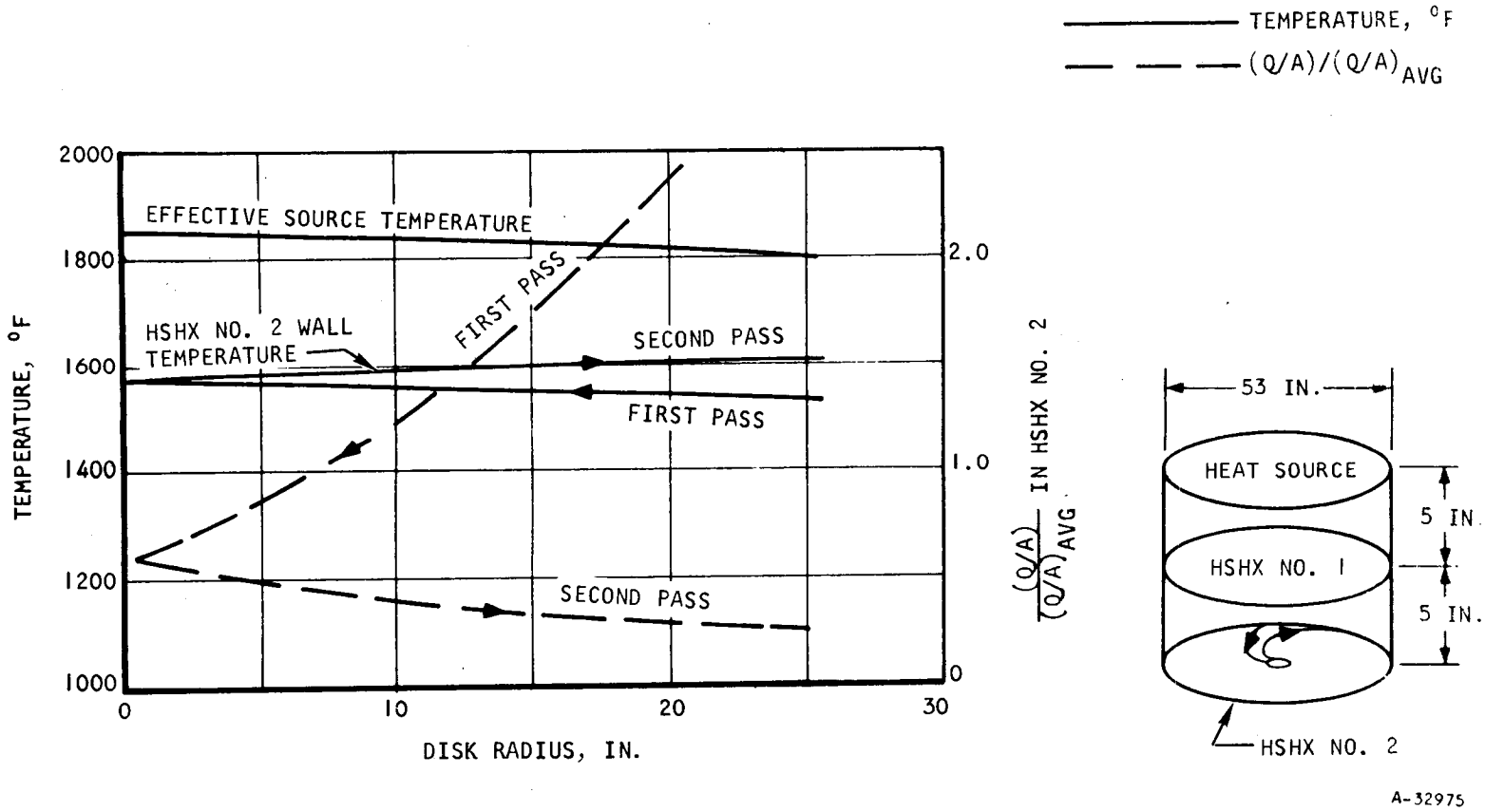

Figure 5.2–43. Temperature Distributions, Two-Pass, Involute HSHX

The two-pass HSHX design eliminates the exit duct problem that exists for System 1A. In the present design, the Brayton fluid both enters and exits at the periphery of the heat exchanger; Figure 5.2-44 is a sketch of this configuration. The fluid enters alternate tubes, follows an involute path to the center, where it enters a header box, and then reenters adjacent tubes and flows back out to the periphery of the heat exchanger. This flow configuration results in a more uniform temperature distribution over the surface of the heat source than the one-pass system (1A).

5.2.5.1.3 System 1C: Single-Pass, Radial, Plate-Fin -- A plot of the temperature and heat flux distribution for System 1C is shown in Figure 5.2-45. These values were obtained using the approximate method outlined in Appendix C. The variations of the wall temperature and the effective source temperature are more significant in this case than in System 1A. Moreover, the maximum effective source temperature is higher than that in System 1A. These differences between the two systems are due to the fact that the flow is radial in the present case, while it is spiral in System 1A.

Figure 5.2-46 is a sketch of a single-pass, radial-flow, plate-fin heat exchanger. The fluid enters at the periphery, flows radially inward, and leaves through an exit duct on the under side of the unit. As for System 1A, this outlet duct interferes with the radiant heat interchange during operation of the secondary Brayton cycle system.

5.2.5.1.4 System 1D: Two-Pass, Radial, Plate-Fin -- Figure 5.2-47 shows the variation of the Brayton fluid and average wall temperature in HSHX 2 as well as the variation of the effective source temperature. Figure 5.2-48 illustrates a two-pass, radial-flow, plate-fin heat exchanger for which the fluid enters and exits at the periphery of the unit. In addition to eliminating the ducting problem that is associated with the single-pass configuration, the two-pass design makes the temperature distribution more uniform over the surface of the heat source.

5.2.5.2 System 2: Rectangular Planar

System definition:

a. Rectangular-planar, 60-deg cone

b. 63- by 34-in. source array

The assumptions used in developing the heat source heat exchangers are as follows:

a. The separation distance between the heat source, HSHX 1 and HSHX 2 is equal to 5 in.

b. Conduction temperature drop in HSHX 1 = 50^{o} F.

c. Effective surface emissivity = 0.85.

d. Maximum source temperature = 2000^{o} F with HSHX 2 in operation at full power.

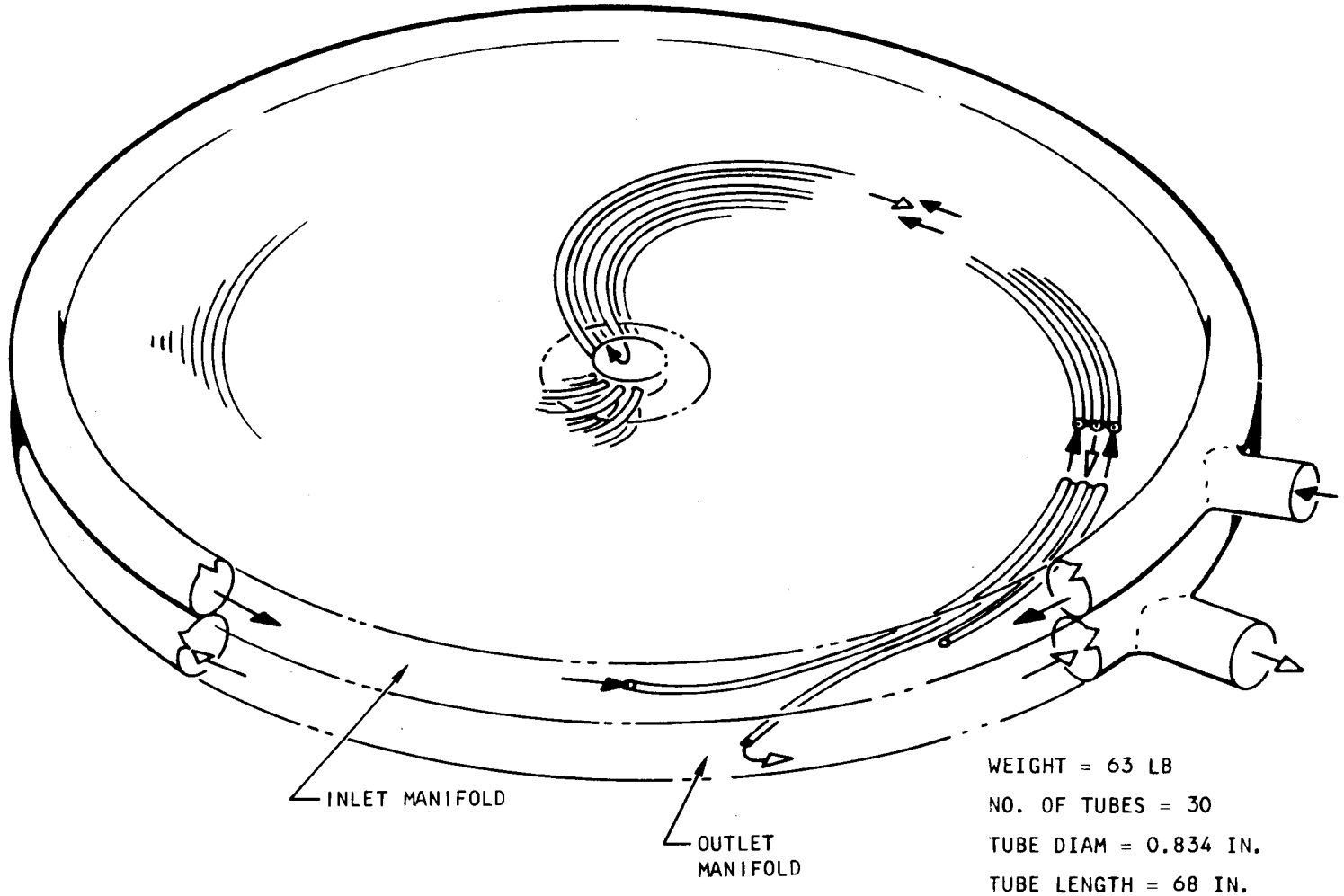

Figure 5.2–44. Two-Pass, Involute, Tube-Fin HSHX

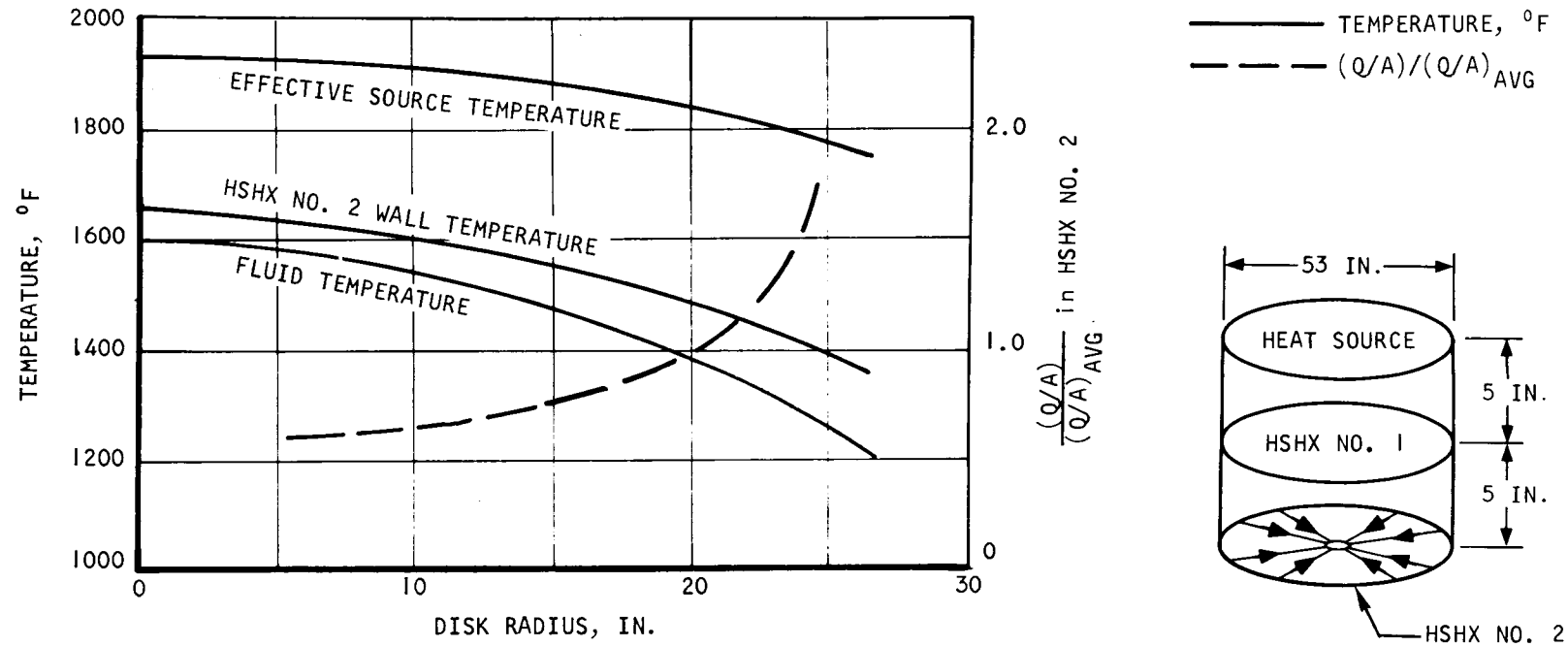

A-32977

Figure 5.2–45. Temperature Distributions, One-Pass, Radial HSHX

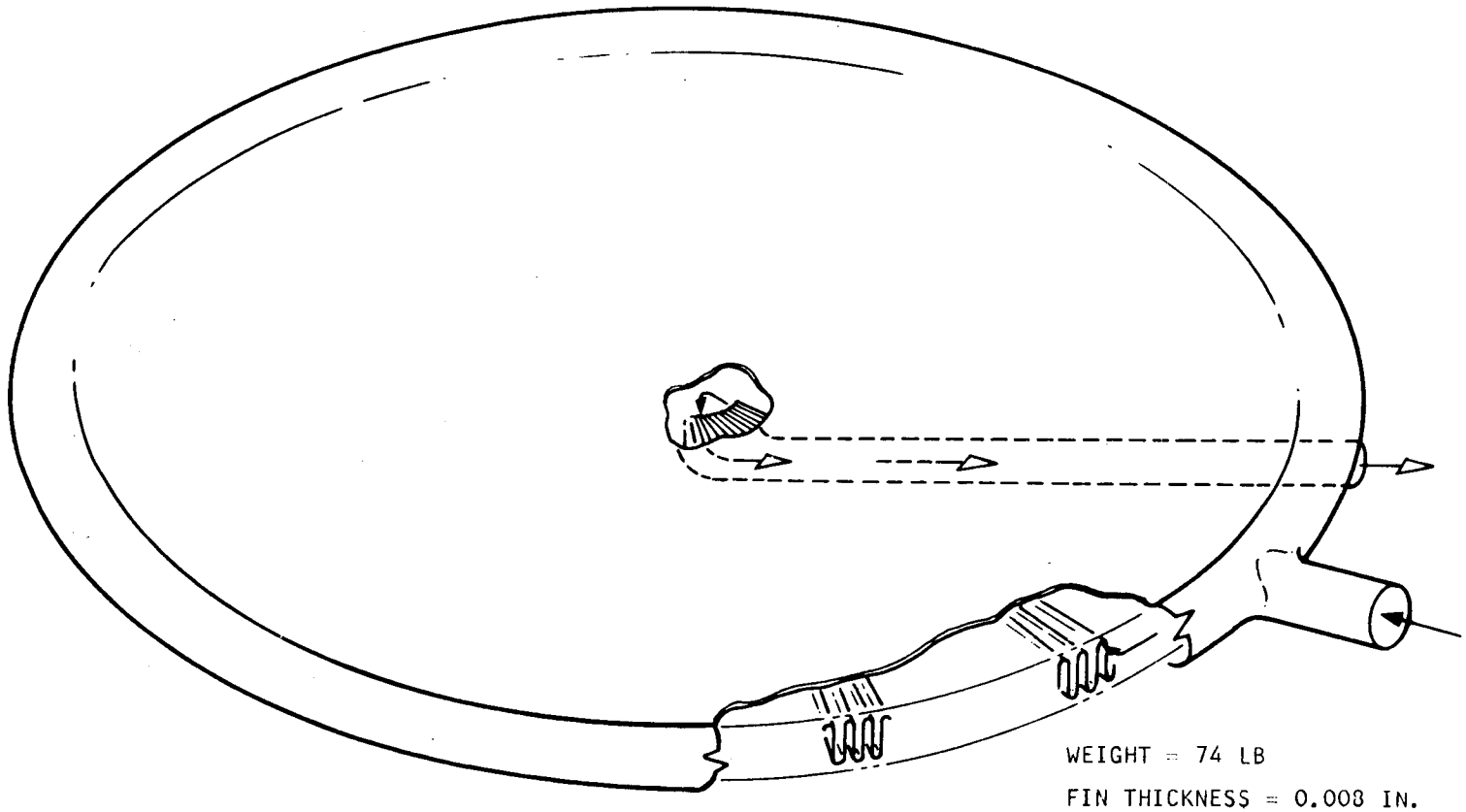

WEIGHT = 74 LB
FIN THICKNESS = 0.008 IN.
FIN HEIGHT = 0.40 IN.
FINS PER INCH = 14
$\Delta P/P$ = 1.6%

4-32978

Figure 5.2–46. One-Pass, Radial, Plate-Fin HSHX

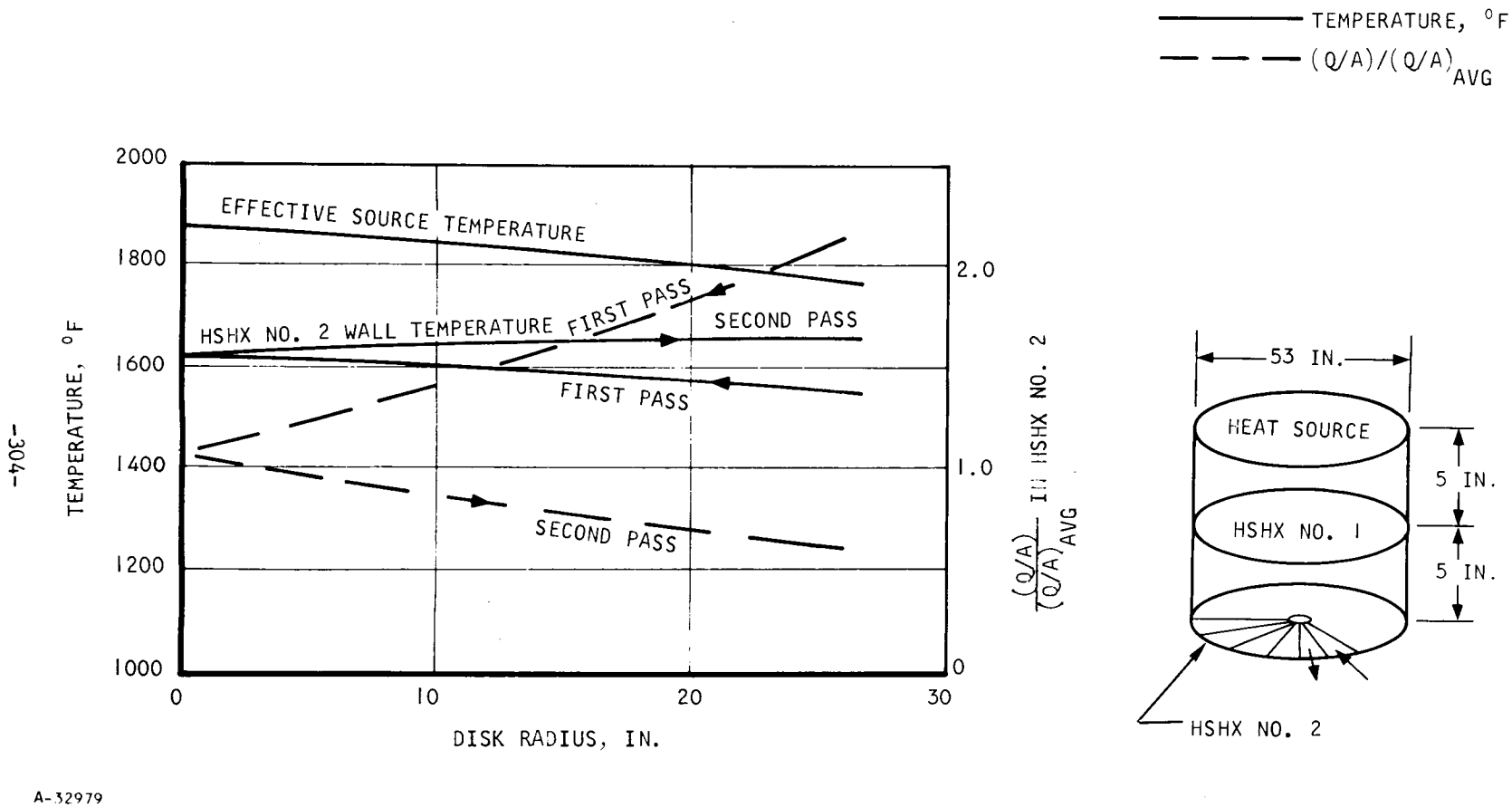

Figure 5.2–47. Temperature Distributions, Two-Pass, Radial HSHX

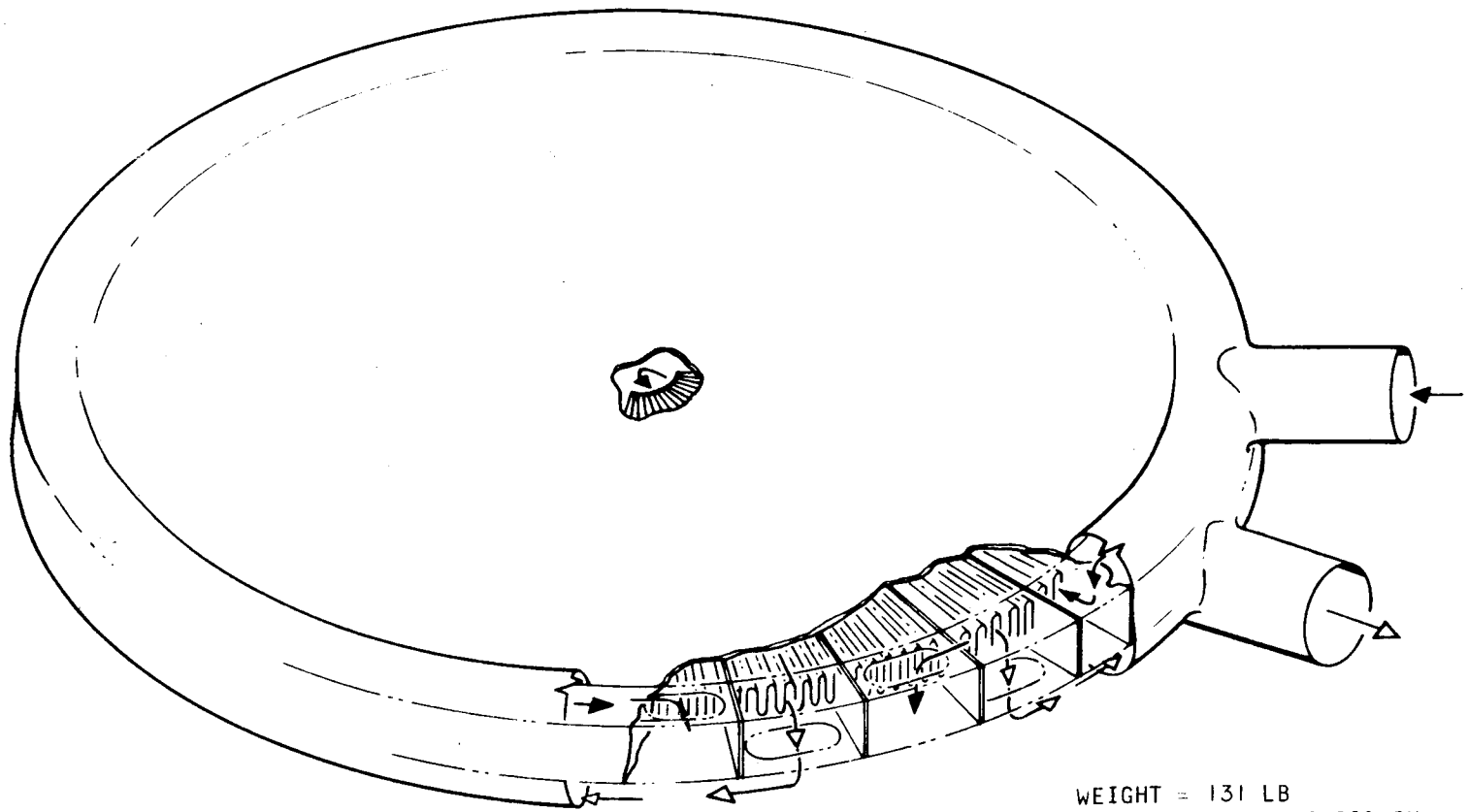

Figure 5.2–48. Two-Pass, Radial, Plate-Fin HSHX

5.2.5.2.1 System 2A: Single-Pass, Tube-Fin -- Figure 5.2-49 shows the HSHX 2 wall temperature, effective source temperature, and heat flux in HSHX 2 versus the dimensionless distance along the flow length. The values shown in this figure were obtained using the approximate method explained in Appendix C. The effective wall temperature of HSHX 2 was taken as 30° F higher than the indicated wall temperatures.

For this particular case, a comparison was made between the results of the approximate and exact methods for computing temperature distributions. (See Appendix C.) Figure C-2 shows this comparison for the effective source temperatures. The agreement between the two results is good and gives confidence in the results obtained by the approximate method.

A sketch of System 2A is shown in Figure 5.2-50. It is of tube-fin construction with Brayton fluid making one pass along the 34-in. dimension.

5.2.5.2.2 System 2B: Two-Pass, Tube-Fin -- In order to obtain a more uniform temperature distribution and a lower maximum temperature over the surface of the heat source, System 2B was designed. A plot of the temperature and heat flux is shown in Figure 5.2-51 and a sketch of the HSHX is shown in Figure 5.2-52. In contrast to System 2A, this is a two-pass configuration with the fluid entering alternate tubes, flowing in the 34-in. direction, entering a tubular header, turning, and then entering adjacent tubes where it flows back along the 34-in. dimension and exits on the same side as it enters.

5.2.5.2.3 System 2C: Single-Pass, Plate-Fin -- Figure 5.2-53 illustrates a single-pass plate-fin HSHX that is analogous to System 2A. The temperature and heat flux map is identical to that in Figure 5.2-49.

5.2.5.2.4 System 2D: Two-Pass, Plate-Fin -- Figure 5.2-54 illustrates a two-pass plate-fin HSHX that is analogous to System 2B. The temperature and heat flux distributions are approximately the same as for System 2A (see Figure 5.2-51).

5.2.5.3 System 3: Conical

System definition:

a. Conical, 60-deg cone

b. 53-in.-dia source

It was shown in Section 5.2.2 of this report that for the 53-in.-dia conical heat source, the radiation characteristics are essentially identical to those of the circular, planar heat source. Because of this, the HSHX designs obtained for the planar heat source array can also be utilized in conjunction with the conical array, obviating the need to design additional HSHX configurations. Hence, the four heat exchanger designs in this case are as follows:

a. System 3A Single-pass, involute, tube-fin

b. System 3B Two-pass, involute, tube-fin

c. System 3C Single-pass, radial, plate-fin

d. System 3D Two-pass, radial, plate-fin

For the description of the above heat exchanger refer to Figures 5.2-41 through 5.2-48.

The principal operation and design characteristics of the various circular and rectangular HSHX configurations are summarized in Table 5.2-III. Based on the comparisons made, the two-pass, tube-fin construction appears the most attractive for meeting the design requirements imposed on the IRV and Brayton cycle system. Therefore, no other type of heat exchanger construction was studied for the final two heat source arrays.

5.2.5.4 System 4: Doughnut Geometry

System definition:

a. Conical configuration, 60-deg cone

b. Source, 61.8-in. OD

29.8-in. ID

Figure 5.2-55 illustrates the HSHX that was designed for the doughnut heat source. The Brayton fluid enters alternate tubes at the periphery of the HSHX, and then follows an involute path towards the center. It enters a toroidal header, is turned, enters adjacent tubes, and then flows back to the periphery of the heat exchanger.

5.2.5.5 System 5: Rectangular Pincushion

System definition:

a. Rectangular, pyramidal

b. Source, 48- by 40-in. array

The HSHX design that was evolved for the rectangular pincushion heat source array is shown in Figure 5.2-56. For the design presented, each passage between the fuel capsule rows contains legs from both the primary and secondary Brayton cycle system; therefore, operation of either the primary or secondary system is equivalent from the standpoint of heat transfer and system temperature distribution. Each heat exchanger consists of nine legs, with a leg extending between each row of fuel capsules. Each leg consists of several tubes and connecting fin. The fluid enters alternate tubes on one end of the heat exchanger, flows along the 48-in. dimension, turns in a tubular header and then flows back in the adjacent tubes (see Figure 5.2-57).

5.2.5.6 Effect of HSHX Weight on Source Temperature

The HSHX designs that have been presented for the various heat source configurations are the minimum-weight solutions that meet the design requirements imposed on the system. The most significant of these requirements is the 2000° F maximum fuel capsule temperature. This temperature can be reduced somewhat at the expense of additional weight in the HSHX's.

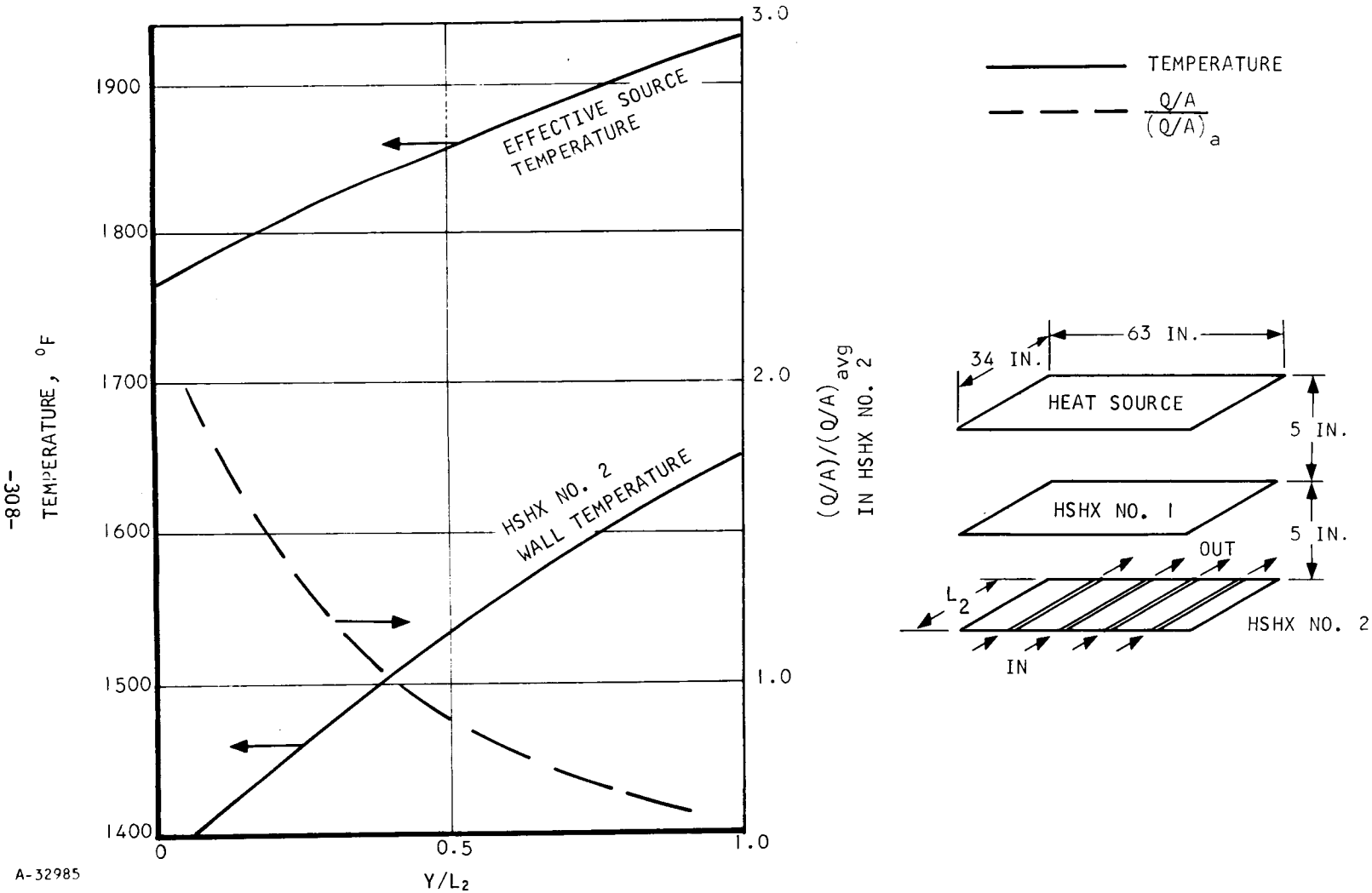

Figure 5.2–49. Temperature Distributions, One-Pass. Rectangular HSHX

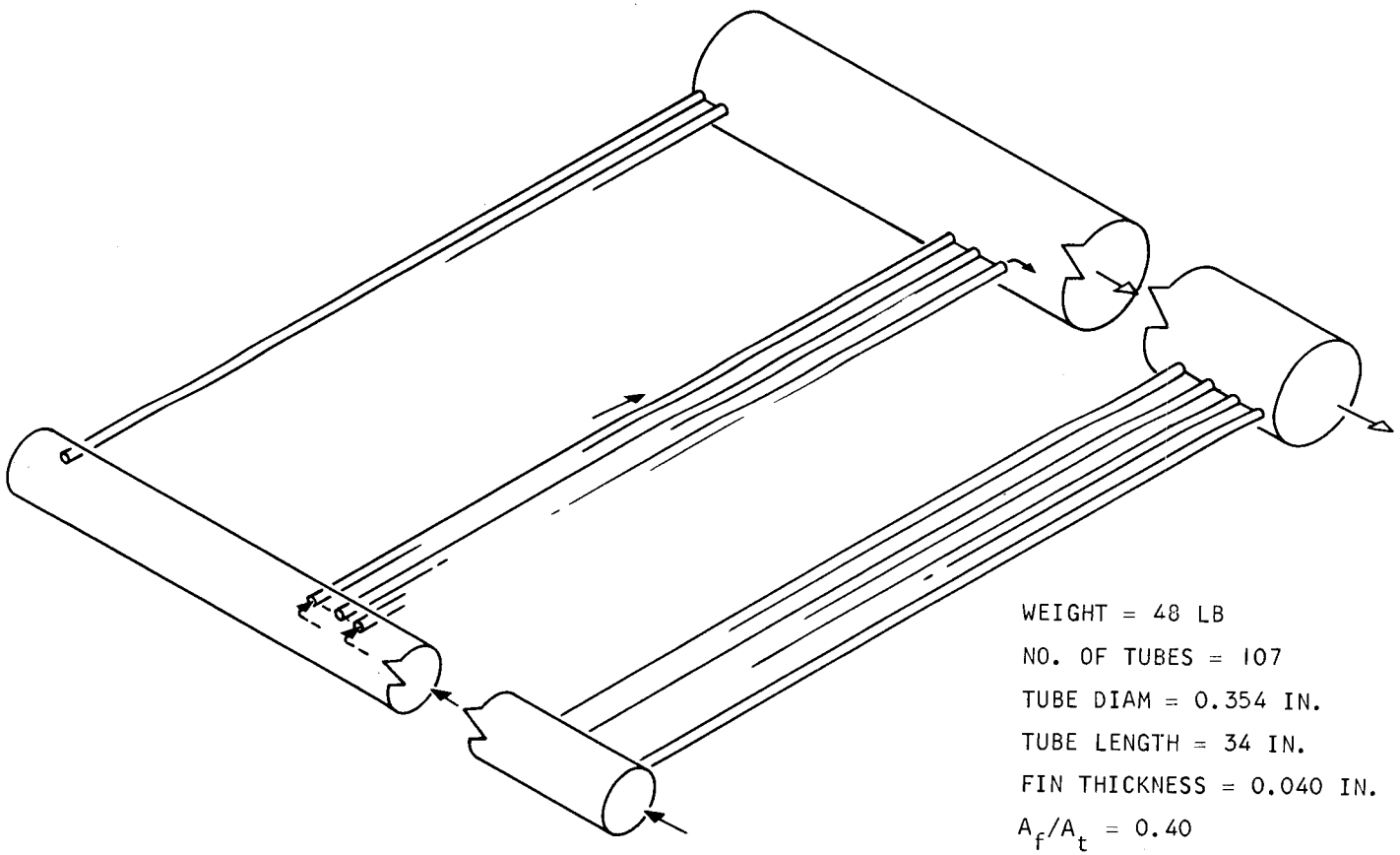

WEIGHT = 48 LB
NO. OF TUBES = 107
TUBE DIAM = 0.354 IN.
TUBE LENGTH = 34 IN.
FIN THICKNESS = 0.040 IN.
A_f/A_t = 0.40
$\Delta P/P$ = 1.6%

A-32986

Figure 5.2-50. Single-Pass, Rectangular, Tube-Fin HSHX

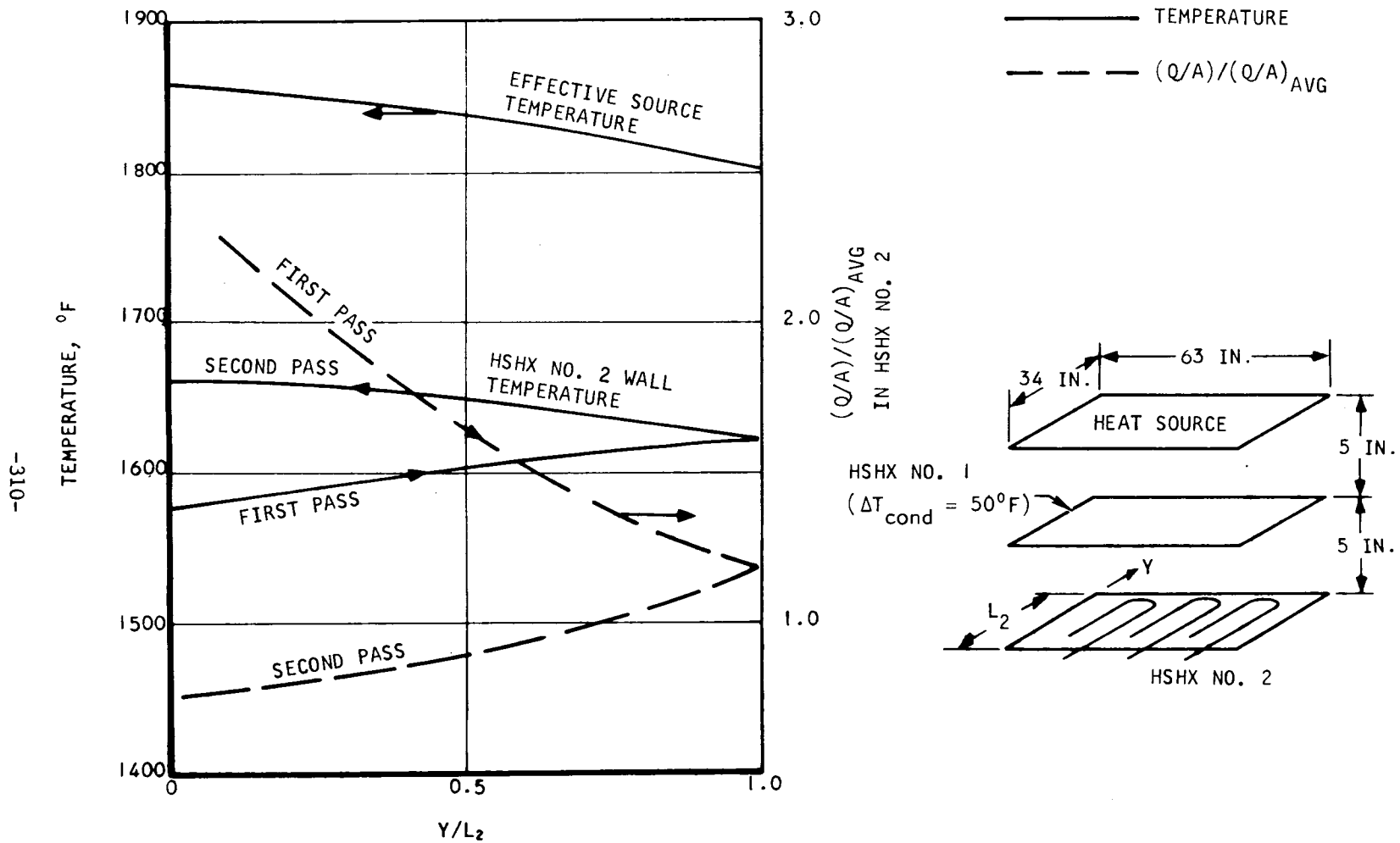

Figure 5.2–51. Temperature Distributions, Two-Pass, Rectangular HSHX

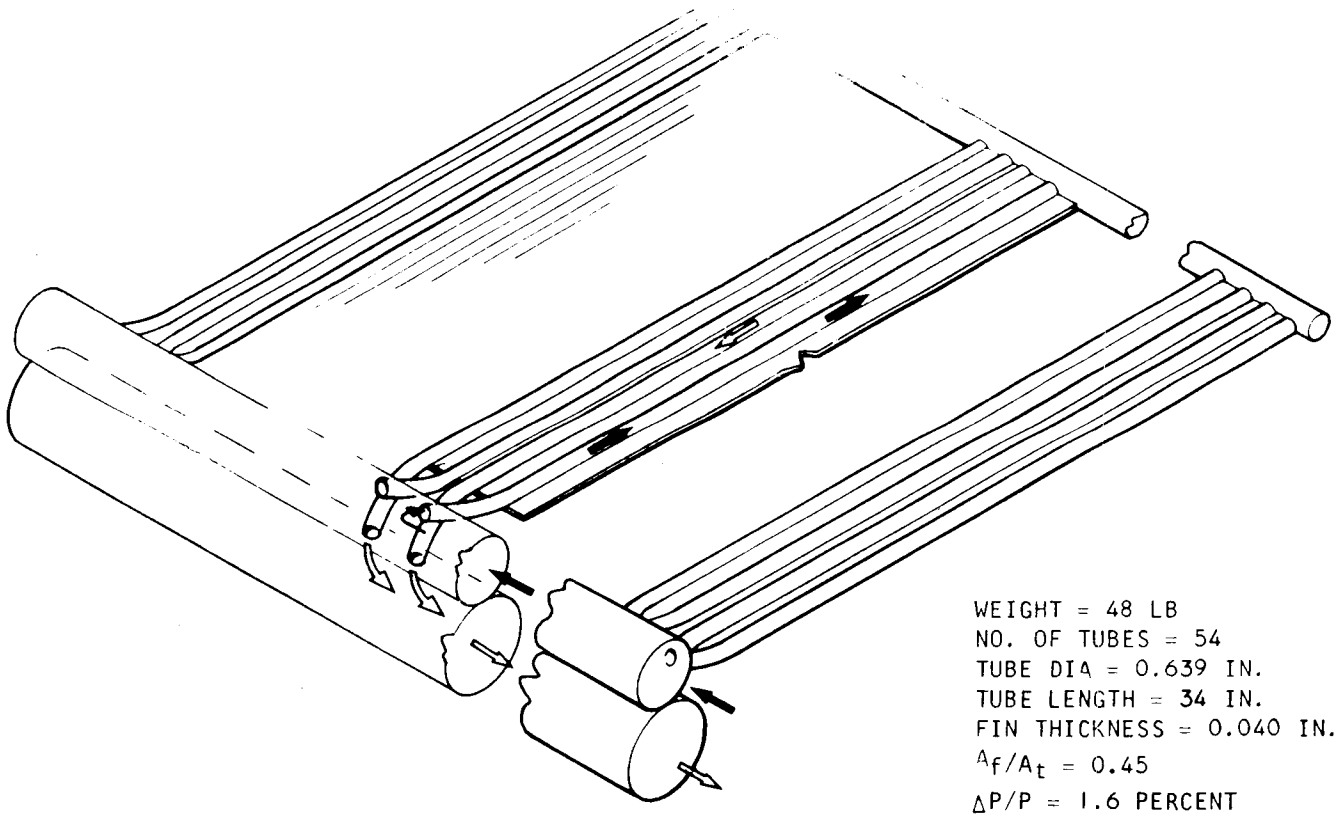

A-32989

Figure 5.2–52. Two-Pass Rectangular, Tube-Fin HSHX

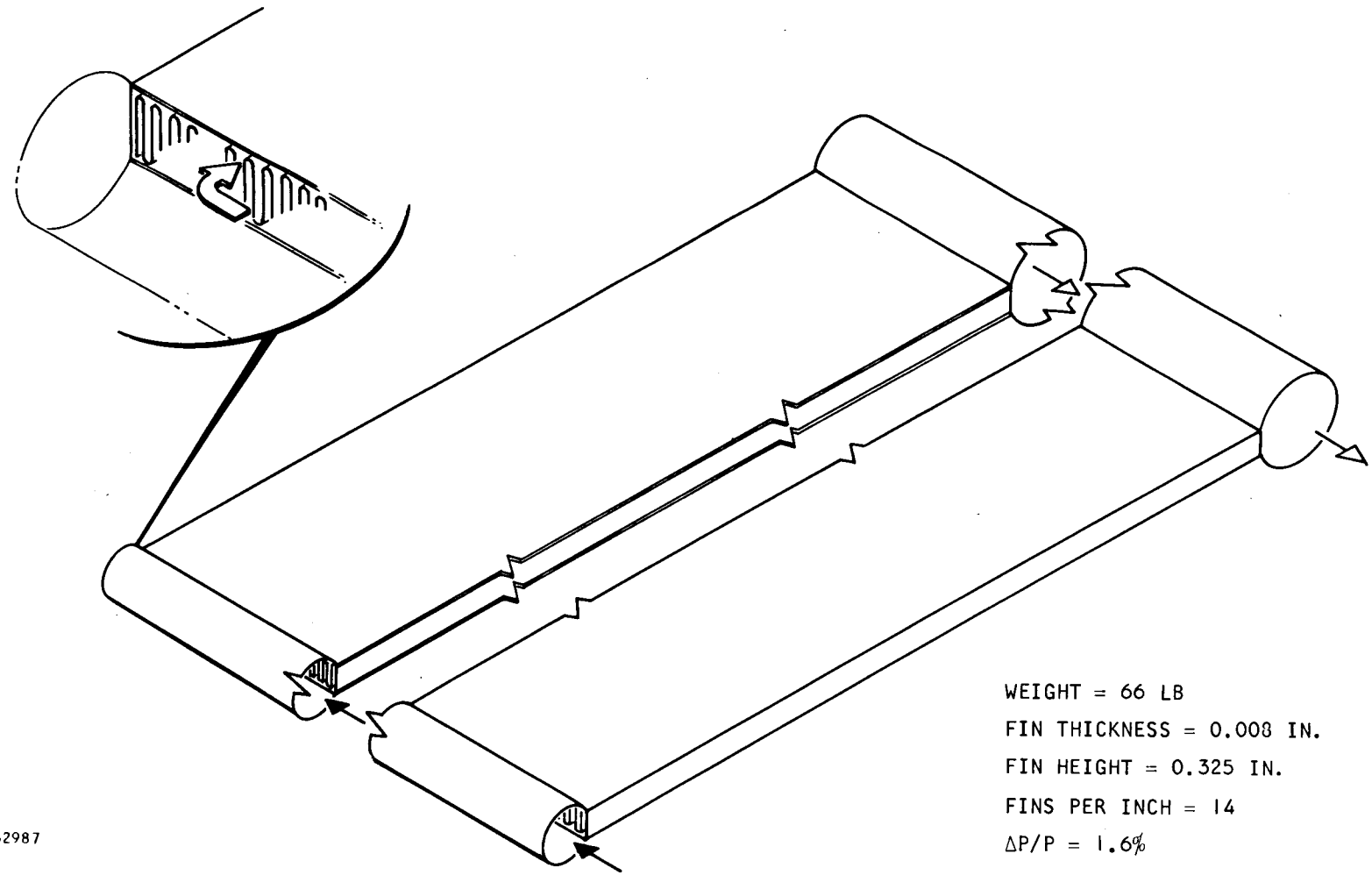

Figure 5.2–53. Single-Pass, Rectangular, Plate-Fin HSHX

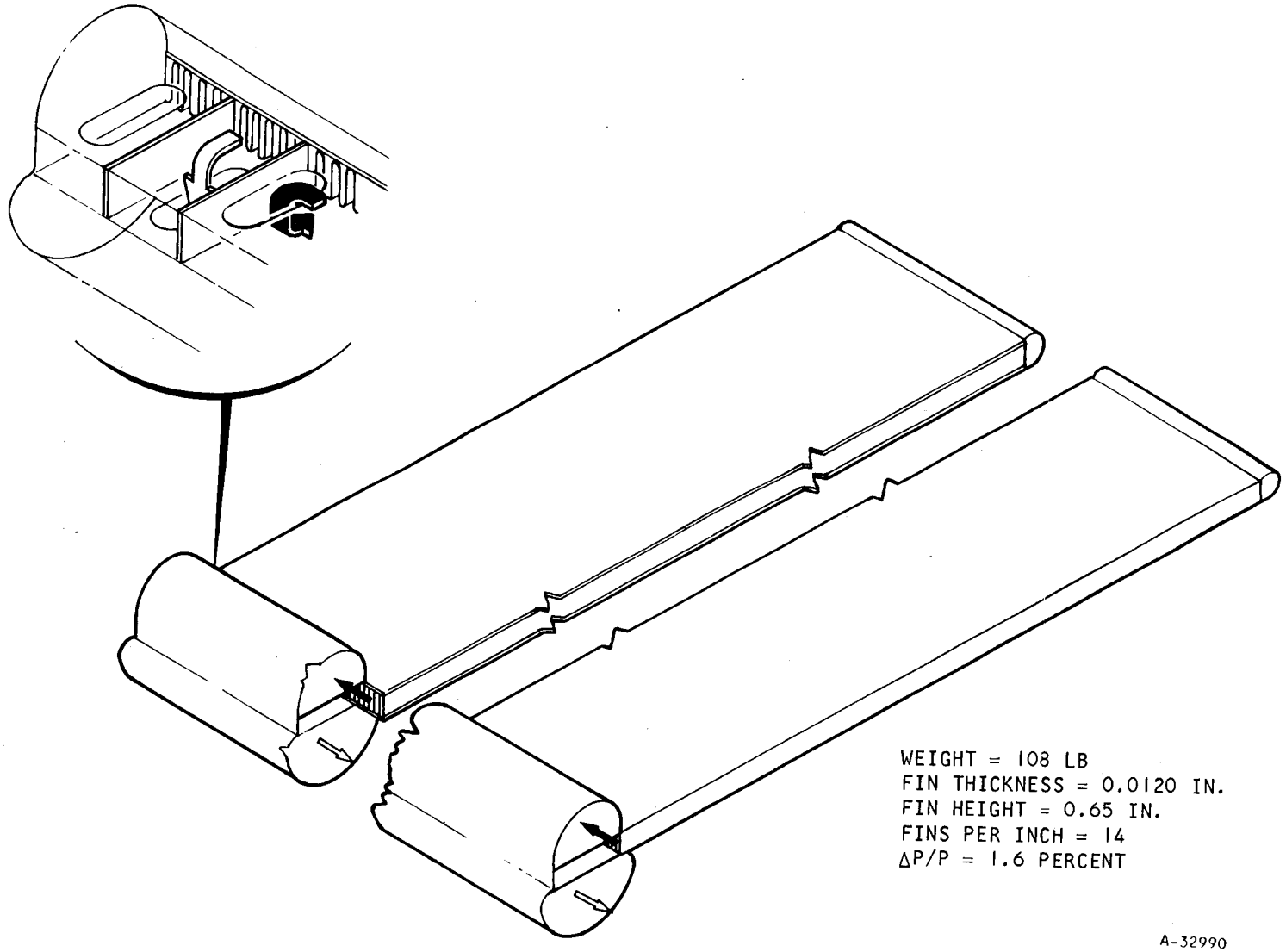

Figure 5.2–54. Two-Pass, Rectangular, Plate-Fin HSHX

TABLE 5.2-III

CIRCULAR AND RECTANGULAR HSHX DESIGN SUMMARY

	Circular				Rectangular			
	Tube-Fin		Plate-Fin		Tube-Fin		Plate-Fin	
	Involute 1-Pass	Involute 2-Pass*	Radial 1-Pass	Radial 2-Pass	1-Pass	2-Pass*	1-Pass	2-Pass
Weight, lb (core only)	63	63	74	131	48	48	66	108
Maximum source temperature, °F	2000	2000	2000	2000	2000	2000	2000	2000
ΔT across source, °F	100	45	180	110	165	55	165	55
ΔT across heat exchanger, °F	220	70	260	110	250	85	250	85
Manifold arrangement	Poor	Good	Poor	Good	Good	Good	Good	Good
Construction	Simple	Simple	Complex	Complex	Simple	Simple	Complex	Complex

*Recommended design approaches.

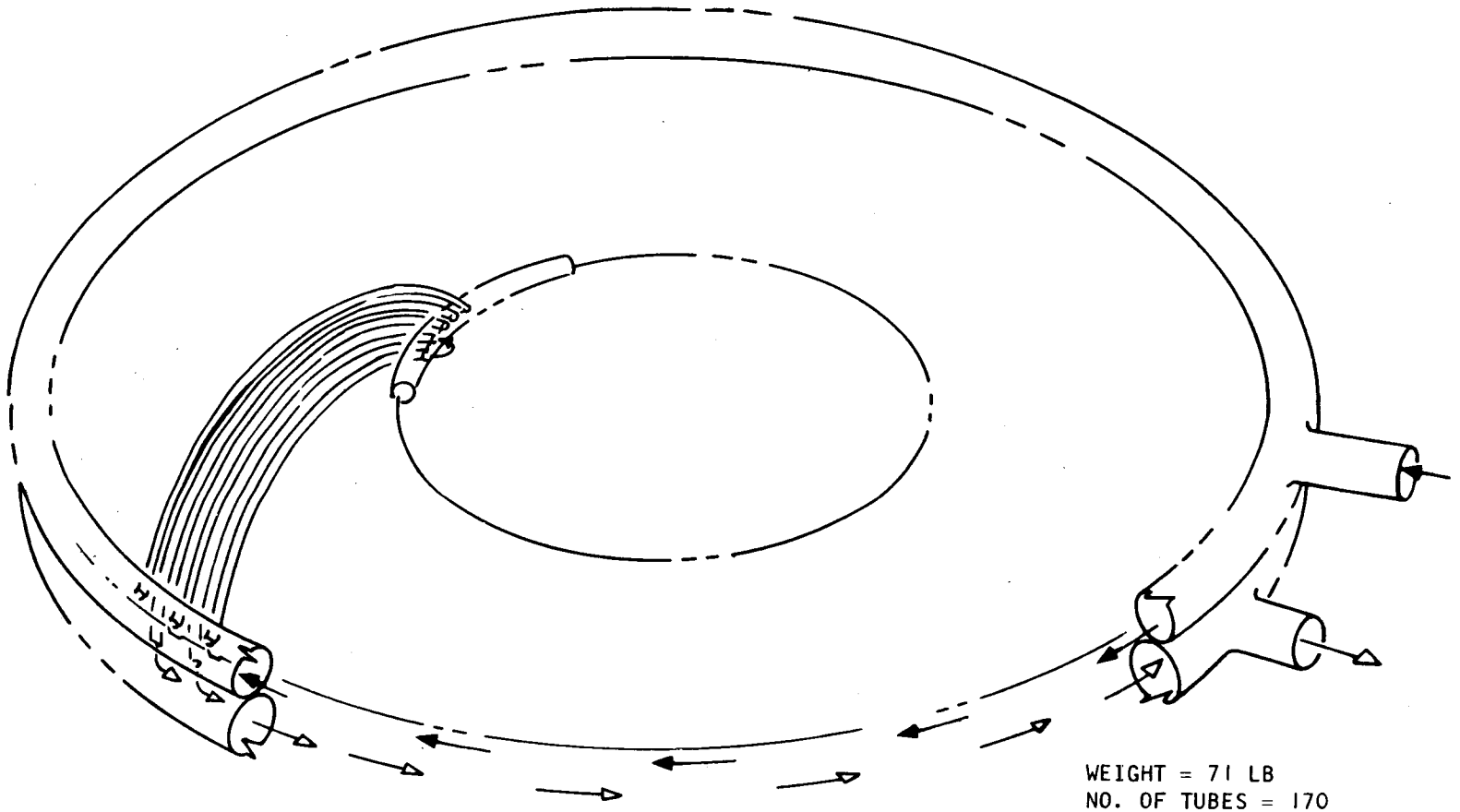

WEIGHT = 71 LB
NO. OF TUBES = 170
TUBE DIA = 0.389 IN.
TUBE LENGTH = 29.1 IN.
FIN THICKNESS = 0.040 IN.
A_f/A_t = 0.29
$\Delta P/P$ = 1.6 PERCENT

A-32995

Figure 5.2–55. System 4: Doughnut, Two-Pass, Tube-Fin HSHX

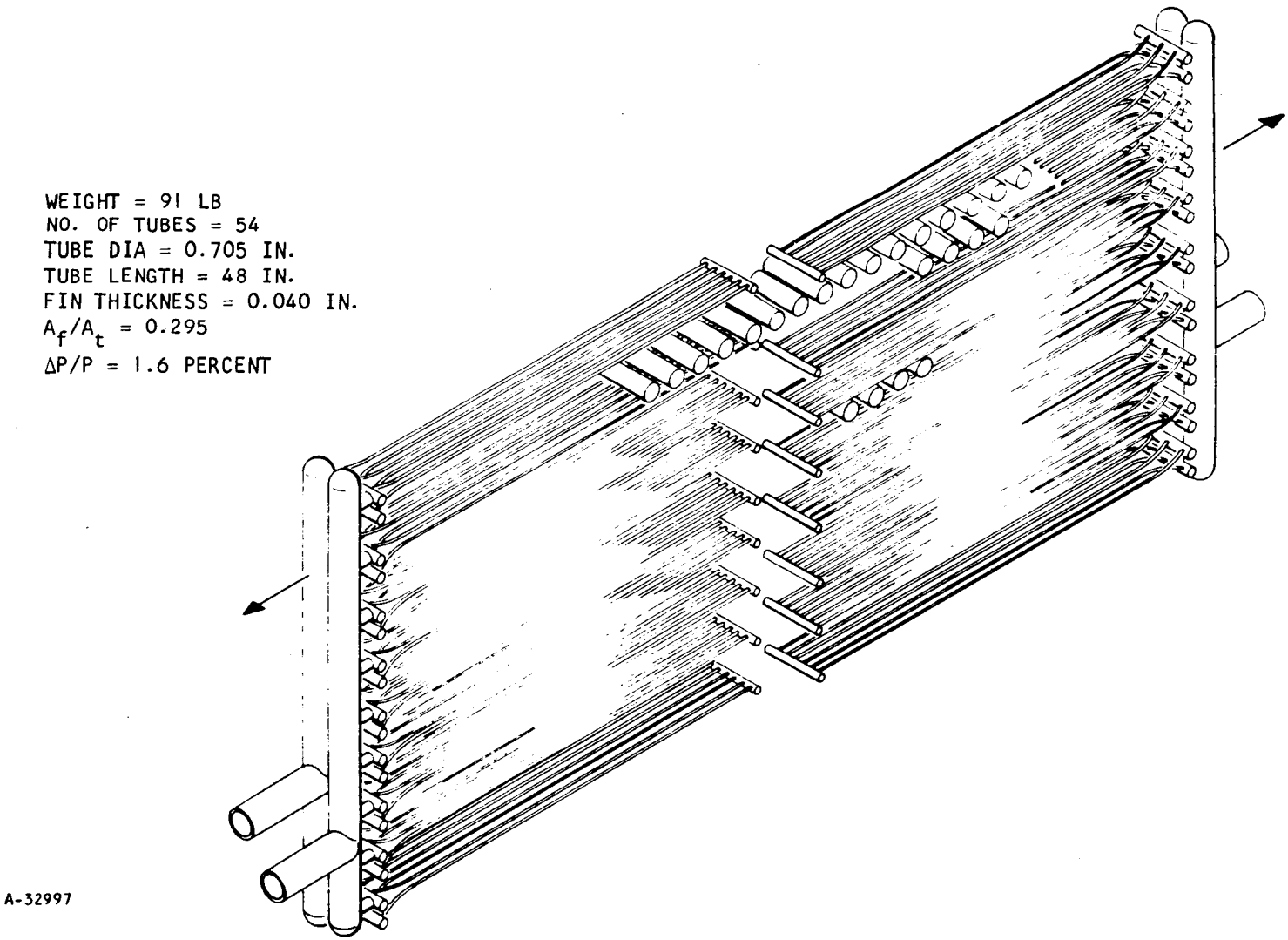

Figure 5.2–56. System 5: Pincushion, Two-Pass, Tube-Fin HSHX

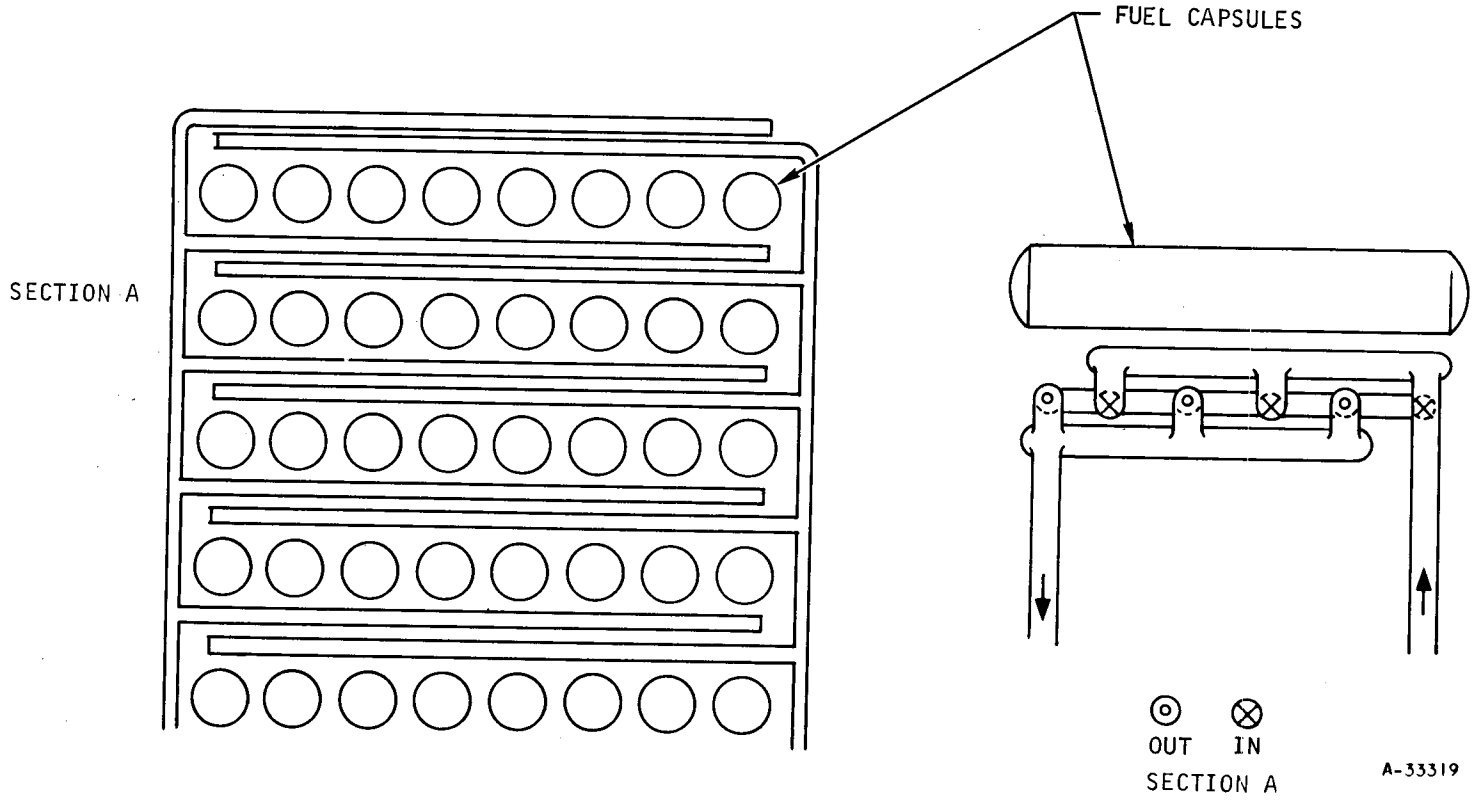

Figure 5.2–57. System 5: Pin Cushion, Two-Pass, Tube-Fin HSHX (Flow Configuration)

Figure 5.2-58 presents this weight and temperature tradeoff for the planar, circular, and rectangular fuel source arrays. By approximately doubling heat exchanger weight, both configurations can realize about a 50° F reduction in source temperature.

5.2.6 Installation Study

For the five IRV configurations selected for a more detailed investigation, a design study was undertaken of the problems of integrating the HSHX with the BHXU package as well as the different IRV designs.

The current BHXU package is shown in Figure 5.2-59 and consists of the recuperator, heat sink heat exchanger, and the Brayton cycle rotating unit (BRU), which comprises the turbine, alternator, and compressor. For the purposes of this design effort, the BHXU was assumed to be enclosed in a structural frame with the dimensions as shown on Figure 5.2-59. The arrangement of the equipment internal to this frame was considered fixed; however, the inlet and outlet ducts were allowed to pivot to effect the most desirable ducting arrangement between the HSHX and the BHXU. Beyond this minor perturbation, the internal layout of the BHXU equipment was held constant. The type of vehicle considered for installation of the BHXU-HSHX was the Atlas/Centaur.

An installation drawing was prepared for each of the five IRV designs with the specific heat exchangers selected for each. These configurations were as follows:

a. Circular planar

b. Rectangular planar

c. Conical

d. Conical doughnut

e. Rectangular pincushion.

In addition to the above five systems, the best plate-fin heat exchanger designs were also laid out for Systems 1 and 2. This was done to further identify any potential problem areas or advantages of the plate-fin design over the tube-fin approach when considering the integration problem.

The installation concept developed for the circular planar system is schematically illustrated in Figure 5.2-60. The installation schemes developed for all seven systems are similar to the one illustrated in this figure, but differ in some details.

The support structure consists of three major rings, the IRV support ring, a shield support ring, and a mounting ring, which carries the loads down to a straight cylindrical section allocated to the system radiators. These three rings are attached by two tubular truss networks, one on each side, which leaves a large central opening free to accept the two BHXU-HSHX assemblies, as indicated in Figure 5.2-60. The BHXU-HSHX assemblies are inserted from opposite sides and the HSHX, with its insulation system, fits between the radiation

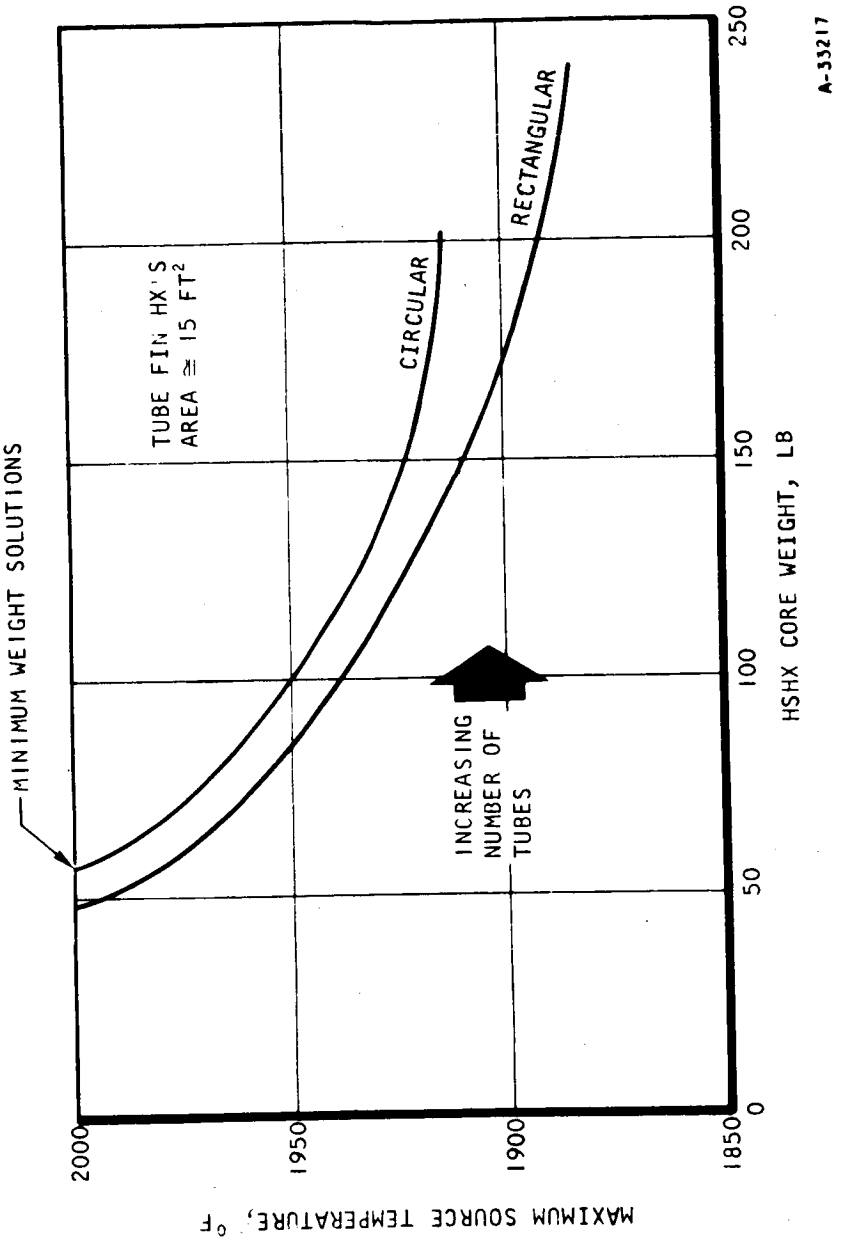

Figure 5.2–58. Effect of HSHX Weight on Source Temperature

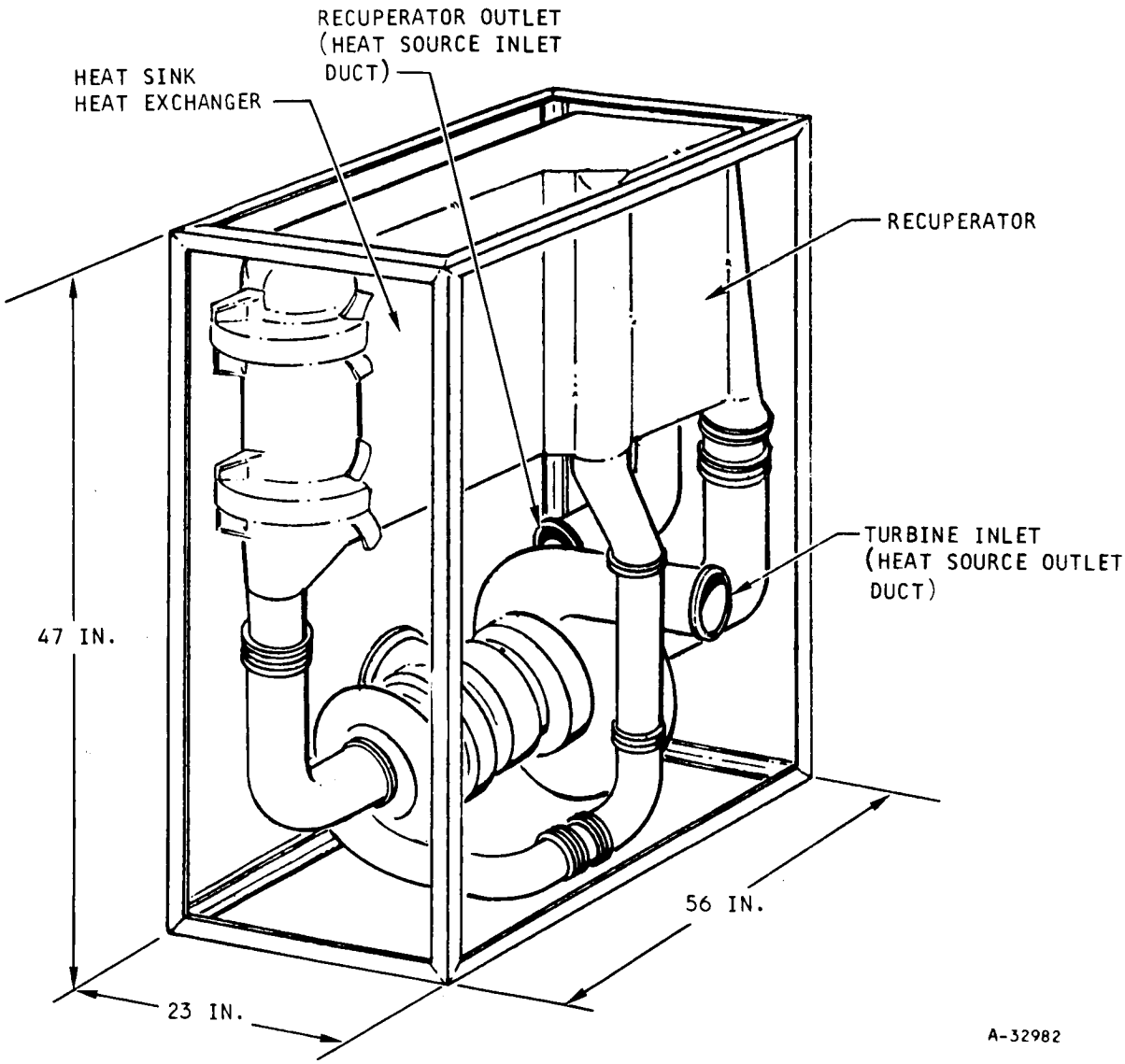

Figure 5.2–59. Brayton Cycle Power Conversion Package (PCS)

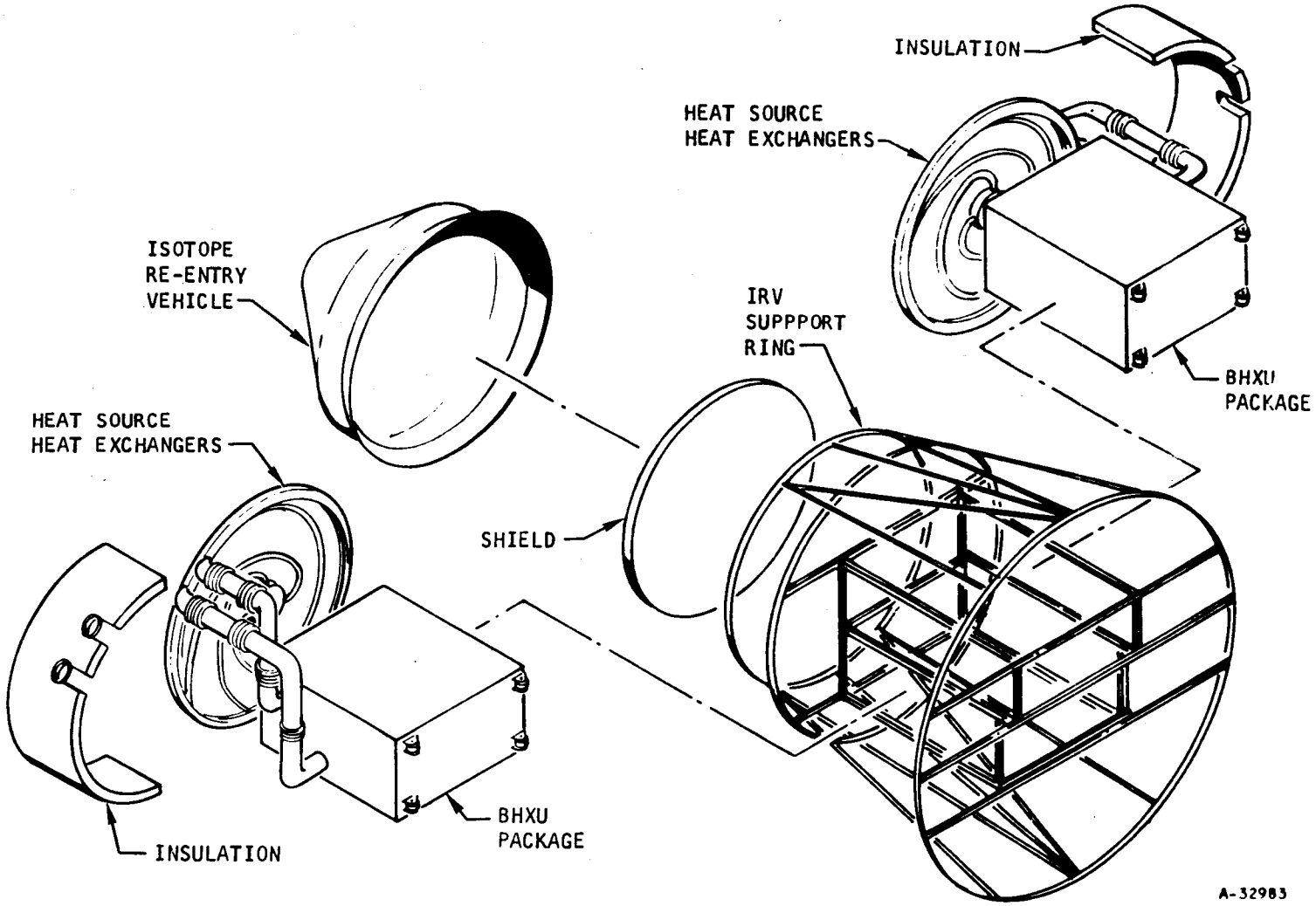

Figure 5.2–60. System I: Circular Planar Atlas/Centaur Installation

shield and the IRV, while the BHXU fits below the radiation shield. A box-like structure located between the shield support ring and the mounting ring provides the support structure for the two BHXU packages. The two BHXU packages sit side-by-side in this box frame, and quick-disconnect clamping and locking devices hold the BHXU packages in place. The heat source heat exchanger is supported from the BHXU frame as well as from the shield support ring (or IRV support ring, depending on which heat exchanger is immediately adjacent to the IRV). The BHXU-HSHX assemblies are installed offset in the vehicle axial direction by an amount sufficient to allow the overlapping of the two heat source heat exchangers; thus, one system can be interchanged with the other. The insulation system is attached to the HSHX in such a manner that when the two power systems are in place, the cavity between the isotope source plate and the radiation and the shield forms a closed insulated compartment (see Section 5.2.8).

The following drawings (SK51433 through SK51439) show the detailed HSHX designs as well as the installation concepts developed for the seven systems considered.

The details of the structural attachment of the HSHX with the BHXU and the HSHX with the IRV-radiation shield are given in Section 5.2.7 of this report, as are the internal structural considerations of the HSHX and the interconnecting duct design.

Details of the overall insulation system and the heat leaks attendant on each of the seven systems are given in Section 5.2.8.

5.2.7 Structural Considerations

5.2.7.1 Structural Problem Areas

The principal problem areas for the HSHX are (1) long-time containment of the working gas and (2) structural integrity for the various applied load conditions during the service life of the unit. The most severe short-duration loads and stresses occur during launch and lift-off.

A circular two-pass involute configuration was analyzed with regard to the following specific considerations:

a. Heat exchanger mounting and assembly

b. Long-time pressure containment

c. Detailed tube-to-fin joint design

d. Interconnecting ducting design

5.2.7.2 Heat Exchanger Mounting and Assembly

The essential details of the heat exchanger mounting concept and the assembly sequence are illustrated in Figure 5.2-61. The cold inlet duct, just prior to its joint with the HSHX inlet manifold, is used as an anchor point for the HSHX. A conical adapter section is welded at its small end to the inlet duct and at its large end to a mount flange. The mount flange is, in turn, bolted

to a semicircular corrugated (or honeycomb sandwich) panel, which contains a matching flange. The panel structure is locally reinforced by gusset plates to form a mounting bracket for attachment to the vehicle support structure. Figure 5.2-61 shows the bracket resting on the lithium hydride shield structure, which would have to be reinforced to accept the loads from the HSHX and related equipment.

The corrugated cold panel skin would, in turn, provide for the mounting and support of the superinsulation. The superinsulation would be held in place by an open-grid type of inside liner structure, which would be supported from the cold panel by mounting clips. The exact details of the superinsulating mounting will require careful study to determine the number and type of mounting clips.

The HSHX attachment bracket will be connected to the BHXU-BRU frame structure by a bridging structure. This will permit separate assembly into a single integral unit of the entire power conversion gas loop. The entire package can then be installed into the launch vehicles as a unit. This also means the PCS can be ground-checked before installation without necessitating subsequent disassembly and reassembly.

An aft mount for the HSHX is shown in Figure 5.2-61. The stress analysis for launch loads revealed excessive bending stresses at the anchor point for the high-g launch-liftoff forces. The aft mount provides restraint for vertical loads (normal to the plane of the HSHX) and for side loads. It does not constrain axial displacement; this feature permits free thermal expansion of the HSHX away from the anchor point. The aft mount is shown as a permanent part of the launch vehicle. For the lower HSHX, it would be supported from the radiation shield structure, and for the upper HSHX, it would be supported from the same structure required to support the IRV assembly.

The final design feature shown on Figure 5.2-61 is the interconnecting ducting arrangement from the HSHX to the BHXU and the BRU. This ducting will undergo the thermal expansion from ambient temperature at installation to final operating temperatures. The connecting flange points on the BHXU and BRU will also experience appreciable thermal motions with respect to the tiedown points of these components. The concept shown in Figure 5.2-61 utilizes an offset bend in the piping with three gimbal-type expansion joints. This allows the piping to act as a three-hinge kinematic mechanism that will absorb all three directions of relative end-to-end deflections as well as angular movement in any direction. This ducting arrangement has been compared to a straight duct with a single bellows in Figure 5.2-62. The comparisons indicate that the offset bend piping is decidedly preferable. The design of the bellows will be greatly simplified by this design arrangement.

5.2.7.3 HSHX Stress Analysis

The involute-tube two-pass HSHX was analyzed for several of the initial problem areas. The following stress ground rules were used for this analysis:

a. Use launch and liftoff loads for Centaur launch vehicle

   Maximum axial acceleration = 6.4 g

   Maximum normal acceleration = 2.3 g

b. Limit load factors - 1.25 x acceleration g's

c. Stress limits

For short-duration loads

Factor of safety versus 0.2-percent yield stress = 1.15

Factor of safety versus ultimate stress = 1.50

For stress rupture (long-time pressure containment)

Factor of safety versus 50,000-hr stress to rupture = 2.0

d. Fundamental resonant frequency $\geq$ 50 cps

The following pertinent material properties were used for Cb-IZr:

a. At R.T. f_{ty} = 35,000 psi; E = 16 x 10^6 psi

b. At 1700° F F_{ty} = 29,000 psi; E = 14 x 10^6 psi

c. 50,000-hr stress to rupture at 1700° F = 4050 psi

d. Elongation = 10 to 12 percent over entire temperature range

e. Expansion coefficient

1) R.T. to 500° F, α = 4.2 x 10^{-6} in./in./°F

2) R.T. to 1700° F, α = 4.5 x 10^{-6} in./in./°F

The involute tubular array was considered a plate with orthotropic stiffness properties. The moment of inertia for tube bending was taken to be that of the tube cross-section properties. The bending stiffness in the weak direction is substantially lower, and it was taken to be essentially zero. The tube direction relative to a radial line from the center of the HSHX constantly changes. The plate was analyzed as an equivalent isotropic structure with the average of the weak and strong direction inertia (or half of the inertia in the strong direction). The maximum plate-bending stress was determined to be 133 psi/g. For a limit load acceleration of 6.4 x 1.25 = 8 g's, the peak stress due to launch is 1067 psi, which is well within the material strength capability.

The circular inlet manifold provides for the support of the HSHX tube array. Stresses at the anchor point without the aft mount were computed to be 12,600 psi/g. This allows for cantilevering the entire heat exchanger from the anchor point during ground handling and system assembly. Stresses due to the 8-g launch load factor would be approximately 100,000 psi, which accounts for the need to have the aft mount support. Launch stresses were also computed with the aft mount. A summary of stress results is shown in Figure 5.2-63.

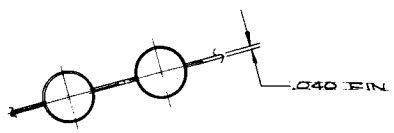

A-A
SCALE 1/1

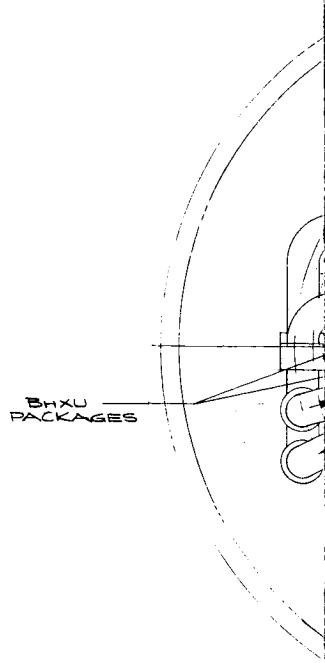

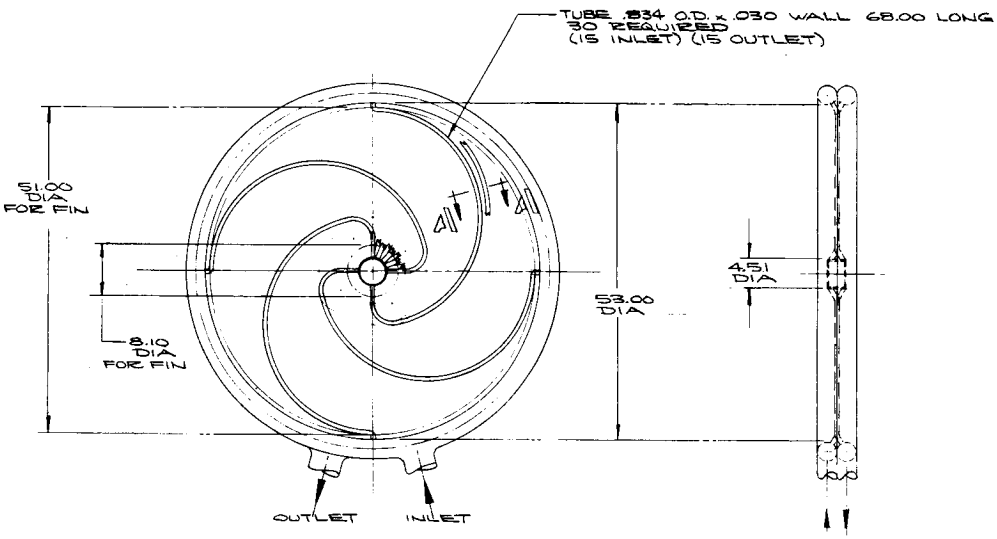

HEAT SOURCE
HEAT EXCHANGER DETAIL

FOLDOUT FRAME

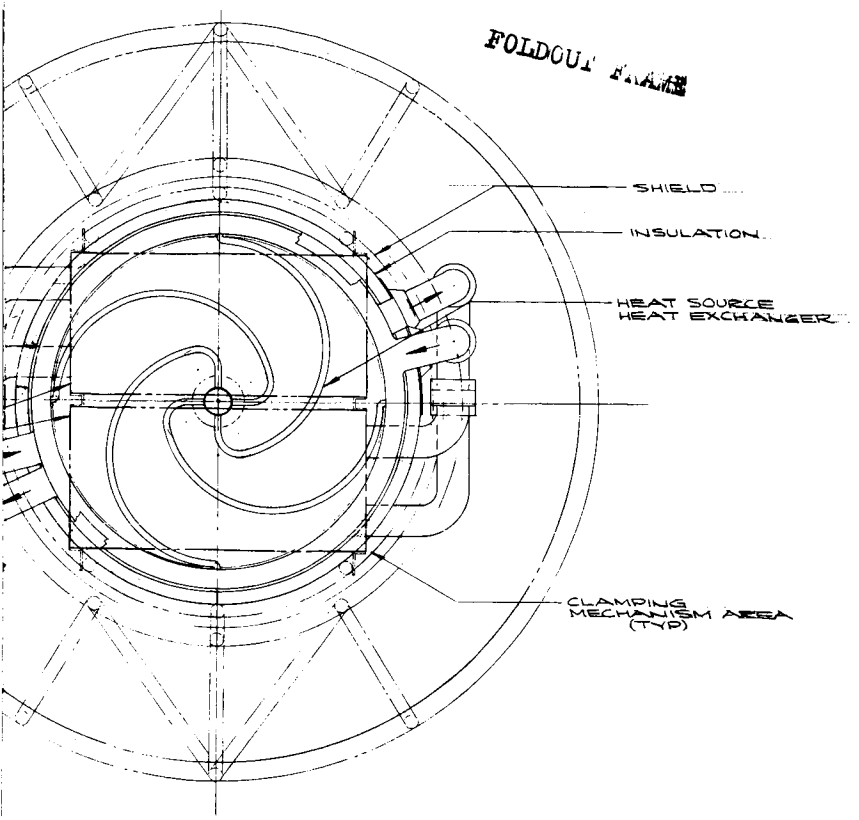

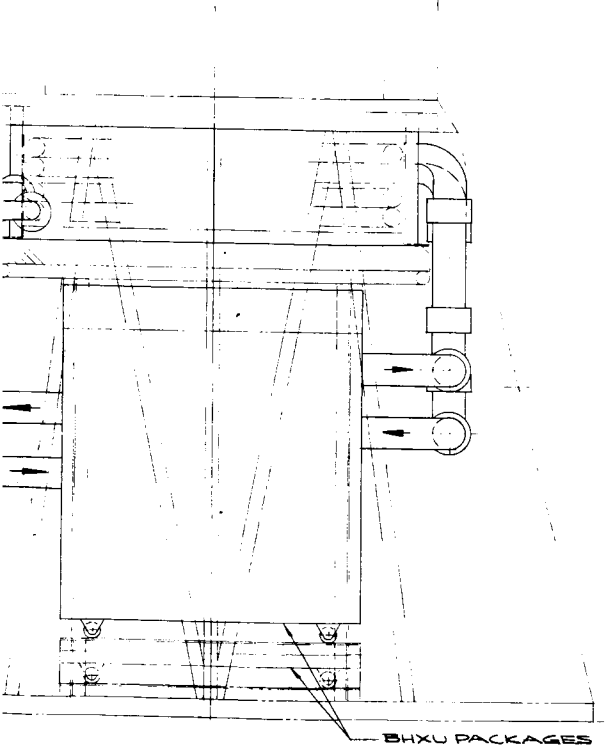

FOLDOUT FRAME 2

FOLDOUT FRAME

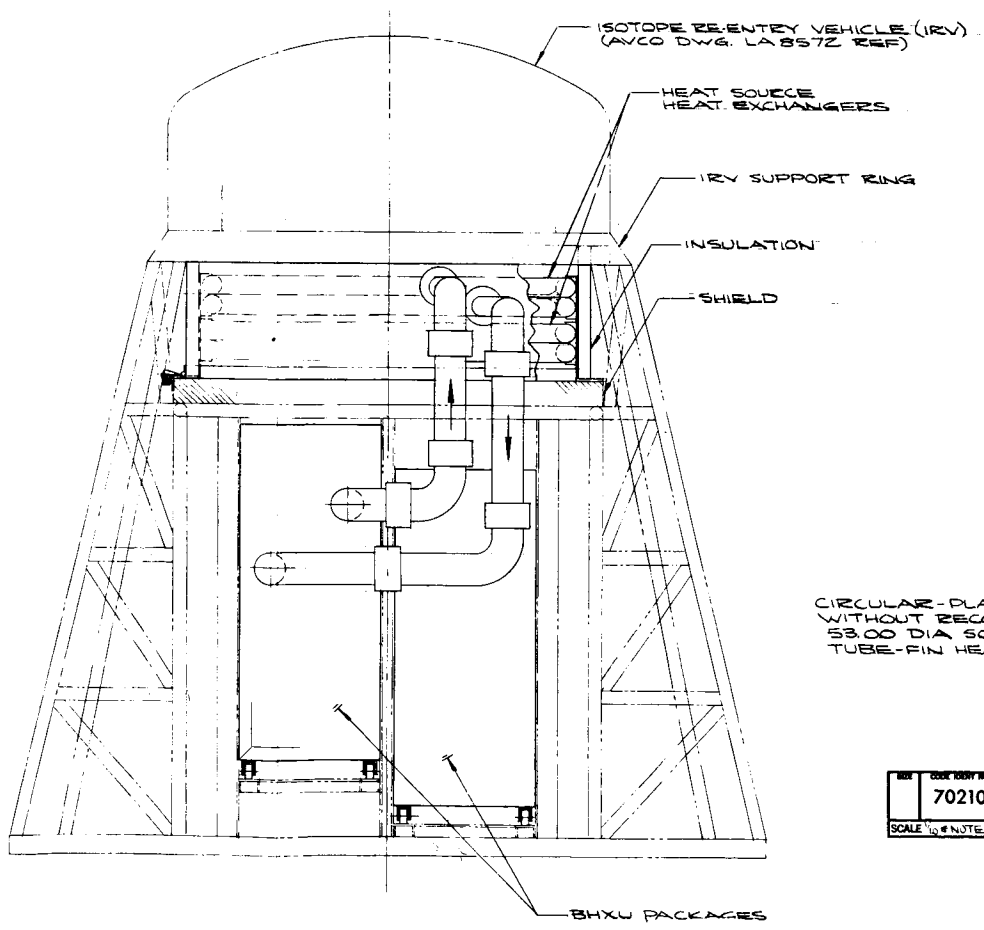

CIRCULAR - PLANAR - 60° CONE
WITHOUT RECOVERY AIDS
53.00 DIA SOURCE
TUBE-FIN HEAT EXCHANGER

SYSTEM NO. 1B

SIZE	CODE IDENT NO.	DWG NO.
	70210	SK 51433
SCALE 1/0 IF NOTED		SHEET 1 OF 1

FOLDOUT FRAME 3

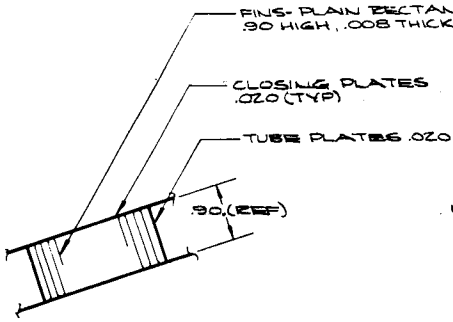

A-A
NO SCALE

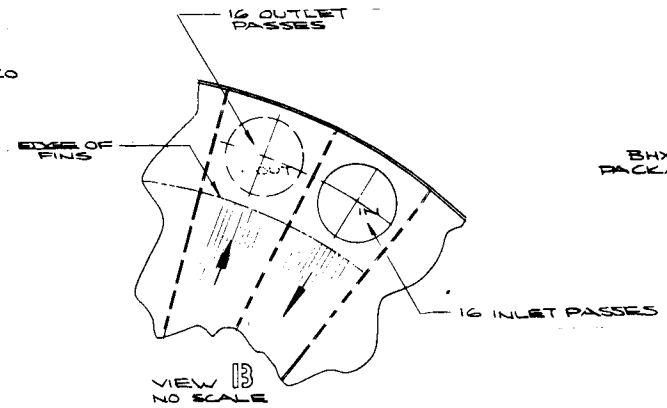

VIEW 13
NO SCALE

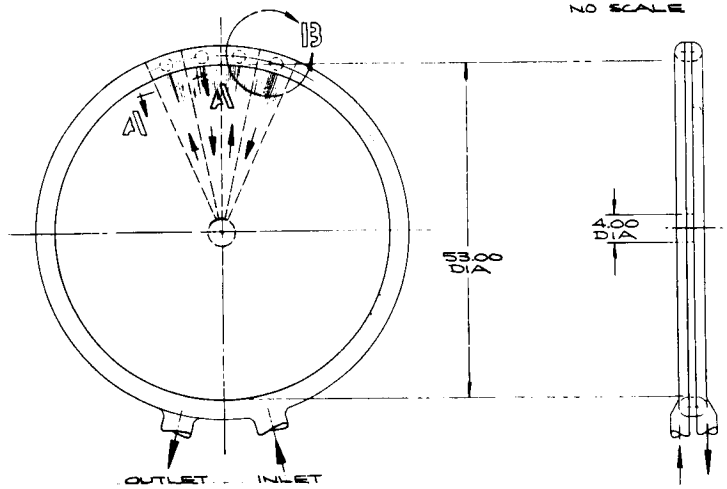

HEAT SOURCE
HEAT EXCHANGER DETAIL

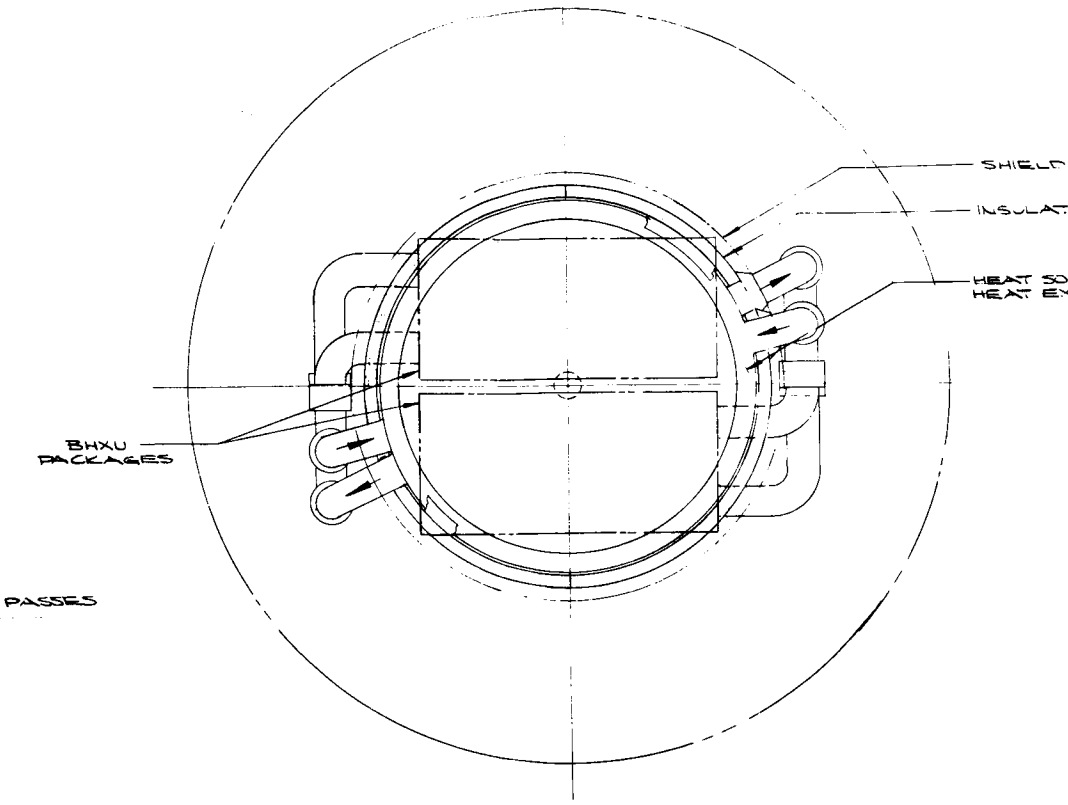

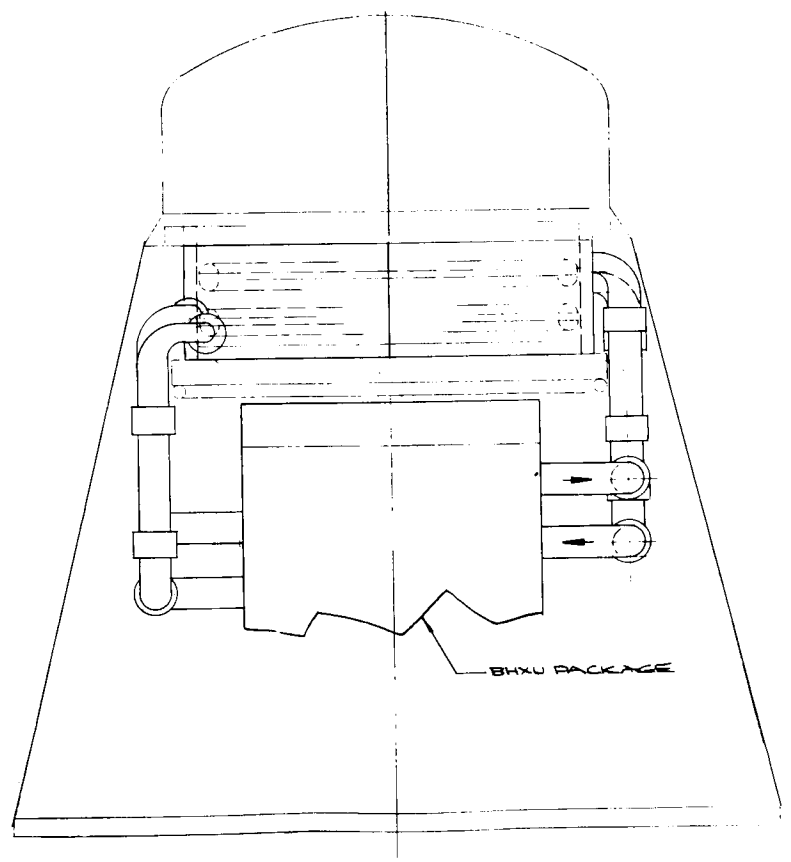

FOLDOUT FRAME 1

FOLDOUT FRAME 2

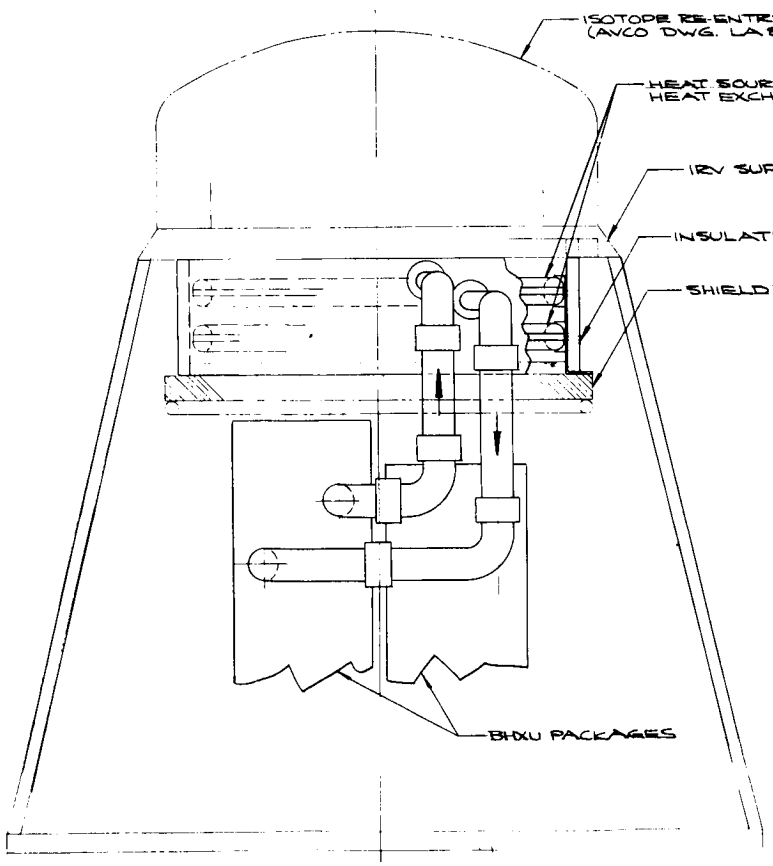

SIMILAR TO SK 51433 EXCEPT FOR HEAT SOURCE HEAT EXCHANGERS

CIRCULAR-PLANAR-60° CONE WITHOUT RECOVERY AIDS
53.00 DIA SOURCE
PLATE-FIN HEAT EXCHANGER

SYSTEM NO. 1D

	70210	SK 51434
SCALE		SHEET 1 OF 1

FOLDOUT FRAME

Foldout Frame 3

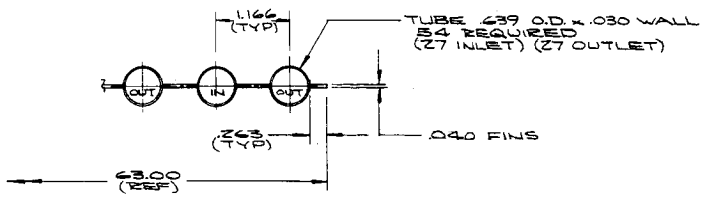

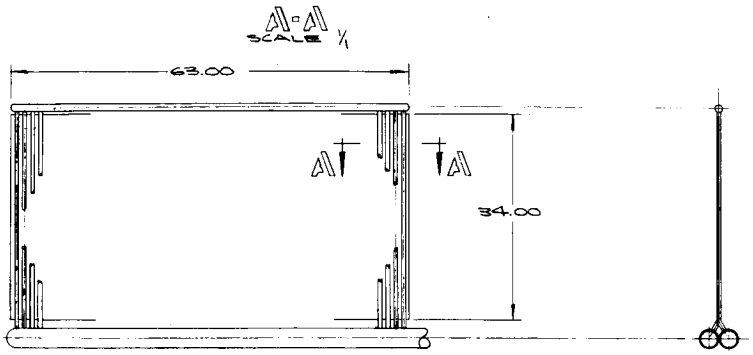

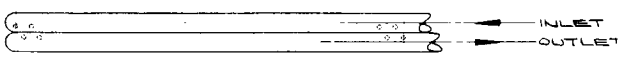

HEAT SOURCE
HEAT EXCHANGER DETAIL

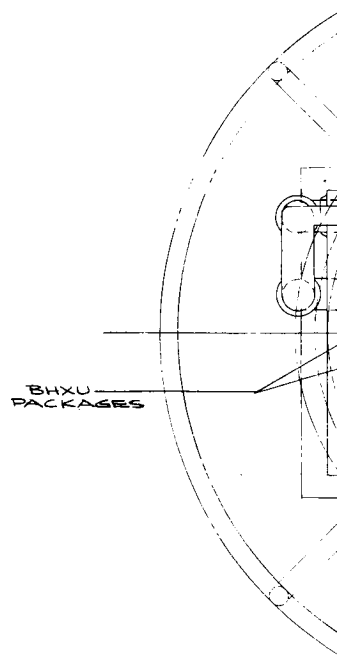

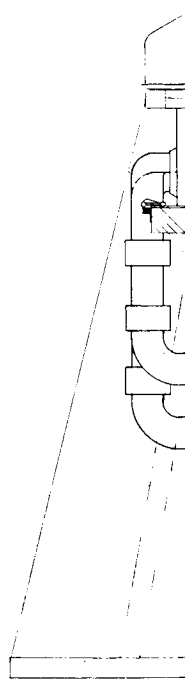

FOLDOUT FRAME 1

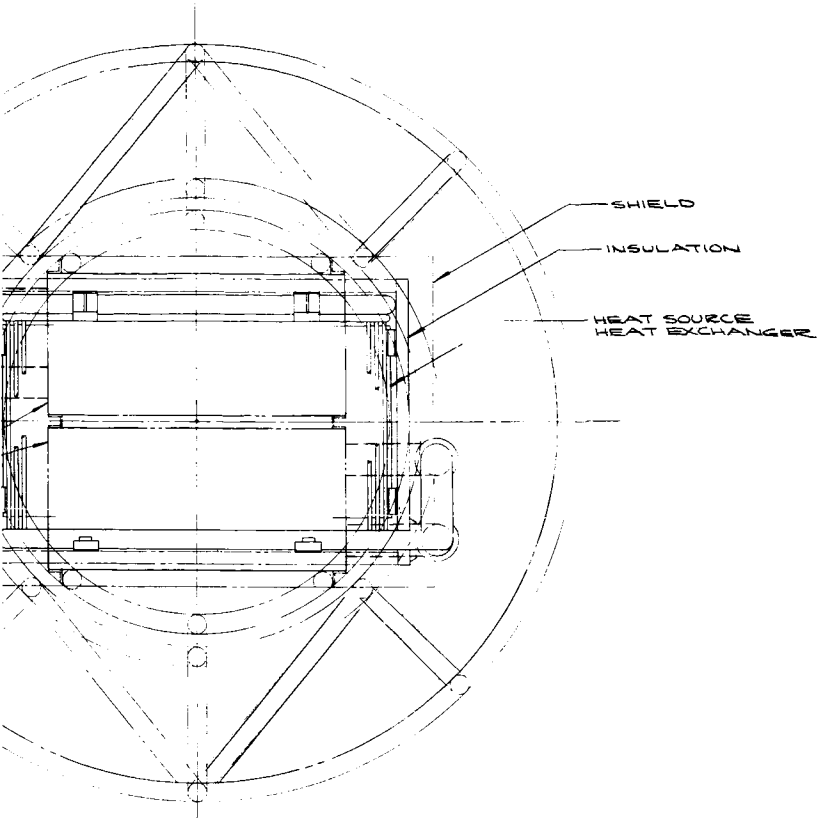

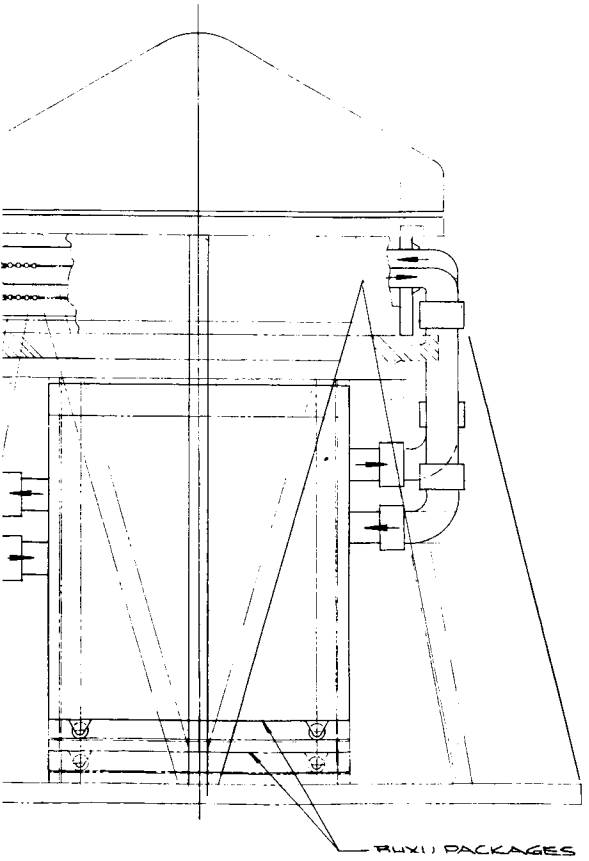

FOLDOUT FRAME 2

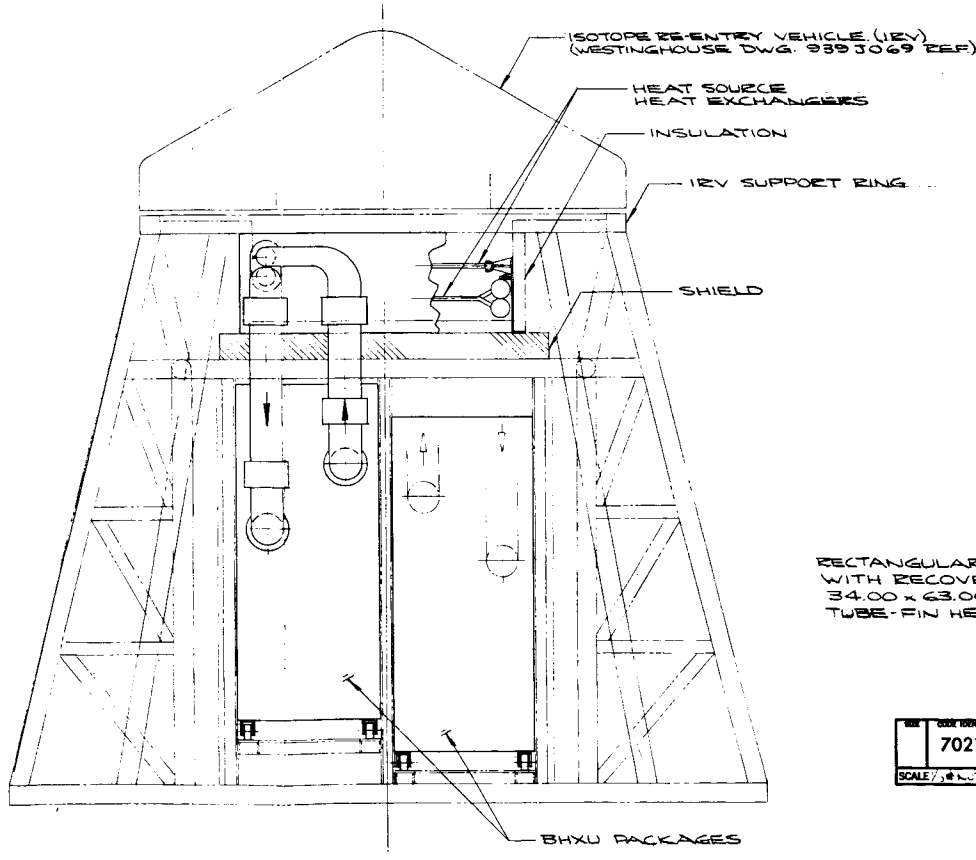

RECTANGULAR-PLANAR-60° CONE
WITH RECOVERY AIDS
34.00 x 63.00 SOURCE
TUBE-FIN HEAT EXCHANGER

SYSTEM NO. 2B

SIZE	CODE IDENT NO.	DWG NO.
	70210	SK 5 435
SCALE		SHEET 1 OF 1

FOLDOUT FRAME 3

FOLDOUT FRAME 1

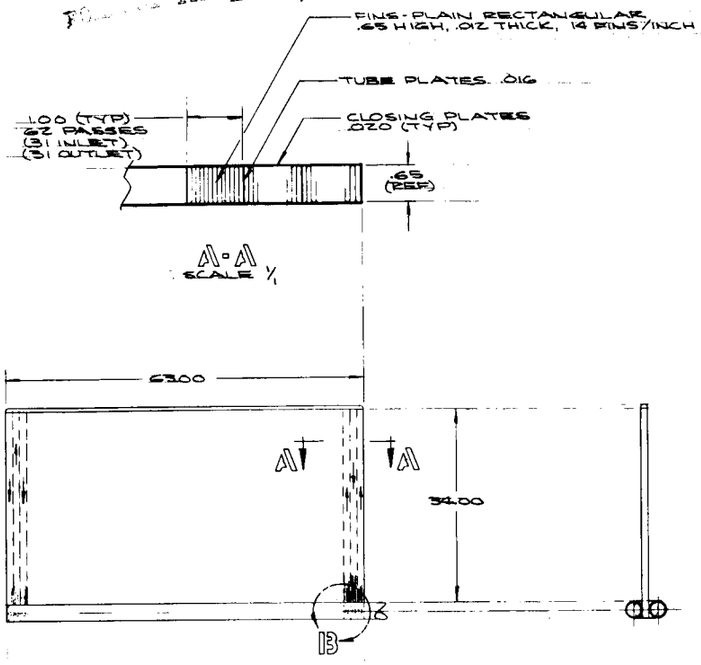

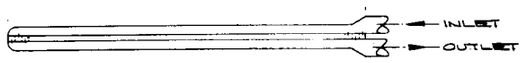

HEAT SOURCE HEAT EXCHANGER DETAIL

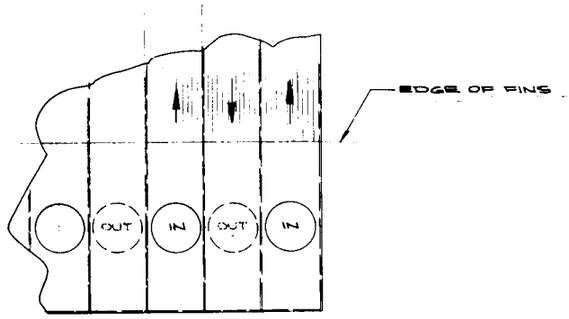

VIEW 13
SCALE 1/1

FOLDOUT FRAME 2

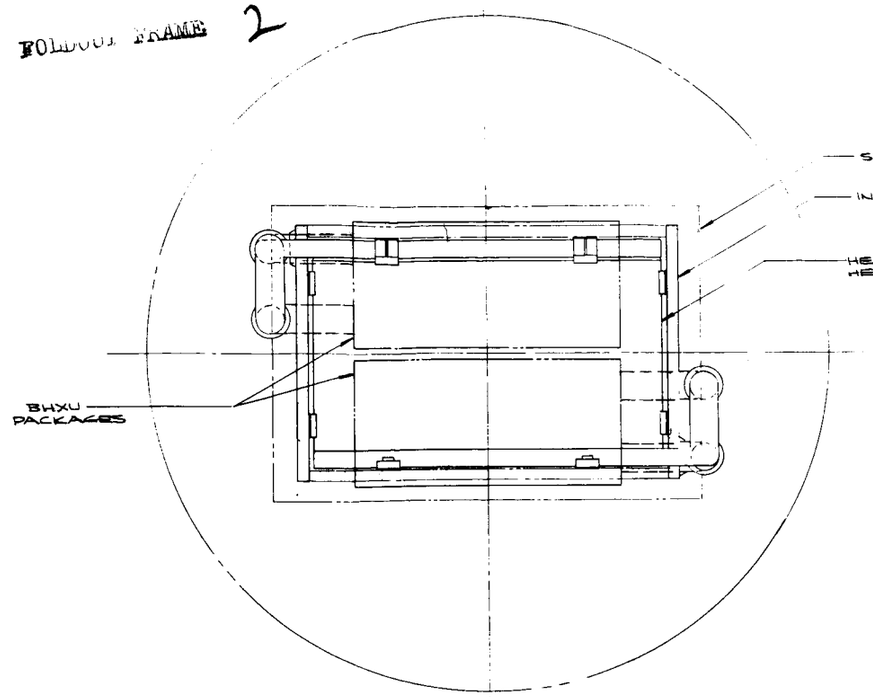

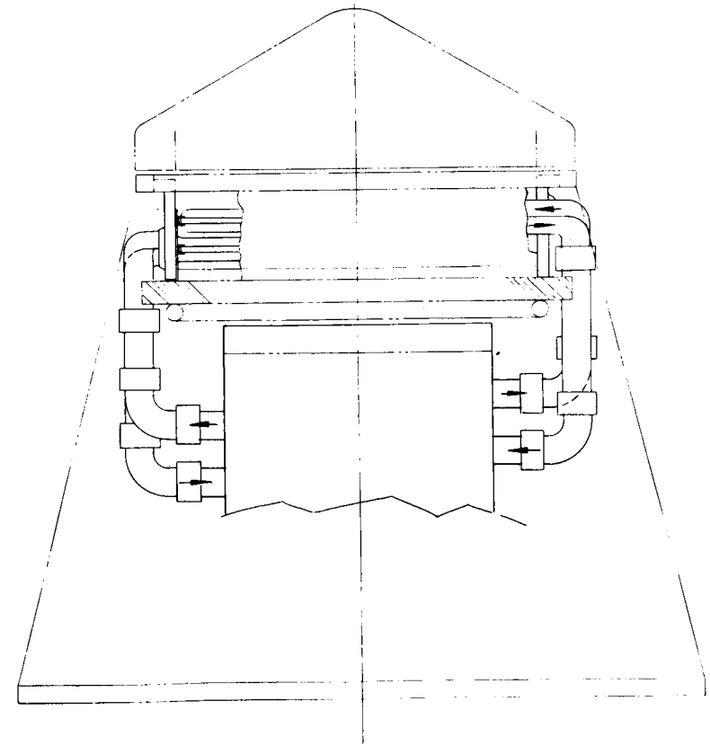

ELD

ULATION

T SOURCE
T EXCHANGER

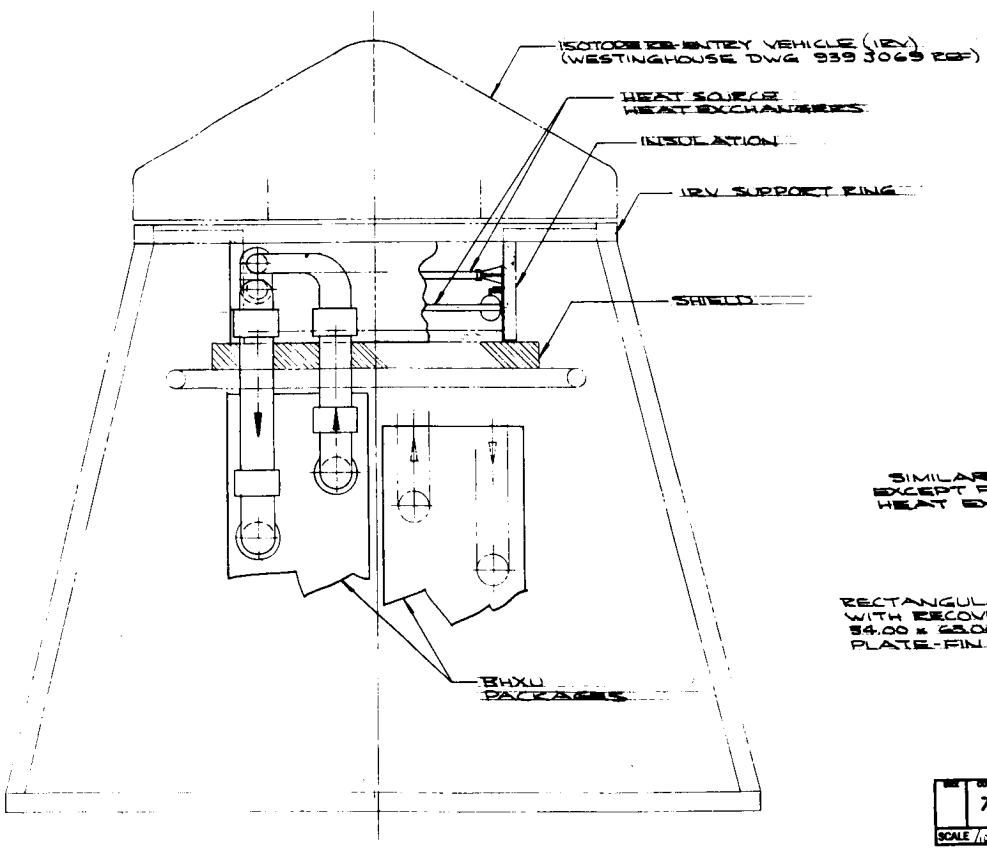

SIMILAR TO SK 51435
EXCEPT FOR HEAT SOURCE
HEAT EXCHANGERS

RECTANGULAR - PLANAR - 60° CONE
WITH RECOVERY AIDS
94.00 x 65.00 HEAT SOURCE
PLATE-FIN HEAT EXCHANGER

SYSTEM NO. 2D

	70210	SK 51436
SCALE NONE NOTED		SHEET OF

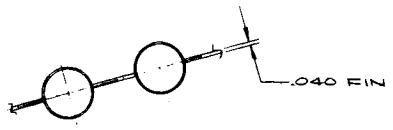

A-A
SCALE 1/1

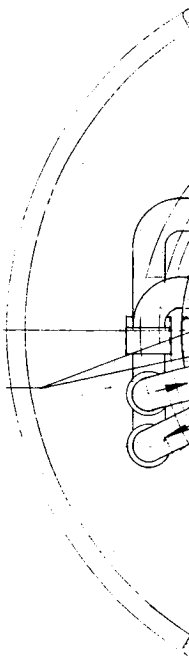

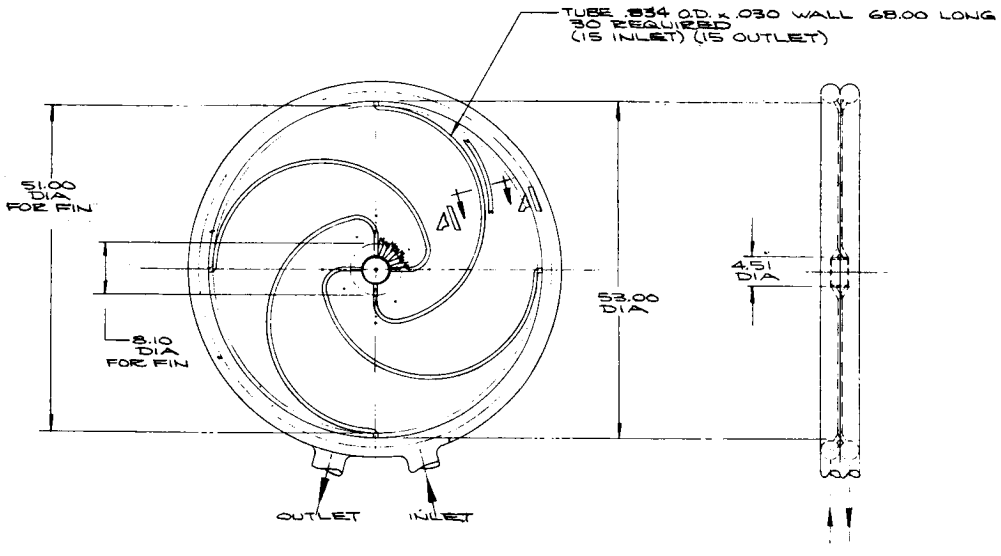

HEAT SOURCE
HEAT EXCHANGER DETAIL

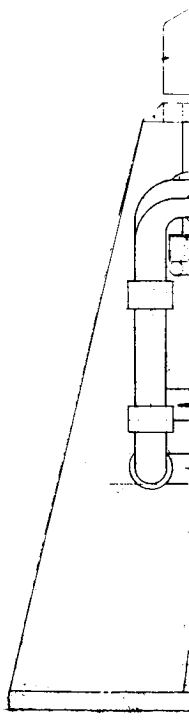

FOLDOUT FRAME 1

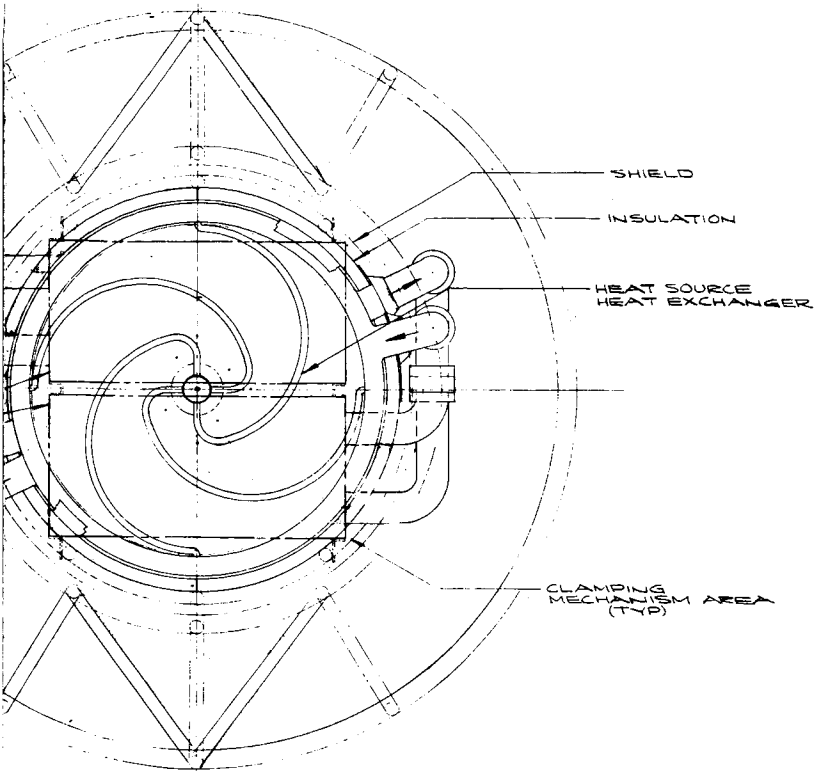

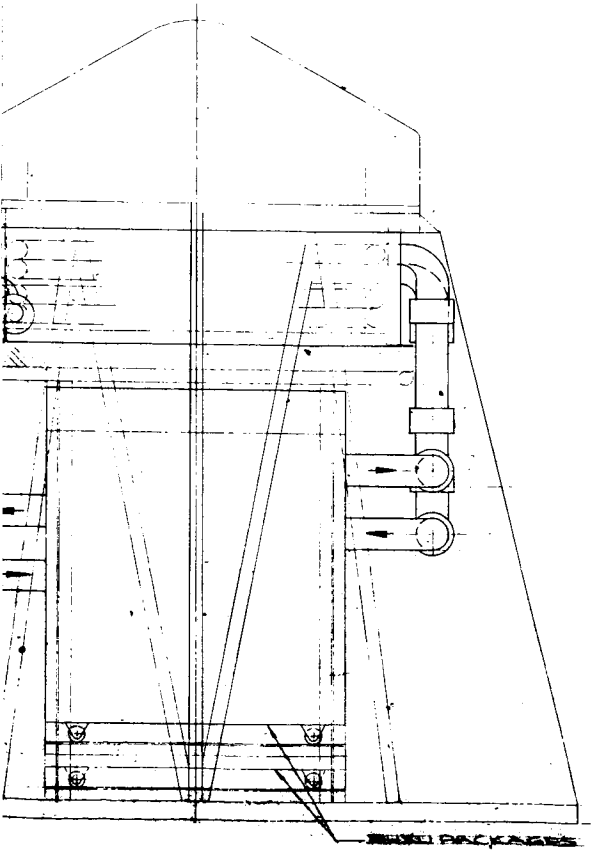

FOLDOUT FRAME 2

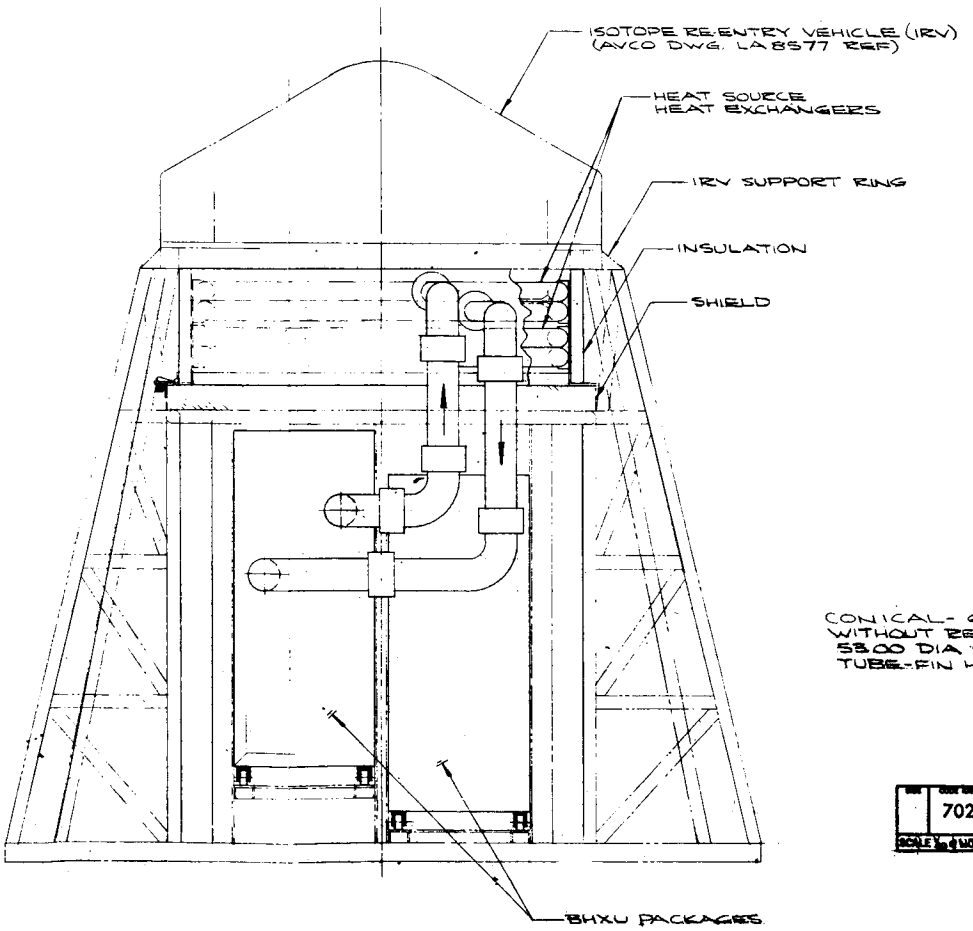

CONICAL- 60° CONE
WITHOUT RECOVERY AIDS
53.00 DIA SOURCE
TUBE-FIN HEAT EXCHANGER

SYSTEM NO. 3

	70210	SK 51437
SCALE		SHEET 1 OF 1

FOLDOUT FRAME 3

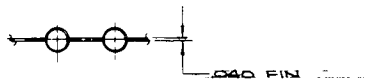

A-A
SCALE 1/1

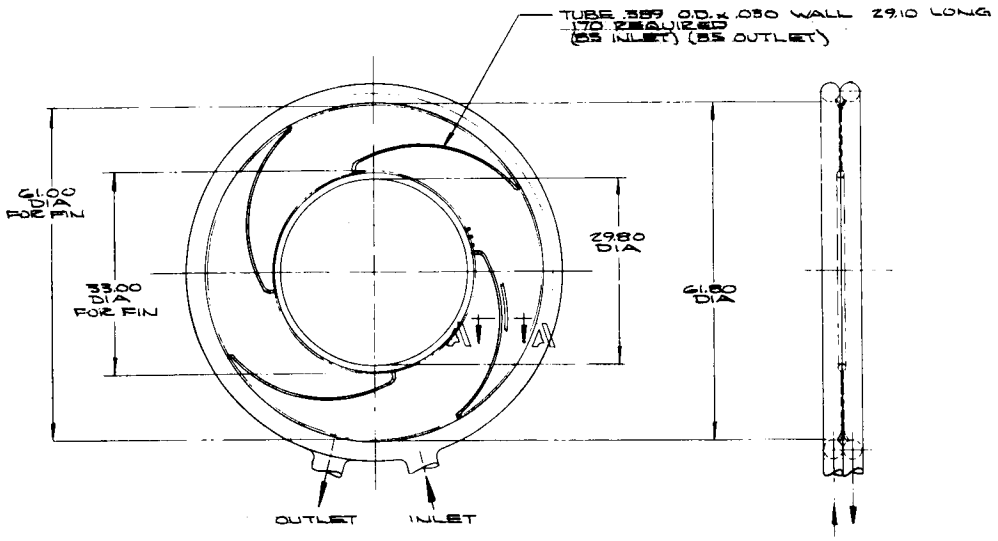

HEAT SOURCE
HEAT EXCHANGER DETAIL

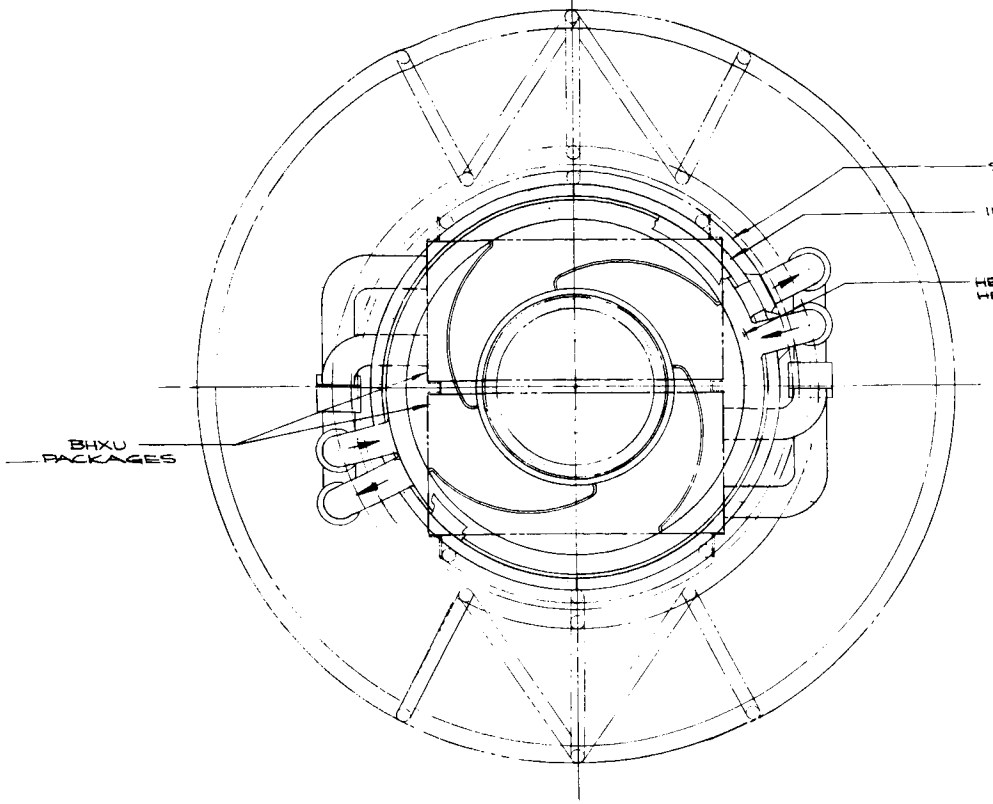

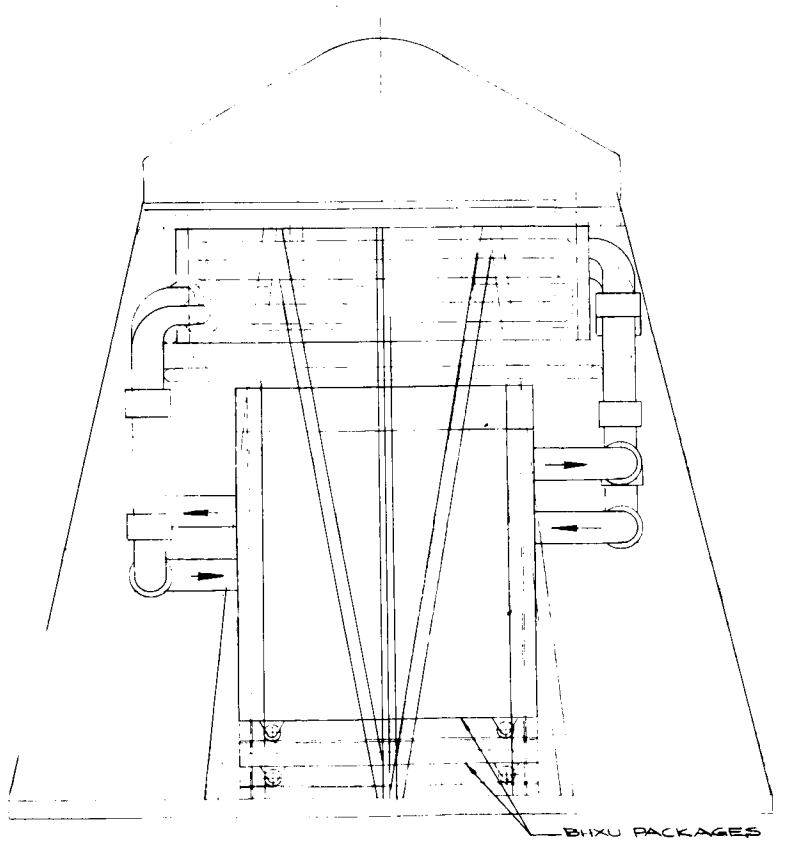

FOLDOUT FRAME 1

FOLDOUT FRAME 2

ELD

ULATION

T SOURCE
T EXCHANGER

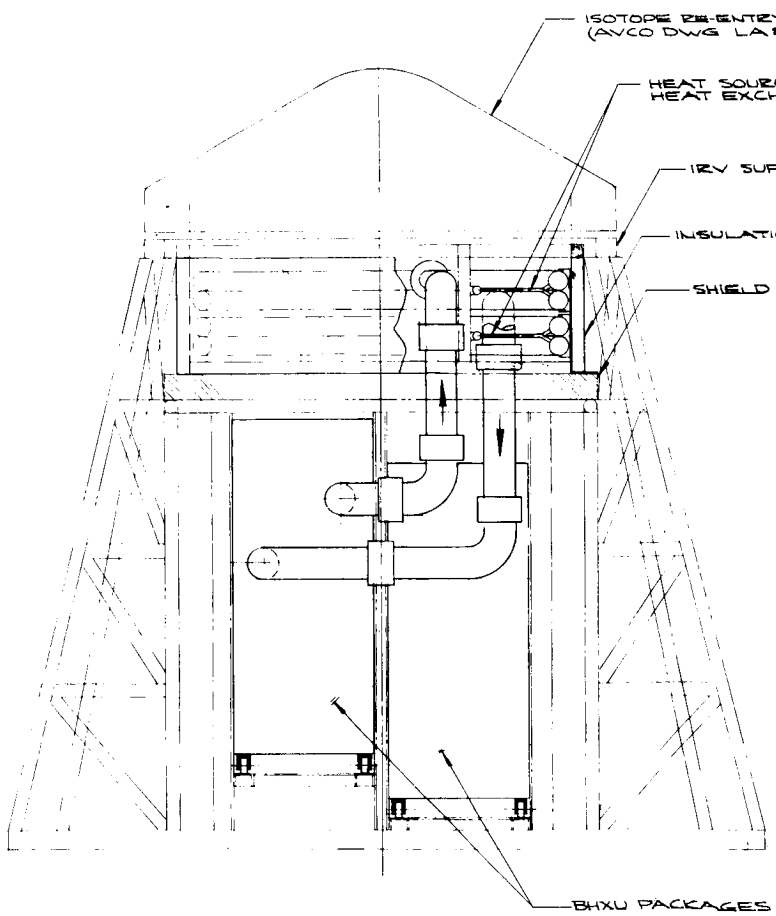

CONICAL - 60° CONE
CENTRAL RECOVERY AIDS
62.00 DIA SOURCE
TUBE-FIN HEAT EXCHANGER
SYSTEM NO. 4

SIZE	CODE IDENT NO.	DWG NO.
	70210	SK 51438
SCALE 1/10 UNLESS NOTED		SHEET 1 OF 1

FOLDOUT FRAME 3

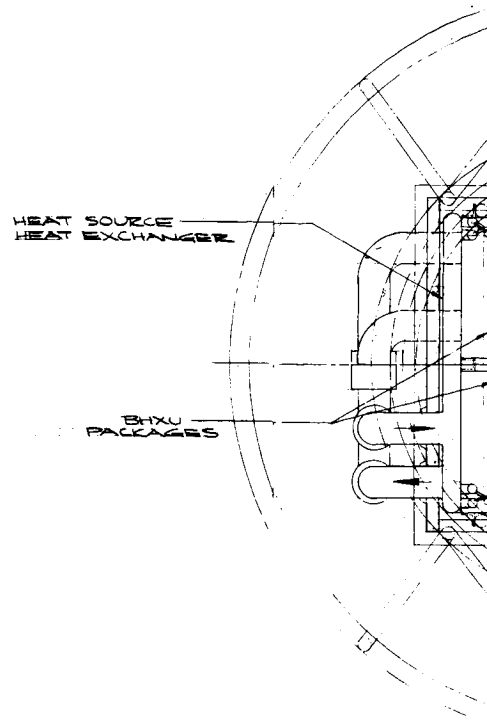

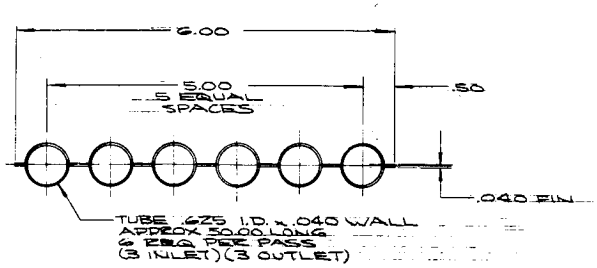

A-A
(TYP 3 PASSES)
SCALE: 1/1

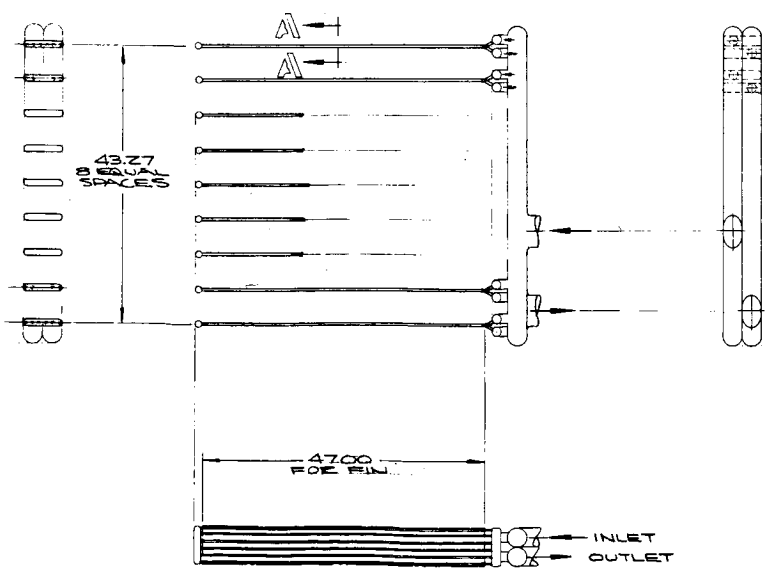

HEAT SOURCE
HEAT EXCHANGER DETAIL

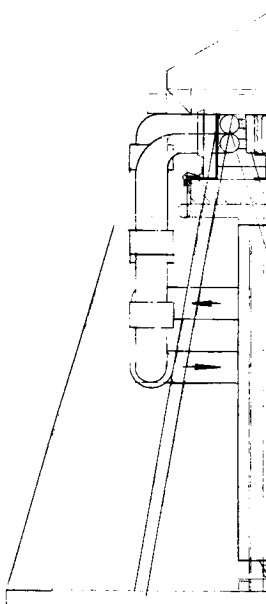

FOLDOUT FRAME /

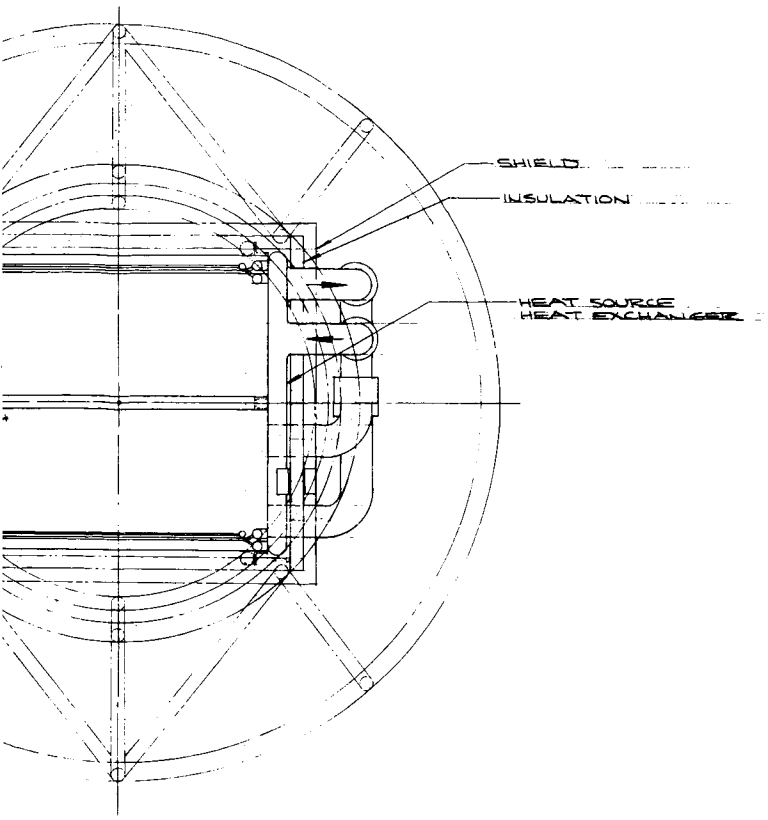

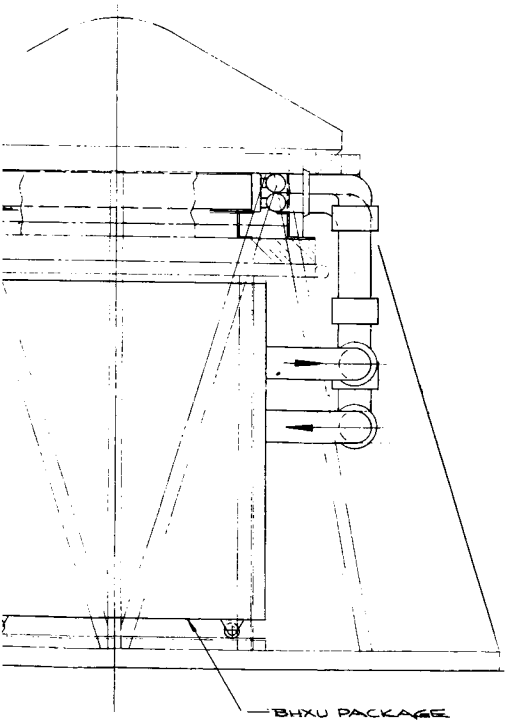

FOLDOUT FRAME 2

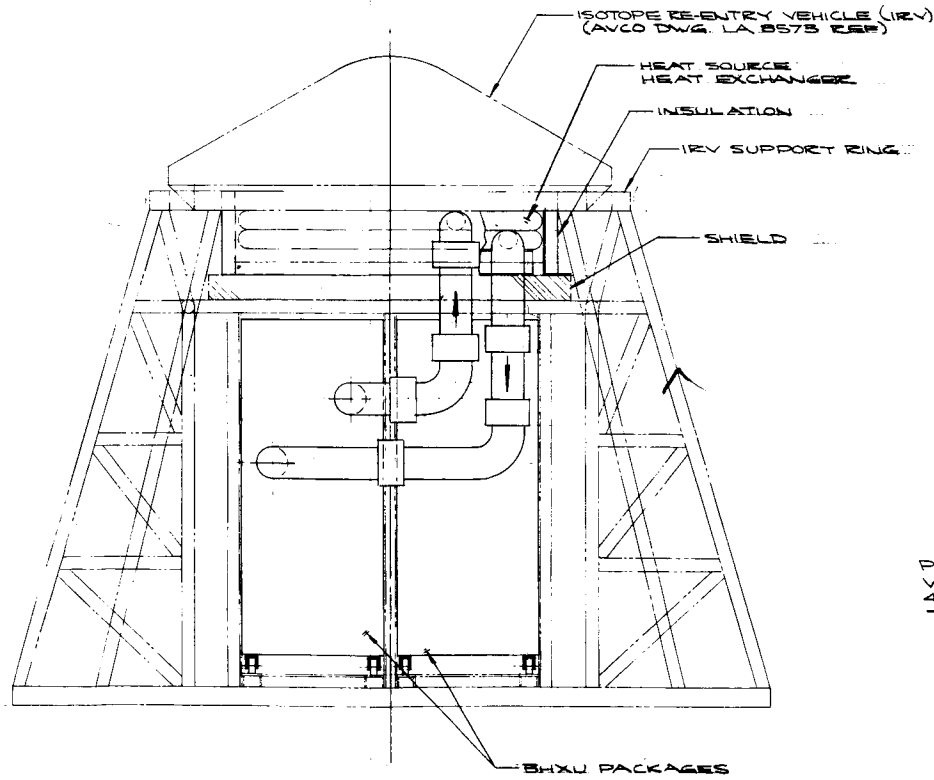

PIN CUSHION
WITHOUT RECOVERY AIDS
40.00 x 48.00 SOURCE
TUBE-FIN HEAT EXCHANGER

SYSTEM NO. 5

	70210	UK 51439
SCALE		SHEET 1 OF 1

FOLDOUT FRAME 3

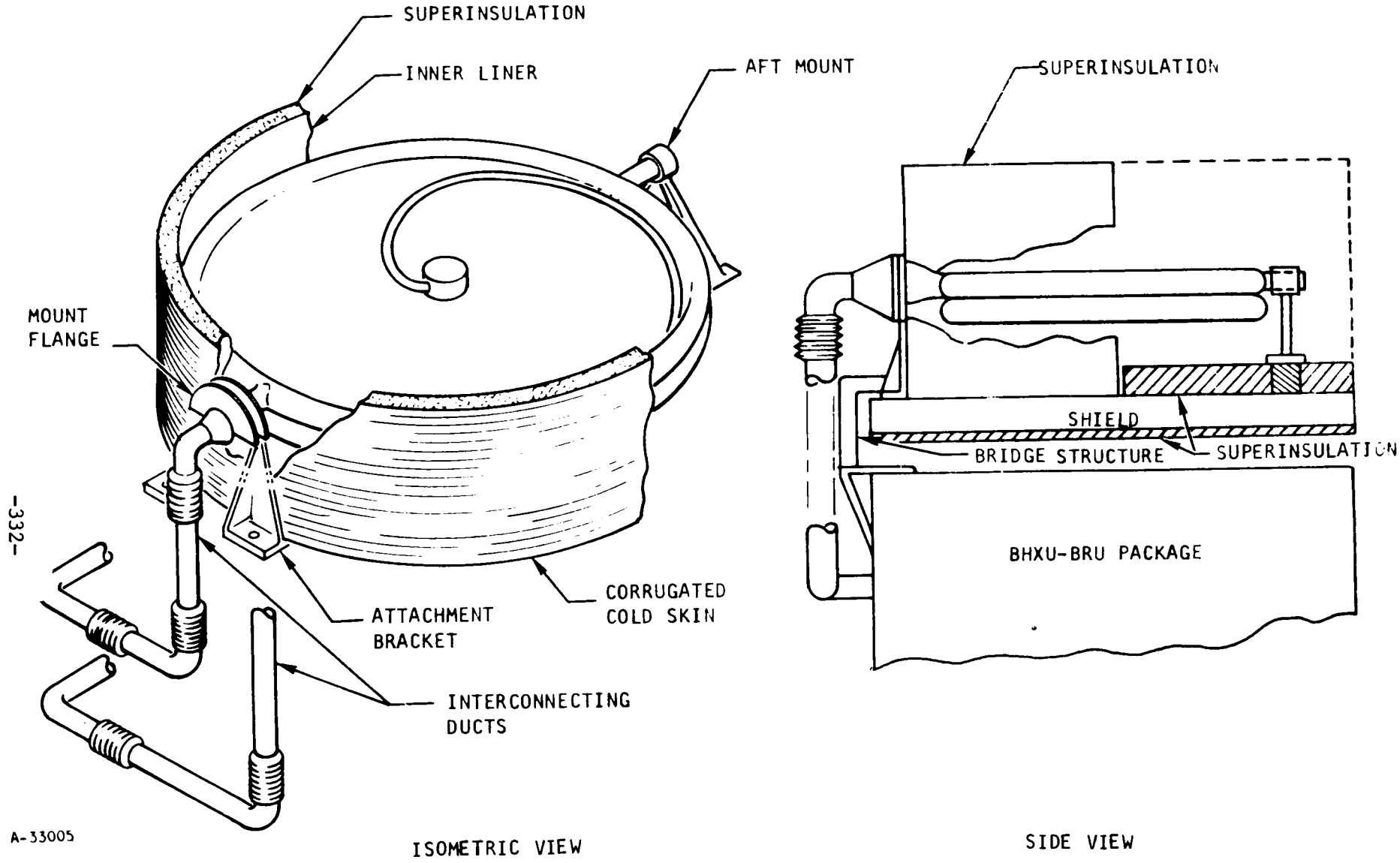

Figure 5.2-61. HSHX Assembly and Mounting

FOLDOUT FRAME

1. STRAIGHT DUCT WITH SINGLE BELLOWS

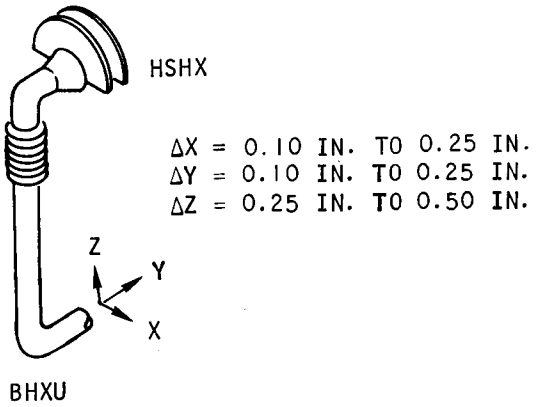

- EQUIV AXIAL MOVEMENT ≅ 1.0 IN. TO 1.5 IN.
- BELLOWS MUST BE FLEXIBLE
- PIPE END JOINTS MUST RESIST PRESSURE FORCES ≅ 700 LB
- SEVERE BELLOWS SQUIRM PROBLEM
- BELLOWS MUST HAVE LOW SPRING RATE

2. OFFSET BEND WITH 3 GIMBAL JOINTS

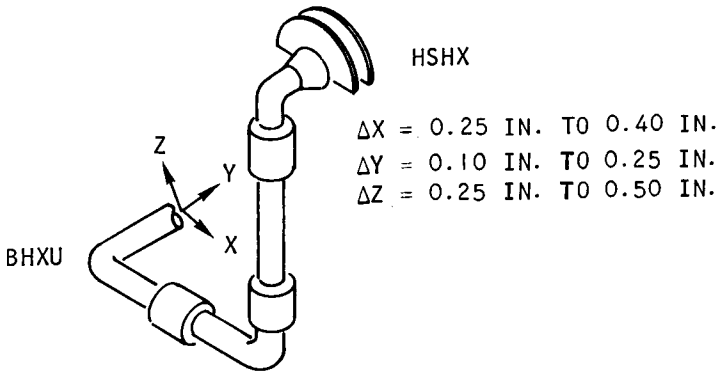

- OFFSET PIPING BEHAVES AS A 3 HINGE MECHANISM
- EQUIV AXIAL BELLOWS MOVEMENT = 0.75 IN.
- PRESSURE LOADS CONTAINED BY GIMBAL STRUCTURE
- BELLOWS MAY HAVE HIGH SPRING RATE
- LOADS AT BHXU AND HSHX DUE TO THERMAL MOVEMENTS ARE SMALL

A-33004

Figure 5.2-62. Interconnecting Ducts

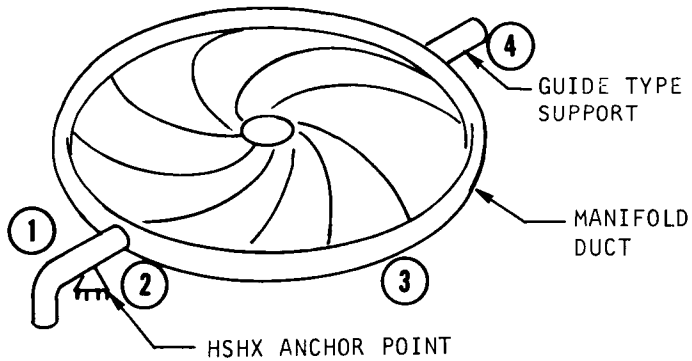

INVOLUTE TUBE ARRAY - ANALYZED AS AN EQUIVALENT ISOTROPIC PLATE

FUNDAMENTAL FREQUENCY = 59.5 CPS
PLATE BENDING STRESS = 133 PSI/G
MAXIMUM AT TUBE TO MANIFOLD JOINTS

MANIFOLD DUCT STRESSES

WITHOUT GUIDE TYPE SUPPORT

$\sigma_{①}$ = 12,600 PSI/G

WITH GUIDE TYPE SUPPORT

$\sigma_{②} = \sigma_{④}$ = 2010 PSI/G
$\sigma_{⑤}$ = 1160 PSI/G

A-33007

Figure 5.2–63. Stress Results for Two-Pass Involute

5.2.7.4 Tube-to-Fin Joint Detail

Several tube-to-fin joint concepts are shown on Figure 5.2-64. The first concept shows a flat plate with individual machined spacers. The spacers could be either welded or brazed to the tubes and the plate. This design is quite costly and heavy, and it provides an unsymmetrical heat flow from the tubes to the fin.

A second design employs bent sheet metal strips that could be welded from one tube to the next. This would be relatively weak for structural loads, and it also produces unsymmetical heat flow and poor fin-tube contact.

A third concept uses machined and formed connector strips. These strips can be welded and/or brazed between tubes for improved thermal contact. This design is readily adaptable to varying fin length. This design is structurally better than the first two designs.

Another possibility for attaining a tube-and-fin construction is to use two matching half-plates that are formed into the tubular configuration. The two half-plates would then be joined by use of spot-welding or continuous-seam welding along the fins. The concept relies upon structural integrity of the welded joints for pressure containment. A localized weld failure could lead to a progressive propagation of the separation and failure of the HSHX. The three designs shown in Figure 5.2-64 do not rely on welded joints or seams for pressure containment, and hence they would inherently have better reliability than a welded construction.

5.2.8 HSHX Insulation Study

The main areas to be insulated are the heat exchanger cavity, inlet and outlet ducts to both heat exchangers, and structural supports to heat exchangers.

Super Insulation, a product of the Linde Division of Union Carbide Corporation, has been selected as a candidate insulating material for the heat exchanger cavity. The thermal conductivity of the Super Insulation is at least one order of magnitude less than that of any of the available conventional insulating materials. Moreover, Super Insulation systems have shown excellent performance while withstanding rigorous conditions of mechanical shock, vibration, and severe radiation and temperature environments.

The principal parts of a Super Insulation system are the vacuum envelope, mechanical support members, reflective shields, fibrous separators, and either getters or adsorbents for vacuum maintenance. As shown in Figure 5.2-65, the Super Insulation itself consists of reflective shields (A) and fibrous separators (B or B-1), all of which are usually held in a vacuum (see Reference 39).

(A) A moderate number of oriented, highly reflective shields are used to minimize the flow of radiant energy. These shields are constructed from aluminum foil for low- or moderate-temperature regions of the insulation system, and copper, nickel, gold, tantalum, and other high-melting-point metals in high-temperature regions. The shields are as thin as is mechanically practical, to permit minimum weight and flexible contour-fitting of the finished insulation.

1. ATTACHMENT TO FLAT PLATE WITH MACHINED SPACERS

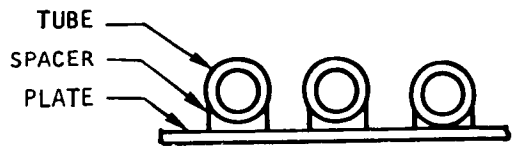

- COSTLY
- HEAVY
- NONSYMMETRIC HEAT FLOW

2. BENT STRIPS BETWEEN TUBES

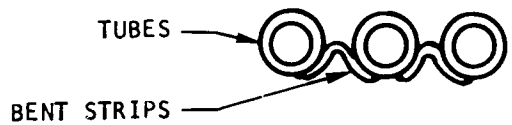

- STRUCTURALLY WEAK
- NONSYMMETRIC HEAT FLOW
- POOR FIN CONTACT

3. MACHINED & FORMED CONNECTOR STRIPS

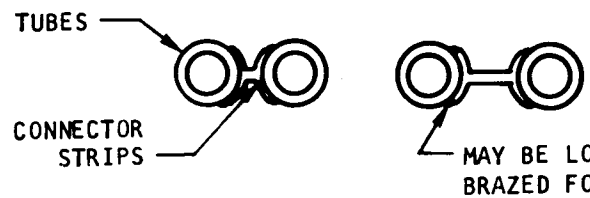

- STRUCTURALLY ADEQUATE
- SYMMETRIC HEAT FLOW
- GOOD FOR ANY TUBE SPACING

A-33000

Figure 5.2–64. Tube-to-Fin Joint Details

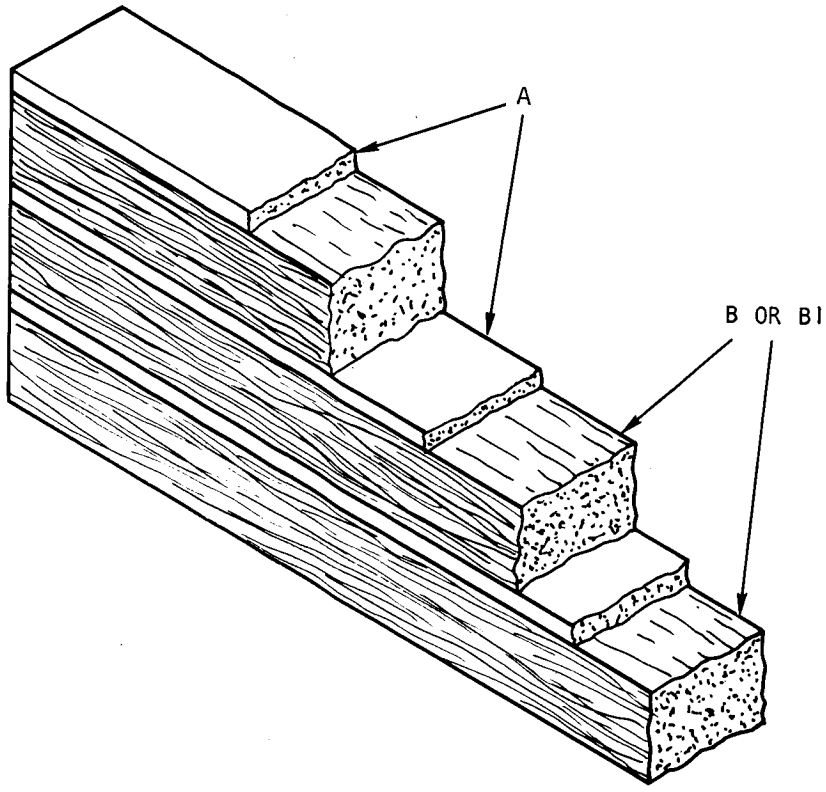

A-33322

Figure 5.2–65. Schematic Diagram of Superinsulation Shows Alternate Layers of Foil (A) and Fibrous Mats (B or B-I)

(B) Fibrous separators of glass fiber at low temperature levels, or quartz, at high temperature levels, separate the shields. Other ceramic fibers and crystals have also been used and are being investigated further for application as high-temperature separators. Thin fibers are used to reduce the area of the contact points, thus increasing the length of conduction paths through the fibers. In addition, smaller voids are produced this way, minimizing residual gaseous condition.

(B-1) Special fibrous mats of the materials mentioned, containing a uniform dispersion of minute metallic flakes, have been developed by Union Carbide Corporation to impede radiant as well as conduction heat flow. These flakes are secured and effectively isolated from one another by the individual fibers in the mat. The resulting arrangement has a solid conductance equivalent to that for a plain mat, coupled with a much higher resistance to radiant energy flow. The thermal performance of Super Insulations containing opacifiers in place of plain fibrous mats is thus appreciably improved. In addition, the unique thermal impedance property of opacified fibrous mats is utilized to advantage, with different foil arrangements, in facilitating insulation applications. The opacified mats contain flakes from copper, nickel, or other high-melting-point materials for high temperatures.

Thermal conductivity performance data for load-bearing and non-load-bearing Super Insulation is presented in Figure 5.2-66. Load-bearing insulation has higher thermal conductivity, due to an increased solid conduction. This difference is less significant at the higher temperatures, where radiation becomes a dominant mode of heat transfer.

The Super Insulation is mounted on the inner surface of the boundary of the HSHX cavity and will be constructed in two halves.

Flexible MIN-K 2000, a product of Johns-Manville, has been selected to insulate inlet and outlet ducts. MIN-K is a fibrous material which contains appreciable quantities of exceedingly fine particulate matter. The pore structure of MIN-K is so minute that it has a thermal conductivity lower than the molecular conductivity of still air. The thermal conductivity decreases appreciably at higher altitudes. For example, Figure 5.2-67 shows that the conductivity decreases at an altitude of 10 miles, by as much as 50 percent. This characteristic is directly attributable to the extremely small pore size of MIN-K. Figure 5.2-68 shows the thermal conductivity of MIN-K 2000 versus temperature in air, helium, and hydrogen.

A thickness of 2-1/2 in. of flexible MIN-K 2000 was estimated to be satisfactory for the insulation of the ducts and to cover the flanges (see Figure 5.2-69). The MIN-K will have stainless steel with gold coating as a facing material. This will decrease the heat lost by radiation to the environment.

A thickness of 1 in. of asbestos is used between the flanges of the inlet and outlet ducts to reduce the heat conducted along the tube walls. While the HSHX is not in operation, the asbestos minimizes the heat conducted to the BHXU. The supports of the BHXU act as heat leaks, dissipating the small amount of heat conducted to the BHXU through the ducts. Hence no significant temperature rise will occur in the inoperative BHXU unit.

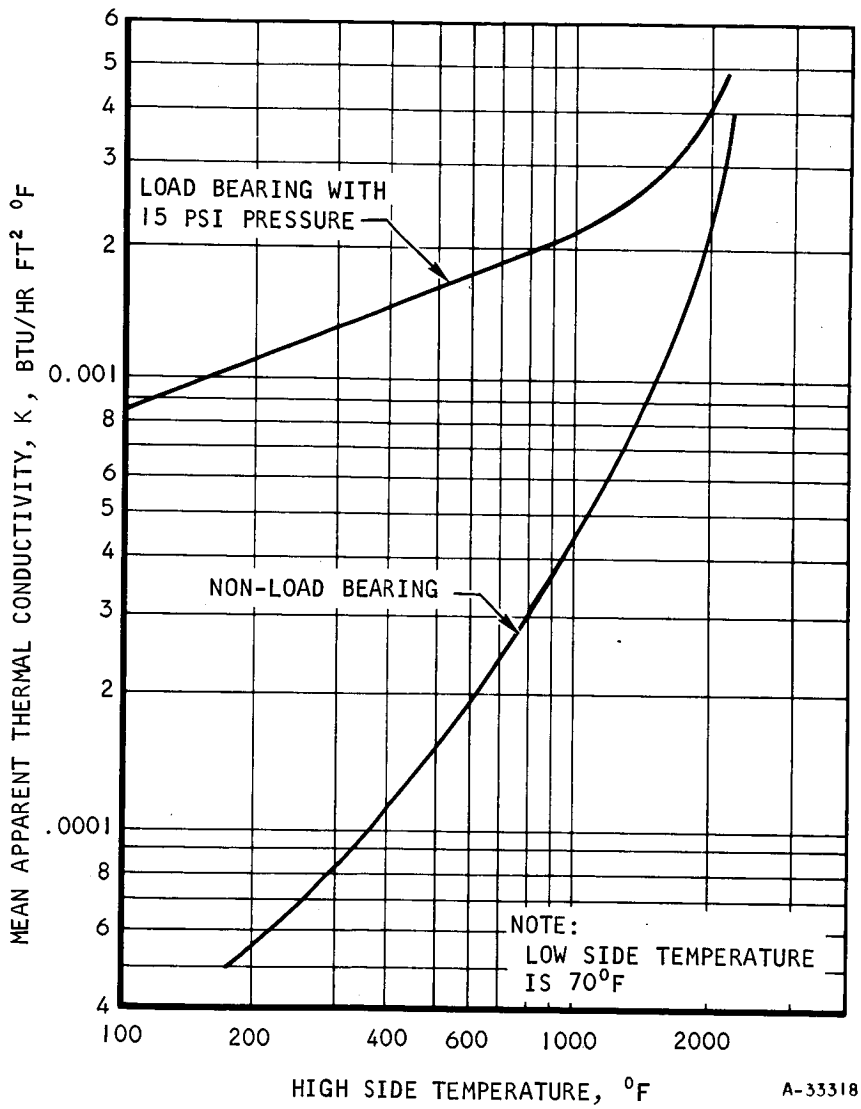

Figure 5.2-66. Thermal Conductivity vs Temperature as a Function of Bearing Load

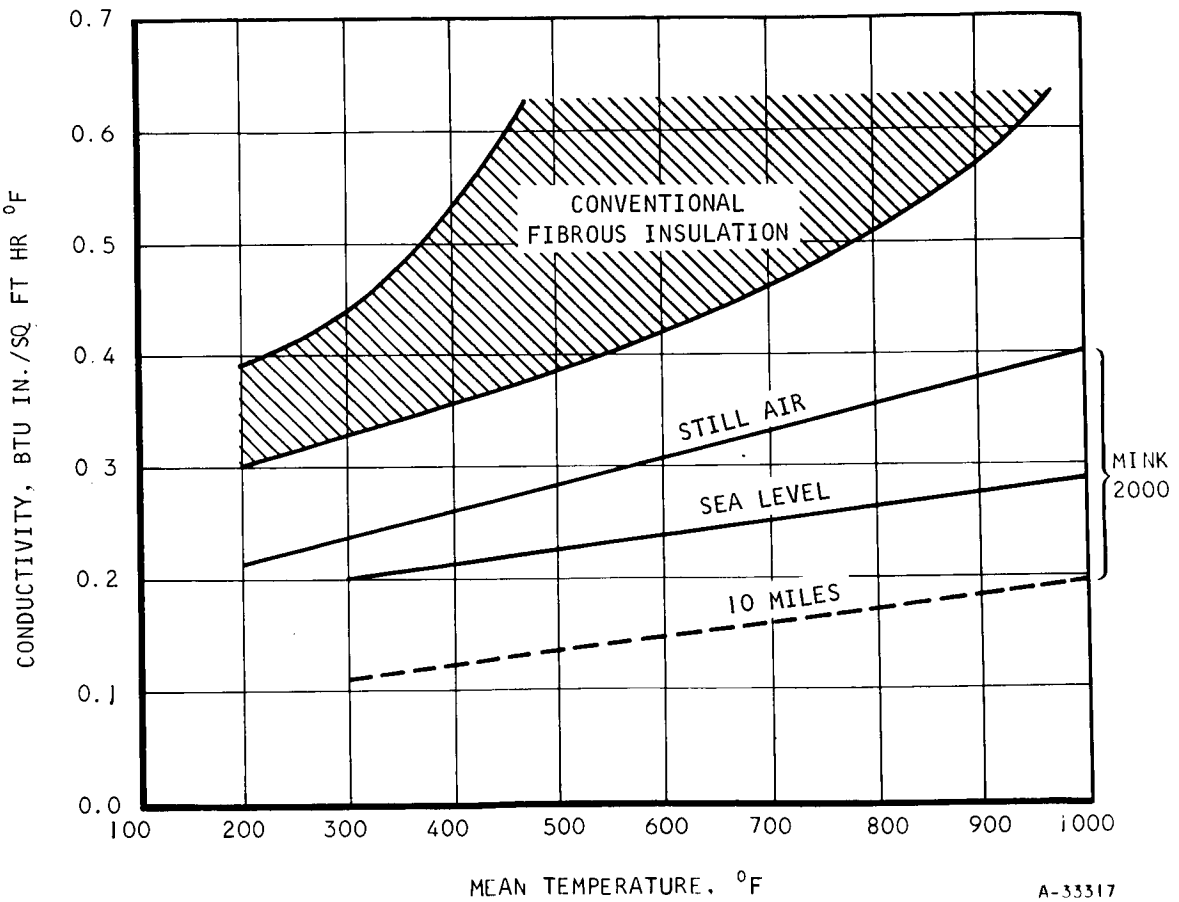

Figure 5.2–67. Thermal Conductivity Comparison

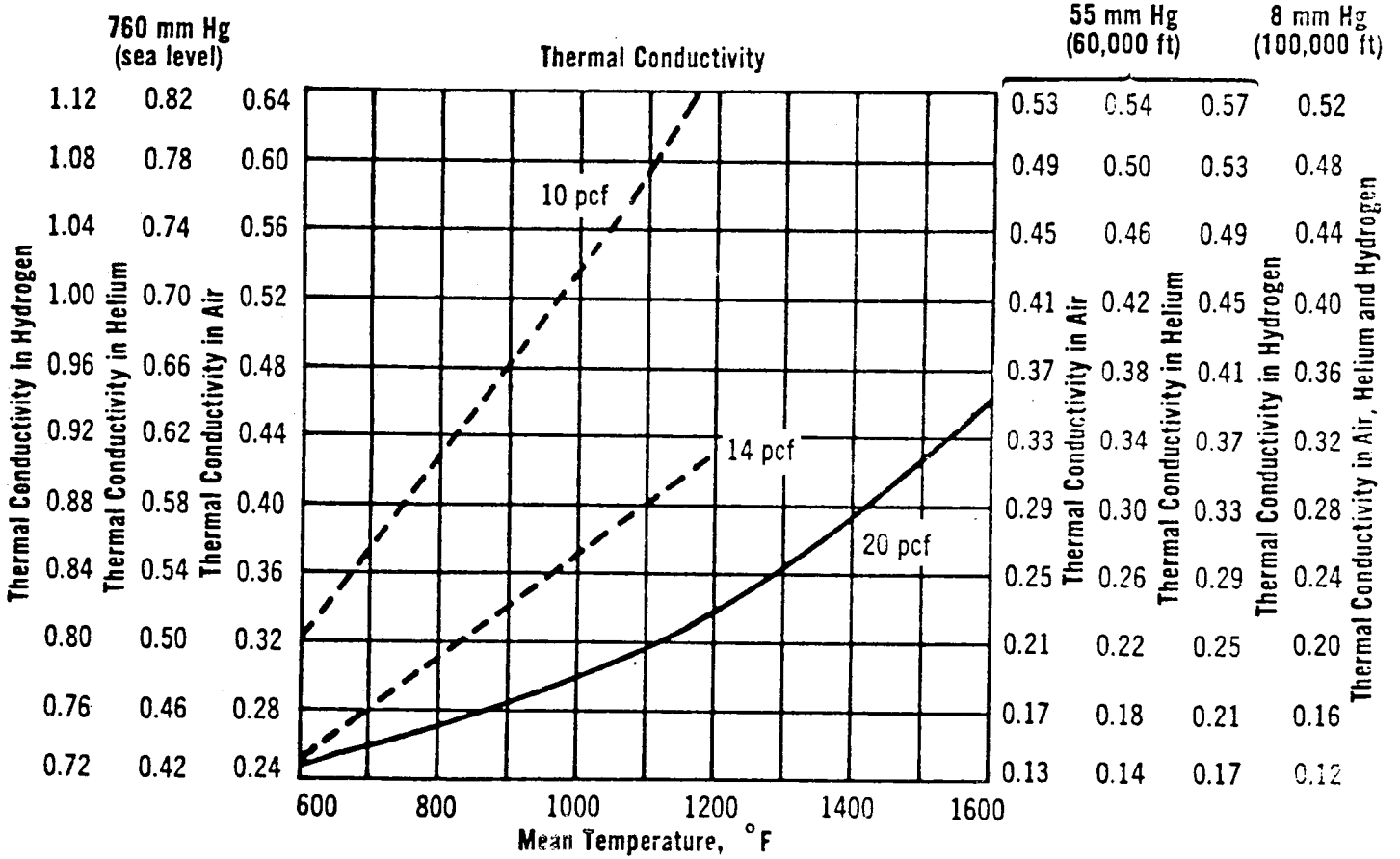

Figure 5.2–68. Thermal Conductivity of Min-K 2000

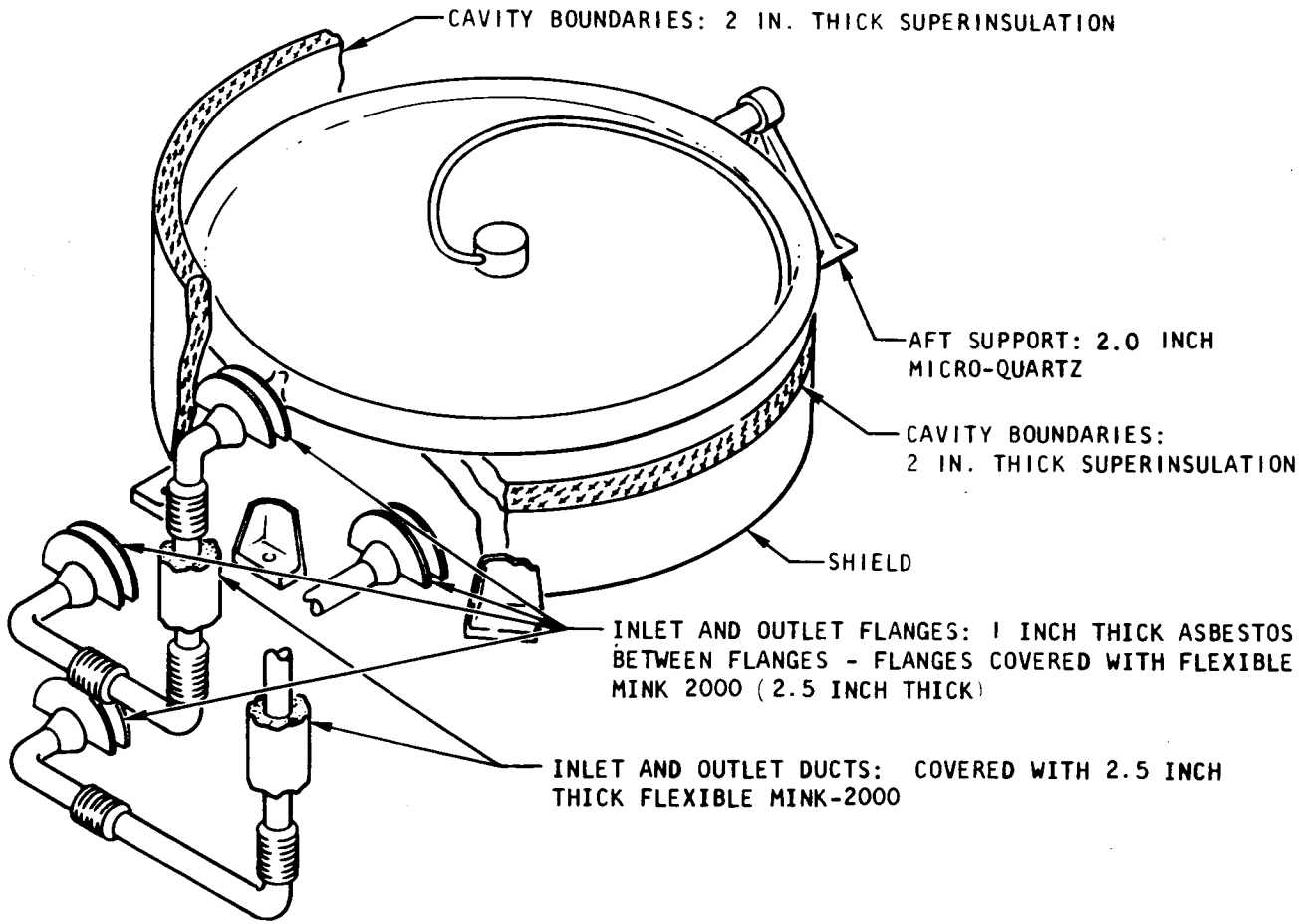

A-33006

Figure 5.2–69. Assumptions for Heat Leak Estimates

Figure 5.2-69 shows the various areas of heat leaks, and Table 5.2-IV lists the magnitude of these leaks for the various systems considered. The heat leaks given in this table do not include those associated with the mating surfaces of the removable portions of the Super Insulation (i.e., the insulation which is attached to the HSHX). One approach to this problem is illustrated in Figure 5.2-70, where there is a fixed piece of Super Insulation between the radiation shield and the IRV, which has two large openings, one on each side, to accept the HSHX's. The insulation on the individual HSHX's is sized to overlap the fixed insulation attached to the vehicle at all boundaries, thus completely sealing the cavity. The amount of overlap and the associated heat leaks will be determined by the specific IRV mounting and attachment scheme, and will be determined at a later date.

TABLE 5.2–IV

ESTIMATED HEAT LEAK

		Heat Leak (w) to 0°F Environment				
System	Geometry	Cavity Boundaries	Aft Support	Flanges +Support	Ducts	Total
1	Circular	305	105	125	453	988
1 (plate fin)	Circular	305	105	125	453	988
2	Rectangular	234	105	118	427	884
2 (plate fin)	Rectangular	234	105	118	427	884
3	Conical	305	105	125	431	966
4	Doughnut	351	87	125	453	1016
5	Pincushion	212	121	120	394	847

A-32998

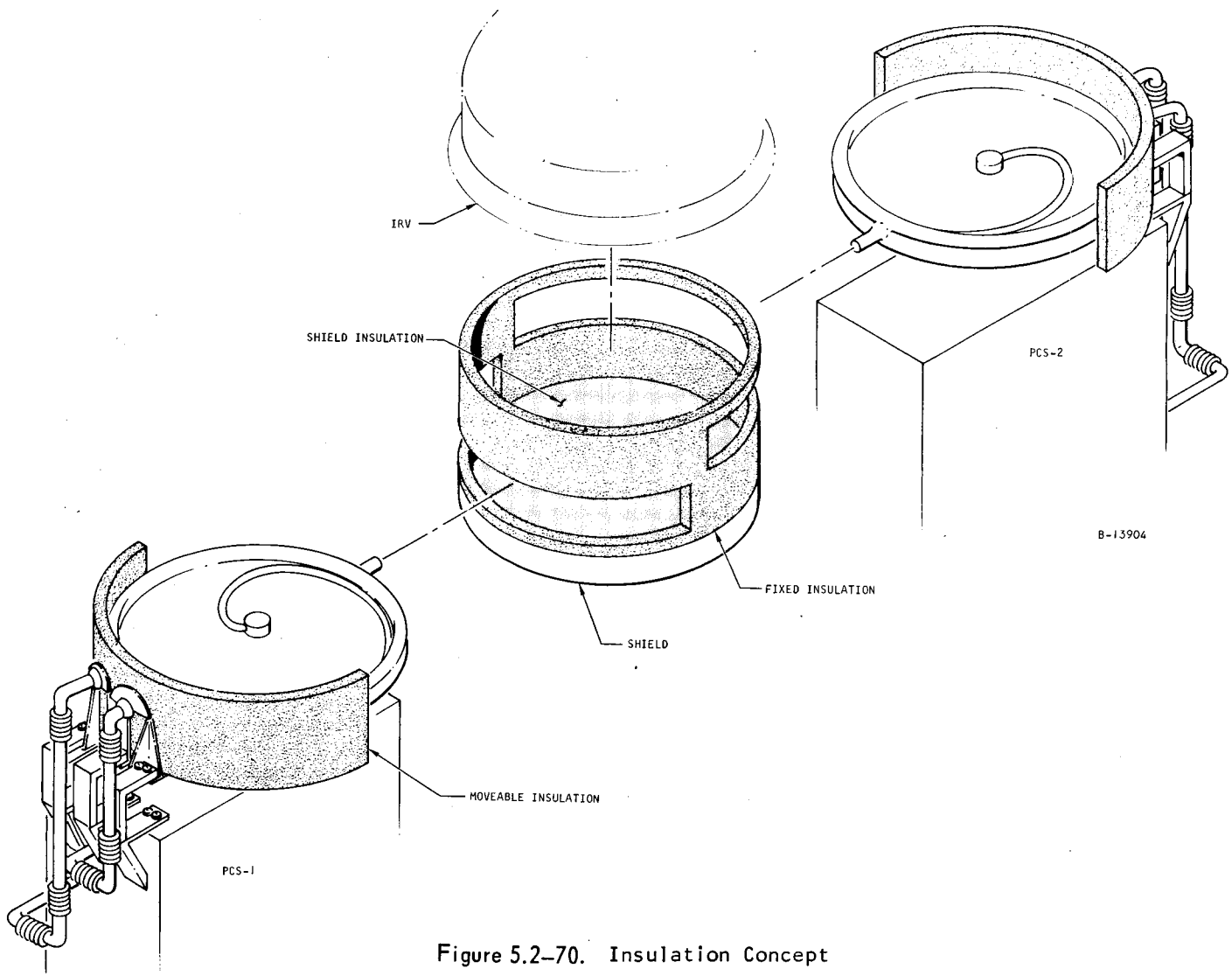

Figure 5.2-70. Insulation Concept

5.3 HEAT SOURCE SUPPORT/AEROSHELL ATTACHMENT SCHEMES

5.3.1 Design Considerations

In the selection of the heat source/aeroshell attachment method, the several controlling factors that must be considered are discussed below:

a. The design must be capable of withstanding the environmental loads. During ascent the primary loads can be transmitted either as compressive or tension (separate launch) or as shear (integral launch) and are at the level of approximately 10 g's. During entry the significant loads are axial and reach 32 g's (with a 1.25 safety margin).

b. The heat leaks must be kept to acceptable levels and in addition temperatures throughout the design (including the aeroshell interface) must be compatible with the materials used.

c. The possibility of the support system causing catastrophic failure of the capsules at impact should be minimized.

During the Phase IA effort four basic attachment schemes were evaluated and these are shown in Figure 5.3-1a,b,c, and d. Figure 5.3-1a,b,c, and d show the truss, peripheral, four point ring and crushup attachments schemes, respectively. The design of the crushup system will, of course, influence the relative performance of the schemes particularly in Figure 5.3-1d where the crushup itself is used for support. If the crushup material is used only locally it is very possible that this latter design would be incompatible and have to be eliminated from consideration.

In the following sections, a discussion of the structural and thermal aspects of the various designs is presented. The final section presents a summary of the advantages and disadvantages of the concepts together with recommendations. While the comments are specifically applicable to the circular planar heat source, the general conclusions reached also apply to the conical and pincushion classes of heat source configurations.

5.3.2 Structural Analyses

The four basic support concepts considered for the heat source and shown in Figures 5.3-2 through 5.3-5 were analyzed to determine preliminary sizes and weights. Sizing of the major component of each concept was necessary to evaluate the heat leakages and temperature distributions. Each concept is briefly discussed in the following paragraphs to explain the manner in which launch and reentry loads are supported.

In the truss support system, both the axial and shear loads of the heat source during launch and reentry are carried by the truss members in either direct tension or compression. These members, consequently, must be sized for both direct stress and Euler buckling under the most critical condition. In order to distribute the concentrated loads that are transmitted by the truss system over the aeroshell circumference, the truss members must be attached to a relatively stiff ring on the aeroshell. This ring must be capable of resisting both in-plane and out-of-plane bending produced by the four point loading.

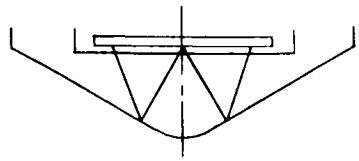

PLANAR ARRAY - TRUSS SUPPORT

(a)

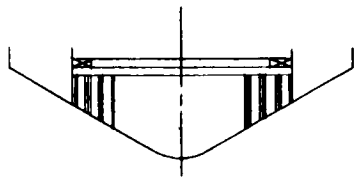

PLANAR ARRAY - PERIPHERAL ATTACHMENT AND CRUSHUP

(b)

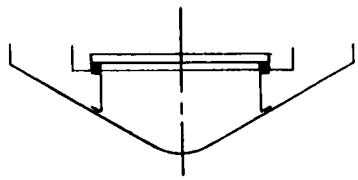

PLANAR ARRAY - PERIPHERAL RING SUPPORT

(c)

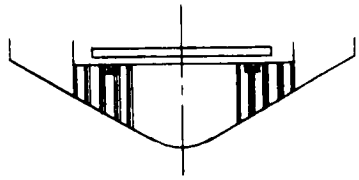

PLANAR ARRAY - FOUR POINT ATTACHMENT TO CRUSHUP SUPPORT

(d)

78-1422

Figure 5.3-1 SUPPORT AND ATTACHMENT CONCEPTS

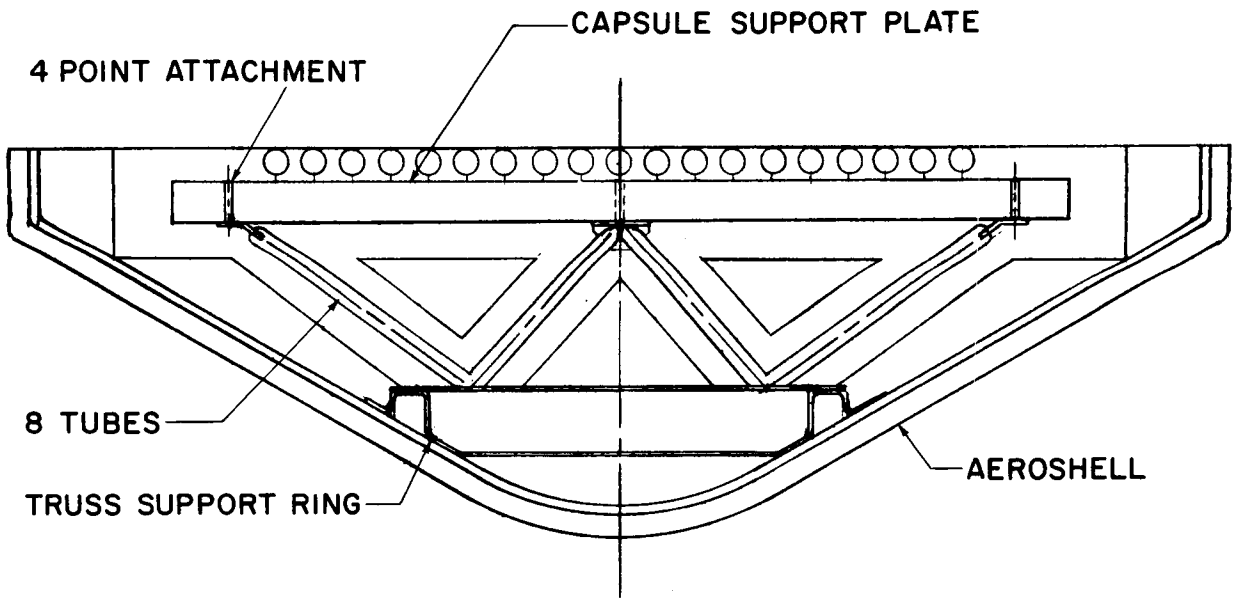

78-0065

Figure 5.3-2 TRUSS/AEROSHELL INTERFACE

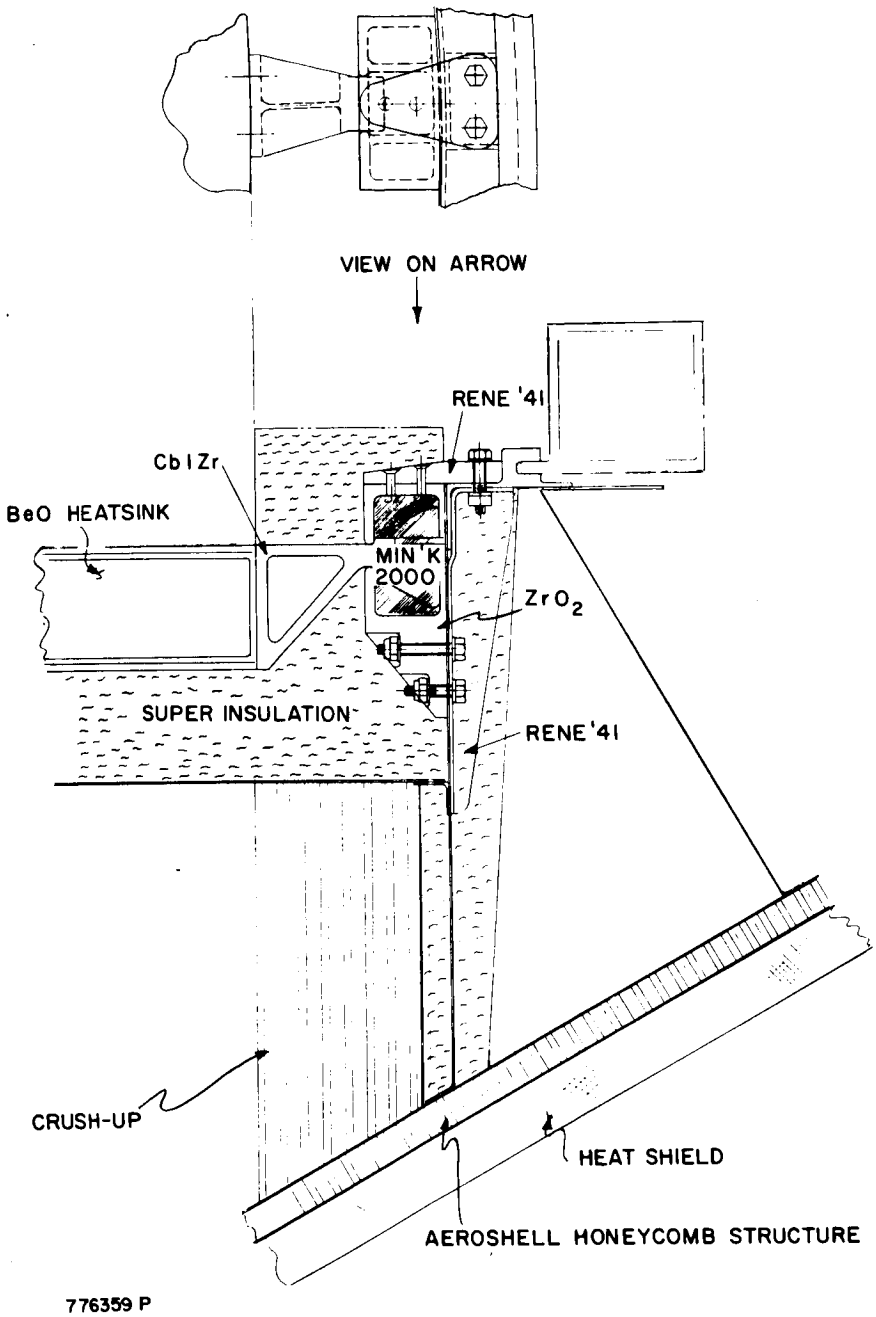

Figure 5.3-3 PERIPHERAL ATTACHMENT -- HEAT SOURCE TO AEROSHELL

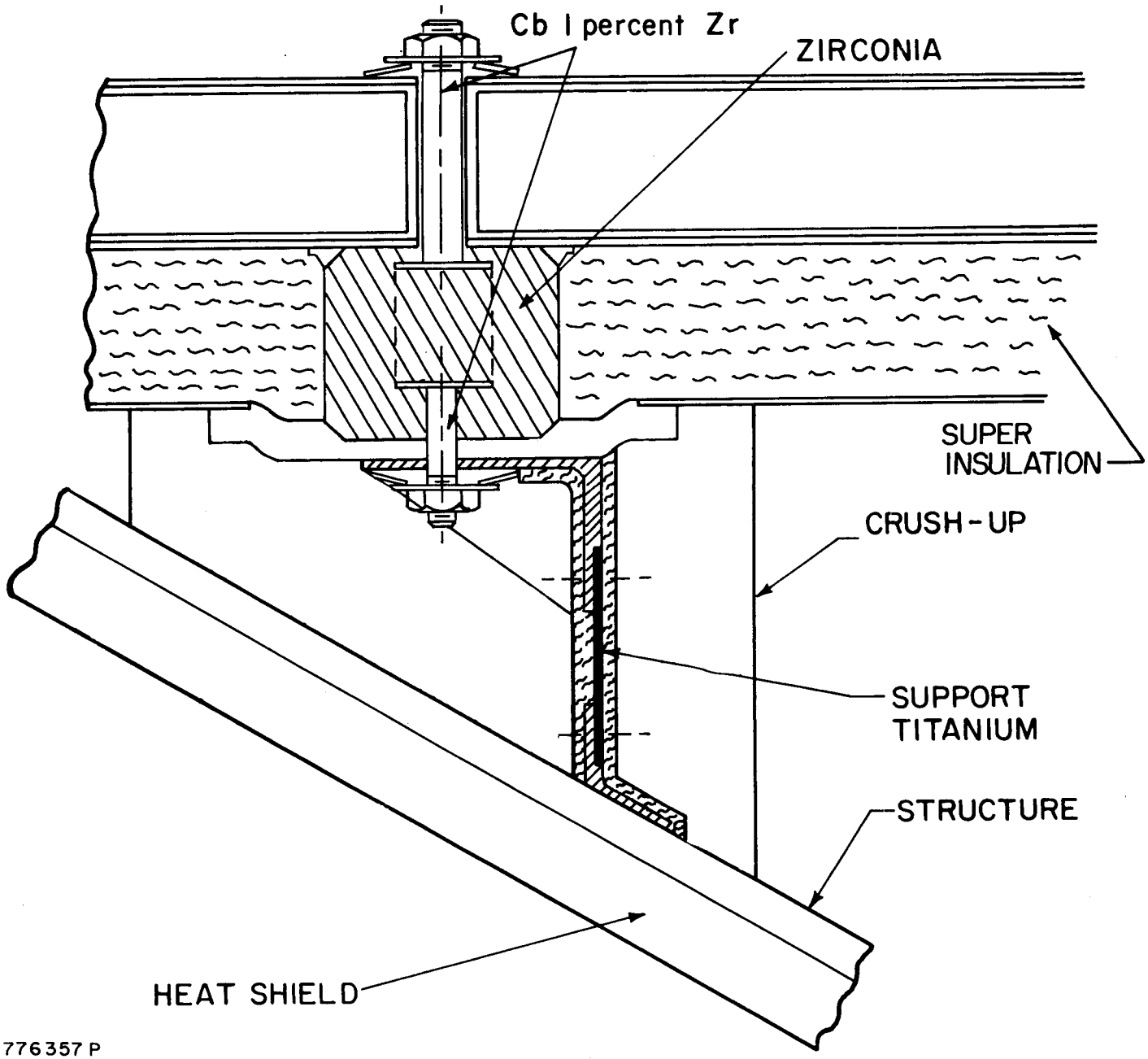

Figure 5.3-1 SUPPORT AND ATTACHMENT CONCEPTS

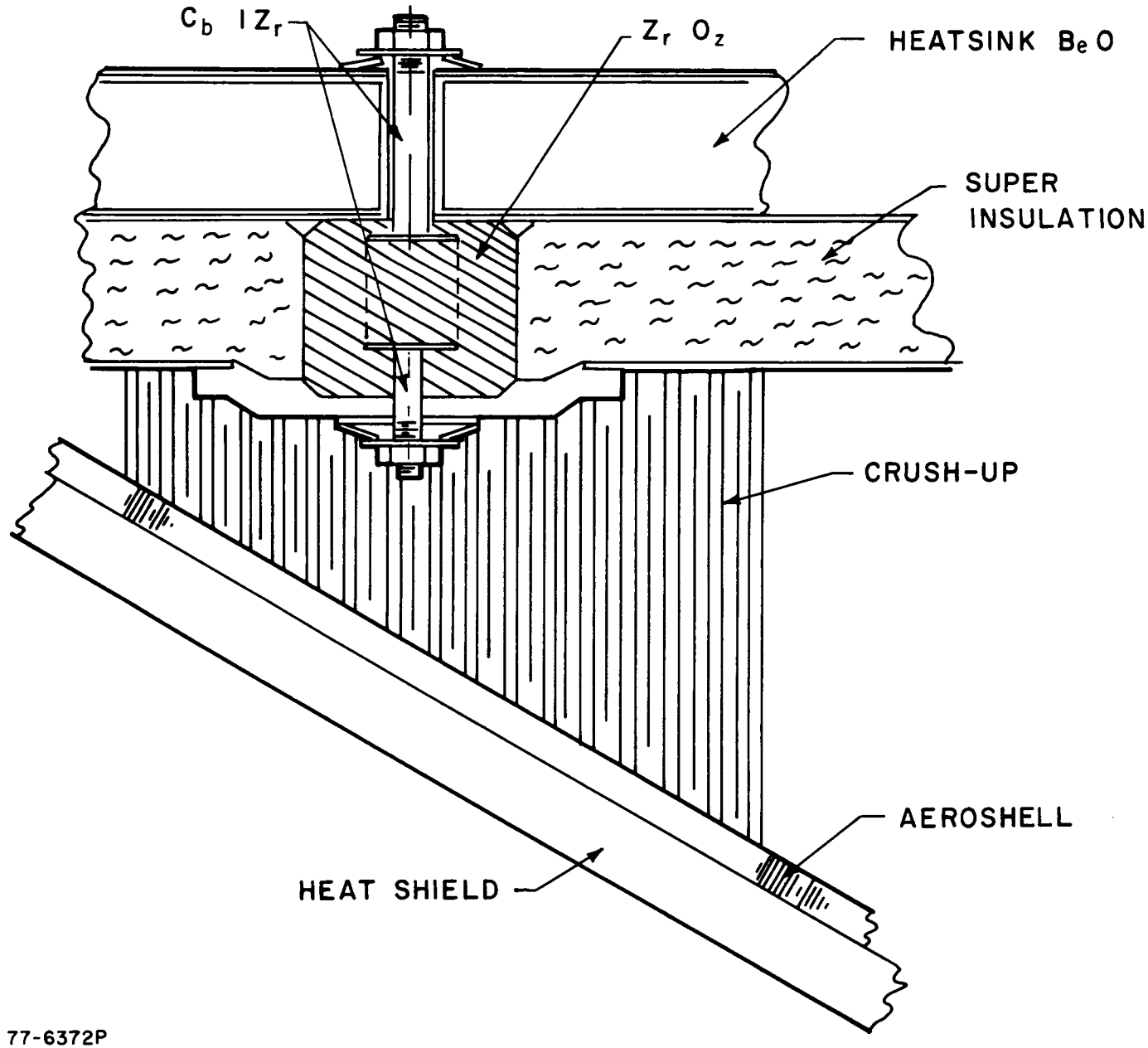

Figure 5.3-5 TYPICAL ATTACHMENT TO CRUSH-UP

The basic truss design recommended consists of an eight-leg truss system attached to the support plate and loaded to the aeroshell through a stiff ring. The truss support has been designed to withstand launch and reentry loads, but will fail at impact at the connection to the support plate, ensuring that capsule damage through "spearing" (i.e., impalement of individual capsules by truss members) will be minimized.

To minimize the heat loss through the truss support, the individual struts can be designed from two different materials. T-111 can be used in the top section where temperatures are in the region of 1800° F, and super alloy (Rene 41) can be used in the lower section where temperatures are below 1000° F. A mechanical connection is required between the two sections at this point. For a 22 in. long strut, this bi-metal joint is located approximately 15 in. from the hot end.

The inclusion of crush-up material into the support system to absorb the kinetic energy expected under impact conditions, and to reduce the high "g" loading on the heat source support plate and the fuel capsules has also been considered during Phase IA.

Figures 5.3-6 and 5.3-7 show schematics of possible truss/crushup combinations. The major pros and cons are listed below:

TRUSS SUPPORT WITH CRUSH-UP IN SERIES

Advantages	Disadvantages
1. Heat loss, 684 watts	1. Possible intrusion into heat sink or capsule at impact
2. Greater heat sink support at all conditions	2. Difficult assembly

TRUSS SUPPORT WITH CRUSH-UP IN PARALLEL

Advantages	Disadvantages
1. Heat loss, 503 watts	1. Possible intrusion into heat sink on impact may require stringent strength requirements on nose cone
2. Greater heat sink support at reentry conditions only	2. Difficult assembly

In comparison the heat leak through the eight-leg truss system is only 150 watts. The possible impact attenuation benefits achievable with the combined truss/crushup systems are only available at a significant penalty in both heat leak and IRV weight. A more efficient impact attenuation concept is described in Section 5.4 following. No further consideration will be given to combined truss/crushup support systems.

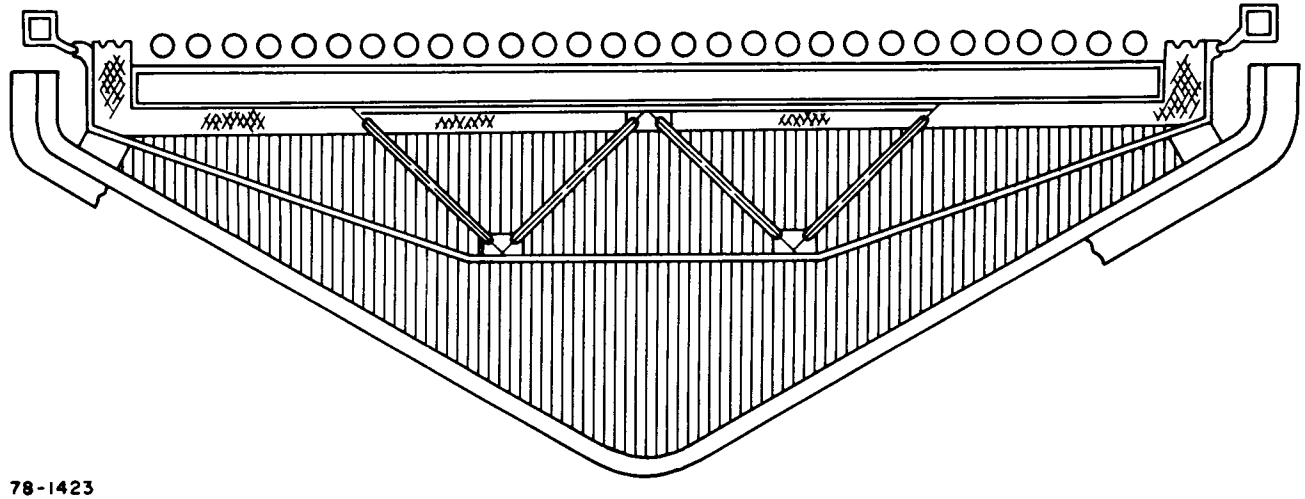

78-1423

Figure 5.3-6 TRUSS SUPPORT WITH CRUSH-UP IN SERIES

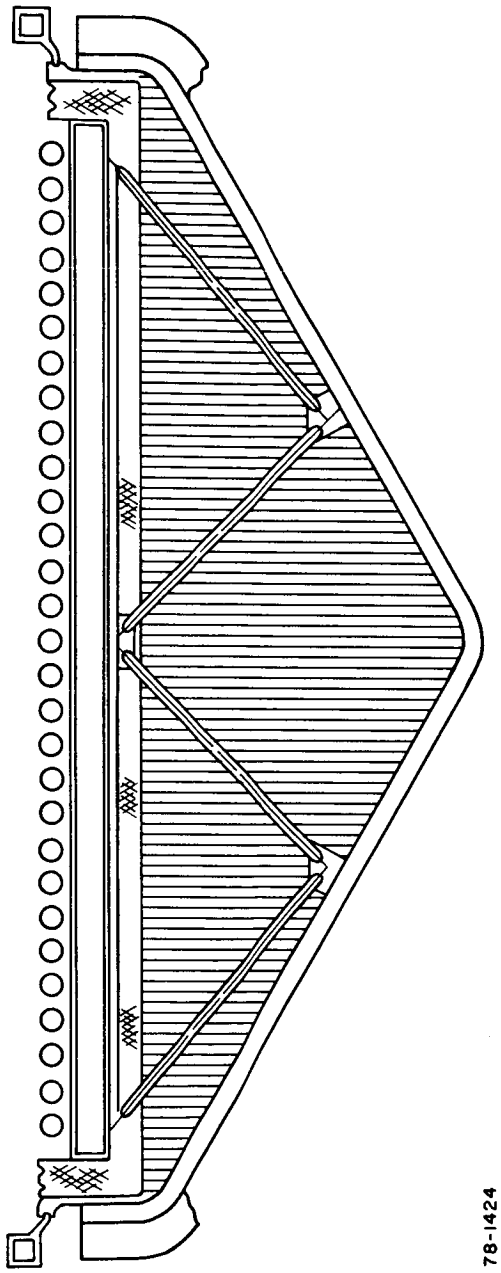

78-1424

Figure 5.3-7 TRUSS SUPPORT WITH CRUSH-UP IN PARALLEL

The peripheral support concept (Figure 5.3-3) features eight support tabs of Cb-1%Zr material on the periphery of the heat source plate. These tabs mate to a Rene 41 cylindrical support shell through an enclosed system of zirconia bearing pads. The zirconia bearing pads, while allowing free radial thermal growth, react against all axial, shear and torque loads imposed by acceleration of the heat source. The zirconia bearing pads provide both direct contact with the hot heat source structure and a sufficient temperature drop to allow the use of a shell support structure of Rene 41 which because of its lower conductivity will depress local temperatures and the overall heat leak relative to Cb-1%Zr. The Rene 41 support cylinder will carry only the reentry loads of the heat source if the reentry vehicle attachment ring is as shown in Figure 5.3-3 but would carry the launch loads as well in the event the reentry vehicle attachment ring is at the vehicle periphery. The support shell is sized for both stress and buckling under the critical load environments.

No provision for a special heavy attachment ring is required at the interface of the support shell and aeroshell as was the case in the truss concept.

A third concept (Figure 5.4-4) features the heat source supported on four zirconia bearing pads located at the plate periphery which in turn transmit loads to either a support shell or ring. The special feature of this concept is the use of the zirconia pads or spacers to carry the tensile loads during launch as well. To accomplish this, special wide head Cb-1Zr bolts as shown in Figure 5.4-4 are embedded in each end of the zirconia spacers and these bolts will fasten to both the upper heat source structure and the lower support shell or ring.

Launch acceleration loads applied in the direction of the reentry vehicle center line will be resisted by tensile forces in all four zirconia pads while acceleration loads applied normal to vehicle center line will be carried by the pads in shear. Torque loads on the heat source are also resisted by the zirconia spacers in shear. During reentry, axial inertia loads due to deceleration cause the plate to bear down on these four spacers which in turn compress the support structure. Since the support structure will tend to distribute the loads uniformly, no special rigid attachment ring is required at the aeroshell.

The bolt holes in the plate would be designed to the proper tolerances and radially oriented flats would be machined on the spacers which would mate into radial tracks or ridges on the plate, such that free radial growth of the plate is not restrained whereas rigid body rotation and translation in any direction is minimized. With this system, however, only those pads that are oriented at an angle to the line of applied lateral load will resist in shear. For example, if the lateral load is applied in line with two spacers, only the two perpendicularly oriented spacers will resist shear.

The fourth concept (Figure 5.4-5) features the same ceramic spacers to support the fuel plate in the manner described for the previous four point concept but uses the crushup material instead of a support ring to transmit loads from the spacers to the aeroshell. A chordal plate with local increased thickness under the spacers is required to distribute the applied loads over a large area of the crushup. Although this system is readily capable of transmitting both shear and compression loads there may be a problem in supporting the tensile forces experienced during launch. A modification to this system which would strengthen its tensile capability would be to include tension ties between the spacer pads

and the aeroshell. This, however, would require a special rigid ring on the aeroshell to distribute the concentrated loads transmitted through the tension ties to the aeroshell. The results of the preliminary structural analyses of these four concepts are summarized in Table 5.3-I. The major components of each concept were evaluated to determine the critical load environments and then preliminary structural dimensions were computed based on the critical failure mode.

5.3.3 Heat Loss Analysis

5.3.3.1 Concept Tradeoff Study

During Phase IA a thermal analysis was performed on the four attachment schemes (Figures 5.3-2 through 5.3-5). The purpose of this analysis was to determine the heat leaks and temperatures at critical locations within the system. In some cases redesign was initiated to produce a more efficient concept. After the optimization procedure was conducted, heat leaks and temperatures for all four systems were calculated and compared. In addition an in-orbit thermal parametric study was performed using the truss as the reference design. This study provides the truss resistance required and the effects of various thermal control coatings.

Table 5.3-II presents the results of the study made to compare the various attachment schemes in terms of heat leaks. It is apparent that the truss design is the best from a thermal standpoint while the crushup concept results in rather high losses. The peripheral and four point systems are comparable but could provide significant development problems relative to the truss. The calculations were based on steady state conditions and a 2000° F heat source temperature. In cases where all heat was transfered into a local area of the heat shield (truss bases, support shells, etc. without consideration of conductive crush-up material), one-dimensional heat balances were performed using confined heat shield radiative areas such as shown for the truss in Table 5.3-III. In the cases where conduction between the structural support members and crushup material took place, (System 4) calculations were based on the total heat shield area. It is apparent that the heat loss is a strong function of geometry and materials involved in the heat path between source and sink as well as of the radiating ablator area. The data presented in this section have been generated to investigate the magnitude of heat losses for the various design concepts under comparable conditions. They should be considered relative to one another and do not necessarily represent the absolute optimum in heat path design.

5.3.3.2 Attachment Thermal Control Analysis (Truss)

Table 5.1-III shows the configuration and assumptions used in the truss tradeoff study while Figures 5.3-8 and 5.3-9 show the results. Figure 5.3-8 indicates the local temperature at the strut/aeroshell interface as a function of the resistance per strut for various environmental and surface coating characteristics. As can be seen the curves are very steep in the lower resistance regions (where we presently are) and that the effect of the sun is significant (on a hot spot basis). Figure 5.3-9 shows that while the heat leak is a strong function of the resistance it is a relatively weak function of the environment and surface characteristics. The effect of the surface absorptivity can be seen in Figure 5.3-10 with the strut resistance as the parameter. From these curves we can obtain the required strut resistance once the acceptable aeroshell structure temperature has been defined.

TABLE 5.3-I

SUMMARY OF PRELIMINARY STRUCTURAL EVALUATION OF CANDIDATE SUPPORT CONCEPTS

Attachment Support Concept	Component	Material	Critical Load Environment	Failure Mode	Structural Requirements
1. Truss Support System	Truss Members	Tantalum T-111 or T-111 + Rene'41	Reentry (A_x = 32 g's)	Compressive Yield	Area* (Cross Section) = .25 $in.^2$
	Aeroshell Attachment Ring	Aluminum	Reentry (A_x = 32 g's)	Out of Plane Bending	Box Section Ring 1.8 in. x 1.8 in. x .1 in.
2. Peripheral Attachment	Plate Tabs	Columbium 1 percent Zirconium	Saturn Launch A_n = 10 g's	Bending	Maximum Cross Section Flanges: 2.1 in. x .2 in. Web: 2.0 in. x .1 in.
	Bearing Pads	Zirconia	Reentry	Bearing Shear	Contact Area = .05 $in.^2$; Minimum Cross Section Area = .65 $in.^2$
	Top Clamping Piece	Rene'41	Atlas Launch A_x = 10 g's	Bending	Cross Section 1 in. x .30 in.
	Support Cylinder**	Rene'41	Reentry A_x = 32 g's	Buckling	R = 28.5 in. Thickness = .02 in.
3. 4-Point With Support Shell	Bolts	Columbium 1 percent Zirconium	Atlas Launch A_x = 10 g's	Tension	.5 in. Dia.
	Bearing Pads or Spacers	Zirconia	Saturn Launch A_n = 10 g's	Shear	1.3 in. Dia.
	Support Shell**	Columbium 1 percent Zirconium	Reentry 32 g's	Buckling	R = 26.5 in. Thickness = .065 in.
4. 4-Point With Crushup	Bolts	Columbium 1 percent Zirconium	Atlas Launch	Tension	.5 in. Dia.
	Pads	Zirconia	Saturn Launch A_n = 10 g's	Shear	2.0 in. Dia.
	Plate Under Pads	Steel	Reentry	Bending	Thickness = .185 in.

* Area is dependent on truss $\measuredangle$ (45° $\measuredangle$ assumed here).
** Will require a cap ring and additional stiffeners to distribute point loads over complete support shell.

TABLE 5.3-II

SUMMARY OF HEAT LEAK DATA ON IRV VEHICLE 47-INCH-DIAMETER PLANAR HEAT SOURCE

ATTACHMENT SYSTEM		SEAL AND SUPERINSULATION HEAT LEAK (WATTS)	BRAYTON CYCLE SYSTEM HEAT LEAK (WATTS)	TOTAL HEAT LEAK (WATTS)
METHOD	HEAT LEAK (WATTS)			
1. TRUSS	150	250	990	1390
2. PERIPHERAL	250	250	990	1490
3. FOUR POINT	200	250	990	1440
4. CRUSHUP	700	250	990	1940

78-0006

TABLE 5.3-III

SUMMARY OF ASSUMPTIONS AND CONSTRAINTS

1. Assumptions

Heat source temperature	$t_1 = 2000^{\circ}$ F
Thermal model (typical for truss concept)	One-dimensional conduction through attachment system section of AL - support ring, Al - Honeycomb and low density ablator.

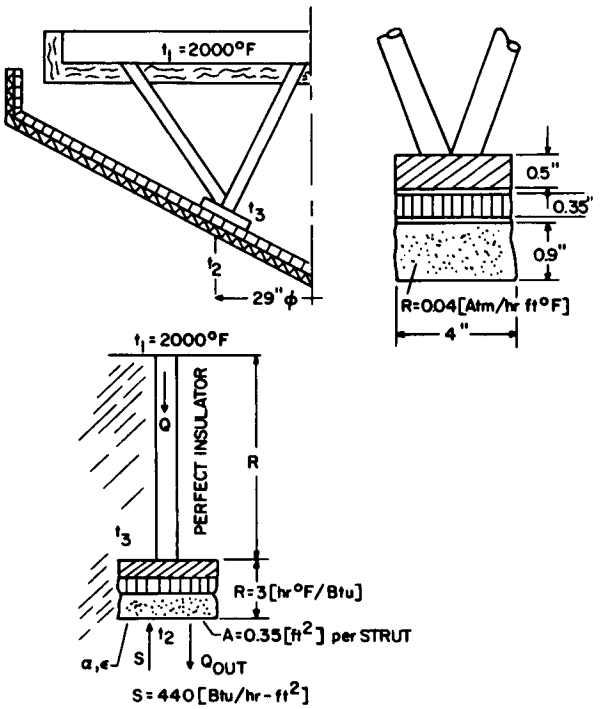

External thermal environment	a. Full-time space exposure b. Full-time sun exposure, sun perpendicular to surface ("worst case"); earth thermal effects neglected.
Aeroshell coating	a. No coating: $\alpha = 0.6$; $\epsilon = 0.9$ b. Undegraded coating: $\alpha = 0.2$; $\epsilon = 0.9$ c. Degraded coating: $\alpha = 0.4$; $\epsilon = 0.9$ "Stable" white coating (zinc oxide/potassium silicate)

2. Constraints

Design temperature (aeroshell)	Maximum: 300° F Preferably: 200° F

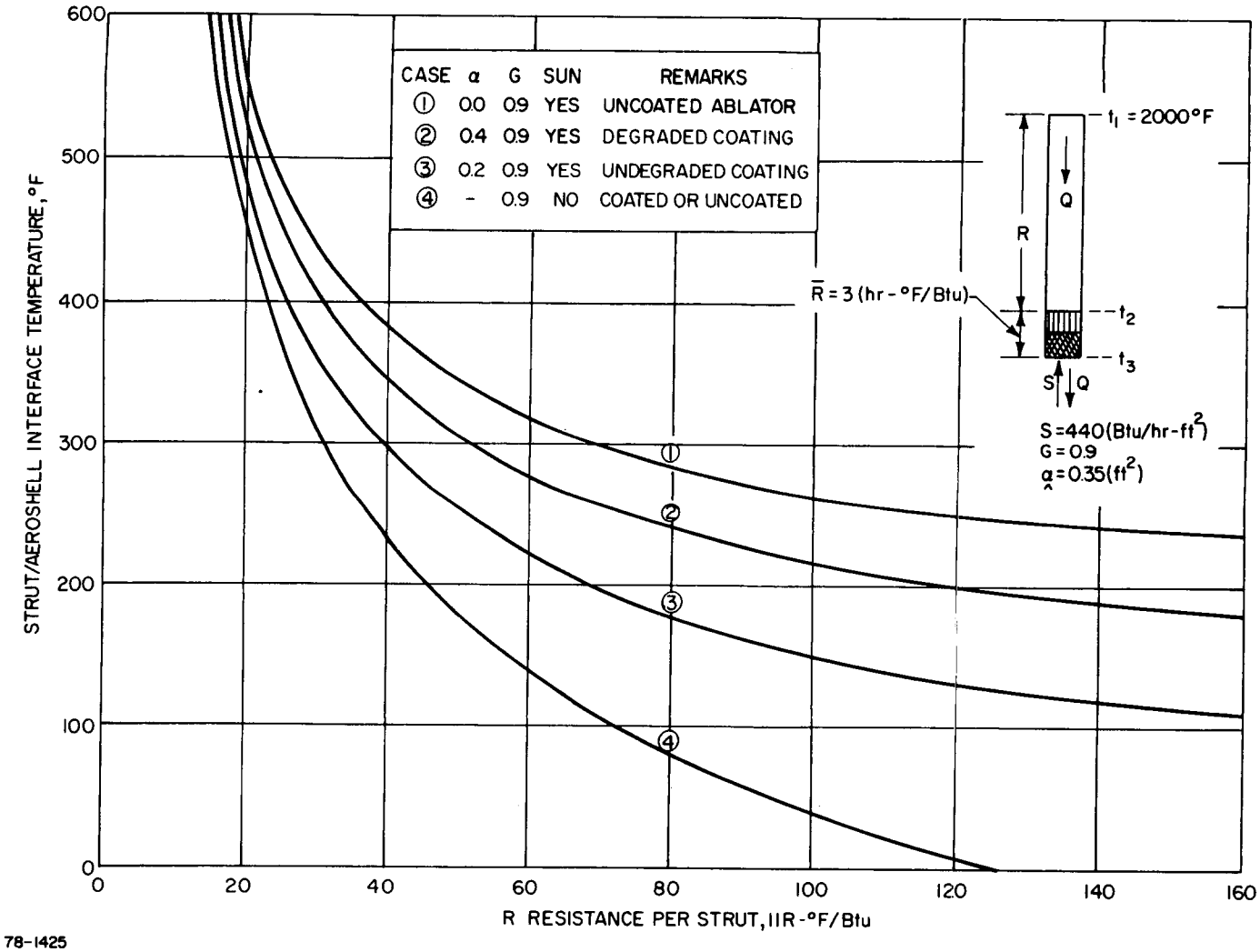

Figure 5.3-8 STRUT/AEROSHELL INTERFACE TEMPERATURE VERSUS STRUT RESISTANCE

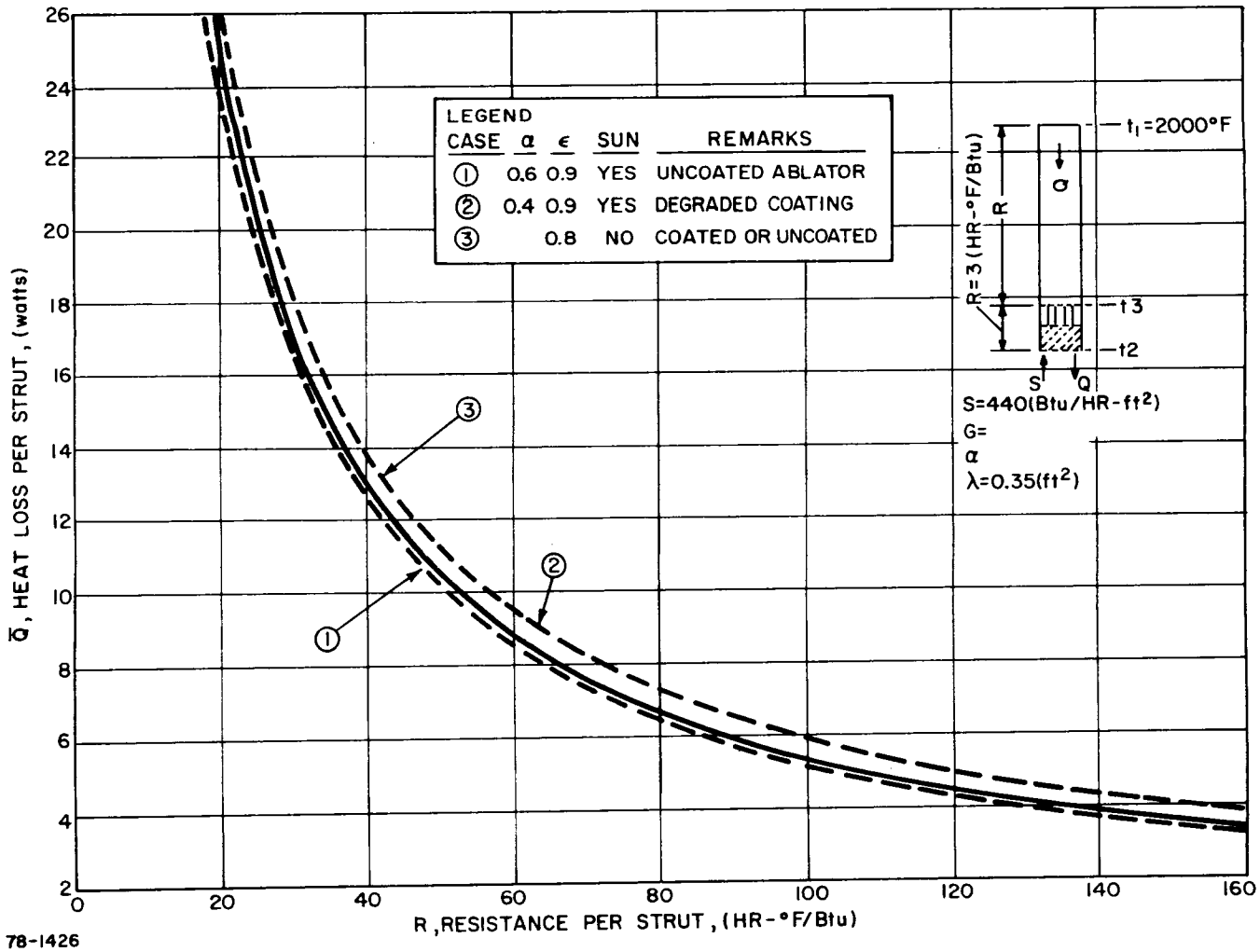

Figure 5.3-9 HEAT LOSS PER STRUT VERSUS STRUT RESISTANCE -- TRUSS CONCEPT

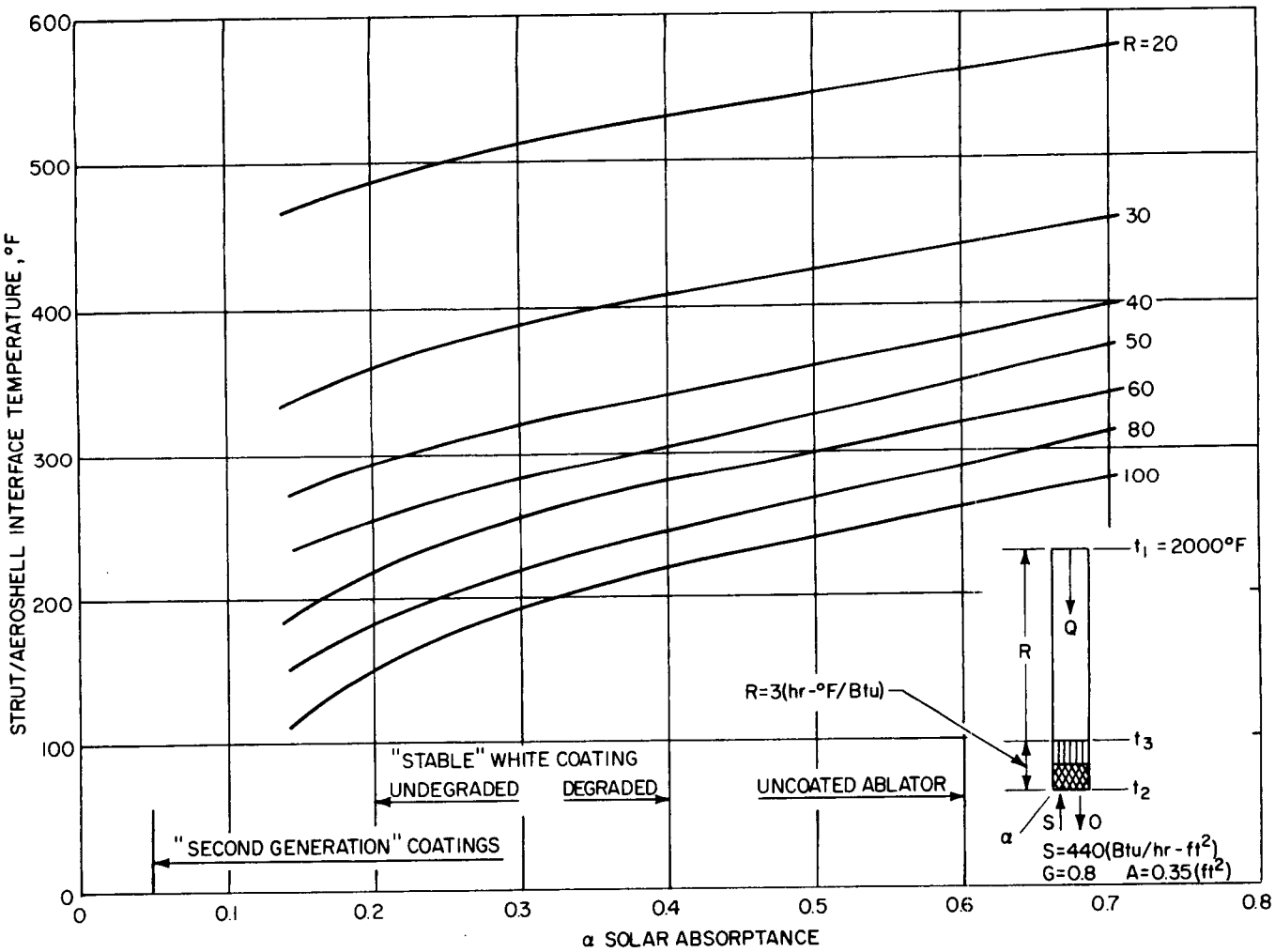

Figure 5.3-10 STRUT/AEROSHELL INTERFACE TEMPERATURE VERSUS α OF HEAT SHIELD COATING

The hot spot temperature that exists at the base or aeroshell end of the attachment points is of major concern. Considerations for limiting these hot spot temperatures include degradation in mechanical properties of both the ablator adhesive and substructure material and outgassing of the ablator itself under the long-time exposure to elevated temperatures and the hard vacuum of space. Although, in general, it is felt that 250° F is a feasible long time design temperature limitation for the candidate low-temperature ablator, ablator adhesives and substructure construction, it would be desirable to design for substantially lower temperatures (<100° F) since this would provide a more confident situation from the material standpoint and also reduce the thermal protection requirements related to the 250° F case.

The "stable" white coating (zinc oxide/potassium silicate, refs. 40 and 41) appears to be the only suitable coating at the present time. This coating has been extensively tested in space and on the ground. Properties are shown in Table 5.3-III. The coating selection may have to be revised as initial research is continuing with "second generation" thermal control coatings. These coatings consist of a silver deposit overcoated with silica in a vapor deposition process (ref. 42). The optical properties of those coatings ($\alpha \approx 0.05$, $\epsilon \approx 0.8$) would make them preferable to other coating systems.

The preceding analysis was performed for two extremes, an uncoated ablator ($\alpha = 0.6$) and an undegraded "stable" white coating ($\alpha = 0.2$). The latter case is optimistic and a literature search has indicated that the value of α is rising with degradation of the coating. Thus, an $\alpha = 0.4$ is assumed as a reasonable value for a degraded coating. This value may eventually approach that of the uncoated ablator ($\alpha = 0.6$), while the ϵ - value ($\epsilon \approx 0.9$) remains essentially constant in any case.

5.3.4 Summary

Table 5.3-IV presents a comparison of the four concepts on an overall basis. While it appears that all of the concepts are acceptable, the truss system was selected for its overall simplicity and lack of potential problem areas. The peripheral design could encounter thermal problems if the contact area and tolerances are not held very close. The four point pad system, while providing good distribution of loads to the aeroshell, provides a higher heat leak and could produce capsule degradation difficulties on impact. The crushup design has the highest heat leak of all the concepts and is only useful if the impact attenuation requirements are compatible.

Some redesign of the present truss system will be required due to the tradeoff study shown in Figures 5.3-8 through 5.3-10. A strut made out of two materials to increase strut resistance to acceptable levels is necessary. However, this problem is minor compared with the difficulties one could expect from the other three systems.

The heat loss analysis was based on the following considerations:

1) Full-time space exposure, no sun

2) Steady-state conditions

TABLE 5.3-IV

HEAT SOURCE ATTACHMENT TRADE-OFF MATRIX

CONCEPT	ATTACHMENT HEAT LEAK*	LAUNCH LOADS	REENTRY LOAD	IMPACT G'S	THERMAL EXPANSION	HEAT SOURCE DEFLECTION
1) TRUSS 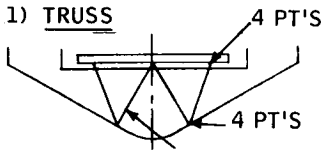	150 WATTS	GOOD	GOOD	FAIR	GOOD	GOOD
2) PERIPHERAL 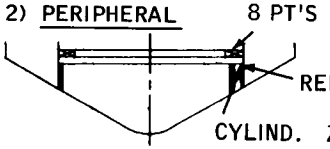	250 WATTS	BEST	GOOD	FAIR	FAIR	POOR
3) 4 POINT 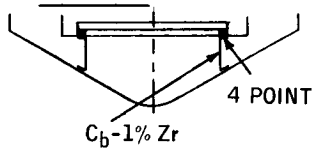	200 WATTS	GOOD	GOOD	POOR	FAIR	FAIR
4) 4 POINT AND CRUSH UP ** 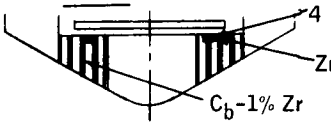	700 WATTS	FAIR	BEST	BEST	FAIR	GOOD

78-0019

* Relative heet loss data in accordance with Section 5.3.3.1 for comparison only.

** The crush up material is part of the heat source support structure.

3) Ablator radiative area restricted to region near attachment points (one-dimensional analysis).

4) Full utilization of the thermal resistance of the structure between source and sink, i.e., perfect structure insulation in case of the truss and four-point concept.

5) Minimization of radiative interchange through protective insulation layers where feasible (an important consideration for the peripheral design).

6) Consideration of heat flow through the crushup material in case of the four-point and crushup concept where the crushup material is part of the heat source support structure.

It has been pointed out that the actual heat loss is a strong function of geometry and materials involved in the heat path between source and sink as well as of the radiating ablator area. During this study phase, a one-dimensional thermal analysis has been performed to investigate the relative magnitude of heat losses for the various design concepts. A three-dimensional mode analysis, considering the total vehicle, is recommended in order to establish accurate heat loss data for a particular design and will be performed during the following study period.

5.4 IMPACT CONSIDERATIONS

5.4.1 Introduction

The need to investigate the ground impact situation has been established in section 3.3.5. This section reviews the basic design criteria, the capsules' structural limitations under impact, and the results of weight and performance tradeoff studies on several impact system concepts.

The following ground rules have been established for the impact system analysis:

a. The stability characteristics of the IRV, the descent wind profile, and the average surface slope of the earth result in impact conditions ranging from nose-on (0^{o} angle of attack) to angled impact up to 30 degrees angle of attack.

b. The IRV configurations under consideration have terminal impact velocities of 150 to 200 fps.

5.4.2 Requirements and Constraints

The major hazard considerations at impact, which were discussed in detail in section 3.3.5, are the release of radioactive fines due to rupture at impact or a post-impact melt-down of the fuel capsule container which could lead to an accidental criticality.

In order to prevent either accident, an obvious requirement of the fuel capsule is that it retain its structural integrity for both the high impact forces and post-impact temperature excursions.

Failure of the fuel capsule can be defined as any one of the following modes: a rupture of the fuel capsule container resulting from either high impact forces or debris penetration, penetration of the thin platinum coating which protects the refractory metal capsule container from catastrophic oxidation, or a melt-down of the fuel capsules due to inadequate heat dissipation in the event of ground burial.

A preliminary failure analysis of the fuel capsules established that the capsule failure limit was strongly affected by the method in which the capsule was supported at impact. The failure limits in terms of G's determined from the analysis are summarized in Figure 5.4-1 for a variety of support modes. The results of this analysis indicated that the fuel capsule could readily survive the extremely high loads imposed on them during impact providing they were properly supported in a cradle-like fashion along their entire length by the retention system, whereas the capsules would fail at relatively low impact G's when improperly supported at concentrated points. In addition, the probability of the capsule oxidation coating also surviving impact increase considerably where loads are transmitted uniformly to the capsule by the retention system rather than at concentrated points.

After impact, there is a definite requirement to effectively cool the fuel capsules. Normal orientation of the heat source (e.g., IRV nose in contact with the ground surface) poses no problem since radiation and convective cooling to the atmosphere provide adequate heat removal. However, burial or an upsidedown orientation of the heat source could lead to capsule melt-down and subsequent release of radioactive material. Provisions for reliably controlling post-impact orientation or effectively removing the heat are, hence, requirements in the design of the heat source. The analyses for post-impact heat rejection are not completed at this time and will be included in the Phase 1B investigation.

5.4.3 Impact Concepts

The impact concepts are as follows:

a. Pre-impact capsule dispersal

b. Dispersal on impact (fracturable plate)

c. Intact plate.

Of these three, the intact plate appeared to offer the greatest promise and was selected for more detailed design and analysis. The results are summarized in the following paragraphs.

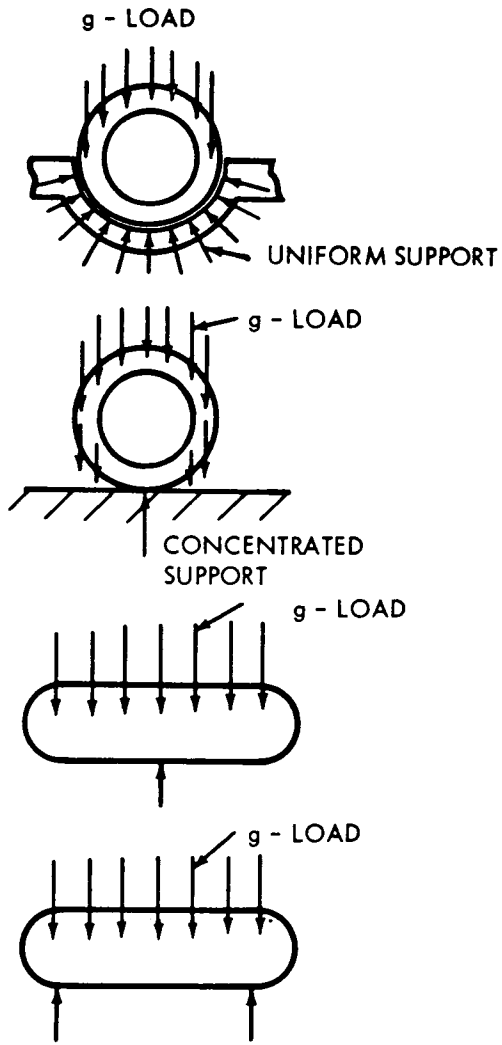

		g-LOAD
1	UNIFORM CRADLE SUPPORT	> 27,300g
2	CONCENTRATED SUPPORT FROM FLAT PLATE	1110g
3	BENDING LOAD-CENTER SUPPORT	2800g
4	BENDING LOAD-SUPPORT AT ENDS	2800g

NOTE: EFFECT OF INTERNAL PRESSURE INCLUDED

612204-1B

Figure 5.4-1 g-LOAD CAPABILITY OF CAPSULE SIDE-ON IMPACT

5.4.4 Intact Plate Concept Design Criteria

The design criteria used for the intact-plate concept are presented in this section.

It is assumed that the capsules are properly supported by a complete cradle retention system and, hence, based on the results of Figure 5.4-1, can survive the impact loads. In order to realize this, however, the fuel plate must be sufficiently rigid structurally such that bending stresses in the plate will not exceed the allowable yield strength for the operating temperature. The plate temperature at impact was taken as 2000^{o} F. Since impact loads are applied very abruptly, the static yield strength for Columbium 1% zirconium, the plate material, was increased 50% from 20,000 psi to 30,000 psi in evaluating plate failure.

For the impact study, a maximum impact incidence angle of 30 degrees is specified. This was considered a realistic design limit in accounting for wind gusts before impact, terminal angle of attack, and terrain slope. The 30 degree design limit coincides with side impact for the IRV blunt cone aeroshell. The impact surface was assumed to be a non-yielding one which would tend to maximize energy absorption requirements for the IRV system. The major vehicle design constraints on the impact attenuation system are vehicle diameter and weight.

In the case of the 60^{o} blunt cone, selected as the IRV aeroshell configuration, every inch of vertical height or stroke required for impact energy absorption could be magnified into approximately a three and a half inch increase in vehicle diameter. Consequently, stroke requirements appear to be crucial to the IRV design. Minimization of stroke, on the other hand, tends to increase the structural requirements of the plate and correspondingly the weight. A weight increase of the plate in addition to being undesirable to the overall IRV system, results in increased stroke requirements since the increase in kinetic energy of the heat source must also be absorbed.

5.4.5 Design and Evaluation of the Intact Plate Concepts

In this section, the basic intact-plate concepts for impact are discussed and evaluated. These concepts include (1) a crush-up system which will absorb the total kinetic energy of the heat source and prevent the heat source from impacting the ground, (2) a beefed-up plate concept without crush-up, and (3) a partial crush-up system at the plate periphery which is designed primarily to rotate the plate (plate rotation concept) in the event of side impact of the IRV such that the plate will impact flat. The planar heat source configuration was evaluated for all three intact-plate concepts. The conical heat source was evaluated only in terms of the total energy absorption concept; the rotation concept cannot be tailored to the conical heat source configuration.

5.4.5.1 Total Energy Absorption System - Planar Heat Source

The energy absorption system for the planar heat source employs crush-up material in the total volume under the heat source to protect the heat source for a range of vehicle impact orientations from head-on or frontal to side

impact. Of these, the side impact represents the most critical condition since the stroke distance between the heat source and ground is at a minimum as is the effective volume of crush-up material available to absorb the kinetic energy of the heat source. In order to provide the required energy absorption capability for side impact without resorting to large stroke penalties, it is necessary to select a crush-up material with a very high strength in the impact direction. In contrast, however, a high strength crush-up material acting over the full area of the heat source during head-on impact would transmit very high G-loads to both the fuel plate and fuel capsules.

To best meet the requirements for both frontal and side impact, a corrugated aluminum honeycomb crush-up material has been selected because of its extremely high strength (Figure 5.4-2). The honeycomb is considered to be oriented radially to the shell. In this way, a portion of the high strength material is always oriented in the preferred direction for any possible side impact condition. At the same time, the G-loads associated with frontal impact are minimized as a result of the known anisotropic behavior of honeycomb systems which is illustrated in figure 5.4-3. In this figure S/S_m is the ratio of the crush-up stress capabilities for a load applied at an angle "0", to the peak stress capabilities of the material. An artist's concept of impact history of this concept for the critical side impact condition is shown in figure 5.4-4. On impact, the aeroshell will collapse and the aluminum honeycomb directly above the impact plane will begin to crush. The impact force, which will increase as the plane of crushing increases, will also stress the fuel plate. The honeycomb on the opposite side of the impact plane is not considered to contribute any significant energy absorption since the rigidity of the vehicle shell is not enough to react against the moving plate.

In evaluating this concept it is assumed that the fuel plate does not rotate during side impact. In reality, some rotation will occur before the corner of the plate actually impacts the ground. Neglecting rotation tends to make the evaluation conservative. In addition, the anisotropy of the aluminum honeycomb has been assumed to be significant, as indicated in figure 5.4-3. Hence, only crushable material within plus or minus ten degrees ($\pm 10^o$) of the perpendicular to the impact plane is considered effective. Stroke and volume requirements based on this assumption are also considered on the conservative side since it is anticipated that the degree of anisotropy for higher density honeycomb such as the corrugated aluminum with its more rigid cell wall construction would not be as pronounced as a low density material.

An impact trade-off study for the total energy absorption concept was made for the side impact condition to evaluate the two critical design parameters, system weight and crush-up stroke or height. For the study, a terminal velocity of 150 feet per second was assumed. The results of the study are presented in figure 5.4-5.

In this analysis, the heat source support plate structural requirements and weight were first developed as a function of the maximum force, in terms of G's, which is exerted by honeycomb of various densities. The plate requirements were based on bending stresses in the plate due to the total impact or crush-up force. Figure 5.4-5 shows the increases in plate weight as a function of crush-up force in terms of G's. The weight values for the heat source shown in figure 5.4-5

include a fixed weight of approximately one thousand pounds for fuel capsules, capsule retainers, beryllium oxide, and insulation. Crush-up stroke requirements and corresponding crush-up weights were determined for kinetic energies associated with the variable plate weights. These parameters are also plotted in figure 5.4-5 as is the total system weight. The results of this impact study indicate that minimum system weight can be achieved only with a penalty of excessive crush-up height and weight.

5.4.5.2 Strengthened Plate Concept - Planar Heat Source

A second impact concept evaluated in the IRV study is the strengthened-plate concept, illustrated in figure 5.4-6. This concept features no crush-up material to provide load relief, but employs a very rigid plate designed to survive impact without yielding. By resisting yielding due to bending moments, the plate with a cradle retention system supporting the fuel capsules would distribute the impact forces to the capsules in the preferred manner shown in figure 5.4-1. The analyses of the fuel plate was based on side impact of the IRV which results in edge impact shown in figure 5.4-6 and critical bending of the plate. The weight penalty for the beefed-up plate is shown in figure 5.4-7 as a function of impact force. This impact force, based again on a fixed weight of 1000 pounds, is shown in terms of G's. For the case of impact on a non-yielding surface, the impact force could reach many thousands of G's. Based on the results in figure 5.4-6, forces of this level would result in unrealistic plate weights.

5.4.5.3 Total Energy Absorption System - Conical Heat Source

The total energy absorption system for the conical heat source was also evaluated using aluminum honeycomb oriented normally to the IRV aeroshell. The terminal velocity of the IRV aeroshell was again assumed as 150 feet per second.

The results of the trade-off study for this design are shown in figure 5.4-8. The conical plate weight and crush-up height is plotted as a function of crush-up strength. The plate weights reflect the increase in plate structure required to withstand the forces imposed on it by the crush-up material. The structure was sized for circumferential bending; yield strength was defined as the failure criteria.

A fixed weight value of approximately 1000 pounds has again been assumed. The results indicate that the plate weights increase greatly with crush-up strength since the conical plate configuration is not an ideal structure in view of the modes of applied loading at impact. The crush-up height requirements are based on both the crush-up strength and the plate weights. Although increased crush-up strength should normally reduce crush-up height requirements, this trend is significantly hampered by the resulting increased plate weights which, in turn, increase the energy absorption requirements.

In addition, providing sufficient crush-up volume to attenuate the nose-on impact case is difficult due to the small available volume at this location in this plate configuration. This problem can only be alleviated at a significant cost in vehicle diameter.

Based on the results, it can be concluded that a reasonable impact design for the conical heat source in terms of combined system weight and crush-up height does not appear feasible where fuel plate integrity is to be maintained in order to achieve an intact system.

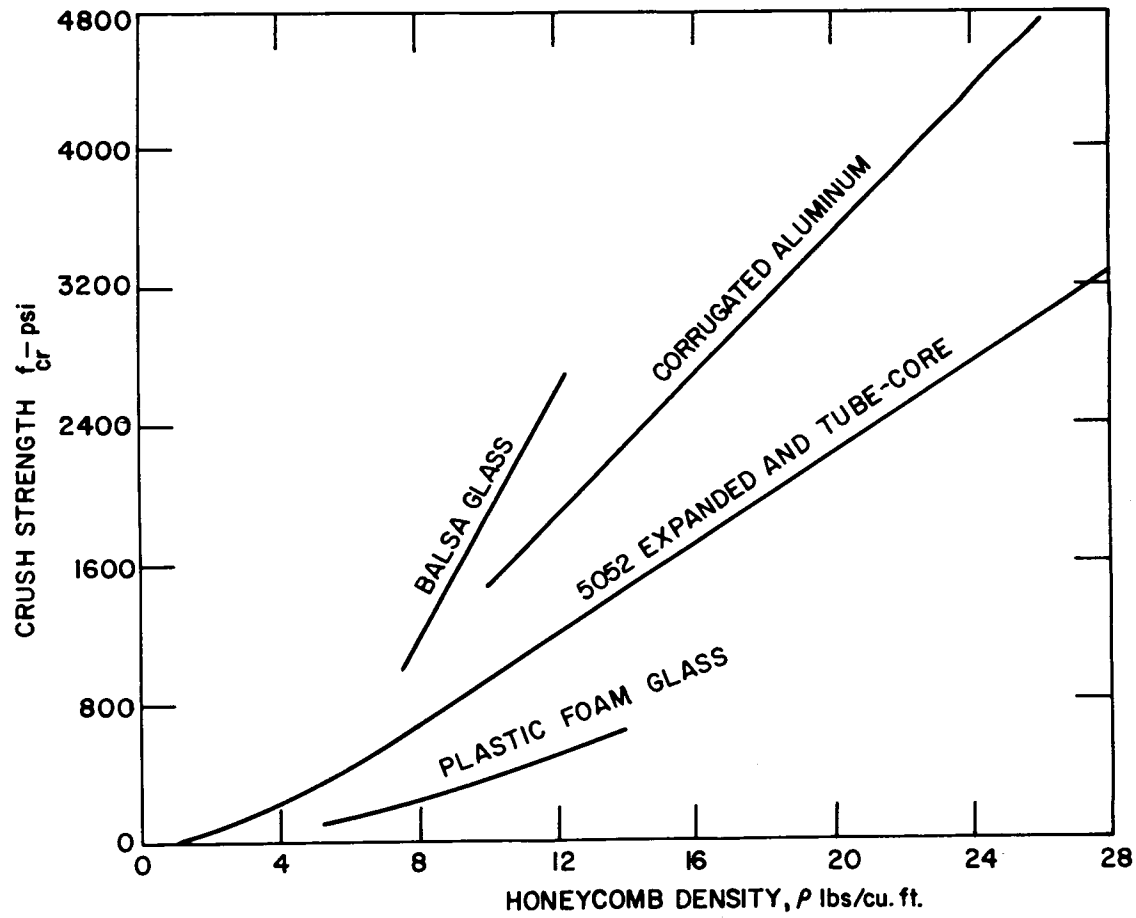

78-0055

Figure 5.4-2 CRUSH-UP MATERIAL

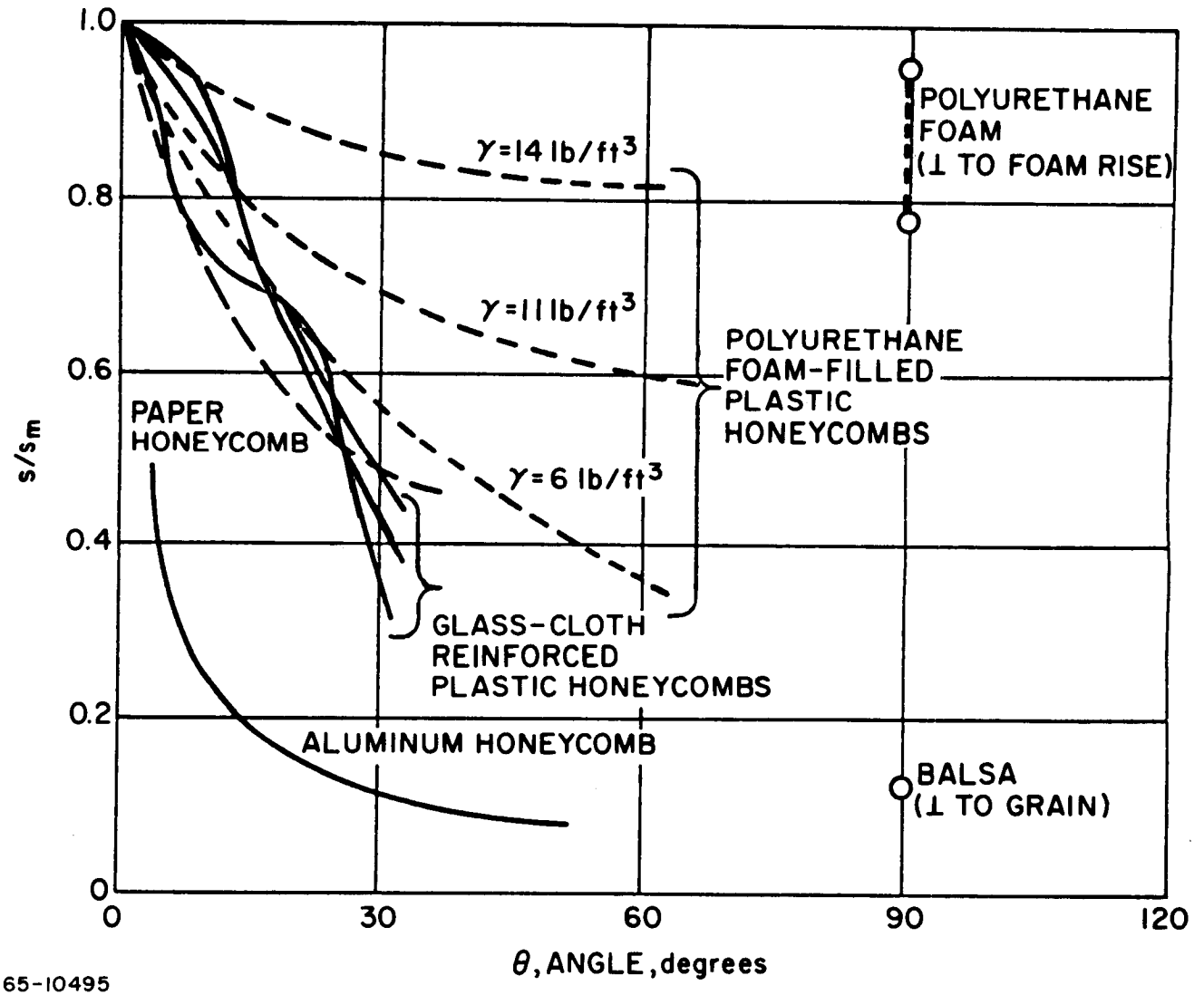

Figure 5.4-3 ANISOTROPHY OF CRUSHABLE MATERIALS

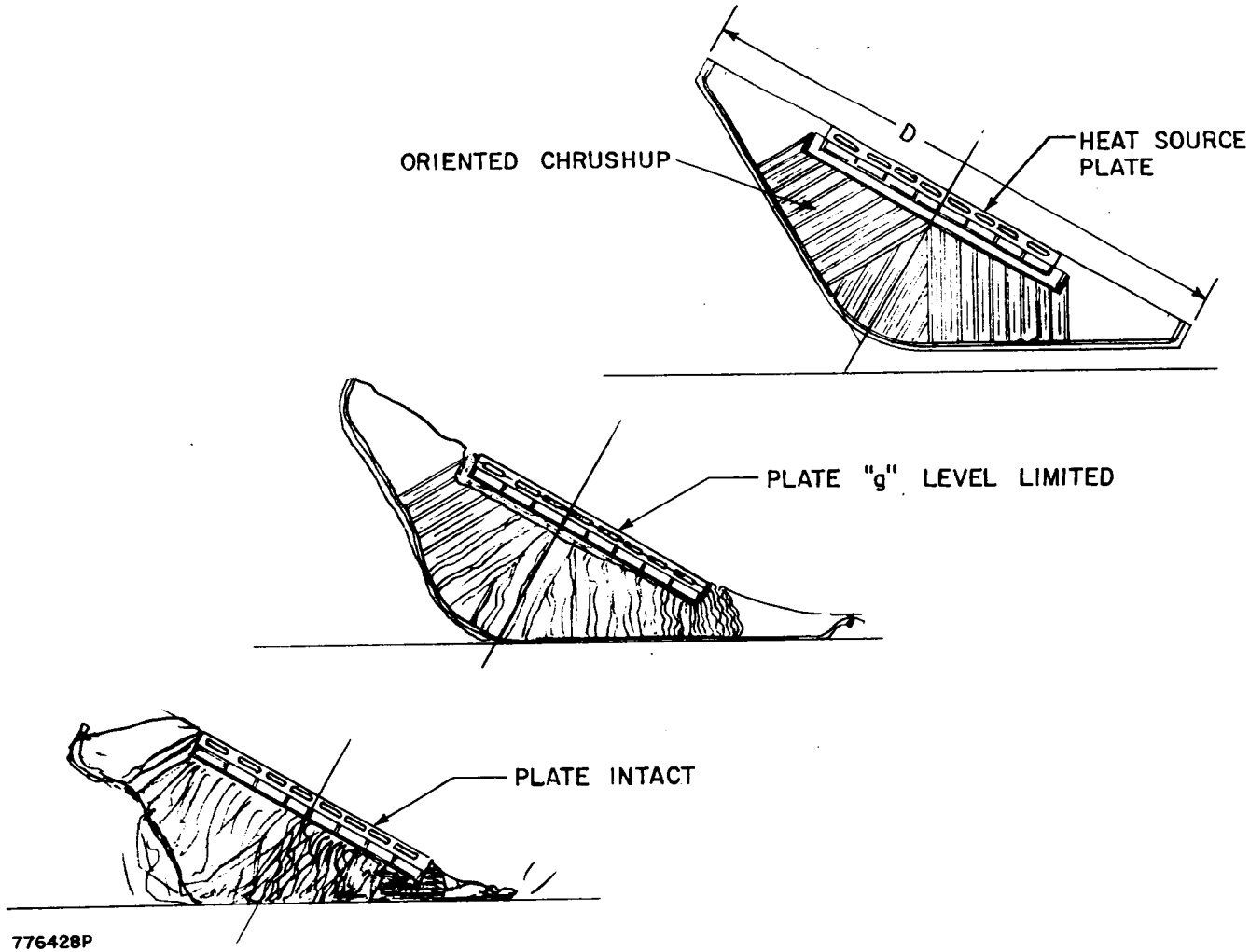

Figure 5.4-4 IRV IMPACT ATTENUATION CONCEPT (NO. 1)

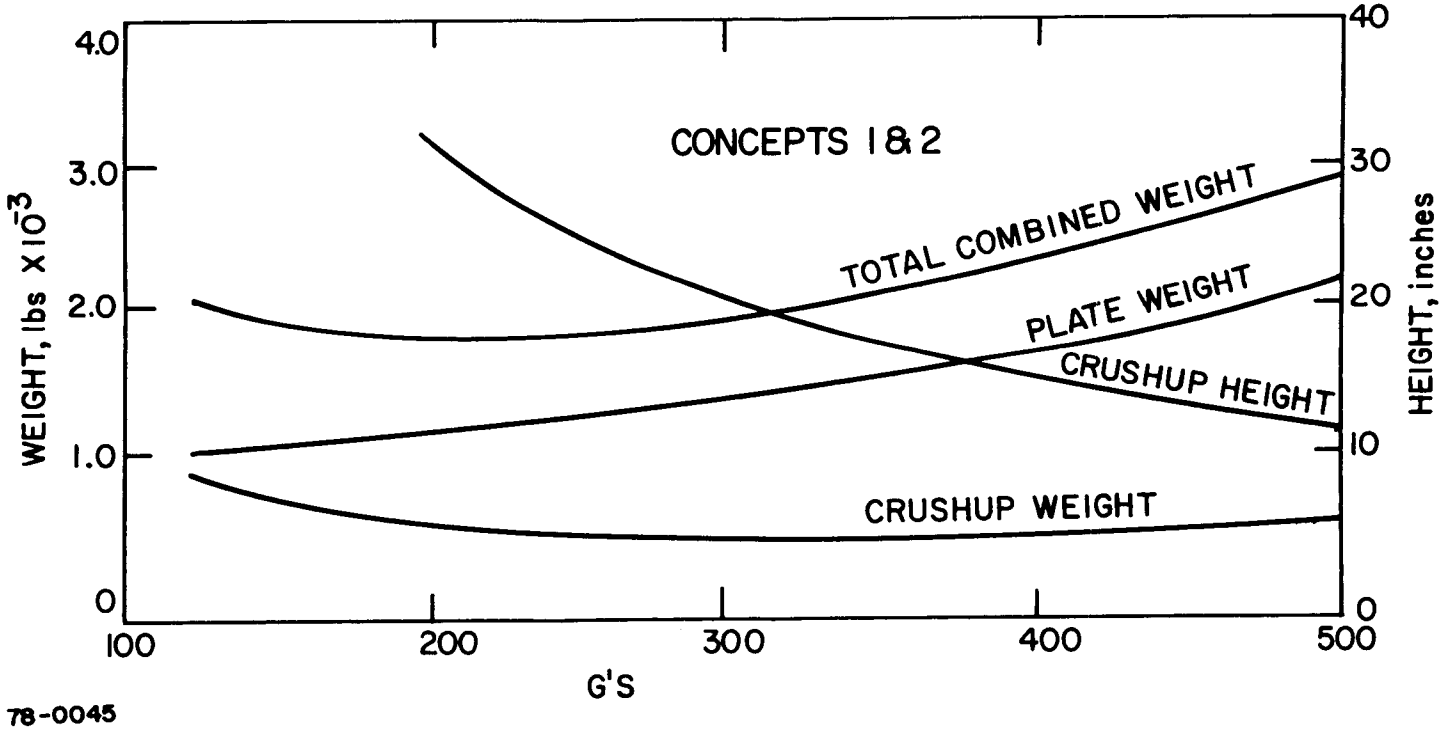

Figure 5.4-5 IMPACT TRADE-OFF STUDY -- INTACT IMPACT -- TOTAL ENERGY ABSORPTION CONCEPT

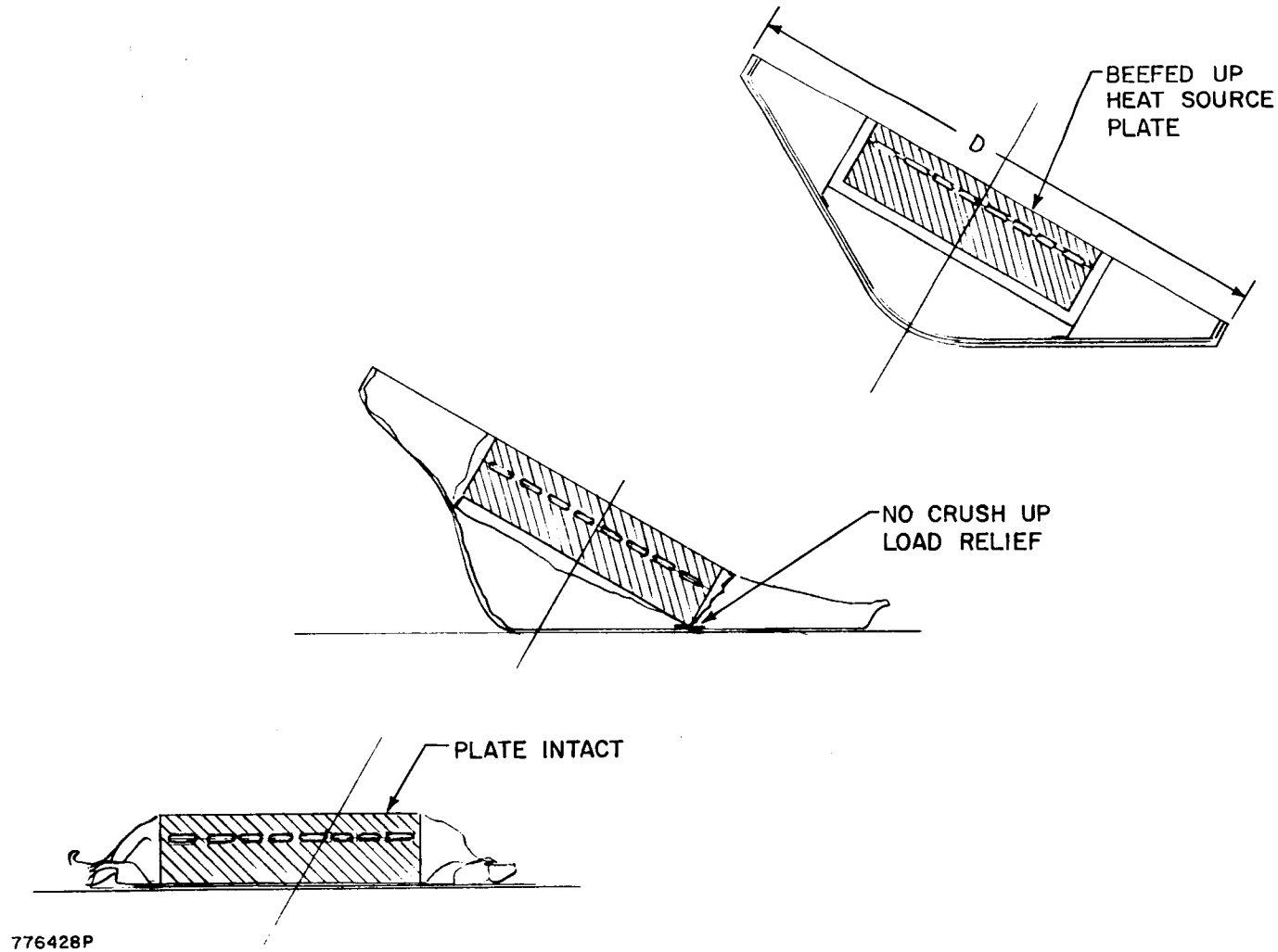

Figure 5.4-6 IRV IMPACT CONCEPT NO. 2 (STRENGTHENED PLATE ALONE)

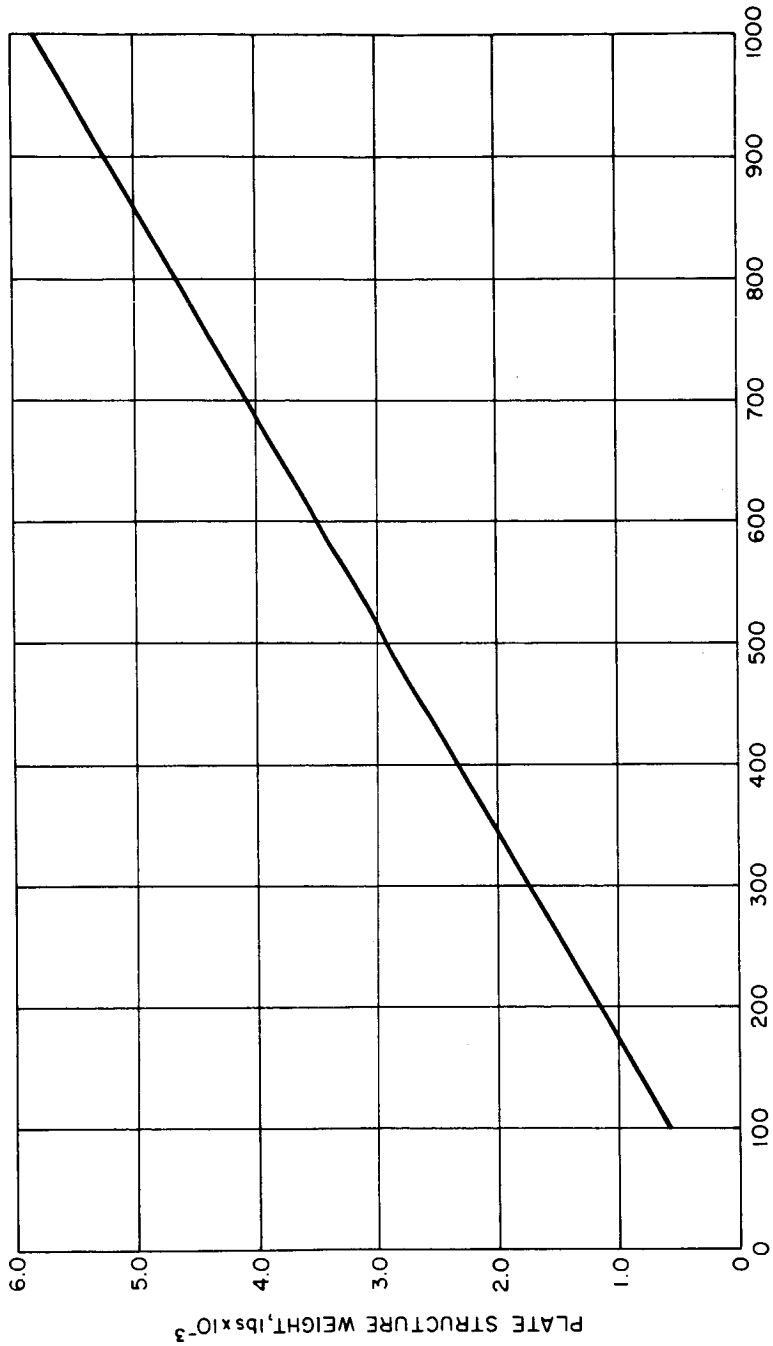

Figure 5.4-7 PLATE STRUCTURE WEIGHT PENALTY STUDY -- STRENGTHENED PLATE CONCEPT

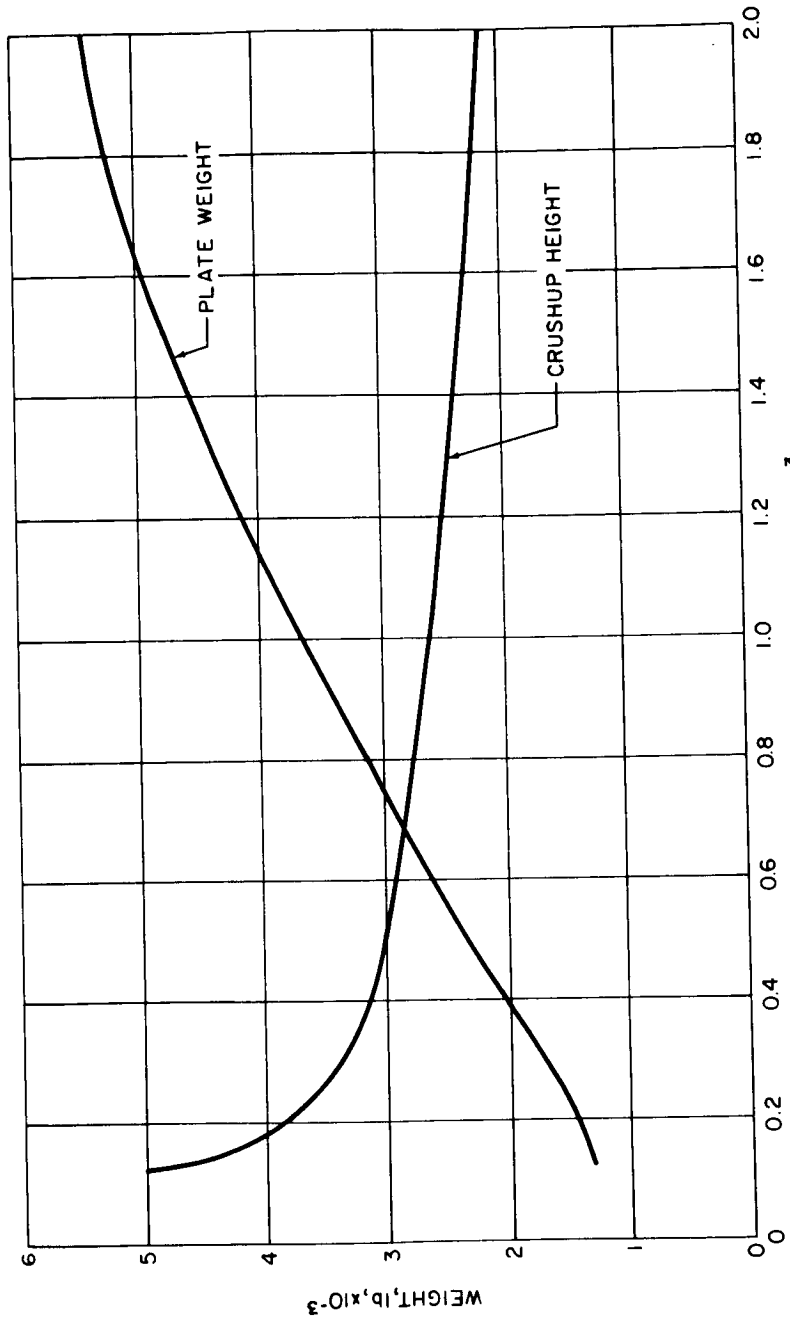

Figure 5.4-8 IMPACT TRADE-OFF STUDY -- INTACT IMPACT -- CONICAL HEAT SOURCE

5.4.5.4 Rotational Plate Concept -- Planar Heat Source

The failure mechanism of the heat source plate, as pointed out in section 4, is chiefly a flexural failure produced by the angled, or edge-on ground impact. This situation gave rise to an idea which could significantly improve the impact capabilities of the plate. That is, ideally if the plate could be made to hit flat so that the impact loads are applied as an evenly distributed pressure over the plate bottom, no bending moments would result and, consequently, flexural failure could not occur. The plate would simply tend to flatten. This situation would be obtained as a natural result for nose-on impact but introduction of plate rotation is necessary for the angled impact. Figure 5.4-9 presents "the rotating plate concept". The first view depicts a cross section of the IRV just prior to impact. The section includes a ring of crush-up material attached to the outside edge of the plate, the heat source plate, and the aeroshell. The second view shows a portion of the crush-up material deforming as the IRV impacts the ground. This causes a relatively concentrated load to be applied to the edge of the heat source plate creating bending moment in the plate, but at the same time causing the plate to rotate in the desired direction of flat impact (shown in the third view.) The concentrated load is controlled or dictated by the selection of the crush-up material and its geometry. The load must be made large enough to cause sufficient rotation of the plate before final impact, but not so large as to cause flexural failure of the plate before full rotation has been achieved. The basic trade-off is then between the required plate strengthening to withstand a given concentrated load and the decrease in load due to increasing the crush-up stroke. Strengthening the plate results in a direct structural weight penalty, while increasing the crush-up stroke results in a vehicle diameter penalty and consequent weight penalty. The results of the trade-off are shown in figure 5.4-10 along with pertinent analysis ground rules. The analysis is presented in Appendix A.

5.4.6 Impact System Selection

As noted in the Systems Analysis discussion, the seemingly best approach for minimizing damage to the capsules is to maintain heat source support plate structural integrity during impact. Two general approaches have been taken to accomplish this design requirement:

a. Limit the load transmitted to the plate

b. Control the manner in which the load is applied to the plate.

The total energy absorption concept evaluated in section 5.4.5 is designed to limit the loads transmitted to the plate whereas the rotating plate concept is an attempt to accomplish the second requirement; namely, to control the method of loading. A comparison of these concepts can be made in figure 5.4-11 which presents a trade-off of vehicle weight and diameter. The rotating plate concept offers the lowest weight by far of the two concepts. The fracturable plate concept results are also shown for comparison, but this system is not considered a good approach since a plate failure could result in an unfavorable pile-up of fuel capsules.

It is apparent from the preceding analyses that approach 1) leads to impractical designs. Approach 2), the rotating plate concept, has resulted in reasonable

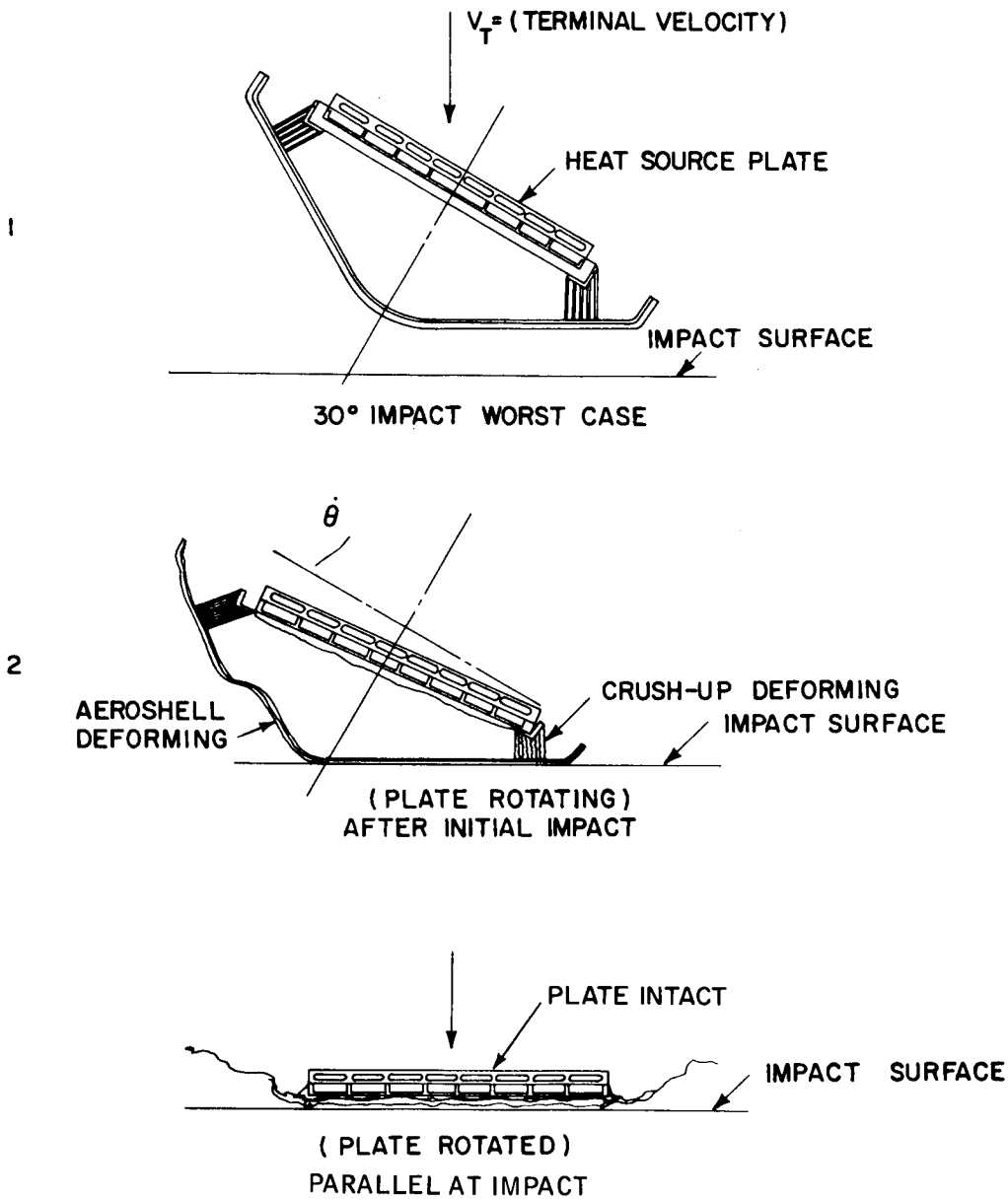

Figure 5.4-9 IRV ROTATIONAL IMPACT ATTENUATION SYSTEM CONCEPT

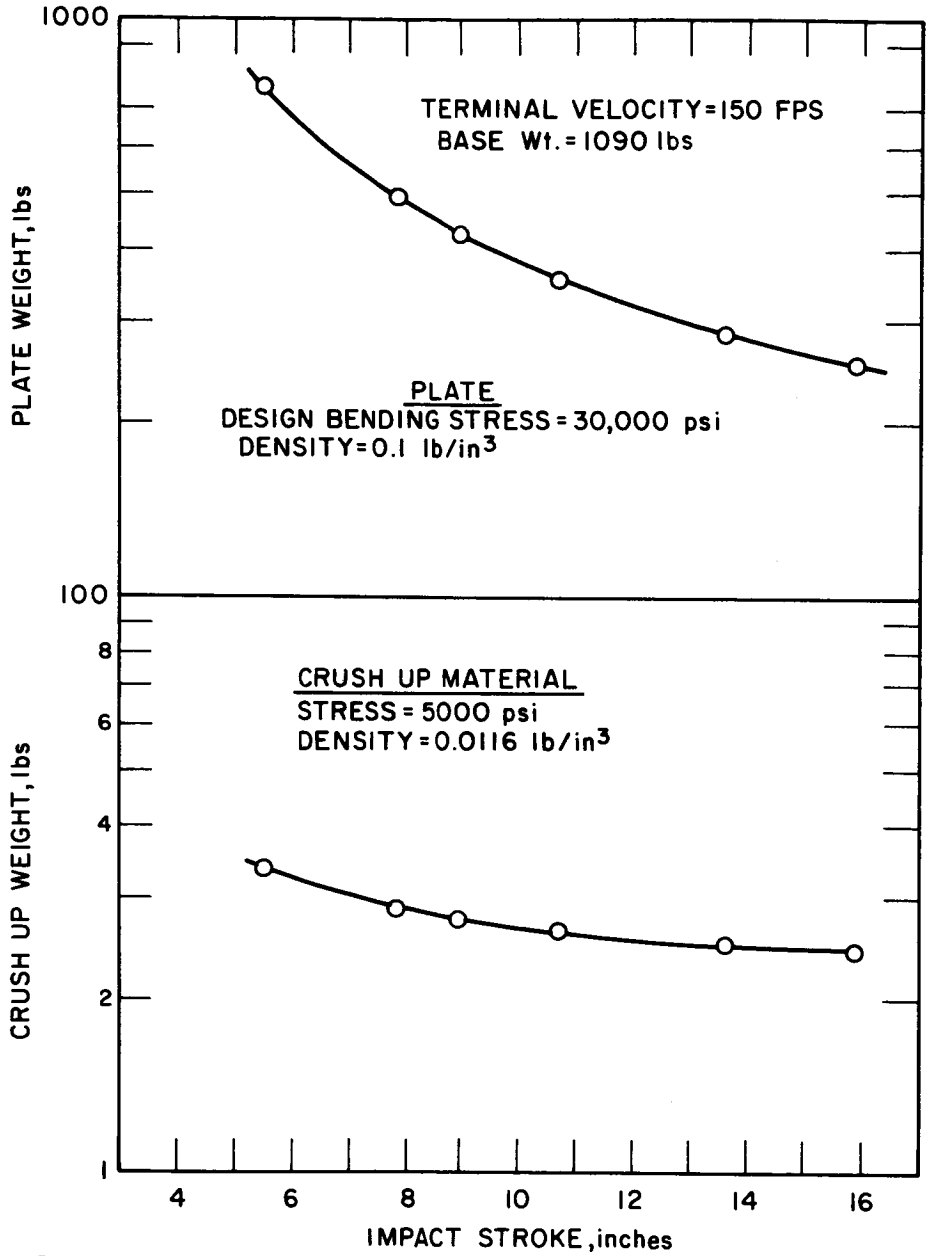

Figure 5.4-10 IMPACT ATTENUATION WEIGHT PENALTIES

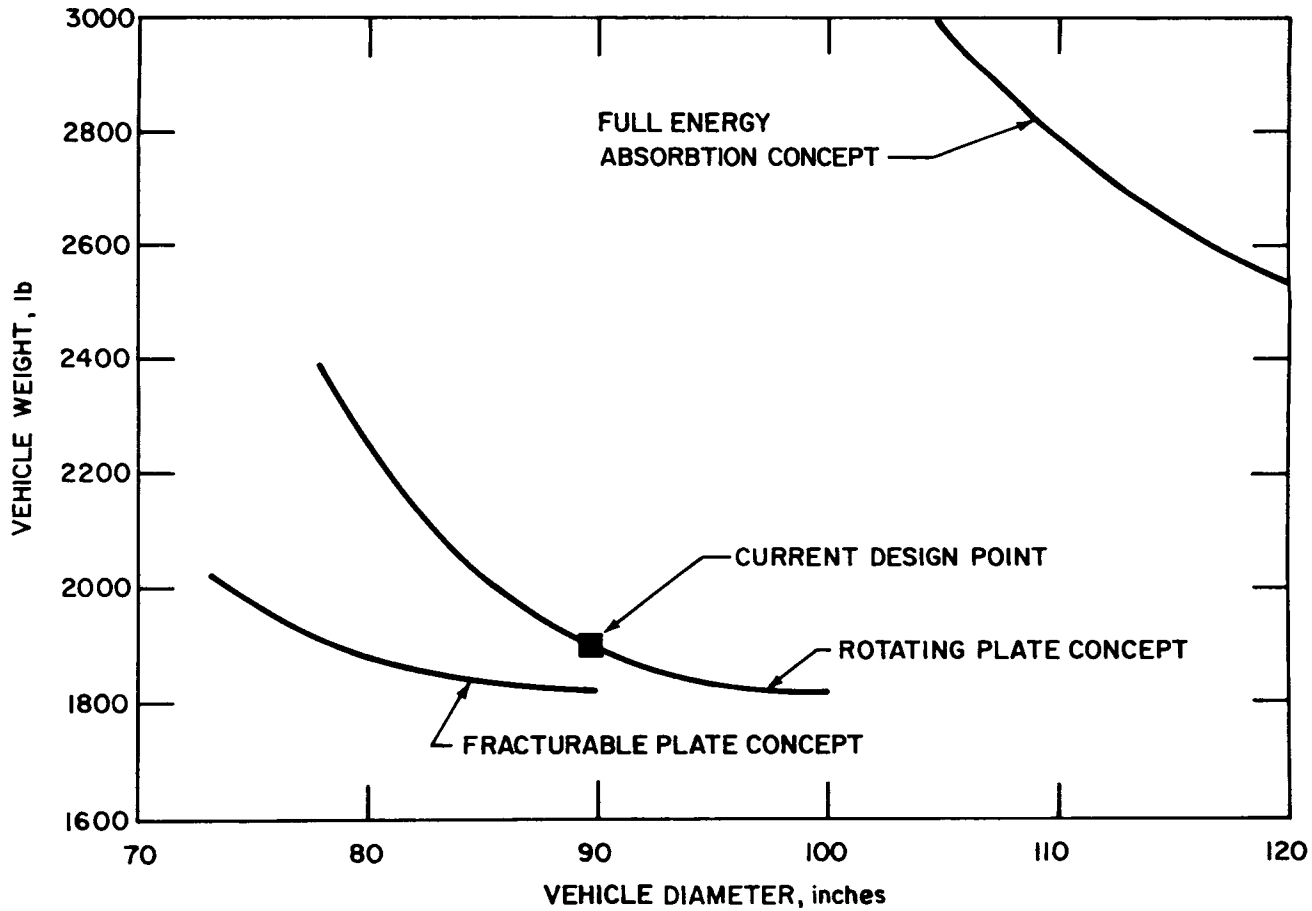

7800-14

Figure 5.4-11 IMPACT ATTENUATION ANALYSIS TRADE-OFF -- 47-INCH PLANAR HEAT SOURCE $Lc/R_B = 0.15$

design configurations and has been selected for further design effort. Effort will continue in this area to develop a lighter weight impact attenuation system.

It is recognized that the preceding analyses and results are based upon idealized dynamical models. Many simplifying assumptions have been made to ease the complexity of the analytical treatment. Some of the physical phenomena which have not been considered at this time are the following:

a. Rough terrain (rocks, gullies, etc.)

b. Soft soil

c. Bounce or ricochet

d. Elastic or plastic deformation of the structures other than the crush-up material.

The analyses do, however, indicate very promising conceptual designs and further effort will be made in subsequent phases of the contract to refine and improve the analytical treatment of the impact problem.

5.4.7 Testing

Verification of the proposed methods of impact attenuation could be obtained by test and much could be learned from small model tests before full-size impact tests need be conducted.

5.5 DECELERATION AND RECOVERY AIDS

5.5.1 Introduction

Several IRV configurations, with and without packaged deceleration and recovery aids, have been analyzed. These aids can be stored in peripheral or central locations of the reentry vehicles at some penalty to overall system size, weight and optimum vehicle configuration. In addition, the study showed that aerial recovery is feasible for planned and controlled reentry. The United States Air Force has acquired considerable experience and success using parachute arrangements for final deceleration and air-to-air recovery of reentry vehicles. Under such conditions, up to 2500 pounds can be air snatched. However, there is a size restriction of sixty-six inches in diameter for reeling the package on-board the aircraft after air snatch (aircraft). An alternate is to tow the package behind the aircraft after air snatch to a soft drop area. Because of the time required to plan the recovery aircraft and support ships, aerial recovery is considered unfeasible for unplanned, uncontrolled and/or random IRV reentry.

A ballute final deceleration unit or a combination of ballute and parachute final deceleration and aerial recovery unit are still under investigation. One of these arrangements may prove superior to a pure parachute deceleration and aerial recovery unit from a safety viewpoint; since possibility of the vehicle tumbling during final descent and becoming tangled in the parachute lines has not been eliminated.

Ballutes will be evaluated during Phase IB. The following paragraphs only consider potential parachute deceleration and aerial recovery systems.

5.5.2 A Typical Deceleration and Recovery Arrangement

The United States Air Force's teams engaged in aerial recoveries of reentry vehicles prefer a minimum of 25 minutes of descent on the parachute before air-to-air pickup to allow sufficient time for acquisition, tracking, and pickup. To achieve this, initiation of final deceleration must occur at altitudes slightly greater than 50,000 feet. A baroswitch can be employed to activate a thruster (mortar) and mortar parachute somewhere between 60,000 and 50,000 feet, taking into account instrument and prediction errors; therefore, the total time on target recommended by the United States Air Force can readily be achieved. A backup baroswitch will be employed to activate the thruster and mortar parachute at 35,000 feet; this will permit the recovery aircraft to make at least one recovery pass after acquisition and pickup. Aerodynamic studies indicate that for normal and planned deorbits, the reentry vehicles will be subsonic and stable when it reaches 75,000 feet, such that a subsonically deployed parachute arrangement can be used.

5.5.2.1 Aerial Recovery

The small mortar parachute will be deployed by a thruster between 60,000 and 50,000 feet. The main functions of the mortar parachute are, 1) to initiate deceleration and 2) to deploy the air-pickup parachute. When the air-pickup parachute, which also serves as the main drogue parachute, is inflated, it will reorient the main structure of the reentry vehicle to a more favorable attitude for deployment of the main parachute. Presently, the main parachute is sized for a 1500 pound reentry vehicle including the deceleration and recovery aids.

A timer will provide the signal for release of the air-pickup parachute from the reentry vehicle structure, and thus deploy the main parachute which remains attached to the air-pickup parachute by 200 foot lines.

Chaff is dispersed, and a radio beacon, flashing light, radar corner reflector, and spot light are deployed with a multicolored main parachute, to facilitate detection and tracking of the reentry vehicle.

The reentry vehicle will be descending at a rate of 25 feet/second at an altitude of 10,000 feet; a typical descent rate for air-to-air pickup. A swivel is incorporated in the riser line of the main parachute in order to prevent parachute fouling due to residual spin. The aircraft picks up the air-pickup parachute.

5.5.2.2 Water Impact

In the event of an unsuccessful air-pickup or an unplanned, uncontrolled, or random reentry, a fast acting saltwater switch will disconnect the parachute arrangement and will initiate inflation of a flotation bag if impact is on water.

The salt-water will also activate a salt-water battery which will provide electric power to activate location aids, mounted on the flotation bag, such as a blinking light and a radio beacon, to facilitate recovery operations. Passive location aids such as dye marker and a high-visibility, multicolored flotation

bag will be used for final visual contact. The reentry vehicle, as a heat source will also act as a recovery aid; that is, it could be located with IR detectors.

A scuttle unit, containing a corrosion plug could sink the flotation bag and reentry vehicle 48 to 60 hours after water impact.

5.5.2.3 Land Impact

In the event of a land impact, an impact device could be used to release the parachutes on impact to eliminate the possibility of the parachutes dragging the reentry vehicle over the ground in strong winds; on the other hand, if a vehicle ground orientation stabilizing device is incorporated into the reentry vehicle, it may be desirable to leave the parachutes attached to the reentry vehicle in the hope that parachute will burn and thus provide an additional visual recovery aid. This concept of leaving the parachute attached to the reentry vehicle requires further analysis to assure that forest fire hazards are minimized and convective cooling will not be retarded. In any event, an impact device will be used to prevent deployment of the flotation bag on impact in order to insure that the reentry vehicle is not placed in an undesirable orientation after impact. This does not preclude the deployment of other recovery aids such as beacons and flashing lights on impact. The reentry vehicle, as a heat source, will act as a recovery aid.

The reentry vehicle could also contain impact attenuating material, at the expense of vehicle configuration and weight, to reduce the impact shock in the event of malfunction of the deceleration device and reentry vehicle free fall.

Table 5.5-I shows a typical deceleration and recovery system.

5.5.3 Problem Areas

5.5.3.1 Heat and Radiation Environment

The temperature of the deceleration and recovery aid compartment aboard the reentry vehicle is still a problem which requires further analysis. Some of the aids such as batteries, thruster, and electronics must be packaged and stored at temperatures of less than 160° F; while other items such as the parachutes and flotation gear can be stored at much higher temperatures.

Analyses indicate that the radiation levels in the deceleration and recovery aid compartment will be less than critical at all times. (Five year integrated dose $< 2 \times 10^{12}$ neutrons/sq cm -- $< 10^{5}$ rads).

5.5.3.2 Time in Orbit

Most of the deceleration and recovery aids have a three year storage life. Certain items may be replaced during the mission in order to support a full five year mission.

TABLE 5.5-I

DECELERATION AND RECOVERY AIDS

	Weight (lb)
Thruster and Mortar Chute	5
Drogue Chute	50
Main Chute	50
Baroswitch	2
Radar Reflector	1
Flashing Light	1 (2 each)
Dye Marker	3
Battery	25
Junction Box	1.5
Flotation Bag	15
Salt Water Switch	0.25 (2 each)
Salt Water Battery	10
Shark Repellent	2

5.6 AEROSHELL HEAT SHIELD

5.6.1 Environment Summary

During this phase of the study several trajectories were analyzed, reflecting a variety of IRV entry and abort conditions. The environments ranged from a ballistic reentry of 23,125 feet per second at an angle of $\gamma_E = -10^o$ lasting 77 seconds, to a double skip trajectory with an initial velocity of 26,000 feet per second entering (on the final phase) at $\gamma_E = -0.7^o$ lasting 10,600 seconds. Table 5.6-I presents a summary of the significant parameters at the stagnation point for all trajectories.

Referring to the table, it is seen that the maximum cold wall stagnation heating rate occurs during the steepest trajectory ($\gamma_E = -10^o$) while the maximum total integrated heating is associated with the double skip trajectory. The double skip trajectory is by far the longest in duration and in addition permits thermal

TABLE 5.6-I

IRV ENVIRONMENT SUMMARY

60° Blunt Cone
$W/C_DA = 30\ lb/ft^2$
$R_N = .72$ ft

Trajectory	Total Time (sec)	Maximum Heating Rate (Stag. Pt.) (BTU/ft^2-sec)	Total Integrated Heating (Stag. Pt.) (BTU/ft^2)	Maximum Stag. Pt. Pressure (Atm.)	Maximum Aerodynamics Study (lb/ft^2)
$\gamma_E = 0^o$ $V_E = 25,685$ fps	3070	193	50,000	.26	3.1
$\gamma_E = -2^o$ $V_E = 25,840$ fps	330	263	33,750	.26	4.3
$\gamma_E = -5^o$ $V_E = 25,400$ fps	160	365	20,300	.48	5.9
$\gamma_E = -10^o$ $V_E = 23,125$ fps	77	370	10,900	.81	6.0
Nominal Case $\gamma_E = -2.25^o$ $V_E = 25,876$	320	270	31,500	.28	5.2
Double Ship $\gamma_E = -.70^o$ $V_E = 26,000$ fps	10,600	195	55,000	.22	3.1

soaking during the skip maneuvers. The last portion of the trajectory is ballistic in nature and will require proper ablation performance from the heat shield. The total integrated heating value of 55,000 Btu/ft^2 is 10 percent higher than the next highest value listed (γ = 0°). Therefore, based on previous experience and the facts presented, it was decided to utilize the double skip trajectory for preliminary heat shield performance calculations with periodic checks on the other trajectories.

Of additional concern is the level of pressure and aerodynamic shear experienced on the vehicle since this could possibly influence the selection of the thermal protection system. The pressure and shear levels as given in the table are not considered excessive and, therefore, should not eliminate any candidate heat shield materials.

The values of the parameters presented in the table are for the stagnation point of a 69-inch diameter 60-degree blunt cone. The stagnation point heating on the modified Apollo configuration is approximately one-third the blunt cone values while the maximum pressure and shear levels will be about the same. It should not be concluded from this statement that the modified Apollo will produce a lower weight heat shield since the heating distribution is such that for a given vehicle diameter only a small difference in total weight will result.

5.6.2 Thermal Design Criteria

In the definition of thermal protection requirements for any vehicle a set of ground rules (or criteria) must be established. These criteria involve allowable structural and bond temperatures and, in addition, uncertainties in heat shield material properties and design methods.

The heat shield must restrict the structure to a temperature where the properties are adequate for the environment and configuration. Some metals may operate at elevated temperatures (i.e., titanium) while others are limited to lower values (i.e., aluminum). State-of-the-art bonds (epoxy, silicone) maintain their integrity from 600° to 800° F. The reference IRV design employs an aluminum honeycomb structure and for the environments considered is limited to a maximum temperature of 350° F during entry. It should be noted that if other structural materials are employed the design condition would be limited by a short-time bond temperature (600° F) regardless of the allowable structure temperature. For the conditions of the IRV no steep temperature gradients exist near the rear of the heat shield and, therefore, the bond and structure maintain similar temperature levels.

To account for uncertainties in material properties and design methods a safety factor of 1.20 on heat shield thickness was used. This factor appears reasonable in view of ground test data scatter and results from reentry vehicle flight tests.

5.6.3 Thermal Protection Concepts

5.6.3.1 Low Density Charring Ablator

Investigation of the IRV environments coupled with past experience indicates that a low density charring ablator (ρ = 25-30 lb/ft^3) may offer the most

efficient thermal design. This class of material provides the combination of a low conductivity coupled with relatively high re-radiation losses due to the carbonaceous char which is formed during the ablation process. Among the main concerns in the utilization of these materials are the pressure, pressure gradient, and aerodynamic shear levels experienced during flight; since past testing has indicated that this class of ablator may not perform well unless restrictions are placed on these parameters. For the range of IRV trajectories, however, the levels of pressure and shear are below the threshold level.

It should be noted that while cork silicone appears to be a suitable material other candidates include Avcoat 5026-39 (Apollo material), Purple Blend, and Avcoat 5026-99 will be evaluated. All of these materials would result in approximately the same weight heat shield. Some additional weight saving may be realized by utilizing a super low density material (ρ = 16 lb/ft^3) currently being developed at Avco/SSD and calculations with this material are currently in process.

Figure 5.6-1 shows the local weight at the stagnation point for the cork silicone and the other candidates described below. For the cork silicone, oblique tape wound Refrasil and carbon phenolic (RAD6300), a 0.35 inch aluminum honeycomb structure was assumed while for the ATJ molded graphite and beryllium no structure was used.

5.6.3.2 Oblique Tape Wound Refrasil (OTWR)

The second ablative material considered was OTWR, which is a high density silaceous compound reinforced with phenolic resin. This material has been used successfully for high performance reentry vehicle heat shields and may be characterized as a charring ablator with silica vaporization occurring at the surface. The weight requirements for the OTWR are shown in Figure 5.6-1 and the weight penalty is quite obvious when compared with the low density ablators.

5.6.3.3 Carbon Phenolic

A third material considered was RAD6300 carbon phenolic. This material is constructed of carbon cloth layers impregnated with phenolic resin. Previous experience with this material on high performance ballistic vehicles showed it to be an excellent ablative performer in high heat flux, high enthalpy environments. The material is characterized by charring (internal pyrolization) and carbon oxidation or sublimation at the surface.

Results of the calculations performed with carbon phenolic are shown in Figure 5.6-1. Again, the local heat shield weight required is much higher than the low density reference ablator. As with OTWR, the problem is the high product of thermal conductivity and density and it is readily concluded that for both of these materials, the heat shield insulative requirement is higher than the ablative one.

5.6.3.4 Beryllium Heat Sink

To allay any doubts as to whether a heat sink might do the job of thermal protection for the IRV vehicle, beryllium requirements were calculated at the stagnation point for the double skip trajectory. It was assumed that the beryllium

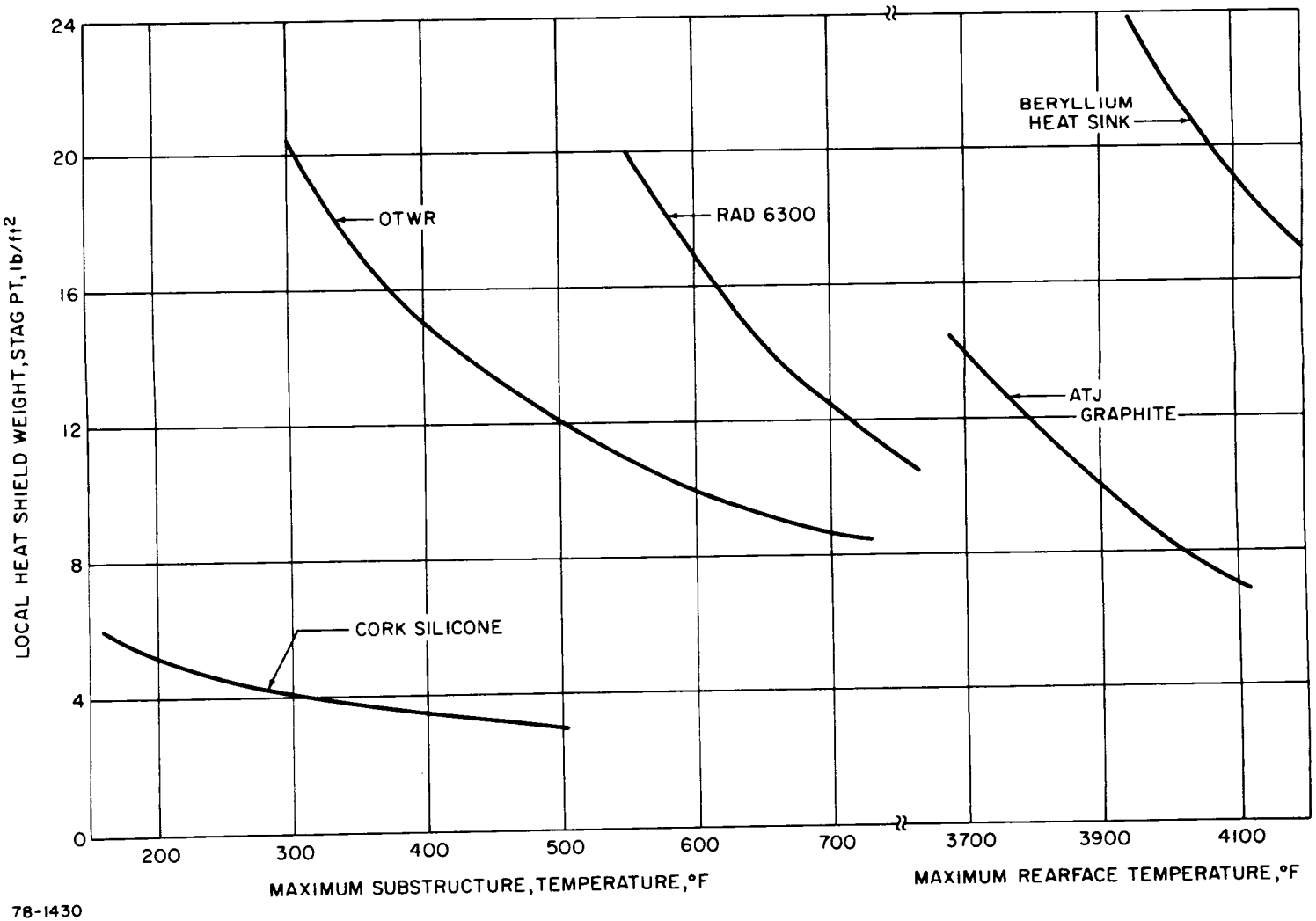

Figure 5.6-1 SUMMARY OF IRV HEAT SHIELD REQUIREMENTS FOR 60° BLUNT CONE DOUBLE SKIP TRAJECTORY $W/C_DA = 30$ lb/ft^2

acted as a structure as well as the thermal protection system. Referring to Figure 5.6-1, it is seen that weight requirements are excessive even if the heat sink is allowed to reach 4000° F at the backface. For beryllium, of course, the melting temperature is only about 2300° F which would make the weight even more prohibitive.

5.6.3.5 ATJ or 3-D Graphite

The final heat shield materials studied were ATJ and precharred 3-D graphite. These materials were selected for their superior stability in the space environment and excellent ablative performance. Calculations were done with the appropriate carbon oxidation model at the stagnation point.

Since the graphite has a very high value of the product of thermal conductivity and density, the weights obtained were clearly not competitive with the design based on a limiting structure temperature of 350° F. The ATJ or 3-D concept is only considered competitive if a high temperature integrated wall system is to be used. However, even if backface temperatures in the order of 4000° F are allowed, a large weight penalty is evident relative to the low density ablator.

5.6.3.6 Ablating Radiation Shield

An additional thermal protection concept considered was an ablating radiation shield. This system operates with a high temperature, low surface recession rate ablator as a surface material with low thermal conductivity, low density insulator as a backup material. The function of the high temperature ablator is to reject heat at the surface by re-radiation at high temperatures, and the insulator serves to block the flow of conducted heat toward the structure. The concept best approximates the ideal marriage of high performance ablation and low weight insulation.

The initial configuration considered used pyrolytic graphite over carbon felt to protect a honeycomb structure. Pyrolytic graphite was selected mainly because of its low thermal conductivity perpendicular to the basal planes and its known high temperature performance. Calculations were performed using a carbon oxidation model and results are shown in Figure 5.6-2. Weight requirements for a 0.17 inch thick pyrolytic graphite shell and carbon felt are only 4.5 lbs/ft^2 and thereby competitive with the low density ablator. Figure 5.6-2 also indicates the weight penalty associated with increasing the pyrolytic graphite thickness on total weight required.

Unfortunately, use of pyrolytic graphite (or any other graphite system as the outside material) would probably present structural problems due to attachment requirements. There remains the possibility that the composite could be designed to permit higher structural temperatures if a material such as steel or titanium were utilized. Although this approach would tend to reduce local hot spot problems at connections, thermal mismatch problems would still exist.

5.6.3.7 Summary

Table 5.6-II shows a comparison of the various concepts on a local weight basis. As can be seen, the low density ablator system provides the best performance

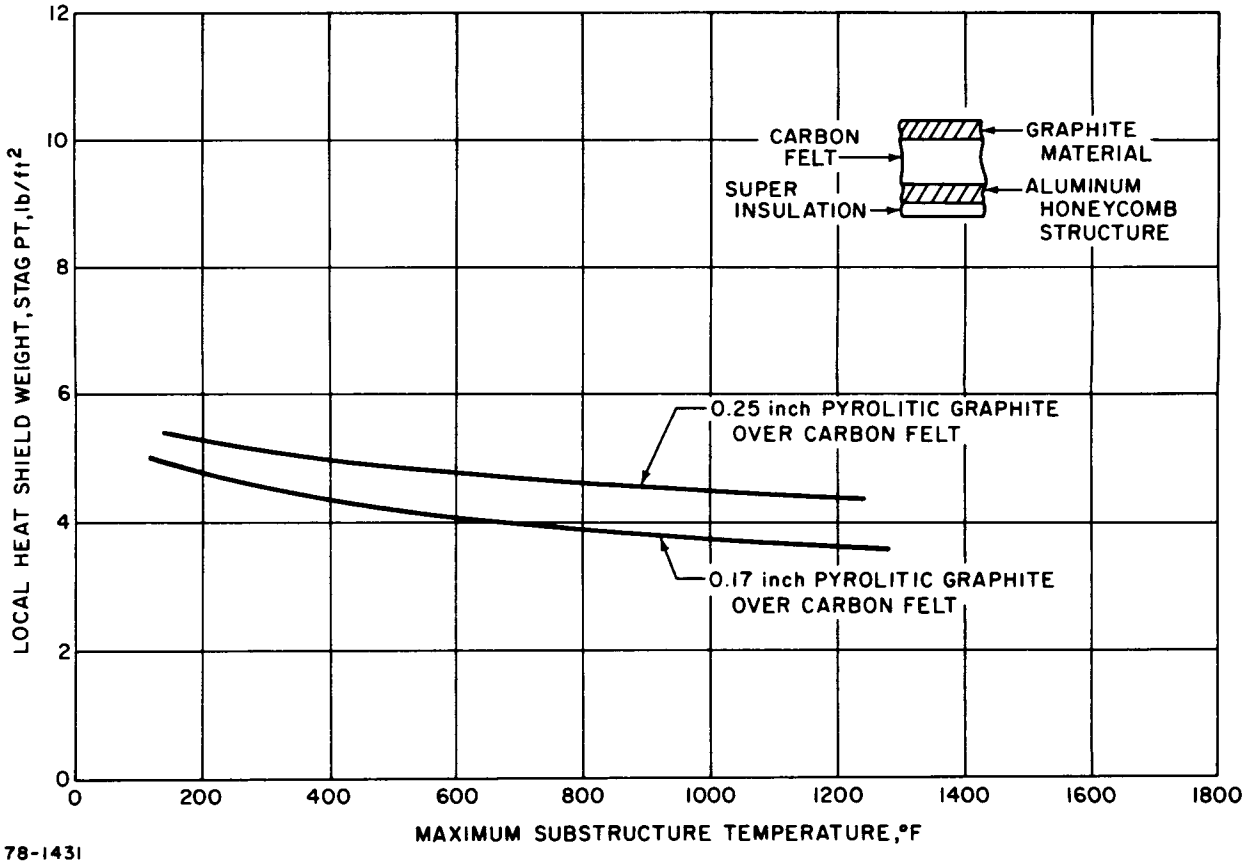

Figure 5.6-2 ABLATING RADIATION SHIELD REQUIREMENTS IRV FOR 60° BLUNT CONE DOUBLE SKIP TRAJECTORY $W/C_DA = 30$ lb/ft^2

TABLE 5.6-II

THERMAL PROTECTION SYSTEM WEIGHT COMPARISON

60^0 BLUNT CONE STAGNATION POINT

DOUBLE SKIP TRAJECTORY (Q = 55, 000 BTU/FT^2)

SYSTEM	LOCAL WEIGHT REQUIRED (lb/ft^2)	SURFACE RECESSION (INCHES)	MASS LOSS (lb/ft^2)
CORK SILICONE OVER Al/HC	4	1.07	2.80
3-D GRAPHITE (INTEGRATED WALL)	5	.11	0.80
GRAPHITE OVER INSULATOR OVER Al/HC	6	.07	0.80
QUARTZ PHENOLIC OVER Al/HC	17	.10	2.30
CARBON PHENOLIC OVER Al/HC	30	.17	2.70
BERYLLIUM HEAT SINK	50*	------	------

*SURFACE MELTS

but the high temperature integrated wall or ablation radiation systems are somewhat competitive. However, in the case of the integrated wall molded graphite system, local attachment problems exist and the insulation requirements must be established. The ablation radiation system could produce thermostructural problems due to the rather large insulation thickness required to make the system competitive. Table 5.6-III shows a summary of the various thermal protection systems and materials that were considered in the study.

At the present time the recommended approach would be to use a low density charring ablator. Advanced designs in which the capsules are actually imbedded in the heat shield material (probably 3-D graphite) and operating in orbit at elevated temperatures (2000° F) could possibly produce a lower weight and diameter design. This latter concept is currently under investigation.

5.6.4 Reference Design

Figures 5.6-3 and 5.6-4 indicate the heat shield thickness requirements as a function of vehicle diameter and location for the 60 degree blunt cone and modified Apollo shapes, respectively. These calculations were based on the following assumptions:

a. Ballistic coefficient (W/C_DA) = 30 lb/ft^2. This will vary with the vehicle diameter but this variation is not well defined at this time.

b. Maximum structural allowable temperature of 350° F. The structure is 0.35-inch aluminum honeycomb.

c. Initial ablator entry temperature = 100° F.

d. Safety factor = 1.2 on heat shield thickness.

The calculations were performed for the maximum integrated heating trajectory (double skip) and utilized a low density charring ablator heat shield (cork silicone - ρ = 30 lb/ft^3). These thicknesses and weights are typical of other low density ablators (e.g., purple blend, 5026-39, etc.).

It is interesting to note that the modified Apollo has essentially a flat thickness requirement over the aeroshell while the distribution on the cone drops off sharply. The thickness requirements in the area of the shoulder are shown in Figures 5.6-3 and 5.6-4 and it is at this location where the maximum aerodynamic shear occurs.

5.7 AEROSHELL STRUCTURE

5.7.1 Requirements and Constraints

The major function of the aeroshell structure is to support the ablative thermal protection system, particularly during the critical entry phase, when surface forces in the form of aerodynamic pressure, are maximum. The aeroshell structure must transmit these aerodynamic pressure loads to the remaining entry vehicle system, which primarily is the heat source assembly, through the intermediate support structure. In addition, the aeroshell structure must be designated to withstand all other mission environments prior to reentry without

TABLE 5.6-III

CANDIDATE THERMAL PROTECTION SYSTEMS

SYSTEM	MATERIAL DESCRIPTION	REMARKS
A. ABLATIVE	1. MOLDED GRAPHITE	STABLE IN VACUUM IN INERT ATMSOPHERE TO OVER 5000°F.
	2. PYROLITIC GRAPHITE	ANISOTROPIC PROPERTIES-STABLE BUT FLIGHT TESTS INDICATE ERRATIC BEHAVIOR DURING ENTRY
	3. CARBON OR QUARTZ PHENOLIC	LONG TIME LIMITING EXPOSURE TEMPERATURE OF 400°F UNLESS PRE-CHARRED.
	4. 3-D CARBON OR QUARTZ PHENOLIC	SAME AS NO. 3 BUT WITH HIGH INTERLAMINAR STRENGTH
	5. LOW DENSITY CHARRING ABLATORS	VERY EFFICIENT THERMALLY BUT MAY HAVE LONG TERM STABILITY PROBLEMS.
B. GRAPHITE-INSULATION COMPOSITE	PRE-CHAR GRAPHITE OVER CARBON FELT INSULATION	COMPETITIVE WEIGHTWISE WITH LOW DENSITY CHARRING ABLATORS.
C. RADIATION	HIGH MELTING POINT MATERIALS (RENE 41, REFRACTORIES)	HEATING RATES ON IRV TOO HIGH FOR UTILIZATION.
D. HEAT SINK	HIGH SPECIFIC HEAT METALS (E. G. BERYLLIUM)	VERY INEFFICIENT THERMALLY BASED ON IRV HEATING CONDITIONS.

78-0063

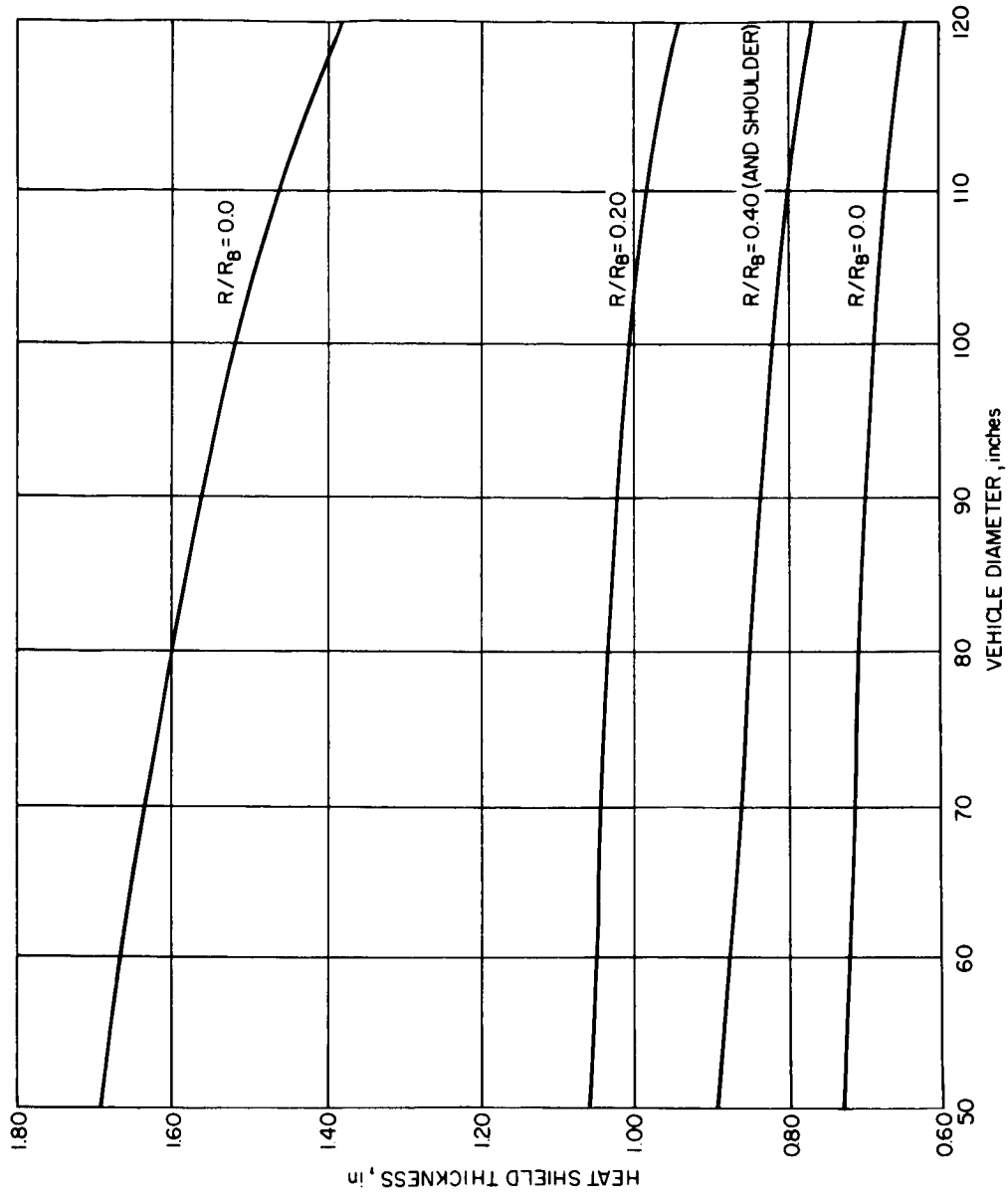

Figure 5.6-3 HEAT SHIELD REQUIREMENT FOR 60° BLUNT CONE MATERIAL -- CORK SILICONE -- SAFETY FACTOR = 1.20 (DOUBLE SKIP TRAJECTORY)

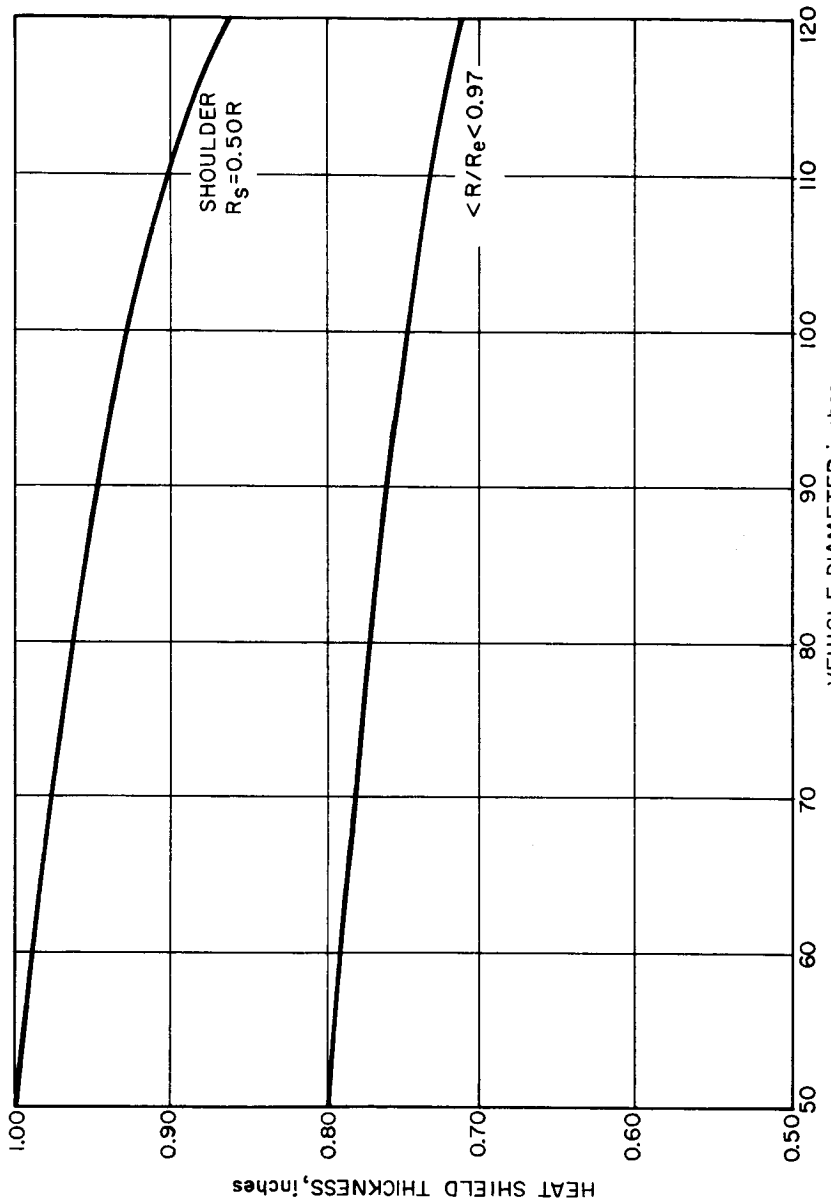

Figure 5.6-4 HEAT SHIELD REQUIREMENT FOR MODIFIED APOLLO SHAPE MATERIAL -- CORK SILICONE -- SAFETY FACTOR = 1.20 (DOUBLE SKIP TRAJECTORY)

sacrifice to its reentry performance. During the launch phase, in addition to supporting itself and the heat shield, it may be required to support the inertia loads of the heat source. The structure must also survive the long-time exposure to elevated temperature, particularly hot-spot temperatures at the heat source support structure, during the orbital phase without suffering a significant degradation of its strength capabilities.

The environmental loading conditions considered in the conceptual design phase are summarized in Table 5.7-I.

Of these load environments, reentry is the most critical and hence was used to establish the shell requirements of the aeroshell. There are, however, local areas such as the IRV tie-down, interface ring, and cylindrical skirt which have not been thoroughly evaluated as yet but which will be checked for both launch and reentry conditions.

The major design requirement was minimum weight subject, of course, to practical design constraints, such as minimum face sheet and core density. In addition, the aeroshell study was focused on practical structural materials whose mechanical properties were well known and manufacturing technology well developed.

5.7.2 Design Criteria

The blunt cone aeroshell was designed such that neither the allowable yield stresses nor the critical buckling loads were exceeded when the critical reentry loads were imposed.

The general buckling or instability evaluation of conical and spherical homogeneous shell was based on the theoretical and experimental data presented in references 43 to 48. The general instability of shells of sandwich construction was evaluated on the same basis using the concept of equivalent flexural and extensional rigidities. For the ring-stiffened conical shell, general stability was based on the orthotropic buckling theory given in reference 49.

The stiffness requirements for the base ring necessary for the conical shell to develop its ultimate buckling capability were based on the inextensional buckling analysis of a combined shell-ring structure described in reference 50.

In the stress and buckling analyses, it was assumed that the ablator material offers no load carrying contribution.

5.7.3 Structural Concepts and Material Selection

The types of shell construction that were considered for the IRV blunt cone aeroshell were monocoque, ring-stiffened and honeycomb sandwich. These design concepts were evaluated for the critical reentry load conditions shown in Table 5.7-I, as a function of reentry vehicle diameter. The monocoque, ring-stiffened, and honeycomb aeroshell weights are compared in Figure 5.7-1. The comparison is based on aluminum as the structure material; a structure temperature of 350° F was assumed.

In order to obtain as realistic a comparison as possible, the honeycomb shell weights include a factor of 1.7 to account for splices, closeouts, and the effect of bending stresses.

TABLE 5.7-I

ANTICIPATED LOAD FACTORS IN TERMS OF G'S

For design, multiply values by 1.25 unless otherwise specified.

A. Launch

1. Atlas-Centaur

(a)	Maximum Axial Load Condition (includes vibration component)	$A_x = 6.4$ $A_n = 0.5$
(b)	Maximum Lateral Load Condition (includes vibration component)	$A_x = 2.3$ $A_n = 2.0$

2. Saturn I-B

A_x* = 4.7 } Does not include
A_n* = 1.0 } vibration components

*For design, assumed ultimate load factors of $A_x = 10$ and $A_n = 2.0$ to cover vibration.

B. Abort

A_x (with respect to IRV) = 10

C. Reentry

$A_x = 25.6$

$A_n = 2.0$

P_s (stagnation pressure) = 16.2 psi

D. Chute Deployment and Air Snatch

$A_x = 8.0$

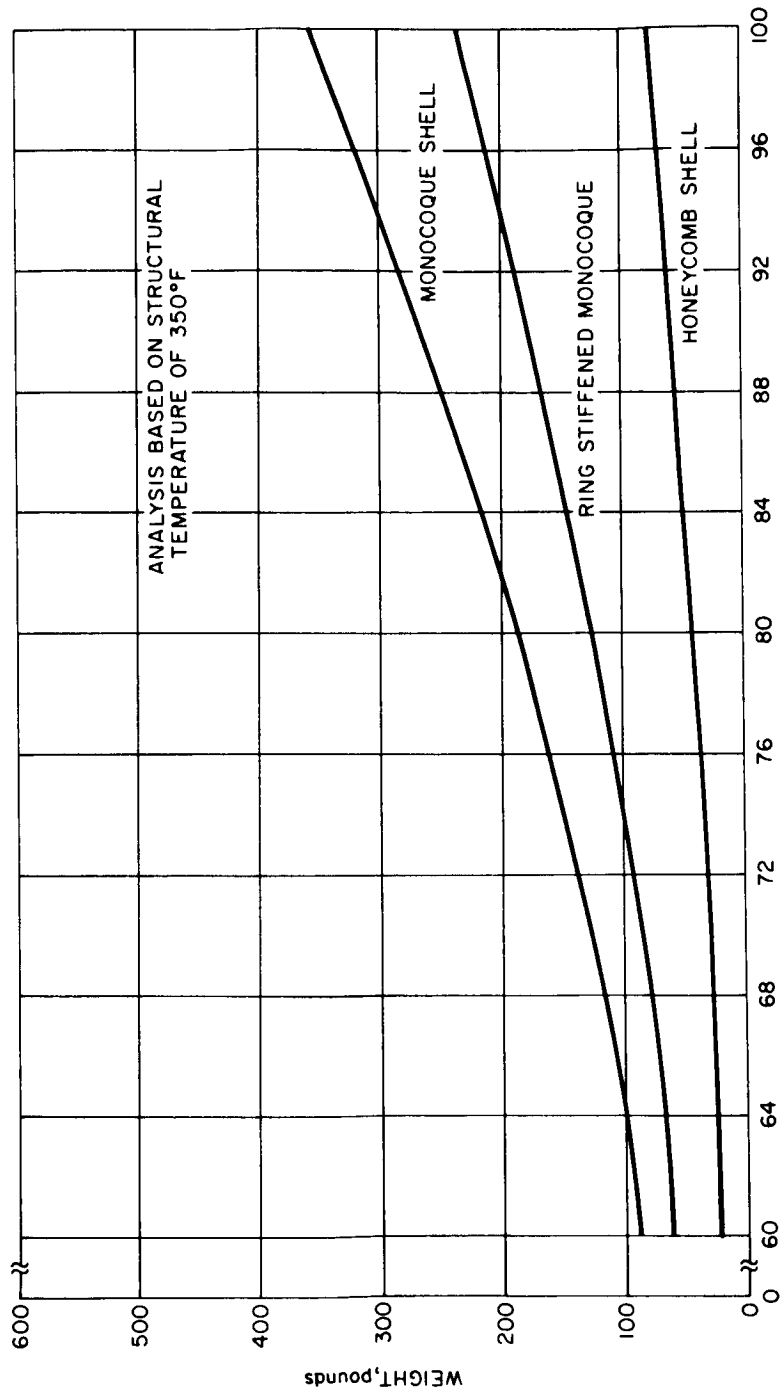

Figure 5.7-1 STRUCTURAL WEIGHT FOR VARIOUS ALUMINUM SHELL DESIGNS -- 60° BLUNT CONE

The weights shown in Figure 5.7-1, however, do not include either an attachment ring for the support structure of the heat source or the base ring required for optimum cone stability; these components are essentially a fixed weight.

The results demonstrate that the honeycomb is the most efficient construction for the IRV aeroshell by offering significant weight-saving over the other two, particularly at the larger diameters.

The aeroshell weights for various candidate structural materials are compared in Figure 5.7-2 again based on the maximum critical trajectory loads and a structure temperature of 350° F. In the case of steel, titanium and beryllium, however, the weight values in Figure 5.7-2 would apply up to 600° F, the bond temperature limitation, since their mechanical properties do not change significantly. For the comparison, the minimum facesheet thickness was taken as .016-inches and the minimum core as .10 inches. The results indicate that aluminum is a more efficient structural material than either titanium or steel based on the above constraints, but not as efficient as the magnesium or beryllium with a steel core.

In order to evaluate weight saving for reduced face sheet thickness, the steel honeycomb weights were computed and also plotted in Figure 5.7-2 based on a minimum face sheet thickness of .008 inches. The high yield strength of steel would permit the use of a .008 inch face sheet for the critical IRV loads. The aluminum, however, still results in a lower weight structure. In addition, it may be possible to further optimize the aluminum honeycomb structure by reducing the face sheet thickness as well, when a preliminary design is evolved and more detailed stress analyses are performed.

5.7.4 Selected Reference Configuration

Although the magnesium and beryllium resulted in a lower weight aeroshell than aluminum, aluminum was selected as the reference structural material primarily because of its well developed manufacturing technology. In addition, the weight advantage of magnesium over aluminum in terms of actual pounds is small and, because of the low yield strength of magnesium, could disappear altogether when local stiffening of the face sheets due to bending and shear loads are considered.

As shown in Figure 5.7-1, the honeycomb construction offers a considerable weight-saving advantage over ring-stiffened and monocoque constructions. It is felt that the manufacturing problems for sandwich construction are not any more severe and could actually be less than for the ring-stiffened construction with its many small rings and thin gage.

Hence, the selected configuration for the IRV aeroshell is an aluminum honeycomb structure utilizing .016 inch face sheets. The corresponding core depth requirements to ensure stability are given in Figure 5.7-3. Further detailed shell analysis to be performed may indicate the need for thicker face sheets in local regions such as the heat source support attachment which is subjected to bending and concentrated shear loads.

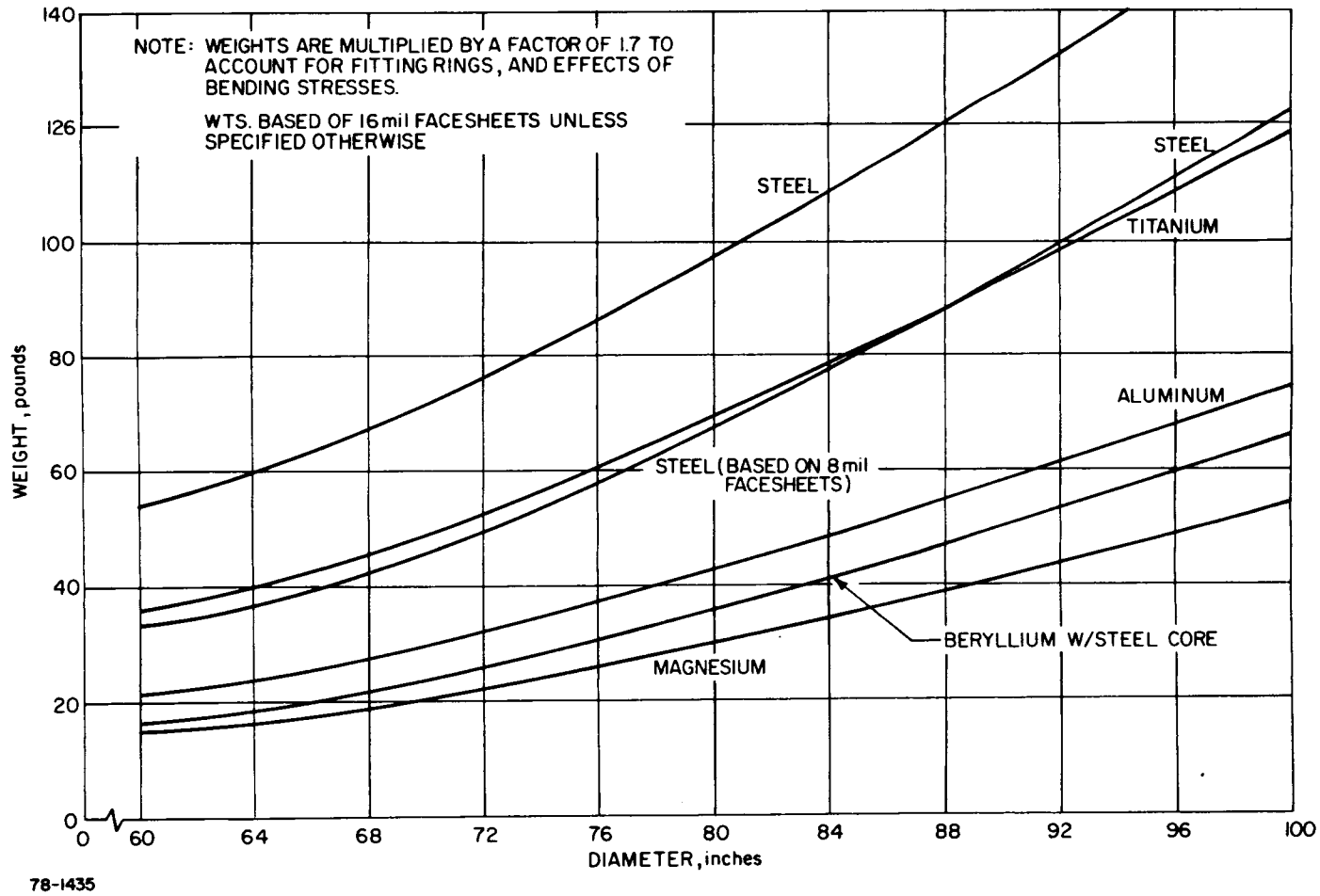

Figure 5.7-2 STRUCTURAL MATERIAL TRADE-OFF FOR HONEYCOMB CONCEPTS

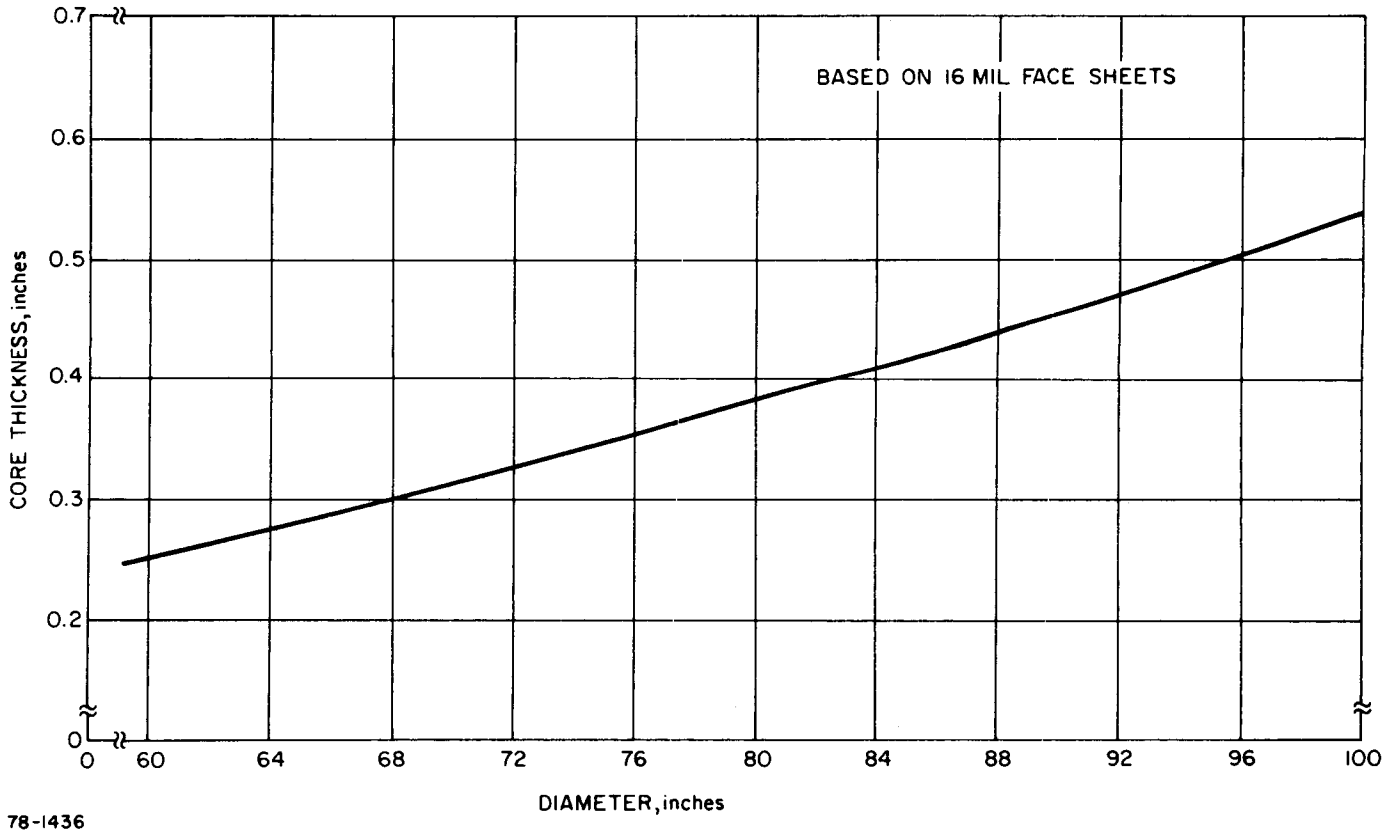

Figure 5.7-3 BLUNT CONE CORE THICKNESS VERSUS VEHICLE DIAMETER -- ALUMINUM HONEYCOMB

5.8 SEPARATION SUBSYSTEM

5.8.1 Function

In reducing the quantity of candidate IRV configurations to be studied during the conceptual design phase, separation subsystem design details are not a primary consideration. However, separation as a function was considered in the sequence of operations of all of these vehicle configurations.

The function of separation is required to detach the support ring, within which the IRV is mounted, from either the launch vehicle or the space orbiting laboratory, for both an abort or normal deorbit mode. The designs considered also assume a second separation function to detach the IRV from the support ring, including the attached propulsion hardware and support structures. This second separation is not critical to abort operations on the launch pad but is necessary for space operations, to increase the probability of predicted aerodynamic performance of the IRV at reentry into the atmosphere.

Other related operations which require some form of a separation function, depending on the overall concept, are the removal of a selected portion of the ascent fairing critical to abort emergencies, and latching operation of the support ring when the IRV is to be disengaged from the heat exchanger for other than emergency operations.

5.8.2 Performance/Design Requirements

The performance/design requirements to be considered in the selection of a specific design solution for each of the separation functions include nominal space vehicle criteria plus the following special criteria:

a. Mission Life -- 5 year minimum, 10 year design goal (periodic maintenance, replacement or repair may be considered).

b. Critical environment -- 5 year minimum at 200° F maximum, hard space vacuum and nominal particle radiation (primarily neutron and gamma emission).

c. During normal deorbit maneuvers the separation subsystem operation is part of the guidance and control sequence whereby separation anomalies contribute to the recovery site accuracy.

d. All of the separation subsystem functional approaches shall be compatible with the Atlas/Centaur launch vehicle resupply/rendezvous concept and/or the Saturn I-B launch vehicle integral space vehicle concept.

5.8.3 Design Alternatives/Technical Approach

The specific hardware solutions for each of the separation functions fall in the following categories:

a. Explosive release mechanisms

1) Explosive bolts

2) Explosive nuts with springs

3) Gas generating squibs

b. Explosive cutting charges

1) Mild detonating fuse (MDF)

2) Flexible linear shaped charge (FLSC) with springs

c. Mechanical release mechanisms

1) Ball lock joint with springs

2) Marman clamp with springs

3) Cable clamp with springs

These various separation techniques each have their advantages and disadvantages. The mechanical systems are generally less reliable than the explosive systems especially after extended exposure to the thermal and hard vacuum environment of the IRV. The explosive release mechanisms are more reliable than the explosive cutting charges since block redundancy is more easily incorporated with a minimal increase in weight and complexity. The explosive release mechanisms are far more easily safety monitored during all pre-operation phases. It seems highly desirable for the separation system to be contained such that debris from the separation event is minimized, if not eliminated. Explosive separation systems except for the FLSC can be designed to contain this debris. Personnel hazards due to inadvertent operation of the explosive release mechanism class of devices is considerably less than for the explosive cutting charges. The explosive release mechanisms are also readily replaceable if the IRV five year lifetime makes periodic replacement of pyrotechnics a necessity.

Each of the above approaches can be stored and operated in the space environment typical of the IRV operation. The five year integrated radiation environment ($< 2 \times 10^{12}$ neutrons/cm^2 and $< 10^5$ rads) is below the threshold of damage for all of these devices.

The resultant dynamic motions (tip-off rates) after separation are not significantly different for a well designed separation system of any of the above types.

A multiple hard point attachment with explosive bolt separation appears to be the best approach for the IRV separation functions. However, the actual design of each separation joint must be compatible with the requirements of the interfacing stage or vehicle. Further design and analysis during phases 1b and 2 of the program will serve to better define the separation systems to be used.

5.9 PROPULSION SUBSYSTEM

5.9.1 Function

The function of the propulsion subsystem is to provide a velocity increment to the IRV as part of an operational deorbit maneuver (Deorbit Mode) and to provide

a safe separation distance of the IRV from the potentially explosive propellants in case of a launch vehicle malfunction (Abort Mode).

5.9.2 Performance/Design Requirements

5.9.2.1 General Requirements

The performance/design requirements to be considered in the selection of the propulsion subsystem design include nominal launch/space operations criteria plus the following special criteria:

a. Mission Life -- 5 year minimum, 10 year design goal (periodic maintenance, replacement or repair may be considered).

b. Critical environment -- 5 year minimum at 150° F maximum, hard space vacuum and nominal particle radiation (primarily neutron and gamma emission).

c. No active attitude control subsystem is available during the Deorbit Mode or Abort Mode operation of the propulsion subsystem. Thrust Vector Control (TVC) during rocket engine thrusting shall be maintained by vehicle spin developed by the propulsion subsystem, either by use of spin rockets mounted to the vehicle or application of propulsion forces to both the spin and transverse axes from a multi-stage operation of the prime propulsion subsystem.

d. The propulsion subsystem shall include all safing, arming, and ignition sequencing components necessary to control the operation of all of the propulsion hardware when initiated by the application of a discrete deorbit or abort signal.

e. The propulsion subsystem shall be compatible with the Atlas/Centaur launch vehicle resupply/rendezvous concept and/or the Saturn I-B launch vehicle/integral space vehicle concept.

5.9.2.2 Typical Requirements

The following propulsion subsystem requirements have resulted from the system engineering trade-off studies of a nominal system operation:

a. Abort Mode

1) Velocity increment - 100 to 125 fps

2) Spin rate - 7 to 10 rpm (applied before abort rocket thrust buildup)

3) Abort rocket burn time - 9 to 11 seconds

b. Deorbit Mode

1) Velocity increment - 500 to 600 fps

2) Spin rate - 7 to 10 rpm (applied before deorbit rocket thrust buildup)

3) Deorbit rocket burn time - 9 to 11 seconds.

5.9.3 Design Alternatives/Technical Approach

Applying the propulsion system requirements to the various configurations studied resulted in a deorbit/spin rocket engine combination with the following characteristics for a 1500 pound nominal weight IRV:

a. Deorbit velocity increment - 500 fps

b. Deorbit rocket thrust - 2800 pounds

c. Deorbit rocket total impulse - 27,500 lb-sec

d. Deorbit rocket burn time - 10 seconds

e. Deorbit rocket thrust application angle - less than 1/4° off axis

f. Spin rocket thrust (4 units) - 215 pounds each

g. Spin rockets burn time - 1.00 second

h. Spin rate - 7.25 rpm

Current state-of-the-art solid propellant propulsion techniques were considered in the synthesis of the propulsion subsystem hardware to accomplish the above systems operation. The Atlantic Research Corporation Mark 6, 1.0 KS 210, control rocket is typical of hardware which can supply the spin forces. A variety of spherical motors are available from the Thiokol Chemical Company which can be adapted specifically to the IRV application depending on the actual weight and velocity requirements of the vehicle configurations.

Design solutions which use the deorbit rockets for performing the abort function as well, are preferable to reduce the overall propulsion hardware requirements. In the case above, with the 1500 pound IRV and the 27,500 pound-seconds total impulse deorbit rocket used at sea level as an abort rocket, a separation distance of over 200 feet from the launch vehicle can be attained for either separate or integral launch concept. However, if configuration selections result in the application of a separate abort propulsion concept, a total impulse of approximately 7000 pound-seconds is all that would be required for safe abort of a 1500 pound IRV.

Continuing system configuration trade-offs of the IRV, discussed in section 6, are divided into four basic propulsion subsystem installations:

a. Multiple rocket motors installed on the periphery of the IRV for abort/deorbit and spin functions.

b. A single rocket motor internally located on center in the rear of the IRV for abort/deorbit functions, plus multiple rocket motors located on the periphery for the spin function.

c. A multi-nozzled single rocket motor located on a tower in front of the IRV for abort/deorbit functions, plus multiple rocket motors located on the periphery for the spin function.

d. A single rocket motor located on the front of the IRV for the deorbit function, and multiple rocket motors installed on the periphery for the abort/spin functions.

In each case the implementation of the propulsion subsystem hardware details is functionally similar, although physically different, and not limited by propulsion hardware capability. Total system configuration trade-offs of weight, size, thermal control, packaging complexity and operational flexibility will be the primary factors in the selection of the propulsion subsystem which is compatible with the overall systems approach.

6.0 IRV DESIGN SYNTHESIS

As has been described in the preceding discussion (Section 5.0) many different combinations of subsystem alternatives have been considered during Phase IA. The matrix of different alternatives has been evaluated primarily on the basis of the criteria listed in Table 1.0-II. These criteria have been employed where necessary as the basis for specific recommendations in the various individual subsystems described in Section 5.0. It must be noted, however, that once basic approach feasibility has been established, e.g., temperature capability, or allowable stress levels are not exceeded, the evaluation criteria quickly reduce to weight, diameter and relative complexity (or reliability) of competitive systems.

Several items must be investigated concurrently in order to produce the most beneficial IRV concept. The most efficient system may not necessarily be the minimum weight or diameter vehicle since other factors (e.g. impact attenuation requirements) may be of such importance that their penalty must be assumed. Table 6.0-I summarizes the major factors that influence the design of the IRV. It should be noted that while tradeoffs can be obtained on most of the factors individually, the final design recommendations have been developed on the basis of the integrated effect.

Section 6.1 summarizes the effect of these major factors on the candidate IRV systems. Weight and diameter tradeoffs are developed in Section 6.2. Finally, the recommended IRV concepts are described briefly in Section 6.3. Weight and diameter penalties associated with different variations from the basic vehicles are also identified in Section 6.3.

6.1 CONFIGURATION AND PACKAGING FACTORS

6.1.1 Heat Source

The most significant parameter of those described in Table 6.0-I is the heat source configuration simply because any change in configuration will directly alter the vehicle diameter if all other parameters remain fixed. Figure 6.1-1 shows the various configurations studied during Phase 1A. It should be noted that these variations were developed as a result of attempts to minimize the IRV diameter and weight, while providing desired aerodynamic performance. There is no particular advantage solely accruing to the Heat Source per se from any of these variations. The circular planar heat source (Figure 6.1-2) is the basic configuration from which the others evolved. This shape has the advantage of being symmetrical and, thereby, does not introduce any inertia asymmetries, which is more favorable for stability. This is undoubtedly the simplest configuration to integrate into the IRV.

The rectangular planar concept (Figure 6.1-3) was investigated because it appeared to offer significant design advantages, if recovery aids are to be incorporated, due to the comparatively large, useful volume available on two sides of the heat source (i.e., parachute storage requirements favor cubical packaging envelopes). Disadvantages include non-uniform moments of inertia and the design of the impact attenuation structure in the corner regions.

TABLE 6.0-I

MAJOR DESIGN FACTORS

1. Heat Source Configuration
2. Reentry Vehicle Shape
3. Impact Attenuation Requirement
4. Heat Source Recess Requirement
5. Recovery Aids
6. Abort and De-Orbit Rocket System

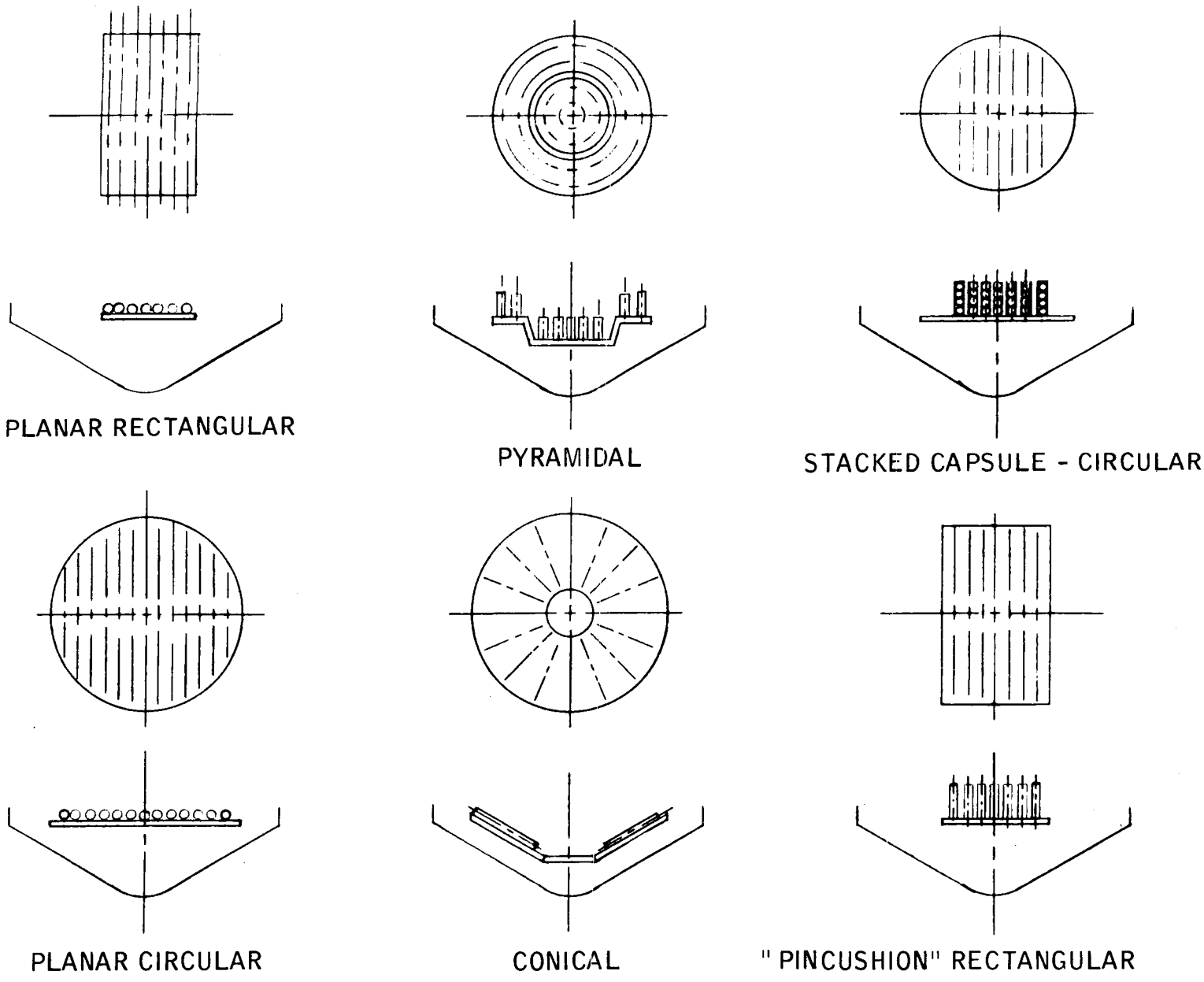

Figure 6.1-1 CANDIDATE IRV AND HEAT SOURCE CONFIGURATIONS

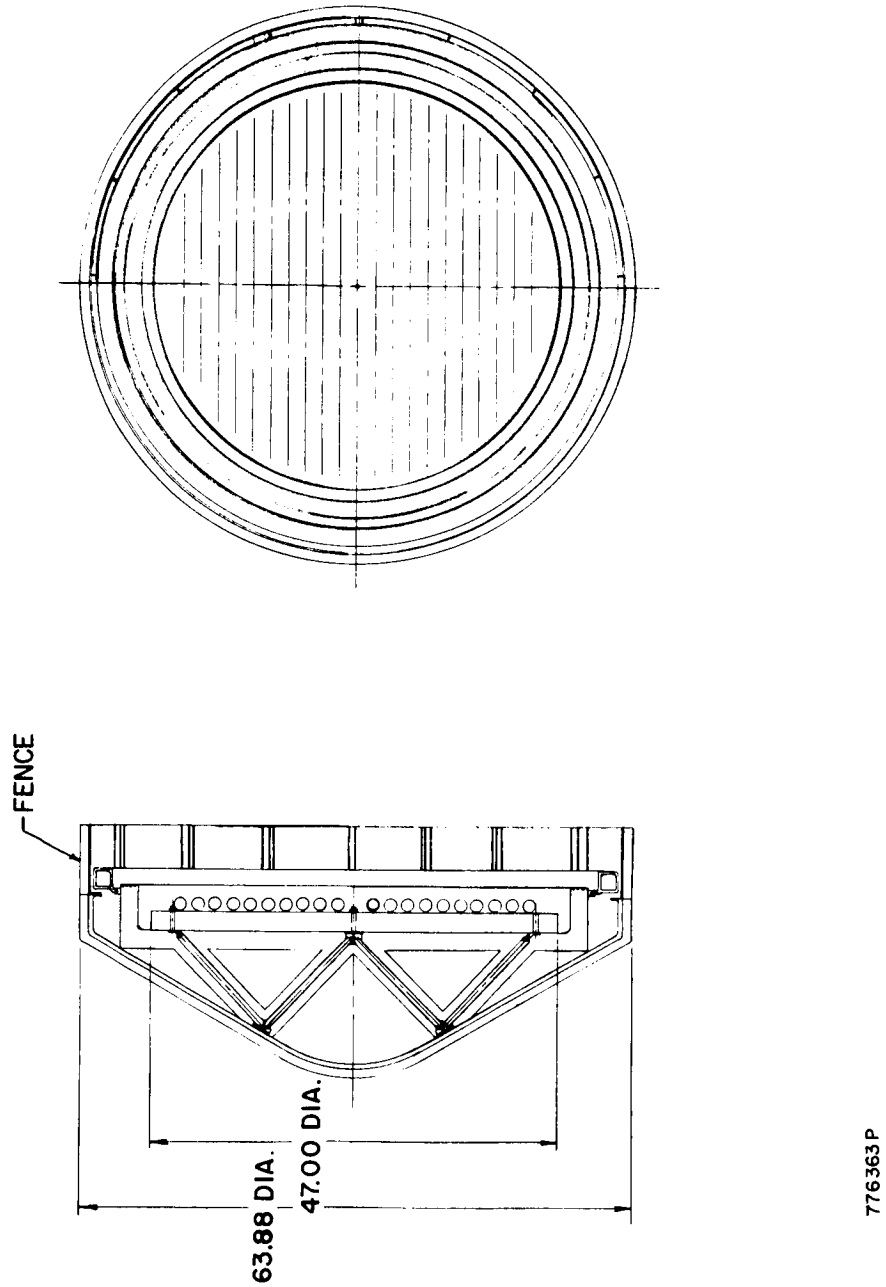

Figure 6.1-2 60° BLUNT CONE MINIMUM DIAMETER -- 47-INCH CIRCULAR PLANAR ARRAY

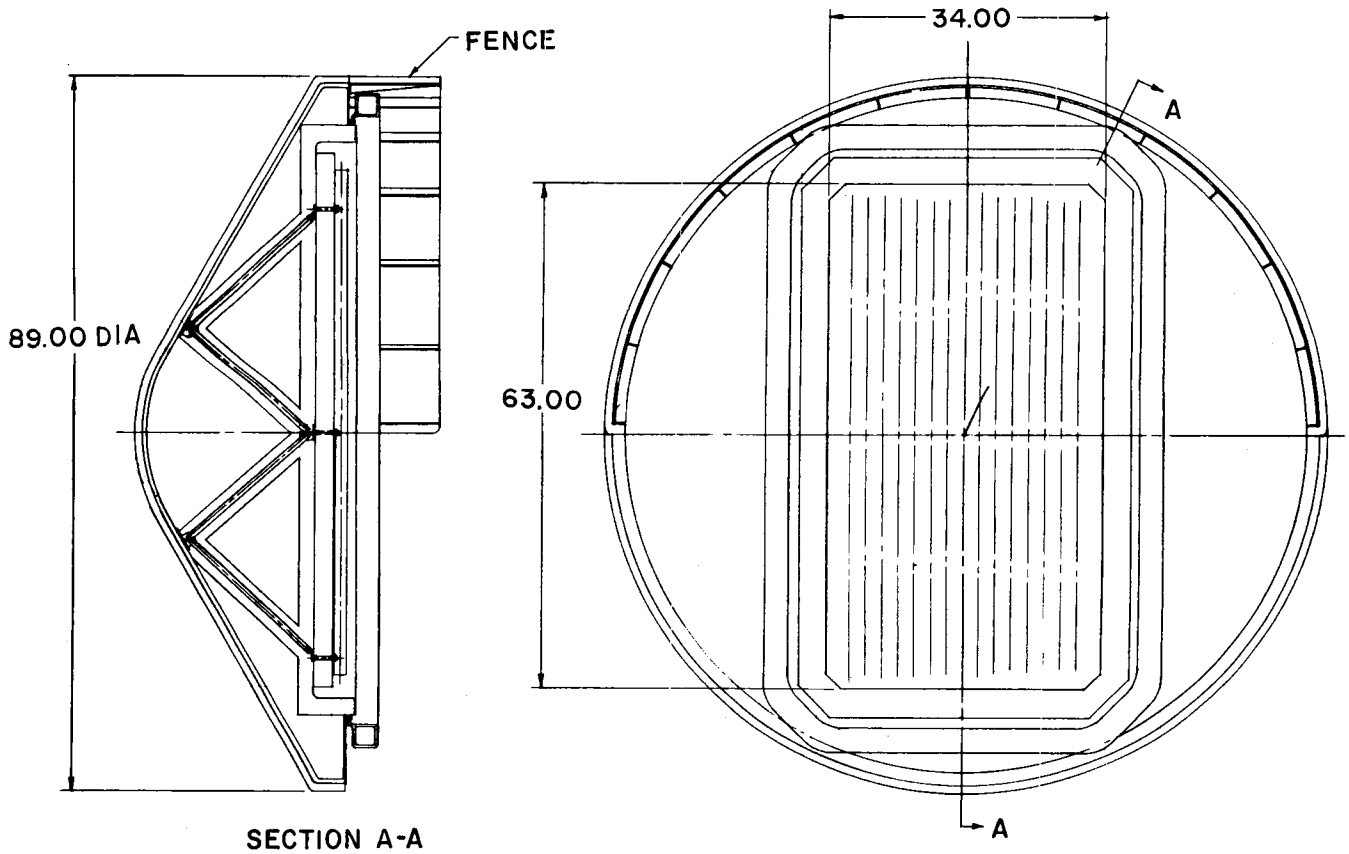

Figure 6.1-3 60° BLUNT CONE -- RECTANGULAR ARRAY (IC)

Both of these configurations require additional stiffening to meet the desired fundamental frequency requirement of 200 hertz or greater.

The conical configuration (Figure 6.1-4) was evaluated because it offered promise of improved aerodynamic performance, i. e., a more favorable forward (toward the nose) C.G. location and static margin. These benefits are achievable only for a large cost in vehicle diameter and weight. The "bare" vehicle is approximately one foot larger in diameter and weighs 150 pounds more than the comparable minimum diameter (47 in.) circular planar Heat Source IRV (Figure 6.1-2). The total diameter and weight required for the conical system will undoubtedly grow as the current short thermal path indicated in the Figure 6.1-4 truss must be increased to provide an acceptable temperature range at the truss/aeroshell attachment point. In addition, the conical configuration requires a complex ACHX design to remove the heat in the apex of the cone.

A pyramidal concept, Figure 6.1-5, at first appeared attractive due to potential gains in system diameter, weight, and aerodynamic performance. Detailed review of the concept proved that these potential gains were illusory, and that the difficulties occasioned in HSHX design were not commensurate with the advantages. In addition, the HSHX could not be inplace redundant and removable with one degree of freedom.

The initial redesign led to the rectangular pin cushion concept. In this concept parallel rows of vertical capsules make up the Heat Source array (Figure 6.1-6). The most advantageous (squarest) arrangement is a 32 by 56 inch configuration. This did not offer any diameter gains. Figure 6.1-7 shows another variation of capsule arrangement in the attempt to achieve a minimum diameter Heat Source Array. This is a stacked capsule array in which capsules are stacked like logs, four deep in each row. The rows' lengths are sized so that the total array approximates a circle. HSHX tubes and fins are interleaved with the capsule rows to assure adequate heat removal and temperature distributions. This particular concept has been based on the use of graphite block retention of the capsules. It appears to offer promise of weight and diameter savings. However, these savings are achieved at considerable penalty in system complexity. This system should be reviewed in detail in Phase 1B of the study to develop more realistic weight, size, and design data.

An additional concept investigated during Phase 1A was the "donut" design where the recovery aids and abort rocket were placed in the center of the vehicle. This design offered the advantage of better system reliability since it eliminated the problems associated with peripheral attachment of these subsystems (see Section 5.8 for a description of these problems). However, the added structural weight penalty due to the large variance in Heat Source diameter is so great as to make this concept extremely unattractive in comparison with the other concepts. Therefore, primary emphasis has been placed on attachment of the rockets external to the IRV.

6.1.2 Reentry Vehicle Shape

One of the basic tradeoffs considered during this phase of the study has been the choice of aerodynamic shape of the IRV. Two basic candidates have been considered - a 60° Blunt Cone and a Modified Apollo Vehicle. The relative aerodynamic performance of these two shapes is treated in Section 4.0. Preliminary

study indicated that the Modified Apollo shape might be slightly more efficient (in terms of vehicle diameter requirement) than the 60° Blunt Cone. In addition the stagnation point convection heating rates on the Modified Apollo are approximately one-third of the rate on the 60° Blunt Cone. However, the heating is similar at station outboard of the vehicle stagnation points; therefore, heat shield weights are comparable.

The potential diameter advantages are also illusory in that for a given stability requirement, e.g., subsonic angle-of-attack oscillation envelope, and consequent cylindrical section length limitation, the Modified Apollo Vehicle is larger in diameter than the Blunt Cone. This is due to the greater cost in diameter growth per incremental inch of vertical dimension for the Modified Apollo configuration. Figure 6.1-8 shows a minimum diameter circular planar Heat Source Array in a Modified Apollo shape. The overall vehicle diameter for the "bare" vehicle (no recess or recovery aids) is only slightly larger than the Blunt Cone. But this difference grows rapidly with increasing vertical dimension requirement as is discussed in Section 6.2 and shown in Figure 6.2-2. It should also be noted that temperature control requirements may dictate increased truss leg lengths above the dimensions shown in Figure 6.1-8.

6.1.3 Impact Attenuation

Section 5.4 has summarized the study effort performed in developing an impact attenuation system concept. Impact attenuation (crushup), recessing, and recovery and packaging requirements have significant impact on IRV diameter (and weight) separately or when combined. This is due to the vertical dimension requirement and subsequent diameter growth for crushup and recess; and to packaging volume on the periphery of the vehicle for recovery and retardation systems.

Even the "rotating plate" concept discussed in Section 5.4 results in significant weight and diameter penalties, as illustrated in Figure 5.4-11. Use of this system requires modification of the current Heat Source support plate and inclusion of a ring of honeycomb crushup around the periphery of the Heat Source plate as is shown in Figure 6.1-9. The diameter penalty shown here, 2 feet, is typical for crushup inclusion. Effort in Phase 1B will be devoted to a tradeoff analysis to develop an optimum system, i.e., the lightest weight vehicle, considering such factors as vehicle weight, impact velocity, diameter, and crushup stroke.

6.1.4 Heat Source Recess Requirement

In order to maintain acceptable capsule temperatures ($< 2500^{\circ}$ F) during entry for any possible vehicle attitude, some recessing may be required (See Section 4.0). The incorporation of this recess into the design will, of course, mean a potential increase in vehicle diameter and weight. At the same time, a more favorable center of gravity situation could be obtained.

6.1.5 Recovery Aids

The inclusion of recovery aids in the vehicles also has a significant effect on vehicle diameter and weight. Enough volume and length must be provided to ensure that adequate space exists for the various aids including parachutes, flotation bag, etc. In addition, another penalty associated with the aids is

the increased thermal protection required to protect the devices from both long term heat source and short term reentry heating. A brief review of recovery aid location and packaging requirements included consideration of centrally located recovery aids as shown in Figure 6.1-10. Although this approach was conceptually attractive, the weight and diameter penalties are clearly unacceptable.

6.1.6 Propulsion Subsystem Integration Tradeoffs

Figure 6.1-11 illustrates four concepts for integration of the propulsion system. Concept 1 shows several peripherally mounted solid rockets used for both de-orbit and abort. While this concept provides the easiest integration into the IRV, it can exhibit an intolerable failure mode. The failure of a single rocket could result in a pitch rate well in excess of 1000 rpm at entry which cannot be stopped during entry by a reasonably sized turn-around device on the IRV. This, however, is an extremely low probability event.

Consideration of the above failure mode led to concepts 2 through 4, each using a single rocket or cluster of rockets. Concept 2 shows a central internal location for the rocket. This concept requires a central hole in the heat source plate through which the rocket is installed. The central hole forces the heat source diameter to increase to maintain the same power level (23 KW_t). The larger diameter heat source significantly increases the IRV diameter and weight. There are also severe problems in maintaining the temperature of the rocket compartment within tolerable limits for the five year orbital lifetime of the IRV.

Concept 3 places the single rocket or rocket cluster on an abort tower structure forward of the IRV. For separate launch on the Atlas/Centaur launch vehicle, this abort tower fits easily within the ascent shroud. However, integration of the IRV with abort tower into the integral launch concept appears difficult since the IRV is mounted on the side of the MORL with the abort tower extending laterally.

The fourth concept illustrates a single rocket or cluster of rockets mounted against the IRV heat shield and directed in an opposite sense than in the previous three concepts. This concept is applicable for de-orbit, but requires a separate propulsion system for launch pad and ascent abort. The abort rockets can be mounted as shown in Concept 1 and would only be used under circumstances in which the high tumble rate failure mode is acceptable, e.g., pad aborts. The abort rockets need only provide about 100 feet per second velocity increment; the prime requirement being a high thrust level for fast exit from a launch vehicle explosion. During the de-orbit sequence using concept 4, about 1/2 orbit delay is necessary from IRV separation and spin-up until the application of the de-orbit ΔV to place the IRV in the proper orientation for ΔV application without having the space station in the path of the de-orbiting IRV.

6.1.7 Summary

In summary, all of the aforementioned factors influence to varying degrees the vehicle diameter and weight. In certain situations, it is possible that use of the above parameters do not affect the vehicle diameter at all simply because the inclusion of another parameter allows its incorporation without any penalty. Examples of this will be shown in section 7.0.

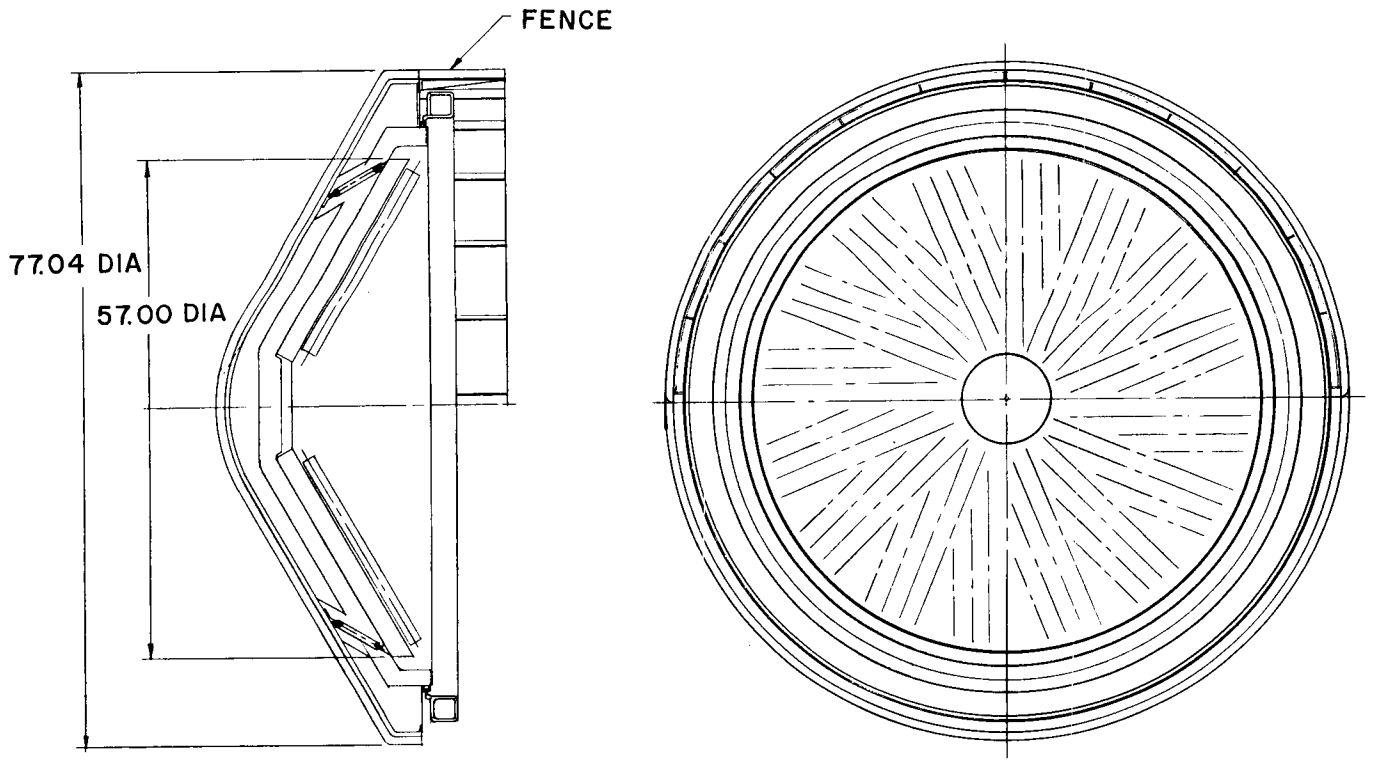

Figure 6.1-4 60° BLUNT CONE -- CONICAL ARRAY WITH TRUSS SUPPORT (2A)

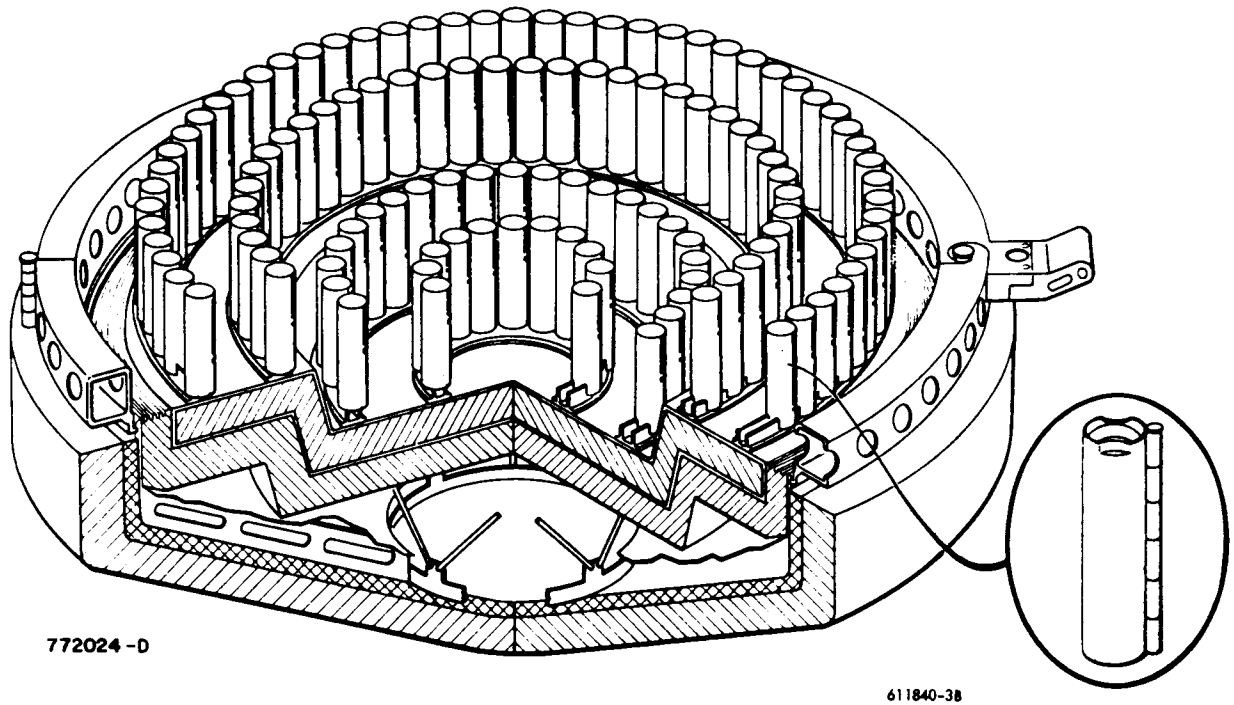

Figure 6.1-5 ISOTOPE REENTRY VEHICLE: SYSTEM 4

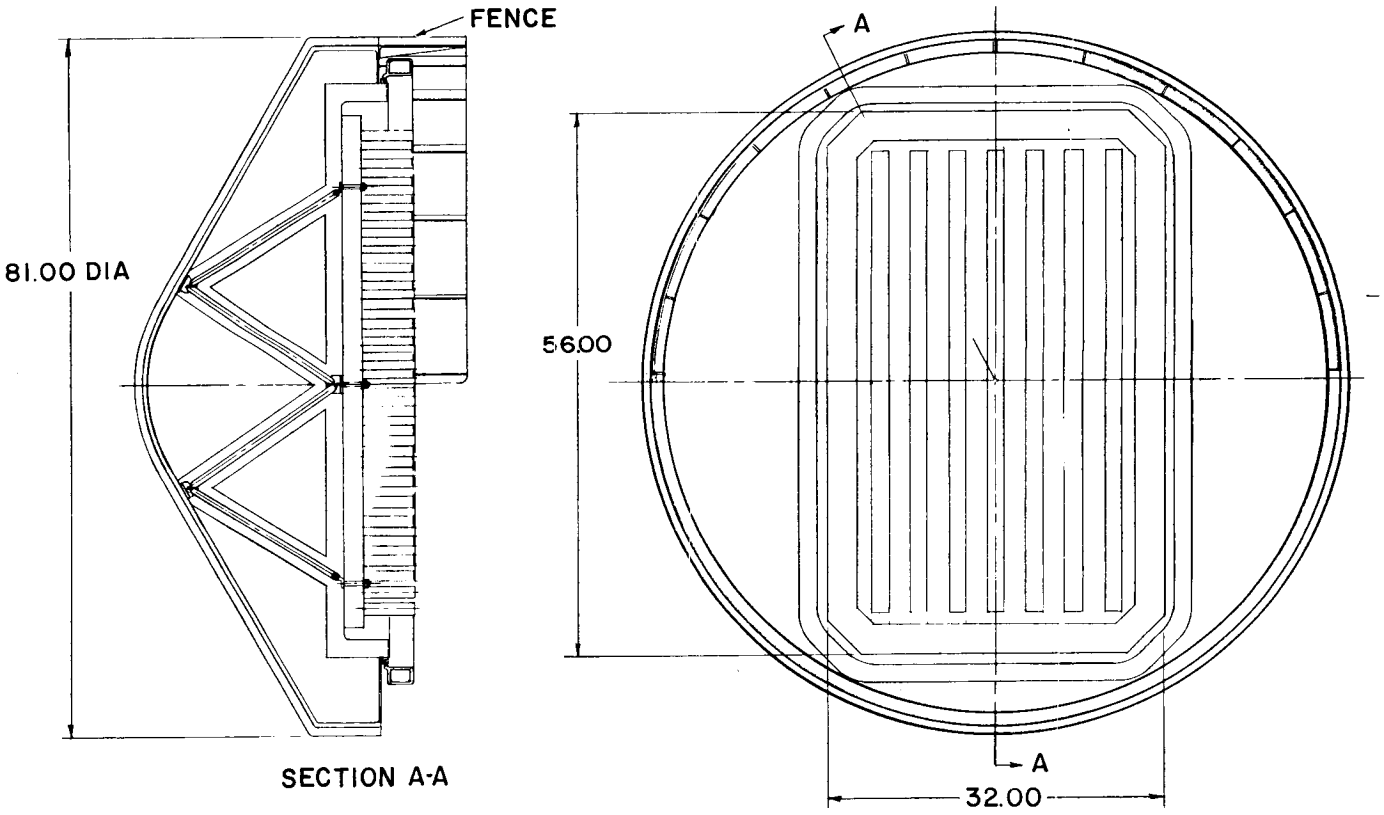

Figure 6.1-6 60° BLUNT CONE -- RECTANGULAR -- VERTICAL CAPSULE ARRAY

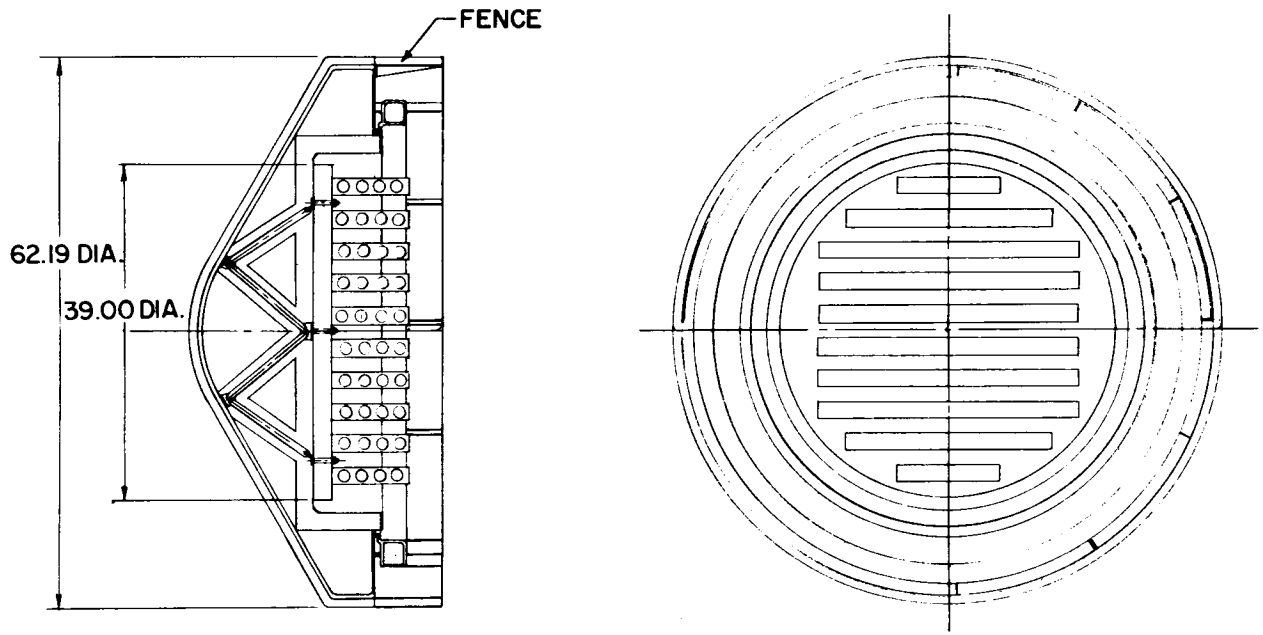

776371P

Figure 6.1-7 60^{0} BLUNT CONE -- CIRCULAR -- STACK CAPSULE ARRAY (3A)

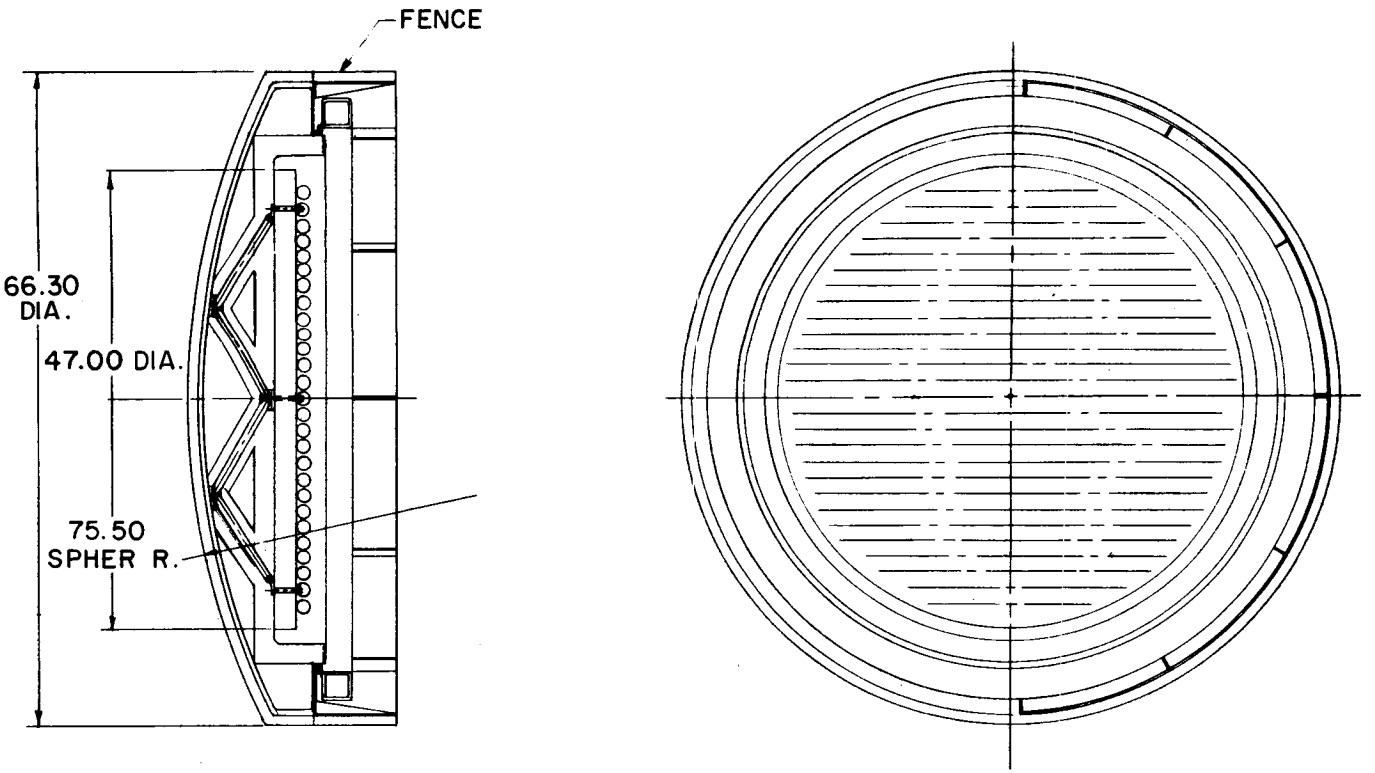

776378P

Figure 6.1-8 MODIFIED APOLLO -- 47-INCH CIRCULAR PLANAR ARRAY (4A)

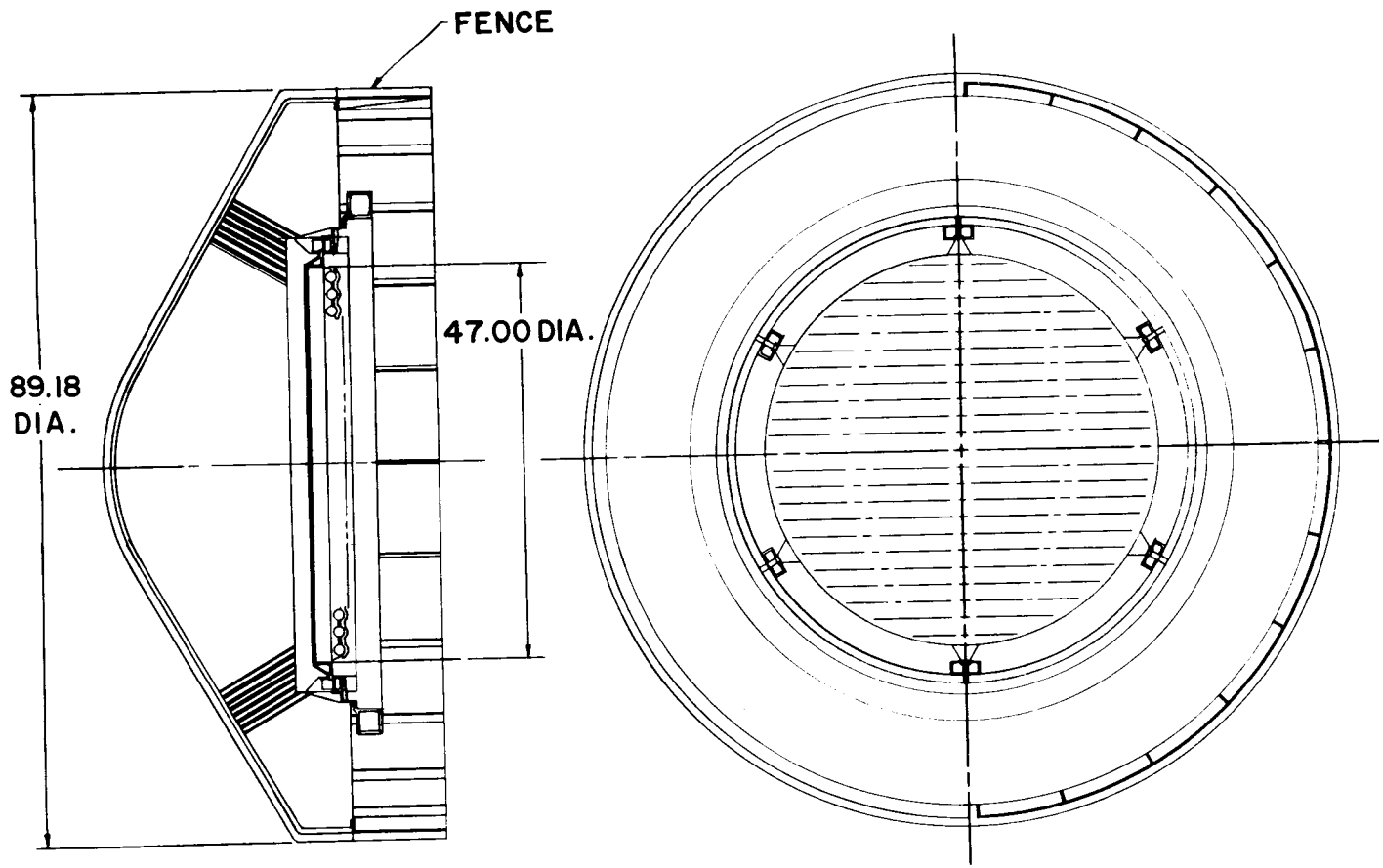

78-0051

Figure 6.1-9 60° BLUNT CONE -- CIRCULAR PLANAR ARRAY WITH CRUSH-UP (1A)

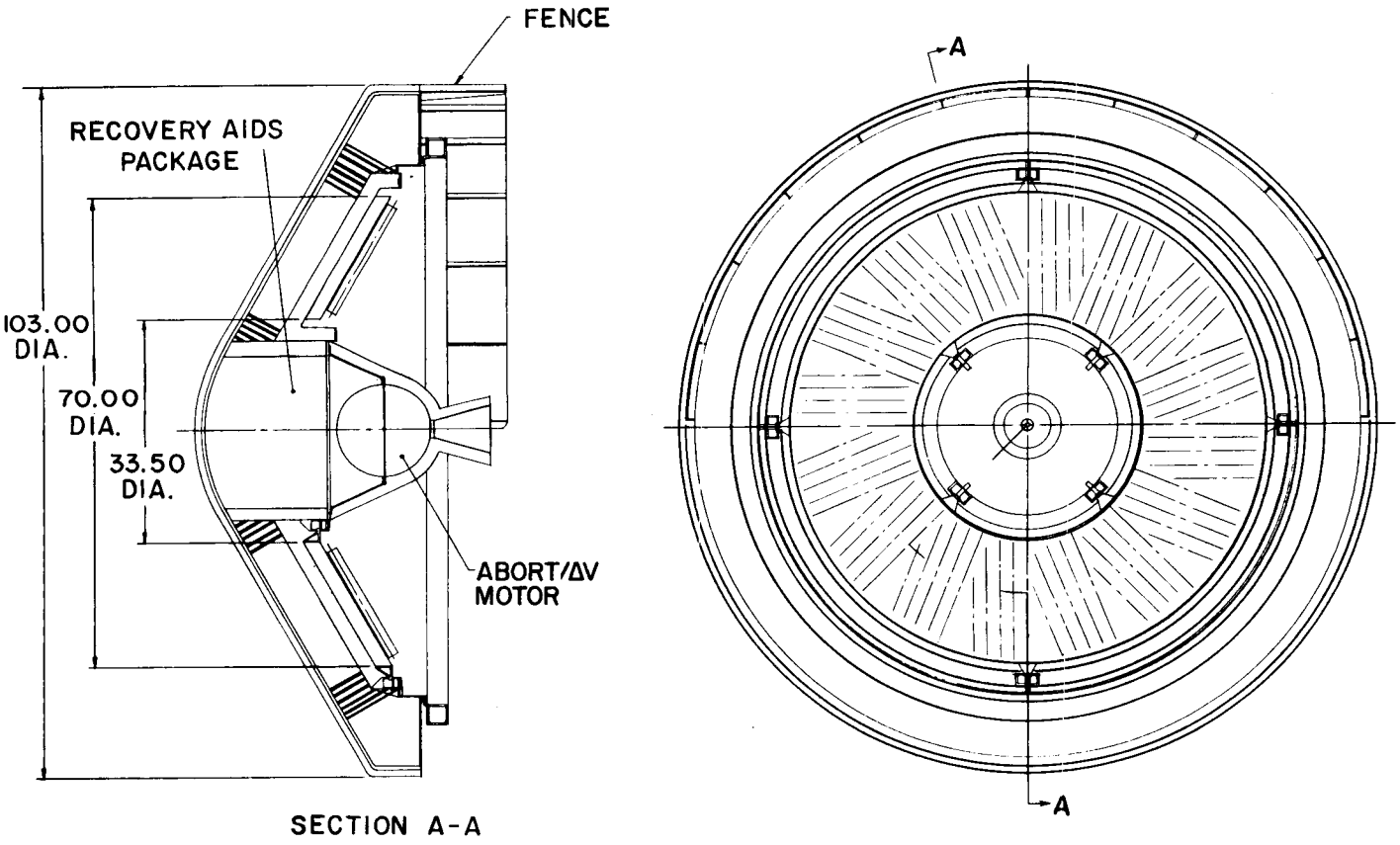

Figure 6.1-10 60° BLUNT CONE -- CONICAL ARRAY -- CENTRAL RECOVERY AIDS (2B)

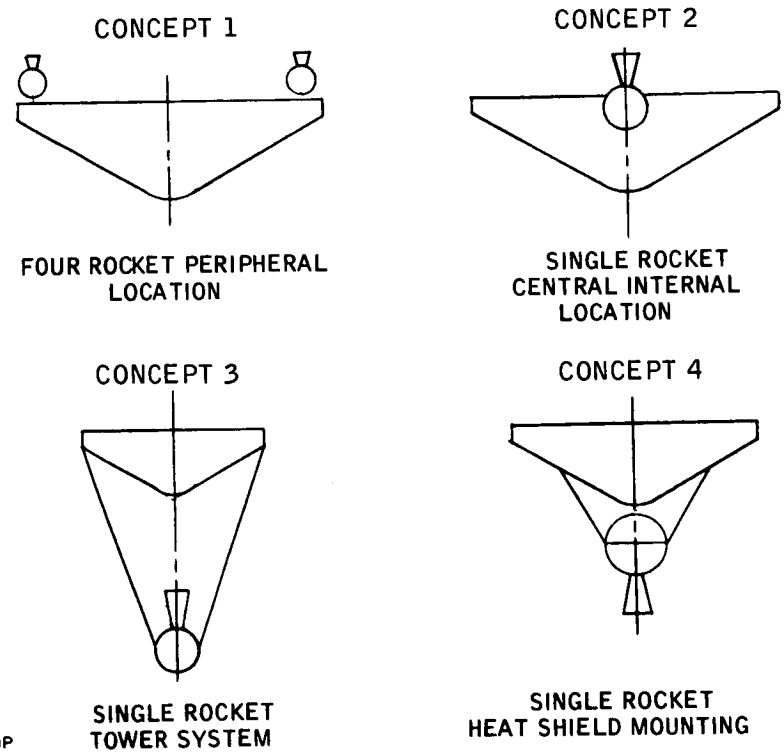

Figure 6.1-11 DEORBIT AND ABORT ROCKET INTEGRATION CONCEPTS

A significant problem area centers about the outer periphery of the vehicle where the support ring, recovery aids, aerodynamic fence and possibly abort rockets are situated. The design details of this region could result in a situation where another small diameter penalty may have to be paid to produce an overall efficient design.

Figure 6.1-12 presents a summary of the various concepts including diameter and weight data for the case of no crushup or recess. These data provide an indication of the minimum diameter vehicle one should expect from the heat source configurations studied during Phase 1A. The diameter and weight effects of recess, crushup material and recovery aids will be discussed in the next section for the various concepts.

6.2 VEHICLE TRADE-OFF STUDIES

Table 6.2-I indicates the IRV minimum size vehicle for the candidate heat source concepts. The table shows that the vehicle diameter ranges between 62 and 81 inches while the weight varies between 1140 and 1416 pounds. The concepts are rated as to their simplicity of integration with the heat exchanger and attachment and support schemes. While this table is informative, it is necessary to determine the penalties associated with the designs by including recess, crushup and recovery aids.

Figure 6.2-1 shows a parametric study of the required vehicle diameter for the case of the 47 inch diameter circular planar heat source with a 60 degree blunt cone configuration. The cylinder length as defined by the ratio Lc/R_B is considered the variable and would be defined by aerodynamic stability considerations. For the purposes of selecting a reference design an Lc/R_B value of 0.15 was chosen as being acceptable and a vertical line at this value is shown dotted in the figure. The effects on diameter of adding recess, recovery aids, crushup or combinations thereof are indicated.

The recess is defined as the top of the heat source support plate being three capsule diameters below the base plane of the vehicle. The crushup requirement is consistent with that defined in section 5.4 for the intact rotating plate concept. The horizontal dotted line refers to the minimum vehicle diameter that can be obtained with the 47 inch planar heat source accounting for supports, superinsulation and aeroshell.

Inspection of Figure 6.2-1 indicates that the crushup requirement is such as to provide the largest diameter penalty of all the parameters. In fact, if the crushup requirement as now defined is used the incorporation of recovery aids would produce only a weight penalty and would not effect the size of the vehicle. Another interesting fact is that the selection of the $Lc/R_B = 0.15$ as a reference is compatible with the minimum diameter bare vehicle design.

The effect of the aerodynamic stability requirements can be seen by noting that as the Lc/R_B varies between 0.20 to 0.05 the vehicle diameter increases by approximately 16 inches.

A comparison in the tradeoffs for the circular planar heat source with the Modified Apollo shape is shown in Figure 6.2-2. It is obvious in comparing

Figures 6.2-1 and 6.2-2 that for the conditions here the Modified Apollo produces a weight penalty relative to the blunt cone and that this penalty grows larger as the Lc/R_B is decreased.

Figure 6.2-3 shows similar information for the 57 inch diameter conical heat source. As in the planar case. the inclusion of the crushup material allows recovery aids with no diameter penalty. However, in the conical case, it is noteworthy that the minimum diameter vehicle (defined by the attachments, etc.) is 77 inches and capsule recess can be obtained with no diameter or weight penalty. Comparing Figures 6.2-1 and 6.2-3 it is apparent that while the minimum vehicle for the circular planar source is 13 inches less than the conical configuration the difference between the two is considerably less as crushup, recess or recovery aids is added. Note that for the conical heat source, however, the crushup does not provide intact plate impact as in the planar case.

Figure 6.2-4 indicates the variation in vehicle diameter for the planar heat source as a function of crushup stroke. Also shown on the curve are the added effects of recess and the current crushup design point for the plate intact impact attenuation concept. Note that every inch of added crushup stroke is transferred into a 3.5 inch increase in vehicle diameter.

For the calculation of the diameter increase required for recovery aids, it was assumed that a 6000 $in.^3$ volume with a minimum axial length of one foot was required to package the equipment. In addition, only 45^o of circumference was considered usable for the aids.

Table 6.2-II provides a complete summary of diameter and weight for the various configurations studied during Phase 1A. In addition to the penalties incurred by adding crushup, recess, and recovery aids the effect of incorporating the recovery aids in the center of the vehicle (donut design) was evaluated. Inspection of Table 6.2-II leads to the following conclusions:

a. The Modified Apollo configuration offers no advantage over the blunt cone even for the minimum case with a 47 in. circular heat source. As more requirements are imposed the penalties associated with the use of the Apollo shape become larger.

b. The rectangular planar source produces weight and diameter penalties relative to the circular planar configuration even when only recovery aids are considered.

c. The central recovery aid design results in a significant diameter penalty and a severe weight increase over comparable designs with the recovery aids placed in the outer periphery. This is true for both the planar and conical heat source configurations.

d. Use of the conical heat source results in vehicle diameters from 2 to 13 inches larger than the circular planar concept depending on recess, crushup and recovery aid incorporation. In addition, the conical design results in a weight penalty of between 90-170 lbs relative to the planar design again depending on the design.

	A	B	C
1	CIRCULAR PLANAR 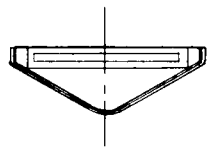 DIA 64.00 WT 1500	CIRCULAR PLANAR CENTRAL R/A 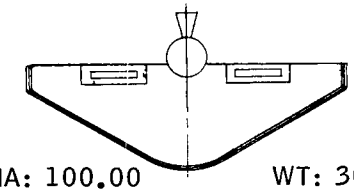 DIA: 100.00 WT: 3000	RECTANGULAR PLANAR 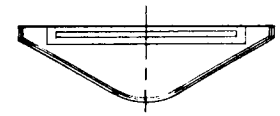 DIA: 89.00 WT: 1890
2	CONICAL 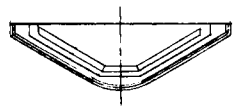 DIA: 77.00 WT 1660	CONICAL CENTRAL R/A 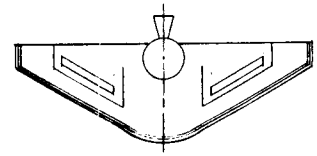 DIA: 103.00 WT 3160	
3	CIRCULAR PLANAR PIN CUSHION 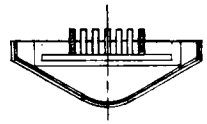 DIA: 62.00 WT: 1320		RECTANGULAR PIN CUSHION 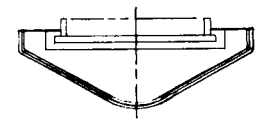 DIA 81.00 WT: 1435
4	APOLLO CIRCULAR PLANAR  DIA: 66.30 WT 1500	APOLLO CENTRAL R/A 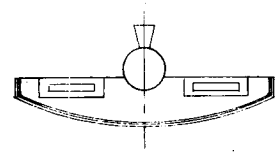 DIA: 100.00 WT: 3000	APOLLO RECTANGULAR 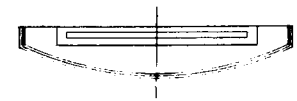 DIA: 89.00 WT: 1890

78-0054

Figure 6.1-12 IRV CANDIDATE CONFIGURATION SUMMARY

TABLE 6.2-I

BASIC IRV CONCEPTS - CHARACTERISTICS SUMMARY

	 B. C. CIRC PLANAR	 B. C. CONICAL	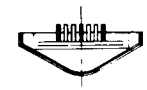 B. C. CIR. PIN CUSHION	 MOD APOLLO PLANAR	 B. C. RECT. PIN CUSHION (32 x 56)
DIAMETER (IN)	64	77	62	66	81
ENTRY WEIGHT (LBS)	1500	1660	1320	1500	1435
HEAT SOURCE WEIGHT (LBS)	1304	1416	1140	1304	1180
W/C_DA (LBS/FT^2)	43	31	41	45	25
SOURCE TEMP (^{0}F) (NORMAL OP.)	1980	1865	2000	1980	2000
HSHX WEIGHT (LBS)	200	200	200	200	200
ATTACHMENT AND SUPPORT	G	G	F	G	F
HSHX INTEGRATION	G	G	P	G	P

78-0053

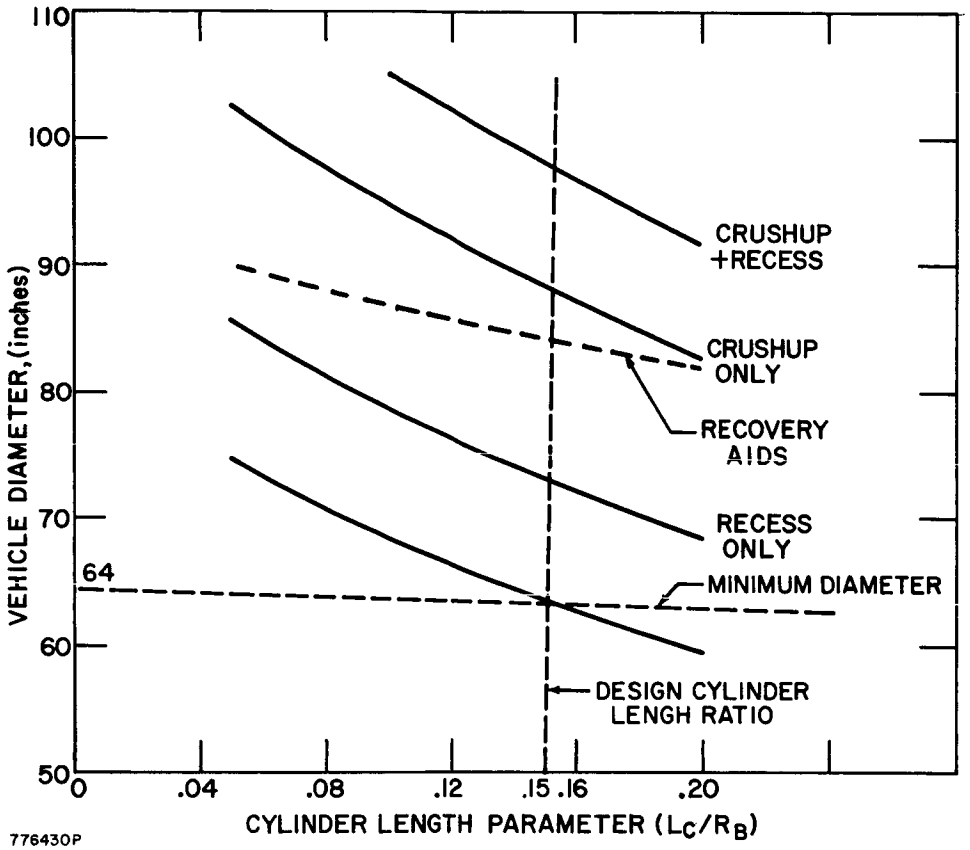

Figure 6.2-1 VEHICLE DIAMETER TRADE-OFF -- 47-INCH CIRCULAR PLANAR HEAT SOURCE

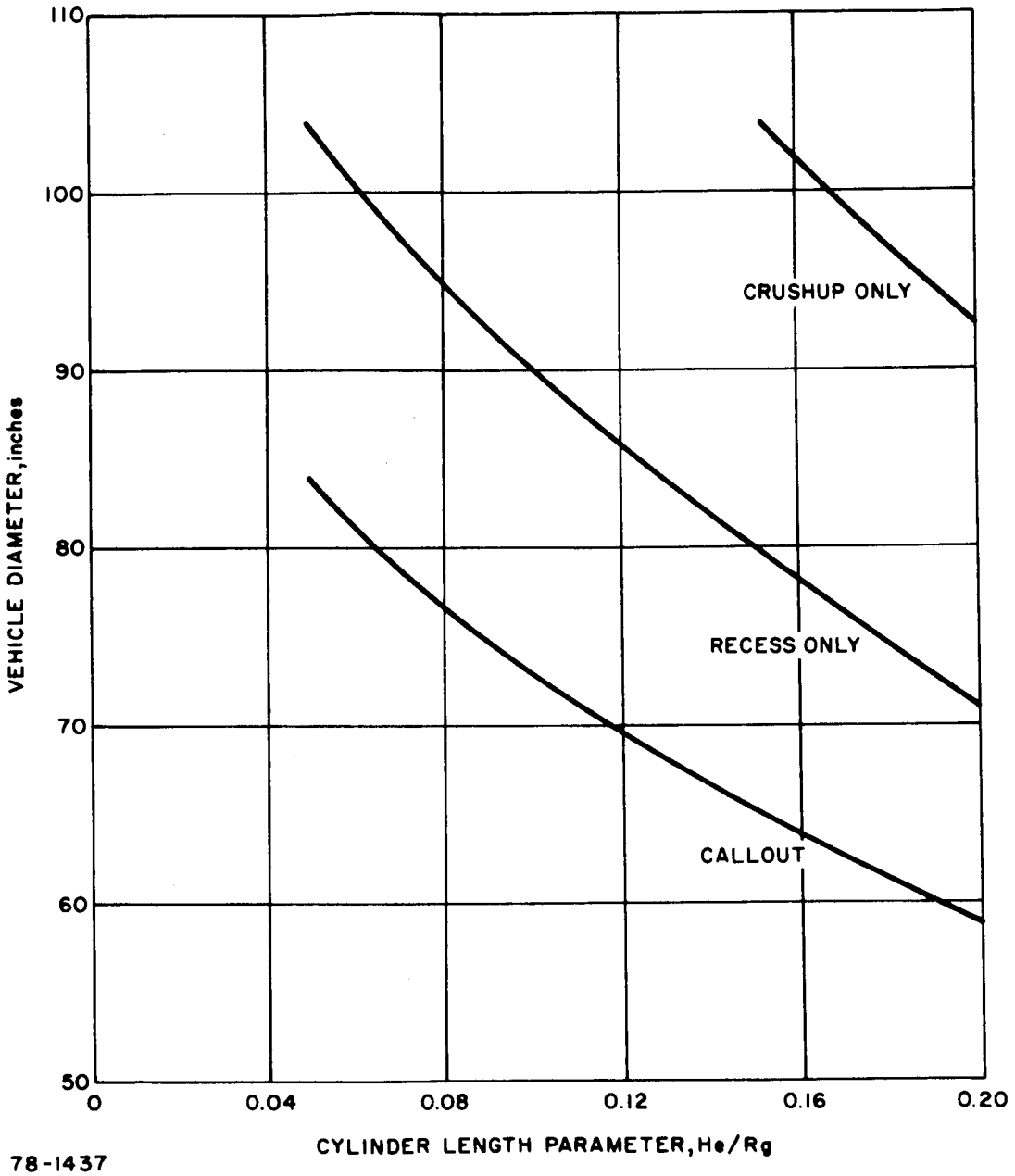

Figure 6.2-2 VEHICLE DIAMETER TRADE-OFF -- 47-INCH CIRCULAR PLANAR HEAT SOURCE -- MODIFIED APOLLO

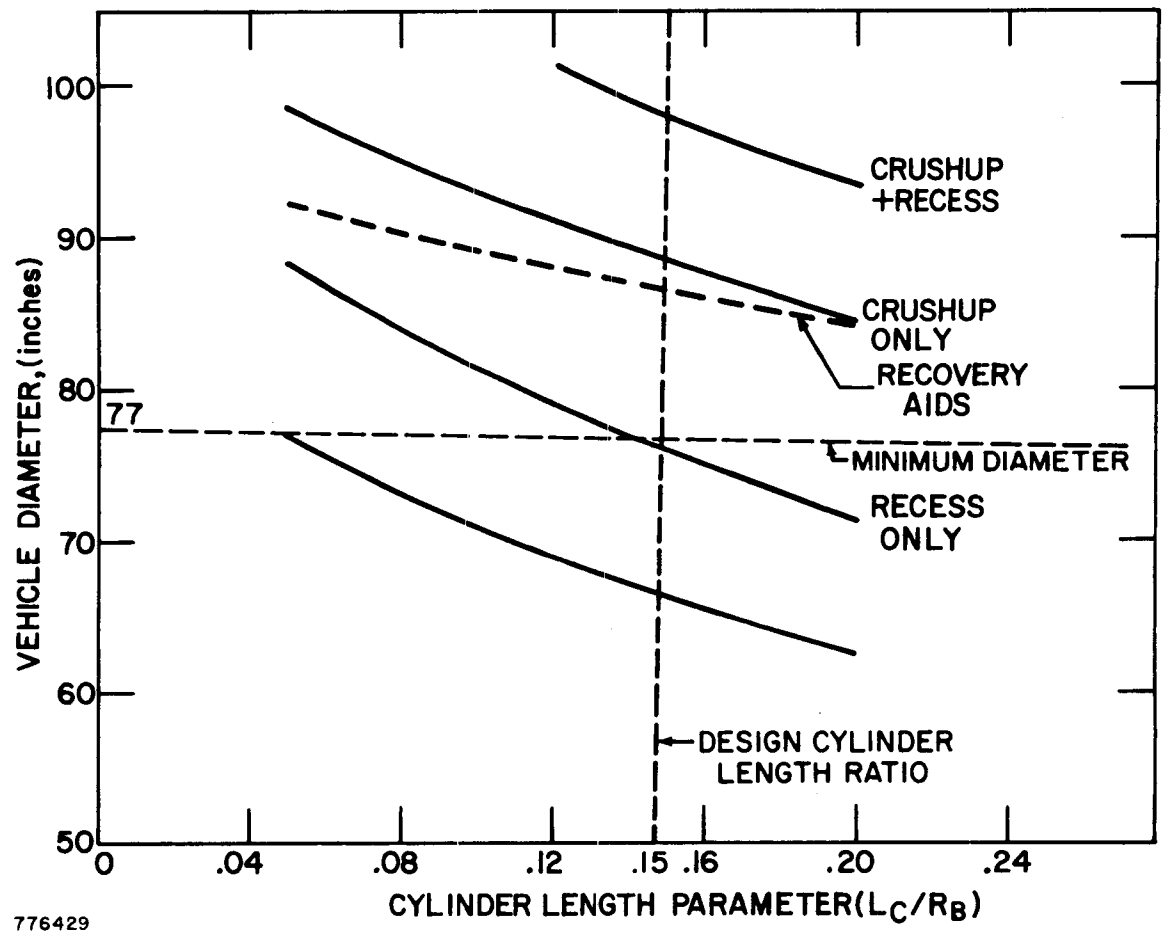

Figure 6.2-3 VEHICLE DIAMETER TRADE-OFF -- 57-INCH CONICAL HEAT SOURCE

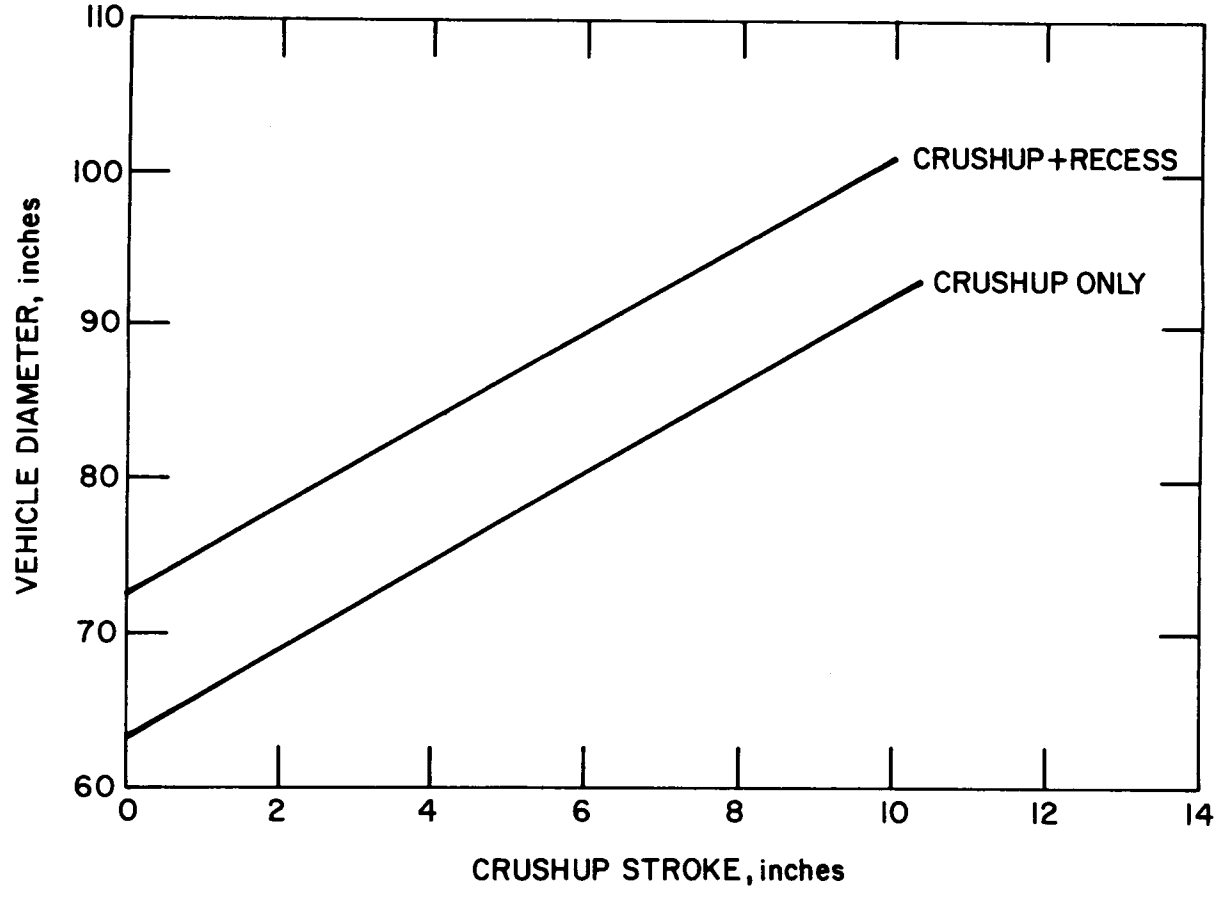

776439 P

Figure 6.2-4 VEHICLE SIZE AS A FUNCTION OF IMPACT ATTENUATION

TABLE 6.2-II

SUMMARY OF WEIGHT AND DIAMETER CHARACTERISTICS

CONFIGURATION	VEHICLE		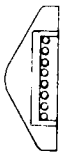	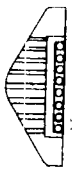	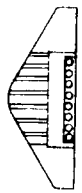	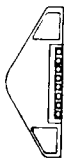	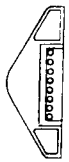	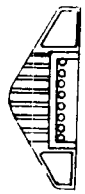	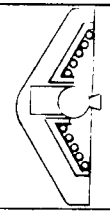
HEAT SOURCE		FLUSH	RECESSED (3 CAPSULE DIAMETER)	CRUSH-UP	FLUSH CRUSH-UP	FLUSH RECOVERY AIDS	RECESSED RECOVERY AIDS	RECESSED CRUSH-UP RECOVERY AIDS	CRUSH-UP RECOVERY AIDS
		DIA. WT.	DIA. WT.	DIA. WT.	DIA. WT.	DIA. WT.	DIA. WT.	DIA. WT.	DIA. WT.
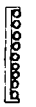	CIRCULAR 47" DIA.	64" 1500	73" 1530	89" 1900	98" 1950	84" 1690	84" 1690	98" 2080	113" 3210
	RECTANGULAR 63" X 34"	89" 1690	92" 1710	107' 2080	116" 2140	89" 1800	92" 1830	116" 2290	---- ----
	CONICAL 57" DIA.	77" 1660	77" 1660	91" 2030	101" 2040	94" 1860	94" 1860	101" 2190	103" 3160
	39" DIA. 4" PROTRUSION 20% CYL.	62" 1320	---- ----	---- ----	---- ----	85" 1520	---- ----	---- ----	---- ----
	32x56 RECT. 4" PROTRUSION 20% CYL.	81" 1435	---- ----	---- ----	---- ----	81" 1535	---- ----	---- ----	---- ----
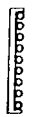	CIRCULAR 47" DIA. APOLLO	66" 1500	80" 1550	102" 1950	119" 2040	92" 1710	92" 1710	119" 2180	---- ----

78-0018

e. The circular pin cushion design is comparable in vehicle diameter to the circular planar concept but offers a weight reduction of about 180 pounds with and without recovery aids. The rectangular pin cushion is only compatible with the aforementioned concepts if recovery aids are used because of the diameter.

In the evaluation of the pin cushion concepts presented in Table 6.2-II it should be noted that the allowable cylinder length ratio has been increased to the $Lc/R_B = 0.20$ and the "stacks" have been permitted to protrude four inches beyond the base of the vehicle. Of additional interest is that the diameter and weight values given in the table do not include the effect of abort or de-orbit rockets.

6.2.1 Preferred Concepts

As a result of the trade-offs conducted in the previous section, it appears that the circular planar, conical and circular pin-cushion heat source configurations offer the best opportunity for minimizing overall vehicle diameter and weight. As mentioned previously, the 60 degree blunt cone aerodynamic shape is chosen simply because the modified Apollo configuration offers no diameter or weight advantage and in fact introduces large penalties when recess crushup and recovery aids are added. The design study indicates that incorporation of recovery aids and the interface problems with the fence would probably be the same for the three concepts. Also, the conical design could present a heat leak and temperature problem due to the short heat path and in addition complication if crushup is added (which would have to be penetrated by the truss).

Table 6.2-III shows a detailed weight breakdown for the three preferred concepts. The controlling factor in the vehicle weight is the heat source, of course, with the aeroshell accounting for only 14 percent of the total. Also shown in the table are the weight penalties associated with adding various items and the factors leading to the increased weight. The inertia properties for the three concepts are also shown in the table, with the most favorable center of gravity location found with the conical heat source system.

TABLE 6.2-III

MASS PROPERTIES COMPARISON

Recommended IRV Concepts

	Configuration			Remarks
	47 inch Circular Planar Heat Source	57 inch Conical Heat Source	39 inch Pin Cushion Heat Source	
AEROSHELL	200	249	202	
Heatshield	60	75	60	Low density charring ablator (link silicone)
Bond	4	5	4	Epon 931
Structure	62	94	64	Aluminum honeycomb
Truss	70	70	70	
Hardware	4	5	4	
ISOTOPE HEAT SOURCE	1304	1416	1140	
Capsules and Fuel	750	736	750	During Phase I(B) the designs will utilize a pickup on the aeroshell thus eliminating the chordal plate.
Capsule Support	216	255	100	
Capsule Retention	60	94	240	
Chordal Plate	98	135	--	
BeO	140	140	--	
Insulation	40	56	50	
TOTAL	1504	1665	1342	
CONTINGENT WEIGHT PENALTIES Relative to Minimum Diameter Design				Factors Effecting Weight Increase
Recess	30	--	--	Aeroshell (increased diameter)
Crushup	400	370	--	Aeroshell (inc. dia.) crushup, beefed up support, plate
Recessed Crushup	450	380	--	Aeroshell (inc. dia.) crushup, beefed up support plate
Flush Recovery Aids	190	200	200	Aeroshell (inc. dia.) recovery aids (7% entry vehicle, etc.)
Recessed Recovery Aids	190	200	--	Aeroshell (inc. dia.) recovery aids
Recessed Crushup - Recovery Aids	580	530	--	Aeroshell (inc. dia.) crushup, beefed up support plate, recovery aids.
MOMENTS OF INERTIA HEAT SOURCE AND AEROSHELL	1504	1665	1342	
C.G. (in. from nose)	26.2	23.1	25.1	
IX (Slug-Ft^2)	120	186	77	
IY (Slug-Ft^2)	92	112	69	

7.0 IRV/LAUNCH VEHICLE/SPACECRAFT INTEGRATION

7.1 SEPARATE LAUNCH

Figure 7.1-1 shows a concept for the integration of the IRV-Brayton Cycle system with the Centaur utilizing the OAO fairing. As can be seen the abort tower (≈ 100 inches long) which can be packaged within the OAO shroud is shown attached to pads on the aeroshell ablator surface. This abort tower attachment could be provided around the periphery of the vehicle but since the former scheme is currently used on the Apollo vehicle no unacceptable design problems are anticipated. It would also appear advisable to minimize any more design complications in the peripheral area because of the existing problems introduced by the interface requirements of the fence, support ring, abort rockets, and recovery aids (if used).

The primary radiator must provide the main interface with the Centaur. This interface must meet mechanical and electrical requirements and resist the loading resulting from the launch environment and be capable of supporting axial and lateral loads from the IRV system. The radiator must be approximately 500 square feet in surface area and fit within the 110 inch diameter OAO shroud. Since the primary radiator is considered a load carrying system, the main consideration will be to ensure that peripheral loading to the radiator be provided by the design of the section between the IRV and radiator.

The HS heat exchanger and Brayton Cycle are mounted between the primary radiator section and the reentry vehicle. The attachment made between the Brayton Cycle equipment and the radiator requires no in-flight separation but does provide proper mechanical, electrical, and associated interfaces. As a result of assembly, accessibility, and maintenance requirements of the various components, the primary support structure between the radiator and the IRV appears to logically warrant an open truss or framework rather than a stiffened sheet construction. This open truss would culminate in a circular ring for rigidity and alignment with the adjacent section.

The interface between the IRV and the spacer section must provide an in-flight separation system, hinges for pivoting the IRV in addition to mechanical and electrical interfaces. It is presently planned to provide this capability through a short spacer section approximately 8 inches in length. The hinging latching, and operating mechanism for pivoting the IRV away from the heat exchanger will be contained completely within this spacer. The spacer must be capable of resisting both loading from the Brayton section truss support as well as from the IRV and properly distribute these loads through the hinge and latch mechanism. The structural attachment between spacer and Brayton engine section will be through permanent bolting, whereas the IRV structural attachment will be through explosive bolts or other separable hardware. The latching/release and remote pivoting may be accomplished through the use of cams and a geared electrical motor. In addition, thermal insulation and a radiation shield will be required, both of which must hinge and separate in the proper sequence.

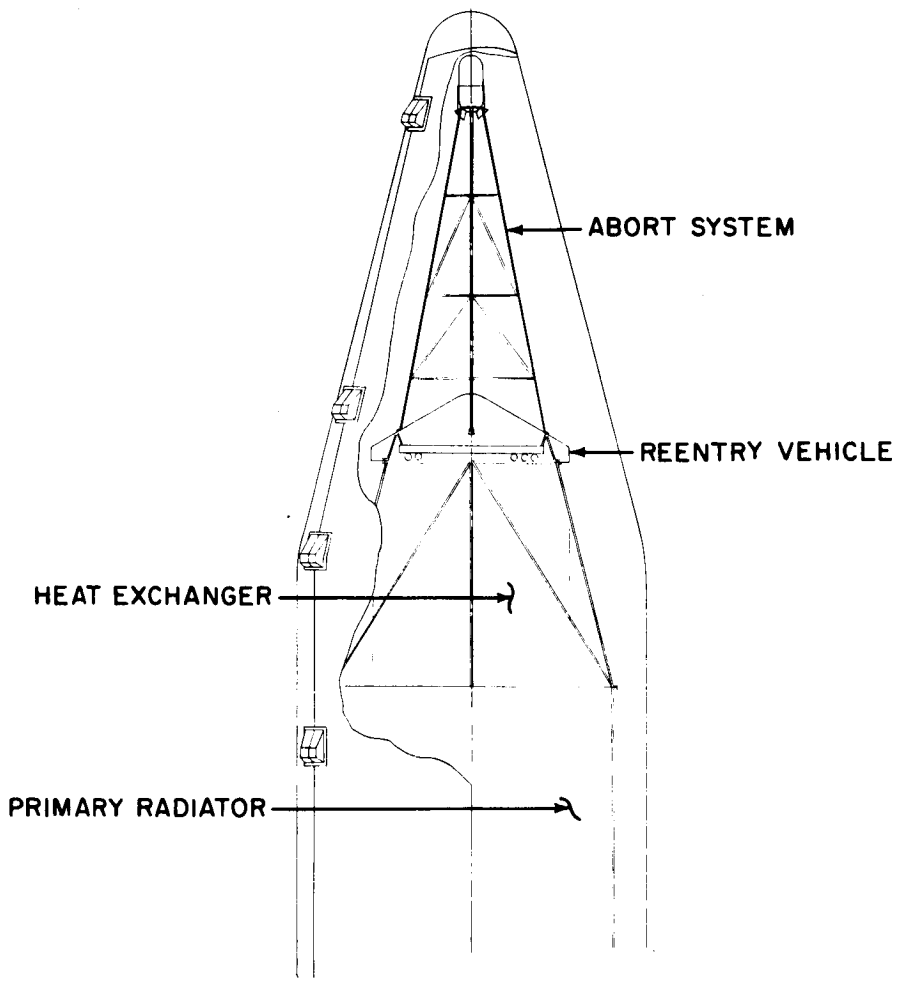

776381P

Figure 7.1-1 BOOSTER INTEGRATION OAO NOSE FAIRING

7.2 INTEGRAL LAUNCH

Figure 7.2-1 shows the IRV-Brayton Cycle system conceptually integrated with the Saturn IV-B in the MORL configuration. Results of the MORL design study (ref. 51) indicate that the full IRV system (including abort tower) can be packaged within the radiator as indicated. A method of hinging the system to swing the heat source out in the event of Brayton Cycle failure in orbit can be seen in Figure 7.2-2. A problem exists in this area since it may be necessary to keep the Saturn attached for some time in orbit to make trajectory corrections which would make swinging out of the vehicle impossible. A possible added penalty which has not been evaluated here, with the integral launch, is the weight of the lithium hydride necessary to protect personnel from radiation.

The work described above was performed to obtain preliminary estimates of integration problems. During Phase 1B a more detailed investigation of the interface problems will be conducted.

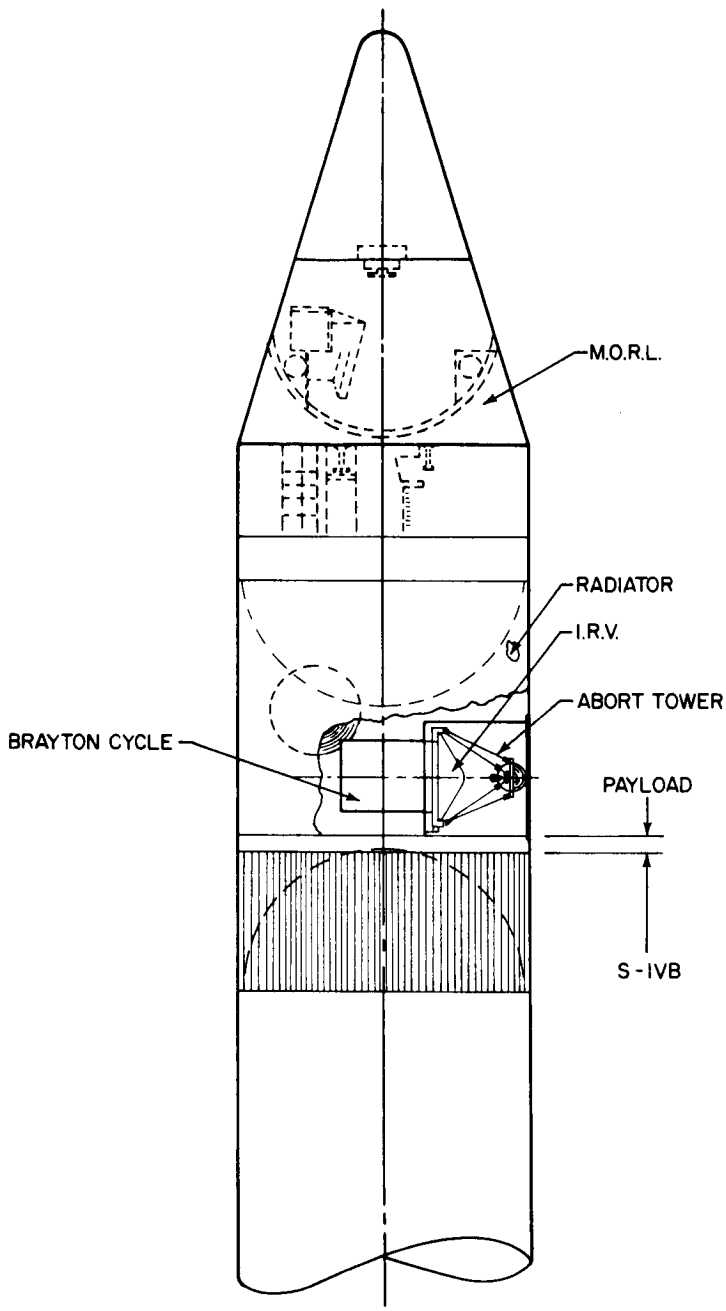

Figure 7.2-1 SATURN 1B -- LAUNCH INTEGRATION

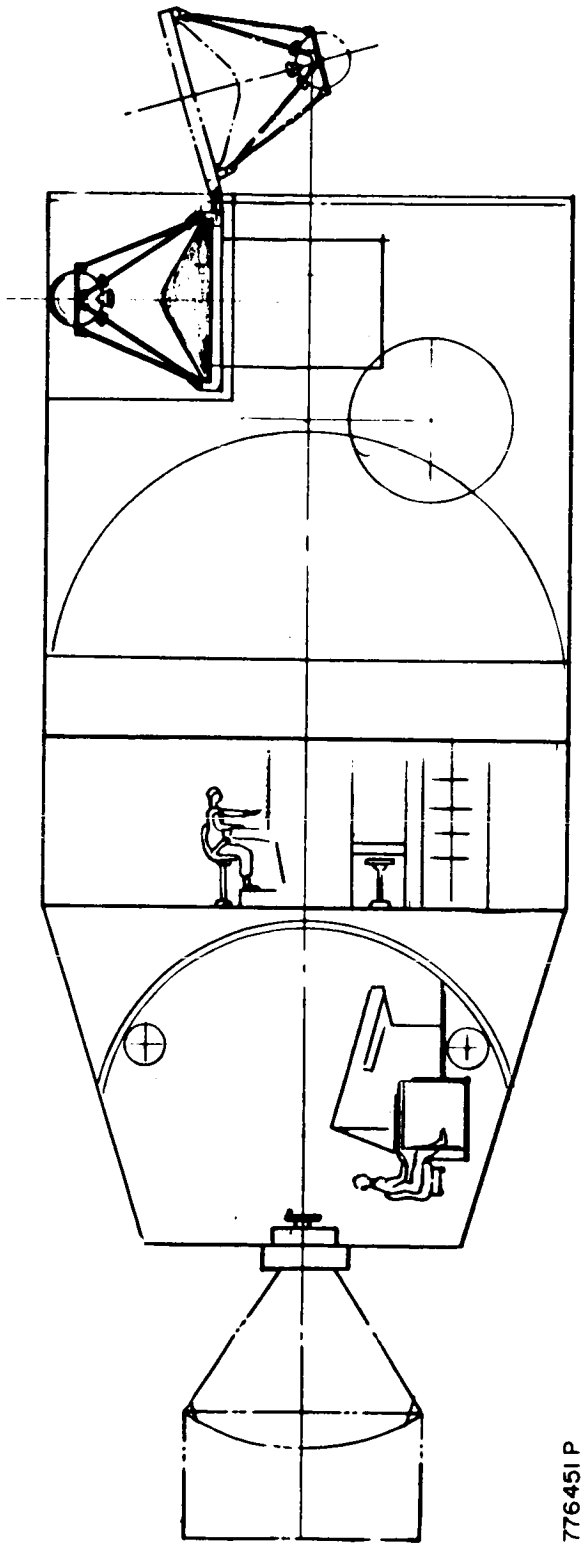

776451 P

Figure 7.2-2 ORBIT-NONCRITICAL FAILURE (ALTERNATE COOLING MODE SHOWN)

APPENDIX A

FUEL CAPSULE IMPACT ANALYSES

The determination of the loadings imposed on the fuel capsule and the actual fuel capsule capacity to resist damage are difficult to quantify with analytical procedures. This appendix describes the approach followed in developing the reference fuel capsule impact performance during Phase I(A). It also contains a brief discussion of the limitations inherent in the applicable basic analytical impact theories.

A list of the variables affecting impact behavior of the capsules is presented in Table A-I.

TABLE A-1

VARIABLES AFFECTING IMPACT BEHAVIOR OF FUEL CAPSULES

1) Velocity

2) Wall thickness

3) Total mass

4) Cylindrical shell mass

5) Material

6) Weld joint design, efficiency, weaknesses, etc.

7) Type head (spherical, elliptical, etc.) and the thickness

8) Impact orientation (sidewise, head-on, in-between angles)

9) Internal pressure
   a) if low - negligible effect
   b) if high - could cause explosion or help prevent cave-in of vessel walls

10) Capsule shape and design, also size effects

11) Temperature at impact

12) Target of impact (water, concrete, granite, etc.)

13) Capsule support (flat plate, cradle), if any

14) Energy absorption and/or damaging effects of all intermediate material between the ground and the capsule

15) Cylinder radius to thickness and length to radius ratios

16) Effect of previous high temperature history and/or creep history of capsule

A1.0 MAIN THEORIES

The three main theories that could be utilized for capsule impact analysis are as follows:

a. Energy Method

b. Stress Wave Method

c. Static Analysis with Equivalent G-Load

For the region of moderate impact velocities, both the wave propagation effects and local indentations and/or deformations at the contact zone are significant, and a thorough analysis would have to account for both types of processes. The time-dependent force and deformations relationships, however, are beyond definition for complex and multi-component structures. Any resultant deformation means that plastic flow theories and plastic wave theories must be integrated with the impact analysis. However, such an analysis, even if it were possible to solve, would still require experimental verification.

The resulting deformations due to impact may be either brittle or ductile in nature, depending on the material, temperature, and effective loading rates. Simulated capsule impact tests* generally show significant plastic deformation, indicating ductile behavior. However, capsules often rupture at weld joints, indicating 1) a defective weld, 2) a joint design weaker than adjacent walls, or 3) a brittle behavior in the weld as opposed to ductile behavior in the adjacent capsule walls.

However, these three theories are often used, and some times with success. The difficulties associated with three theories are listed below:

a. Impact Energy - Strain Energy Theory Shortcomings

1) No "true" stress-strain diagram for the material at impact temperature is available.

2) Failure is by bending plus tension/compression, hence, stress-strain diagrams must be identical for such stresses, but they often are not.

3) Stress-strain diagrams must account for loading rate, but this information is generally not available.

4) The entire material must be stressed uniformly.

5) The material must be homogeneous (no welds, etc.), although this is generally not the case.

6) Numerous variables are not taken into account - shape, impact angle, internal pressure, etc.

* For example, see Sandia Report No. SC-RR-65-9

7) No consideration is given to the energy required to initiate a crack and the energy required to propagate a crack (whether a ductile or brittle failure); the energy required to initiate a crack may be 10 percent to 90 percent of the total required to split open the vessel.

8) The actual amount of impact energy load is somewhat uncertain.

9) The energy which is absorbed by each of the various components involved (head, cylindrical portion, internal components) is generally indeterminable.

10) The energy absorbed by the target itself is indeterminable.

b. Difficulties with Using Stress Wave Theories

1) The impact produces elastic and plastic stress waves; plastic stress wave phenomena is less understood than elastic wave theory (for instance, the subject of magnitude of the plastic stress wave velocity has not been settled), and the combination of the two is very complex and generally beyond the state-of-the-art.

2) Precise impact conditions are required or assumed which are obviously unobtainable.

3) The shape of the impacting body and the angle of impact set up the numerous stress waves which rebound, add, subtract, etc., in their history. This history determines the behavior, yet the history of such complex nature is impossible to define for other than the simplest shapes.

4) If the resulting impact produces any deformation, plastic flow theories and/or viscoelastic theories must be incorporated into the analysis along with the plastic wave theories, all of which further complicate the analysis.

5) The use of elastic and plastic material constants that are required introduces errors due to the assumed material model (i.e., like assuming an elastic-perfectly plastic solid) and also due to the fact that static material data often does not satisfactorily represent the true dynamic material behavior properties.

6) Most physical behavior models are chosen on the mathematical simplifications and have little experimental verification.

c. Difficulties with Using Static G-Load Analysis

1) It assumes that the stress and strain under impact is the same as under static loading. This is false and is worse for the higher loading rates, since the material has not had time to distribute the loading as it would be distributed in a static case.

2) Most material behaviors are strain rate dependent, and the material data is lacking for such high rates of loading (ultimate strength and elastic strains generally increase with loading rate).

3) A system experiences a load magnification with dynamic load compared to a static load.

4) The actual resultant G-loading is varying with time and with position over the various components involved, but it is assumed constant with time and uniform over the system.

A2.0 A JUSTIFICATION FOR USING STATIC G-LOAD ANALYSIS OF THE IMPACT OF THE FUEL CAPSULE

Although there are numerous methods of analyzing high velocity impact, of the three main methods discussed, the method of determining a component's equivalent static G-load capability will most generally be used. It is generally the simplest method to use and the assumptions utilized in overcoming the difficulties associated with such an analysis are usually on the conservative side. For instance, assuming that the standard stress-strain curve is applicable is generally conservative since high loading rates usually increases the material's allowable stresses, especially if the load is of a short duration as for an impact load. Also, assuming a uniform maximum G-loading over a structure is generally conservative since in actuality the maximum G-loading of a component is usually not simultaneously a maximum, but rather various areas experience a maximum at different distinct times. Also, it is well known that structures generally can carry a greater dynamic load (over a limited time period) than the structures could statically. For example, the axial impact buckling load of a cylindrical shell is normally greater than its static buckling load.

It is a generally accepted criteria to employ a static G-load analysis when the natural period of a structure is less than one third of the time of load application. Impact loading of the capsule at a terminal velocity of 180 fps meets this criteria as shown below:

The natural period of a heavy-walled cylinder is given by:

$$T = \frac{\pi (b + a)}{c}$$

where

$b = 0.737$ in.

$a = 0.562$ in.

$$c = \sqrt{\frac{E}{\rho}}$$

$c = 10{,}000$ ft/sec for T-111 material

$T = 4.04\ (10^{-4})$ sec

Time duration of load application is

$$t = \frac{S}{V_{ave}}$$

assuming uniform deceleration. Let the stopping distance of the heat source equal one foot and let the initial velocity be 180 ft/sec, then the time t of load application can be determined.

V_{ave} = 90 ft/sec

$t = 1/90 = 1.11\ (10^{-2})$ sec

The IRV as a whole would have a much lower period of vibration and hence would be considered as undergoing a complex impact load history.

Now consider the magnitude of strain under the condition of a fuel capsule impacting a 180 ft/sec. The elastic stress wave propagates at the speed of sound in the material. For a capsule of T-111 material the elastic stress wave propagates at a velocity given by:

$$C = \sqrt{\frac{E}{\rho}}$$

C = 10,000 ft/sec

Impact velocity = 180 ft/sec

$$\frac{V}{C} = 0.0178$$

$\therefore$ Impact strain = 17,800 μin./in.

This is beyond the elastic strain range hence the impact will plastically deform a capsule if it impacts at a rigid surface with no intermediate structure. Hence, it is desirous to have the capsules impact with some structure (preferably with high energy absorbing capability) between the capsules and earth if plastic deformation is to be avoided.

A3.0 ANALYSIS OF SIDEWISE IMPACT OF THE FUEL CAPSULE

Impact of the IRV with the capsules orientated horizontally (i.e., axis nearly perpendicular to the direction of travel) on a heat source support plate will load the capsules radially. The exact loading on the capsule depends on many unknowns such as the capsule support plate, and if it fails on impact, then the plate's mode of failure. For a tubular capsule, it is desirous to adequately support the capsule in a manner to prevent any tendency for the tube to flatten out or rupture, and could be approximated by a cradle support. The worst support

would be if the tube was supported by a rigid flat plate. Although a cradle will be included in the design, since the cradle may undergo bending or deformation on impact, the case of line impact is not necessarily impossible. But, then the capsule would tend to deform (plastically) to occupy the cradle. Hence, any case between line support and half tube (cradle) support is possible and represents the bounds for the capsule loading capability.

Now the end caps will affect the behavior of the cylindrical tube portion near the ends of the fuel capsule on impact, and as a result the center portion will be the weakest zone during impact. The question of whether the end caps affect the center span can be determined from beam-on-elastic foundation theory, where it is generally accepted that a λL value greater than π determines a long beam or cylinder with the end conditions not affecting the major portion of the cylinder. For the capsule with radius R and thickness t:

$$\lambda = 1.285 \frac{1}{\sqrt{Rt}} = 3.66$$

Now the length of the cylinder is five inches (see figure 3.0-1).

So: $\lambda L = 18.3$.

For a λL this large, the fuel capsule is a long cylinder and hence the middle portion of the cylinder will not be affected or reinforced by the end caps. Hence, under a high uniform load (G-loading), the center span of the tube will probably yield or buckle in first. This will be the first failure made on impact; how much the tube can collapse before a breach will occur is indeterminable.

A3.1 CASE A: G-LOAD CAPABILITY WITH A CRADLE SUPPORT

Consider the desirable case of the cradled fuel capsule as shown. Neglect initial tensile stress due to the internal pressure (conservative).

If the cradle-plate assembly furnishes maximum support for the capsule at impact, the following case is a reasonable assumption; otherwise, it is optimistic and hence represents an upper limit.

Load = (g-load)(wt)

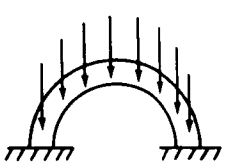

Assume the sudden load magnification factor will cancel out the yield stress magnification factor (overlaod factor). Also assume failure of the capsule wall will be defined by the buckling or yielding of the capsule wall, whether rupture occurs or not.

Now the case of vertical loading on the semi-circular arch as shown is conservatively approximated by an arch with normal pressure loading P as shown above.

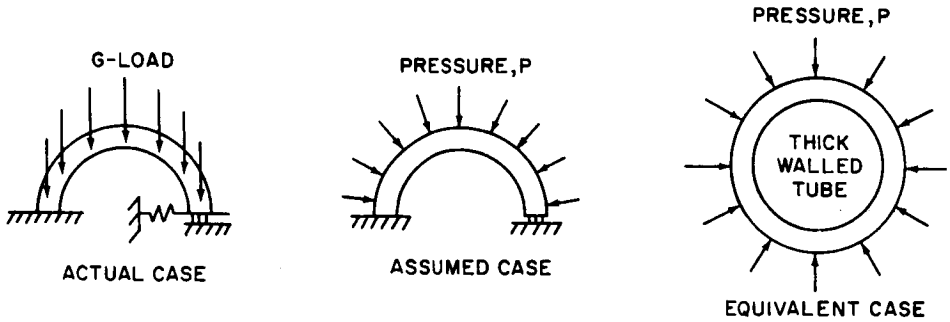

Where the assumed case represents a lower bound of the actual case due to the assumed normal load in place of the vertical loading and the allowable radial displacement of arch at the one support whereas in reality the cradle and adjacent capsules would tend to restrict such radial motion.

Thus the critical buckling pressure is approximated by

$$P_{cr} = \frac{E\,h^3}{4(1-\nu^2)\,R^3}$$

$$P_{cr} = 1.29\ (10^5)\ \text{psi}$$

where

E = Young's Modulus

h = Thickness

R = Mean Radius

P_{cr} = Buckling Pressure

But this is greater than the yield stress, σ_{YP}, hence the critical pressure is given as

$$P_{cr} = \frac{h}{R}\ \frac{\sigma_{YP}}{1 + 4\ \frac{\sigma_{YP}}{E}\left(\frac{R^2}{h^2}\right)}$$

$$P_{cr} = 8100\ \text{psi}$$

Assume T-111 material and use σ_{YP} = 35 ksi at 2000° F for T-111 shell material. This is rather conservative since the capsule temperature at impact will be much cooler than 2000° F and the yield stress could be as high as 45 ksi at impact.

Now to initiate yielding of the inner surface, the critical pressure P_{cr} is approximated by that for a thick-walled cylinder under uniform external pressure. Neglecting any internal pressure (conservative) -

$$P_{cr} = \frac{\sigma_{YP} [(O.D.)^2 - (I.D.)^2]}{2(O.D.)^2}$$

$$P_{cr} = 7350 \text{ psi}.$$

Hence, of the three values, the limiting value is

$$P_{cr} = 7350 \text{ psi}.$$

Assuming that the fuel weight is uniformly carried by the capsule wall on impact, the load per unit area on the cylinder is (ρhg). Thus,

$$P_{cr} = \rho hg = 7350$$

where

ρ = density of fuel and shell combined

ρ = 1.538 lb/in.^{3}

h = thickness = 0.175 in.

Hence, the G-load capability is

G-load = 27,300

Result: For a cradle support, the capsule can withstand over 27,000 g's before yielding of the fuel capsule occurs.

A3.2 CASE B: G-LOAD CAPABILITY WITH A FLAT PLATE SUPPORT

Consider the most undesirable case, where the capsule is supported by a flat plate with no distributed support. Hence the capsule will see a line-load impact as shown.

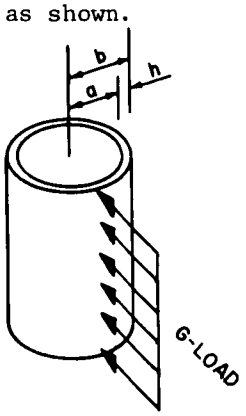

Assume the case of ring as shown.

Maximum moment = $M_m = \frac{3}{2} w R^2$

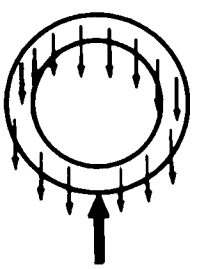

where: considering the weight of the shell only,

w = (load/inch circumference/unit depth) $g = g\rho h = 0.1058\ g\ \text{lb/in.}^2$

So:

$M_m = 0.0778\ g\ \text{in. lb/in.}$

Assume internal pressure 1800 psi.

The tensile stress due to an internal pressure is:

$$\sigma_p = \frac{P(a^2 + b^2)}{b^2 - a^2} = 6800\ \text{psi}$$

Then the allowable stress,

$$\sigma_A = \sigma_{YP} - \sigma_p$$

$$= 28{,}200\ \text{psi}$$

Equating the stress due to the bending moment M_m and the allowable stress

$$\sigma_A = \frac{6M_m}{h^2}$$

and substituting numerical gives

$g = 1840.$

Result: Maximum G-Load to yield the material is 1840 g's.

Now to rupture the vessel, the allowable load is

$$\sigma_{\text{Allowable}} = \sigma_{US} - \sigma_{\text{pressure}} = (50{,}000\ \text{psi at } 2000^\circ\text{F}) - 6800$$

$$= 43{,}000\ \text{psi}$$

Thus: Load Capability = 2820 g's; however, this is a lower limit since theory assumes elastic behavior to the rupture stress; a thorough analysis would require a plasticity analysis.

Result: Minimum G-load to rupture the capsule is 2820 g's.

Now assume that the fuel adds to the density of the shell (conservative assumption). An approximate density for the shell and fuel combined is $1.538\ \text{lb/in.}^3$

Thus,

$M_m = 0.198\ \text{in. lb/in.}$

For an allowable stress of 28,000 psi (accounts for internal pressure), then G-load = 722.

Result: The g-load to yield material ≥ 722 g's. For the g-load to rupture the capsule,

$$\sigma_{\text{allowable}} = \sigma_{US} - \sigma_{\text{pressure}} = 43 \text{ ksi}$$

Assume elastic behavior to the rupture stress value results in g-load = 1110. Again, this is a lower limit since the material will take more strain than the assumed elastic strain here; a complex elastic-plastic analysis would be required for a more accurate value.

Result: The g-load to rupture capsule ≥ 1110 g's.

A3.3 CASE C: CRADLED ENDS SUPPORTED ONLY (OR CRADLED CENTER SUPPORTED ONLY)

Consider the case if the capsule support plate bends somewhat on impact (especially nonvertical impact), then the local load on certain capsules as shown is possible.

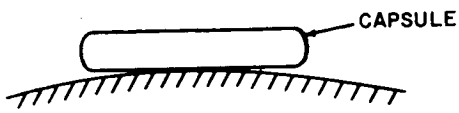

The worst case is a local load directly at the center of the capsule, away from the hemispherical caps. Attempt at an analysis of the local load effect using Hertz's contact pressure demonstrates that local yielding occurs almost immediately until the capsule is adequately supported by cradle. Consequently, a simple bending of the capsule as a beam simply supported at the middle by the cradle is considered. Assume the internal pressure has no effect and neglect local effects at the contact point of the capsule on the bent plate; i.e., nil indentation so we have the case of a tube bending.

Thus:

$$I = \frac{\pi}{64} [(\text{O.D.})^4 - (\text{I.D.})^4] = 0.153 \text{ in}^4$$

$$M_{max} = 1/2 \text{ WL} = 3.37 g$$

So:

$$\text{max} \cdot = \frac{M_{max} (\text{O.D.})}{21}$$

Allowable Stress= $\sigma_{\text{yield}} - \sigma_{\text{axial tensile stress}}$

$$\sigma_{ATS} = \frac{(O.D.)^2 P}{(O.D.)^2 - (I.D.)^2} = 4300 \text{ psi}$$

$$\sigma_A = 35{,}000 - 4300 = 30{,}700 \text{ psi}$$

Hence:

g-load capability = 1900 g's

Result: The capsule will take 1900 g's before yielding and over 2800 g's before rupturing.

Or, also consider the case of a capsule cradle supported with the plate bending opposite of that just considered, hence, the case is that shown below.

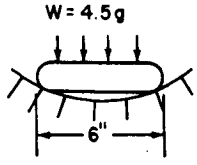

Assume: Internal pressure negligible with respect to cylindrical tube stability. Neglect localized effects. Consider tube-bending only.

Thus:

$$M_{max} = \frac{WL}{8}$$

$$\sigma_{max} = \frac{M_{max}(O.D.)}{2I}$$

Thus:

$$g = 1900$$

This result is the same as above which it should be.

Note that the internal pressure would help prevent bending of the tube and buckling-in of the tube. However, the capsule is in the thick-walled tube range and the effect is thus minimized; hence neglecting the beneficial effect of the internal pressure is conservative and presents less than one percent error.

A4.0 ENERGY THEORY ANALYSIS

The kinetic energy versus strain energy criteria of analyzing impact phenomena is often used and has had sufficient experimental correlation in some areas to merit its consideration.

The kinetic energy of an impacting capsule must be dissipated in elastic and/or plastic deformation of material and in certain cases by heat energy dissipation, such as melting or vaporization of material or frictional dissipation. An example of frictional dissipation is the impact force of a hammer on a nail being dissipated by frictional heat between the nail and wood. Melting and/or vaporization phenomena are usually only encountered at ultra-high impact velocities. Hence, the kinetic energy of an impacting capsule must be dissipated in elastic and plastic material deformation. Consider the impact of a lone capsule.

KE = (elastic and plastic deformation of capsule shell)

+ (elastic and plastic deformation of encapsulated material)

+ (elastic and plastic deformation of the target)

Since the second type of deformation is undesirable (fragmentation of fuel spheroids, etc.), minimize this quantity and assume negligible. The last type of deformation is the most desirable and can be the main energy absorbing quantity, but unfortunately, this is not controllable and may result in a negligible quantity, such as if the target was granite. Hence, the kinetic energy must be absorbed by the capsule shell in elastic and/or plastic deformation. Now the elastic component may be undesirable since this may imply rebound; also, its total magnitude is generally insignificant compared to the plastic deformation. The general equation for the strain energy capability of a capsule is: $S = \frac{1}{24}(\sigma_u + \sigma_y)\epsilon_u V$ which assumes a linear work hardening stress-strain curve with the negligible elastic strain compared to the ultimate strain ϵ_u, with:

σ_u = Ultimate strength, psi

σ_y = Yield strength, psi

ϵ_u = Strain at σ_u, in./in.

V = Material volume, $in.^3$

S = Strain energy, ft-lb

The general impact energy is given by

$$KE = \frac{W V^2}{2 g_c}$$

where

V = Impact velocity, ft/sec

W = Capsule Weight, lb

g_c = Acceleration of gravity, 32.2 ft/sec^2

KE = Impact kinetic energy

Now both energy values are attenuated before being set equal to each other. That is:

$$K_1(S) = K_2(KE)$$

where

K_1 = Fudge factor to account for the fact that not all of the material is effectively strained to the maximum when failure occurs.

K_2 = Fudge factor to account for the fact that not all of the impact energy need be absorbed by the capsule, but that intermediate structures and the target itself (the ground) absorb part of the kinetic energy of the capsule.

The conservative case is to assume all energy must be absorbed by the capsule ($K_2 = 1.0$) which applies for a capsule impacting against hard material such as granite. However, if crushable material was incorporated either integrable with the capsule or merely spaced between the capsule and the target, K_2 would tend toward zero and hence the deformation of the capsule would be minimized.

For the factor K_1, a value may be assumed ≤ 1.0, but a true value can be obtained only experimentally since the K_1-value depends on many parameters, including capsule shape, impact velocity, etc.

Assume a capsule with a total weight of 4.5 pounds and an impact velocity of 180 ft/sec, with $K_2 = 1.0$ and $K_1 = 0.5$, then

$$(\sigma_u + \sigma_y)\ \epsilon_u\ V = \frac{24\ W V^2}{g_c}$$

$$= 109{,}000 \text{ in. lb.}$$

Now if 3 pounds in the capsule shell weight

$$\frac{(\sigma_u + \sigma_y)\ \epsilon_u}{\rho} = 36{,}300 \text{ in. lb/lb}$$

where

ρ = density, lb/in.^{3}

For an optimistic assumption of $K_1 = K_2 = 1.0$,

$$(\sigma_u + \sigma_y)\ \epsilon_u\ V = 54{,}500 \text{ in. lb.}$$

or

$$\frac{(\sigma_u + \sigma_y)\epsilon_u}{\rho} = 18{,}000 \text{ in. lb/lb.}$$

Consequently, the desired range of material parameter for capsule shell to survive impact is from 18,000 in. lb/lb to 36,200 in. lb/lb.

A4.1 CAPABILITY VERSUS MATERIAL

The strain energy expression is a function of the yield stress, ultimate strength, fracture strain, and material density. Since these are all material properties, a single combination of these define a material property which is proportional to its strain energy capacity = C.

$$C = \frac{(\sigma_y + \sigma_u)(\epsilon_u)}{\rho}$$

A list of material C-values is shown below for the temperatures indicated.

$$C = \frac{(\sigma_y + \sigma_u)\epsilon_u}{\rho}, \left(\frac{\text{in lb}}{\text{lb}}\right)$$

Material	1500° F	2000° F
T-111 Alloy (Recrystallized)	21,000	29,000
TZM Alloy	79,000	63,000
B-66 Niobium Alloy	108,000	108,000
Cb-752 Alloy	660,000	600,000

Since T-111 has a C-value between that previously calculated as desirable (1800 to 3600 in. lb/lb), survival of impact appears feasible by this method of analysis. In order to enhance the survival capability of T-111 capsules, it is desirous that some energy absorbing material be used to absorb a good portion of the impact energy. It should be noted that for a vented capsule where the long term creep properties are not an overriding consideration, then some other material than T-111 would be more desirable to use.

A4.2 CAPABILITY VERSUS VOLUME

From the preceding discussion, it can be seen from

$$KE = K_1 \frac{(\sigma_u + \sigma_y)\ \epsilon_u\ V}{24}$$

that for a given material and a given amount of kinetic energy to absorb, only K_1 and V are variables. That is, the capsule design must be made such that K_1

and V are large enough to satisfy the equation. They both are dependent on design; that is, the amount of material used in the capsule (V) and the shape of capsule (K_1) are now limited by the above requirement.

Increasing the volume (i.e., mass) of the material used for the fuel capsule shell generally increases its strength, lifetime, and impact integrity; however, it also adds to the weight, which may be deleterious. The actual effect on change in K_1 by a design change or increasing the mass is determinable only by experimental testing.

A5.0 EXPERIMENTAL TEST RESULTS OF CAPSULE IMPACT TESTS

Although no tests are conducted under this program, other isotope projects have conducted some impact tests on their capsule design. Although such data is not directly applicable here, these results do furnish some guides.

General conclusions of capsule impact tests conducted by Sandia Corporation, General Electric, and Atomics International are as follows:

a. Damage increases with impact velocity.

b. Off-center angular impact is generally worse than a perfect head-on or side-on impact.

c. Welds are an inherent weak point and hence it is more desirable to locate welds at the midspan rather than at the ends.

d. Higher ductility is more important than higher strength.

e. For a given impact velocity, the thickness required increases with higher L/D ratios.

f. Any intermediate material between the fuel capsule and the target tends to reduce damage to the fuel capsule and hence increase the critical impact velocity.

g. Heavy end cap wall thickness is desirable for head-on impact.

h. The fuel particles tend to break into finer particles on impact.

The test data is best summarized by Figure A-1 from the Sandia test report.

From Figure A-1, the ORNL capsule with $X_1 = 4.0$ and $X_2 = 0.175$ inch should be able to survive V_{10} of 360 fps, if it was made of 4130 steel as the Sandia test capsule (see Figure A-2). Now to extrapolate these room temperature test results of head-on impact of 4130 steel to a room temperature, head-on impact of a T-111 capsule, from the preceding section, it can be shown that for the same K_1 and K_2 values

$$\left(\frac{S}{KE}\right)_{T-111} \simeq \left(\frac{S}{KE}\right)_{4130}$$

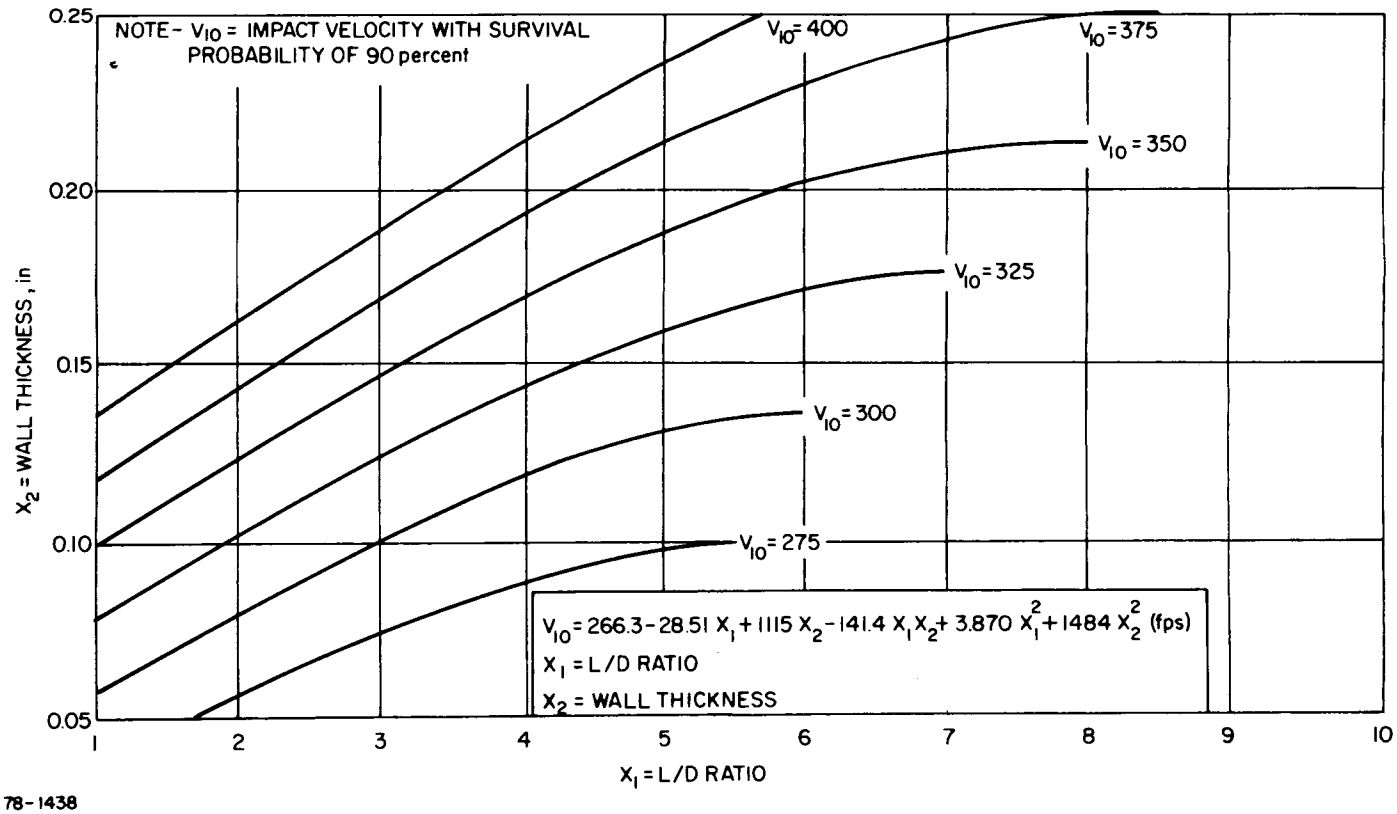

Figure A-1 L/D RATIO VERSUS WALL THICKNESS, PROBIT ANALYSIS
(TAKEN FROM SANDIA REPORT SC-RR-65-9)

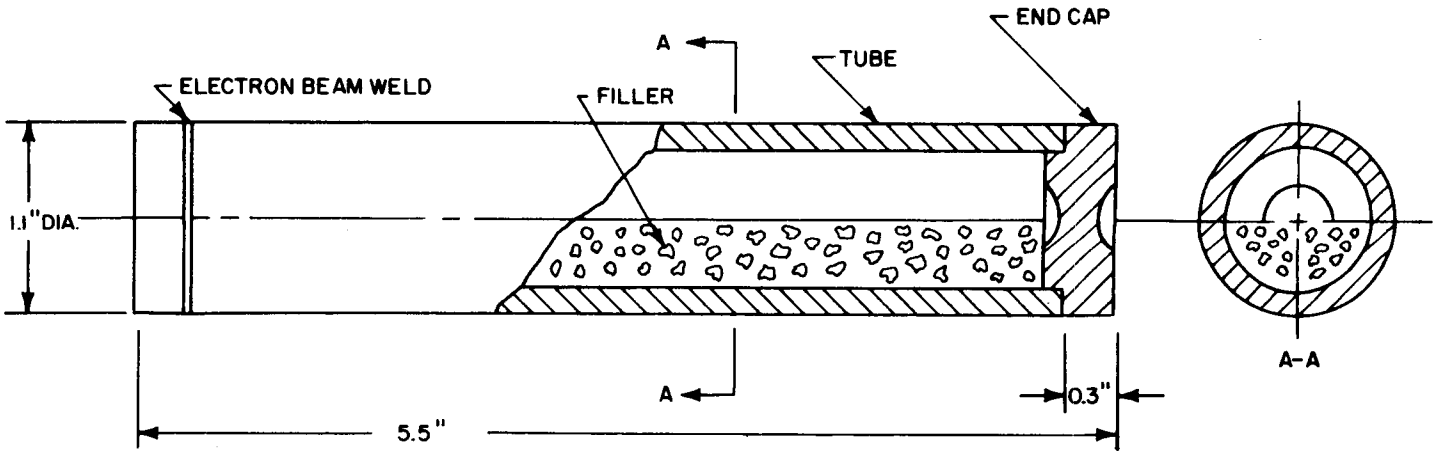

MATERIALS

1. TUBE – 4130 STEEL. NORMALIZED AT 1600°F.
2. END CAP – 4340 STEEL. HARDENED TO ROCKWELL "C" READING OF 48.
3. FILLER – LEAD IMPREGNATED WITH TUNGSTEN PUNCHINGS

78-1439

Figure A-2 TYPICAL TEST SPECIMEN, CONTAINMENT CAPSULE IMPACT SAFETY STUDY, CC/SS

or

$$\left(\frac{S}{W V^2}\right)_{T-111} \simeq \left(\frac{S}{W V^2}\right)_{4130}$$

where, for T-111 capsule at room temperature

$S = 19{,}900$ ft-lb

$W = 3$ lb

and for the ORNL capsule (4130 steel) at room temperature

$S = 9400$ ft-lb

$W = 0.77$ lb

$V_{10} = 360$ fps

Hence:

$$V_{T-111} = V_{4130} \left[\left(\frac{19900}{9400}\right)\left(\frac{0.77}{3}\right)\right]^{1/2}$$

$$V_{T-111} = 265 \text{ fps}$$

Hence for the same type of test, 90 percent of the ORNL capsules should be able to withstand an impact velocity of 265 fps.

APPENDIX B

PRELIMINARY SUPPORT PLATE RESONANT FREQUENCY CALCULATIONS

B1.0 FUEL CAPSULE SUPPORT PLATE - CIRCULAR PLANAR DESIGN

B1.1 The vibration of sector between reinforced ribs is possible assuming no contact with the beryllium oxide.

Assume sector is rectangular with all four sides approximating the fixed edge conditions.

Let

$$a = \frac{d}{4} = 13.25 \text{ in.}$$

$$b = \frac{\pi d}{\text{no. sectors}} = 4.62 \text{ in.}$$

where

$d = 53$ in. diameter

Thus:

$$\frac{a}{b} = 2.87$$

From "Thin Plate Natural Frequencies" by M. Vet, Machine Design, June 10, 1965; June 9, 1966; and April 13, 1967, the resonant frequency can be expressed as

$$f = a \frac{h}{a^2} \sqrt{\frac{E}{(1 - \nu^2)}}$$

Then a = 175 where for clamped edges and a/b = 2.87

Let:

$h = 0.125$ in.

$a = 13.25$ in.

$E \simeq 5(10^6)$ psi for Cb 1 Zr at temperature

Hence,

$f_1 = 535$ hertz

Therefore, the fundamental frequency of panel vibration is above 200 hertz.

B1.2 Vibration of the plate as a whole, considering the plate as free at the edges with the support struts not influencing model shape and with the beryllium oxide contributing to the weight of the plate but not the stiffness of the plate.

Now

$$f_n = \frac{a}{2\pi}\sqrt{\frac{D}{\mu r^4}}$$

where

$$r = 26.5$$

and

$$D = \int_{-h/2}^{h/2} \frac{E z^2 \, dz}{(1 - \nu^2)}$$

where

D = plate stiffness per unit width

E = Young's Modulus, $5(10^6)$ psi

ν = Poisson's Ratio, 0.3

h = thickness

Where beryllium oxide may contribute to stiffness or may not, it will be assumed that it does not. Plate stiffness per unit width, assuming that the beryllium oxide and rib spacers make the cover plates act as a homogeneous plate yet neglect their stiffening effect and any capsule retention stiffening effect

$$D = \frac{2E}{1 - \nu^2} \int_{1}^{1.125} z^2 \, dz$$

$$D = 1.55\ (10^6)\ \text{in.lb.}$$

Now, μ (mass per unit area) is a maximum of approximately 0.545 lb/in^2.

Hence, for the circular plate

$$f_n = 7.51a$$

Now, the lowest mode is the umbrella mode with a = 3.75; hence, the fundamental frequency is

f_1 = 28 hertz

Therefore, additional stiffening would be required to increase the final design to over 200 hertz.

B2.0 RESONANT FREQUENCY OF THE RECTANGULAR HEAT SOURCE SUPPORT PLATE

Assume the rectangular plate is 63 in. x 44 in. Also assume:

a. Wt/area = 0.56 lb/in^2

b. I of plate $\simeq$ 0.304 in^4/in (neglect beryllium oxide)

c. Simply-supported Edge Conditions (from Den Hartog, "Mechanical Vibrations", for the vibration of a rectangular plate)

$$f_r = \frac{\pi}{2}\left(\frac{m^2}{L_1^2} + \frac{n^2}{L_2^2}\right)\sqrt{\frac{D}{\mu}}$$

Assume

$E \simeq 5(10^6)$ psi

Then, the flexural stiffness is

$D = 1.67\ (10^6)$

Therefore

f_1 = 41 hertz

So the rectangular plate requires additional stiffening before the final design.

B3.0 CONICAL STRUCTURE VIBRATION ANALYSIS

B3.1 There is generally a flat plate at the apex of conical frustum structures. The resonant frequency of this plate is:

For a circular plate:

$$f_n = \frac{a}{2\pi}\sqrt{\frac{D}{\mu r^4}}$$

here

$r = 5$ in.

$D = 895$ in.lb.

$\mu = 0.0375$ lb/in^2

Thus

$$f_n = 19.5\ a$$

Now the plate joins to a reinforced cone so that the end condition should be close to the clamped edge condition.

Thus

$$a = 10.21$$

So

$$f_n = 200 \text{ hertz}$$

Hence, a slightly thicker plate may be desirable.

B3.2 Flutter-vibration of panels in cone between support ribs, neglecting damping of superinsulation, assume the panel is essentially a rectangular plate (a x b) with sides b clamped and sides a simply-supported.

$a = 8.25$ in.

$b = 27.5$ in.

Thus, the ratio $a/b = 0.3$ and the thickness is 0.125 in.
From the paper by M. Vet, referenced previously,

$$a/b = 0.3$$

then

$$a \simeq 21$$

with

$$f_n = a_n \frac{t}{a^2} \sqrt{\frac{E}{\rho(1-\nu^2)}}$$

$$f_n = 7.88\ a_n$$

So

f_1 = 165 hertz

Hence, closer rib spacing will be required in the final design.

B3.3 Vibration of the Conical Structure as a Whole

The conical support structure approximates a free conical frustum as a lower bound in vibration since the actual designs contemplated have some restrictions at the ends of the frustum. To get an approximate value for the fundamental frequency, the complex structure must be assumed to be a thin-walled homogeneous conical frustum; then, the results of W. C. Hu* can be utilized. The frequency and mode functions depend on six parameters. The natural frequency is given by

$$f = \frac{\Omega}{2\pi a}\sqrt{\frac{E}{\rho(1-\nu^2)}}$$

Where:

Ω = Frequency parameter

Ω = $\Omega(a, S_2/S_1, h/a, \nu, n, m)$

h = Thickness

a = Major base radius

ρ = Density

E = Young's Modulus

ν = Poisson's Ratio

m = Axial wave number

n = Circumferential wave number

S_2/S_1 = Ratio of distances from apex to major base and minor base

Assuming:

$\left.\begin{array}{l}\nu = 0.3 \\ E = 5 \times 10^6 \text{ psi} \\ \rho = 0.3 \text{ lb/in}^3\end{array}\right\}$ For Cb 1 Zr at temperature

* Hu, W.C., Free Vibrations of Conical Shells, NASA TN D-2666(1965).
Hu, W.C., and U. Lindholm, Nonsymmetric Tranverse Vibrations of Truncated Conical Shells, Proc. AIAA Symposium on Structural Dynamics and Aeroelasticity (1965), pp. 389-99.

and using the following values to represent the conical structure:

$a \simeq 28$ in.

$a \simeq 60^{\circ}$

$S_2/S_1 = 4.6$

$h \geq 0.125$ in.

$h/a \geq 0.00446$

Now for non-torsional axisymmetric vibrations of free conical frustums, $n = 0$ and the bending rigidity has negligible effect on the lower modes, hence for $S_2/S_1 = 4.0$, then $\Omega \geq 0.6$.

Thus:

$$f = \frac{0.6}{2\pi a}\sqrt{\frac{E}{\rho(1-\nu^2)}}$$

$f = 286$ hertz

Therefore, the resonant frequency for the case assumed is greater than 200 hertz, although later stage efforts must consider other possible mode shapes. Note also that this analysis considered the density of Cb 1 Zr whereas the plate structure as a whole should include the capsule weight as did part 1 and part 2. This more than doubles the effective density; hence, the conical structure will also have a resonant frequency less than 200 hertz.

APPENDIX C

THERMAL ANALYSIS

An analysis of the heat transfer between the heat source and the heat source exchangers should consider the radiant heat interchange between the heat source and HSHX1, as well as between HSHX1 and HSHX2, conduction across the heat exchangers, and convection between the Brayton fluid and the walls of the HSHX in operation. The interaction between radiation, conduction, and convection results in a very complex heat transfer process. Therefore, an accurate determination of the temperature distribution over the heat source and the heat source heat exchangers requires the use of computers.

Two methods were used to obtain the temperature distributions. The first method employs two computer programs and will be referred to as the exact method. The second method, which will be referred to as the approximate method, was used before the computer programs became operational.

C1.0 EXACT METHOD

To demonstrate this method, case 2A is considered (rectangular configuration; single-pass tube-fin HSHX). The heat source and both the heat exchangers are divided in elements, as shown in Figure C-1, and the following assumptions are made:

a. Each element is isothermal and assumes one discrete temperature.

b. Each surface is gray.

c. The radiation reflected and emitted from each element is diffusely distributed. The effect of reflectivity of each element is accounted for by assuming an effective emissivity $\epsilon \cong 0.74$.

d. The top surfaces of the heat source, the sidewalls, and the lower surface of HSHX2 are perfectly insulated. (This assumption is unnecessary and can be eliminated in the analysis of the final systems.)

e. A prescribed and uniform heat flux exists at the elements of the heat source.

f. Heat is transferred between the two halves of the heat exchanger by conduction. A suitable value of the thermal resistance between the two halves was determined by separately analyzing the tube and fin combination.

g. The Brayton fluid in HSHX2 is also divided into elements. Heat is transferred between each element and the two halves of the HSHX by convection.

h. Heat transfer coefficient inside the tubes of the HSHX is constant.

Using assumptions (a) and (c), the radiation view factors between various elements in Figure C-1 are computed by a computer program CONFAC-II (Reference 1), see Appendix D. Knowing these view factors and using the remainder of the above

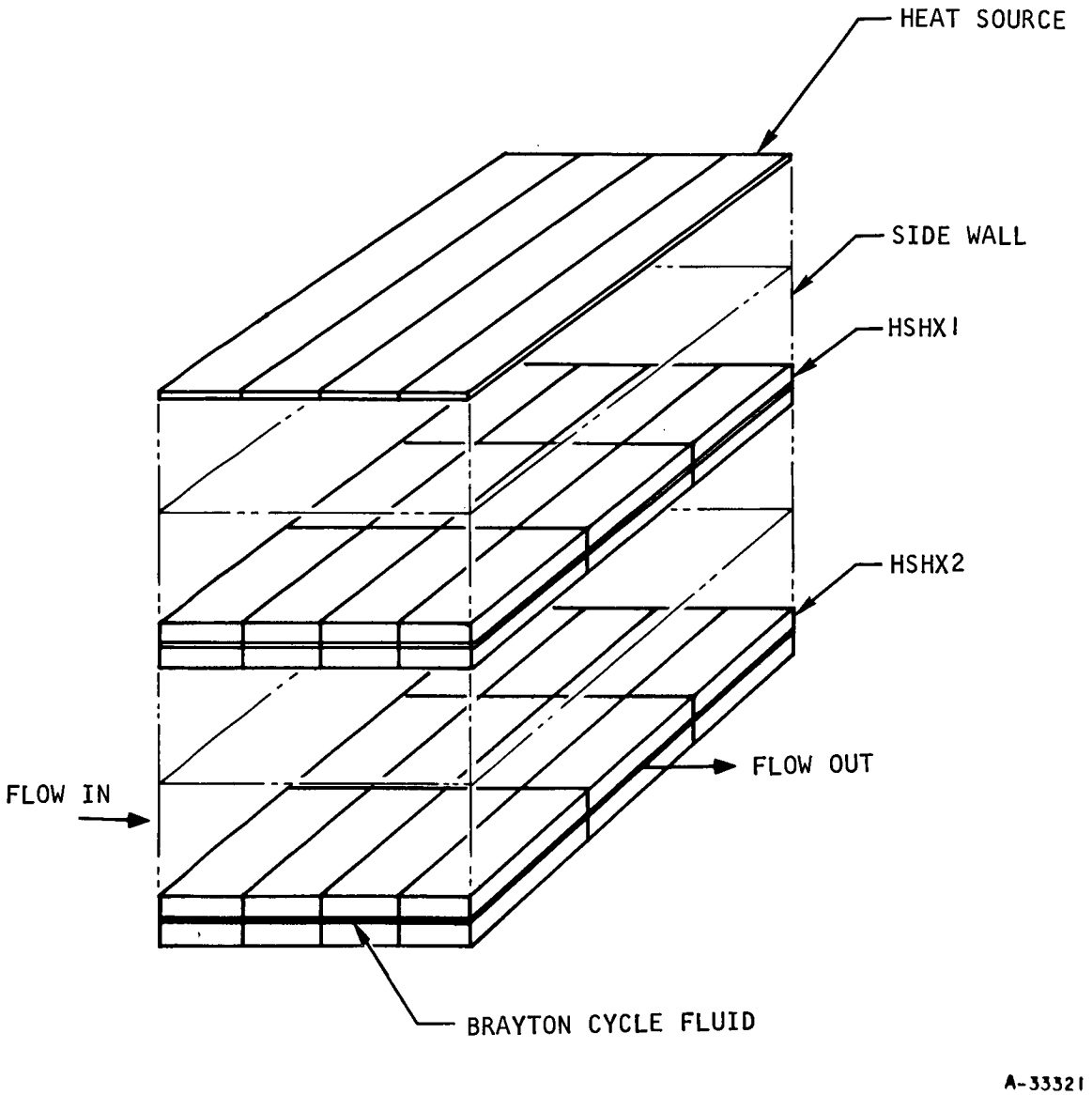

Figure C-1. Model for Thermal Analysis

assumptions, the various elements are represented as discrete nodes in an electric network simulating the heat transfer process. This, in turn, is analyzed using a second computer program MLFTHAN-MARK-I (Reference 35) to obtain the temperature distribution for the physical system shown in Figure C-1, both in the transient and steady-state conditions.

It may be noted that slight modification of the MARK-II program was necessary to allow for the large number of the radiation resistances in the present application. A brief description of this program and the modifications is given in Appendix E.

This analysis was carried out only for System 2A, and the result of the temperature distribution over the heat source is shown in Figure C-2 for steady-state conditions.

C2.0 APPROXIMATE METHOD

To design the heat exchangers for the various systems described in this report, it was necessary to determine, at least in an approximate way, the variation of the temperature and heat flux over the heat exchangers.

This was accomplished by an approximate analysis, which will be outlined in the following paragraphs for the particular case of System 2A (Figure C-1).

In the approximate method, the various surfaces are divided in a smaller number of elements than what is shown in Figure C-1, and the simultaneous interaction between radiation, conduction, and convection is not considered. The radiation shape factors between various elements are obtained from Reference 36, together with shape factor algebra (Reference 37).

The same assumptions, (a) through (f), are used. The assumption of an effective emissivity is unnecessary in this case and the actual emissivity is used. For convenience, suppose that the radiating surfaces are numbered so that those with prescribed temperatures are designated as $1 \leq i \leq N_1$, while those with prescribed heat fluxes are designated as $(N_1 + 1) \leq i \leq N$.

For each of the first N surfaces, one can write the radiant flux balances as (Reference 38):

$$B_i = \epsilon_i \sigma T_i + (1 - \epsilon_i) \sum_{j=1}^{N} B_j F_{i-j}, \quad 1 < i < N_1 \tag{C-1}$$

where B_i is the radiosity at a surface i , T is the absolute temperature, and F_{i-j} is the shape factor which designates the fraction of the radiation leaving i that arrives at j . It is assumed that the radiosity is uniform over each element. The unknown surface heat flux is related to the known surface temperature by:

$$\frac{Q_i}{A_i} = \frac{\epsilon_i}{1 - \epsilon_i} (\sigma T_i^4 - B_i), \quad 1 \leq i \leq N_1 \tag{C-2}$$

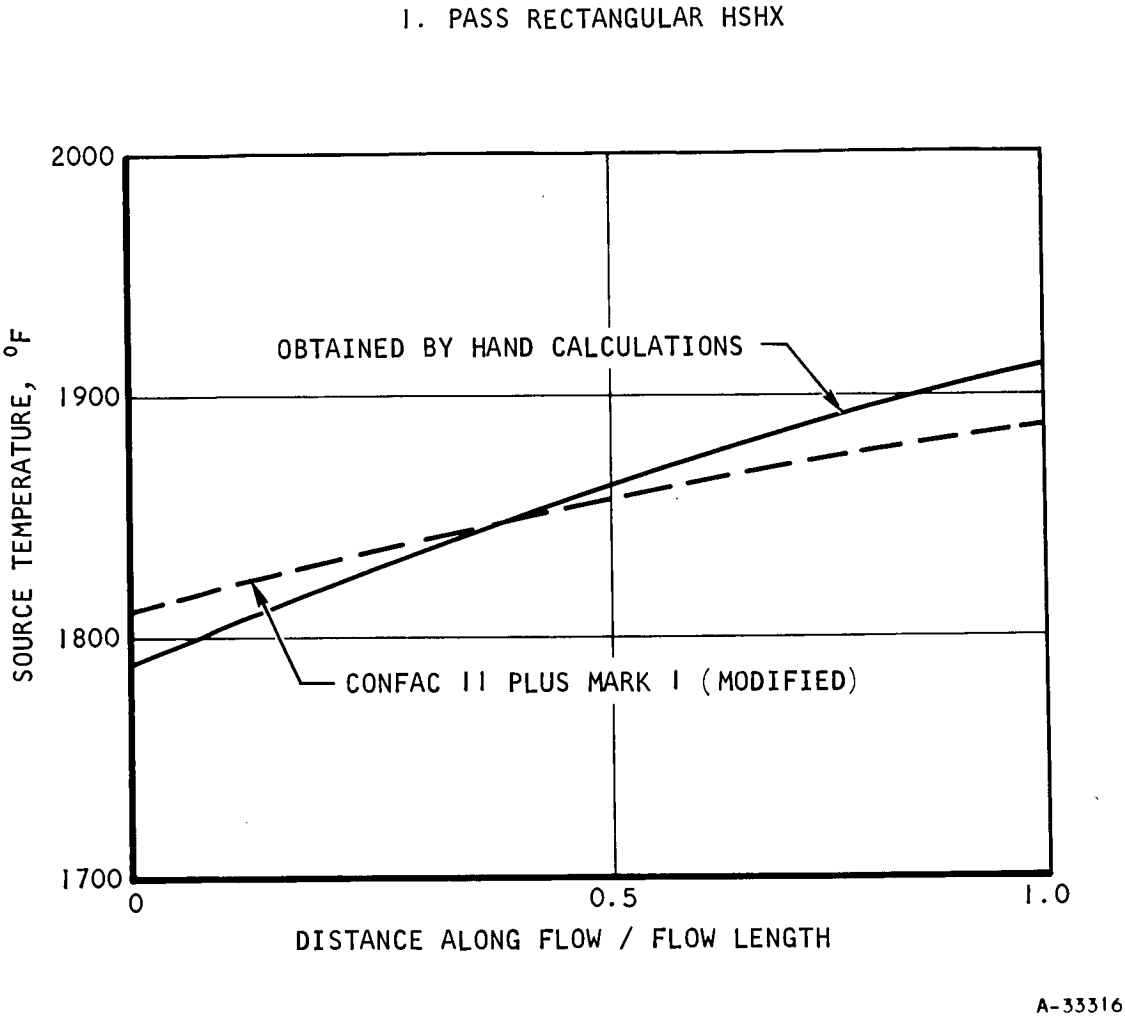

Figure C–2. Comparison of Computer Calculations

For the second group of surfaces $(N_1 + 1) \leq i \leq N$, the unknown surface temperature is related to the known surface heat flux by (C-3)

$$\sigma T_i^4 = \frac{1 - \epsilon_i}{\epsilon_i} \frac{Q_i}{A_i} + B_i, (N_1 + 1) \leq i \leq N \quad \text{(C-4)}$$

The emissivity ϵ_i for both the heat source and the heat exchanger surfaces is assumed equal to 0.85.

Equations such as (C-1) and (C-3) are written for each of the N surfaces of the enclosure. In this way, N linear, algebraic equations are generated for the N unknown radiosities $B_1, B_2, -- B_N$. For a small number of surfaces, the equations can be easily solved. For a large number of surfaces, the equations are solved on a digital computer by matrix inversion methods. (Such a computer program is available at computer libraries.) The unknown heat flux or surface temperatures are then determined from Equation (C-2) or (C-4).

Now, consider the enclosure composed of the lower surface of HSHX 1 and HSHX 2, and neglect the temperature drop, due to conduction, across HSHX 2 (see Figure C-1). Assume a temperature distribution over both heat exchangers and use Equations (C-1) and (C-2) to determine the heat flux distribution along HSHX 2. Knowing the heat transfer coefficient inside the tubes of HSHX 2, the outlet temperature can be checked against the desired temperature (1600° F). The process is repeated until agreement is obtained.

Conduction across HSHX 1 is accounted for approximately by adding a suitable temperature drop to the temperature at the lower surface of HSHX 2.

Now knowing the temperatures at the upper surface of HSHX 1, the enclosure composed of the heat source and HSHX 1 is considered. The surface of the heat source is assumed to have a prescribed heat flux. Hence, by using Equations (C-1), (C-3), and (C-2), the temperature distribution over the heat source is determined.

A comparison between the results of the approximate and exact methods is shown in Figure C-2 for System 2A. The agreement between the exact method and the approximate method is reasonably good.

APPENDIX D

COMPUTER PROGRAM FOR THE DETERMINATION OF RADIANT INTERCHANGE CONFIGURATION AND FORM FACTORS - CONFAC II

This computer program calculates the geometric radiant-interchange factors used in radiant heat transfer and illumination of the basis of a simple numerical method. The program is written in FORTRAN IV and provides a rapid and accurate means of computation of configuration and form factors. Simplicity of data entry, flexibility of application, and economy of operation are principal features of this program.

The source of heat may be any general plane polygon, and the receiver may be any general plane or nonplanar polygon, the surface of an arbitrary polyhedron, or an arbitrary combination of such surfaces.

It is also possible to accurately determine configuration and form factors from a plane surface to another surface occluded by complex intervening surfaces. Form factors are computed rapidly - averaging less than two seconds on the IBM 7094 for simple, unobstructed plane surfaces and less than 30 seconds for simple polyhedra. Also, means are provided to internally generate a variety of regular polygons or polyhedra and to transform surface spatial coordinates for convenience of data entry and/or motion simulation.

The data classification handled by CONFAC II are as follows:

Class 1: plane polygon (silhouette developed directly from input surface coordinate data)

Class 2: nonplane polygon (silhouette developed directly from input surface coordinate data)

Class 3: internally generated polygon (silhouette developed directly from internally generated data)

Class 4: plane polygon (silhouette internally computed from input coordinate and connections data)

Class 5: nonplane surface or solid (silhouette internally computed from input coordinate and connections data)

Class 6: internally generated polygon or solid (silhouette internally computed from internally generated coordinate and connections data)

Class 7: sphere (closed-form factor solution)

Class 8: multisurface (silhouette developed from input or internal coordinate and connections data of a group of surfaces taken together)

Class 9: transformation data.

APPENDIX E

MLFTHAN - LMSC THERMAL NETWORK ANALYZER

This computer program (Reference 35) produces a temperature history for a physical system which has, through the concept of lumped parameters, been expressed as the electrical analog of the heat transfer problem using finite difference techniques.

The vast majority of heat flow problems may, by lumping the physical parameters, be represented by a thermal resistance-thermal capacitance network with the capability of heat input at any of the discrete "nodes" in the network. This program solves n-dimensional transient heat flow problems through the use of an electrical analog of the thermal network. An example of the reduction of a two-dimensional slab heat flow problem to its electrical analog is shown below:

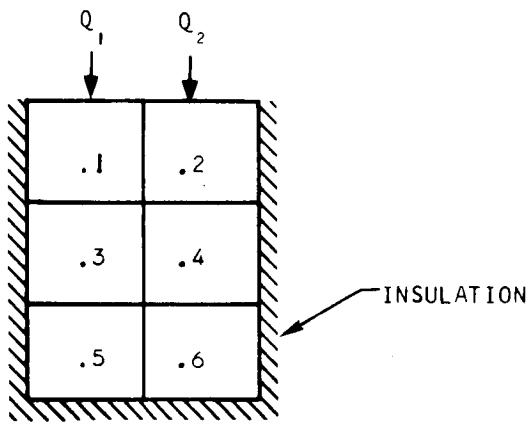

Electrical analog (with the simplifying use of T rather than voltage):

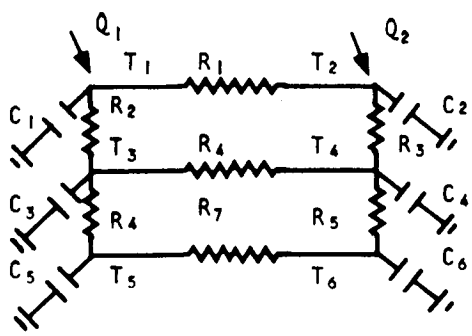

The units for the above network parameters are

T - ^{o} F

C - BTU ^{o} F

R - sec*^{o} F/BTU

Q - BTU sec*

The MLFTHAN-LMSC Thermal Network Analyzer (Reference 35) has been modified at AiResearch, and a summary of these modifications is given below:

1. The maximum number of the radiation resistance that can be used is increased 400.

2. The number of tables that can be used is increased to 100. The size of each table is increased to 65 pairs of variables.

3. If more than one node has identical initial temperatures and capacitances, input data need not be repeated for each node.

4. Input format for output specification has been simplified extensively. For example, if temperatures of all 700 nodes need to be printed out, 700 input cards are necessary for H2361;**however, for H2804*** one card is sufficient. (One can still use 700 input cards for this condition in this program if desired.) This simplification can also be applied to the output specifications for resistance, capacitance and heat input.

5. Print-out format has been improved for H2804. The user can now identify the variables and number of nodal points of the output data immediately. There is no confusion or possibility of getting lost in the large output data, as occurred frequently when using H2361.

6. Any number (less than 700) can be designated as the Resistance Identification Number. The input card of the resistances can be arranged at random. It is not necessary to arrange them in numerical sequence. Similarly, the input cards of initial temperatures and capacitances can also be arranged at random in their respective groups.

7. A steady-state criterion has been added to this program. The machine can stop the computation when this criterion is reached, and a cut-off message is printed out for your information. This criterion is the change of temperature in degrees per unit time. The units of degrees and time should be consistent with other input data. This criterion is assigned as Problem Constant No. 12 in Function No. 9 of the input.

8. Final temperatures of all nodes for each computer run can also be punched out on IBM cards in the same format as the initial temperatures. These cards can be used directly as input cards for computer runs later on. The control

---

* or consistent time units

** This is the program of Reference 35.

*** This is the AiResearch-modified version.

of this punched out operation is assigned as Problem Constant No. 14 in Function No. 9 of the input. Assigning this constant a value anything larger than zero will instruct the machine to punch out final temperature on cards.

9. A heading card is necessary in H2804 to insure proper identification for the input deck and output. This card should be placed in the very beginning of each set of data.

10. All the regulations about the input procedure for H2361 can also be applied to H2804, except for the necessary heading card.

The above mentioned modifications are believed to be very useful and can save a tremendous amount of the engineer's time.

APPENDIX F

SPIN STABILIZATION FOR THRUST VECTOR CONTROL

F1.0 DISCUSSION

In order to have controlled intact reentry, the velocity increment vector for deorbit must be applied within certain angular error bands. This requires some form of thrust vector control (TVC) and the simplest form is spin stabilization. The principal contributors for down range dispersion at the reentry altitude are as follows:

1) Initial orbital position accuracy

2) Initial orbital velocity vector accuracy

3) ΔV timing errors

4) Spacecraft attitude rates

5) Separation dynamics

   a) Tipoff rates due to separation force misalignments

   b) Tipoff rates due to IRV center of gravity offsets

6) The time interval between separation and spin-up

7) Spin-up thrust vector misalignments

8) IRV dynamic imbalance

9) ΔV thrust vector misalignments.

Items 1) through 4) are at this stage of the contract undefined. Items 5) through 9) are, however, part of the system design and are considered in this section.

F2.0 SEPARATION DYNAMICS

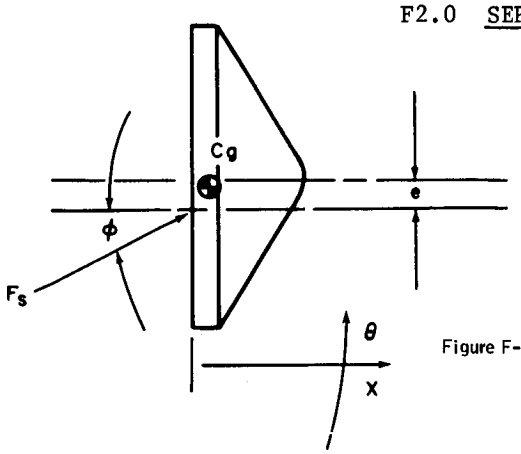

The separation force is assumed to be supplied by compressed springs located on the attachment bolts around the periphery of the IRV.

Figure F-1 SEPARATION MODEL

In the figure:

F_s = separation force

e = IRV c.g. offset plus separation force misalignment.

Assuming ϕ is small

$$F_x = M\ddot{X} \qquad M_{cg} = I_{cg}\ddot{\theta} \tag{1}$$

$$M\ddot{X} = F_o - k(X + e\theta) \qquad I\ddot{\theta} = e[F_o - K(X + e\theta)] \tag{2}$$

where:

k = separation mechanism spring constant

F_o = preload in the springs.

Assuming $e\theta$ is small compared to X , the differential equations of motion decouple and the solutions are:

$$V_s = \frac{F_o}{M\omega} = \text{separation velocity} \tag{3}$$

$$\Omega_T = \frac{eF_o}{\omega I} = \text{tip-off rate} \tag{4}$$

where

$$\omega = (k/M)^{1/2} \tag{5}$$

Figure F-2 presents the relationsiip between separation velocity, transverse tip-off rate and e , the allowable combined c.g. offset and resultant separation spring force offset for a typical IRV configuration.

The time interval between separation and spin-up, and the spin-up thrust vector misalignment are assumed small when compared to the other contributing factors.

The remaining contributors to ΔV vector misalignment are the result of:

a. Thrust vector misalignment

b. Dynamic imbalance

c. Static c.g. offset

d. Transverse tip-off rates

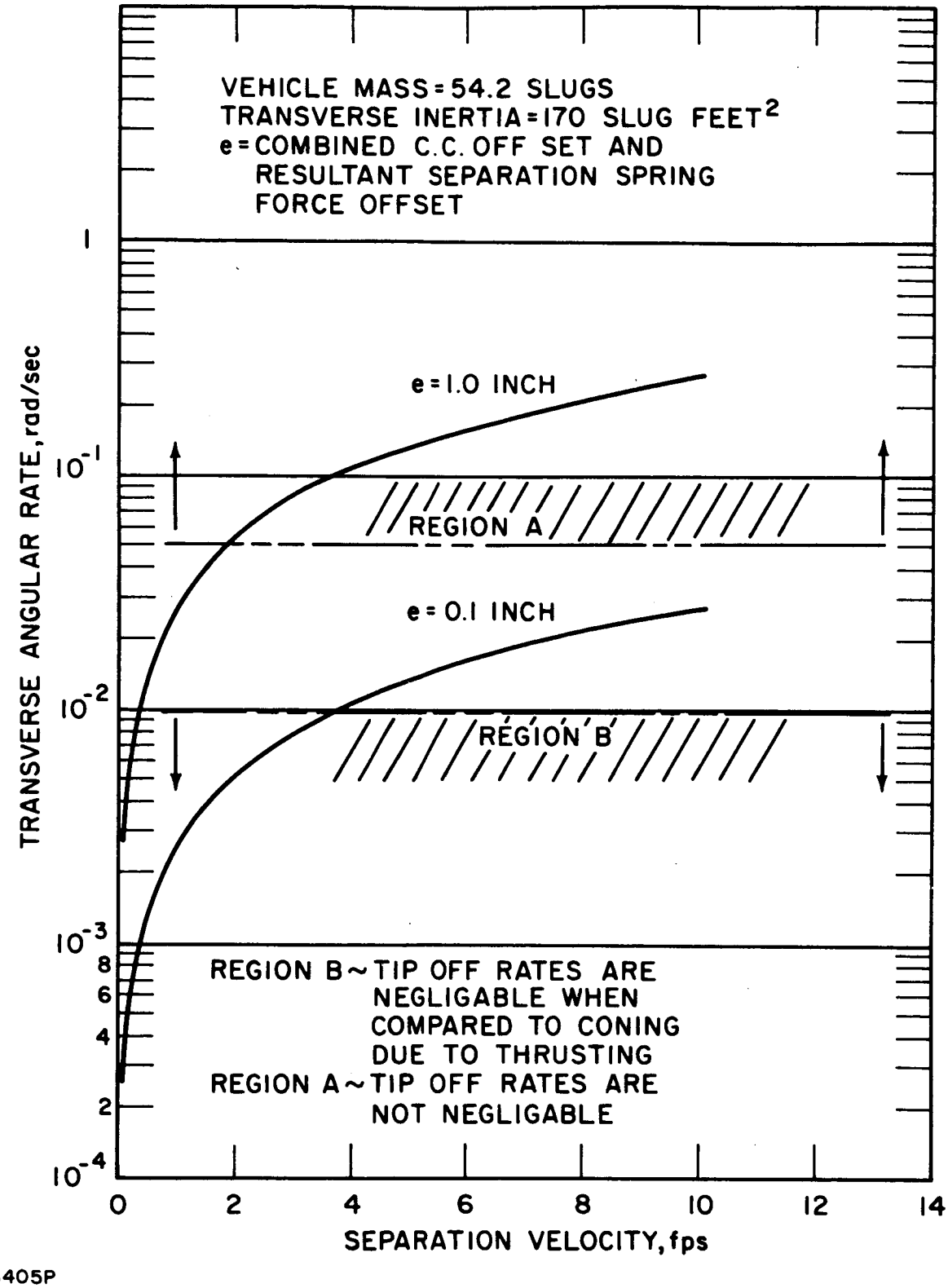

776405P

Figure F-2 TIPOFF RATES

The worst combination of these anomalies occurs when they are directly additive, i.e.

$$M_Z = d_1 T \sin\beta + d_2 T + 2mr\omega_X^2 d_3 \quad (6)$$

where:

M_Z = the applied transverse moment ~ in-pounds

T = deorbit thrust level ~ pounds

β = thrust misalignment angle ~ degrees

d_1 = distance between IRV longitudinal axis and thrust application point ~ inches

d_2 = IRV c.g. offset

m = equivalent mass dynamic imbalance ~ lb sec^2/in

r = radius of "m" measured from longitudinal axis ~ inches

ω_X = IRV spin rate ~ rad/sec

d_3 = distance between IRV c.g. and "m" along longitudinal axis ~ inches.

M_Z is a body fixed moment, and can be simplified to:

$$M_Z = dT \quad (7)$$

where d takes into account the contribution of the other moments.

The general rotational equations of motion in terms of a body axis coordinate system where the axis coincides with the principal axis, and the center of mass are:

$$I_x\dot{\omega}_x + (I_z - I_y)\omega_z\omega_y = 0 \quad (8)$$

$$I_y\dot{\omega}_y - (I_y - I_x)\omega_x\omega_z = 0 \quad (9)$$

$$I_z\dot{\omega}_z + (I_z - I_x)\omega_x\omega_y = M_Z \quad (10)$$

Simplifying and noting $I_y = I_z$, they become:

$$\dot{\omega}_x = 0$$

$$\dot{\omega}_y + k\,\omega_z = 0 \tag{12}$$

$$\dot{\omega}_z - k\,\omega_y = M \tag{13}$$

where:

$$k = -\frac{(I_y - I_x)\,\omega_x}{I_y} \tag{14}$$

$M = M_Z / I_y$

I_x = roll inertia

$I_y = I_z$ = transverse inertia.

The solutions to the above equations with initial conditions of $\omega_y(o)$ and $\omega_z(o)$ (the tip-off rates) are:

$$\omega_z(t) = \omega_z(o)\cos k\,t + \frac{M + k\,\omega_y(o)}{k}\sin k\,t \tag{15}$$

$$\omega_y(t) = \omega_y(o)\cos k\,t - \omega_z(o)\sin k\,t - \frac{M}{k}(1 - \cos k\,t) \tag{16}$$

$$\omega_x(t) = \omega_x = \text{constant} \tag{17}$$

These are motions relative to the body. In order to determine the motion of the IRV relative to a set of coordinate axes fixed in space a transformation must be performed relating the two coordinates.

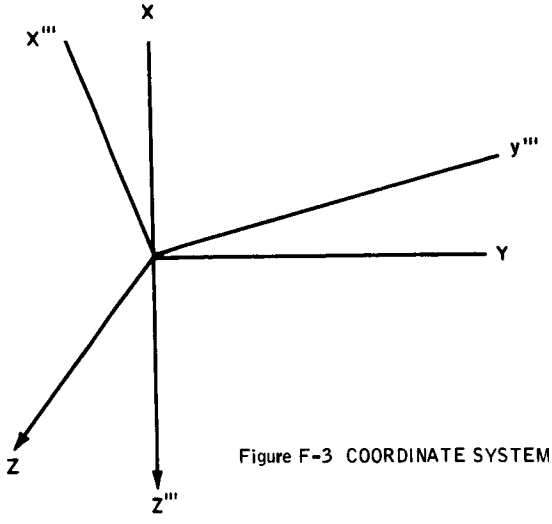

Figure F-3 COORDINATE SYSTEM

Performing xyz rotations in Figure F-3 results in:

$$\begin{vmatrix} \omega_x^{111} \\ \omega_y^{111} \\ \omega_z^{111} \end{vmatrix} = \begin{vmatrix} C\theta & -S\theta & 0 \\ S\theta & C\theta & 0 \\ 0 & 0 & 1 \end{vmatrix} \begin{vmatrix} C\psi & 0 & S\psi \\ 0 & 1 & 0 \\ -S\psi & 0 & C\psi \end{vmatrix} \begin{vmatrix} 1 & 0 & 0 \\ OC & \phi & -S\phi \\ 0 & S\phi & C\phi \end{vmatrix} \begin{vmatrix} \omega_x \\ \omega_y \\ \omega_z \end{vmatrix} \tag{18}$$

where:

C = cosine

S = sine

$$\theta = \int \omega_z^{111} \, dt$$

$$\psi = \int \omega_y^{111} \, dt$$

$$\phi = \int \omega_x^{111} \, dt = \omega_x \, t = \omega t$$

Assuming the motions to remain small results in:

$$\omega_x^{111} = \omega_x \tag{19}$$

$$\omega_y^{111} = \omega_y \, C\phi - \omega_z \, S\phi \tag{20}$$

$$\omega_z^{111} = \omega_y \, S\phi \tag{21}$$

Substituting Equations 14, 15 and 16 into the above gives:

$$\omega_z^{111} = \sin \omega t \left[\omega_y(o) - \omega_z(o) \sin k t - \frac{M}{k} (1 - \cos k t) \right] + \cos \omega t \left[\omega_z(o) \cos k t + \frac{M + k \omega_y(o)}{k} \sin k t \right] \tag{22}$$

$$\omega_y^{111} = \cos \omega t \left[\omega_y(o) \cos k t - \omega_z(o) \sin k t - \frac{M}{k} (1 - \cos k t) \right]$$

$$- \sin \omega t \left[\omega_z(o) \cos k t + \frac{M + k \omega_y(o)}{k} \sin k t \right] \quad (23)$$

Simplifying and using the trigonometric identies leaves:

$$\omega_z^{111} = \omega_y(o) \sin (k + \omega) t + \omega_z(o) \cos (k + \omega) t - \frac{M}{k} \sin \omega t$$

$$+ \frac{M}{k} \sin (k + \omega t) \quad (24)$$

$$\omega_y^{111} = \omega_y(o) \cos (\omega + k) t - \omega_z(o) \sin (\omega + k) t - \frac{M}{k} \cos \omega t$$

$$+ \frac{M}{k} \cos (\omega + k) t \quad (25)$$

Integrating:

$$\psi = \frac{\omega_y(o)}{\omega + k} \sin (k + \omega) t + \frac{\omega_z(o)}{\omega + k} \cos (\omega + k) t$$

$$- \frac{M}{k\omega} \sin \omega t + \frac{M}{k(\omega + k)} \sin (\omega + k) t - \frac{\omega_z(o)}{\omega + k} \quad (26)$$

$$\theta = \frac{-\omega_y(o)}{\omega + k} \cos (\omega + k) t + \frac{\omega_z(o)}{\omega + k} \sin (\omega + k) t + \frac{M}{k\omega} \cos \omega t$$

$$- \frac{M}{k(k + \omega)} \cos (k + \omega) t + \frac{M}{k(\omega + k)} - \frac{M}{k\omega} \quad (27)$$

θ and ψ, therefore, represent the motions of the longitudinal axis of the IRV as a function of time, transverse moment, tip-off rates, spin rate and the inertial characteristics of the vehicle. The incremental velocity misalignment is defined as the average amplitude of θ and ψ during a thrusting time, τ. This is determined mathematically by integrating Equations 26 and 27 over a time, τ, and dividing by τ.

Figure F-4 presents this incremental velocity vector misalignment as a function of thrust level and spin rate for typical IRV characteristics, i.e.:

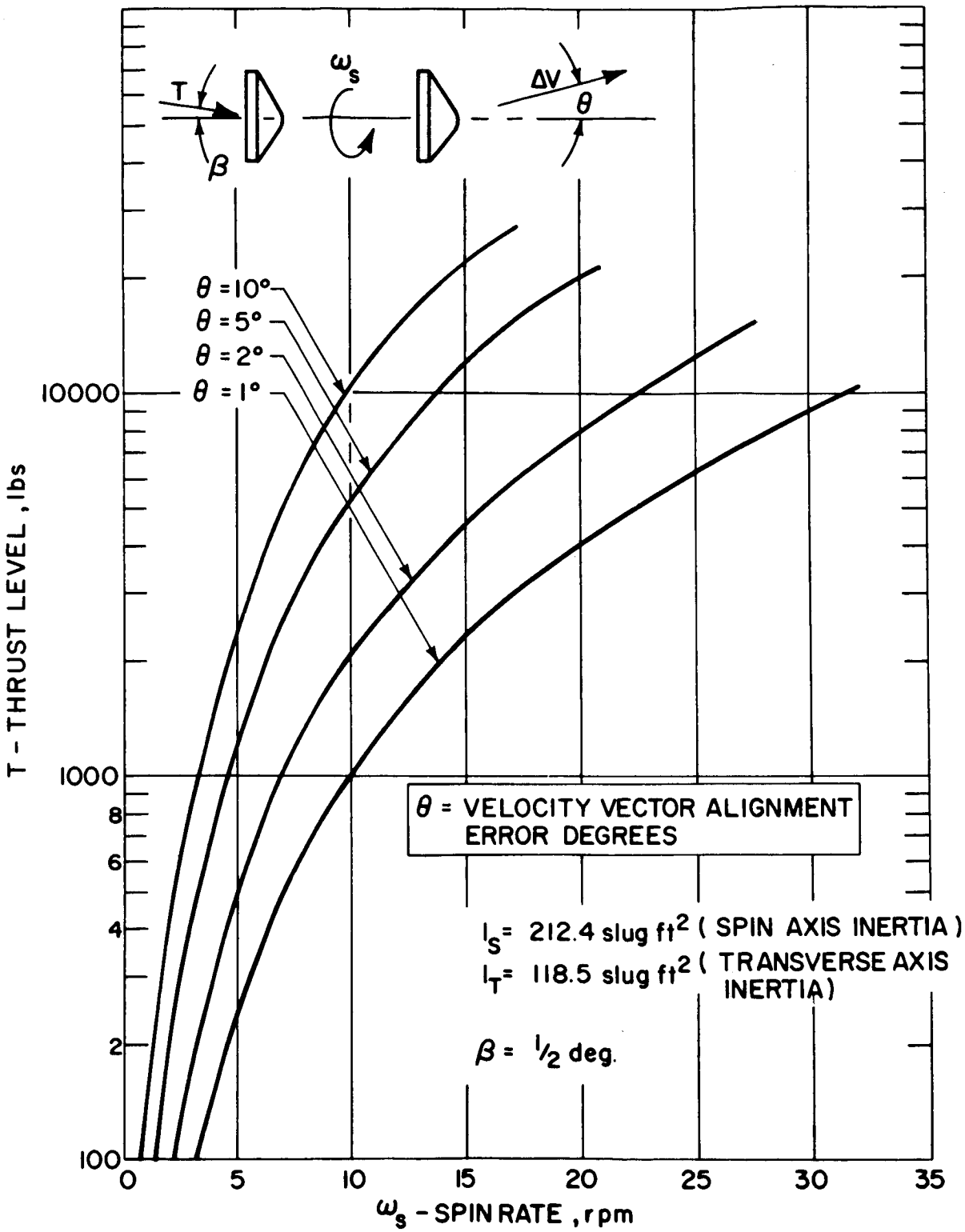

776404P

Figure F-4 SPIN STABILIZATION REQUIREMENTS

$d = 4.8 \times 10^{-2}$ in.

$I_x = 212.4$ slug ft^2

$I_y = 118.4$ slug ft^2

F3.0 PAD ABORT

The objective of the pad abort system is to get the isotope heat source clear of the launch configuration. This can be accomplished practically only by the use of rockets and the minimum system would be one which utilized the deorbit TVC and ΔV rockets. As the requirements for the deorbit system are fairly specific, it is of interest to see if these could be used as they stand for the pad abort function.

In view of the need to use the ΔV rocket to separate from the launch vehicle while on the pad, prior spin stabilization for TVC cannot be achieved. Spin-up while thrusting, therefore, will be the case, and larger dispersion angles of the longitudinal axis will be the result.

The thrust level of 2800 pounds is adequate to lift the IRV away from the launch configuration but it remains to be determined whether the resulting separation distance of the IRV from the launch pad is adequate.

Assuming:

a. ΔV is applied 5 degrees from the vertical (conservative)

b. That drag can be neglected,

the IRV reaches an altitude of approximately 1,000 feet and impacts the ground approximately 200 feet from the launch pad.

For the Saturn configuration, with the IRV coming out horizontally, the separation distance achieved is again approximately 200 feet.

APPENDIX G

IMPACT ANALYSIS FOR ROTATIONAL PLATE CONCEPT

Figure G-1 presents the dynamical model to be analyzed.

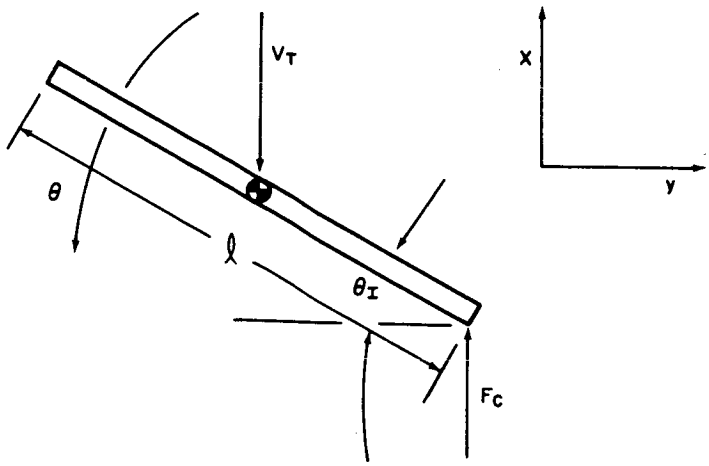

Figure G-1 ROTATION MODEL

where:

V_T = terminal velocity

F_c = crush-up force

ℓ = diameter of heat source plate

W = plate weight

θ_I = maximum impact angle.

Assuming the plate acts as a rigid body, the angular motion is established by:

$$\sum M_{cg} = I_{cg} \ddot{\theta} \tag{1}$$

$$I_{cg} \ddot{\theta} = F_c \ \ell/2 \cos\theta \tag{2}$$

where:

$$I_{cg} = \frac{ML^2}{12}$$

with small angle approximations:

$$\ddot{\theta} = \frac{6 F_c}{M \ell} \tag{3}$$

with solutions:

$$\dot{\theta} = \frac{6 F_c t}{M \ell}$$

$$\theta = \frac{3 F_c t^2}{M \ell}$$

The translational motion of the C_g of the plate is established by:

$$\sum F_x = M\ddot{X} \tag{6}$$

$$M\ddot{X} = F_c \tag{7}$$

$$\ddot{X} = F_c/M \tag{8}$$

with solutions:

$$\dot{X} = F_c/M\, t - V_T \tag{9}$$

$$X = F_c/2M\, t^2 - V_T\, t \tag{10}$$

The analysis is valid up until the time the velocity of point A becomes zero, and the displacement of point A at this time corresponds to the maximum crush-up height h needed to cause a rotation of θ.

The velocity of point A is:

$$V_A = \dot{X} + \ell/2\,\dot{\theta} \tag{11}$$

$$= \frac{F_c}{M} t - V_T + \frac{\ell}{2}\left(\frac{6F_c}{M\ell}\right) t \tag{12}$$

$$V_A = \frac{F_c}{M} t - V_T + \frac{3F_c}{M} t \tag{13}$$

when V_A is zero, therefore:

$$t = \frac{MV_T}{4F} \tag{14}$$

In time t point A has traveled a distance h

$$h = X + \ell/2\,\theta \tag{15}$$

Substituting for X and θ:

$$h = \frac{F_c t^2}{2M} - V_T t + \frac{\ell}{2}\left(\frac{3F_c}{M\ell}\right) t^2 \tag{16}$$

Substituting for t results in:

$$h = -\frac{M V_T^2}{8 F_c} \tag{17}$$

The crush-up force F_c, which is the only undefined term in Equation 17, is the limiting force which can be applied to the edge of the plate without causing its failure.

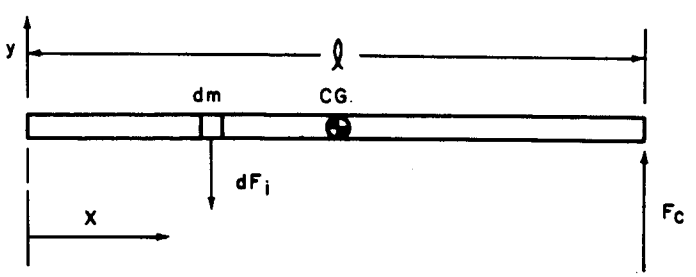

Figure G-2 PLATE LOADING FREE BODY DIAGRAM

Free body diagram of the plate experiencing the crush-up load is shown in Figure G-2. The inertial force dF_i is made up of two components:

$$dF_i = dm\ddot{y} - (\ell/2 - X)\, dm\ddot{\theta} \tag{18}$$

As before, $$\ddot{y} = F_c/M \tag{19}$$

$$\ddot{\theta} = \frac{F_c \ell}{2 I_{cy}} = \frac{6 F_c}{M \ell} \tag{20}$$

$$\text{or, } dF_i = \frac{dmF_c}{M} \left(\frac{6X}{\ell} - 2\right) \tag{21}$$

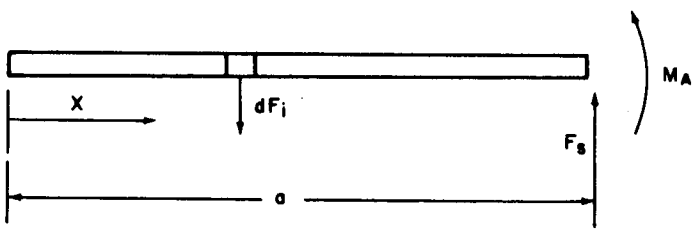

Figure G-3 PLATE SECTION

Figure G-3 shows the plate cut at an arbitrary point A, and the bending moment M_a and shear force F_s are needed to put the section in equilibrium.

Taking moments about A gives:

$$M_a = \int_{X=0}^{X=a} dF_i\ (a - X) \tag{22}$$

$$= \frac{F_c}{M} \int_0^a \left(\frac{6X}{\ell} - 2\right) (a - X)\ dm \tag{23}$$

let

$$dm = \rho\, dX$$

$$M = \rho\, \ell$$

$$M_a = \frac{F_c}{\ell} \int_0^a \left(\frac{6Xa}{\ell} - 2a - \frac{6X^2}{\ell} + 2 \times \right) dX \tag{24}$$

integrating

$$M_a = \frac{F}{\ell} \left(\frac{a^3}{\ell} - a^2 \right) \tag{25}$$

From above, M_a is maximum at $a = 2/3\,\ell$ or

$$M_{max} = \frac{4F_c\,\ell}{27} \tag{26}$$

The stress in the plate caused by this moment is:

$$\sigma = \frac{M_{max}\, C}{I} \tag{27}$$

Figure G-4 represents an idealized cross section of the plate

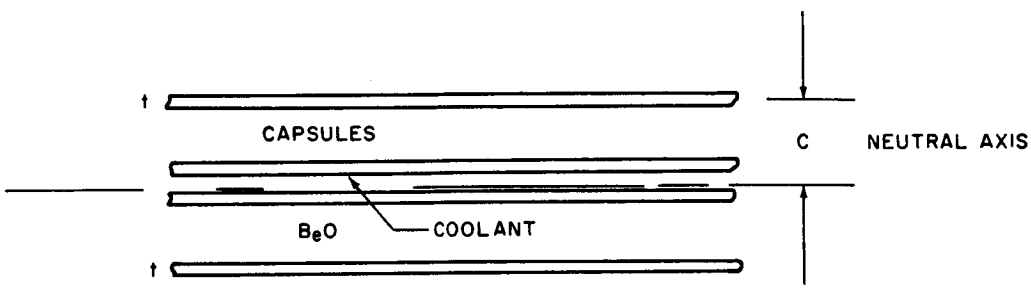

Figure G-4 ASSUMED HEAT SOURCE SUPPORT PLATE CROSS SECTION

From the section, C is found to be:

$$C = 1.75$$

and

$$I = 288\,t \tag{27a}$$

The weight of the plate is made up of a fixed weight plus a variable which is determined by the thicknesses t .

(Columbium 1 percent Zr) = 0.31 lb/in^3 = $82\,t + 0.62\,\ell^2\,t$

$$h = \frac{4.2 \times 10^{-5} (W_f + 0.62\,\ell^2\,t)\, V_T^2\, \ell}{t\sigma} \qquad (28)$$

G1.0 TYPICAL DESIGN CONDITIONS

Let W_f = fixed plate = 82

capsules = 744 lbs.

insulation = 58

BeO = $\frac{140}{1029}$ lbs.

σ = 30,000 psi

V_T = 150 fps $\qquad V_T^2 = 2.25 \times 10^4$

ℓ = 47 $\qquad \ell^2 = 2.21 \times 10^3$

t = 0.3

Substituting these values into Equation 28 gives

h = 7.1 inches

This analysis has assumed that the translational motion of the corner of the plate on the side of the vehicle which impacts the ground first must be brought to zero.

This crush up height is the height required to bring the corner (point A) to rest. If in doing so, the plate rotates more than necessary, then too much stroke has been provided.

Determine how far the plate does rotate:

From Equations:

(27a) I = 86.5 in.^{4}

(27) M_{max} = 1.48×10^6 in.lbs

(26) F_c = 2.13×10^5 in. lbs

(14) t = 0.0312 sec

(5) θ = 0.3 RAD

θ = 17.2°

Because point A has come to rest, the plate can continue to rotate the full amount required by pivoting about point A.

Therefore, the value of crush-up height h as computed is the minimum height which will accomplish the required rotation of 30° and this approach will, in general, be the case.

The plate as previously designed would weigh approximately 300 lbs.

The beefed up plate as designed by this analysis would weigh 492 lbs which indicates a weight penalty of 192 lbs.

The crush-up weight penalty is determined as follows:

Although the above analysis has assumed a square plate for simplicity, the crush-up design should be established for a circular plate.

Assume that only 60° of arc will be effective in producing the crush-up force F_c .

From Figure G-5, typical aluminum honeycomb material crushing stress is linear with density, i.e.,

$$\sigma_c = k\rho$$

where:

$$k = \frac{5000}{28} = 178.5$$

Assuming a ring of 4 inch thickness located around the periphery of the heat source plate, the effective area is:

$$A = r\theta W = \left(\frac{47}{2}\right)\left(\frac{60}{57.3}\right) 4 \simeq 100 \text{ in.}^2$$

The stress level required is:

$$\sigma_c = F_c/A = \frac{2.13 \times 10^5}{100} = 2.13 \times 10^3 \text{ psi}$$

which is within the performance capabilities of aluminum honeycomb materials. The crush-up material density is:

$$\rho = \frac{2.13 \times 10^3}{178.5} = 12.1 \text{ lb/ft}^3$$

The height of the crush-up material was computed to be 7.1 inches but 25 percent of this height is ineffective. Consequently, the height required is

$$h = \frac{7.1}{0.75} = 9.5 \text{ inches}$$

The total volume needed is:

$$V = \frac{(\pi)(47)(4)(9.5)}{1728} = 3.25 \text{ ft}^3$$

and the crush-up weight is:

$$W = (3.25)(12.1) = 39.3 \text{ lbs.}$$

The total weight penalty for the crush-up system is therefore

$$W = 39.3 + 192.0 = 231 \text{ lbs.}$$

REFERENCES

1. MLM-1387, Supplement (C), Mound Laboratory.

2. Broecher, W., Radioisotopes and Large-Scale Oceanic Mixing, The Sea Vol. 2, Interscience Publishers (1963).

3. Environmental Parameters of an Aborted Launch, Data from Accidental Atlas/Centaur Disintegration on the Pad, N6636552 (2 March 1965).

4. Booster Rocket Altitude Abort Program, Final Report, SC-CR-66-2047 (July 1966).

5. Brayton Cycle Radioisotope Heat Source Design Study Phase I (Conceptual Design) Report, Oak Ridge National Laboratory, ORNL TM-1691 (NASA CR-72090).

6. Bendura, R. J., Low Subsonic Static and Dynamic Stability Characteristics of Two Blunt 120° Cone Configurations, NASA TN D-3853 (February 1967).

7. Campbell, J. F., Longitudinal Aerodynamic Characteristics of Several High-Drag Bodies at Mach Numbers from 1.50 to 4.63, NASA TN D-3915 (April 1967).

8. Davenport, E. E., Some Supersonic Aerodynamic Characteristics of 120° Cones and a Tension Shell Model, NASA/Langley Working Paper 391 (April 1967).

9. Krumins, M. V., A Ballistic Range Study of Aerodynamic Characteristics of Mars Probe/Lander Shapes, AIAA Paper 67 - 167.

10. Keyes, J. W., Longitudinal Aerodynamic Characteristics of Blunted Cones at Mach Numbers of 3.5, 4.2 and 6.0, NASA TN D-2201 (February 1964).

11. Comparative Studies of Conceptual Design and Qualification Procedures for a Mars Probe/Lander, Final Report, Vol. V, Book 2, Avco/SSD (11 May 1966).

12. Rose, P. H., and Stankevics, J. O., Stagnation Point Heat Transfer Measurements in Partially Ionized Air, Avco/Everett Research Laboratory, RR 143 (April 1963).

13. Hoshizaki, H., Heat Transfer in Planetary Atmospheres at Super-satellite Speeds, ARS Journal, 32 (October 1962).

14. Rose, P. H., and Stark, W. I., Stagnation Point Heat Transfer Measurements in Dissociated Air, Journal of Aero/Space Science, 25, 2 (February 1958).

15. Warren, W. R., Rodgers, D. A., and Harris, C. J., The Development of an Electrically-Heated Shock-Driven Test Facility, MSVD General Electric TIS Report R62SD37 (April 1962).

16. Offenhartz, E., Weisblatt, H., and Flagg, R. F., Stagnation Point Heat Transfer Measurements at Super-Satellite Speeds, Journal Royal Aeronautical Society (January 1962).

17. Scala, S. M., and Warren, W. R., Hypervelocity Stagnation Point Heat Transfer, ARS Journal, 32 (January 1962).

18. Pallone, A., and Van Tassell, W., The Effects of Ionization on Stagnation-Point Heat Transfer in Air and in Nitrogen, Avco Research and Advanced Development Division, Technical Memorandum RAD TM 62-75 (September 1962).

19. Cohen, N., Boundary Layer Similar Solutions and Correlation Equations for Laminar Heat Transfer Distribution in Equilibrium Air at Velocities up to 41,000 Feet Per Second, NASA Technical Report R-118 (1961).

20. Fay, J. A., and Kemp, N. H., Theory of Stagnation Point Heat Transfer in a Partially Ionized Diatomic Gas, Avco Everett Research Laboratory, Research Report 144 (December 1962), presented at IAS Annual Meeting, New York (January 1963). IAS Preprint No. 63-60.

21. Detra, R. W., and Hidalgo, H., Generalized Heat Transfer Formulae and Graphs, Avco Everett Research Laboratory, RR72 (March 1960).

22. Nestler, D., and Musser, I., Correlations for Convective Heat Transfer, Pressure Distribution, and Shock Detachment Distance for Blunt, Axisymmetric Forebodies, Aerophysics Tech. Memo., 149, General Electric/MSD (January 1960).

23. Gudonov, S., Zabrodin, A., and Prokopov, G., The Difference Schemes for Two Dimensional Unsteady Problems in Gas Dynamics and the Calculation of Flows with a Detached Shock Wave, Journal of Computing Mathematics and Mathematical Physics, Academy of Sciences, USSR, Vol. I, No. 6 (November - December 1961); translation by T. Strelkoff.

24. Masson, B., Two-Dimensional Flow Field Calculations by the Godunov Method, Tech. Report 3575, Picatinny Arsenal, Dover, New Jersey (July 1967).

25. Schurmann, E., Engineering Methods for the Analysis of Aerodynamic Heating, Avco/RAD Technical Memorandum RAD-TM-63-68 (11 November 1963).

26. Marvin, J., and Sinclair, A., Convective Heating in Regions of Large, Favorable Pressure Gradient, AIAA Journal (November 1967), pp. 194049.

27. Brower, W. G., Jr., Leading Edge Separation of Laminar Boundary Layers in Supersonic Flow, Aerodynamics Section Memo No. 189, Avco/RAD (17 March 1959).

28. Tobak, M., and Peterson, V. L., Theory of Tumbling Bodies Entering Planetary Atmospheres with Application to Probe Vehicles and the Australian Tekites, NASA TR-R-203 (July 1964).

29. Brower, W., Jr., Leading Edge Separation of Laminar Boundary Layers in Supersonic Flow, Aerodynamics Section Memo No. 189, Avco/RAD (17 March 1959).

30. Chapman, D., Kuehn, D., and Larson, H., Investigation of Separated Flows in Supersonic and Subsonic Streams with Emphasis on the Effect of Transition, NACA Report 1356 (1958).

31. Charwat, A., Roos, J., Dewey, F., Jr., and Hitz, J., An Investigation of Separated Flows - Part I; The Pressure Field, J. Aerospace Sciences (June 1961).

32. Erdos, J., and Pallone, A., Shock-Boundary Layer Interaction and Flow Separation, Avco Technical Report RAD-TR-61-23 (15 August 1961).

33. Erdos, J., Hand Calculation Procedures for Estimation of Occurrence and Extent of Flow Separation, Avco Aerodynamics Section Technical Release, T510-TR-62-20 (1 February 1962).

34. Toups, K. A., A General Computer Program for the Determination of Radiant, Interchange Configuration and Form Factors - CONFACT II, Report No. SID 65-1043-2, North American Aviation, Inc. (October 1965).

35. Fick, J. L., MLFTHAN-LMSC Thermal Network Analyzer Mark I, Distribution No. 1295.

36. Hamilton, D. C., and Morgan, W. R., Radiant-Interchange Configuration Factors, NACA TN-2836.

37. McAdams, W. H., Heat Transmission, 3rd ed., McGraw-Hill Book Company, Inc., New York (1954).

38. Sparrow, E. M., and Cess, R. D., Radiation Heat Transfer, Brooks/Cole Publishing Company, Belmont, California (1966).

39. Quarterly Progress Report of Research and Development in a Thermal Insulation Study, Report No. ALO 3632-14, Union Carbide Corporation - Linde Division (January-March 1967).

40. Pearson, B. D., Preliminary Results from the Ames Emissivity Experiment on OS-II, Progress in Astronautics and Aeronautics, 18, Academic Press (1966), pp. 459-72.

41. Streed, E. R., and Arvesen, J. C., A Review of the Status of Spacecraft Thermal Control Materials, SAMPE Volume II (Society of Aerospace Material and Process Engineers), Western Periodicals Co. (1967), pp. 181-92.

42. Greenberg, S. A., Vance, D. A., and Streed, E. R., Low Solar Absorptance Surfaces with Controlled Emittance: A Second Generation of Thermal Control Coatings, papers No. 67-343, AIAA Thermophysics Specialist Conference, New Orleans (April 1967).

43. Weingarten, V. I., and Seide, P. Elastic Stability of Thin-Walled Cylindrical and Conical Shells Under Combined External Pressure and Axial Compression, AIAA Journal, 3 (1965), pp. 913-20.

44. Batdorf, S. B., A Simplified Method of Elastic Stability Analysis for Thin Cylindrical Shells, NACA Report No. 874 (1947).

45. Timoshenko, S., and Gere, J. M., Theory of Elastic Stability, Second Edition, Sections 7.10 and 11.13, McGraw-Hill Book Company (1961).

46. Homewood, R. H., Brine, A. C., and Johnson, A. E., Instability of Monocoque Shells, Society for Experimental Stress Analysis, Paper No. 457, presented at Washington, D.C. (May 1959).

47. Kaplan, A., and Fung, Y. C., A Nonlinear Theory of Bending and Buckling of Thin Elastic Shallow Spherical Shells, NACA TN-3212 (1954).

48. Kloppel, K., and Jungbluth, O., Beitrag zum Durchslag Problem Dunn wandiget Kungelschalen, Der Stahlbau, 22, Springer, Berlin (1935), pp. 121-30, 288.

49. Serpico, J. C., Elastic Stability of Orthotropic Conical and Cylindrical Shells Subjected to Axisymmetric Loading Conditions, AIAA Journal, 1 (1963), pp. 128-37.

50. Comparative Studies of Conceptual Design and Qualifications Procedure for a Mars Probe/Lander, Vol., Book 2, AVSSD-0006-66-RR, Contract NASA-5224.

51. Preliminary Design of the PU-238 Isotope Brayton Cycle Power System for MORL, Missile and Space Division, Douglas Aircraft Co., Santa Monica, California (September 1965).

REPORT DISTRIBUTION LIST FOR CONTRACT NAS3-10938

NASA Lewis Research Center
21000 Brookpark Road
Cleveland, Ohio 44135
Attention:

Lloyd I. Shure (3)
Mail Stop 500-201

W. T. Wintucky (1)
Mail Stop 500-201

H. O. Slone (1)
Mail Stop 500-201

B. Lubarsky (1)
Mail Stop 500-201

T. A. Moss (1)
Mail Stop 500-201

J. E. Dilley (1)
Mail Stop 500-309

P. E. Foster (1)
Mail Stop 3-19

Library (2)
Mail Stop 60-3

Report Control Office (1)
Mail Stop 5-5

Technology Utilization Office (1)
Mail Stop 3-19

NASA Lewis Research Center
Plum Brook Station
Taylor Road
Sandusky, Ohio 44870
Attention:

J. C. Nettles (1)
Mail Stop 7141-6

National Aeronautics & Space Adm.
Washington, D. C. 20546
Attention:

B. Leefer RNP (1)
T. B. Kerr RNS (1)
T. Hagler MTY (1)
H. Rochen RNP (1)

NASA Scientific & Technical Information Facility (1)
Post Office Box 5700
Bethesda, Maryland 20014
Attention:

Acquisitions Branch (SQT-34054)

NASA Ames Research Center (1)
Moffett Field, California 94035
Attention: Library

V. Peterson (1)
E. Katzen (1)
G. Goodwin (1)

NASA Goddard Space Flight Center (1)
Greenbelt, Maryland 20771
Attention: Library

NASA Manned Spacecraft Center (1)
Houston, Texas 77058
Attention: Library

NASA Marshall Space Flight Center (1)
Huntsville, Alabama 35812
Attention: Library

Air Force Systems Command (1)
Aeronautical Systems Division
Wright-Patterson Air Force Base, Ohio
45433
Attention: Library

Power Information Center (1)
University of Pennsylvania
3401 Market Street, Room 2107
Philadelphia, Pennsylvania 19104

NASA Langley Research Center (1)
Langley Station
Hampton, Virginia 23365
Attention: Library

NASA Manned Spacecraft Center
Houston, Texas 77058
Attention:
Tony Redding EP-5 (1)
E. Olling EP-4 (1)

Jet Propulsion Laboratory (1)
4800 Oak Grove Drive
Pasadena, California 91103
Attention: Library

Battelle Memorial Institute (1)
505 King Avenue
Columbus, Ohio 43201
Attention: Library

Institute for Defense Analyses (1)
400 Army-Navy Drive
Arlington, Virginia 22202
Attention: Library

Aerojet-General Corporation (1)
Von Karman Center
Azusa, California 91702
Attention: Library

The Boeing Company (1)
Aero-Space Division
Box 3707
Seattle, Washington 98124
Attention: Library

Aerospace Corporation (1)
P. O. Box 95085
Los Angeles, California 91745
Attention: Library

General Electric Company (1)
Reentry Systems Department
3198 Chestnut Street
Philadelphia, Pennsylvania 19104
Attention: Mr. R. Brast

SAMSO
Los Angeles Air Force Station
Los Angeles, California 90045
Attention: Library (1)
Maj. H. M. Butler (1)

Douglas Aircraft Company (1)
3000 Ocean Park Blvd.
Santa Monica, California 90406
Attention: Library

General Electric Company (1)
Flight Propulsion Division
Cincinnati, Ohio 45215
Attention: Library

McDonnell Douglas Corporation (1)
Missile & Space Systems Division
3000 Ocean Park Blvd.
Santa Monica, California 90406
Attention: Library

General Motors Corporation (1)
Indianapolis, Indiana 46206
Attention: Library

Lockheed Missiles & Space Co. (1)
P. O. Box 504
Sunnyvale, California 94088
Attention: Mr. H. Greenfield

Pratt & Whitney Aircraft (1)
400 Main Street
East Hartford, Connecticut 06108
Attention: Library

Sunstrand Denver (1)
2480 West 70 Avenue
Denver, Colorado 80221
Attention: Library

Martin Marietta Corp.
P. O. Box 988
Baltimore, Maryland 21203
Attention: Mr. Barney Mead (1)
Mail Stop 836

McDonnell-Douglas Corp. (1)
Lambert Field
St. Louis, Missouri 63166
Attention: Library

NASA-Langley Research Center
Langley Station
Hampton, Virginia 23365
Attention:

Mr. W. Hayes, MORL Studies Office (1)
Mr. P. J. Bobbitt, Applied Mech. Br. (1)

TRW Systems Division (1)
One Space Park
Redondo Beach, California 90278
Attention: Library

U. S. Atomic Energy Commission
Space Nuclear Systems Div.
Washington, D.C. 20545
Attention:

Dr. L. Topper (1)
Mr. R. L. Carpenter (1)
Mr. G. Newby (1)
Dr. J. A. Powers (1)

Sandia Corporation
Sandia Base
Albuquerque, New Mexico 87115
Attention: Library (1)
Mr. A. J. Clark, Dept. 9330 (1)
Mr. R. W. Hanke, Dept. 9331 (1)
Mr. J. W. McKiernan, Dept. 9331 (1)

Donald Douglas Laboratories
McDonnell-Douglas Corp.
Richland, Washington 99352
Attention: Library (1)

Bellcomm, Inc. (1)
1100 17th St. N.W.
Washington, D. C. 20036
Attention: Mr. C. Witze

Department of the Navy (1)
Naval Facilities Engineering Command
Nuclear ENgineering Div.
Washington, D. C. 20390
Attention: Mr. M. Starr

Atomics International
P. O. Box 309
8900 DeSoto Ave.
Canoga Park, Calif. 91304
Attention: Mr. W. Botts (1)

USAF Aeropropulsion Lab.
Wright-Patterson AFB, Ohio 45433
Attention: Mr. G. Thompson (APIP-I) (1)

Research Library - Lowell	(3)
Research Library - Wilmington	(1)
Reports Distribution Center	(46)

Unclassified

Security Classification

DOCUMENT CONTROL DATA - R&D

(Security classification of title, body of abstract and indexing annotation must be entered when the overall report is classified)

1. ORIGINATING ACTIVITY *(Corporate author)*
Avco Missiles, Space and Electronics Group
Space Systems Division
Lowell Industrial Park
Lowell, Massachusetts 01851

2a. REPORT SECURITY CLASSIFICATION
Unclassified

2b. GROUP

3. REPORT TITLE
Isotope Reentry Vehicle Design Study
Conceptual Design -- Phase IA--Topical Report

4. DESCRIPTIVE NOTES *(Type of report and inclusive dates)*
Topical Report

5. AUTHOR(S) *(Last name, first name, initial)*

6. REPORT DATE	7a. TOTAL NO. OF PAGES	7b. NO. OF REFS
May 1968	528	51

8a. CONTRACT OR GRANT NO.	9a. ORIGINATOR'S REPORT NUMBER(S)
NAS3-10938	AVSSD-0071-68-CR
b. PROJECT NO.	
c.	9b. OTHER REPORT NO(S) *(Any other numbers that may be assigned this report)*
d.	NASA CR-72366

10. AVAILABILITY/LIMITATION NOTICES

11. SUPPLEMENTARY NOTES	12. SPONSORING MILITARY ACTIVITY
	Technical Management NASA Lewis Research Center Cleveland, Ohio

13. ABSTRACT

This document summarizes the Phase IA conceptual design effort on the Isotope Reentry Vehicle (IRV) study. The major objective of the study is to develop a preliminary design of a 25 KW_t Pu 238 IRV. Major design emphasis is on system safety and developability. The IRV is configured to meet minimum practical diameter and weight limits. During Phase IA various IRV, heat source, and heat-source heat exchanger concept combinations have been developed and evaluated. Three IRV systems have been recommended for detailed conceptual design evaluation in Phase IB.

DD FORM 1 JAN 64 1473

Unclassified

Security Classification

14 KEY WORDS	LINK A		LINK B		LINK C	
	ROLE	WT	ROLE	WT	ROLE	WT
Isotope Reentry Vehicle						
Brayton Cycle Power Supplies						
Plutonium 238 Fuel Capsule						
Heat Shields						
Refractory Metal Structure						
Impact Attenuation						

INSTRUCTIONS

1. ORIGINATING ACTIVITY: Enter the name and address of the contractor, subcontractor, grantee, Department of Defense activity or other organization *(corporate author)* issuing the report.

2a. REPORT SECURITY CLASSIFICATION: Enter the overall security classification of the report. Indicate whether "Restricted Data" is included. Marking is to be in accordance with appropriate security regulations.

2b. GROUP: Automatic downgrading is specified in DoD Directive 5200.10 and Armed Forces Industrial Manual. Enter the group number. Also, when applicable, show that optional markings have been used for Group 3 and Group 4 as authorized.

3. REPORT TITLE: Enter the complete report title in all capital letters. Titles in all cases should be unclassified. If a meaningful title cannot be selected without classification, show title classification in all capitals in parenthesis immediately following the title.

4. DESCRIPTIVE NOTES: If appropriate, enter the type of report, e.g., interim, progress, summary, annual, or final. Give the inclusive dates when a specific reporting period is covered.

5. AUTHOR(S): Enter the name(s) of author(s) as shown on or in the report. Enter last name, first name, middle initial. If military, show rank and branch of service. The name of the principal author is an absolute minimum requirement.

6. REPORT DATE: Enter the date of the report as day, month, year; or month, year. If more than one date appears on the report, use date of publication.

7a. TOTAL NUMBER OF PAGES: The total page count should follow normal pagination procedures, i.e., enter the number of pages containing information.

7b. NUMBER OF REFERENCES: Enter the total number of references cited in the report.

8a. CONTRACT OR GRANT NUMBER: If appropriate, enter the applicable number of the contract or grant under which the report was written.

8b, 8c, & 8d. PROJECT NUMBER: Enter the appropriate military department identification, such as project number, subproject number, system numbers, task number, etc.

9a. ORIGINATOR'S REPORT NUMBER(S): Enter the official report number by which the document will be identified and controlled by the originating activity. This number must be unique to this report.

9b. OTHER REPORT NUMBER(S): If the report has been assigned any other report numbers *(either by the originator or by the sponsor)*, also enter this number(s).

10. AVAILABILITY/LIMITATION NOTICES: Enter any limitations on further dissemination of the report, other than those imposed by security classification, using standard statements such as:

(1) "Qualified requesters may obtain copies of this report from DDC."

(2) "Foreign announcement and dissemination of this report by DDC is not authorized."

(3) "U. S. Government agencies may obtain copies of this report directly from DDC. Other qualified DDC users shall request through _____."

(4) "U. S. military agencies may obtain copies of this report directly from DDC. Other qualified users shall request through _____."

(5) "All distribution of this report is controlled. Qualified DDC users shall request through _____."

If the report has been furnished to the Office of Technical Services, Department of Commerce, for sale to the public, indicate this fact and enter the price, if known.

11. SUPPLEMENTARY NOTES: Use for additional explanatory notes.

12. SPONSORING MILITARY ACTIVITY: Enter the name of the departmental project office or laboratory sponsoring *(paying for)* the research and development. Include address.

13. ABSTRACT: Enter an abstract giving a brief and factual summary of the document indicative of the report, even though it may also appear elsewhere in the body of the technical report. If additional space is required, a continuation sheet shall be attached.

It is highly desirable that the abstract of classified reports be unclassified. Each paragraph of the abstract shall end with an indication of the military security classification of the information in the paragraph, represented as *(TS), (S), (C), or (U)*.

There is no limitation on the length of the abstract. However, the suggested length is from 150 to 225 words.

14. KEY WORDS: Key words are technically meaningful terms or short phrases that characterize a report and may be used as index entries for cataloging the report. Key words must be selected so that no security classification is required. Identifiers, such as equipment model designation, trade name, military project code name, geographic location, may be used as key words but will be followed by an indication of technical context. The assignment of links, rules, and weights is optional.